Current Clinical Urology
Series Editor: Eric A. Klein

Pat F. Fulgham
Bruce R. Gilbert *Editors*

Practical Urological Ultrasound

Second Edition

Humana Press

Current Clinical Urology

Eric A.Klein, MD, Series Editor
Professor of Surgery
Cleveland Clinic Lerner College of Medicine Head,
Section of Urologic Oncology
Glickman Urological and Kidney Institute
Cleveland, OH

More information about this series at http://www.springer.com/series/7635

Pat F. Fulgham • Bruce R. Gilbert
Editors

Practical Urological Ultrasound

Second Edition

Humana Press

Editors
Pat F. Fulgham
Department of Urology
Texas Health Presbyterian Dallas
Dallas, TX, USA

Bruce R. Gilbert
Hofstra North Shore LIJ
Smith Institute for Urology
Great Neck, NY, USA

ISSN 2197-7194 ISSN 2197-7208 (electronic)
Current Clinical Urology
ISBN 978-3-319-43867-2 ISBN 978-3-319-43868-9 (eBook)
DOI 10.1007/978-3-319-43868-9

Library of Congress Control Number: 2016956231

Printed on acid-free paper

This Humana Press imprint is published by Springer Nature
The registered company is Springer International Publishing AG
The registered company address is: Gewerbestrasse 11, 6330 Cham, Switzerland

To: Edwin Darracott Vaughan, M.D.
(May 13, 1939–April 22, 2016), beloved mentor
and friend who will always be an enduring inspiration.

Preface

The first edition of *Practical Urological Ultrasound* was an outgrowth of a campaign to teach practicing urologists the basic techniques for performing and documenting ultrasound examinations on urologic patients. An emphasis on an organ-based approach was intended to mimic what was encountered in daily practice and to extend the principles learned to intraoperative applications.

The more pervasive use of MRI in conjunction with radionuclide studies and, more recently, for MRI-guided prostate biopsy would seem to render a fundamental understanding of ultrasound less vital. To the contrary, the skillful use of ultrasound is critical to the co-registration of images for MRI-TRUS fusion biopsy of the prostate, for identification of lesions for focal therapy of the prostate, and for intraoperative guidance during complex renal surgery.

In fact, multi-parametric ultrasound (gray scale, Doppler, contrast-enhanced, and elastography) may function as well as MRI-based procedures in a variety of clinical situations at a fraction of the cost. In the short time since our first edition, improvements in transducers and overall image quality have made ultrasound a fundamental part of daily urologic practice and have the potential to replace axial imaging for some applications and procedures.

Central to urologist-performed imaging and imaging-based procedures is a thorough understanding of the physics underlying ultrasound imaging. We hope this edition will continue to enlighten urologists and encourage them to personally perform these procedures on behalf of their patients.

Dallas, TX, USA — Pat F. Fulgham

Acknowledgments

The subject of this book has been a passion of mine for the past 10 years, and, like many roads in life, it would not have been possible without the support and tutelage of mentors, colleagues, and friends. I dedicate this book to the memory of Dr. E. Darracott Vaughan. He has always been my mentor and inspiration for the love of knowledge and teaching. In particular, for his vision, encouragement, and belief in me when I was a postgraduate research fellow in physiology, I owe my medical career to him.

This book was the vision of my coeditor, colleague, and friend Dr. Pat Fulgham. Through his leadership over these past years, he has helped elevate the art of urologic ultrasound to a subspecialty within urology. He is a gifted surgeon, articulate spokesman, and tireless academician who accepts nothing less than perfection from himself, which is contagious among all that have had the great fortune to work with him.

To the authors of this book, I am indebted. They have tirelessly given their precious time away from family and their busy clinical practices to share their experience. Their teachings as expressed in this text form the basis of urologic ultrasound.

My wife, and best friend, Betsy has been the most supportive and loving partner throughout the late nights and endless weekends involved in this project. She is, and has always been, my source of inspiration.

Bruce R. Gilbert

Contents

Contributors

John Samuel Banerji, MD, MCh (Urology), DNB (Urology) Section of Urology and Renal Transplantation, Virginia Mason, Seattle, WA, USA

Z. Chad Baxter, M.D. Department of Urology, UCLA David Geffen School of Medicine, Santa Monica, CA, USA

Akhil Das, M.D. Department of Urology, Sidney Kimmel Medical College at Thomas Jefferson University, Philadelphia, PA, USA

Majid Eshghi, M.D., F.A.C.S., M.B.A. Department of Urology, New York Medical College, Westchester Medical Center, New York, NY, USA

Farzeen Firoozi, M.D., F.A.C.S. Department of Urology, Hofstra Northshore–LIJ School of Medicine, The Arthur Smith Institute for Urology, Center of Pelvic Health and Reconstructive Surgery, Northwell Health System, Lake Success, NY, USA

Pat Fox Fulgham, M.D., F.A.C.S. Department of Urology, Texas Health Presbyterian Hospital of Dallas, Dallas, TX, USA

Bruce R. Gilbert, M.D., Ph.D. The Smith Institute for Urology, Northwell Health System, New Hyde Park, NY, USA

Etai Goldenberg, M.D. Urology Consultants, Ltd., Saint Louis, MO, USA

Nikhil K. Gupta, M.D. Smith Institute for Urology, Hofstra University, Northwell Health System, Lake Success, NY, USA

Adam Howe, M.D. Division of Pediatric Urology, Hofstra Northwell School of Medicine, Cohen Children's Medical Center of New York of the Northwell Health System, Lake Success, NY, USA

Fernando J. Kim, M.D., M.B.A., F.A.C.S. Department of Urology, Denver Health Medical Center and University of Colorado Denver, Denver, CO, USA

Xialong Shawn Liu, M.D. Department of Urology, Tufts Medical Center, Boston, MA, USA

Lane S. Palmer, M.D., F.A.C.S. Division of Pediatric Urology, Hofstra Northwell School of Medicine, Cohen Children's Medical Center of New York of the Northwell Health System, Lake Success, NY, USA

Ricardo Palmerola, M.D. Department of Urology, Hofstra Northshore–LIJ School of Medicine, The Arthur Smith Institute for Urology, Center of Pelvic Health and Reconstructive Surgery, Northwell Health System, Lake Success, NY, USA

Rodrigo R. Pessoa, M.D. Department of Urology, Denver Health Medical Center and University of Colorado Denver, Denver, CO, USA

Christopher Robert Porter, M.D., F.A.C.S. Section of Urology And Renal Transplantation, Virginia Mason, Seattle, WA, USA

Soroush Rais-Bahrami, M.D. Departments of Urology and Radiology, University of Alabama at Birmingham, Birmingham, AL, USA

Gideon D. Richards, M.D. Arizona State Urological Institute, Chandler, AZ, USA

Daniel B. Rukstalis, M.D. Department of Urology, Wake Forest Baptist Medical Center, Winston-Salem, NC, USA

Jennifer Simmons, M.D. Department of Urology, Geisinger Health System, Danville, PA, USA

Whitney Smith, M.D. Department of Urology, Sidney Kimmel Medical College at Thomas Jefferson University, Philadelphia, PA, USA

R. Ernest Sosa, M.D. Division of Urology, Veterans Administration Healthcare System, New York, NY, USA

Edouard J. Trabulsi, M.D. Department of Urology, Sidney Kimmel Medical College of Thomas Jefferson University, Philadelphia, PA, USA

Vinaya Pavithra Vasudevan, M.D. Smith Institute of Urology, Northwell Health Systems, New Hyde Park, NY, USA

Nikhil Waingankar, M.D. Department of Urology, Mt. Sinai Hospital, Astoria, NY, USA

Department of Population Health Science and Policy, Mt. Sinai Hospital, Astoria, NY, USA

History of Ultrasound in Urology

1

Vinaya Vasudevan, Nikhil Waingankar,
and Bruce R. Gilbert

Introduction

Ultrasound is the portion of the acoustic spectrum characterized by sonic waves that emanate at frequencies greater than that of the upper limit of sound audible to humans, 20 kHz. A phenomenon of physics that is found throughout nature, ultrasound is utilized by rodents, dogs, moths, dolphins, whales, frogs, and bats for a variety of purposes, including communication, evading predators, and locating prey [1–4]. Lorenzo Spallanzani, an eighteenth century Italian Biologist and physiologist, was the first to provide experimental evidence that non-audible sound exists. Moreover, he hypothesized the utility of ultrasound in his work with bats by demonstrating that bats use sound rather than sight to locate insects and avoid obstacles during flight; this was proven in an experiment where blind-folded bats were able to fly without navigational difficulty while bats with their mouths covered were not. He later determined through operant conditioning that the Eptesicus fuscus bat can perceive tones between 2.5 and 100 kHz [5, 6].

The human application of ultrasound began in 1880 with the work of brothers Pierre and Jacques Curie, who discovered that when pressure is applied to certain crystals, they generate electric voltage [7]. The following year, Gabriel Lippmann demonstrated the reciprocal effect that crystals placed in an electric field become compressed [8]. The Curies demonstrated that when placed in an alternating electric current, the crystals underwent either expansion or contraction and produced high frequency sound waves, thus creating the foundation for further work on piezoelectricity. Pierre Curie met his future wife Marie—with whom he later shared the Nobel Prize for their work on radioactivity [9]—in 1894 when Marie was searching for a way to measure the radioactive emission of uranium salts. She turned to the piezoelectric quartz crystal as a solution, combining it with an ionization chamber and quadrant electrometer; this marked the first time piezoelectricity was used as an investigative tool [10].

The sinking of the RMS Titanic in 1912 drove the public's desire for a device capable of echolocation, or the use of sound waves to locate hidden objects. This was intensified 2 years later with the

V. Vasudevan, M.D. (✉)
Smith Institute of Urology, Northwell Health Systems, 450 Lakeville Road,
New Hyde Park, NY 11042, USA
E-mail: vvasudevan@northwell.edu

B.R. Gilbert, M.D., Ph.D.
Hofstra Northwell School of Medicine, The Arthur Smith Institute for Urology, 450 Lakeville Road, Suite M41, New Hyde Park, NY 11042, USA
E-mail: bgilbert@gmail.com

N. Waingankar, M.D.
Department of Urology, Mt. Sinai Hospital, 25-10 30th Ave, Astoria, NY 11102, USA

Department of Population Health Science and Policy, Mt. Sinai Hospital, 25-10 30th Ave,
Astoria, NY 11102, USA
E-mail: WaingankarMD@gmail.com

P.F. Fulgham, B.R. Gilbert (eds.), *Practical Urological Ultrasound*, Current Clinical Urology,
DOI 10.1007/978-3-319-43868-9_1

beginning of World War I, as submarine warfare became a vital part of both the Central and Allied Powers' strategies. Canadian inventor Reginald Aubrey Fessenden—perhaps most famous for his work in pioneering radio broadcasting and developing the Niagara Falls power plant—volunteered during World War I to help create an acoustic-based system for echolocation. Within 3 months he developed a high-power oscillator consisting of a 20 cm copper tube placed in a pattern of perpendicularly oriented magnetic fields that was capable of detecting an iceberg 2 miles away, and being detected underwater by a receiver placed 50 miles away [11].

A contemporary of Fessenden and student of Pierre Curie, Paul Langevin was similarly interested in using acoustic technology for the detection of submarines in World War I. Using piezoelectricity, he developed an ultrasound generator in which the frequency of the alternating field was matched to the resonant frequency of the quartz crystals. This resonance evoked by the crystal produced mechanical waves that were transmitted through the surrounding medium in ultrasonic frequency, and were subsequently detected by the same crystals [12, 13]. Dubbed the "hydrophone," this represented the first model of what we know today as sound navigation and ranging, or SONAR. Although there were only sporadic reports on the use of SONAR in sinking German U-boats, SONAR was vital to both the Allied and Axis Powers during World War II [14].

In 1928, Russian scientist Sergei Sokolov further advanced the applicability of ultrasound in his experiments at Ulyanov Electrotechnical Institute. Using a "reflectoscope," Sokolov directed sound waves through metal objects, which were reflected at the opposite side of the object and traveled back to the reflectoscope. He determined that flaws within the metals would alter the otherwise predictable course of the sound waves. Sokolov also proposed the first "sonic camera," in which a metal's flaw could be imaged in high resolution. The actual output, however, was not adequate for practical usage. These early experiments describe what we now know as through transmission [15]. Sokolov is regarded by many as the "Father of Ultrasonics," and was awarded the Stalin prize for his work [13].

In 1936, German scientist Raimar Pohlman described an ultrasonic imaging method based on transmission via acoustic lenses, with conversion of the acoustic image into a visual entity. Two years later, Pohlman became the first to describe the use of ultrasound as a treatment modality when he observed its therapeutic effect when introduced into human tissues [16]. Austrian neurologist Karl Dussik is credited with being the first to use ultrasound as a diagnostic tool. In 1940 in a series of experiments attempting to map the human brain and potentially locate brain tumors, transducers were placed on each side of a patient's head, which along with the transducers, was partially immersed in water. At a frequency of 1.2 MHz, Dussik's "hyperphonography" was able to produce low resolution "ventriculograms" [17]. Other investigators were unable to reproduce the same images as Dussik, sparking controversy that this may have not been true images of the cerebral ventricles, but rather, acoustic artifact. Dussik's work led MIT physician HT Ballantyne to conduct similar experiments, where they demonstrated that an empty skull produces the same images obtained by Dussik. They concluded that attenuation patterns produced by the skull were contributing to the patterns that Dussik had previously thought resulted from changes in acoustic transmission caused by the ventricles. These findings led the United States Atomic Energy Commission to conclude that ultrasound had no role in the diagnosis of brain pathology [18, 19].

In 1949, John Wild, a surgeon who had spent time in World War II treating numerous soldiers with abdominal distention following explosions, used military aviation-grade ultrasonic equipment to measure bowel thickness as a noninvasive tool to determine the need for surgical intervention. He later used A-mode comparisons of normal and cancerous tissue to demonstrate that ultrasound could be useful in the detection of cancer growth. Wild teamed up with engineer John Reid to build the first portable "echograph" for use in hospitals (see Fig. 1.1) and also to develop a scanner that was capable of detecting breast and colon cancer by using pulsed waves to allow display the location and reflectivity of an object, a mode that would later be described as "brightness mode," or simply B-mode [13, 20, 21].

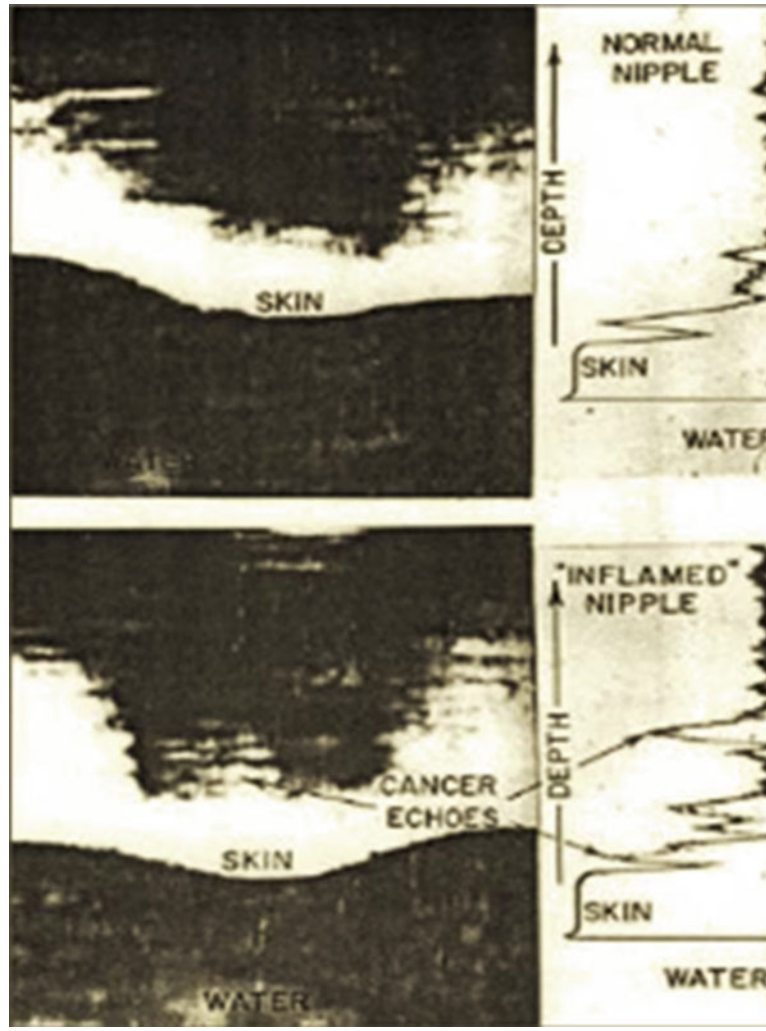

Fig. 1.1 An example of one of Wild and Reid's original echographs, pictured above, was used to measure skin thickness as compared to breast cancer tissue thickness to determine a diagnosis of breast cancer [22]. *Reproduced with permission from Hill CR, Early days of scanning: Pioneers and Sleepwalkers, in Radiography. 2009 (15): p. 15–22, courtesy of Elsevier*

Following the post-World War II resurgence of interest in cardiac surgery, Inge Edler and Hellmuth Hertz began to investigate noninvasive methods of detecting mitral stenosis, a disease with relatively poor results at the time. Using an ultrasonic reflectoscope with tracings recorded on slowly moving photographic film designed by Hertz (see Fig. 1.2), they were able to capture moving structures within the heart. Dubbed "Ultrasound Cardiography," this represented the first echocardiogram, which was capable of differentiating mitral stenosis from mitral regurgitation, and detecting atrial thrombi, myxomas, and pericardial effusions [23, 24].

With the support of the Veterans Administration and United States Public Health Service, Holmes et al. described the use of ultrasound to detect soft tissue structures with an ultrasonic "sonascope." This consisted of a large water bath in which the patient would sit, a sound generator mounted on the tub, and an oscilloscope which would display the images. The sonascope was capable of identifying a cirrhotic liver, renal cyst, and differentiating veins, arteries, and nerves in the neck. Consistent with the results of their predecessors, however.

The use of ultrasound in obstetrics and gynecology began in 1954 when Ian Donald became interested in the use of A-mode, or amplitude-mode, which uses a single transducer to plot echoes on a screen as a function of depth; one of the early uses of this was to differentiate solid from cystic masses.

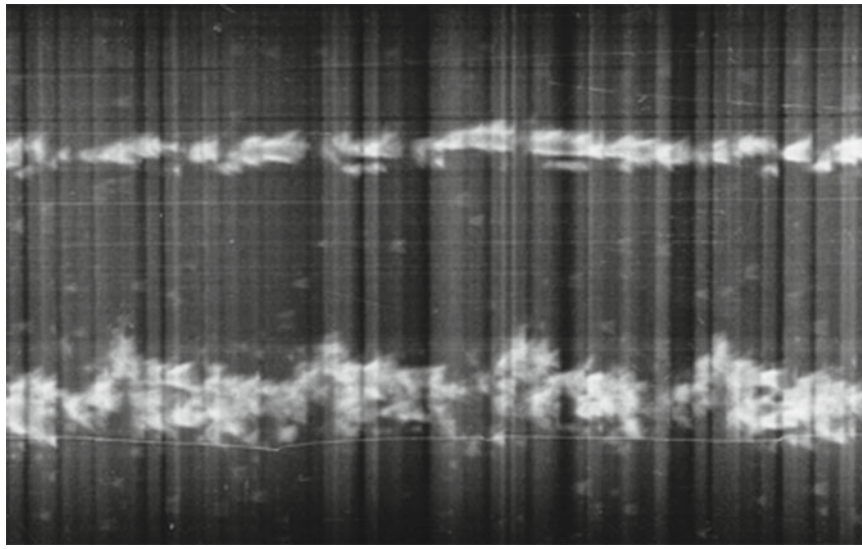

Fig. 1.2 The first echocardiographic recording is displayed as a "motion-mode," or M-mode, tracing displaying ultrasonic tracings of the left ventricular posterior wall [24]. *Reproduced with permission from Fraser, A.G., Inge Edler and the origins of clinical echocardiography. Eur J Echocardiogr, 2001. 2(1): p. 3–5, courtesy of Oxford University Press*

Using a borrowed flaw-detector, he initially found that the patterns of the two masses were sonically unique. Working with the research department of an atomic boilermaker company, he led a team that developed the first contact scanner. Obviating the need for a large water bath, this device was hand-operated and kept in contact with skin and coupled with olive oil. Captured on Polaroid® film with an open shutter, abdominal masses could be reliably and reproducibly differentiated using ultrasound. Three years later, Donald collaborated with his team of engineers to develop a means to measure distances on the output on a cathode ray tube, which was subsequently used to determine fetal head size [13, 25–27].

History of Doppler Ultrasound

In 1842, Christian Johann Doppler theorized that the frequency of light received at a distance from a fixed source is different than the frequency emitted if the source is in motion [28]. More than 100 years later, this principle was applied to sound by Satomura in his study on cardiac valvular motion and peripheral blood vessel pulsation [29]. In 1958, Seattle pediatrician Rushmer and his team of engineers further advanced the technology with their development of transcutaneous continuous-wave flow measurements and spectral analysis in peripheral and extracranial brain vessels [30]. Real-time imaging—developed in 1962 by Homes—was born out of the principal of "compounding," which allowed the sonographer to sweep the transducer across the target to continuously add information to the scan; the phosphordecay display left residual images from the prior transducer position on the screen, allowing the entire target to be visualized [13]. The first commercially available real-time scanner was produced by Siemens, and its first published use was in the diagnosis of hydrops fetalis [31, 32].

Bernstine and Callagan were the first to report the obstetric utility of Doppler in their 1964 report on ultrasonic detection of fetal heart movement, thus laying the foundation for continuous fetal monitoring [33]. The same year, Buschmann was the first report "carotid echography" for the diagnosis of carotid artery thrombosis [34], although debate ensued as to whether ultrasound was capable of identifying the carotid bifurcation or its branches into the internal and external carotid arteries [35–37].

In 1966, Kato and Izumi developed directional Doppler that was capable of determining direction of flow [32, 38]. The following year, McLeod reported similar findings using phase shift in the United States [30, 39, 40]. By 1967, the use of Doppler ultrasound had spread to Europe, where continuous-wave ultrasound (which does not allow precise spatial localization) was being used to diagnose occlusive disease of neck and limb arteries, venous thrombosis, and valvular insufficiency with accuracy [41]. Pulsed Doppler soon provided the capability of sampling specific Doppler signals in target tissues, a function that quickly became clinically applicable in the detection of valvular motion and differential flow rates within the heart [42].

The addition of color flow mapping to Doppler ultrasound allowed real-time mapping of blood flow patterns [43]. The limitations of color flow, including angle dependence and difficulty assessing flow in slow-flow states, were soon appreciated. These were overcome with the advent of an alternative form of Doppler, termed "Power Doppler." This alternative to routine color flow was found to be useful in confirming or excluding difficult cases of testicular or ovarian torsion and vascular thrombosis [44].

Researchers next turned their attention to techniques to improve the clarity and reduce artifact within ultrasound-guided images. In 1980, real-time compound sonography was developed by using the probe to obtain multiple images from different viewing angles. Computed beam steering technology is then used to combine multiplanar images into one compound image in real time. Summation of these images reduced artifact and improved delineation of surfaces. This technique was expanded from linear array to curved array transducers, making it more accessible for abdominal and pelvic imaging. Now, compound sonography is used for musculoskeletal, vascular, hepatobiliary, and pelvic imaging [45].

In 1989, Baba and colleagues reported on the first production of a three-dimensional ultrasonic image. Using a real-time straight or curved transducer, they were able to obtain positional information with an ultrasound device that was connected to a microcomputer, which reconstructed the data into a three-dimensional output. The authors hypothesized that this system would be ideal for the screening of fetal anomalies and abnormalities in intrauterine growth [44]. Following the development of von Ramm's three-dimensional ultrasound device, Sheikh et al. published the first use of real-time three-dimensional acquisition and presentation of data in the United States in 1991. This proved to be useful in cardiology for assessment of perfusion and ventricular function [46].

In 1996, several authors including Burns et al. began exploring the realm of tissue harmonic sonography (see Fig. 1.3) as a means to overcome image degradation [45, 47]. During the initial investigation, the authors explored microbubble

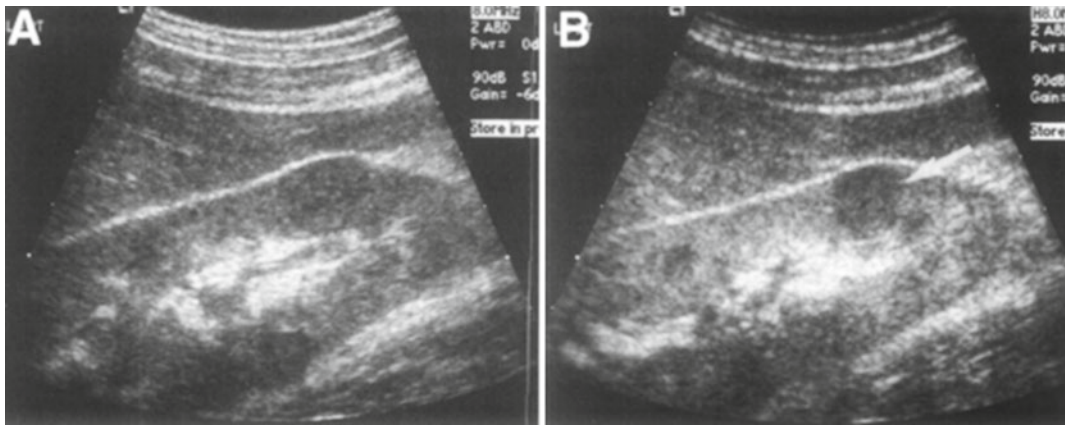

Fig. 1.3 Here, a fundamental mode image of the kidney reveals a focal contour of an abnormality seen in the lower pole, while the harmonic mode image, to the *right*, reveals that the lesion is solid in nature [47]. *Reproduced with permission from Desser, T.S., et al., Tissue Harmonic Imaging Techniques: Physical Principles and Clinical Applications. Seminars in Ultrasound, CT, and MRI. 2001.* ***22****(1): 1–10, courtesy of Elsevier*

ultrasound contrast media to improve contrast agent-specific images, with the result that the harmonic signal was stronger from the microbubbles than the signal from tissue. Now, harmonic mode has developed as a gray scale ultrasound mode that employs echoes at twice the transmitted frequency. This technique has resulted in improved image clarity and decreased artifact, and has proven invaluable in diagnosis of pathology in the hepatobiliary tree and genitourinary tract, most importantly in determining distinguishing characteristics of cystic and solid lesions.

Electronic steering of the ultrasound beam is the process of using parallel beams oriented along multiple directions from an array transducer along different directions. This is also referred to as multibeam imaging. The arrays obtained from each direction are compounded into a single image, which increases the lateral resolution and reduces the noise levels [48].

History of Ultrasound in Urology

Prostate

In 1963, Japanese Urologists Takahashi and Ouchi became the first to attempt ultrasonic examination of the prostate. However, the image quality that resulted was not interpretable and thus carried little medical utility [49]. Wild and Reid also attempted transrectal ultrasound, but were met with the same result. Progress was not made until Watanabe et al. demonstrated radial scanning that could adequately identify prostate and bladder pathology. Using a purpose-built device modeled after a museum sculpture entitled "Magician's Chair," Watanabe seated his patients on a chair with a hole cut in the center such that the transducer tube could be passed through the hole and into the rectum of the seated patient [50]. Images from Watanabe's seated probe are displayed in Fig. 1.4a; it is evident in Fig. 1.4b

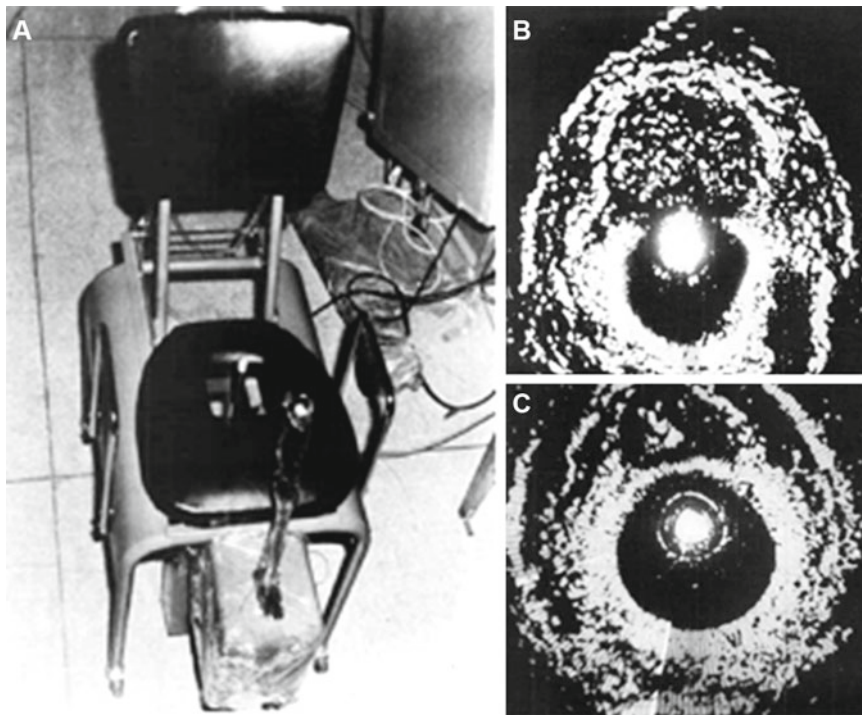

Fig. 1.4 (**a**) Images from Watanabe's seated probe are displayed [50], revealing (**b**) an area of circumscribed symmetric echogenicity, representing BPH, (**c**) an asymmetric area of hyperechogenicity, representing prostate cancer. In these images, note that resolution was poor, and images displayed extreme contrast. *Reproduced with permission from Watanabe, H., et al., Development and application of new equipment for transrectal ultrasonography. J Clin Ultrasound, 1974. 2(2): p. 91–8, courtesy of John Wiley and Sons*

(demonstrating an area of circumscribed symmetric echogenicity, representing BPH) and Fig. 1.4c (demonstrating an asymmetric area of hyperechogenicity, representing prostate cancer) that resolution was poor and images displayed extreme contrast. Subsequent development of biplane, high frequency probes has created increased resolution and has allowed for transrectal ultrasound to become the standard for diagnosis of prostatic disease.

In 1974, Holm and Northeved introduced a transurethral ultrasonic device that would be interchangeable with conventional optics during cystoscopy for the purpose of imaging the prostate and bladder. Their other goals for this device included the ability to determine depth of bladder tumor penetration, prostatic volume, evaluation of prostatic tumor progression, and to assist with transurethral resection of prostate [51].

More recently, several other techniques have come to light in the diagnosis of prostate cancer.

The concept of multiparametric MRI, in which MRI images are electronically superimposed in real time on transrectal ultrasound (see Fig. 1.5), has further revolutionized the ability to detect high-risk prostate cancer [52].

Histoscanning has also been used to more accurately define prostatic lesions. This involves three steps: a motorized transrectal ultrasound, a software analysis to define the region of concern, and a color-coded analysis of tissue detailing all region suspicion [54].

Finally, sonoelastography, a technique for assessing tissue elasticity to distinguish cancer tissue from prostate parenchyma, has been shown to improve detection rates when ultrasound-guided biopsies alone are insufficient to define the target

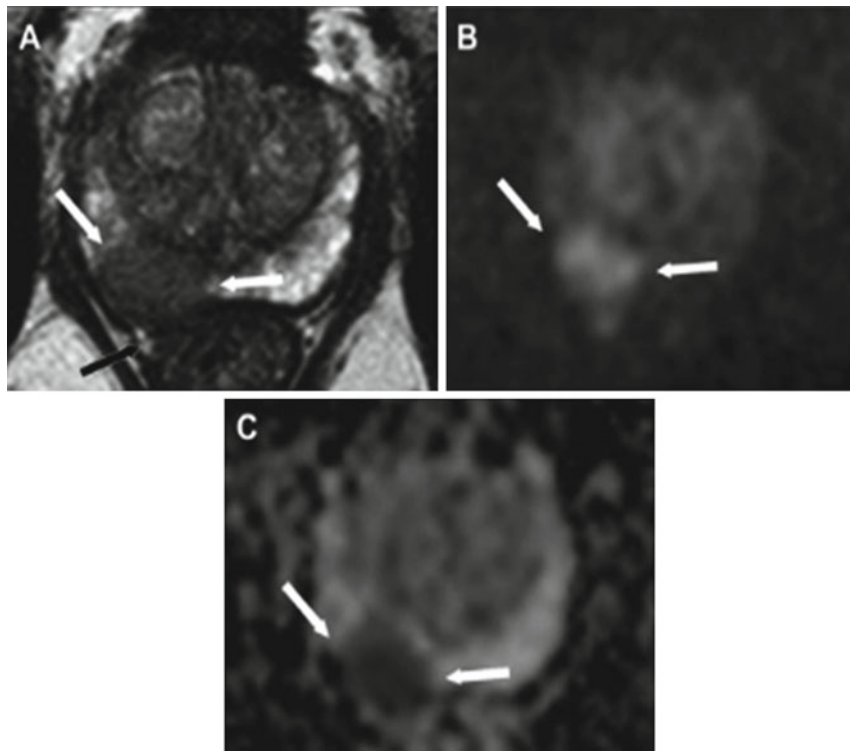

Fig. 1.5 In this example, a multiparametric MRI, T2 weighted, was obtained and outlines a suspicious lesion. (**a**) A hypointense lesion in the right peripheral zone of the prostate is noted with extracapsular extension. The lesion is hyperintense on DWI imaging. (**b**) A TRUS-guided biopsy, performed with the ADC map shown here (**c**), revealed Gleason grade 9 (4 + 5) disease in this patient [53]. *Reproduced with permission from Oliveira Neto JA, Parente DB. Multiparametric Magnetic Resonance Imaging of the Prostate. Magnetic Resonance Imaging Clinics of North America. 2013 (21): p. 409–26, courtesy of Elsevier*

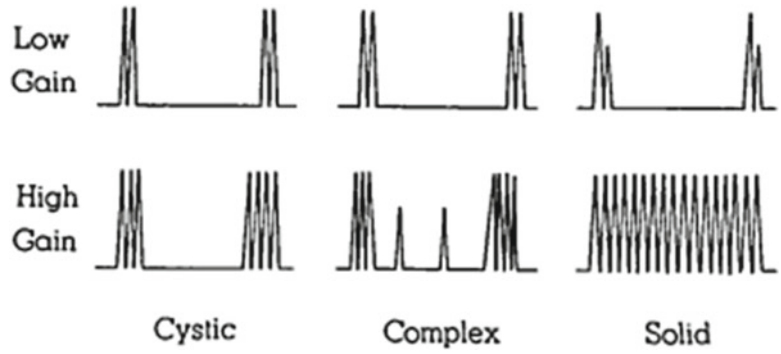

Fig. 1.6 This is a diagrammatic representation of the three types of ultrasound patterns obtained from masses. In this way, ultrasound has been able to distinguish the differences between the solid, cystic, and necrotic masses (a mixture of solid and cystic masses) [57]. *Reproduced with permission from Goldberg, B.B. and H.M. Pollack, Differentiation of renal masses using A-mode ultrasound. J Urol, 1971. 105(6): p. 765–71, courtesy of Elsevier*

[55]. A sensitivity of 0.81, specificity of 0.69, and accuracy of 0.74 for detection of prostate cancer were found by Boehm et al. [56], which is similar to that of MRI.

Kidney

In 1971, Goldberg and Pollack, frustrated with the inability of IVP to differentiate benign from malignant lesions, turned to A-mode ultrasound. In their report on "nephrosonography," they demonstrated in a series of 150 patients the capability of ultrasound to discern solid, cystic, and complex masses with an accuracy of 96 %. The diagrammatic representation of the three ultrasound patterns they found is depicted in Fig. 1.6 [57]. In cystic lesions, the first spike represents the striking of the front wall of the cyst and the second spike represents the striking of the back wall. More complex lesions therefore have return of more spikes.

Scrotum

Perri et al. were the first to use Doppler as a sonic "stethoscope" in their workup of patients with an acute scrotum. While they were able to identify patients with epididymitis and torsion of the appendix testis as having increased flow, and patients with spermatic cord torsion as having no blood flow, they also reported that false negatives in cases of torsion could result from increased flow secondary to reactive hyperemia [58, 59].

Further Advancements

Watanabe and colleagues demonstrated that Doppler could be used to identify the renal arteries in a noninvasive way in 1976 [60], and 5 years afterward, Greene and colleagues documented that Doppler could adequately differentiate stenotic from normal renal arteries [61]. In 1982, Arima et al. used Doppler to differentiate acute from chronic rejection in renal transplant patients, noting that acute rejection is characterized by the disappearance of diastolic phase, with reappearance being indicative of recovery from rejection. The authors concluded that Doppler could guide the management of rejection as an index for steroid therapy [62].

In the early 1990s, a number of authors investigated the therapeutic uses of high-intensity focused ultrasound, or HIFU. Following prior reports of histologic changes following HIFU [63], Marberger and colleagues were the first to

report the safety and efficacy of HIFU in symptomatic BPH patients [64]. Its utilities in the treatments of testicular cancer [65], early prostate cancer [66], recurrent prostate cancer [67], and renal cell cancer (transcutaneously [68] and laparoscopically [69]) were soon explored as well.

The field of urology continues to demand and discover novel uses for ultrasound technology. Chen et al. used transrectal ultrasound guidance to inject botulinum toxin into the external urethral sphincters of a series of patients with detrusor external sphincter dyssynergia [70]. Ozawa and colleagues used perineal ultrasound videourodynamics to accurately diagnose bladder outlet obstruction in a new, noninvasive method [71]. The possibilities for the application of ultrasound in diagnosing or treating urologic patients remain endless.

Conclusion

Ultrasound is a cost-effective, accurate, and nearly ubiquitous easy to use diagnostic tool that produces meaningful results instantly. As a standard in the urologist's office armamentarium, it can be applied to the workup of pathology of the genitalia, pelvic floor, bladder, prostate, and kidneys. Specific uses within each organ system will be detailed throughout this book.

The history of ultrasound is quite extensive and has involved a number of groundbreaking discoveries and new applications of basic physical principles (see Fig. 1.7). In the future, multiparametric imaging and multidimensional real-time ultrasound will allow for enhanced diagnostic and therapeutic utility of ultrasound in multiple different clinical settings. This homage to the innovators of the past serves both to recognize prior achievements and to acknowledge that future work in the development of new applications for ultrasound will always be needed.

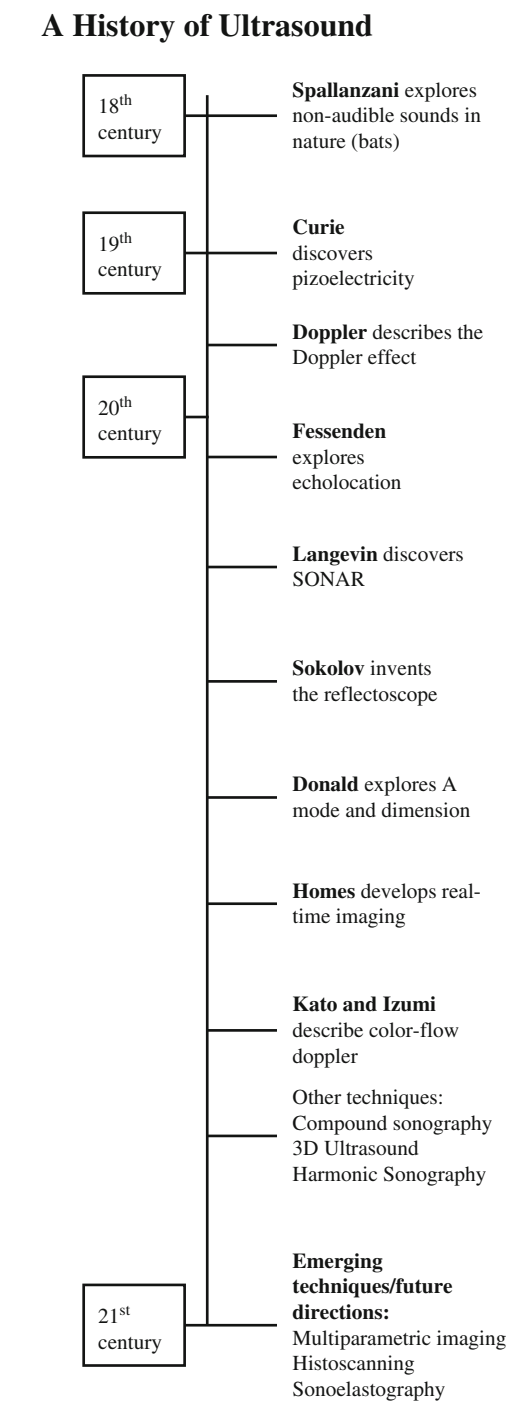

Fig. 1.7 A timeline detailing the history of important contributions to the field of ultrasonography

References

1. Corcoran AJ, Barber JR, Conner WE. Tiger moth jams bat sonar. Science. 2009;325(5938):325–7.
2. Dunning DR, Roeder KD. Moth sounds and the insect-catching behavior of bats. Science. 1965;147:173–4.
3. Mackay RL, Liaw HM. Dolphin vocalization mechanisms. Science. 1981;212(4495):676–8.
4. Ruttimann J. Frogs chat in ultrasound. Nature News. 2006.
5. Galambos R. The avoidance of obstacles by flying bats: Spallanzani's ideas (1794) and later theories. Isis. 1942;34(2):132–40.
6. Dijkgraaf S. Spallanzani's unpublished experiments on the sensory basis of object perception in bats. Isis. 1960;51(1):9–20.
7. Curie J, Curie P. Sur 'electricite polaire dans cristaux hemiedres a face inclinees. C R Seances Acad Sci. 1880;91:383.
8. Katzir S. The discovery of the piezoelectric effect. In: The beginnings of piezoelectricity: a study in mundane physics. Netherlands: Springer; 2006. p. 15–64.
9. Curie P. Radioactive substances, especially radium. In: Nobel Lecture. 1905.
10. Diamantis A, Magiorkinis E, Papadimitriou A, Androutsos G. The contribution of Maria Sklodowska-Curie and Pierre Curie to nuclear and medical physics. A hundred and ten years after the discovery of radium. Hell J Nucl Med. 2008;11(1):33–8.
11. Seitz F. The cosmic inventor: Reginald Aubrey Fessenden (1866–1932). Am Philos Soc. 1999;89:41–6.
12. Chilowsky C, Langevin M. Procedes et appareils pour la production de signaux sous-marins diriges et pour la localisation a distance d'obstacles sous-marins. 1916.
13. Martin J. History of ultrasound. In: Sanders R, Resnick M, editors. Ultrasound in urology. Baltimore: Williams and Wilkins; 1984. p. 1–12.
14. Zimmerman D. Paul Langevin and the discovery of active sonar or asdic. North Mar. 2002;12(1):39–52.
15. Sokolov SY. The ultra-acoustic microsocpe. Zh Tekh Fiz. 1949;19:271.
16. Jagannathan J, et al. High-intensity focused ultrasound surgery of the brain: part 1—a historical perspective with modern applications. Neurosurgery. 2009;64(2):201–10. discussion 210–1.
17. Dussik K. Uber die Moglichkeit, hochfrequente mechanische Schwingungen als diagnostische Mittel zu verwerten. Z Ges Neurol Psych. 1941;174:153–68.
18. Thomas AMK, Banerjee A, Busch U. Uber die Moglichkeit, hochfrequente mechanische Schwingungen als diagnostische Mittel zu verwerten. In: Banerjee A, Thomas AMK, Busch U, editors. Classic papers in modern diagnostic radiology. Berlin: Springer; 2005. p. 144–61.
19. Shampo MA, Kyle RA. Karl Theodore Dussik—pioneer in ultrasound. Mayo Clin Proc. 1995;70(12):1136.
20. Thomas AMK, Banerjee A, Busch U. Application of echo-ranging techniques to the determination of structure of biological tissues. In: Banerjee A, Thomas AMK, Busch U, editors. Classic papers in modern diagnostic radiology. Berlin: Springer; 2005. p. 162–9.
21. Wild JJ, Reid JM. Application of echo-ranging techniques to the determination of structure of biological tissues. Science. 1952;115(2983):226–30.
22. Hill CR. Early days of scanning: pioneers and sleepwalkers. Radiography. 2009;15:15–22.
23. Edler I, Hertz CH. The use of ultrasonic reflectoscope for the continuous recording of the movements of heart walls. Clin Physiol Funct Imaging. 2004;24(3):118–36.
24. Fraser AG. Inge Edler and the origins of clinical echocardiography. Eur J Echocardiogr. 2001;2(1):3–5.
25. Holmes JH, et al. The ultrasonic visualization of soft tissue structures in the human body. Trans Am Clin Climatol Assoc. 1954;66:208–25.
26. Donald I, Macvicar J, Brown TG. Investigation of abdominal masses by pulsed ultrasound. Lancet. 1958;1(7032):1188–95.
27. Thomas AMK, Banerjee AK, Busch U. Investigation of abdominal masses by pulsed ultrasound. In: Thomas AMK, Banerjee AK, Busch U, editors. Classic papers in modern diagnostic radiology. Berlin: Springer; 2005. p. 213–23.
28. Doppler C. Über das farbige Licht der Doppelsterne und einiger anderer Gestirne des Himmels. Abh Königl Böhm Ges Wiss. 1843;2:465–82.
29. Satomura S. Ultrasonic Doppler method for the inspection of cardiac function. J Acoust Soc Am. 1957;29:1181–5.
30. Coman IM. Christian Andreas Doppler—the man and his legacy. Eur J Echocardiogr. 2005;6(1):7–10.
31. Hofmann D, Hollander HJ. Intrauterine diagnosis of hydrops fetus universalis using ultrasound. Zentralbl Gynakol. 1968;90(19):667–9.
32. Woo J. A short history of the development of ultrasound in obstetrics and gynecology. http://www.ob-ultrasound.net/site_index.html.
33. Bernstine RL, Callagan DA. Ultrasonic Doppler inspection of the fetal heart. Am J Obstet Gynecol. 1966;95(7):1001–4.
34. Buschmann W. On the diagnosis of carotid thrombosis. Albrecht Von Graefes Arch Ophthalmol. 1964;166:519–29.
35. Brinker RA, Landiss DJ, Croley TF. Detection of carotid artery bifurcation stenosis by Doppler ultrasound. Preliminary report. J Neurosurg. 1968;29(2):143–8.
36. Grossman BL, Wood EH. Evaluation of cerebrovascular disease utilizing a transcutaneous Doppler technic. Radiology. 1968;90(3):586–7.
37. Strandness Jr. D. Ultrasonic velocity determination in the diagnosis and evaluation of peripheral vascular disease. In: Symposium on ultrasound. Indiana University; 1968.
38. Kato K, Izumi T. A new ultrasonic flowmeter that can detect flow direction. In: Proceedings of the tenth scientic meeting of the Japan Society of Ultrasonics in Medicine; 1966. p. 78–9.
39. Maroon JC, Campbell RL, Dyken ML. Internal carotid artery occlusion diagnosed by Doppler ultrasound. Stroke. 1970;1(2):122–7.

40. McLeod F. A directional Doppler flowmeter. In: Digest of the seventh international conference on medical electronics and biological engineering; 1967. p. 213.
41. Bollinger A, Partsch H. Christian Doppler is 200 years young. Vasa. 2003;32(4):225–33.
42. Baker DW, Johnson SL, et al. Doppler echocardiography. In: Waag R, Gramiak R, editors. Cardiac ultrasound. St. Louis: CV Mosby; 1974. p. 24.
43. Maulik D, et al. Doppler color flow mapping of the fetal heart. Angiology. 1986;37(9):628–32.
44. Hamper UM, et al. Power Doppler imaging: clinical experience and correlation with color Doppler US and other imaging modalities. Radiographics. 1997;17(2):499–513.
45. Oktar SO, et al. Comparison of conventional sonography, real-time compound sonography, tissue harmonic sonography, and tissue harmonic compound sonography of abdominal and pelvic lesions. AJR. 2003;181:1341–7.
46. Sheikh K, et al. Real-time, three-dimensional echocardiography: feasibility and initial use. Echocardiography. 1991;8(1):119–25.
47. Desser TS, et al. Tissue harmonic imaging techniques: physical principles and clinical applications. Semin Ultrasound CT MR. 2001;22(1):1–10.
48. Chan V, et al. Basics of ultrasound imaging. In: Atlas of ultrasound-guided procedures in interventional pain management, vol. 1. New York: Springer; 2011. p. 13–9.
49. Takahashi H, Ouchi T. The ultrasonic diagnosis in the field of urology. Proc Jpn Soc Ultrason Med. 1963;3:7.
50. Watanabe H, et al. Development and application of new equipment for transrectal ultrasonography. J Clin Ultrasound. 1974;2(2):91–8.
51. Holm HH, Northeved A. A transurethral ultrasonic scanner. J Urol. 1974;111(2):238–41.
52. Siddiqui M, Rais-Bahrami S, Turkbey B, et al. Comparison of MR/ultrasound fusion-guided biopsy with ultrasound-guided biopsy for the diagnosis of prostate cancer. JAMA. 2015;313(4):390–7.
53. Oliveira Neto JA, Parente DB. Multiparametric magnetic resonance imaging of the prostate. Magn Reson Imaging Clin N Am. 2013;21:409–26.
54. Koh J, et al. Additional targeted biopsy in clinically suspected prostate cancer: prospective randomized comparison between contrast-enhanced ultrasound and sonoelastography guidance. Ultrasound Med Biol. 2015;41(11):2836–41.
55. Yen C-L, et al. The benefits of comparing conventional sonography, real-time spatial compound sonography, tissue harmonic sonography, and tissue harmonic compound sonography of hepatic lesions. Clin Imaging. 2008;32:11–5.
56. Boehm K, Salomon G, Beyer B, Schiffmann J, Simonis K, Graefen M, Budaeus L. Shear wave elastography for localization of prostate cancer lesions and assessment of elasticity thresholds: implications for targeted biopsies and active surveillance protocols. J Urol. 2015;2014(193):794–800.
57. Goldberg BB, Pollack HM. Differentiation of renal masses using A-mode ultrasound. J Urol. 1971;105(6):765–71.
58. Perri AJ, et al. Necrotic testicle with increased blood flow on Doppler ultrasonic examination. Urology. 1976;8(3):265–7.
59. Perri AJ, et al. The Doppler stethoscope and the diagnosis of the acute scrotum. J Urol. 1976;116(5):598–600.
60. Watanabe H, et al. Non-invasive detection of ultrasonic Doppler signals from renal vessels. Tohoku J Exp Med. 1976;118(4):393–4.
61. Greene ER, et al. Noninvasive characterization of renal artery blood flow. Kidney Int. 1981;20(4): 523–9.
62. Arima M, et al. Predictability of renal allograft prognosis during rejection crisis by ultrasonic Doppler flow technique. Urology. 1982;19(4):389–94.
63. Burgess SE, et al. Histologic changes in porcine eyes treated with high-intensity focused ultrasound. Ann Ophthalmol. 1987;19(4):133–8.
64. Madersbacher S, et al. Tissue ablation in benign prostatic hyperplasia with high-intensity focused ultrasound. Eur Urol. 1993;23 Suppl 1:39–43.
65. Madersbacher S, et al. Transcutaneous high-intensity focused ultrasound and irradiation: an organ-preserving treatment of cancer in a solitary testis. Eur Urol. 1998;33(2):195–201.
66. Chapelon JY, et al. Treatment of localised prostate cancer with transrectal high intensity focused ultrasound. Eur J Ultrasound. 1999;9(1):31–8.
67. Berge V, Baco E, Karlsen SJ. A prospective study of salvage high-intensity focused ultrasound for locally radiorecurrent prostate cancer: Early results. Scand J Urol Nephrol. 2010;44(4):223–7.
68. Kohrmann KU, et al. High intensity focused ultrasound as noninvasive therapy for multilocal renal cell carcinoma: case study and review of the literature. J Urol. 2002;167(6):2397–403.
69. Margreiter M, Marberger M. Focal therapy and imaging in prostate and kidney cancer: high-intensity focused ultrasound ablation of small renal tumors. J Endourol. 2010;24(5):745–8.
70. Chen SL. Transrectal ultrasound-guided transperineal botulinum toxin a injection to the external urethral sphincter for treatment of detrusor external sphincter dyssynergia in patients with spinal cord injury. Arch Phys Med Rehabil. 2010;91(3):340–4.
71. Ozawa H, et al. The future of urodynamics: non-invasive ultrasound videourodynamics. Int J Urol. 2010;17(3):241–9.

Physical Principles of Ultrasound

2

Pat F. Fulgham

Introduction

The use of ultrasound is fundamental to the practice of urology. In order for urologists to best use this technology on behalf of their patients, they must have a thorough understanding of the physical principles of ultrasound. Understanding how to tune the equipment and to manipulate the transducer to achieve the best-quality image is crucial to the effective use of ultrasound. The technical skills required to perform and interpret urologic ultrasound represent a combination of practical scanning ability and knowledge of the underlying disease processes of the organs being imaged. Urologists must understand how ultrasound affects biological tissues in order to use this modality safely and appropriately. When the physical principles of ultrasound are fully understood, urologists will recognize both the advantages and limitations of ultrasound.

The original version of this chapter was revised. An erratum to this chapter can be found at DOI 10.1007/978-3-319-43868-9_18

P.F. Fulgham, M.D., F.A.C.S. (✉)
Department of Urology, Texas Health Presbyterian Dallas, 8210 Walnut Hill Lane Suite 014, Dallas, TX 75231, USA
e-mail: pfulgham@airmail.net

The Mechanics of Ultrasound Waves

The image produced by ultrasound is the result of the interaction of mechanical ultrasound waves with biologic tissues and materials. Because ultrasound waves are transmitted at frequent intervals and the reflected waves received by the transducer, the images can be reconstructed and refreshed rapidly, providing a real-time image of the organs being evaluated. Ultrasound waves are **mechanical waves** which require a physical medium (such as tissue or fluid) to be transmitted. Medical ultrasound imaging utilizes frequencies in the one million cycles per second (or MHz) range. Most transducers used in urology vary from 2.5 to 18 MHz, depending on the application.

Ultrasound waves are created by applying alternating current to piezoelectric crystals within the transducer. Alternating expansion and contraction of the piezoelectric crystals creates a mechanical wave which is transmitted through a coupling medium (usually gel) to the skin and then into the body. The waves that are produced are **longitudinal waves**. This means that the particle motion is in the same direction as the propagation of the wave (Fig. 2.1). This longitudinal wave produces areas of rarefaction and compression of tissue in the direction of travel of the ultrasound wave.

The compression and rarefaction of molecules is represented graphically as a sine wave alternating between a positive and negative

P.F. Fulgham, B.R. Gilbert (eds.), *Practical Urological Ultrasound*, Current Clinical Urology,
DOI 10.1007/978-3-319-43868-9_2

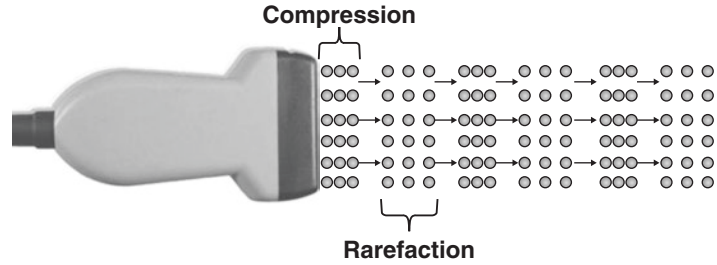

Fig. 2.1 Longitudinal waves. The expansion and contraction of piezoelectric crystals caused by the application of alternating current to the crystals causes compression and rarefaction of molecules in the body

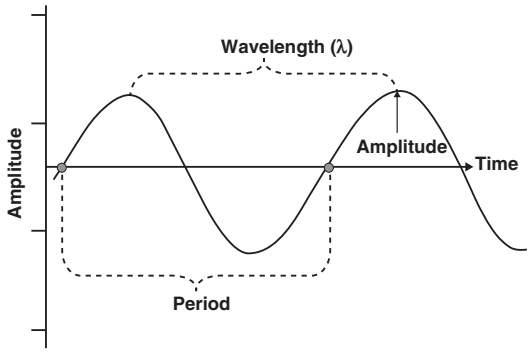

Fig. 2.2 Characteristics of a sound wave: the amplitude of the wave is a function of the acoustical power used to generate the mechanical compression wave and the medium through which it is transmitted

deflection from the baseline. A **wavelength** is described as the distance between one peak of the wave and the next peak. One complete path traveled by the wave is called a **cycle**. One cycle per second is known as 1 Hz (Hertz). The **amplitude** of a wave is the maximal excursion in the positive or negative direction from the baseline, and the **period** is the time it takes for one complete cycle of the wave (Fig. 2.2).

The velocity with which a sound wave travels through tissue is a product of its frequency and its wavelength. The velocity of sound in tissues is constant. Therefore, as the frequency of the sound wave changes, the wavelength must also change. The average velocity of sound in human tissues is 1540 m/s. Wavelength and frequency vary in an inverse relationship. Velocity equals frequency times wavelength (Fig. 2.3). As the frequency diminishes from 10 to 1 MHz, the wavelength increases from 0.15 to 1.5 mm. This has important consequences for the choice of transducer depending on the indication for imaging.

$$\upsilon = f\lambda$$

velocity = frequency x wavelength

Fig. 2.3 Since the velocity of sound in tissue is a constant, the frequency and wavelength of sound must vary inversely

Ultrasound Image Generation

The image produced by an ultrasound machine begins with the transducer. **Transducer** comes from the Latin **transducere**, which means to convert. In this case, electrical impulses are converted to mechanical sound waves via the **piezoelectric effect**.

In ultrasound imaging the transducer has a dual function as a sender and a receiver. Sound waves are transmitted into the body where they are at least partially reflected. The piezoelectric effect occurs when alternating current is applied to a crystal containing dipoles [1]. Areas of charge within a piezoelectric element are distributed in patterns which yield a "net" positive and negative orientation. When alternating charge is applied to the two element faces, a relative contraction or elongation of the charged areas occurs resulting in a mechanical expansion and then a contraction of the element. This results in a mechanical wave which is transmitted to the patient (Fig. 2.4).

Reflected mechanical sound waves are received by the transducer and converted back into electrical energy via the piezoelectric effect. The electrical energy is interpreted within the ultrasound instrument to generate an image which is displayed upon the screen.

For most modes of ultrasound, the transducer emits a limited number of wave cycles (usually two to four) called a pulse. The frequency of the two to

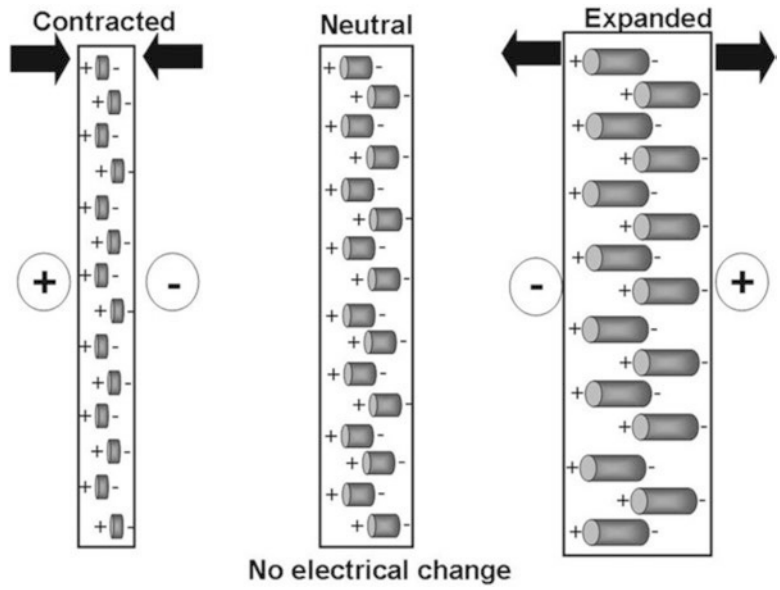

Fig. 2.4 Piezoelectric effect. Areas of "net" charge within a crystal expand or contract when current is applied to the surface, creating a mechanical wave. When the returning wave strikes the crystal, an electrical current is generated

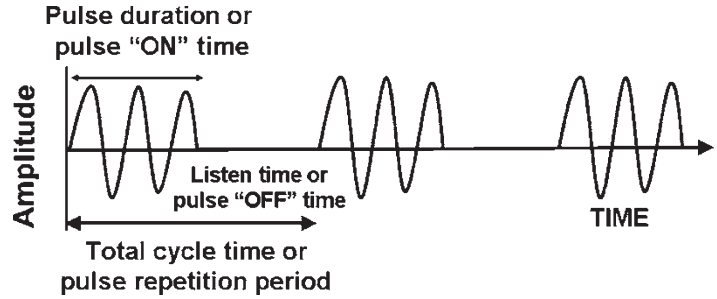

Fig. 2.5 The pulsed-wave ultrasound mode depends on an emitted pulse of 2–4 wave cycles followed by a period of "silence" as the transducer awaits the return of the emitted pulse

four waves within each cycle is usually in the 2.5–14 MHz range. The transducer is then "silent" as it awaits the return of the reflected waves from within the body (Fig. 2.5). The transducer serves as a receiver more than 99% of the time.

Pulses are sent out at regular intervals usually between 1 and 10 kHz which is known as the **pulse repetition frequency** (**PRF**). By timing the pulse from transmission to reception, it is possible to calculate the distance from the transducer to the object reflecting the wave. This is known as **ultrasound ranging** (Fig. 2.6). This sequence is known as **pulsed-wave ultrasound**.

The amplitude of the returning waves determines the brightness of the pixel assigned to the reflector in an ultrasound image. The greater the amplitude of the returning wave, the brighter the pixel assigned. Thus, an ultrasound unit produces an "image" by first causing a transducer to emit a series of ultrasound waves at specific frequencies and intervals and then interpreting the returning echoes for duration of transit and amplitude. This "image" is rapidly refreshed on a monitor to give the impression of continuous motion. Frame refresh rates are typically 12–30 per second. The sequence of events depicted in Fig. 2.7 is the basis for all "scanned" modes of ultrasound including the familiar gray-scale ultrasound.

Interaction of Ultrasound with Biological Tissue

As ultrasound waves are transmitted through human tissue, they are altered in a variety of ways including loss of energy, change of direction, and change of frequency. An understanding of these interactions is necessary to maximize image quality and correctly interpret the resultant images.

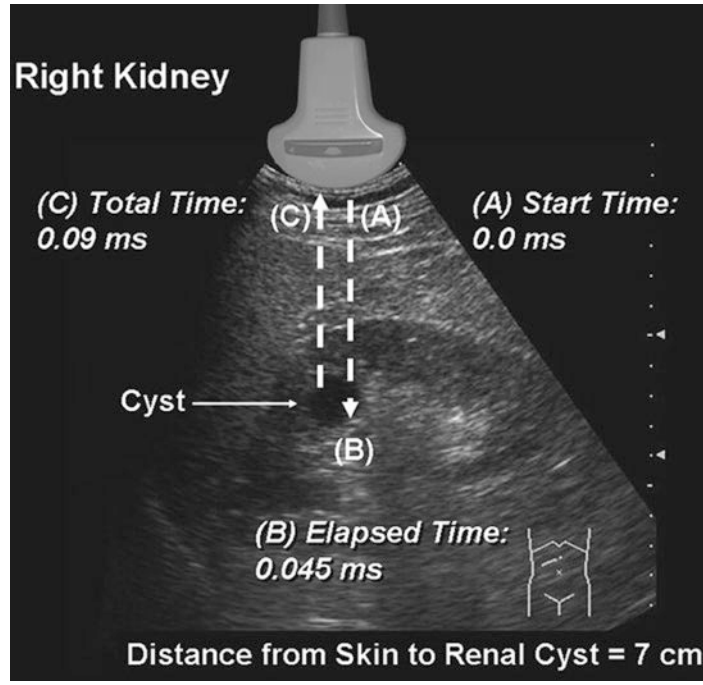

Fig. 2.6 Ultrasound ranging depends on assumptions about the average velocity of ultrasound in human tissue to locate reflectors in the ultrasound field. The elapsed time from pulse transmission to reception of the same pulse by the transducer allows for determining the location of a reflector in the ultrasound field

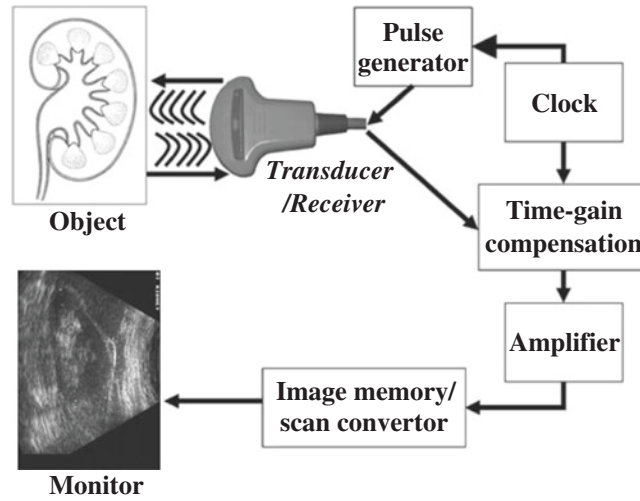

Fig. 2.7 Schematic depiction of the sequence of image production by an ultrasound device

Attenuation refers to a loss of kinetic energy as a sound wave interacts with tissues and fluids within the body [2]. Specific tissues have different potentials for attenuation. For example, water has an attenuation of 0.0 whereas kidney has an attenuation of 1.0 and muscle an attenuation of 3.3. Therefore, sound waves are much more rapidly attenuated as they pass through muscle than as they pass through water (Fig. 2.8). (Attenuation is measured in dB/cm/MHz.)

The three most important mechanisms of attenuation are absorption, reflection, and scattering. Absorption occurs when the mechanical kinetic energy of a sound wave is converted to

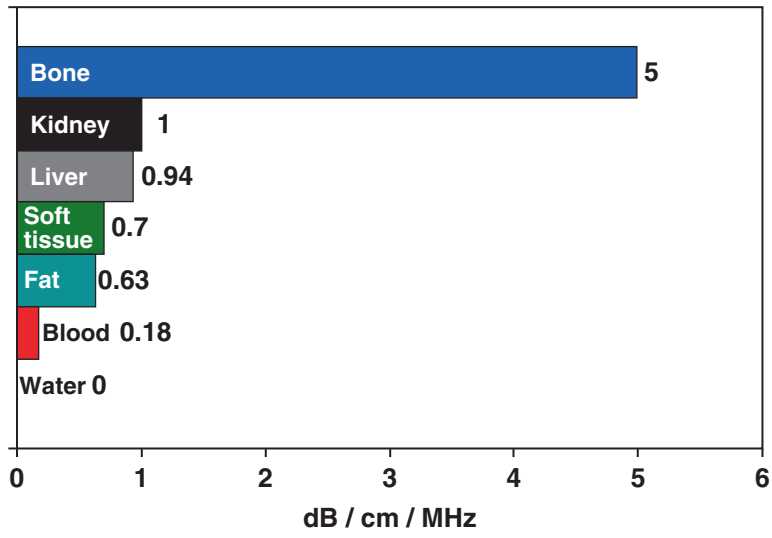

Fig. 2.8 Attenuation of tissue.) (Adapted from Diagnostic Ultrasound, Third Ed., Vol 1). The attenuation of a tissue is a measure of how the energy of an ultrasound wave is dissipated by that tissue. The higher the attenuation value of a tissue, the more the sound wave is attenuated by passing through that tissue

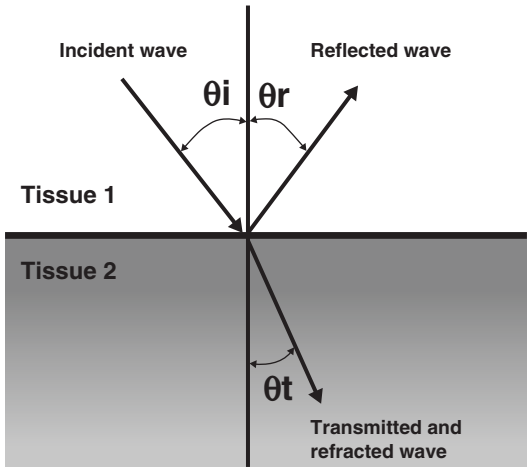

Fig. 2.9 A wave which strikes the interface between two tissues of differing impedance is usually partially reflected and partially transmitted with refraction. A portion of the wave is reflected at an angle (θR) equal to the angle of insonation (θi); a portion of the wave is transmitted at a refracted angle (θt) into the second tissue

heat within the tissue. Absorption is dependent on the frequency of the sound wave and the characteristics of the attenuating tissue. Higher frequency waves are more rapidly attenuated by absorption than lower frequency waves.

Since sound waves are progressively attenuated with distance traveled, deep structures in the body (e.g., kidney) are more difficult to image. Compensation for loss of acoustic energy by attenuation can be accomplished by the appropriate use of gain settings (increasing the sensitivity of the transducer to returning sound waves) and selection of a lower frequency.

Refraction occurs when a sound wave encounters an interface between two tissues at any angle other than 90°. When the wave strikes the interface at an angle, a portion of the wave is reflected and a portion transmitted into the adjacent media. The direction of the transmitted wave is altered (refracted). This results in a loss of some information because the wave is not completely reflected back to the transducer, but also causes potential errors in registration of object location because of the refraction (change in direction) of the wave. The optimum angle of insonation to minimize attenuation by refraction is 90° (Fig. 2.9).

Reflection occurs when sound waves strike an object or an interface between unlike tissues or structures. If the object has a relatively large flat surface, it is called a specular reflector, and sound waves are reflected in a predictable way based on the angle of insonation. If a reflector is small or irregular, it is called a diffuse reflector. Diffuse reflectors produce **scattering** in a pattern which produces interference with waves from adjacent diffuse reflectors. The resulting pattern is called "speckle" and is characteristic of solid organs such as the testes and liver (Fig. 2.10).

When a sound wave travels from one tissue to another, a certain amount of energy is reflected at the interface between the tissues. The percentage

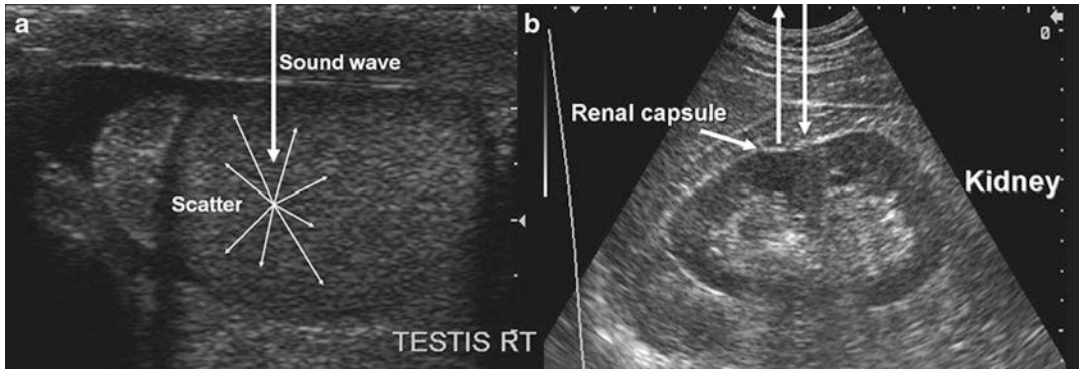

Fig. 2.10 (**a**) Demonstrates a diffuse reflector. In this image of the testis, small parenchymal structures scatter sound waves. The pattern of interference resulting from this scattering provides the familiar "speckled" pattern of testicular echo architecture. (**b**) Demonstrates a specular reflector. A specular reflector reflects sound waves at an angle equal to the incident angle without producing a pattern of interference caused by scattering. In this image of the kidney, the capsule of the kidney serves as a specular reflector

Table 2.1 Impedance of tissue

Tissue	Density (kg/m^3)	Impedance (Rayles)
Air and other gases	1.2	0.0004
Fat tissue	952	1.38
Water and other clear liquids	1000	1.48
Kidney (average of soft tissue)	1060	1.63
Liver	1060	1.64
Muscle	1080	1.70
Bone and other calcified objects	1912	7.8

Adapted from Diagnostic Ultrasound, 3rd Ed, Vol. 1
Impedance (Z) is a product of tissue density (p) and the velocity of that tissue (c). Impedance is defined by the formula: Z (Rayles) = p (kg/m^3) × c (m/s)

of energy reflected is a function of the difference in the **impedance** of the tissues. Impedance is a property of tissue related to its "stiffness" and the speed at which sound travels through the tissue [3]. If two adjacent tissues have a small difference in tissue impedance, very little energy will be reflected. The impedance difference between kidney (1.63) and liver (1.64) is very small so that if these tissues are immediately adjacent, it may be difficult to distinguish the interface between the two by ultrasound (Table 2.1).

Fat has a sufficient impedance difference from both kidney and liver that the borders of the two organs can be distinguished from the intervening fat (Fig. 2.11).

If the impedance differences between tissues are very high, complete reflection of sound waves may occur, resulting in acoustic shadowing (Fig. 2.12).

Artifacts

Sound waves are emitted from the transducer with a known amplitude, direction, and frequency. Interactions with tissues in the body result in alterations of these parameters. Returning sound waves are presumed to have undergone alterations according to the expected physical principles such as attenuation with distance and frequency shift based on the velocity and direction of objects they encountered. The timing of the returning echoes is based on the expected velocity of sound in human tissue. When these expectations are not met, it may lead to image representations and measurements which do not reflect actual physical conditions. These misrepresentations are known as "artifacts." Artifacts, if correctly identified, can be used to aid in diagnosis.

Increased through transmission occurs when sound waves pass through tissue with less attenuation than occurs in the surrounding tissues. For example, when sound waves pass through a fluid-filled structure such as a renal cyst, the waves experience relatively little attenuation compared to that experienced in the

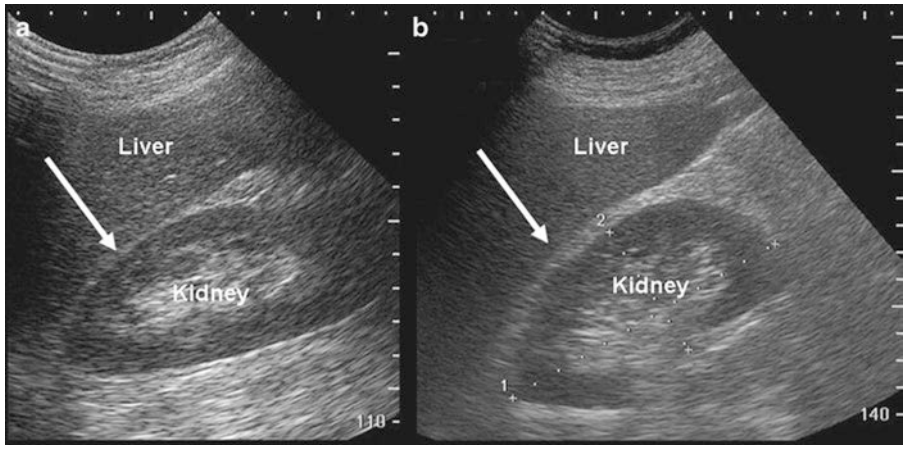

Fig. 2.11 Image (**a**) demonstrates that when kidney and liver are directly adjacent to each other, it is difficult to appreciate the boundary (*arrow*) between the capsules of the kidney and liver. Image (**b**) demonstrates that when fat (which has a significantly lower impedance) is interposed, it is far easier to appreciate the boundary between liver capsule (*arrow*) and fat

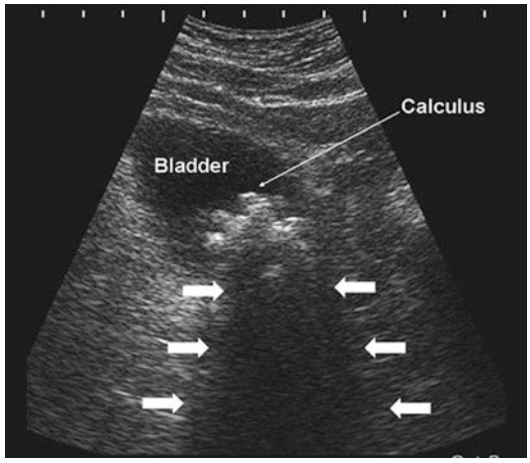

Fig. 2.12 In the urinary bladder, reflection of sound waves as the result of large impedance differences between urine and the bladder calculus (*thin arrow*). Acoustic shadowing results from nearly complete reflection of sound waves (*arrows*)

surrounding renal parenchyma. Thus when the waves reach the posterior wall of the cyst and the renal tissue beyond it, they are more energetic (have greater amplitude) than the adjacent waves. The returning echoes have significantly greater amplitude than waves returning through the renal parenchyma from the same region of the kidney. Therefore, the pixels associated with the region distal to the cyst are assigned a greater "brightness." The tissue appears hyperechoic compared to the adjacent renal tissue even though it is histologically identical (Fig. 2.13). This artifact can be overcome by changing the angle of insonation or adjusting the time-gain compensation settings.

Acoustic shadowing occurs when there is significant attenuation of sound waves at a tissue interface causing loss of information about other structures distal to that interface. This attenuation may occur on the basis of reflection or absorption, resulting in an "anechoic" or "hypoechoic" shadow. The significant attenuation or loss of the returning echoes from tissues distal to the interface may lead to incorrect conclusions about tissue in that region. For instance, when sound waves strike the interface between testicular tissue and a testicular calcification, there is a large impedance difference and significant attenuation and reflection occur. Information about the region distal to the interface is therefore lost or severely diminished (Fig. 2.14). Thus, in some cases spherical objects may appear as crescenteric objects, and it may be difficult to obtain accurate measurements of such three-dimensional objects. Furthermore, fine detail in the region of the acoustic shadow may be obscured. The problems with acoustic shadowing are most appropriately overcome by changing the angle of insonation.

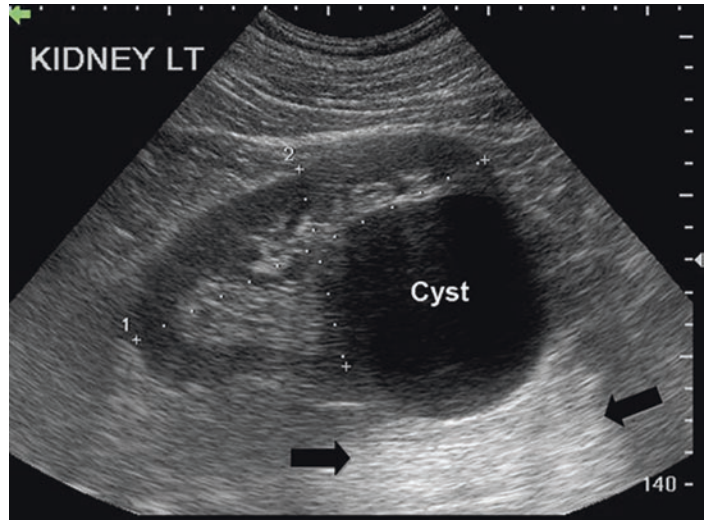

Fig. 2.13 Increased through transmission with hyperechogenicity (*arrow*) as the result of decreased attenuation by the fluid-filled cyst. This is an example of artifactual misrepresentation of tissue characteristics and must be recognized to avoid incorrect clinical conclusions

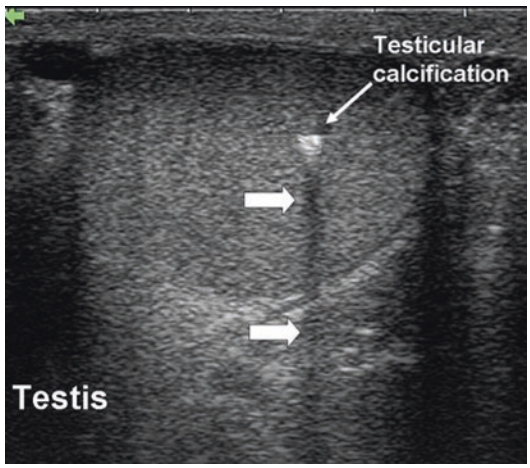

Fig. 2.14 Acoustic shadowing occurs distal to a calcification in the testis (*large arrows*). Information about testicular parenchymal architecture distal to the area of calcification is lost

Edging artifact occurs when sound waves strike a curved surface or an interface at a critical angle. A **critical angle** of insonation is one which results in propagation of the sound wave along the interface without significant reflection of the wave to the transducer. Thus, information distal to the interface is lost or severely diminished. This very common artifact in urology must be recognized and can, at times, be helpful. It is seen in many clinical situations but very commonly seen when imaging the testis. Edging artifacts often occur at the upper and lower pole of the testis as the sound waves strike the rounded testicular poles at the critical angle. This artifact may help differentiate between the head of the epididymis and the upper pole of the testis. The edging artifact is also prominently seen on transrectal ultrasound, where the two rounded lobes of the prostate come together in the midline. This produces an artifact that appears to arise in the vicinity of the urethra and extend distally. Edging artifact may be seen in any situation where the incident wave strikes an interface at the critical angle (Fig. 2.15). Edging artifact may be overcome by changing the angle of insonation.

A **reverberation artifact** results when an ultrasound wave bounces back and forth (reverberates) between two or more reflective interfaces. When the sound wave strikes a reflector and returns to the transducer, an object is registered at that location. With the second transit of the sound wave, the ultrasound equipment interprets a second object that is twice as far away as the first. There is ongoing attenuation of the sound wave with each successive reverberation resulting in a slightly less intense image displayed on the screen. Therefore, echoes are produced which are spaced at equal intervals from the transducer but are progressively less intense (Fig. 2.16).

The reverberation artifact can also be seen in cases where the incident sound wave strikes a series of smaller reflective objects (such as the

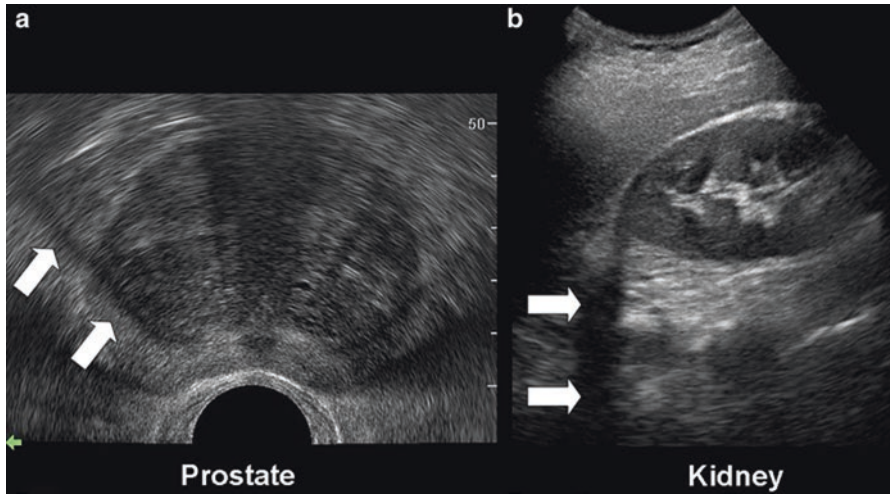

Fig. 2.15 Edging artifact (*arrows*) seen in this transverse image of the prostate is the result of reflection of the sound wave along the curved lateral surface of the transition zone (**a**). Edging artifact (*arrows*) caused by the rounded upper pole of the kidney (**b**)

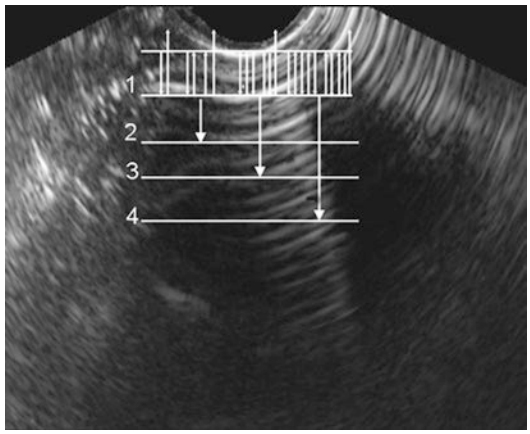

Fig. 2.16 A reverberation artifact occurs when a sound wave is repeatedly reflected between reflective surfaces. The resultant echo pattern is a collection of hyperechoic artifactual reflections distal to the structure with progressive attenuation of the sound wave

gas–fluid mixture in the small bowel) which results in multiple reflected sound waves of various angles and intensity (Fig. 2.17).

This familiar artifact may obscure important anatomic information and is frequently encountered during renal ultrasound. It may be overcome by changing the transducer location and the angle of insonation.

Modes of Ultrasound

Gray-Scale, B-Mode Ultrasound

Gray-scale, B-mode ultrasound (brightness mode) is the image produced by a transducer which sends out ultrasound waves in a carefully timed, sequential way (pulsed wave). The reflected waves are received by the transducer and interpreted for distance and amplitude. Time of travel is reflected by position on the image monitor and intensity by "brightness" of the corresponding pixel. Each sequential line-of-sight echo is displayed side by side and the entire image refreshed at 15–40 frames/s. This results in the illusion of continuous motion or "real-time" scanning. The intensity of the reflected sound waves may vary by a factor of 10^{12} or 120 dB. Although the transducer can respond to such extreme variations in intensity, most monitors or displays have an effective range of only 10^6 or 60 dB. Each of 512×512 or 512×640 pixels may display 2^8 or 256 shades of gray [3]. Most ultrasound units internally process and compress ultrasound data to allow it to be displayed on a standard monitor. Evaluation of

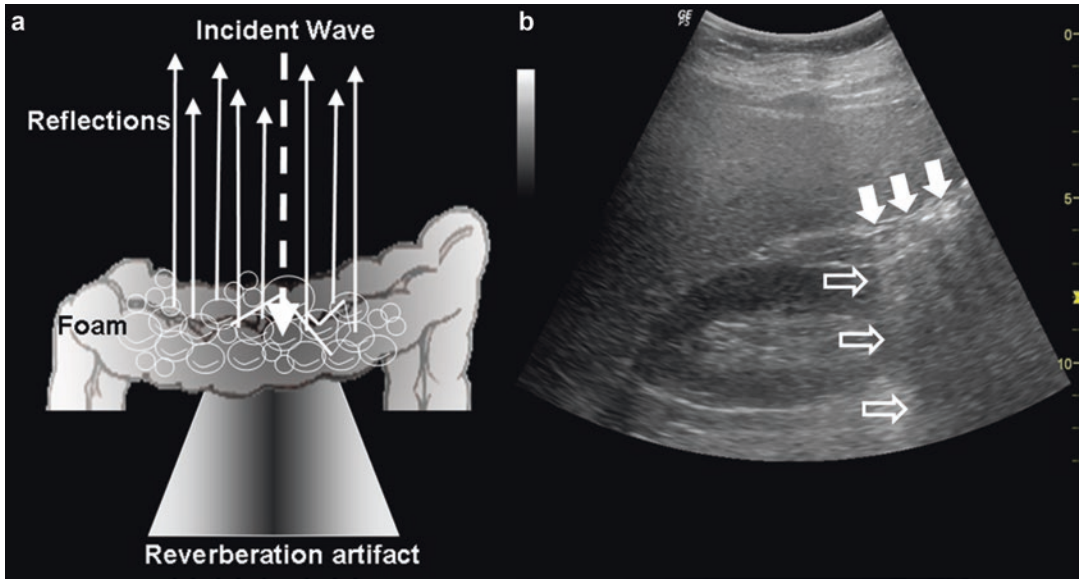

Fig. 2.17 (**a**) Reverberation artifact produced when sound waves strike a mixture of fluid and gas in the bowel. (**b**) This type of reverberation (multipath artifact) is characterized by hyperechoic areas (*open arrow*) and distal attenuation of the incident wave (*closed arrows*)

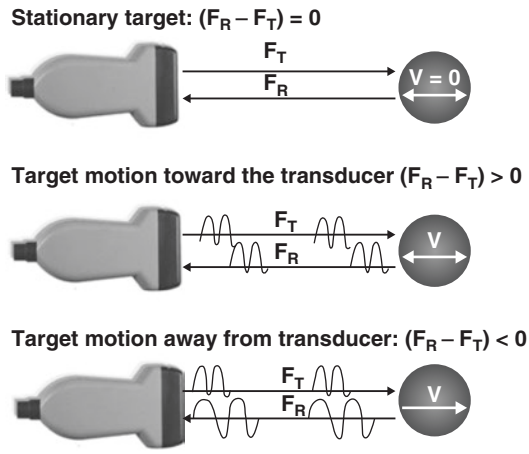

Fig. 2.18 Doppler effect. FT is the transmitted frequency. When the FT strikes a stationary object, the returning frequency FR is equal to the FT. When the FT strikes a moving object, the FR is "shifted" to a higher or lower frequency

gray-scale imaging requires the ability to recognize the normal patterns of echogenicity from anatomic structures. Variations from these expected patterns of echogenicity indicate disorders of anatomy or physiology or may represent artifacts.

Doppler Ultrasound

The Doppler ultrasound mode depends on the physical principle of frequency shift when sound waves strike a moving object. The basic principle of Doppler ultrasound is that sound waves of a certain frequency will be shifted or changed based on the direction and velocity of the moving object as well as the angle of insonation. This phenomenon allows for the characterization of motion, most commonly the motion of blood through vessels, but may also be useful for detecting the flow of urine.

The **Doppler Effect** is a shift in the frequency of the transmitted sound wave based on the velocity of the reflecting object that it strikes. If the reflecting object is stationary relative to the transducer, then the returning frequency will be equal to the transmitted frequency. However, if the echo-generating object is traveling toward the transducer, the returning frequency will be higher than the transmitted frequency. If the object generating the echo is traveling away from the transducer, then the reflected frequency will be lower than the transmitted frequency. This is known as the frequency shift, or Doppler shift (Fig. 2.18).

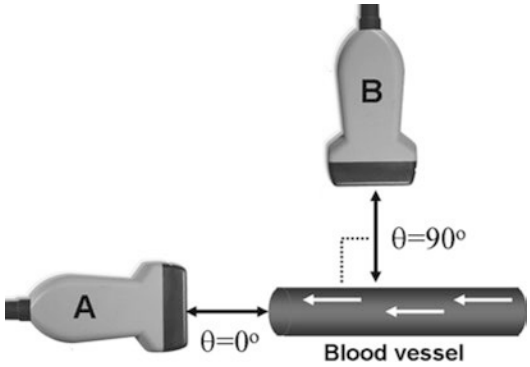

Fig. 2.19 (*A*) Maximum frequency shifts are detected when the transducer axis is parallel to the direction of motion. (*B*) No frequency shift is detected when the transducer axis is perpendicular to the direction of motion

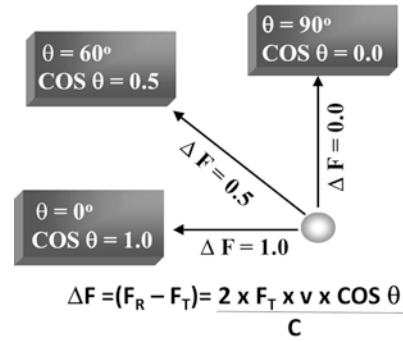

Fig. 2.20 Angle of insonation. The calculated velocity of an object using Doppler shift is dependent on the transducer angle (θ). If the transducer axis is perpendicular to the direction of flow (90°), then the cosine of θ is 0. Based on this formula for Doppler shift (ΔF), the detected frequency change would be 0. Adapted from Radiographics 1991;11:109–119

The frequency shift of the transmitted wave is also dependent on the angle of the transducer relative to the object in motion. The maximum Doppler frequency shift occurs when the transducer is oriented directly on the axis of motion of the object being insonated. That is, when the transducer is oriented parallel (angle θ=0°) to the direction of motion, the shift is maximal. Conversely, when the transducer face is oriented perpendicular to the direction of motion (angle θ=90°), there will be no shift in Doppler frequency detected (Fig. 2.19).

An accurate calculation of velocity of flow depends on the angle θ between the transducer and the axis of motion of the object being insonated (Fig. 2.20).

Color Doppler ultrasonography allows for an evaluation of the velocity and direction of an object in motion. A color map may be applied to the direction. The most common color map uses blue for motion away from the transducer and red for motion toward the transducer (Fig. 2.21).

The velocity of motion is designated by the intensity of the color. The greater the velocity of the motion, the brighter is the color displayed. Color Doppler may be used to characterize blood flow in the kidney, testis, penis, and prostate. It also may be useful in the detection of "jets" of urine emerging from the urethral orifices. An accurate representation of flow characteristics requires attention to transducer orientation relative to the object in motion. Therefore, in most clinical circumstances the angle between the transducer and the direction of motion should be less than or equal to 60° (Fig. 2.22).

When it is not possible to achieve an angle of 60° or less by manipulation of the transducer, the beam may be "steered" electronically to help create the desired angle θ (Fig. 2.23).

Power Doppler ultrasonography is a mode which assigns the amplitude of frequency change to a color map. This does not permit evaluation of velocity or direction of flow but is less affected by backscattered waves. Power Doppler is therefore less angle dependent than color Doppler and is more sensitive for detecting flow [4].

When a sound wave strikes an object within the body, the sound wave is altered in a variety of ways including changes in frequency and changes in amplitude (Fig. 2.24).

While color Doppler assigns the changes in frequency to a color map, power Doppler assigns changes in integrated amplitude (or power) to a color map. It is possible to assign low-level backscattered information to a color which is unobtrusive on the color map, thereby allowing increased gain without interference from this backscattered information (Fig. 2.25). Power Doppler may be more sensitive than color Doppler for the detection of diminished flow [4].

The integrated amplitude (power) of the Doppler signal is signified by the brightness of the color.

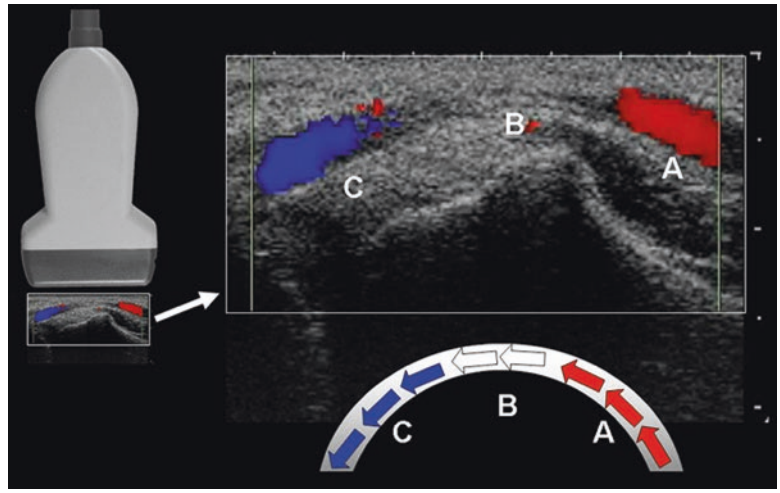

Fig. 2.21 In this image of the radial artery, blood is flowing through the curved vessel from (*A*) to (*C*). Flow toward the transducer (*A*) is depicted in *red*. Flow in the middle of the vessel (*B*) is perpendicular to the transducer axis and produces no Doppler shift; thus, no color is assigned even though the velocity and intensity of flow are uniform through the vessel. Flow away from the transducer (*C*) is depicted in *blue*

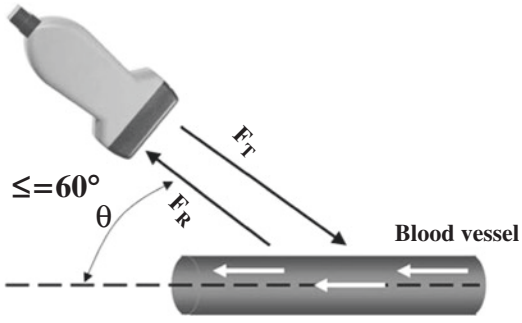

Fig. 2.22 The transducer angle should be ≤60° relative to the axis of fluid motion to allow a more accurate calculation of velocity of flow

Because frequency shift is not displayed in standard power Doppler, the direction and velocity of flow are not indicated.

Color Doppler with spectral display is a mode which allows the simultaneous display of a color Doppler image and representation of flow as a wave form within a discrete area of interrogation. This mode is commonly used to evaluate the pattern and velocity of blood flow in the kidney and testis (Fig. 2.26).

The **spectral waveform** provides information about peripheral vascular resistance in the tissues. The most commonly used index of these velocities is the resistive index (Fig. 2.27).

The resistive index may be helpful in characterizing a number of clinical conditions including renal artery stenosis and urethral obstruction. Since the velocity is represented on a scaler axis, it is necessary to set appropriate scaler limits to prevent artifacts. Therefore, it is necessary to know the expected velocity within vessels pertinent to urologic practice (Table 2.2). The clinical use of resistive index is described in subsequent chapters.

Artifacts Associated with Doppler Ultrasound

The **twinkle artifact** is produced when a sound wave encounters an interface which produces an energetic reflection of the sound wave. In ultrasound modes such as power and color Doppler, this can cause a distortion in the returning sound wave that gives the appearance of motion distal to that interface. The resulting Doppler signal appears as a trailing acoustic "shadow" of varying intensity and direction known as twinkle artifact. Although this artifact may be seen in a variety of clinical circumstances (e.g., twinkle artifact produced by the interaction of an ultrasound wave with a Foley catheter balloon in the bladder), it is most often helpful clinically in evaluating hyperechoic objects in the kidney. Stones often have a twinkle artifact (Fig. 2.28), whereas arcuate vessels and other hyperechoic structures in the kidney usually do not. Not all calcifications display the twinkle artifact. Calcifications of the renal artery and calcifica-

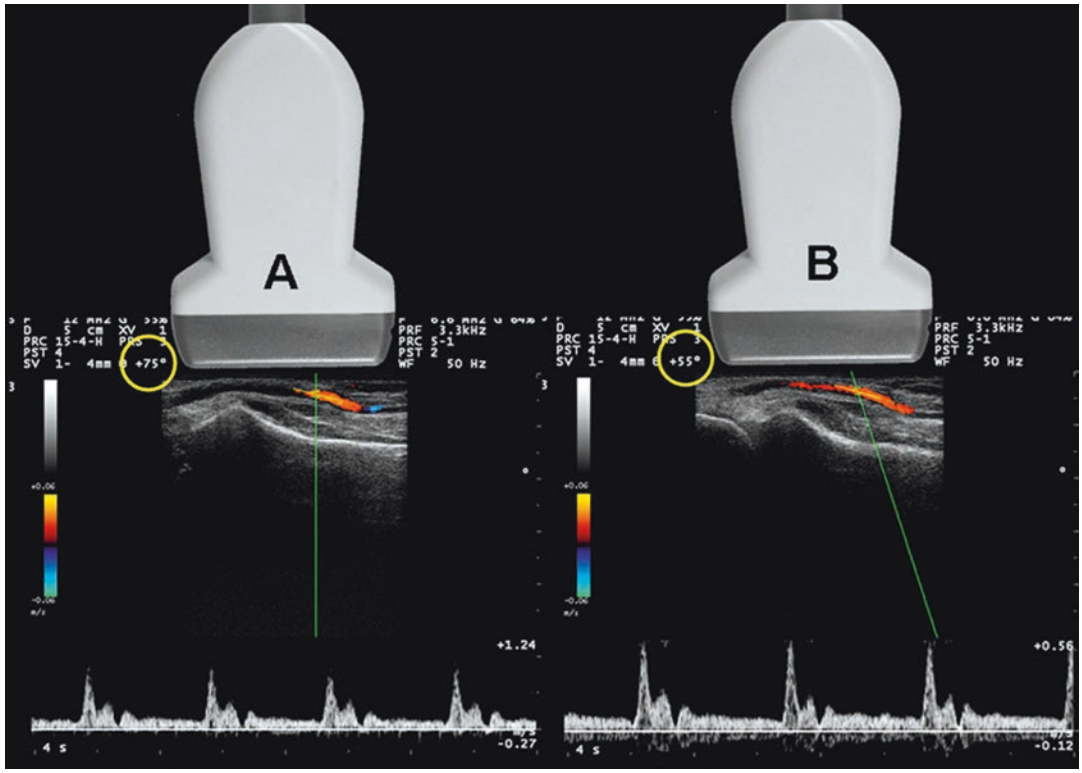

Fig. 2.23 Beam steering. In image (*A*), the angle of insonation is 75° (*yellow circle*) which is unfavorable for accurate velocity calculations. This is because the axis of the transducer is perpendicular to the vessel. In image (*B*) the beam has been "steered" to produce an angle of 55° (*yellow circle*) without changing the physical position of the transducer. The resultant velocity calculation is more accurate at 55°

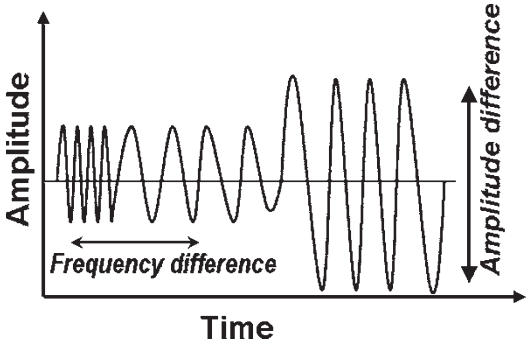

Fig. 2.24 Backscatter is defined as a combination of changes in frequency and amplitude which occur in the reflected sound wave of a primary frequency

tions within tumors and cysts may also produce the twinkle artifact [5].

Aliasing is an artifact which occurs when the ultrasound interrogation (determined by PRF) of an event occurs at a frequency which is insufficient to accurately represent the event. When interrogation occurs at infrequent intervals, only portions of the actual event are depicted. Aliasing occurs when the interrogation frequency is less than twice the shifted Doppler frequency (Fig. 2.29).

Normal laminar unidirectional blood flow is depicted as a single color on color Doppler. Spectral Doppler shows a complete waveform (Fig. 2.30). During color Doppler scanning, aliasing is most commonly seen as apparent turbulence and change in direction of blood flow within a vessel. During spectral Doppler scanning, the aliasing phenomenon is seen as truncation of the systolic velocity peak with projection of the peak below the baseline (Fig. 2.31).

This artifact can be overcome by decreasing the frequency of the incident sound wave, increasing the angle of insonation (θ), or increasing the PRF.

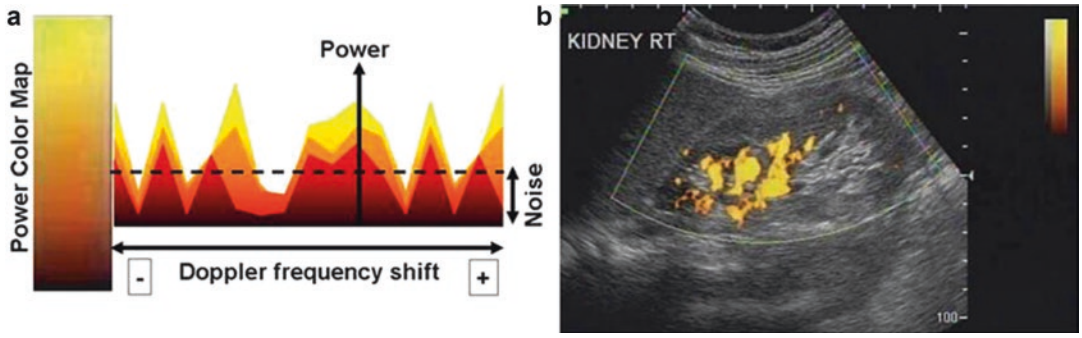

Fig. 2.25 (**a**) For power Doppler the intensity of color is related to changes in amplitude (power) rather than changes in frequency. (**b**) In this sagittal image of the kidney, power Doppler blood flow is demonstrated. Note that the color map depicted to the upper right does not have a scale since quantitative measurement of velocity is not displayed with standard power Doppler

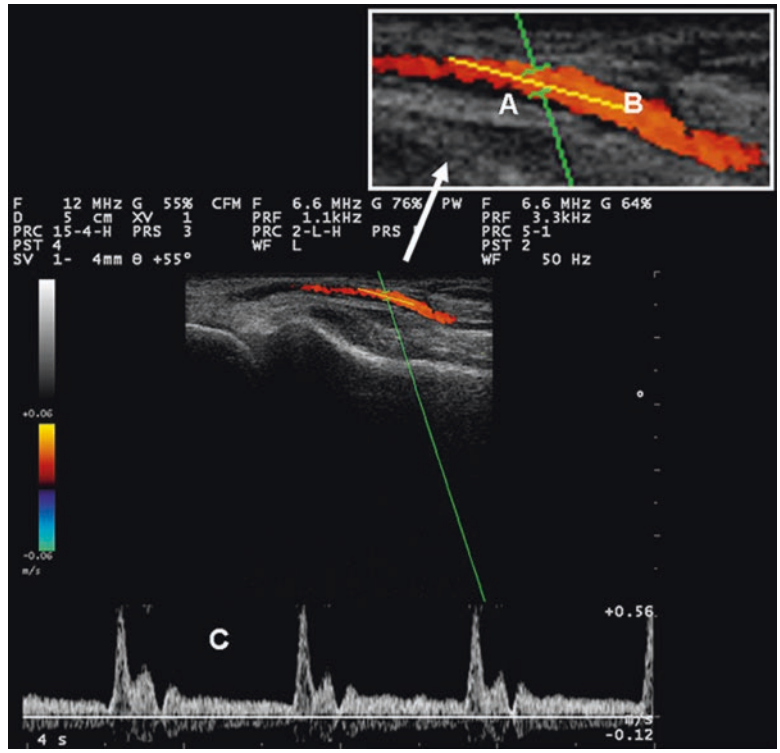

Fig. 2.26 In this example, the radial artery is shown in real-time gray-scale ultrasound with color Doppler overlay. The interrogation box or gate (*A*) is positioned over the vessel of interest. The gate should be positioned and sized to cover about 75 % of the lumen of the vessel. The angle of insonation is indicated by marking the orientation of the vessel with a cursor (*B*). The velocity of the flow within the vessel is depicted quantitatively in the spectral display (*C*)

Harmonic Scanning

Harmonic scanning makes use of aberrations related to the nonlinear propagation of sound waves within tissue. These asymmetrically propagated waves generate fewer harmonics but those which are generated have greater amplitudes (Fig. 2.32).

Since these harmonics are less subject to scattering associated with the incident wave, there is less noise associated with the signal. By selectively displaying the harmonic frequencies which are produced within the body and reflected to the transducer, it is possible to produce an image with less artifact and greater resolution.

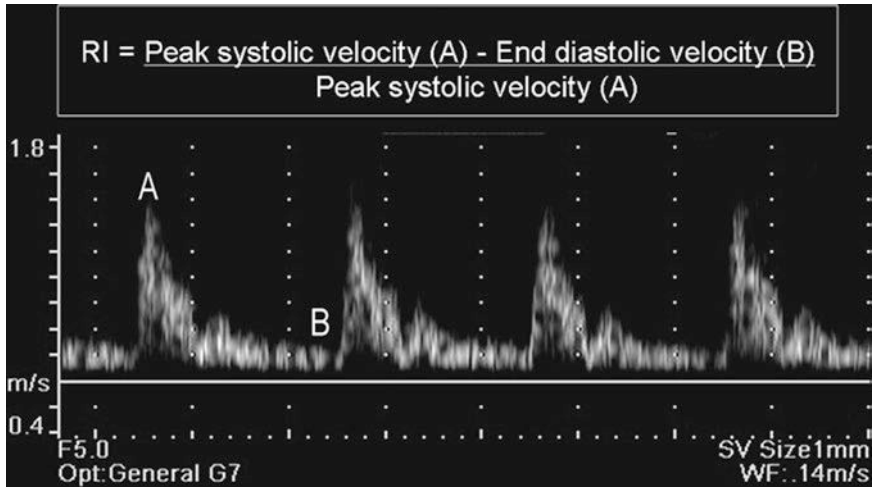

Fig. 2.27 The resistive index (RI) is the peak systolic velocity (*A*) minus the end-diastolic velocity (*B*) over the peak systolic velocity (*A*)

Table 2.2 Expected velocity in urologic vessels

Vessel	Velocity
Penile artery	>35 cm/s (after vasodilators) [10]
Renal artery	<100 cm/s [11]
Scrotal capsular artery	5–14 cm/s [12]

The measured velocity will depend on a variety of physiologic and anatomic variants

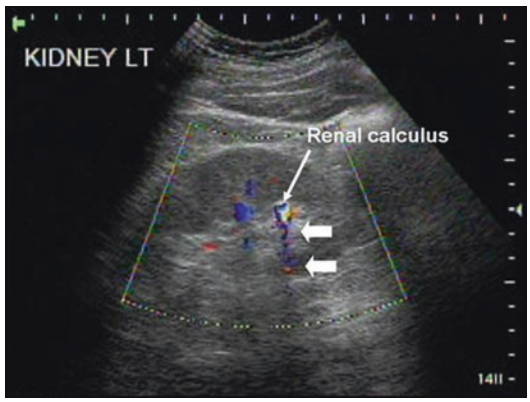

Fig. 2.28 Twinkle artifact. The effect produced by the interaction of sound waves at an interface with high impedance differences (in this case a renal calculus) which produces an artifact suggesting turbulent motion (*large arrows*)

Spatial compounding is a scanning mode whereby the direction of insonation is sequentially altered electronically to produce a composite image. This technique reduces the amount of artifact and noise producing a scan of better clarity [6] (Fig. 2.33).

Three-dimensional (3D) scanning produces a series of images (data set) which can then be manipulated to generate additional views of the anatomy in question. 3D rendering may be important in procedural planning and precise volumetric assessments [7]. 3D scanning may allow the recognition of some tissue patterns which would otherwise be inapparent on two-dimensional scanning [8].

Contrast Agents in Ultrasound

Intravenous compounds containing microbubbles have been used for enhancing the echogenicity of blood and tissue. Microbubbles are distributed in the vascular system and create strong echoes with harmonics when struck by sound waves. The bubbles themselves are rapidly degraded by the interaction with the sound waves. Machine settings producing a low mechanical index (see Chap. 4) are desirable to reduce destruction of the microbubbles. Contrast agents

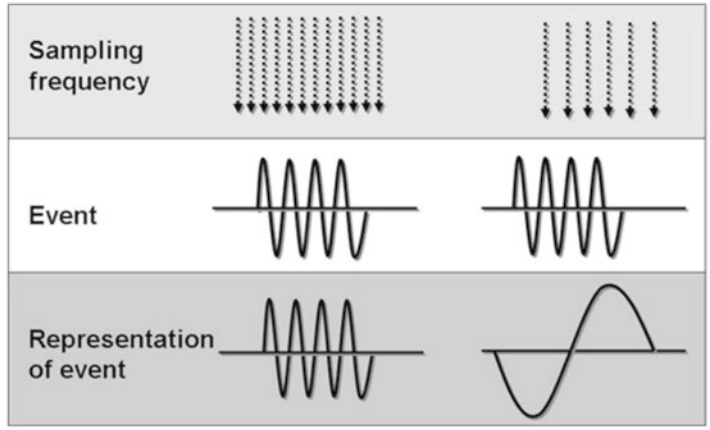

Fig. 2.29 Aliasing. In this illustration where a sine wave is the real-time event and the vertical *arrows* in the *top* panel represent the frequency of interrogation, we see that frequent interrogation produces an accurate representation of the event. An accurate depiction of an ultrasound event must meet the condition: fs ≥ 2b, where fs is the sampling frequency and 2b is the highest frequency in the event. This is known as the Nyquist limit. Less frequent sampling (on the right) results in an incorrect interpretation of the event. (Diagram adapted from Diagnostic Ultrasound, 3rd Ed., Figs. 1–40, p. 33)

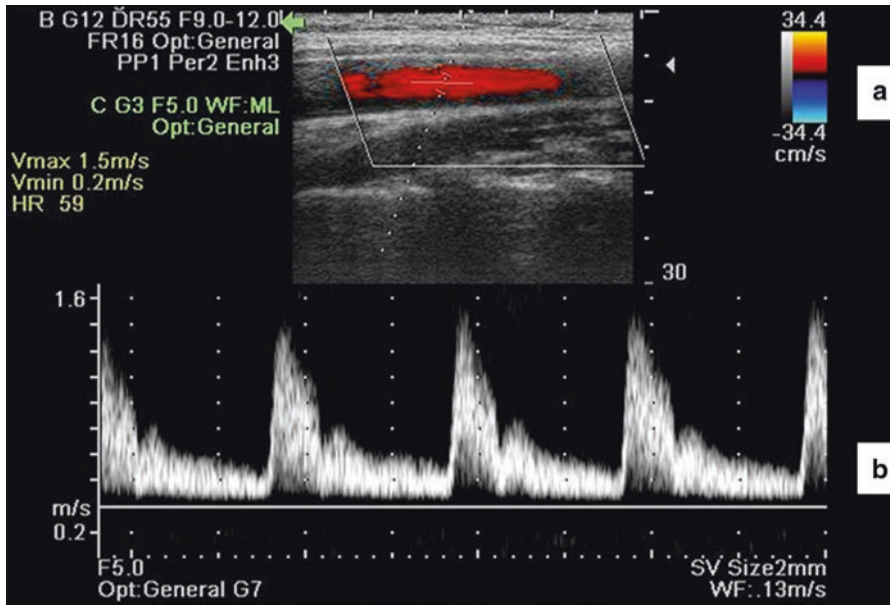

Fig. 2.30 Spectral Doppler. (**a**) Blood flow appears unidirectional on color mapping in this color Doppler image with spectral flow analysis. (**b**) The waveform is accurately depicted on spectral analysis

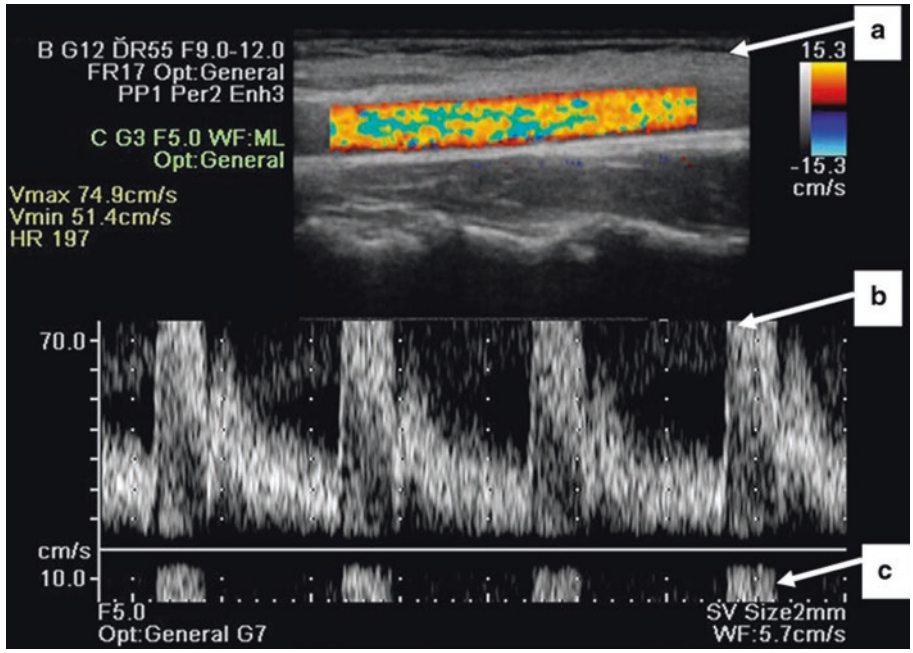

Fig. 2.31 In this color Doppler ultrasound with spectral flow, aliasing is demonstrated by apparent changes in velocity and direction on the color map assigned to the vessel (**a**). Aliasing of the spectral waveform is seen as truncation of the peak systolic velocity (**b**) with projection of the peak below the baseline (**c**)

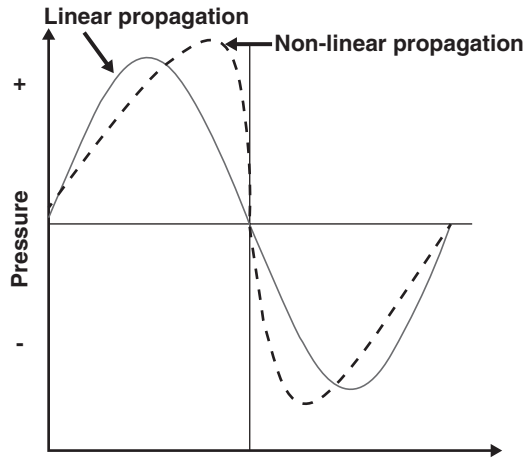

Fig. 2.32 Nonlinear propagation of sound waves in tissue results in fewer but more energetic harmonics which may be selectively evaluated in the returning echo

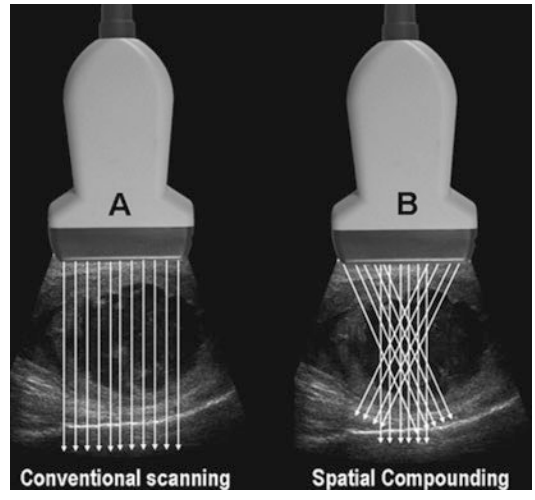

Fig. 2.33 Spatial compounding results in a composite image by combining data from multiple scanning angles produced by automated beam steering. The resulting image is more detailed with less artifact

may be useful in prostatic ultrasound by enhancing the ability to recognize areas of increased vascularity [9]. The use of intravenous ultrasound contrast agents is considered investigational but has shown promise in a number of urologic scanning situations. The ability to demonstrate vascular enhancement without exposure to potential toxic contrast agents or ionizing radiation makes contrast-enhanced ultrasound a promising urologic imaging modality.

References

1. Mason WP. Piezoelectricity, its history and applications. J Acoust Soc Am. 1981;70(6):1561–6.
2. Rumack CM, Wilson SR, Charboneau JW. Diagnostic ultrasound. 3rd ed. St. Louis: Mosby; 2005. p. 8.
3. Rumack CM, Wilson SR, Charboneau JW. Diagnostic ultrasound, vol. 3. St. Louis: Mosby; 2005. p. 12.
4. Rubin JM, Bude RO, Carson PL, et al. Power Doppler US: a potentially useful alternative to mean frequency-based color Doppler US. Radiology. 1994; 190:853–6.
5. Kim HC, Yang DM, Jin W, Ryu JK, Shin HC. Color Doppler twinkling artifacts in various conditions during abdominal and pelvic sonography. J Ultrasound Med. 2010;29:621–32.
6. Merritt CR. Technology update. Radiol Clin North Am. 2001;39:385–97.
7. Ghani KR, Pilcher J, Patel U, et al. Three-dimensional ultrasound reconstruction of the pelvicaliceal system: an in-vitro study. World J Urol. 2008;26:493–8.
8. Mitterberger M, Pinggera GM, Pallwein L, et al. The value of three-dimensional transrectal ultrasonography in staging prostate cancer. BJU Int. 2007;100:47–50.
9. Mitterberger M, Pinggera GM, Horninger W, et al. Comparison of contrast enhanced color Doppler targeted biopsy to conventional systematic biopsy: impact on Gleason score. J Urol. 2007;178:464–8.
10. Rifkin MD, Cochlin DL. Imaging of the scrotum & penis. London: Martin Dunitz; 2002. p. 276.
11. Zucchelli PC. Hypertension and atherosclerotic renal artery stenosis: diagnostic approach. J Am Soc Nephrol. 2002;13:S184–6.
12. Bluth EI, Benson CB, Ralls PW. Ultrasonography in vascular diseases: a practical approach to clinical problems. New York: Thieme Medical; 2008. p. 87.

Bioeffects and Safety

3

Pat F. Fulgham

Urologists who perform and interpret ultrasound in their office must have a thorough knowledge of the potential bioeffects of ultrasound in human tissues and how to maintain the ultrasound equipment to protect patient safety. Diagnostic ultrasound transmits energy into the patient which has the potential to produce biological effects. The maximum output of ultrasound energy by ultrasound devices is regulated by the US Food and Drug Administration (FDA) [1]. In general, these regulations allow enough energy to accomplish diagnostic goals but prescribe a margin of safety. The total energy imparted during an ultrasound examination is controlled by the operator through (1) acoustic output, (2) selection of frequency, (3) mode of ultrasound, (4) technique, and (5) duration of the examination.

Bioeffects of Ultrasound

As ultrasound waves enter biological tissues, some of the energy is transmitted, some is reflected, and some is dissipated as heat. The interaction of ultrasound with human tissue produces **thermal effects** and **mechanical effects**.

P.F. Fulgham, M.D., F.A.C.S. (✉)
Department of Urology, Texas Health Presbyterian Dallas, 8210 Walnut Hill Lane, Suite 014, Dallas, TX 75231, USA
e-mail: pfulgham@airmail.net

Thermal Effects

The most important thermal effect of ultrasound is tissue heating. Tissue heating from ultrasound is a result of **scattering** and **absorption**, two mechanisms of attenuation. Absorption of ultrasound by tissue results in the conversion of mechanical acoustic energy into heat. The amount of heat generated is directly proportional to the frequency of the wave, the amplitude of the wave, and the duration of exposure.

The work performed by ultrasound as it passes through tissue is given in Watts (W) which is a measure of acoustic power per unit of time. The distribution of acoustic power over area is **intensity**. Intensity (*I*) is expressed in w/cm^2. Intensity is influenced by the cross-sectional area of the ultrasound beam. The same amount of acoustic power distributed in a smaller area results in increased intensity. The amount of heating which occurs in human tissue as the result of ultrasound exposure is directly proportional to the intensity. Thus, beam focusing in a specific anatomic region will result in more heating in that area because of increased acoustic intensity at that location.

Temporal factors also influence the amount of tissue heating. The fraction of time that the transducer is producing pulses (called the *duty factor*), and the total amount of time a tissue is exposed to the beam (called the *duration time*) influences tissue heating. A low duty factor and a short duration

P.F. Fulgham, B.R. Gilbert (eds.), *Practical Urological Ultrasound*, Current Clinical Urology,
DOI 10.1007/978-3-319-43868-9_3

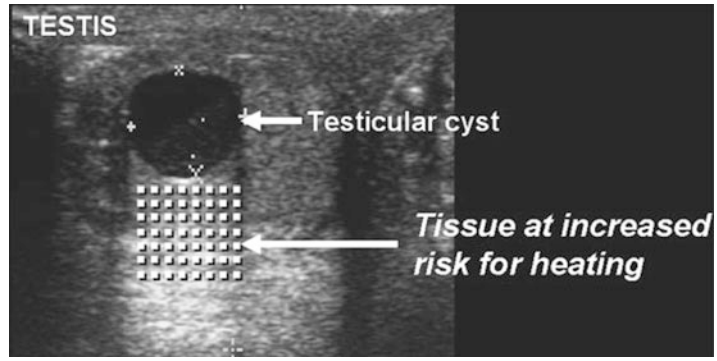

Fig. 3.1 Testicular cyst. The tissue distal to this testicular cyst (*gridded area*) is prone to more tissue heating because sound waves passing through the cyst are less attenuated than those passing through adjacent testicular parenchyma

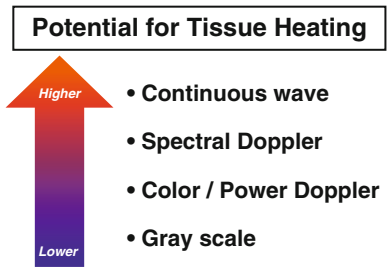

Fig. 3.2 Potential for tissue heating. Relative likelihood of tissue heating by mode of ultrasound is based in part on pulse-repetition frequency and duration of tissue exposure

time reduce tissue heating. In standard scanned modes of ultrasound (e.g., gray scale, power, and color Doppler), the transducer is being moved at frequent intervals, reducing duration time and limiting heating of specific tissue areas. Blood flow in tissues also tends to dissipate heat, resulting in less temperature increase in the tissue.

The type of tissue being insonated influences tissue heating. Tissues which rapidly attenuate sound (i.e., tissue with high impedance, such as bone) experience more heating. Thus, soft tissue immediately adjacent to bony structures may be more prone to tissue heating. Soft tissue heating may also occur when less attenuated waves strike these tissues. This may occur in tissue distal to a fluid-filled structure such as a cyst (Fig. 3.1).

Tissue heating of up to 1 °C may occur during diagnostic imaging at tissue/bone interfaces. Localized tissue heating seems to be safe up to about 2–5 °C [2]. In most diagnostic scanning applications, the amount of tissue heating is negligible. The beneficial effects of tissue heating are utilized in therapeutic ultrasound for joints and muscles. At high intensity levels (e.g., with high-intensity focused ultrasound (HIFU)), the biological effects of heating and cavitation are used to destroy tissue [3].

Standard gray-scale imaging generates the least tissue heating because the pulse duration is short and pulse-repetition frequencies (PRFs) are low. Color flow Doppler and power Doppler produce intermediate tissue heating. Spectral Doppler imaging is an unscanned mode which uses longer pulse durations and higher PRFs (to avoid artifacts such as aliasing) and therefore has an increased potential for heating. Spectral Doppler also involves longer duration times as individual vessels are interrogated in a fixed scanning position (Fig. 3.2) [4]. Tissue heating associated with routine diagnostic ultrasound is not known to produce tissue damage or to cause denaturation of proteins or to have teratogenic effects as long as scanning times are not prolonged and acoustic output restrictions are observed [5].

Mechanical Effects

Ultrasound energy generates an **acoustic field** in tissue. The acoustic field generates mechanical forces which affect tissue at the microscopic and macroscopic levels. Pressure exerted by the field creates **torque** and induces motion called **streaming**. These forces may potentially damage cells or tissues and also contribute secondarily to tissue heating.

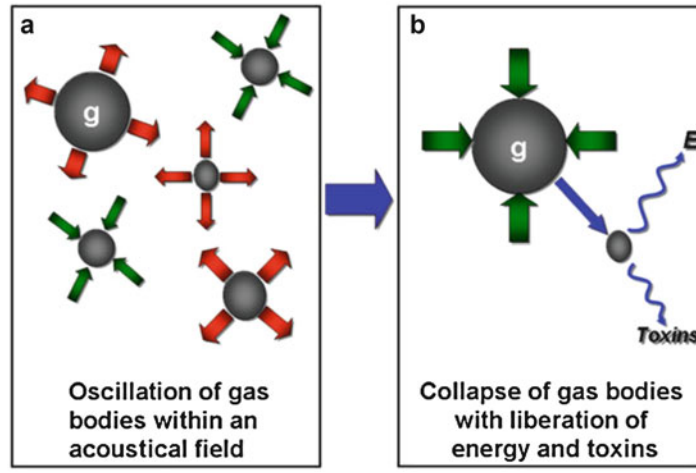

Fig. 3.3 Cavitation. (**a**) The oscillation and collapse of gas bodies (g) is cavitation. (**b**) The result of the collapse of gas bodies is the release of energy (*E*) and chemical toxins which may cause tissue damage

One phenomenon associated with acoustical fields, **cavitation**, deserves special attention since it has been shown to cause tissue damage in animal models [1]. Cavitation occurs when gas bubbles within tissue begin to first oscillate or vibrate in response to ultrasound and then to collapse. This collapse causes a violent movement of individual adjacent particles within the tissue which, in turn, causes tissue damage. This damage may take the form of ruptured cells and blood vessels or may cause chromosomal (ultrastructural) damage. In addition, the heat generated by the rapid collapse of gas bubbles may result in the formation of toxic chemical by-products (Fig. 3.3) [6].

The detrimental mechanical effects of acoustic fields are most likely to occur at gas/fluid interfaces. Thus, cavitation effects (such as petechia formation) would most likely be seen in the lung or bowel. The threshold for cavitation is approximately 1 kW/cm^2 (far higher than the average intensity of 100 mW/cm^2 generated by most clinical scanners) [6].

Patient Safety

For most urologic applications, ultrasound produces energies in human tissues which are within recognized safe limits. *The single most important factor in minimizing potential adverse effects of ultrasound is the well-informed ultrasound operator* [7].

The proper selection of acoustic output, transducer frequency, and mode of ultrasound for a specific indication will mitigate risks. Expeditious and efficient scanning technique is critical to limiting overall exposure. To assist the sonographer in monitoring the bioeffects of ultrasound, the ultrasound community has adopted the output display standard (ODS) [8]. Two values are typically displayed, the **mechanical index** (MI) and the **thermal index** (**TI**) (Fig. 3.4). These indices are *calculated* estimates of the potential for bioeffects of ultrasound based on the mode of ultrasound being used, frequency, power output, and time of insonation. The MI and TI are typically displayed on the monitor during ultrasound examinations and all practitioners should be familiar with the location. It is important to understand that these indices are not safety limits and are not direct measurements.

Mechanical Index

The MI indicates the probability that cavitation will occur. For tissues not containing stabilized gas bodies (lung and intestine), the risk of cavitation is low as long as the MI is ≤0.7.

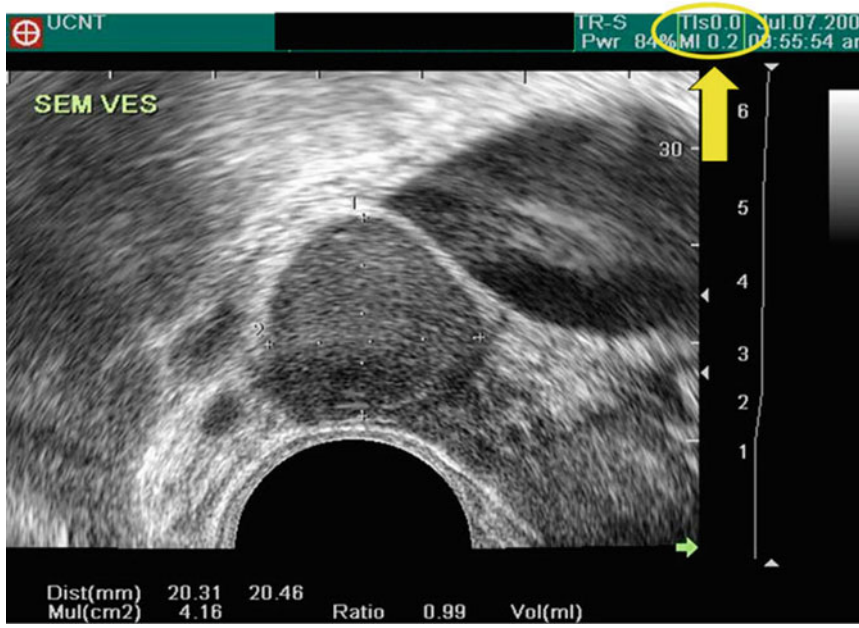

Fig. 3.4 Mechanical and thermal index. The MI and TI (*yellow* cycle) are calculated estimates of the potential for cavitation and tissue heating respectively, based on study parameters and time of study. These are not direct measurements of either heating or pressures in the acoustical field

For structures adjacent to lung or intestine, scanning time should be limited if the MI exceeds 0.4 (Fig. 3.5).

Thermal Index

The TI indicates the probability that tissue temperature within the sonographic field will be increased by 1 °C. The precise consequences of tissue heating are not completely understood, but even tissue temperature elevations of up to 6 °C are not likely to be dangerous unless exposure time exceeds 60 s [2].

ALARA

In general, ultrasound performed by urologists has a low risk for patient harm as long as standard protocols are followed. Although tissue heating may occur, there are no confirmed biologic effects of tissue heating in non-fetal scanning except when they are sustained for extended periods. "No independently confirmed adverse effects caused by exposure from present diagnostic ultrasound instruments have been reported in human patients in the absence of contrast agents. Biological effects (such as localized pulmonary bleeding) have been reported in mammalian systems at diagnostically relevant exposures, but the clinical significance of such effects is not yet known. Ultrasound should be used by qualified health professionals to provide medical benefit to the patient" [9]. Nevertheless, all urologists should endeavor to follow the principles of **ALARA** which stands for "**A**s **L**ow **A**s **R**easonably **A**chievable." The ALARA principle is intended to limit the total energy imparted to the patient during an examination. This can be accomplished by (1) keeping power outputs low, (2) using appropriate scanning modes, (3) limiting exam times, (4) adjusting focus and frequency, and (5) using the cine function during documentation.

Scanning Environment

The physical environment where ultrasound examinations are performed should have adequate room for ultrasound equipment with the ability to control lighting and temperature.

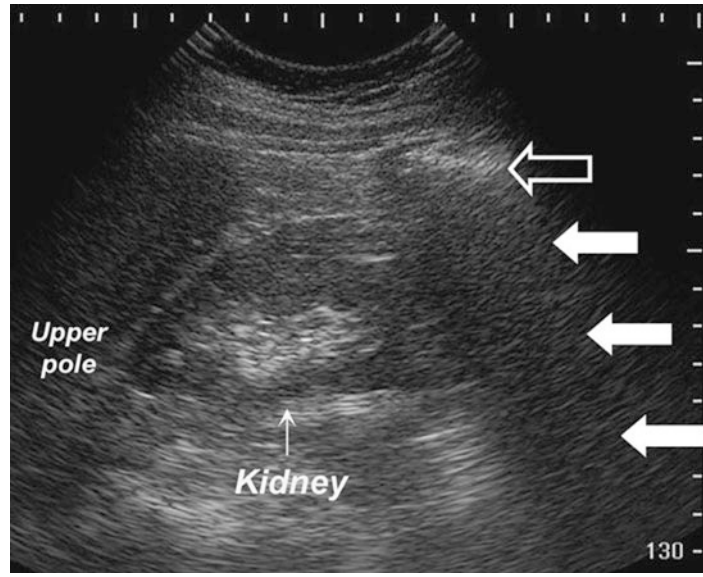

Fig. 3.5 The risk for cavitation is higher in tissues which are in proximity to gas-containing bodies such as the bowel. Here, bowel gas (*open arrow*) and the resultant distal acoustic shadowing (*white arrows*) obscures the *lower* pole of the *right* kidney (*arrow*)

The exam table should have a height adjustment for sonographer comfort and ease of patient access. If there are windows in the exam room, they should have adjustable coverings to reduce the light and glare on the monitor and to preserve patient privacy. Workspace design should include adequate space to allow for safe handling of biopsy needles and specimens. Since the lighting in the room is dimmed, it may be necessary to provide a separate lighting source for the work area where biopsy samples are being transferred into specimen containers.

The goals of the optimum scanning environment should be to protect patient safety and to maximize operator efficiency and reduce the risk for work-related musculoskeletal disorders (MSDs). Occupational Safety and Health Administration (OSHA). OSHA has established an e-tool to provide guidance on operator safety in the performance of ultrasound [10]. Urologists should personally arrange the ultrasound equipment and monitor the environment in pursuit of these goals. Policies and procedures should be in place to provide for the safety of patients and personnel. Infection control policies and procedures should be in place including adherence to universal precautions and proper care, cleaning, and maintenance of ultrasound equipment.

Patient Identification and Documentation

Patient identification should be verified prior to performing ultrasound procedures. When biopsy specimens are taken, a time-out should be conducted to verify patient identity and the accurate labeling of ultrasound images and specimen containers. It is estimated, based on DNA evidence, that up to 1 % of prostate biopsy specimens may be subject to incorrect patient identification [11]. Documentation and image labeling is addressed in further detail in Chap. 2. An ultrasound report should be generated. The report and images should be included in the patient's medical record.

Equipment Maintenance

Ultrasound equipment should be in good operating condition and undergo routine calibration at least once a year [12]. Equipment manufacturer specifications and federal and state guidelines for the maintenance of ultrasound equipment should be followed. Equipment should be routinely inspected and tested for electrical safety. When transporting ultrasound equipment, care should be taken to ensure that transducers are secured to the machine. The transducers are delicate and should not be

dropped. Transducer cables and power cords should be secured to the machine and off the ground to prevent damage to the cables by the machine rolling over them.

Cleaning and Disinfection of Ultrasound Equipment

The ultrasound transducers, cables, and the machine itself should be cleaned immediately following each study. Ultrasound transducers have delicate parts which can be damaged by inappropriate handling, so equipment manufacturer guidelines should be followed when cleaning. The cleaning method and level of disinfection for transducers will depend on the specifics of the procedures and the nature of tissue encountered. The Centers for Disease Control (CDC) publishes guidelines for disinfection and sterilization in healthcare facilities which should be followed [13].

Applications such as abdominal, pelvic, or scrotal ultrasound are considered **non-critical** since they are performed on intact skin. The transducers and transducer holders should be cleaned immediately following the procedure. Allowing gel to dry on the probe makes cleaning more difficult. Staff should wear gloves when cleaning the probes and equipment. The probe should be disconnected from the ultrasound unit when cleaning. Ultrasound gel may be removed from the probe by wiping with a soft cloth. The transducer should be cleaned with mild soap and water or a commercial spray and wiped after every use. The ultrasound manufacturer-approved disinfectant should be used to avoid damaging the probe. When placing the probe under running water, care should be taken to keep water away from the junction of the probe and the cable. The entire body of the transducer may be immersed, but care should be taken to avoid the junction between the transducer body and the cable. Each manufacturer provides specific instructions about the proper immersion levels for probes. A small soft brush may be used to clean crevices, where gel may accumulate.

When an ultrasound procedure is performed in which the probe comes into contact with mucous membranes (e.g., with transrectal ultrasound), a **high-level disinfection** process should be followed. Even when the probe covers are used, high-level disinfection after the procedure is still necessary. When cleaning the transrectal probe and attachments, staff should wear personal protective equipment including gloves and glasses. The FDA has published guidelines for the reprocessing of reusable ultrasound transducer assemblies used for biopsy procedures which should be followed [14]. The AIUM (American Institute of Ultrasound in Medicine) has issued guidelines on the cleaning and preparing of endocavitary ultrasound transducers between patients [15]. Transducer covers and biopsy attachments should be removed and discarded in a biohazard container. The probe should be placed under warm running water to remove residual debris and a small amount of nonabrasive liquid soap used to thoroughly cleanse the probe. Using a small brush, areas of angulation and crevices may be brushed clean. The probe should be rinsed with warm running water prior to being placed in sterilizing liquid. When immersing in a liquid, care should be taken to follow the manufacturer's recommended immersion level so as to not damage the probe. The transducer should be immersed in a disinfectant approved for high-level disinfection and for the specified time recommended by the manufacturer to achieve high-level disinfection. The transducer should not remain immersed in the disinfectant solution for longer than the recommended time as prolonged exposure may damage the transducer. A published list of approved high-level disinfectants for use in processing reusable medical devices is available at US Food and Drug Administration web site [16]. The CDC publishes guidelines on the cleaning of medical devices on their web site [13]. After high-level disinfection has been performed, the transducer should be rinsed thoroughly with sterile water, dried with a paper towel, and stored in a clean environment until its next use.

Critical disinfection is required when blood or body fluids come in contact with the transducer or needle guide. Because blood and tissue pass through prostate biopsy guides, reusable prostate biopsy guides should be heat sterilized. If reusable biopsy guides are not able to be heat

sterilized, then chemical sterilization should be performed [17]. Attachments which are labeled "one-time use" should not be reused and should be disposed of in a biohazard container. When cleaning reusable biopsy attachments, they should be placed immediately into a solution of mild soap and water. A clean and properly sized brush should be used to clean the biopsy channel and lumen of the device checking to make sure no debris remains in the channel or lumen. The attachment should be rinsed and placed in a bag for heat sterilization. Heat sterilization should be performed, and the attachments should remain in the sterile bag until ready for use.

References

1. Guidance for industry and FDA staff-information for manufacturers seeking marketing clearance of diagnostic ultrasound systems and transducers. Document issued on 9 Sept 2008. http://www.fda.gov/MedicalDevices/DeviceRegulationandGuidance/GuidanceDocuments/ucm070856.htm.
2. Bioeffects Committee of the American Institute of Ultrasound in Medicine. American Institute of Ultrasound in Medicine consensus report on potential bioeffects of diagnostic ultrasound: executive summary. J Ultrasound Med. 2008;27:503–15.
3. Susani M, Madersbacher S, Kratzik C, Vingers L, Marberger M. Morphology of tissue destruction induced by focused ultrasound. Eur Urol. 1993;23 Suppl 1:34–8.
4. Rumack CM, Wilson SR, Charboneau JW. Diagnostic ultrasound, Chap. 2. 3rd ed. St. Louis: Mosby; 2005. p. 37.
5. O'Brien WD, Deng CS, Harris GR, Herman BA, Merritt CR, Sanghvi N, et al. The risk of exposure to diagnostic ultrasound in postnatal subjects: thermal effects. J Ultrasound Med. 2008;27:517–35.
6. Church CC, Carstensen EL, Nyborg WL, Carson PL, Frizzell LA, Bailey MR. The risk of exposure to diagnostic ultrasound in postnatal subjects: nonthermal mechanisms. J Ultrasound Med. 2008;27:565–92.
7. Nelson TR, Fowlkes JB, Abramowicz JS, Church CC. Ultrasound biosafety considerations for the practicing sonographer and sinologist. J Ultrasound Med. 2009;18:139–50.
8. American Institute of Ultrasound in Medicine. How to interpret the ultrasound output display standard for higher acoustic output diagnostic ultrasound devices: version 2 [technical bulletin]. J Ultrasound Med. 2004;23:723–6.
9. American Institute of Ultrasound in Medicine Official Statement on Prudent Use Clinical Safety. 2012. http://www.aium.org/resources/statements.aspx. Accessed 29 Jan 2013.
10. United States Department of Labor Occupational Safety and Health Administration: Hospital eTool, Clinical services sonography. http://www.osha.gov/dcsp/products/etools/hospital/sonography/sonography.html.
11. Makary MA, Epstein J, Pronovost PJ, Millman EA, Hartmann EC, Freischlag JA. Surgical specimen identification errors: a new measure of quality in surgical care. Surgery. 2007;141(4):450–5.
12. Routine quality assurance for diagnostic ultrasound equipment. American Institute of Ultrasound in Medicine. 2008. http://www.aium.org.
13. Rutala WA, Weber DJ, The Healthcare Infection Control Practices Advisory Committee (HICPAC). Guidelines for disinfection and sterilization in healthcare facilities. 2008. http://www.cdc.gov/hicpac/pdf/guidelines/Disinfection_Nov_2008.pdf. Accessed 29 Jan 2013.
14. FDA public health notification: reprocessing of reusable ultrasound transducer assemblies used for biopsy procedures. 2006. http://www.fda.gov/medicaldevices/safety/alertsandnotices/publichealthnotifications/ucm062086 Accessed 22 June 2006.
15. AIUM guidelines for cleaning and preparing endocavitary ultrasound transducers between patients. Approved 4 June 2003. http://www.aium.org/resources/statements.asp.x. Accessed 29 Jan 2013.
16. FDA-cleared sterilants and high level disinfectants with general claims for processing reusable medical and dental devices. 2009. http://www.fda.gov/MedicalDevices/DeviceRegulationandGuidance/ReprocessingofSingle-UseDevices/ucm133514.htm.
17. ANSI/AAMI ST58:1005(R)2010. Chemical sterilization and high level disinfection in health care facilities. Developed by the Association for the Advancement of Medical Instrumentation. Approved by the American National Standards Institute.

Maximizing Image Quality: User-Dependent Variables

4

Pat F. Fulgham

Introduction

Ultrasound is a tool used for the diagnosis and management of urologic disease. An ultrasound examination performed and interpreted by the clinician combines a knowledge of the underlying anatomy and disease processes with technical expertise to produce images of superior quality which answer a specific clinical question. The interpretation of urologic images is an integral part of the training of all urologists. The technical performance of the study and the ability to maximize image quality are learned skills. Current ultrasound equipment is a sophisticated combination of mechanical equipment and software which is capable of producing exquisitely detailed anatomic images. Almost all current ultrasound equipment includes preset applications which optimize machine settings for imaging of specific organs or regions of the body. These presets save a great deal of time because they set scanning parameters which are favorable for most patients. However, there are many clinical circumstances in which these presets will need to be adjusted by the individual performing the ultrasound examination. An understanding of the underlying physical principles of ultrasound, proper probe selection, and machine settings is critical to making appropriate adjustments to the equipment.

Tuning the Instrument

The goal of adjusting machine settings is to produce "a good-quality image." Accepted characteristics of a good-quality image include (1) sufficient and uniform brightness, (2) sharp and in focus, (3) adequate size, and (4) oriented and labeled for documentation purposes. Desired attributes of an image may vary from individual to individual, but these general principles should always apply.

Several machine settings can be manipulated by the sonologist. These include but are not limited to gain, time-gain compensation (TGC), frequency, focal zones, depth/size, field of view, and cine function (Fig. 4.1).

This chapter will explore the use of each of these "user-controlled" variables emphasizing the underlying physical principles and defining the clinical circumstances under which these adjustments may be necessary.

Transducer Selection

Selection of the transducer is critical to maximizing image quality. The physical shape of the transducer may be important in certain circumstances.

P.F. Fulgham, M.D., F.A.C.S. (✉)
Department of Urology, Texas Health Presbyterian Dallas, 8210 Walnut Hill Lane, Suite 014, Dallas, TX 75231, USA
e-mail: pfulgham@airmail.net

P.F. Fulgham, B.R. Gilbert (eds.), *Practical Urological Ultrasound*, Current Clinical Urology,
DOI 10.1007/978-3-319-43868-9_4

The image that is produced by a transducer may be recognized by its shape. A linear array transducer produces a rectangular image whereas a curved array transducer produces an image which is trapezoidal in shape (Fig. 4.2).

Linear array transducers are most commonly used in urology for imaging of the testes and male genitalia. The curved array transducer is more frequently used for abdominal scanning. The curved nature of the probe allows gentle pressure on the patient's abdomen or flank resulting in contact of the entire transducer face with the skin. Curved array transducers are useful for imaging between ribs or angling beneath the pubic symphysis.

Transducers are usually multifrequency, meaning the frequency can be switched electronically over a range of frequencies (e.g., 2.5–6 mHz for an abdominal transducer). It is important to select the highest frequency which has adequate depth of penetration for the anatomic area of interest. The higher the frequency of the transducer, the greater the axial resolution and the better the anatomic representation of the image. However, there is a trade-off between frequency and depth of penetration. Imaging of the kidneys requires a lower frequency to penetrate to a depth of 6–14 cm below the surface of the skin. Thus, renal scanning is usually performed with a curved array transducer between 2.5 and 6 mHz. By contrast, because of the close proximity of the testes to the surface of the skin, scanning of the testis can be performed with high frequency transducer, producing excellent axial resolution. A linear array transducer at 12 mHz is often used for testicular ultrasound. Transrectal ultrasound of the prostate often employs a transducer of 7.5 mHz since it offers an optimal combination of depth of penetration and axial resolution for the average-sized gland (Fig. 4.3).

Frequently Used Adjustable Machine Settings

- Gain
- Time-gain compensation
- Frequency
- Focal zones
- Depth / Size
- Field of view
- Cine function

Fig. 4.1 There are a large number of parameters and settings which may be modified by the user. These seven represent commonly used adjustments and functions for manipulating image quality

Scanning Environment

To produce the best-quality image, the sonographer should arrange the scanning environment so that the interfaces between patient, sonographer, and equipment are optimized. The patient should be positioned at a height which allows the sonographer to stand or sit in a comfortable position so

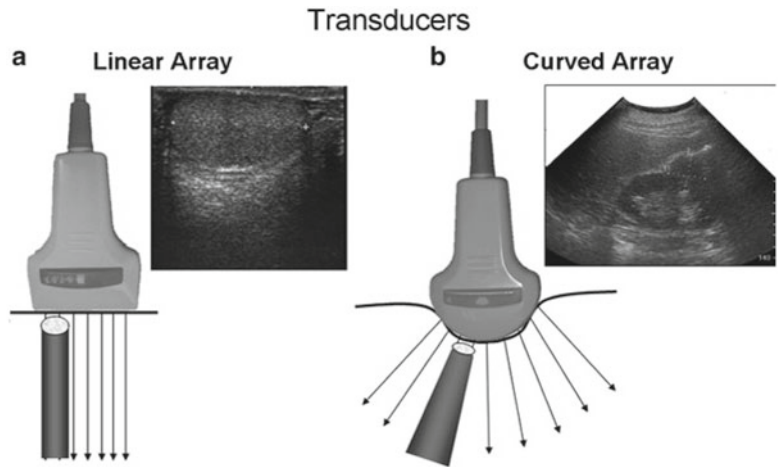

Fig. 4.2 (**a**) The linear array transducer produces a *rectangular* image field. (**b**) The *curved array* transducer produces a *trapezoidal* or *pie-shaped* image. The shape of the transducer affects the divergence of the sound wave as it propagates in the body

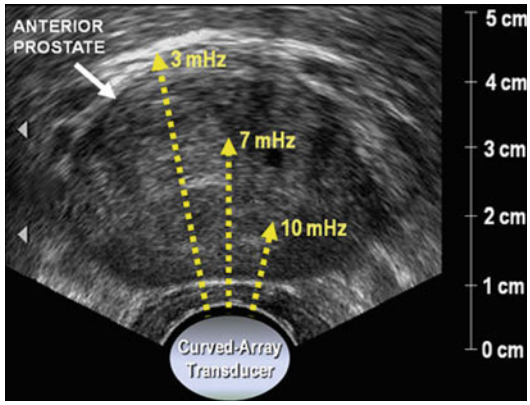

Fig. 4.3 The selection of a transducer with the frequency of 7.5 mHz reflects the trade-off between depth of penetration and good axial resolution. In this axial image of a large prostate, a *lower* scanning frequency may be needed to adequately visualize the anterior prostate

Fig. 4.4 The configuration of the equipment and proximity to the patient are critical in maximizing comfort, efficiency, and accuracy during scanning and documentation

that the sonographer is able to stabilize the transducer against the patient's body. This minimizes unwanted movement of the transducer and allows the sonographer to maintain the orientation and position of the transducer while adjusting machine features (Fig. 4.4).

The sonographer must have the ability to comfortably reach the physical console or touch screen in order to adjust the machine setting. Many ultrasound units provide the ability to freeze and unfreeze the transducer via a button on the transducer itself or by a foot switch. In either case, the sonographer must be able to scan the patient with one hand while manipulating the console and documenting with the other hand.

The sonographer must have a clear direct view of the monitor. The angle of the monitor should be adjusted for viewing by the sonographer. The brightness settings on the monitor need to be adjusted for the conditions under which the scan is being performed. In general, dimming the room lights improves the ability to evaluate the image on the monitor.

Monitor Display

It is important when performing an ultrasound examination to understand the information that is available on the monitor. Patient demographic information, type of exam, and facility should be entered. The monitor will usually display information regarding which probe is active, the frequency of the probe, and the magnification of the image. Information regarding overall gain and other settings is available on the monitor. Typically, there will be a TGC curve displayed on one side of the image as well as color bar which demonstrates the range of pixel brightness or hues available. In addition, there will be gradient markings on one side so that depth of field can be appreciated (Fig. 4.5).

By convention, when scanning organs in the sagittal view, the upper pole of the organ (e.g., kidney or testis) is to the left of the screen and the lower pole is to the right of the screen (Fig. 4.6).

In transverse scanning, the right side of an anatomic structure is displayed on the left side of the image just as it would be when evaluating a conventional radiograph. These conventions should always be followed when documenting an ultrasound examination; however, it may be useful to also demonstrate the orientation of the probe using graphics or icons. When paired structures such as the kidneys or testes are imaged, it is particularly important to designate the organ as right or left.

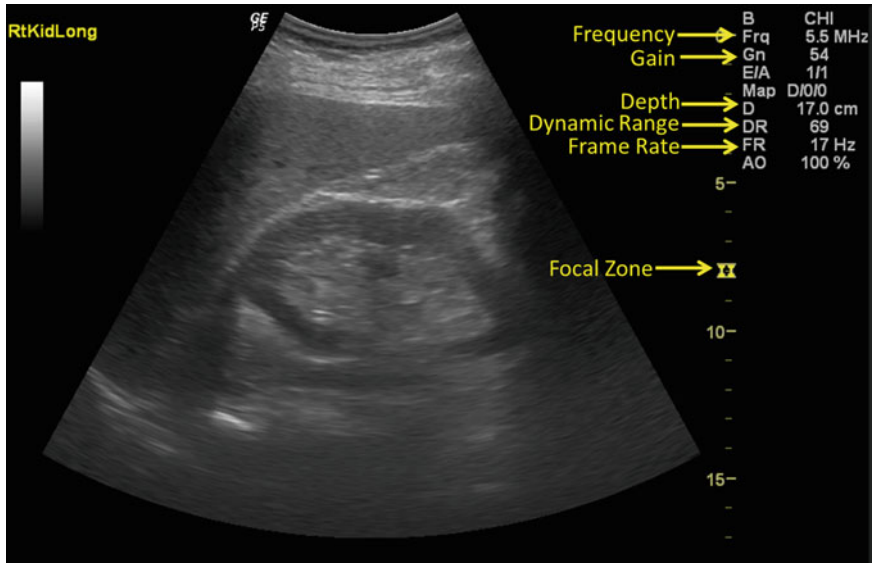

Fig. 4.5 Some of the machine settings are displayed on the monitor. Knowing where these settings are displayed and what they mean assists in optimizing image quality

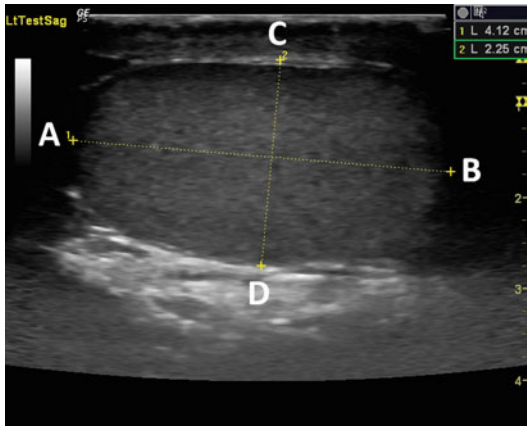

Fig. 4.6 In this sagittal image of the *left* testis, the superior pole of the testis (*A*) is to the *left* and the inferior pole of the testis (*B*) is to the *right*. The anterior aspect of testis (*C*) is at the *top* of the image and the posterior aspect (*D*) is at the *bottom*. Without the label "LtTestSag," there would be no way to distinguish the *right* from the *left* testis

User-Controlled Variables

One of the most commonly required adjustments during ultrasound scanning is an adjustment to the overall **gain**. The gain is a control which determines the degree to which the electrical signal produced by a returning sound wave when it strikes the transducer will be amplified for display. This needs to be differentiated from **acoustic output** which is defined as the power or amplitude of the afferent wave which is generated by the transducer (Fig. 4.7).

Both gain and acoustic power can be controlled by the operator; however, acoustic output is limited by the manufacturer in compliance with industrial safety standards [1]. In general, when the gain is increased the resultant image is brighter or more hyperechoic. When there is excessive overall gain, the image often appears bright and washed out. When there is insufficient overall gain, the image is often dark and it is difficult to distinguish between adjacent structures (Fig. 4.8).

It is generally more desirable to increase or decrease the gain rather than manipulate the acoustic output. However, there may be circumstances (e.g., a very thin or a very heavy patient) where increases or decreases in acoustic output would be appropriate. In every case, manipulations of gain or acoustic output are made to improve image quality. The principle of ALARA (as low as reasonably achievable) should always be honored when making these adjustments, imparting as little acoustic energy into the patient as will provide an adequate image.

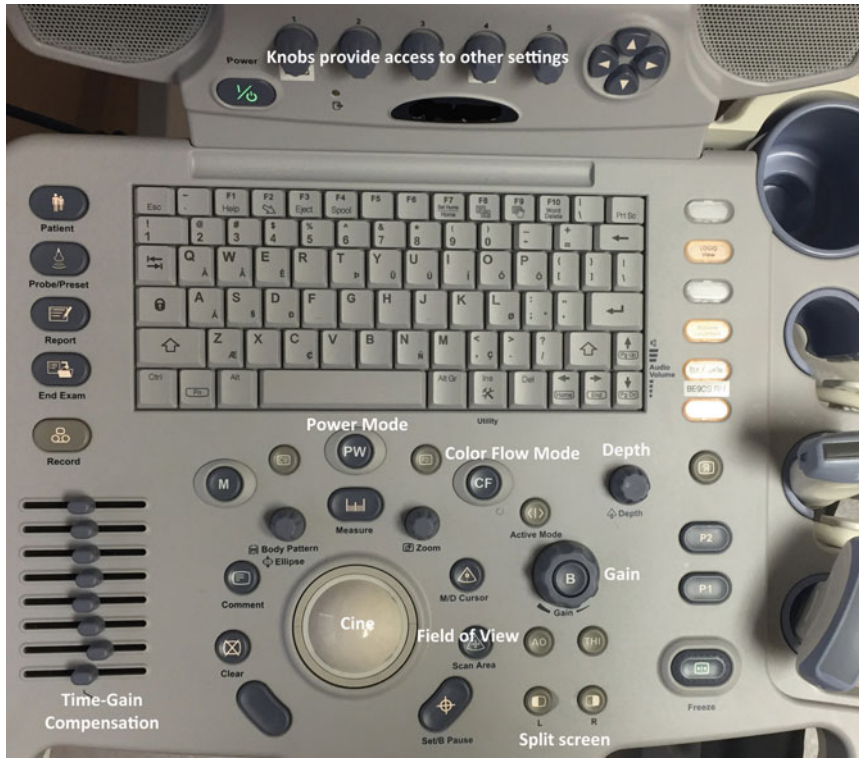

Fig. 4.7 A typical console interface showing common user-controlled variables

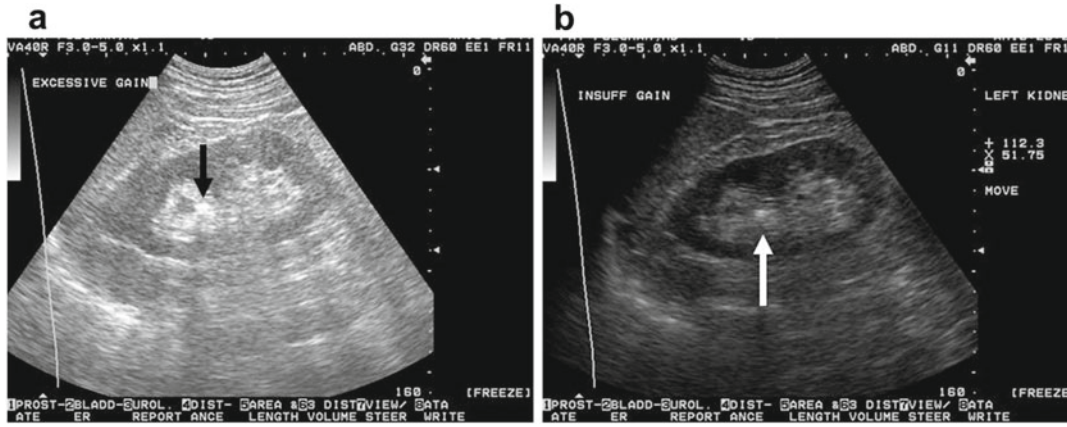

Fig. 4.8 (**a**) Excessive gain settings make it difficult to distinguish the stone (*black arrow*) in the upper pole of the kidney. (**b**) Insufficient gain makes it difficult to appreciate the distinction between the medial renal capsule (*white arrow*) and the perinephric fat

Time-gain compensation is another way to control the amplification of the signal from a returning sound wave. As opposed to overall gain, the amplification of these signals can be adjusted independently by region of the scanned field. That is, the electrical signal generated by sound waves returning from a specific region inside the patient can be individually amplified using TGC controls.

TGC controls usually involve a set of sliding switches which can increase or decrease the amplification of a signal at a particular depth in the scanned field. This is often displayed graphically on the monitor as a line or a curve which corresponds to the position of the physical slides on the console (Figs. 4.9 and 4.10).

TGC is most commonly used to amplify the signal strength from regions of the image where there is high attenuation of the sound waves or to decrease the amplification of the signal strength when there are areas where sound waves are unattenuated. One frequent use of TGC in urologic scanning is to compensate for the hyperechogenicity of tissue distal to a fluid-filled structure such as the bladder or a large renal cyst. It is often necessary to decrease the TGC for that region of the image distal to the fluid-filled structure so that structures in that location can be accurately represented (Fig. 4.11).

Frequency adjustment allows a multifrequency probe to be switched between two and three main frequency ranges during scanning. For instance, a curved array probe for abdominal scanning will often have the ability to adjust from 2–4 to 3.5–5 to 4–6 mHz. These ranges are specifically designed to take advantage of greater axial resolution with the higher frequencies and greater depth of penetration with lower frequencies. It is useful during scanning to change between frequencies to determine which frequency range provides the best overall image quality (Fig. 4.12).

The frequency determines the axial resolution of the scan. Axial resolution is the ability to identify as separate, two objects in the direction of the traveling sound wave. The higher the frequency, the better the axial resolution. The pulse that is sent from a transducer usually consists of two or three wavelengths and, as such, has a physical length. This pulse must fit completely between two objects in the axial plane in order to discriminate those objects as separate (Fig. 4.13).

Therefore, a pulse using a higher frequency wave has a shorter physical length than a pulse using a lower frequency wave. The shorter the pulse length, the better the axial resolution. A 5 mHz transducer produces a pulse length sufficient to produce an axial resolution of approximately 0.9 mm (see Box 4.1).

Dynamic Range

The backscattered echoes in a sonographic field return to the transducer in a large variety of amplitudes. The amplitude of the returning wave

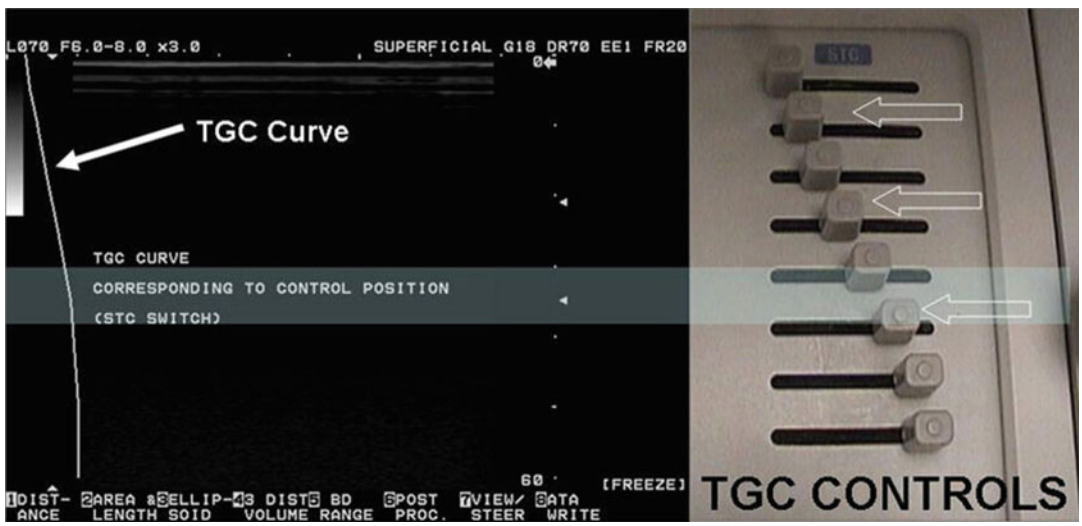

Fig. 4.9 TGC (time-gain compensation). The signal from a reflected (returning) sound wave can be amplified or diminished based on the depth of the reflector within the scanned field. The physical "sliders" (*open arrows*) correspond to the shape of the "TGC curve" (*white arrow*) on the monitor

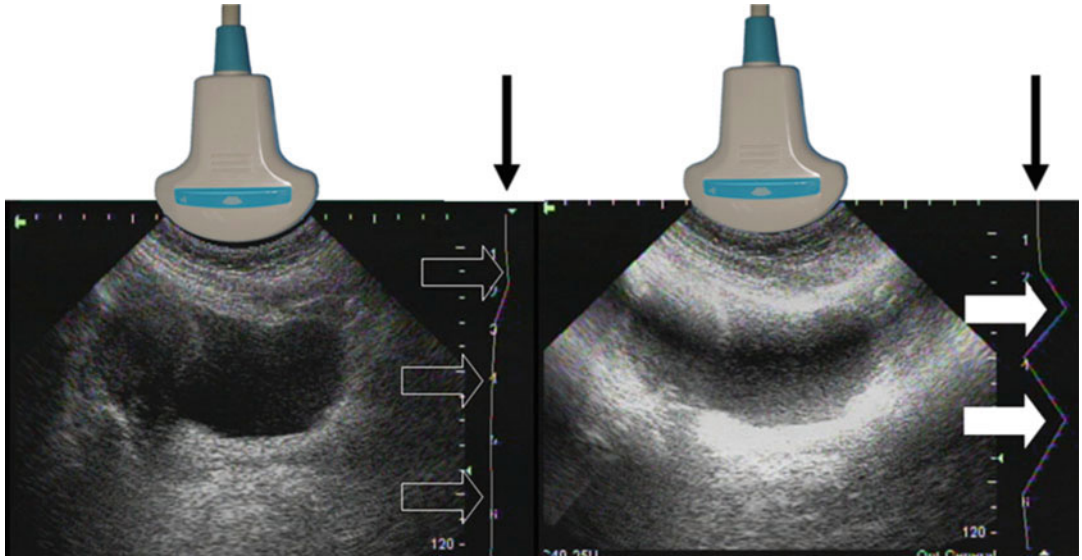

Fig. 4.10 Note how the shape of TGC curve (*black arrows* in the image on the *left*) corresponds to the pixel brightness at given regions of the scanned field. When the TGC curve is deviated to the right, (*large arrows* in the image on the *right*) the signals produced by sound waves returning from that corresponding region of the ultrasound field are amplified and displayed as "brighter" pixels. Acoustic output is unchanged by adjustments in time-gain compensation

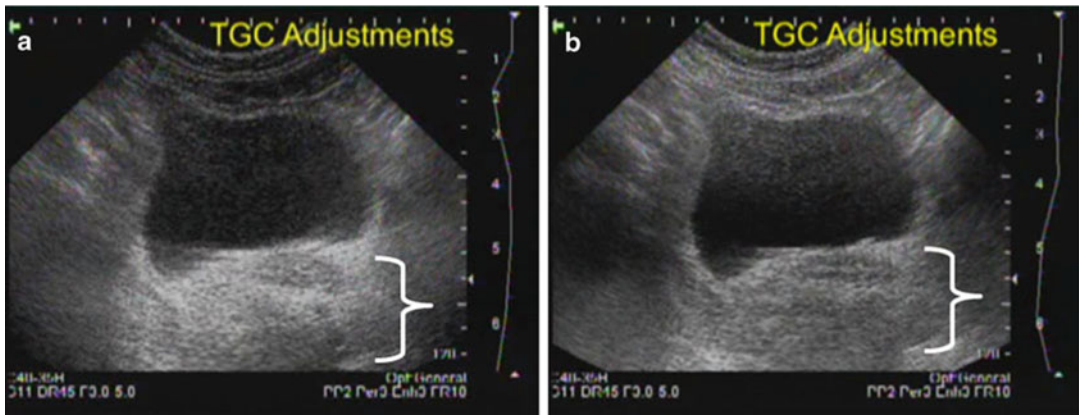

Fig. 4.11 (**a**) The fluid-filled bladder results in a region of decreased attenuation which produces a hyperechoic appearance of tissue posterior to the urinary bladder. (**b**) This artifact called "increased through transmission" can be corrected by decreasing the TGC curve in this region (*brackets*)

is assigned to a shade of gray for each pixel to be displayed on the monitor. The dynamic range is the spectrum of amplitudes to be divided among the normal shades of gray. In general, the larger the dynamic range, the greater the ability to distinguish between subtle differences in the amplitude of the returning echoes and thus between different tissue reflectors (Fig. 4.14).

Focal zone adjustments are made in an attempt to bring the narrowest portion of the ultrasound beam into the location, where maximal lateral resolution is desired. Lateral resolution is defined as the ability to discriminate as separate, two points which are equidistant from the transducer (Fig. 4.15).

Lateral resolution is a function of the width of the sound wave beam. The more focused the

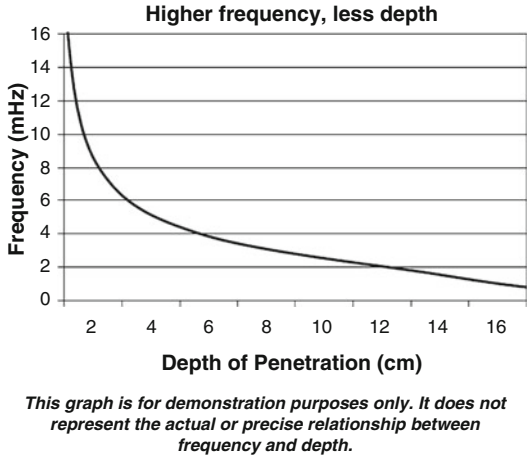

Fig. 4.12 The relative relationship between frequency and depth of penetration. Notice that to image a kidney 12 cm beneath the skin, a frequency of 2–4 mHz would be required to achieve an adequate depth of penetration

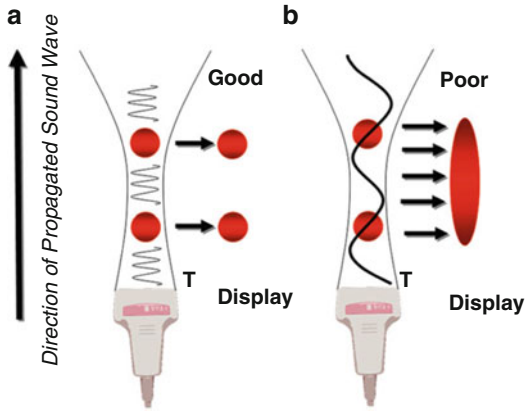

Fig. 4.13 (**a**) The shorter pulse length associated with this higher frequency wave is able to fit between the two objects in the axial plane providing good axial resolution. (**b**) The longer pulse length is unable to fit between the objects, thus depicting the two distinct objects as a single "blurred" echogenic focus

beam, the better the lateral resolution; that is, even closely spaced objects can be differentiated. Most transducers have a focal point producing the best lateral resolution and a focal range producing adequate lateral resolution (Fig. 4.16).

The width of the beam can be controlled by setting the location of focal zones. However, the thickness of the beam (known as the elevation or azimuth) is determined by the characteristics of the transducer crystals and design. In general, the focal zone should be placed at or just distal to the area that is of maximum clinical interest (Fig. 4.17).

It is possible to set multiple focal zones; however, this requires the software to sequentially interpret returning sound waves from specific locations of the scanning field (Fig. 4.18).

Multiple focal zones result in a slower frame refresh rate and may result in a display motion that is discontinuous. In most urologic scanning applications, a slower refresh rate is not a significant liability. Multiple focal zones are most useful in urologic scanning when fine anatomic detail throughout a solid structure is desirable (notably, in testicular scanning). When it is desirable to produce and interpret a twinkle artifact during Doppler scanning, it is useful to place the focus just at or distal to the object producing the twinkle artifact (Chap. 5, p. 63).

Depth/size function allows the user to select that portion of the scanned field which will be displayed on the monitor. By adjusting the depth of field, it is possible to allow the structure of interest to occupy the appropriate proportion of the visual field. By limiting the area of the scanned field from which returning echo signals will need to be interpreted and displayed, the amount of work performed interpreting that returning information will be diminished and frame refresh rates will be improved. The depth/size function has no effect on the axial resolution of the image. Appropriate depth of field adjustments can improve the ability to visually

Box 4.1: Axial Resolution

1 pulse $= 3\lambda$

$\nu = f\lambda$

For normal tissue velocity of 1540 m/s and a frequency of 5 mHz,

$\lambda = \nu / f$

$\lambda = 1540$ m/s/5 mHz

$\lambda = 0.31$ mm

$3\lambda = 0.93$ mm

1 pulse $= 0.93$ mm

Therefore, axial resolution at 5 mHz ≥ 0.93 mm.

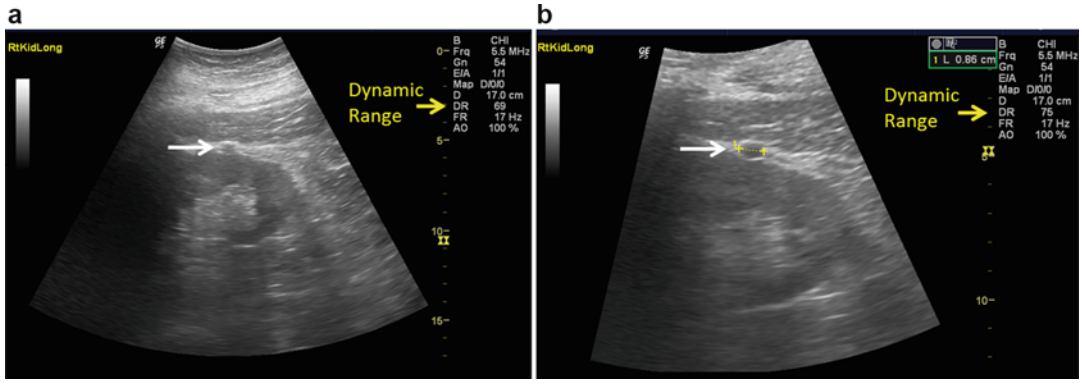

Fig. 4.14 Note the improved contrast and clarity of the cyst on lateral surface of the right kidney in image (**b**) where the dynamic range is 75 vs. image (**a**) where the dynamic range is 69

Fig. 4.15 Lateral resolution is optimized when beam width is narrow enough to fit between two objects equidistant from the transducer. In (**a**), the objects would be correctly displayed as separate objects. In (**b**), the beam width is too thick to fit between the objects, and they would be displayed as a single "blurred" focus

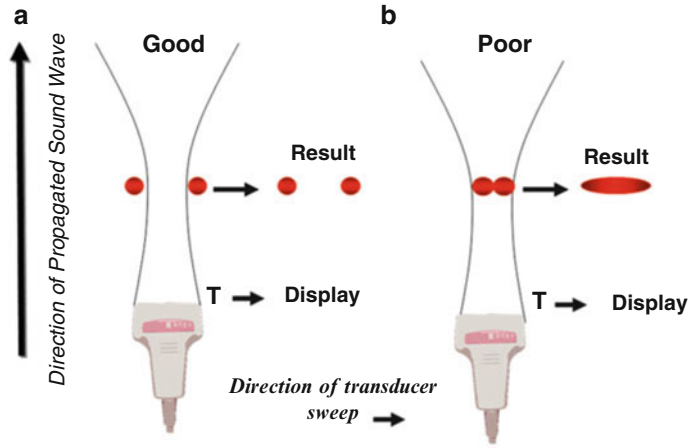

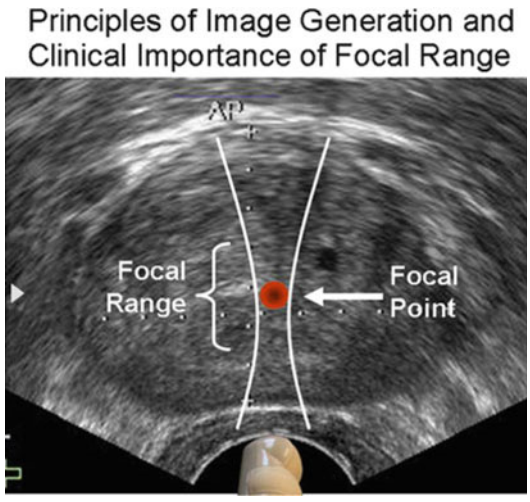

Fig. 4.16 The shape of the ultrasound beam determines its lateral resolution. The narrowest portion of the beam is its focal point or focal zone. The location of the narrowest point of the beam can be adjusted by manually setting foci

discriminate certain structures during urologic scanning and improves the overall performance of the equipment (Fig. 4.19).

Field of view is an adjustment to limit the width of an image so that only a portion of the available ultrasound information is interpreted. As with changes in depth of field, narrowing the field of view will reduce the amount of work necessary to interpret the returning echo data and improve frame refresh rate. It also limits the visual distraction of tissues which are irrelevant to a specific exam. Field of view can be virtually increased in some cases to visualize an entire structure (Fig. 4.20).

The **cine function** of most machines provides an opportunity to save a sequence of frames from the most recent scanning session and allows these frames to be played back one by one. This is a very useful feature when scanning organs such as the kidney which may be

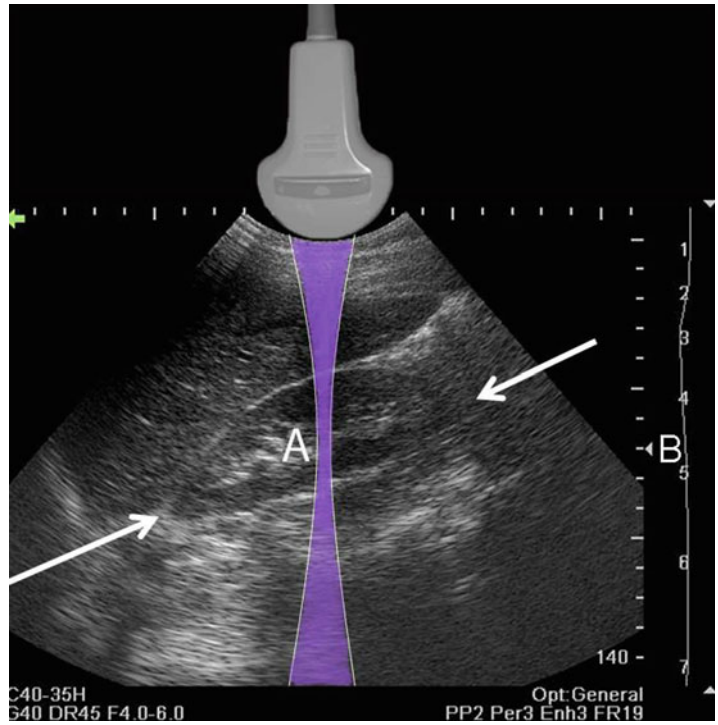

Fig. 4.17 The shape of the ultrasound beam is simulated in this drawing (*purple*). The focal zone (*A*) is located to produce the best lateral resolution of the medial renal cortex (*white arrows*). The location of the focal zone is designated by the *arrowhead* (*B*). The location of the focal zone can be adjusted by the operator

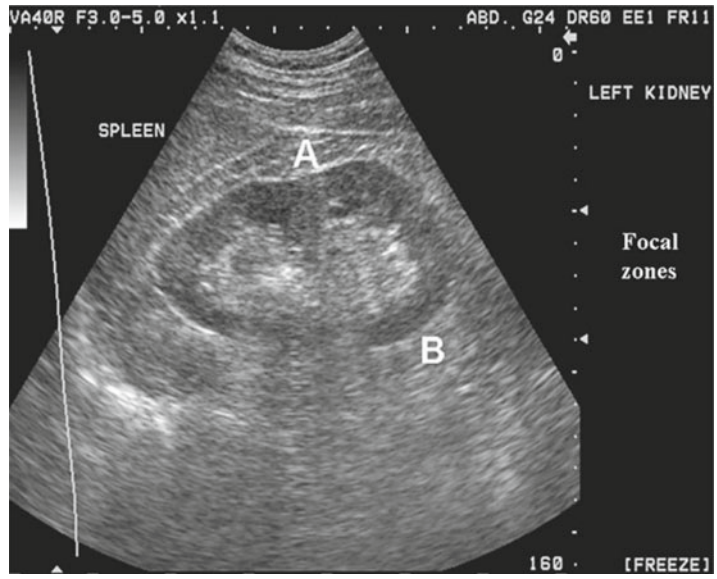

Fig. 4.18 In this sagittal renal ultrasound two focal zones (*arrowheads*) are set to correspond to the (*A*) lateral renal cortex and (*B*) the medial renal vortex

affected by respiratory motion. When a subtle finding is identified, the machine can be placed in the freeze mode and then the sequential images captured in the cine memory can be scanned backwards until the most appropriate image for measurement and documentation is identified. The cine function is invaluable in clinical office urology because it significantly decreases the time necessary to perform and document a complete examination.

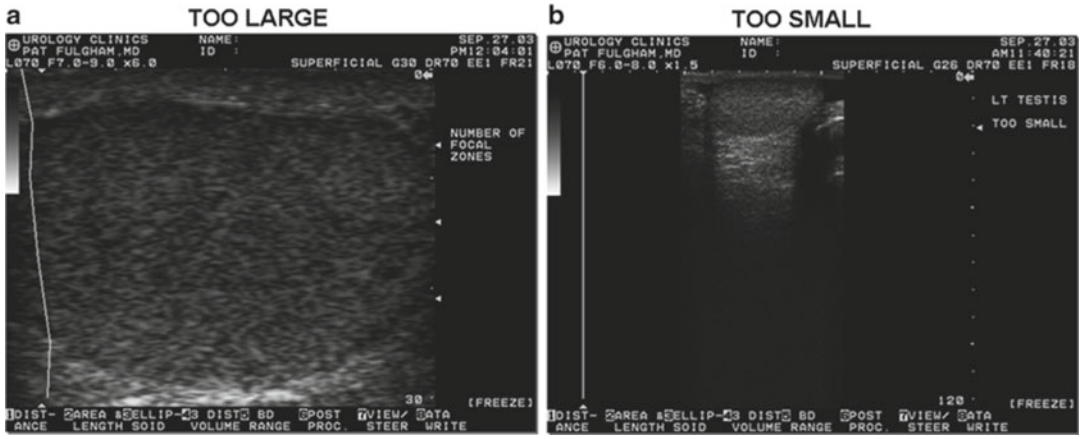

Fig. 4.19 (**a**) Depth of field has been set so that the testis fills the available display space but produces a grainy image. (**b**) Depth of field has been increased so that the testis occupies a very small portion of the available display. Tissue posterior to the testis which is not relevant occupies a large percentage of the display

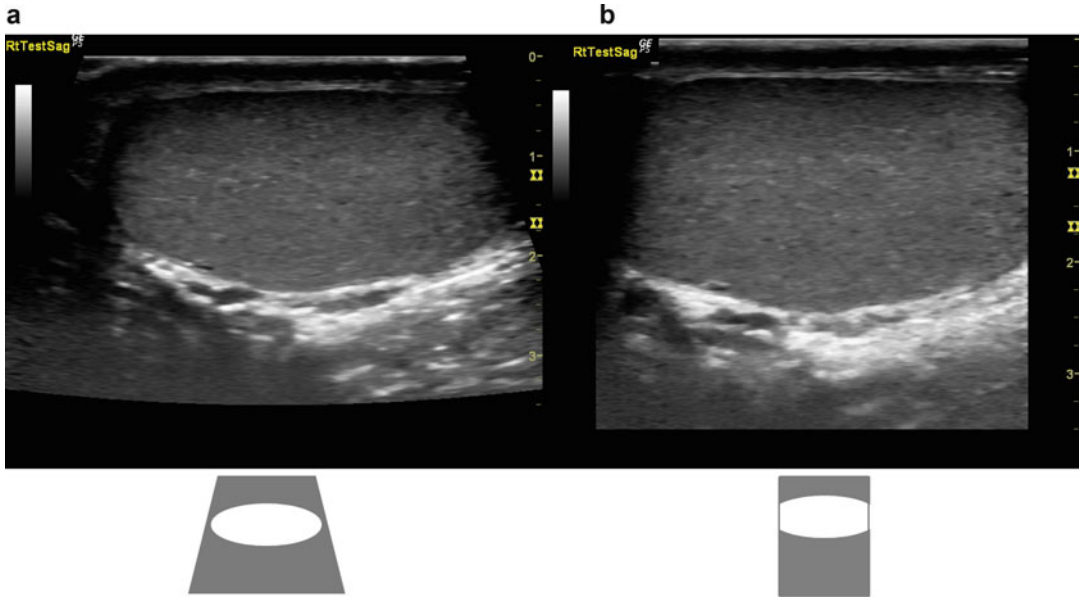

Fig. 4.20 A virtual convex field of view (**a**) includes the entire testis. The traditional view with the linear array probe (**b**) is not able to display the upper and lower poles of the testis simultaneously

Conclusion

Ultrasound equipment has preset applications for imaging of the prostate, kidneys, bladder, and testes. These presets allow scanning of most patients without the need to make individual adjustments. However, there are many clinical circumstances where the ability to make individual adjustments is invaluable to making a clinical diagnosis or clarifying an artifact. Most equipment allows users to store a large number of additional scanning protocols to account for commonly encountered challenges such as obese patients or pediatric patients.

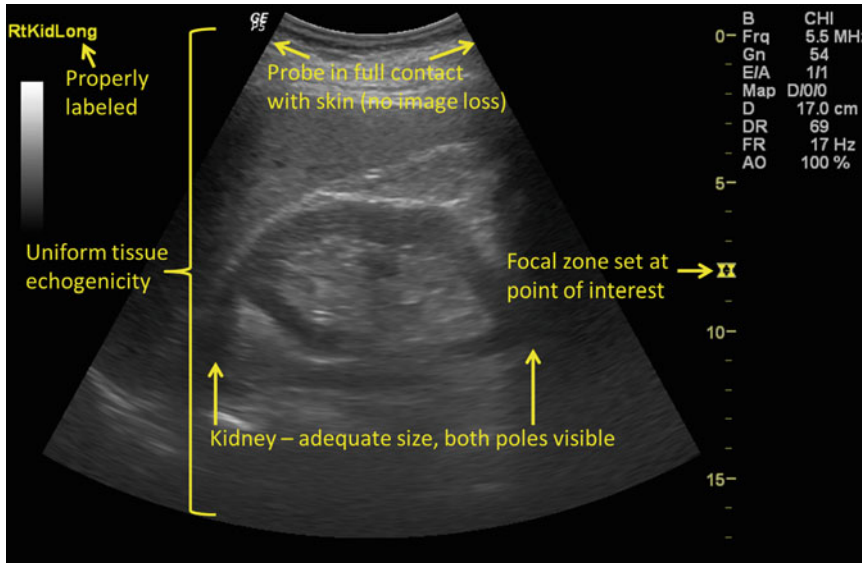

Fig. 4.21 This image displays the characteristics of a good-quality image by virtue of appropriate settings of user-controlled variables as well as proper labeling

Summary

A good-quality image is recognized by certain generally agreed upon characteristics (Fig. 4.21).

Ultrasound is ultimately an exercise in image recognition. Clinicians tend to see what they know and are familiar with. Great care must be taken to ensure optimal image quality so that the unexpected and unfamiliar may also be recognized and correctly diagnosed.

Reference

1. Guidance for industry and FDA staff information for manufacturers seeking marketing clearance of diagnostic ultrasound systems and transducers. 2008. http://www.fda.gov/downloads/MedicalDevices/DeviceRegulationandGuidance/GuidanceDocuments/UCM070911.pdf. Accessed 9 Sept 2008.

Renal Ultrasound

5

Daniel B. Rukstalis, Jennifer Simmons, and Pat F. Fulgham

Introduction

The development of mobile and low-cost ultrasound equipment with the ability to incorporate newer modalities such as improved Doppler vascular analysis and elastography has expanded the diagnostic value of ultrasound in the management of renal disorders. Both safety and economic advantages of ultrasound have been well established yet it appears that ultrasound remains underutilized [1]. In particular, the clinical presentation of renal disorders such as urolithiasis, hematuria, obstruction, and a renal mass represent opportunities for the application of ultrasound. Additionally, ultrasound guidance is likely valuable for renal interventional procedures such as biopsy, ablation, extirpative procedures, and endourologic techniques. This chapter is designed to expand on the advent of point-of-service ultrasound, performed by the urologist during a direct patient encounter, in order to enhance the diagnostic and therapeutic pathway.

Renal ultrasound has been found to be a highly sensitive and specific test for hydronephrosis in both the adult and pediatric population, which can streamline the evaluation of patients with emergent complaints of flank pain, fever, or acute renal injury [2]. Additionally, ultrasound is valuable in the initial evaluation of hematuria and stone disease. Furthermore, asynchronous patient care, defined as an initial clinical encounter separated in time and space from the imaging examination, requires that the physician have access to and remembers to review the imaging study at a second visit. Integration of ultrasound, performed by the urologist, into the initial physical examination likely improves the efficiency of patient care while avoiding the pitfalls of segregating the care pathway into metachronous episodes. This concept has been well illustrated by the application of point-of-service renal ultrasound in the initial emergency room evaluation of patients with colic [3].

This chapter details the applications and techniques of renal ultrasound necessary to integrate this modality into the daily practice of urology. The reader will be able to understand the technical process of generating an ultrasound image of the renal units in response to specific clinical question. In fact, it is the juxtaposition of the physician's

D.B. Rukstalis, M.D. (✉)
Department of Urology, Wake Forest Baptist Medical Center, Medical Center Boulevard, Winston-Salem, NC 27157, USA
e-mail: drukstal@wakehealth.edu

J. Simmons, M.D.
Department of Urology, Geisinger Health System, 100 N Academy Ave, Danville, PA 17822, USA
e-mail: Jsimmons1@Geisinger.edu

P.F. Fulgham, M.D.
Department of Urology, Texas Health Presbyterian Hospital of Dallas, 8230 Walnut Hill Lane Suite 700, Dallas, TX 75231, USA
e-mail: pfulgham@airmail.net

P.F. Fulgham, B.R. Gilbert (eds.), *Practical Urological Ultrasound*, Current Clinical Urology,
DOI 10.1007/978-3-319-43868-9_5

ability to elucidate the clinical concern, develop a differential diagnosis, and determine the potential etiology with ultrasound that makes this technology so valuable to the practicing urologist and each patient.

Point-of-Service Ultrasound

The current structure of medical practice in the United States is codified into established specialty units that provide patient care as individually measurable units. Diagnostic imaging has been cohorted into centers that provide expertise and resources for all forms of imaging. Patient access to these centers for diagnostic testing often necessitates multiple encounters and subsequent complex communication between specialty units. Point-of-service delivery of diagnostic testing and imaging can reduce the inefficiency and cost of these multiple encounters while enhancing the timely diagnosis for patient health concerns.

Medical imaging with ultrasound represents a safe and low-cost approach to the initial evaluation and subsequent follow-up of a variety of urologic conditions [1]. The availability of ultrasound performed by a urologist represents a likely advance for a value-based health care system. The point-of-service ultrasound performed while a patient is visiting with their urologist can often improve the diagnostic accuracy of that encounter. The urologist is then optimally equipped to request additional advanced imaging modalities, if needed, following the history, physical exam, and initial ultrasound. This chapter is based on the premise that renal ultrasound will be performed by practitioners as an integral component of the direct patient encounter.

Indications

The indications for renal ultrasound include [4]:

1. Flank and/or back pain with consideration for urolithiasis and abscess
2. Acute renal injury/failure with concern for obstruction
3. Hematuria
4. Abdominal trauma
5. Evaluation of asymptomatic microscopic hematuria in patients who are not candidates or refuse CT and MRI
6. Active surveillance for renal mass (solid or cystic)
7. Surveillance for known renal and ureteral stones
8. Pretransplant and posttransplant renal evaluation
9. Further evaluation of abnormal findings of the kidney on other imaging studies
10. Follow-up after initial treatment of a low-risk renal malignancy
11. Pediatric indications include evaluation of congenital anomalies, prenatal hydronephrosis, evaluation for vesicoureteral reflux
12. Planning and guidance for interventional procedures including percutaneous nephrostomy tube placement, renal biopsy, renal cyst aspiration/sclerosis, and renal mass ablation
13. Intraoperative renal parenchymal and vascular imaging for ablation or resection of tissue
14. Evaluation and intervention in pregnancy

Equipment

Adequately performing and documenting a renal ultrasound requires familiarity with the basic features of the ultrasound machine. Renal imaging in both adults and children requires a curved array transducer as seen in Fig. 5.1. A smaller width transducer may offer superior contact with the body surface in very thin patients and can facilitate scanning between the ribs. Renal ultrasound scanning is performed at frequencies between 2.5 and 6 MHz. In most adults and many children, the kidney is located far enough beneath the skin surface that lower ultrasound frequencies can give superior penetration and allow visualization of all the parenchyma. The image quality will be reduced as lower frequencies result in a decrease in linear (axial) resolution. A higher frequency can be used for children, thin patients and intraoperative applications.

Most commonly, one or two focal zones are used for renal imaging. The focal zone should correspond to the area of interest in the field of view. The focal zone represents the narrowest

Fig. 5.1 Curved array transducers are used for the performance of renal ultrasound. Seen in this image are two different widths of curved array transducers, large footprint (*left*) and small footprint (*right*)

part of the ultrasound beam and gives the best lateral resolution at the region of interest. Adding focal zones reduces the refresh rate of the image, which can slow down the performance of the ultrasound examination. Several additional ultrasound features are often helpful during a renal examination. These include Doppler mode with calculation of resistive index, cine loop (capture of live images), and measurement calipers.

Patient Preparation

Patient preparation is helpful to facilitate an efficient exam. Fasting decreases intestinal contents and can allow for a more anterior window for imaging the kidney. This can avoid the thicker flank musculature and take advantage of the liver as a window to the right kidney. In the urology office, however, renal imaging is often performed on short notice to investigate an acute problem during the appointment. Thus, it is usually impractical to have the patient fast several hours prior to the exam. For planned examinations, such as upper tract imaging for a hematuria workup or screening for postoperative hydronephrosis after endoscopic stone extraction, the patient should fast for 6 h prior to the examination.

The exam room should have the capability to dim room lights and reduce glare from natural lights. The ultrasound image detail on the screen is dramatically improved by reducing ambient light.

Patient positioning will depend upon the indications for the exam. A focused unilateral follow-up exam such as for a post-ESWL hematoma or for renal trauma can be done efficiently with the patient in supine position. However, larger patients with more truncal obesity are likely best imaged in the lateral position since this allows for both coronal and sagittal (lateral and posterior) imaging of the particular renal unit. A bilateral examination will likely then involve moving the patient from supine or right lateral to left lateral position to image the left kidney. Ultrasound for urolithiasis will involve imaging from the high posterior flank coursing inferiorly to the lower anterior abdominal wall. Ultimately evaluation of the ureterovesical junction (UVJ) will include attempts to locate a distal stone and document ureteral jets.

The ultrasound machine should be positioned so that the screen is easily visible to the operator and that the keyboard and patient can be reached comfortably. Extreme care should be taken to avoid falls caused by rolling patients from side to side on a standard examination table. Typical exam tables are narrow and have no side rails. The physician's attention will likely be focused on the ultrasound monitor so that ancillary staff should observe unsteady patients.

Anatomic Considerations for Renal Imaging

Ultrasound evaluation of each renal unit is influenced by the orientation of the kidney in the retroperitoneum. Figures 5.2 and 5.3 demonstrate the anatomic position of the right and left renal unit. The lower pole of the right kidney is 15° lateral to the upper pole in the coronal plane. The renal hilum is rotated approximately 30° posterior to the horizontal coronal plane when examined transversely. The psoas muscle displaces each kidney such that the lower pole is more anterior

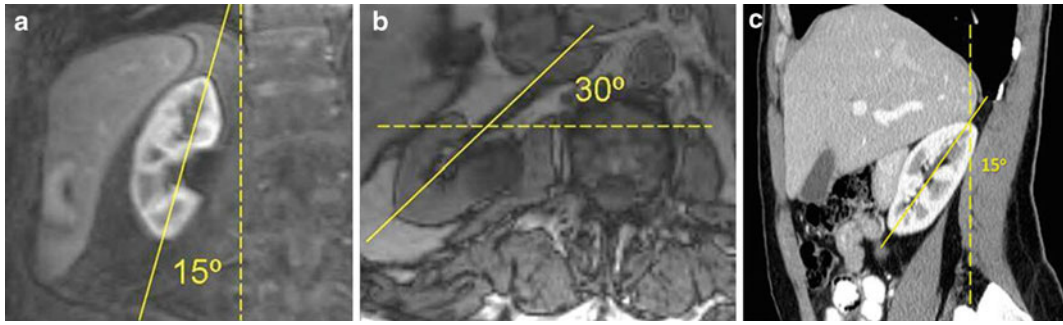

Fig. 5.2 (**a**) Coronal MRI showing that the lower pole is 15° lateral to the vertical plane. (**b**) Transverse MRI at the level of the renal hila showing that the axis of the kidney is 30° posterior to the true coronal plane. (**c**) MRI demonstrating that the lower pole of the kidney is anterior to the upper pole

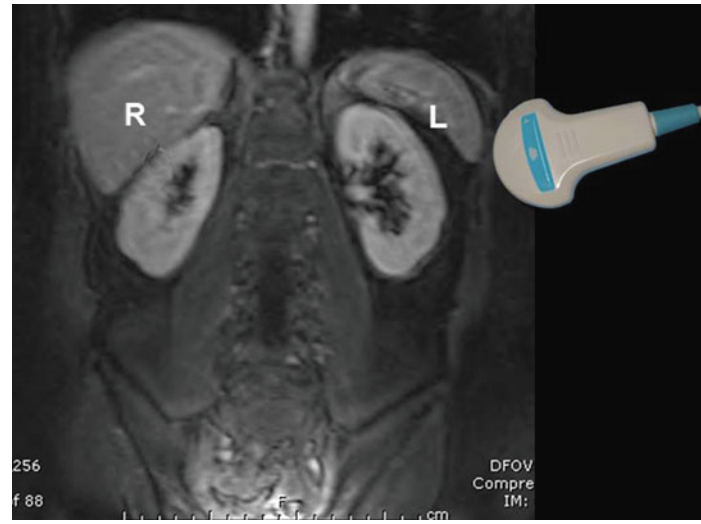

Fig. 5.3 Image of an MRI demonstrating the anatomical position of the kidney in the abdomen and proper position and angle of the ultrasound probe for imaging the left kidney. This probe position would generate a true midsagittal ultrasound image of the left kidney

than the upper pole. For longitudinal views, the orientation of the ultrasound probe should match the long axis of the kidney as depicted in Fig. 5.3. This will allow identification of the true midsagittal plane of the kidney.

Imaging the Right Kidney

Technique

Ultrasound imaging of the right renal unit can be performed in either the supine or flank position. In the flank position, the patient's right arm should be positioned over their head with a possible pillow under the left flank to open the space between the ribs and the iliac crest. The transducer is placed in the midclavicular line at the level of the costal margin. Bowel gas in the transverse colon will often be encountered initially. The flank position can allow lateral imaging (through a coronal plane) or through a posterior window that can avoid the gas. The transducer is swept laterally using the liver as an acoustic window to image the upper portion of the kidney. Figure 5.4 is an example of a right kidney viewed through a liver window. The homogeneous composition of the liver offers excellent transmission of the sound waves with minimal distortion. The echogenicity of the liver also offers a comparison for the appearance of the renal parenchyma. The kidney is expected to be isoechoic or hypoechoic to the liver. The finding of renal parenchyma that is hyperechoic to the liver suggests the presence of renal disease.

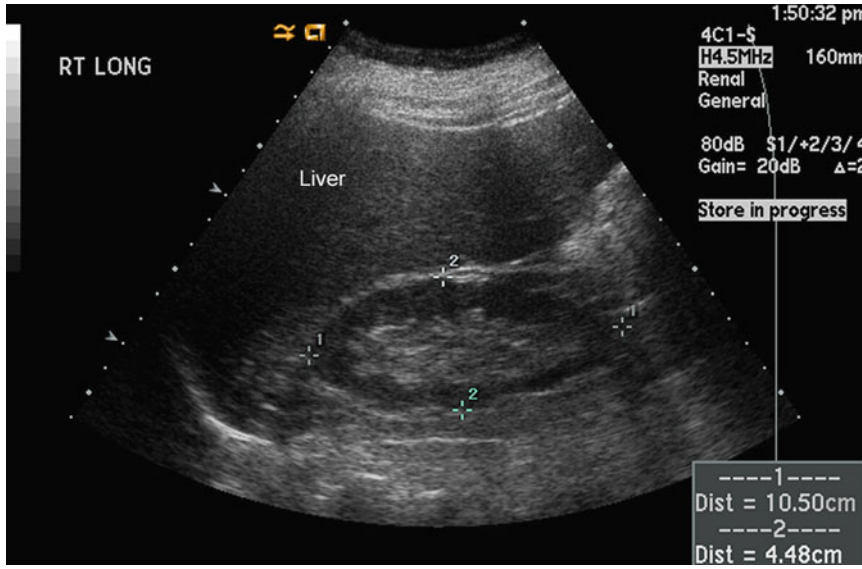

Fig. 5.4 Right kidney viewed using the liver as an acoustic window

The transducer is moved over the kidney in both transverse and longitudinal (both coronal and sagittal) planes from any window provided by the position of the patient. It is helpful to locate the true sagittal section of the kidney. This serves as an anatomic landmark from which the remainder of the scan can be performed. The midsagittal plane of the kidney is characterized by the longest measurable sagittal axis of the kidney. It is important in a routine renal ultrasound examination to document the parenchymal length in this plane. A normal adult renal length is between 9 and 12 cm.

Once the midsagittal plane is located, the kidney should be scanned both anteriorly and posteriorly until the entire renal parenchyma has been evaluated. The upper pole and the midportion of the kidney can usually be viewed through the liver window. The lower pole frequently has to be imaged directly through a more lateral or posterior location. It is also often necessary to have the patient take and hold a deep breath while imaging the full aspect of the renal parenchyma. Figure 5.5 is an example of the lower pole of the left kidney viewed directly from the flank rather than through the spleen as an acoustic window. This is analogous to imaging the right kidney directly through the flank while the patient holds a deep breath.

Once the longitudinal imaging has been completed, the transducer may be rotated to achieve a transverse view of the kidney. The mid-transverse plane can be identified by the characteristic horseshoe-shaped renal parenchyma, which is discontinuous on the medial aspect at the level of the renal sinus and vessels. It is often possible to visualize the renal artery and vein through this window. Although the renal artery is sometimes more difficult to identify than the vein, both vessels may be distinguished with the color flow Doppler analysis. It is in the transverse plane that measurements of parenchymal thickness, as well as cortical thickness, can be obtained and documented. The color Doppler function with spectral display can be used to calculate the resistive index. This measurement may be useful in characterizing renal vascular disease, renal parenchymal disease, and obstruction [5, 6].

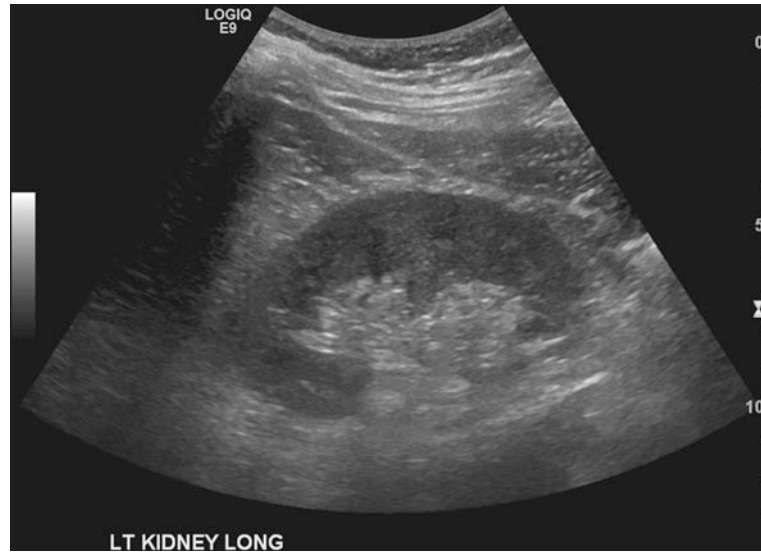

Fig. 5.5 Left kidney viewed directly via lateral flank approach (true midsagittal plane)

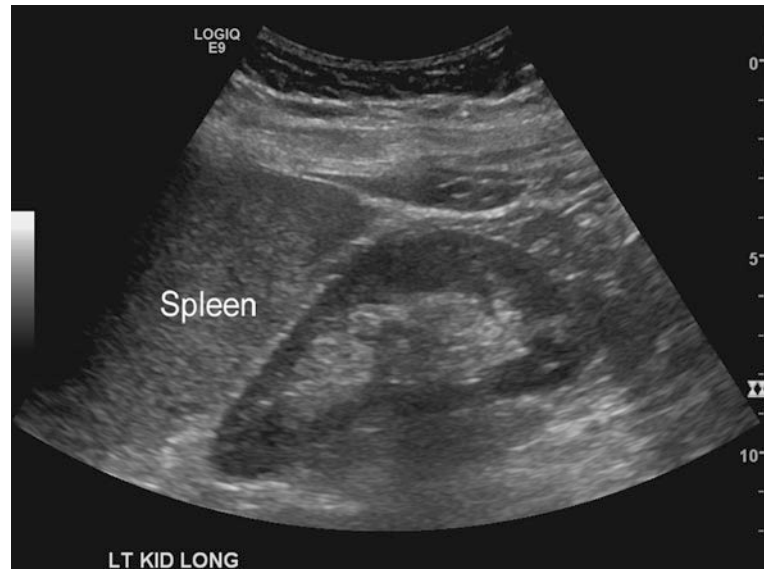

Fig. 5.6 The spleen is seen on this image cephalad to the *left* kidney

Imaging the Left Kidney

Technique

Ultrasound of the left renal unit is typically performed with the patient in a lateral position with the left arm raised overhead to open the intercostal spaces for better imaging. The transducer is placed at the midaxillary or posterior axillary line. Bowel contents commonly prevent an anterior approach to viewing the left kidney. The left kidney image is often less crisp due to attenuation and scattering from muscle in the flank and back. The spleen is frequently seen anterior and superior to the left kidney but is not usually well positioned to use as an acoustic window. This is illustrated in Figs. 5.5 and 5.6. Similar to the right renal ultrasound examination, having the patient take and hold a deep breath often brings both the spleen and the upper aspects of the kidney into view.

The true midsagittal plane of the left kidney is then located. This will be the plane of the longest sagittal parenchymal length. The renal capsule will appear discontinuous at the mid kidney medial at the site of the renal hilum. In the coronal view, cortical tissue is seen as a continuous ring around the hyperechoic pelvic sinus fat except at the renal hilum. Once the anterior and posterior surfaces of the kidney have been fully imaged in the sagittal plane, the transducer is rotated to obtain a transverse image. It is always important to remember standard radiologic convention establishing the medial aspect of the kidney on the left side of the ultrasound monitor. This means that the renal vessels should point towards the left side of the monitor during transverse imaging.

The upper and lower portions of the left kidney are imaged completely by moving the probe cephalad and caudad while asking the patient to hold a deep breath. A deep inspiration and expiration will move the kidney several centimeters. The mobility of the kidney can be assessed for possible evidence of a mass, inflammation, or anatomic abnormalities. Once the kidney has been completely evaluated in all planes, attention is then turned to identifying and documenting normal and abnormal findings in a manner similar to the right renal exam.

The goal of the ultrasound exam is to view the entire renal parenchyma and the entire capsular surface. When imaging in the transverse plane, the entire length of the kidney must be viewed. Through the use of directed patient breathing, a scan can be performed from the adrenal superior to the kidney down to below the lower pole. The cross-sectional diameter of the renal capsule becomes smaller as the lower pole is reached. This then disappears as the imaging beam extends beyond the lower pole. An edging artifact is often encountered at the final rounded edge of each renal pole. This artifact can be eradicated by moving the transducer slightly to complete the imaging of the extent of the renal parenchyma.

A good analogy is the way one would view the renal axial imaging on a CT scan. Images can scroll through the kidney from just cephalad to the upper pole to just below the kidney to avoid missing any exophytic lesions. When imaging in the longitudinal plane, the probe can be fanned both anteriorly and posteriorly (both coronal and sagittal planes) to completely evaluate the renal unit from the anterior surface to the posterior capsule. Figure 5.7 demonstrates an MRI, which depicts a posterior exophytic mass that could be missed with incomplete imaging of the full capsular surface of the kidney.

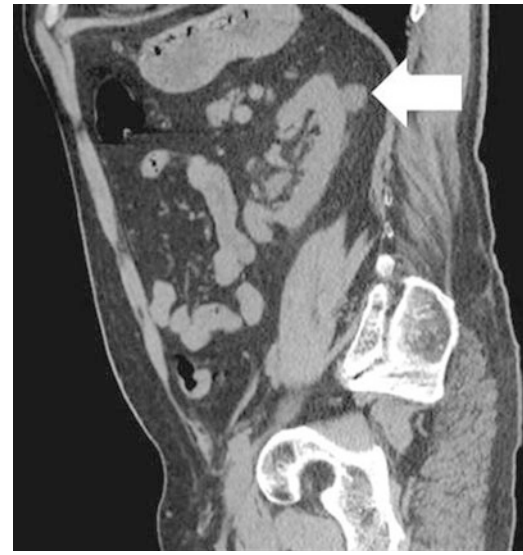

Fig. 5.7 This MRI demonstrates a small exophytic renal cyst (*arrow*) that could easily be missed on ultrasound if the full anterior and lateral surface of the left kidney is not evaluated

Normal Findings

The renal contours should be smooth and of an ovoid reniform shape. Any deviation from a smooth uniform contour should be noted and a representative image saved. All surfaces of the kidney should be scanned from the top to the bottom and from anterior to posterior.

The kidney measurements should be recorded in both transverse and longitudinal planes. The transverse view of the mid kidney should be measured and a representative image saved. These measurements can include parenchymal thickness, cortical thickness, and possibly renal width from lateral capsule to medial extent of renal sinus. An image of the midline longitudinal length should be measured,

including anterior to posterior height as well as length, and saved. Care should be taken to ensure that an accurate midline longitudinal view of the kidney is obtained for measurement of the parenchymal length. It is quite easy to obtain an oblique image that appears to represent the full length of the kidney anatomically with a resultant shorter measured length. Figure 5.8 demonstrates that there may be a substantial difference in the measurement of the long axis of the kidney if the renal unit is measured in a parasagittal plane versus a true midsagittal plane. The true midsagittal plane is characterized by

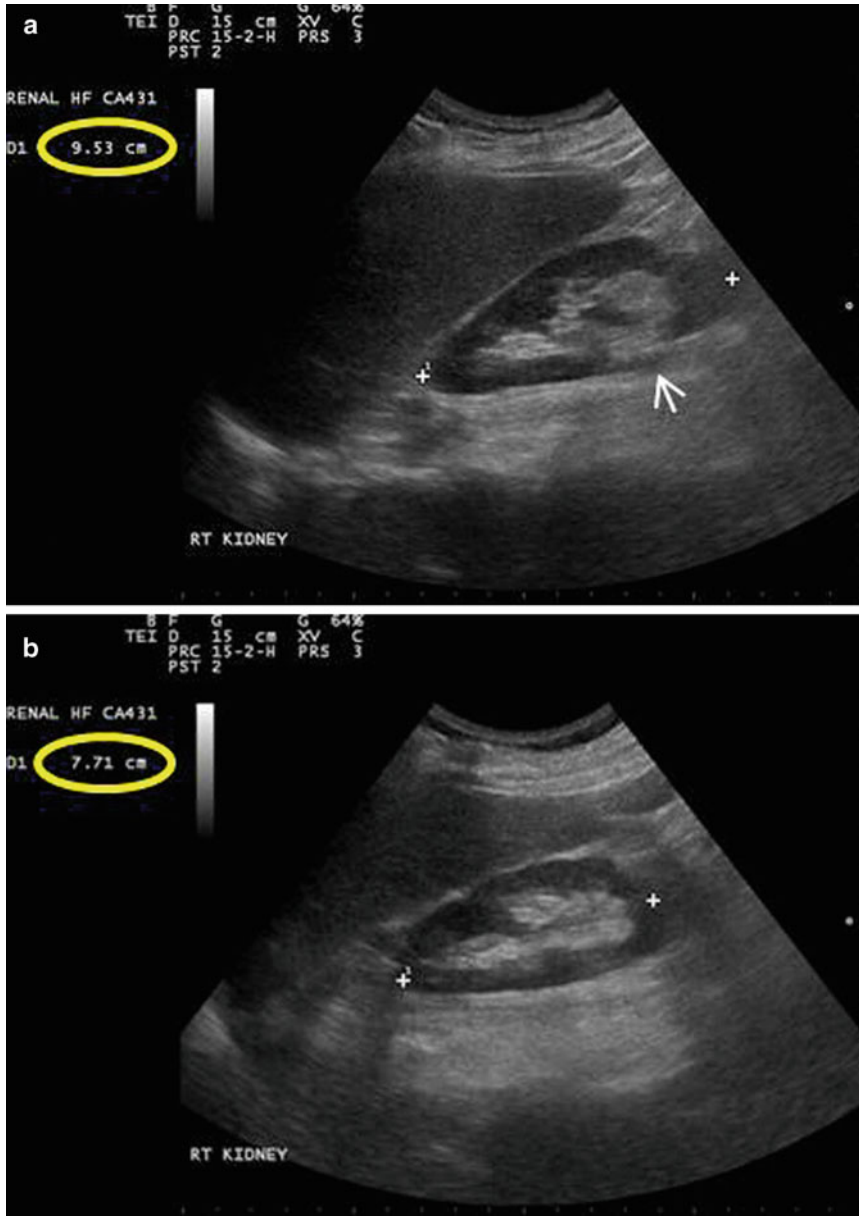

Fig. 5.8 An accurate measurement of renal length depends upon obtaining a truly midline renal image in the sagittal plane. In ultrasound image (**a**) the right kidney is in the true midline as noted by the medial discontinuity of the renal parenchyma. This represents the hiatus through which the renal vessels and collecting system enter and exit (*arrow*). The kidney on this view measures 9.53 cm. Ultrasound image (**b**) demonstrates the measurement of the same right kidney when it is not in the true midline. The kidney measures 7.71 cm

a medial discontinuity of the renal parenchyma representing the hiatus through which the renal vessels and collecting system enter and exit.

Normal adult kidneys measure 9–12 cm longitudinally, 5–7 cm in transverse width and 3 cm in anteroposterior dimension [7]. Han and coworkers also provided information regarding normal renal measurements in pediatric patients [8]. Although there is a normal variation in the anatomy of each renal unit in an individual patient, a difference in length of more than 1.5 cm is considered abnormal [9].

Renal cortical thickness should be uniform throughout the kidney. Any bulges or indentations in the cortex should be noted on the report and captured as an image. Parenchymal and cortical thickness should be noted. The cortical thickness is measured from renal capsule to the base of the triangular medullary pyramids. The parenchymal thickness is measured from the renal capsule to the edge of the renal sinus. In adults, the medullary pyramids are often indistinct on ultrasound imaging making the measurement of cortical thickness inaccurate. Therefore, parenchymal thickness is often easier to measure. A renal parenchymal thickness under 1 cm is considered abnormal [9]. Figure 5.9 demonstrates cortical versus parenchymal thickness measurements.

The echotexture of the kidney should be described. The normal adult renal cortex should appear hypoechoic or isoechoic relative to the normal liver or spleen. The normal cortex should appear homogeneous in echogenicity. The medullary pyramids should be hypoechoic to the renal cortex. This distinction is much more pronounced in children compared to adults.

The renal sinus is hyperechoic compared to the renal parenchyma in normal renal units. The renal sinus is highly echogenic due to its many different reflectors including blood vessels, sinus fat, and the collecting system.

Adjacent Structures

Renal ultrasound by urologists is usually performed for a specific clinical indication and is focused on the kidneys. Adjacent organs will be in the field of view and any remarkable findings of those organs should be noted.

The adrenal gland in adults is not normally visualized on ultrasound. However, specific attention to the tissue anterior and medial to the

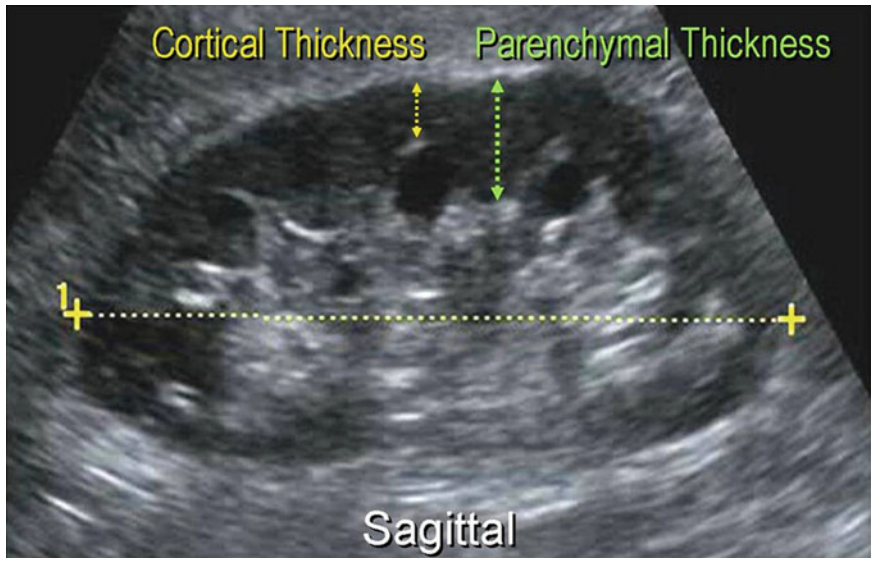

Fig. 5.9 Image demonstrating the difference between the measurement of the cortical thickness and parenchymal thickness

upper pole of each kidney can reveal the normal adrenal gland and represents a potentially useful tool for examining adrenal lesions [10]. A prominent adrenal gland seen on ultrasound should be considered potentially abnormal and further imaging with CT or MRI can be considered.

It is not the intention of a focused urologic examination to provide complete imaging of the liver, gallbladder, spleen, or aorta. However, any abnormalities noted in these organs during the renal exam should be documented and further testing pursued as appropriate. Often the urologist has an ongoing relationship with the patient and may be able to provide valuable information regarding ancillary findings to the patient.

Ultrasound Report

The importance of a detailed and accurate ultrasound report cannot be overstated. The generation of the ultrasound documentation is a critical component of all renal ultrasound examinations and is routinely audited by other entities for clinical information, appropriateness of the examination, and reimbursement. The report has four components: indications, equipment, findings, and impression.

Indications

The clinical history and reason for performing the study should be documented in the indication section.

Equipment

Each ultrasound report should identify the make and model of the machine that is used for the exam. Additionally, the type of probe, frequency, and any pertinent modifications of US power, Doppler and elastography (if applicable) should be mentioned.

Findings

The findings section should include a succinct description of the normal findings as well as any notable abnormalities. Specific aspects of the report can also be reviewed in the AIUM report on urologic ultrasound guidelines [4]. Formal ultrasound terminology should be used with the findings described without an associated diagnosis. The diagnosis should be reserved for the impression section of the report. For example, one should report, "a 9 mm brightly hyperechoic focus in the lower pole of the right kidney with strong posterior acoustic shadowing" in the findings and report "consistent with the appearance of a stone" in the impression.

Impression

The impression portion of the report should include an interpretation of the sonographic findings based on clinical history and associated physical findings. When the urologist is the ordering, performing, and interpreting physician, the impression may also include a plan for subsequent imaging or intervention.

Image Documentation

Representative images of the exam should be captured and saved in the permanent patient record. These can be digital or hard copy images. It may also be possible to capture the actual cine loop of an examination. This approach has been found to improve the subsequent review of the exam by other providers [11]. Minimum image documentation will vary based on the clinical indication for the study but for a full examination of both renal units captured images should include:

1. Right Kidney
   (a) Longitudinal view with length measure ment
   (b) Transverse view of the upper pole
   (c) Transverse view of the lower pole
   (d) Transverse view of the renal pelvis
   (e) View showing the liver and right kidney on the same image, if possible
2. Left Kidney
   (a) Longitudinal view including length measurement

(b) Transverse view of the upper pole
(c) Transverse view of the lower pole
(d) Transverse view of the renal pelvis
(e) View showing the spleen and the left kidney on the same image, if possible

3. Appropriate views of abnormalities, with measurements if indicated

Doppler

Color and power Doppler are useful tools in renal imaging. The ability to confirm normal blood flow in the kidney can be valuable in the follow-up of trauma, partial nephrectomy, and obstruction. The ability to characterize hypoechogenic structures in the kidney relative to blood flow can influence the diagnosis and future intervention. The application of Doppler mode can quickly distinguish between vessels and hydronephrosis (Fig. 5.10). The use of Doppler to demonstrate renal artery stenosis is generally beyond the scope of office urologic practice.

Resistive Index

Resistive index is a calculated metric that represents the degree of downstream resistance to blood flow measured at a specific point in a blood vessel. In the kidney, it is calculated by quantifying the velocity of blood flow from the Doppler waveform of intrarenal arteries. The arcuate arteries running along the junction of the cortex and medulla or the interlobar arteries running between the medullary pyramids are targeted. Color or power Doppler can be used to identify a suitable vessel. The Doppler angle indicator is aligned with the long axis of the blood vessel being interrogated and the gate set at no greater than 75% of the inner diameter of the vessel. The angle of insonation (Ø) should always be ≤60°. The resultant waveform is analyzed (Fig. 5.11). The peak diastolic and end systolic velocities are marked. The formula to calculate resistive index (RI) is peak systolic velocity (PSV) minus the end-diastolic velocity (EDV) divided by the PSV (PSV − EDV/PSV). A value of <0.7 is generally accepted as normal. Higher RIs can be seen normally in children and the elderly. Comparing side-to-side RIs, called resistive ratio, may be useful. A resistive ratio is the ratio between the RI of the affected kidney and the contralateral normal kidney. However, a difference in the RI of >0.1 on the symptomatic side compared to the asymptomatic side may be more important than a resistive ratio clinically [12–14]. Studies have shown acceptable sensitivity and specificity for RI in evaluating obstruction [5]. Ureteral obstruction causes elevated arterial resistance even preceding the development of significant hydronephrosis [15–17]. Nonobstructive causes of renal pelvis dilation tend to demonstrate normal RIs. For example, pregnant women have been demonstrated to have normal RIs despite the development of hydronephrosis of pregnancy [18–20]. These studies suggest that ultrasound calculation of RI can be

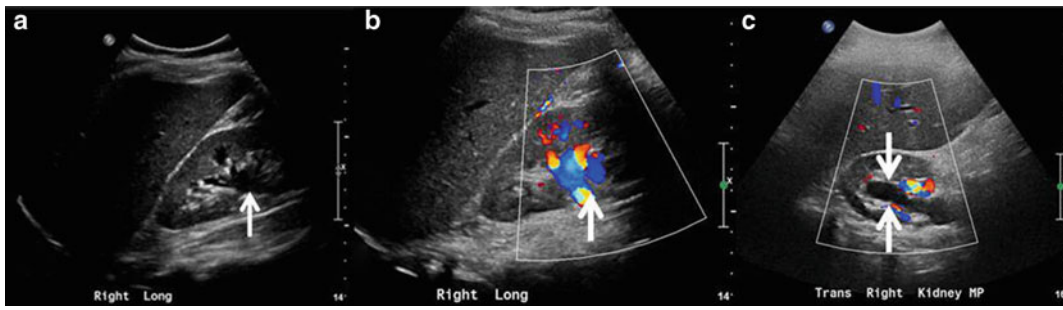

Fig. 5.10 The anechoic area (*arrow*) seen centrally in image (**a**) which has an appearance consistent with hydronephrosis is found to represent hilar vessels by color Doppler in image (**b**). In a different kidney, the central anechoic area (*arrows*) in the transverse image (**c**) remains anechoic (*arrow*) during application of Doppler indicating a dilated collecting system

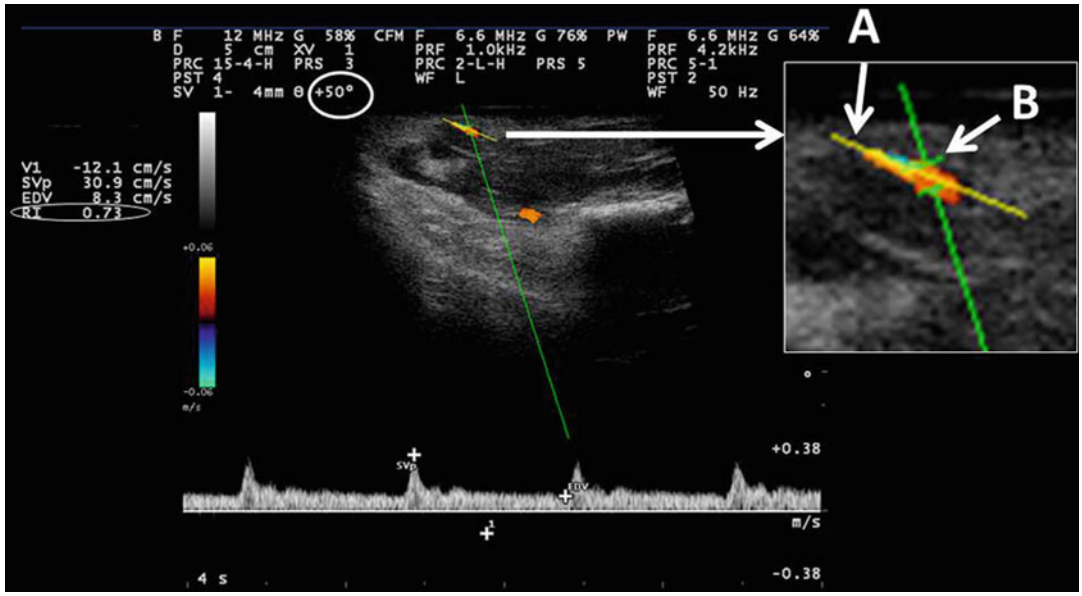

Fig. 5.11 The accurate calculation of the resistive index depends on (**a**) aligning the angle indicator (*yellow line*) with the long axis of the vessel being imaged and (**b**) ensuring that the gate (two parallel *green lines*) is set to about 3/4 of the vessel width. The goal is to achieve an angle of insonation (θ) of $\leq$60°. In this image, the angle is 50° (*circle*). The resistive index is calculated as 0.73

useful in distinguishing physiologic hydronephrosis of pregnancy from renal colic in pregnant woman while avoiding ionizing radiation.

The RI seems to rise reliably only in complete obstruction. Studies which included patients with partial obstruction demonstrated a reduced ability to discriminate between anatomic obstruction from functional dilation [21, 22]. The resistive index is not reliable as an isolated finding to prove or disprove a clinically significant obstruction. Rather, it can be another useful finding of a point-of-service ultrasound examination to support or refute a diagnosis during a clinical patient encounter.

Artifacts

Imaging the retroperitoneum with ultrasound is a challenging task due to anatomic hurdles to sound wave transmission. It is necessary to recognize and account for several common ultrasound artifacts. Ribs may cause posterior acoustic shadowing and prevent accurate visualization of the renal unit beneath that rib. Positioning the transducer between the ribs may be necessary to obtain a complete view of the kidney. Probe manipulation techniques such as fanning may be helpful for directing the beam between the ribs. A small-width curved array transducer is often helpful for imaging between the ribs. Positioning the patient in the lateral decubitus position with the ipsilateral arm extended above the head opens the intercostal spaces adequately in most patients. If additional extension is needed for particularly narrow intercostal spaces, a rolled towel or pillow under the contralateral side may facilitate extension. Figure 5.12 demonstrates a persistent rib shadow. If a more favorable window cannot be found, the examiner will have to move the kidney above or below the shadow with coached breathing to complete the renal examination.

Stones that are 5 mm or larger can be reliably seen on ultrasound as a hyperechoic focus and will usually produce a posterior acoustic window. Small or narrow stones may fail to produce a strong acoustic shadow. Some calculi may display a *twinkle artifact* during interrogation with color Doppler [23]. Twinkle artifact is a mixed color flow signal around and behind a bright specular reflector. Twinkle artifact can be useful when imaging a hyperechoic focus. When it is desireable to interpret

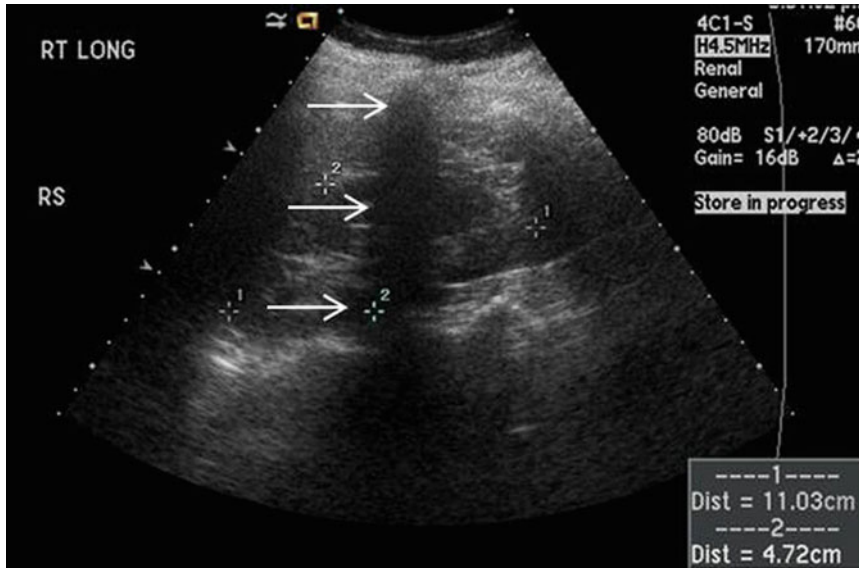

Fig. 5.12 Rib causing posterior acoustic shadowing (*arrows*) across this midsagittal image of the kidney

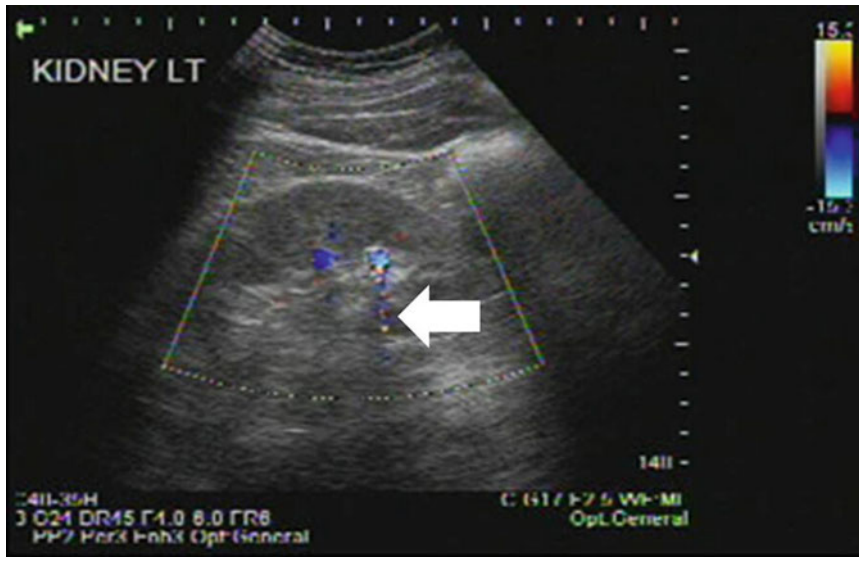

Fig. 5.13 Twinkle artifact (*arrow*) is the result of the interaction of sound waves with a highly echogenic object or an interface of significantly different impedance

an object for twinkle artifact during Doppler scanning, it is useful to place the focus just at or distal to the object producing the twinkle artifact. Blood vessels near the collecting system such as arcuate arteries often appear hyperechoic and can be difficult to distinguish from small stones. The application of color Doppler will often produce a multicolored trail posterior to a stone but not from a blood vessel (Fig. 5.13).

Stones appear differently on ultrasound compared to a CT scan. Larger stones will appear as an intensely hyperechoic leading edge rim with complete shadowing posterior on ultrasound. Therefore it can be difficult to accurately determine the three-dimensional shape and size of a stone with ultrasound (Fig. 5.14).

Reverberation artifact is the indistinct hazy shadow created by bowel gas. The colon lies ante-

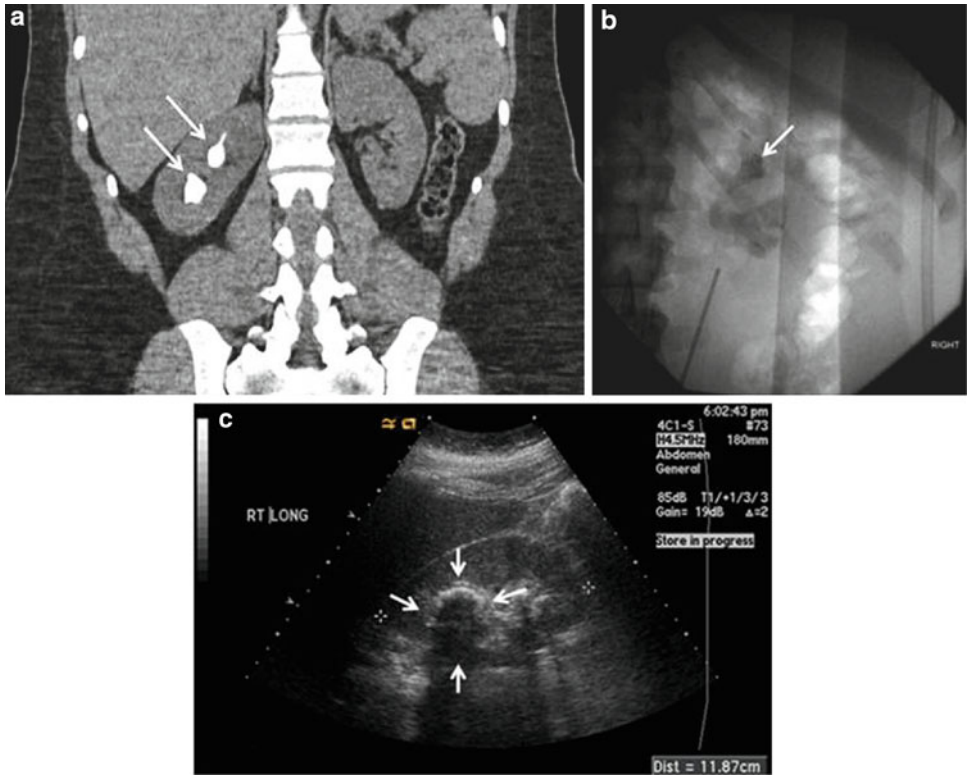

Fig. 5.14 (**a**) CT demonstrating two large caliceal stones in the right kidney (*arrows*). (**b**) Same stones on a plain radiograph. The stone is seen to be a partial staghorn calculus (*arrow*). (**c**) Ultrasound of the stone demonstrating bright leading edge (*top three arrows*) with posterior acoustic shadowing (*bottom arrow*) making it difficult to determine the three-dimensional structure of the stone

rior to each kidney and so this finding is often encountered anterior to medial to the renal unit. Figure 5.15 demonstrates the reverberation artifacts typical of bowel gas. If shadowing from bowel gas is interfering with visualization of the kidney, the probe may be moved laterally and even posteriorly to image around the colon. If the patient is lying in a supine position, it may be useful to ask the patient to reposition to a flank orientation to allow for lateral and posterior imaging.

Edging artifact is often strikingly demonstrated at the pole of the renal units. This artifact can also be seen off the edges of renal cysts (Fig. 5.16). Edging artifact occurs when sound waves strike a rounded surface at an angle, which prevents reflection back to the probe.

Side lobe artifact, also called slice thickness artifact, can be seen as fine, hyperechoic echoes within a renal cyst. To differentiate this artifact from a septum within a complex cyst or with tissue on the edge of the cyst, the ultrasound probe can be moved to change the angle of insonation between the probe and the cyst. If the finding is due to an anatomic structure, the finding will persist regardless of the angle of insonation. The side lobe artifact may also be minimized by adjusting the time gain compensation curve (Fig. 5.17).

Renal Findings

Renal scanning requires a good foundation of knowledge of both normal and abnormal renal anatomy and pathology, which further supports the concept of the urologist performing the point-of-service imaging.

The kidney has a few normal variations, which might be discovered on renal sonography. Some well-known variants are reviewed here. Pathologic findings in the kidney are quite familiar to urologists and may need to be further studied with additional imaging modalities.

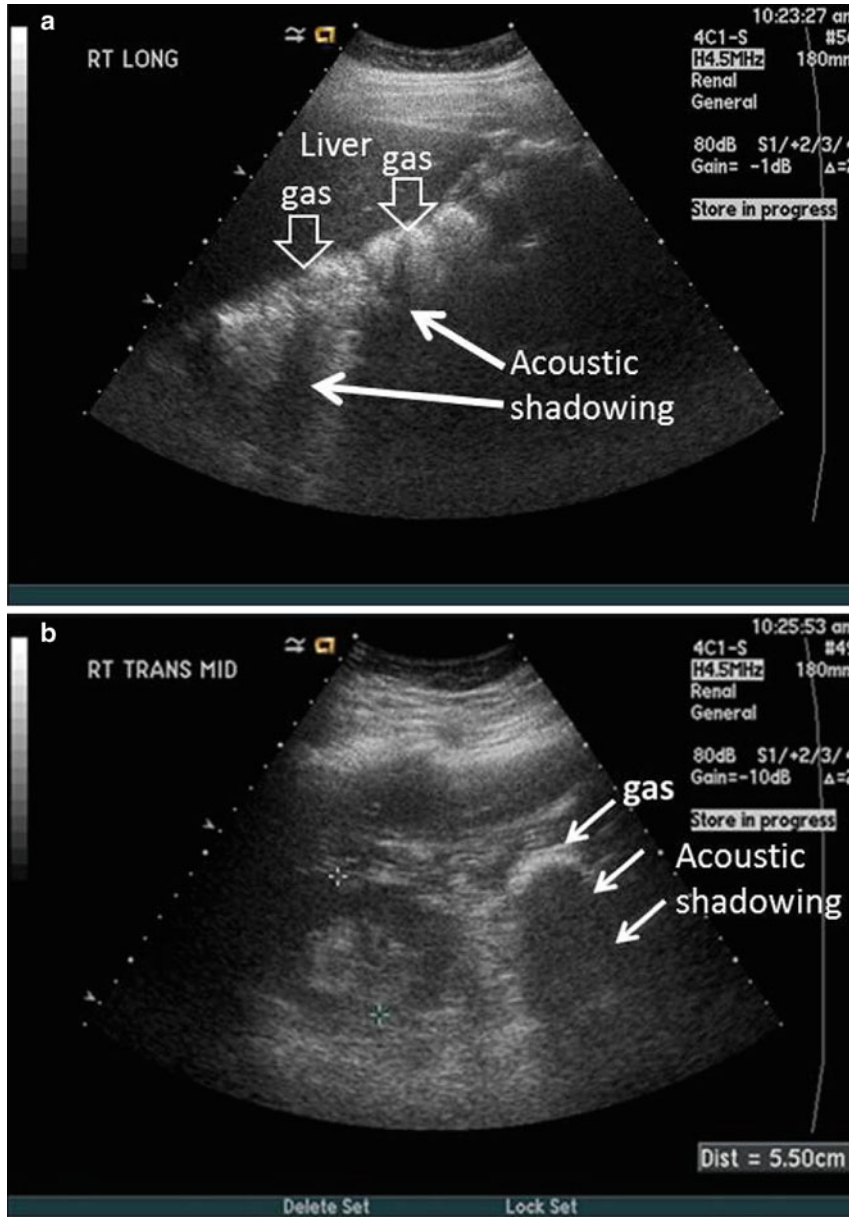

Fig. 5.15 (**a**) The characteristic shadow of bowel gas in the transverse colon shows a hyperechogenic focus corresponding to air bubbles in the bowel contents (*open arrows*) and a tracking black shadow of mixed echogenicity (*closed arrows*). (**b**) Bowel gas (*top arrow*) with dark posterior acoustic shadowing (*bottom two arrows*)

Extrarenal Pelvis

An extrarenal pelvis can also be confused for hydronephrosis. Careful examination should demonstrate lack of dilation of the infundibula and calyces. Ancillary imaging is often necessary to confirm the diagnosis.

Normal Parenchymal Variants

Normal renal units can manifest a spectrum of parenchymal variations that must be distinguished from a pathologic condition. For example, approximately 10 % of left kidneys may contain a thickened region of the lateral parenchyma called

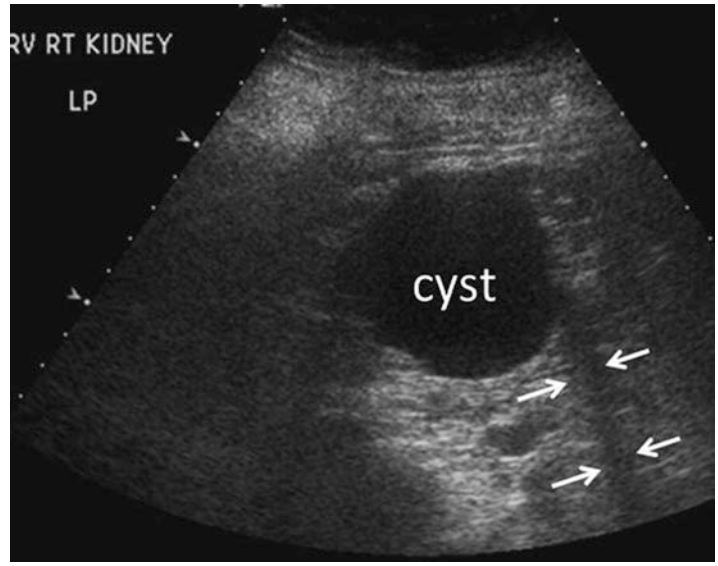

Fig. 5.16 Edging artifact (*arrows*) seen on the trailing edge of a renal cyst

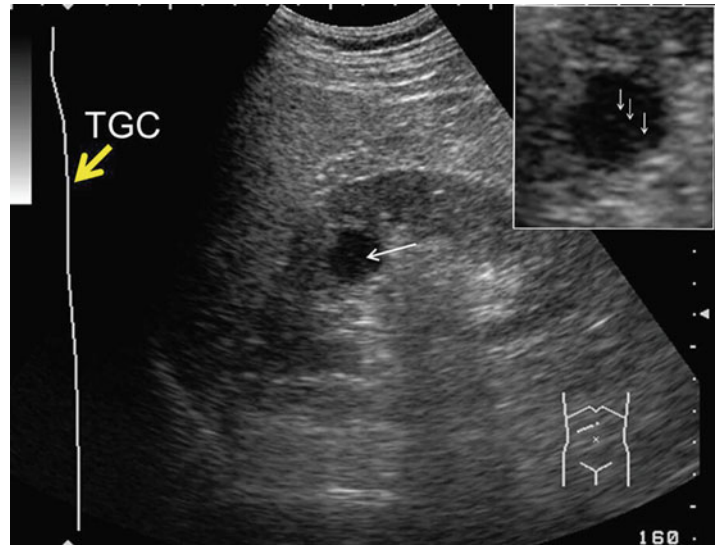

Fig. 5.17 Echoes within this renal cyst represent the side lobe artifact (*white arrows*). The time gain compensation curve (TGC) could be adjusted to minimize this artifact

a dromedary hump (Fig. 5.18). This shape is believed to be the result of pressure from the cephalad-located spleen molding the kidney during nephrogenesis. It is rarely seen on the right side. This normal variant involves bulging of the mid left lateral renal contour. Importantly, uniformity of the parenchymal thickness should be preserved and the tissue remains isoechoic to the adjacent normal parenchyma. Any bulge in this location, which distorts the parenchymal thickness or is varied in echogenicity compared to adjacent tissue, should be considered pathologic.

Hypertrophied columns of Bertin are extensions of the renal cortical tissue that protrude deeply into the renal sinus. These columns are always located between the medullary pyramids and have the same echotexture as adjacent renal cortical tissue (Fig. 5.19).

Junctional defects are areas of discontinuity in the parenchymal rim found most commonly in the anterior superior portion of the right kidney. These defects can rarely be seen on the posterior-inferior aspect of the right kidney as well. The defect has a hyperechoic appearance, slightly

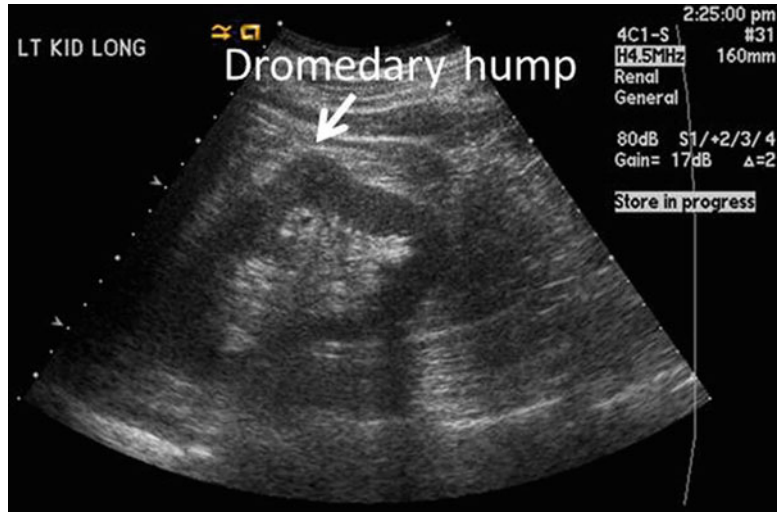

Fig. 5.18 Dromedary hump (*arrow*). The thickness of the renal parenchyma remains constant in dromedary hump

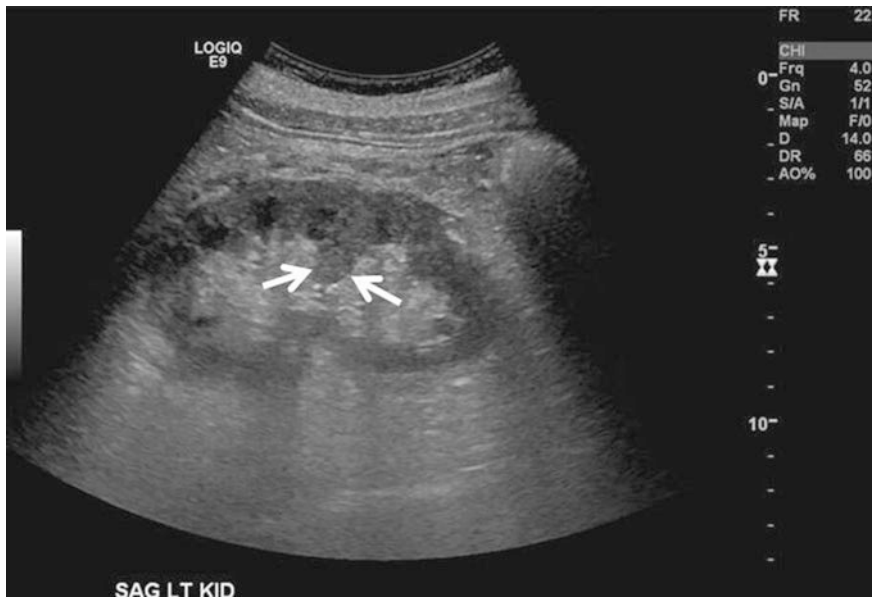

Fig. 5.19 Hypertrophied column of Bertin (*white arrows*). Note the tissue of normal renal parenchymal echogenicity extending into the renal sinus

indents the renal surface, and extends from the renal capsule to the renal sinus. It is often triangular in shape (Fig. 5.20). This anatomic alteration is thought to be secondary to incomplete fusion of the upper and lower pole parenchymal masses during embryologic development. Importantly, this junctional defect can be confused with a cortical scar or the adjacent parenchyma confused for an abnormal mass. The hyperechoic junctional defect should communicate with the renal sinus, whereas cortical scars tend to occur over the medullary pyramids and not reach the sinus.

Persistent fetal lobulations (Fig. 5.21) appear as bulges in the renal capsule over the medullary pyramids with depressions of the surface between the pyramids. The cortex is otherwise normal in thickness and uniform in echogenicity.

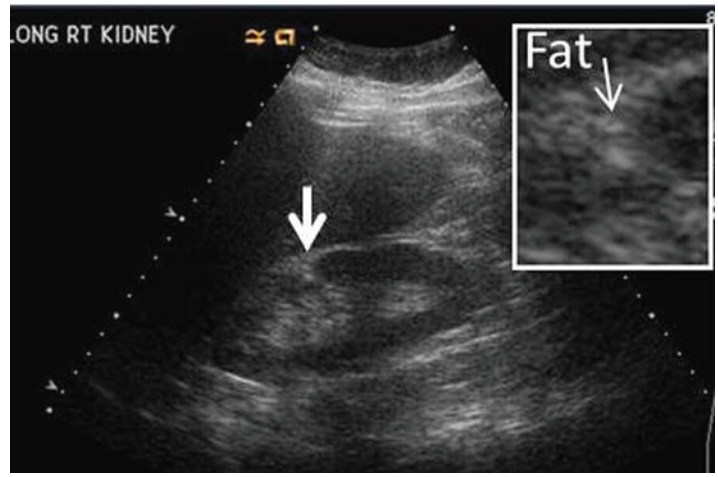

Fig. 5.20 Junctional defect with apparent invagination of the perinephric fat (*arrow*)

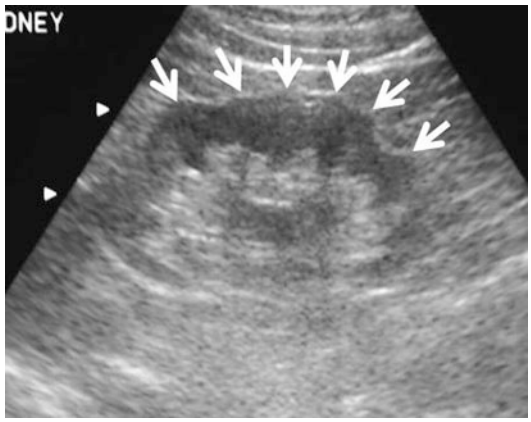

Fig. 5.21 The fetal kidney has 12-15 segments. The shape sometimes persists to adulthood as fetal lobulations (*arrows*)

Ultrasound Diagnosis of Renal Pathology

Renal Cysts

Routine radiologic evaluation of adult patients for a variety of indications, including with ultrasound, has suggested that renal cysts are identified in approximately 5–6 % of cases and may increase to as high as 30 % in adults with renal insufficiency [24, 25]. Renal ultrasound can provide the initial diagnosis of a renal cyst while also providing a safe and low-cost method for surveillance of renal cystic disease [26]. Ultrasound can be useful in distinguishing a benign cystic mass from malignancy both with gray scale imaging and the application of Doppler techniques including contrast-enhanced Doppler [27, 28]. In fact, the combination of gray scale imaging with contrast-enhanced ultrasound may improve the diagnostic accuracy of CT for complex renal masses [29].

A simple cyst is defined by the presence of three ultrasonographic characteristics: (1) cyst contents are anechoic; (2) cyst walls are thin, smooth, and well defined; and (3) there is posterior acoustic enhancement beyond the cyst. The Bosniak classification has been developed for describing cysts on CT scans but is often extended to evaluating the ultrasonographic appearance of a cyst [30]. The Bosniak I renal cyst is a simple cyst as described above (Fig. 5.22). A Bosniak II cyst has small calcifications, thin septations, or internal echoes (Fig. 5.23). A Bosniak III cystic mass contains thick calcifications, solid nodules, or thick septations (which may be vascular on Doppler) as depicted in Fig. 5.24. Bosniak IV lesions are solid with some cystic components (Fig. 5.25). A renal ultrasound lacks the resolution to identify fine abnormal features, which could upstage a cyst from Bosniak I to Bosniak II. Furthermore, gray scale ultrasound will not identify enhancement or vascular flow, which is important in the Bosniak classification system (Table 5.1). However, investigations into Doppler analysis and contrast-enhanced Doppler imaging have suggested a value for ultrasound in distinguishing benign from malignant cystic lesions [28, 31].

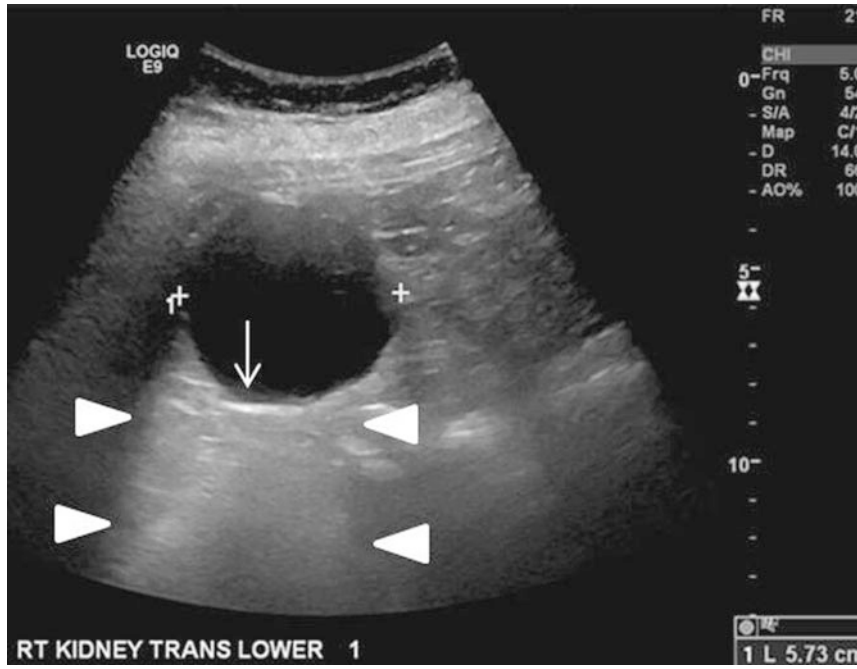

Fig. 5.22 Simple cyst (Bosniak I). Note the anechoic interior, bright back wall (*arrow*), and the increased posterior enhancement (*arrowheads*)

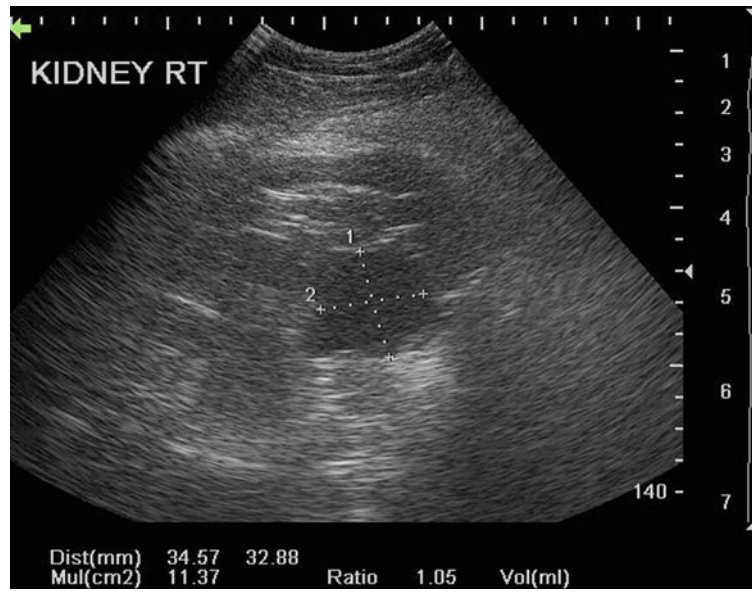

Fig. 5.23 Bosniak II cyst, in this case with irregular shape and thickened posterior wall)

Parapelvic Cysts

Parapelvic cysts are anechoic structures of varying size adjacent to or within the renal sinus. They are easily mistaken for hydronephrosis. The cysts sometimes penetrate deeply into the renal sinus mimicking dilated calyces (Fig. 5.26). One helpful characteristic that may distinguish a parapelvic cyst from the renal collecting system is the location of the cyst in relation to the medullary pyramid. In hydronephrosis, the long axis of the hypoechoic structure tends to line up pointing

towards the renal papilla and pyramid (Fig. 5.27). Parapelvic cysts tend to have their long axis pointing in between the pyramids. However, these structures can be difficult to distinguish from the renal pelvis or from other structures within the renal sinus on either ultrasound, intravenous pyelography, or CT [32, 33].

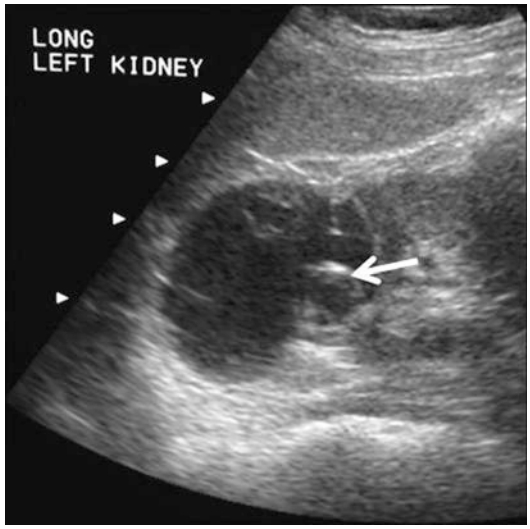

Fig. 5.24 Bosniak III cyst demonstrating a thick mural nodule (arrow) within the cyst

Hydronephrosis

The clinical examination of a patient for the presence of renal collecting system obstruction (hydronephrosis) is likely the most well-established application of renal ultrasound. Research has demonstrated the value of point-of-service renal US performed in a physician's office as well as facilities in which educational programs can equip physicians with the skills to diagnose hydronephrosis [34, 35]. The overall sensitivity of renal ultrasound for hydronephrosis is 70–98 % which is often helpful in the acute evaluation of renal colic in the emergency room [36–38].

In the hands of a urologist, ultrasound is a useful tool for identifying and monitoring hydronephrotic disease processes. The surgeon who repaired the UPJ obstruction, performed a ureteral reimplantation, or treated a ureteral stricture can use ultrasound with a high degree of confidence that hydronephrosis will be visible if present. The classification of hydronephrosis is summarized in Table 5.3 [39]. There have also been ongoing attempts to establish a grading system for pediatric renal pelvic dilation that can be applied to prenatal ultrasound [40]. Finally, renal ultrasound in combination with nuclear

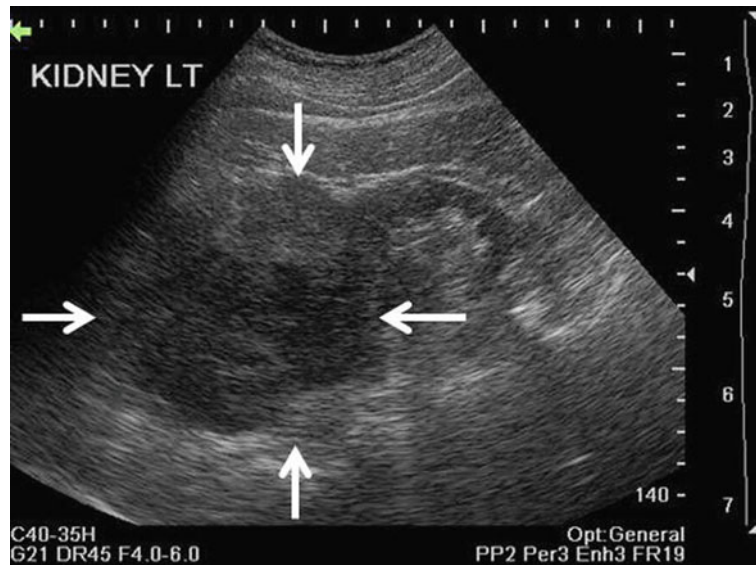

Fig. 5.25 Bosniak IV cyst demonstrating a solid mass (*arrows*) with hypoechogenic cystic components

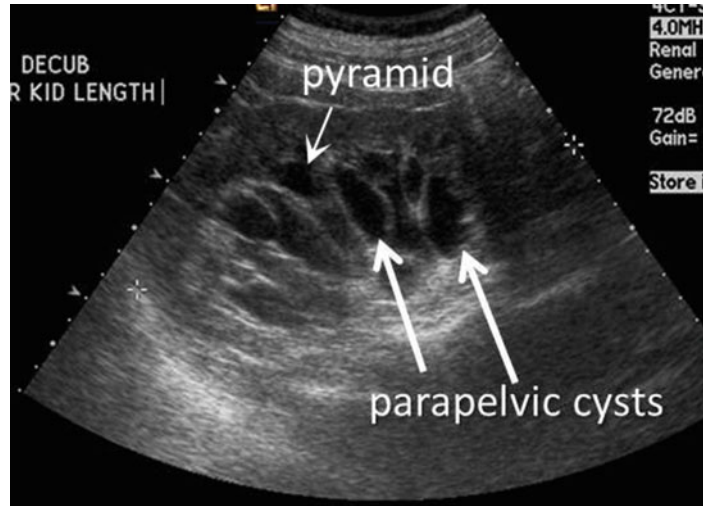

Fig. 5.26 Parapelvic cysts (*bottom two arrows*) with long axes which point between medullary pyramids (*top arrow*)

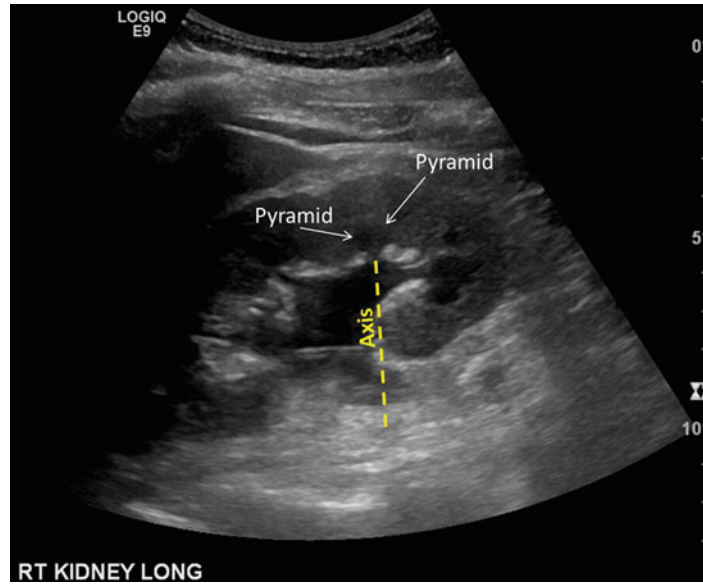

Fig. 5.27 The long axis (*yellow line*) of the hypoechoic pelvis and infundibulum points to a medullary pyramid (*white arrows*)

medicine studies may represent a noninvasive method for the diagnosis of high grade reflux in children [41].

Urolithiasis

Predictive models have demonstrated that the prevalence of urolithiasis is increasing in the United States and currently represents approximately 600,000 emergency room visits each year. A non-contrast CT scan has been designated by the American College of Radiology as the modality with the highest sensitivity and specificity [1]. However, in the spirit of the American Institute for Ultrasound in Medicine (AIUM) program of "Ultrasound First" as well as the concept of ALARA (as low as reasonably achievable) a renal ultrasound is likely an effective initial diagnostic tool for patients with renal colic. Certainly, ultrasound is the primary modality for pregnant women with pain consistent with a renal stone. Smith-Bindman and

coworkers performed a landmark prospective randomized study of ultrasound versus computed tomography for suspected urolithiasis during initial presentation to an emergency room [3]. The study population consisted of 2759 patients at multiple sites with renal colic and were randomized to point-of-service ultrasound by an emergency room physician, radiology-performed ultrasound, or an abdominal CT scan. Ultimately, this study demonstrated that the clinical outcomes for the patients were not altered by the initial imaging study but that ultrasound resulted in reduced radiation exposure and a reduced cost of the clinical pathway.

Retroperitoneal ultrasound can evaluate the involved renal unit, ureter, and bladder for possible hydronephrosis and calculus. The combination of gray scale imaging with Doppler has been found to compare favorably to CT scan for stones larger than 5 mm since these stones are usually associated with the twinkle artifact [23, 42]. An ultrasound examination can be used initially in the diagnosis of abdominal pain when a stone is suspected or in surveillance for monitoring the progression of a ureteral calculus. Hydronephrosis has not been proven to be an absolute diagnostic feature of renal colic so the ultrasonographer should also attempt to locate the stone and assess ureteral jets [15, 43].

A targeted office ultrasound can be helpful with monitoring patients following the initial diagnosis of a renal or ureteral calculus. The exam can quickly establish the persistence or resolution of hydronephrosis and the status of the ipsilateral ureteral jet. Additionally, patients frequently do not recover small stones and renal colic can be episodic in nature. Ultrasound can be helpful in determining if a stone has passed. Distal stones can often be directly imaged posterior to the bladder or in the intramural portion of the distal ureter. Patients without evidence of hydronephrosis or a visible calculus can be assured that the stone has likely passed while individuals with persistent findings can be scheduled for an elective intervention.

Renal Masses

Renal ultrasound has a role as an adjunct to cross-sectional imaging with CT and MRI for the diagnosis, surveillance, and management of renal masses. Ultrasound is not as sensitive as CT or MRI for the initial diagnosis or characterization of a renal mass. However, recent technologic improvements in renal ultrasound have increased the value of this diagnostic modality in the differential diagnosis of a small renal mass, active surveillance of these lesions, and possibly even surgical planning. The application of contrast-enhanced or even improved fine flow Doppler has improved the differential diagnosis of a complex cystic mass in the kidney [28, 44]. Furthermore, the advent of strain elastography offers another opportunity to identify malignant renal lesions without ionizing radiation or the expense of an MRI [45].

Renal ultrasound can be very helpful in the ongoing surveillance of known masses. The dangers of repeated ionizing radiation from CT imaging have been established and ultrasound represents an excellent modality for monitoring a known mass. Finally, renal ultrasound is likely a helpful tool for radiographic surveillance following the definitive management of a renal malignancy. The American Urologic Association clinical guidelines include ultrasound as an option for follow-up imaging in low-risk patients [46]. Finally, the combination of gray scale imaging again with Doppler interrogation is helpful following cryoablation of a renal mass, which can reduce the cost of the surveillance [47].

Angiomyolipomas

Renal ultrasound is an excellent imaging tool for confirming the diagnosis of fat-containing angiomyolipomas (AML) of the kidney [48]. Figure 5.28 is an example of the typical appearance of a fat-rich AML. Ultrasound is likely useful for surveillance of these lesions over time with the attempt to document changes in the size of the mass. Size and possibly identification of arterial venous malformations represent the established criteria for surgical intervention for this benign mass.

Renal Scars

Parenchymal scarring appears as a sharp depression in the outline of the kidney. Scars are always located over renal pyramids. The cortical thickness

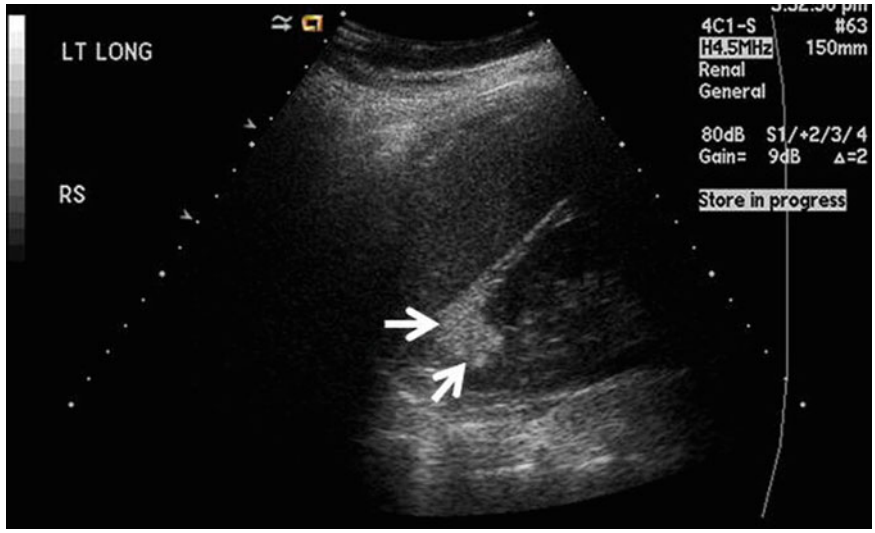

Fig. 5.28 An angiomyolipoma is typically a hyperechoic mass (*arrows*). The hyperechoicism is caused by the high fat content of the tumor

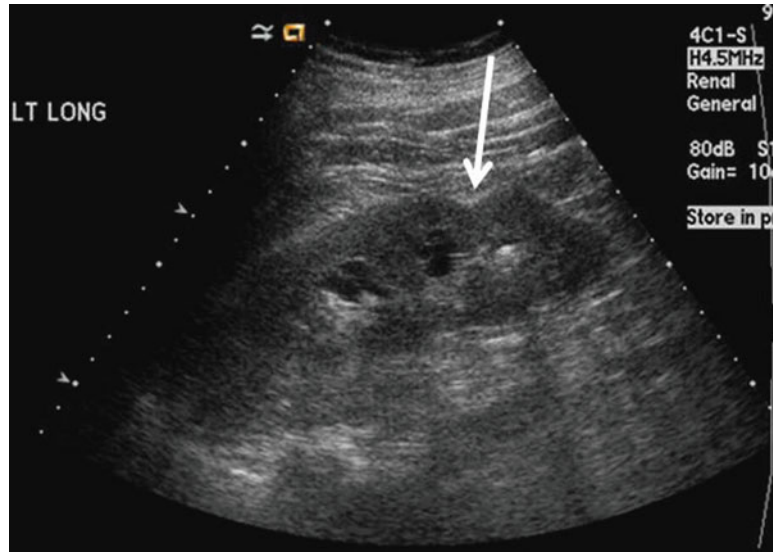

Fig. 5.29 Renal cortical scarring appears as a sharp depression (*arrow*) in the outline of the kidney usually overlying a calyx

is dramatically reduced or absent completely at the scar. Figure 5.29 demonstrates a renal cortical scar.

Medical Renal Disease

Renal ultrasound appears to be a useful tool for the evaluation of patients with evidence of renal parenchyma disease. Table 5.2 lists the various manifestations of renal parenchymal disease on ultrasound imaging. It is now apparent that renal ultrasound can accurately identify hydronephrosis as an underlying etiology for the acute renal injury [49]. Additional gray scale visible alterations include an increased echogenicity of the renal parenchyma and a reduction in parenchymal length or thickness [50]. Figure 5.30 depicts these characteristics.

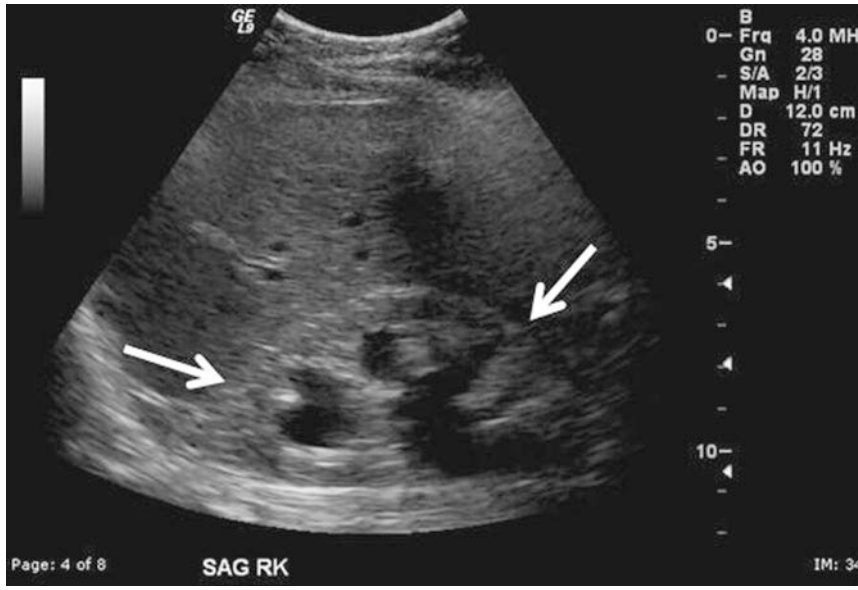

Fig. 5.30 Small hyperechogenic kidney (*arrows*) as a result of medical renal disease

Perhaps more importantly, renal ultrasound has the ability to identify patients at risk for progressive renal dysfunction prior to parenchymal loss. Measurements of RI can identify patients at risk for hypertension-associated renal injury which likely represents a marker for systemic vascular disease [6, 51]. The resistive index is also altered in some patients with diabetes mellitus and could offer an early screening test for these individuals [52, 53].

Applications of Intraoperative Renal Ultrasound

Ultrasound has become established as a valuable adjunct to the operative management of renal disorders particularly during partial nephrectomy, performance of venous thrombectomy and renal tissue ablation. The renal parenchyma appears very similar during intraoperative ultrasound imaging except for the enhanced details that can be achieved with higher ultrasound frequencies. Therefore, the ultrasound imaging of the kidney can more clearly delineate the anatomy of a renal mass, the presence of a pseudocapsule, and any previously unsuspected invasion into adjacent parenchyma.

Doppler analysis of a renal mass, with or without contrast enhancement, has been used in animals during ablation procedures [54]. This may become a useful method for determining the immediate success of a targeted ablation in humans.

Conclusion

The deep familiarity with which a urologist approaches patients with possible renal disorders represents the platform upon which the successful application of point-of-service renal ultrasound is founded. The combination of the patient's history, associated signs and symptoms, and any prior diagnostic testing can now be combined with a low-cost ultrasound examination to streamline the diagnostic pathway.

As discussed in this chapter, renal ultrasound has utility in the emergent evaluation of patients with abdominal pain suggestive of urolithiasis with both an improvement in patient safety and a reduction in the cost of care. Patients with evidence of medical disorders that can result in renal parenchymal disease can now be identified earlier in their disease presentation with

improved opportunities for prevention of progression of renal insufficiency. Finally, the performance of a real-time renal ultrasound by the urologist in the office can further cement the patient–physician relationship.

References

1. Minton KK, Abuhamad A. 2012 ultrasound first forum proceedings. J Ultrasound Med. 2013;32(4):555–66.
2. Surange RS, et al. Bedside ultrasound: a useful tool for the on-call urologist? Int Urol Nephrol. 2001;32 (4):591–6.
3. Smith-Bindman R, et al. Ultrasonography versus computed tomography for suspected nephrolithiasis. N Engl J Med. 2014;371(12):1100–10.
4. American Institute of Ultrasound in Medicine, American Urological Association. AIUM practice guideline for the performance of an ultrasound examination in the practice of urology. J Ultrasound Med. 2012;31(1):133–44.
5. Piazzese EM, et al. The renal resistive index as a predictor of acute hydronephrosis in patients with renal colic. J Ultrasound. 2012;15(4):239–46.
6. Geraci G, et al. Association of renal resistive index with aortic pulse wave velocity in hypertensive patients. Eur J Prev Cardiol. 2015;22(4):415–22.
7. Emamian SA, et al. Kidney dimensions at sonography: correlation with age, sex, and habitus in 665 adult volunteers. AJR Am J Roentgenol. 1993;160 (1):83–6.
8. Han BK, Babcock DS. Sonographic measurements and appearance of normal kidneys in children. AJR Am J Roentgenol. 1985;145(3):611–6.
9. Moghazi S, et al. Correlation of renal histopathology with sonographic findings. Kidney Int. 2005;67(4): 1515–20.
10. Kim KW, et al. Sonography of the adrenal glands in the adult. J Clin Ultrasound. 2012;40(6):357–63.
11. Gaarder M, et al. Standardized cine-loop documentation in renal ultrasound facilitates skill-mix between radiographer and radiologist. Acta Radiol. 2015;56(3): 368–73.
12. Shokeir AA, Abdulmaaboud M. Resistive index in renal colic: a prospective study. BJU Int. 1999;83(4) :378–82.
13. Rawashdeh YF, et al. The intrarenal resistive index as a pathophysiological marker of obstructive uropathy. J Urol. 2001;165(5):1397–404.
14. Shokeir AA, Abdulmaaboud M. Prospective comparison of nonenhanced helical computerized tomography and Doppler ultrasonography for the diagnosis of renal colic. J Urol. 2001;165(4):1082–4.
15. Song Y, Hernandez N, Gee MS et al. Can ureteral stones cause pain without causing hydronephrosis? World J Urol (2016) 34:1285.
16. Nadzri M, et al. Renal doppler assessment in differentiating obstructive from non-obstructive hydronephrosis in children. Med J Malaysia. 2015;70(6):346–50.
17. Tseng FF, et al. Value of Doppler ultrasonography in predicting deteriorating renal function after spinal cord injury. Radiol Med. 2012;117(3):500–6.
18. Andreoiu M, MacMahon R. Renal colic in pregnancy: lithiasis or physiological hydronephrosis? Urology. 2009;74(4):757–61.
19. Nuri Bodakci M, et al. Hydronephrosis during pregnancy: how to make a decision about the time of intervention? Med Glas (Zenica). 2014;11(1):165–9.
20. Pepe F, Pepe P. Color Doppler ultrasound (CDU) in the diagnosis of obstructive hydronephrosis in pregnant women. Arch Gynecol Obstet. 2013;288(3) :489–93.
21. Morcillo E, et al. Experimental study with Doppler ultrasound in partial chronic obstructive uropathy. Actas Urol Esp. 2012;36(3):146–52.
22. Tublin ME, Bude RO, Platt JF. Review. The resistive index in renal Doppler sonography: where do we stand? AJR Am J Roentgenol. 2003;180(4): 885–92.
23. Kielar AZ, et al. Prospective evaluation of Doppler sonography to detect the twinkling artifact versus unenhanced computed tomography for identifying urinary tract calculi. J Ultrasound Med. 2012;31(10):1619–25.
24. Murshidi MM, Suwan ZA. Simple renal cysts. Arch Esp Urol. 1997;50(8):928–31.
25. Gulanikar AC, et al. Prospective pretransplant ultrasound screening in 206 patients for acquired renal cysts and renal cell carcinoma. Transplantation. 1998; 66(12):1669–72.
26. Ozveren B, Onganer E, Turkeri LN. Simple renal cysts: prevalence, associated risk factors and follow-up in a health screening cohort. Urol J. 2016;13(1):2569–75.
27. Xue LY, et al. Contrast-enhanced ultrasonography for evaluation of cystic renal mass: in comparison to contrast-enhanced CT and conventional ultrasound. Abdom Imaging. 2014;39(6):1274–83.
28. Lan D, et al. The value of contrast-enhanced ultrasonography and contrast-enhanced CT in the diagnosis of malignant renal cystic lesions: a meta-analysis. PLoS One. 2016;11(5):e0155857.
29. Nicolau C, et al. Prospective evaluation of CT indeterminate renal masses using US and contrast-enhanced ultrasound. Abdom Imaging. 2015;40(3):542–51.
30. Israel GM, Bosniak MA. An update of the Bosniak renal cyst classification system. Urology. 2005; 66(3):484–8.
31. Ignee A, et al. The value of contrast enhanced ultrasound (CEUS) in the characterisation of patients with renal masses. Clin Hemorheol Microcirc. 2010; 46(4):275–90.
32. Hidalgo H, et al. Parapelvic cysts: appearance on CT and sonography. AJR Am J Roentgenol. 1982; 138(4):667–71.

33. Rha SE, et al. The renal sinus: pathologic spectrum and multimodality imaging approach. Radiographics. 2004;24 Suppl 1:S117–31.
34. Moslemi MK, Mahfoozi B. Urologist-operated ultrasound and its use in urological outpatient clinics. Patient Prefer Adherence. 2011;5:85–8.
35. Caronia J, et al. Focused renal sonography performed and interpreted by internal medicine residents. J Ultrasound Med. 2013;32(11):2007–12.
36. Ellenbogen PH, et al. Sensitivity of gray scale ultrasound in detecting urinary tract obstruction. AJR Am J Roentgenol. 1978;130(4):731–3.
37. Riddell J, et al. Sensitivity of emergency bedside ultrasound to detect hydronephrosis in patients with computed tomography-proven stones. West J Emerg Med. 2014;15(1):96–100.
38. Sheafor DH, et al. Nonenhanced helical CT and US in the emergency evaluation of patients with renal colic: prospective comparison. Radiology. 2000;217 (3):792–7.
39. Fernbach SK, Maizels M, Conway JJ. Ultrasound grading of hydronephrosis: introduction to the system used by the Society for Fetal Urology. Pediatr Radiol. 1993;23(6):478–80.
40. Swenson DW, et al. Characterizing upper urinary tract dilation on ultrasound: a survey of North American pediatric radiologists' practices. Pediatr Radiol. 2015;45(5):686–94.
41. You SK, et al. Prediction of high-grade vesicoureteral reflux in children younger than 2 years using renal sonography: a preliminary study. J Ultrasound Med. 2016;35(4):761–5.
42. Korkmaz M, et al. Investigating the clinical significance of twinkling artifacts in patients with urolithiasis smaller than 5 mm. Jpn J Radiol. 2014;32 (8):482–6.
43. Mos C, et al. The sensitivity of transabdominal ultrasound in the diagnosis of ureterolithiasis. Med Ultrason. 2010;12(3):188–97.
44. Jiang J, et al. Clear cell renal cell carcinoma: contrast-enhanced ultrasound features relation to tumor size. Eur J Radiol. 2010;73(1):162–7.
45. Dalen H, et al. Cardiovascular risk factors and systolic and diastolic cardiac function: a tissue Doppler and speckle tracking echocardiographic study. J Am Soc Echocardiogr. 2011;24(3):322–32.e6.
46. Donat SM, et al. Follow-up for clinically localized renal neoplasms: AUA guideline. J Urol. 2013;190(2):407–16.
47. Zeccolini G, et al. Comparison of Contrast-Enhanced Ultrasound Scan (CEUS) and MRI in the follow-up of cryoablation for small renal tumors. Experience on 25 cases. Urologia. 2014;81 Suppl 23:S1–8.
48. Atri M, et al. Accuracy of contrast-enhanced US for differentiating benign from malignant solid small renal masses. Radiology. 2015;276(3):900–8.
49. Licurse A, et al. Renal ultrasonography in the evaluation of acute kidney injury: developing a risk stratification framework. Arch Intern Med. 2010;170(21):1900–7.
50. Khati NJ, Hill MC, Kimmel PL. The role of ultrasound in renal insufficiency: the essentials. Ultrasound Q. 2005;21(4):227–44.
51. Zhu J, Wen K, He H. Diagnostic value of urinary protein and creatinine in combination with renal ultrasound examination in early renal damage of patients with hypertension. Pak J Med Sci. 2015;31(4):899–902.
52. Muraira-Cardenas LC, Barrios-Perez M. Effect of metabolic uncontrolled diabetes mellitus (DM) on the resistance index of renal (IR) Interlobar arteries assessed with pulsed Doppler. Gac Med Mex. 2016;152(2):213–7.
53. Boddi M, Natucci F, Ciani E. The internist and the renal resistive index: truths and doubts. Intern Emerg Med. 2015;10(8):893–905.
54. Slabaugh TK, et al. Monitoring radiofrequency renal lesions in real time using contrast-enhanced ultrasonography: a porcine model. J Endourol. 2005;19(5):579–83.

Scrotal Ultrasound

6

Etai Goldenberg, Gideon Richards, and Bruce R. Gilbert

Introduction

Portability, safety, economy, and efficiency, together with the ability to accurately and rapidly define pathology, have made ultrasound the primary imaging modality for evaluation of the scrotum, testis, and paratesticular structures. These factors provide for timely diagnosis and treatment. Scrotal ultrasound is essential in the diagnosis of testicular cancer and is particularly helpful when a physical examination is inconclusive or when the disease process prevents adequate examination. The detailed imaging of ultrasonography is often a vital component in the diagnosis of symptoms including scrotal pain, trauma, infertility, and abnormal findings on physical exam. This chapter will explore the techniques and protocols for performing scrotal ultrasounds in order to make the most thorough assessment of patient symptoms leading to diagnosis.

E. Goldenberg, M.D.
Urology Consultants Ltd., 12855 North Forty, Suite 375, Saint Louis, MO 63141, USA
e-mail: egoldenberg@ucl-stl.com

G. Richards, M.D.
Arizona State Urological Institute, 1445 W. Chandler Blvd, Suite, A-5, Gilbert, Chandler, AZ 85295, USA
e-mail: gidrichards@gmail.com

B.R. Gilbert, M.D., Ph.D. (✉)
Hofstra Northwell School of Medicine, The Arthur Smith Institute for Urology, 450 Lakeville Road, Suite M41, New Hyde Park, NY 11042, USA
e-mail: bgilbert@gmail.com

Scanning Technique and Protocol

It is our belief that the ultrasound exam is best performed by a skilled sonographer using defined protocols. In this chapter we present our approach, realizing that many experienced sonographers will modify it to fit in with their needs. Nonetheless, it provides a basis to assure consistency in the exam appropriate documentation.

The scrotal ultrasound is most often performed with the patient in the supine position. There are several different techniques to support the scrotum. The easiest is to use the patient's legs for support. Other approaches use towels placed across the patient's thighs or under the scrotum. The phallus is positioned up on the pubis held by the patient and/or covered by a towel for privacy (Figs. 6.1 and 6.2). The transducer is held with examiner's hand against the patient for stability (Figs. 6.3 and 6.4).

P.F. Fulgham, B.R. Gilbert (eds.), *Practical Urological Ultrasound*, Current Clinical Urology,
DOI 10.1007/978-3-319-43868-9_6

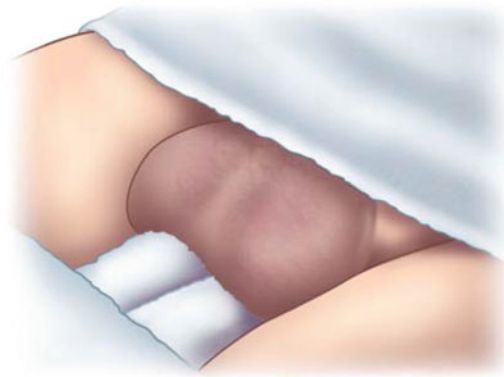

Fig. 6.1 Patient is placed in a supine position with a towel placed under the scrotum

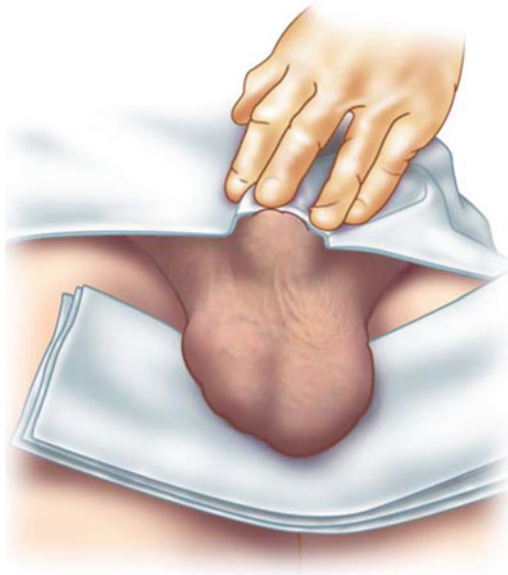

Fig. 6.2 Patient positioning: the phallus is positioned up on the pubis, held by the patient or a towel

Transducer Selection

The choice of the frequency used is determined by a balance between depth of penetration required and the detail of the image required. As the frequency increases the image resolution (axial resolution) improves and the depth of penetration decreases. Broad bandwidth transducers allow for multiple focal zones, eliminating the need for adjustment during the examination. Multiple frequency transducers allow the transducer to be set to several distinct frequencies. A high frequency (7–18 MHz) array transducer is most often used for scrotal scanning. A linear array probe with a "footprint" able to measure the longitudinal length of

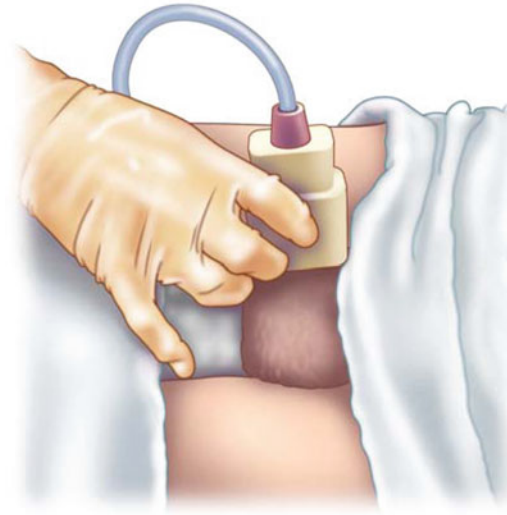

Fig. 6.3 Sonographer performing a longitudinal view of the testis. Note the use of the fifth finger on the patient's thigh to help steady the transducer and minimize movement of the testis in the scrotum

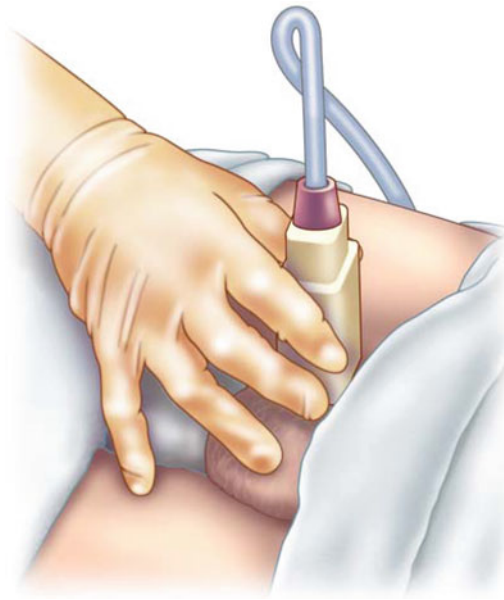

Fig. 6.4 Sonographer positioning the transducer for a transverse view of the testis. Note again, the use of the fifth finger on the patient's thigh to help steady the transducer and minimize movement of the testis in the scrotum

testis is ideal. A curved array probe can be used with a thickened scrotal wall or in the presence of scrotal edema or for a large testis. The curved array transducer is also useful to compare echogenicity of the testes; however, the frequency is usually lower with a curved array probe, resulting in decreased axial resolution. Color and spectral Doppler are essential elements of scrotal ultrasound because they provide documentation of testicular blood flow and paratesticular findings. The highest possible Doppler frequency, typically in the 5–10 MHz range providing the best axial resolution and blood flow detection, should be used [1].

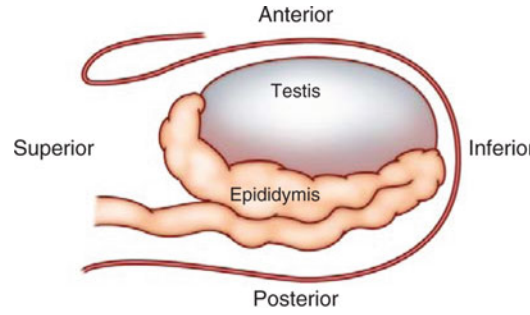

Fig. 6.5 Schematic view of longitudinal scrotal ultrasound

Overview of the Exam

The American Institute of Ultrasound in Medicine (AIUM) guidelines recommend that scrotal ultrasound should be performed in at least two planes: longitudinal and transverse. In the **longitudinal** view, the standard orientation of the image should be with the superior pole of the testis to the left and the inferior pole to the right on the monitor screen (Fig. 6.5). In the **transverse** plane, the standard orientation is for the patient's right testis to be the right side of the screen. Therefore, for the right testis, the lateral aspect is located on the left side of the screen and the medial aspect to the right. Conversely, for the left testis, the lateral aspect should be to the right and the medial aspect to the left (Fig. 6.6).

The evaluation of the scrotal contents should begin with a longitudinal survey scan, progressing medial to lateral to get an overall impression of the testis and paratesticular structures. If the testis is larger than the footprint of the transducer, it is important to document views of the superior and inferior portions of the testis including the epididymis in these regions. The transverse view is obtained by rotating the transducer 90°. A survey scan is performed using the mid-testis as a starting point and proceeding first toward the superior pole then back to the mid-testis before scanning to the inferior pole.

At least one image should visualize both testes to document the presence of two testes and their relative echogenicity (Fig. 6.7) [2]. Measurements of the testicular width and height are taken and documented at the mid-testis. A measurement should also be made of the long axis at the mid-testis and a testicular volume is calculated (Fig. 6.8). If the equipment being used has split-screen capabilities, comparative views of echogenicity can easily be made and documented.

All relevant extratesticular structures should be evaluated, including but not limited to the epididymis, spermatic cord, and scrotal skin. Techniques that improve visualization, such as Valsalva maneuver or upright positioning, may be used as needed.

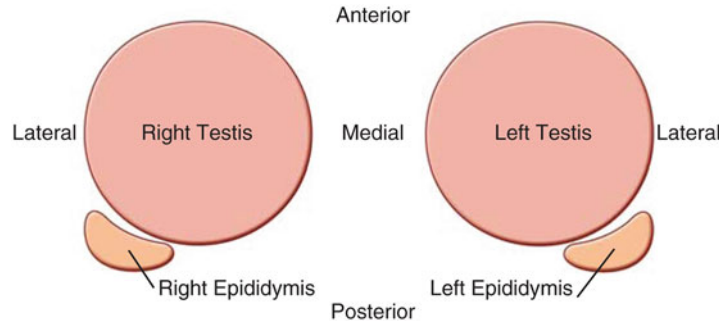

Fig. 6.6 Schematic view of transverse scrotal ultrasound as seen on the ultrasound screen with the right testis on the left and left testis on the right. The relative positions of each epididymis is also demonstrated

Color and Spectral Doppler

Color and spectral Doppler should be considered an integral part of the scrotal US examination. Many inflammatory, neoplastic, and benign conditions have characteristic flow patterns that can assist in diagnosis. At least one side-by-side image containing both testes with identical Doppler settings should be included to evaluate symmetry of flow. If blood flow cannot be visualized on color Doppler (Fig. 6.9a), power Doppler may increase the sensitivity to detect blood flow (Fig. 6.9b) [1].

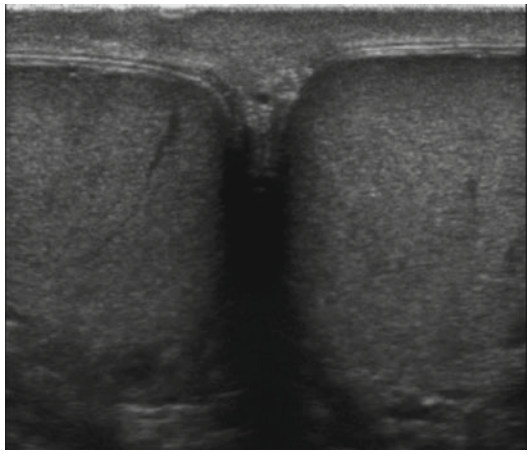

Fig. 6.7 Gray scale side-by-side view of both testes in a single image. This image is important to confirm the presence of two testes

Documentation

The written report and archived images are a reflection of the quality of the examination. The old adage "If it's not documented, it wasn't done" should guide the sonographer in developing a quality report. The static images obtained during the evolving ultrasound exam should represent the sonographer's impression of the findings. If electronic storage space is available and the equipment allows, video clips, which demonstrate important findings and survey scans, can and should be obtained. A quality report can aid in diagnosis and is therefore in the best interest of our patients.

All the measurements and anatomical findings of the exam should be documented. Images should be attached to the report. It is essential to include patient identification information, the exam date, and the indications for performing the exam. The transducer used and its frequency should also be documented. The area of interest should be clearly identified. The orientation and measurements should be labeled along with the pertinent anatomy and any abnormalities. There is no minimum number of images that are required for proper documentation. It is a best practice to provide images that depict the measurements being taken and the pathology being described. The physician who performed the exam should sign the report.

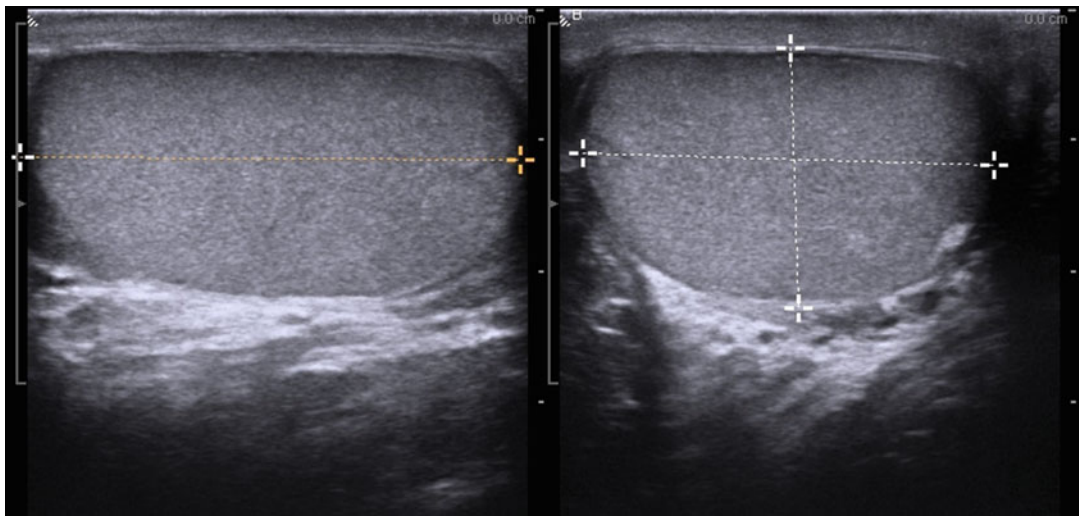

Fig. 6.8 Gray scale ultrasound in transverse and longitudinal planes used to measure the testicular volume

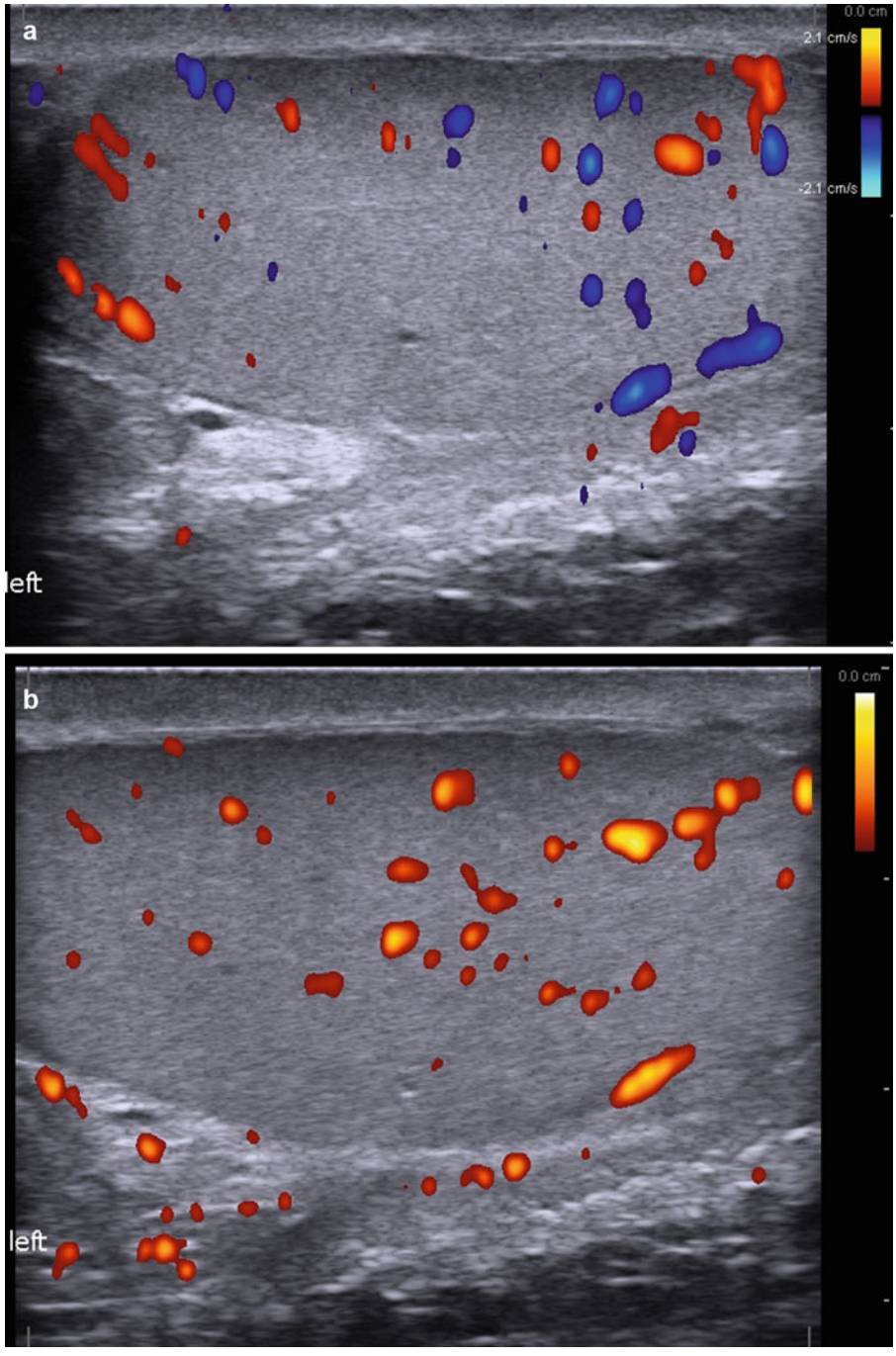

Fig. 6.9 (**a**) Color Doppler Ultrasound demonstrating testicular blood flow. (**b**) Power Doppler Ultrasound demonstrating testicular blood flow. Note lack of directionality with Power Doppler

Indications

There are many specific indications for scrotal ultrasound (Table 6.1). Scrotal ultrasound is often performed when the physical examination is inconclusive or difficult to complete (or both) because of patient discomfort or inability of the examiner to precisely identify the scrotal structures on palpation. In these instances the scrotal ultrasound examination is therefore an integral part of the physical examination of the male genitalia. In other situations, ultrasound evaluation is essential to diagnosis and treatment and is well supported in the literature. However, the decision on whether or not to obtain an ultrasound study is discretionary and without a clearly defined evidence-based approach [3, 4].

Table 6.1 Indications for scrotal ultrasound

1. Assessment of scrotal mass
(a) Painful enlargement
• Epididymitis/orchitis
• Testicular abscess
• Torsion
(b) Nonpainful enlargement
• Testicular tumor
• Hydrocele
• Varicocele
• Spermatocele/epididymal cyst
• Scrotal hernia
• Cyst
2. Evaluation of scrotal trauma
(a) Testicular rupture
(b) Hematocele
3. Evaluation and management
(a) Detection of occult primary tumors in patients with metastatic germ cell tumors
(b) Follow-up of patients with prior primary testicular neoplasms, leukemia, or lymphoma
(c) Evaluation of abnormalities noted on other imaging modalities (CT., MRI, PET, etc.)
(d) Evaluation of intersex conditions
4. Investigation of empty/abnormal scrotal sac
(a) Undescended testis
(b) Thickened scrotal skin
5. Evaluation of male infertility and related issues
(a) Varicocele
(b) Intratesticular microcirculation
(c) Atrophic testis
(d) Microlithiasis
(e) Impaired semen quality
(f) Azoospermia
(g) Antisperm antibody
6. Postoperative follow up
(a) Varicocele
(b) Testis biopsy
(c) Hydrocelectomy
(d) Patients with indeterminate scrotal masses

Normal Anatomy of the Testis and Paratesticular Structures

Scrotum

The normal scrotal wall thickness varies between 2 and 8 mm. The scrotal wall contains the following structures: rugated skin, superficial fascia, dartos muscle, external spermatic fascia, cremasteric fascia, and internal spermatic fascia. The scrotum is separated into right and left hemiscrotal compartments by a septum termed the median raphe. As the testis descends *in utero* from the abdomen, it acquires each layer of the scrotal compartment. The external spermatic fascia is derived from the external oblique fascia and is attached to the external inguinal ring. The cremasteric fascia and muscle derive from the internal oblique muscle. Encasing each testis is the tunica vaginalis, derived from the peritoneum, which consists of parietal and visceral layers. These layers are normally separated by 2–3 mL of straw colored fluid often referred to as a physiologic hydrocele. Ultrasound of this fluid is seen as a thin echo free rim around the head of the epididymis [5] (Fig. 6.10). The parietal and visceral layers join at the posterolateral aspect of the testes where the tunica attaches to the scrotal wall [6].

Testis

The size and shape of the testis changes with the age, influenced by gonadotropic hormones testicular volume gradually rises from birth to up to 5 months of age due to peak in gonadotropic hormones levels [7, 8]. After 5 months of age, the testicular volume steadily declines and

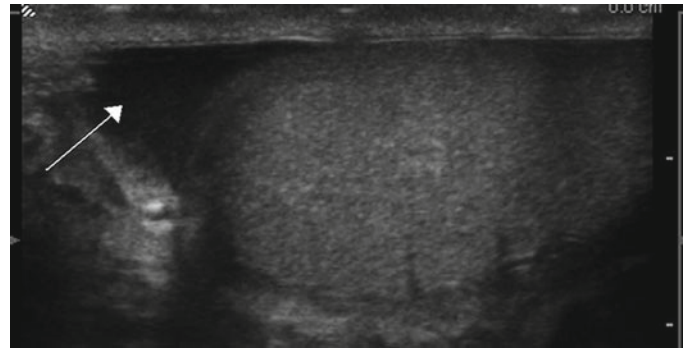

Fig. 6.10 Gray scale ultrasound showing physiologic hydrocele (*arrow*)

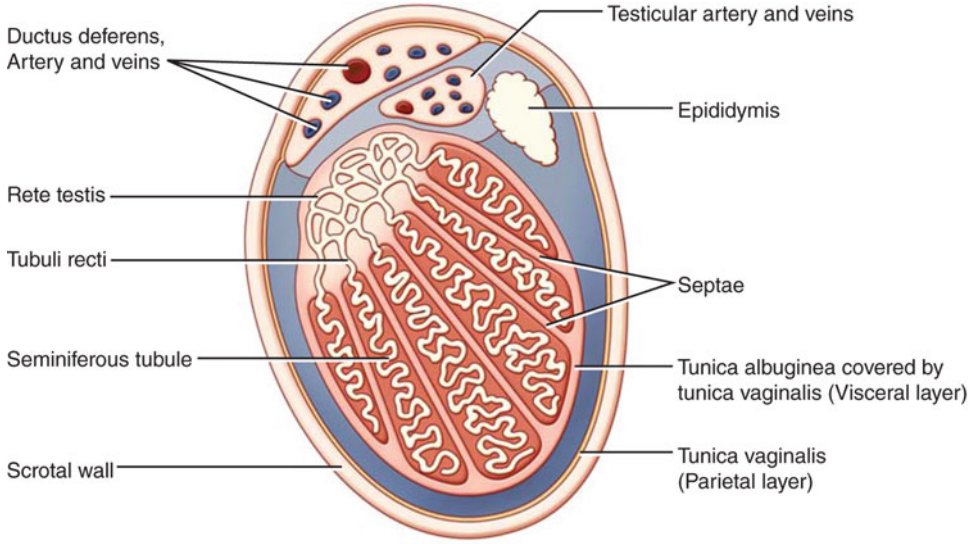

Fig. 6.11 Schematic cross section of the testis

reaches its minimum volume at approximately 9 months of age and remains approximately the same size until puberty [9]. In newborns, the testis is round and gradually becomes ovoid with growth. The echogenicity of the testis increases in puberty due to the development of germ cell elements [10]. The adult testis is a smooth ovoid gland, approximately 4–5 cm long, 3 cm wide, 2–3 cm in the anterior–posterior (AP) dimension, and typically between 20 and 30 mL in volume.

The testis exhibits medium homogenous echogenicity. A dense fibrous capsule the tunica albuginea envelops the testis, which is apparent as a thin echogenic line on ultrasound. Each testis has approximately 200–300 cone-shaped lobules each containing at least one seminiferous tubule [11] (Fig. 6.11). The lobules are separated by the fibrous septa of tunica albuginea that extend from the mediastinum of the testis in to the parenchyma of the testis [12]. Testicular lobules are occasionally identified on ultrasound as lines radiating from the mediastinum testis (Fig. 6.12). The seminiferous tubules contained within the lobules open into dilated spaces called rete testis within the mediastinum. The seminiferous tubules are long V-shaped tubules, both ends of which usually terminate in the rete testis. The rete testis is connected to the head (caput or globus major) of the epididymis with about 8–12 efferent ductules. The normal rete testis is sonographically evident in 18 % of patients as a hypoechoic area with a

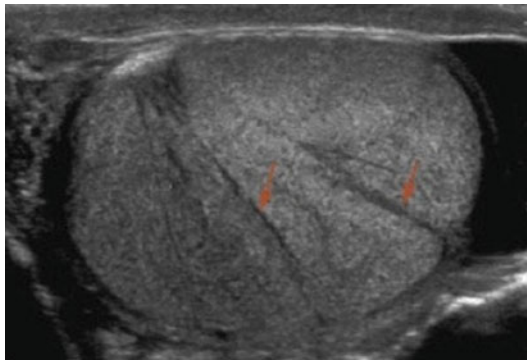

Fig. 6.12 Gray scale ultrasound of a normal testis demonstrating testicular lobules separated by fibrous septa (*arrows*)

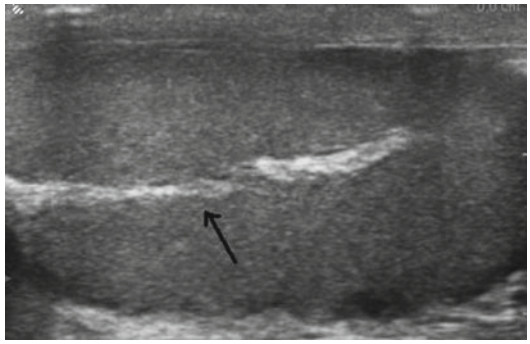

Fig. 6.13 The mediastinum testis appears as an avascular echogenic line (*arrow*)

striated configuration adjacent to the mediastinum testes [13]. The mediastinum testes appear as a linear avascular echogenic band on ultrasonography [14] (Fig. 6.13).

Epididymis

The adult epididymis is 6–7 cm long and has three parts, the head (caput) measuring 10–12 mm in diameter, the body (corpus) measuring 2–4 mm in diameter, and the tail (cauda) about 2–5 mm in diameter. In the normal epididymis, the head is routinely identified at posterolateral to the upper pole of the testis. The caput epididymis is triangular in shape, often has the same echogenicity as the testis (Fig. 6.14). However, it can be heterogenous with areas that are hyper or hypoechogenic. The smaller corpus epididymis can be seen as a

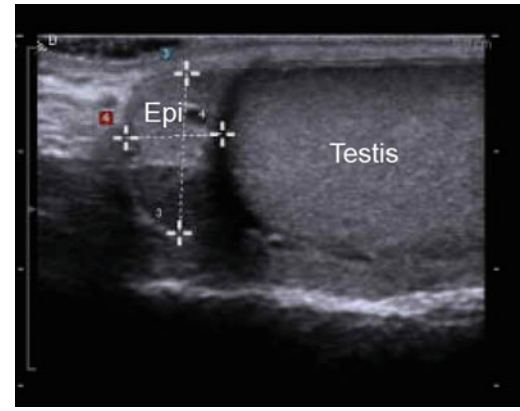

Fig. 6.14 The caput epididymis is triangular in shape (E) and is usually isoechoic or slightly hypoechoic compared to the testis

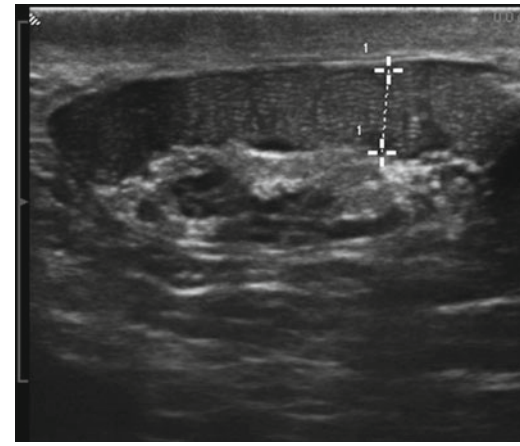

Fig. 6.15 Gray scale image of a dilated corpus epididymis in a vasectomized man

hypoechoic structure containing multiple echogenic linear structures representing the coiled epididymal tubule and lies posteriorly along the long axis of the testis (Fig. 6.15).

Vascular Anatomy

The spermatic cord is normally seen superior to the posteromedial aspect of the testis and contains the vas deferens, the testicular and cremasteric and deferential arteries, the pampiniform plexus of veins, genital branch of the genital femoral nerve, testicular plexus of the sympathetic trunk, and lymphatic vessels [12]. The blood supply to the

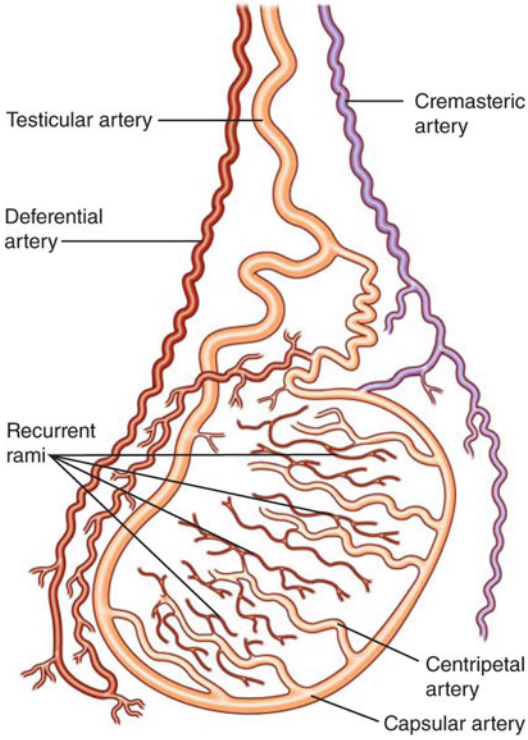

Fig. 6.16 Blood supply of testis. The testis is supplied by three sources of blood supply. (1) The testicular artery, which arises from the aorta. (2) The deferential artery, which arises from the superior vesical artery. (3) The cremasteric artery, a branch of the inferior epigastric artery

scrotal structures is from three primary arteries: the testicular, deferential, and cremasteric arteries (Fig. 6.16). The testicular artery testis or gonadal artery, which arises from the aorta and courses through the scrotum with the spermatic cord, is the major supply to the testis. The deferential artery, which arises from the superior vesical artery and supplies the vas deferens and epididymis. The cremasteric artery, a branch of the inferior epigastric artery, which supplies the scrotal skin and coverings of the spermatic cord. As the testicular artery approaches the posterolateral aspect of the testis it divides. The branches pierce through the tunica albuginea to run in a layer called the tunica vasculosa. Capsular arteries run peripherally in the tunica vasculosa, supplying centripetal arteries that course toward the mediastinum and divide further to recurrent rami that flow away from the mediastinum [14]. The veins draining the testis and epididymis converge to form the pampiniform plexus at the mediastinum on the superior pole of the testis. The pampiniform plexus is primarily drained by the testicular and external pudendal veins [15]. The testicular vein on the left drains into the renal vein and the testicular vein on the right directly into the inferior vena cava [16].

Ultrasonography with Color-Flow imaging provides visualization of the intratesticular, epididymal, and paratesticular blood flow. Under normal conditions, Color Flow images show equivalent vascularity of the bilateral testis. When vascularity is not well visualized, Power Doppler increases the sensitivity of detection. Spectral Doppler is used to calculate the Resistive Index (RI) of intratesticular arteries. The RI of intratesticular arteries has been found to correlate with testicular function.

Embryology Relevant to Ultrasound Imaging of the Scrotum

A basic understanding of the embryologic development male gonad and adnexal structures guide the interpretation of many abnormalities encountered in the scrotal ultrasound. Presented in this section is the embryology relevant to the ultrasound evaluation of the scrotum. There are many excellent textbooks available which present the known elements of male genitourinary development should the reader desire a more comprehensive treatise on the subject [17–20].

Early Gonadal Developmental Anatomy

In the 3-week-old embryo (Fig. 6.17), primordial germ cells, originating in the wall of the yolk sac near the attachment of the allantois, migrate along the wall of the hindgut and through the dorsal mesentery into the urogenital ridge. The urogenital ridge is a protrusion of intermediate mesoderm that indents the coelomic cavity (precursor to the peritoneal cavity) on each side of the mesentery. The kidney precursors, gonads, and the proximal portions of the reproductive

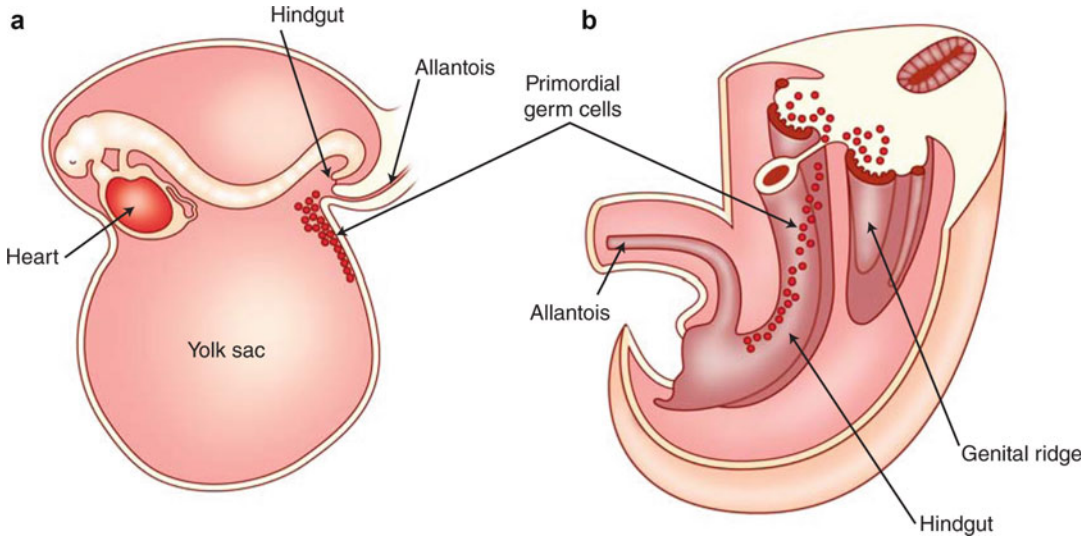

Fig. 6.17 Primordial germ cells at their location in yolk sac as they begin their migration (**a**). The primordial germ cells migrating through the mesentery to the genital portion of the urogenital ridge bulging into the coelomic cavity (**b**)

tracts develop from the urogenital ridge. The unilateral absence of the male reproductive ducts or gonad and reproductive ducts is associated with ipsilateral absence of the kidney in 20–85 % of cases [21]. It is therefore reasonable to evaluate the retroperitoneum for the presence of a kidney in a patient where the unilateral reproductive ducts are absent on ultrasound evaluation.

In the 5-week-old embryo (Fig. 6.18), the two early excretory organ systems (the pronephros and mesonephros) begin to regress. The mesonephros constitutes the lateral portion of the urogenital ridge and consists of mesonephric tubules that interact with glomeruli-like vessels extending from the aorta at one end and drain into a mesonephric duct at the other end. The regression begins at the cranial aspects and continues toward the caudal end where the duct joins the cloaca (and at what will eventually diverge from the cloaca into the urogenital sinus). The ureteric bud (also referred to as the metanephric diverticulum) develops as a dorsal bud of the mesonephric duct near its insertion into the cloaca. The metanephros (precursor to the adult kidney) forms from the interaction of the metanephric diverticulum and a region of cells in the intermediate mesoderm known as the metanephric cell mass.

At 7 weeks (Fig. 6.19), the reproductive ducts of embryo remain devoid of phenotypic manifestations of sexual differentiation. There are two, roughly parallel pairs of genital ducts: in addition to the mesonephric (Wolffian) ducts there are the paramesonephric (Müllerian) ducts, which are located more laterally. Along the medial portion of the urogenital ridge, cords of coelomic epithelium termed sex cords have invaginated in to the ridge and house the primordial germ cells. This portion of the urogenital ridge becomes the gonadal ridge and the most superficial aspects of the sex cords regress to completely separate the sex cords from the rest of the coelomic epithelium.

It is the presence of a Y chromosome gene, called the sex-determining region Y gene (SRY), that results in the development of testes and the initiation of phenotypic sexual differentiation. The testis forms in the gonadal ridge and Sertoli cells differentiate from cells within the epithelial sex cords. By week 8, the developing fetal testis produces at least two hormones. The first has been referred to as Müllerian-inhibiting substance or factor (MIS, MIF) and, in other reports, as anti-Müllerian hormone (AMH). It is produced by the fetal Sertoli cells and suppresses the development of the paramesonephric duct (which in

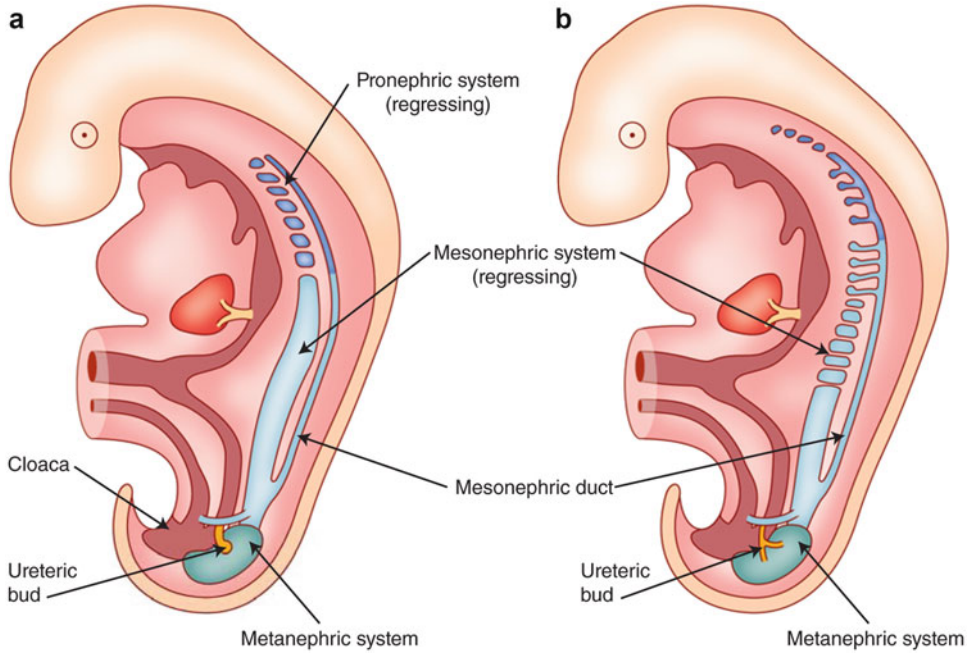

Fig. 6.18 Development of the early excretory system. Regression of the pronephros (**a**) and mesonephros (**b**) with the development of the metanephric system

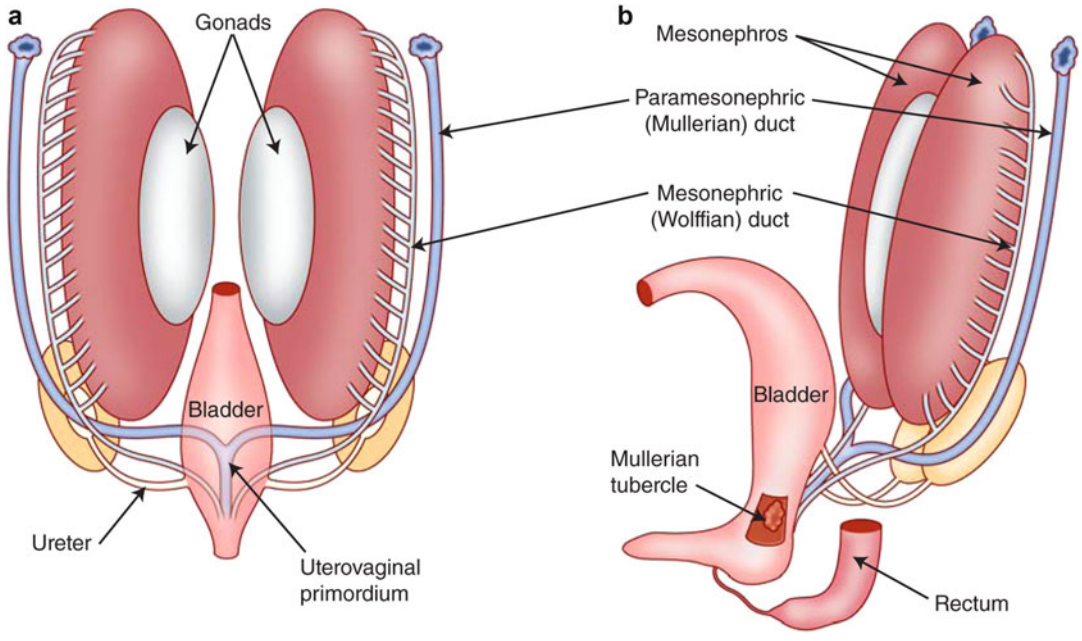

Fig. 6.19 The reproductive ducts and their relationship to the developing gonads after the incorporation of the distal mesonephric ducts into the urogenital sinus

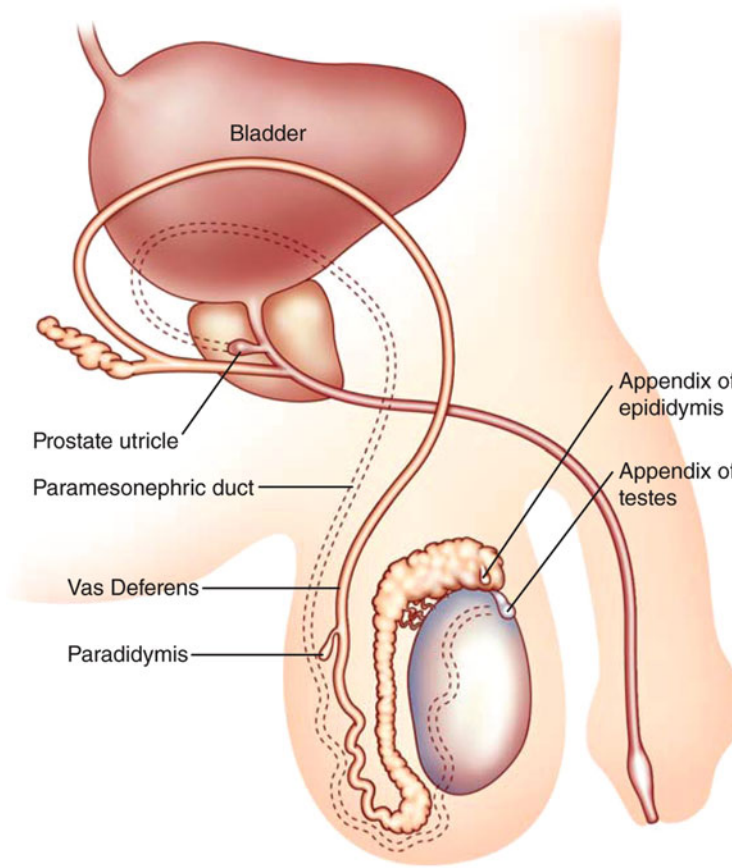

Fig. 6.20 Schematic showing the most frequent location of testicular and epididymal appendages and other vestigial remnants of the mesonephric and paramesonephric ducts in the male genitalia

the absence of this suppression would develop into the upper female reproductive tract organs). The other, testosterone, stimulates development of the mesonephric ducts into components of the male genital tract. Vestigial remnants of portions of these ducts (Fig. 6.20) often can be visualized sonographically.

Remnants of the most cranial aspects of the regressed paramesonephric ducts can persist beyond the embryologic period as the appendix of the testis in and be demonstrated on ultrasound (Fig. 6.21). The most caudal vestiges of the paramesonephric ducts form midline structures and are often found in the prostate, which is derived from the embryonic urogenital sinus. The prostatic utricle is such a structure and when enlarged, be demonstrated on ultrasound. In addition, midline cysts derived from vestiges of the paramesonephric ducts may also be demonstrated. These midline paramesonephric remnants have also been found to obstruct the ejaculatory ducts and result in dilation of the seminal vesicles (anterior–posterior distance greater than 15 mm).

The deepest aspects of the sex cords converge on what will become the mediastinum testis. The mesenchyme between each of the cords gives rise to the interstitial cells of Leydig and the septa of the testis that radiate out from the mediastinum testis. The sex cords develop into tubules composted of the germ cells and Sertoli cells and the inner ends of these tubes are referred to as the tubuli recti. The gonadal ridge, throughout its development, slowly separates from the mesonephros. The mesonephric structures develop under the paracrine influence of the testosterone produced in the neighboring testis. The mesonephric tubules adjacent to the testis develop into the ductuli efferentia and meet the tubuli recti at the rete testis. The mesonephric ducts develop into the epididymides, vasa deferentia, and ejaculatory ducts. The seminal vesicles develop as a diverticulum of this tube. Residual mesonephric structures can persist as a

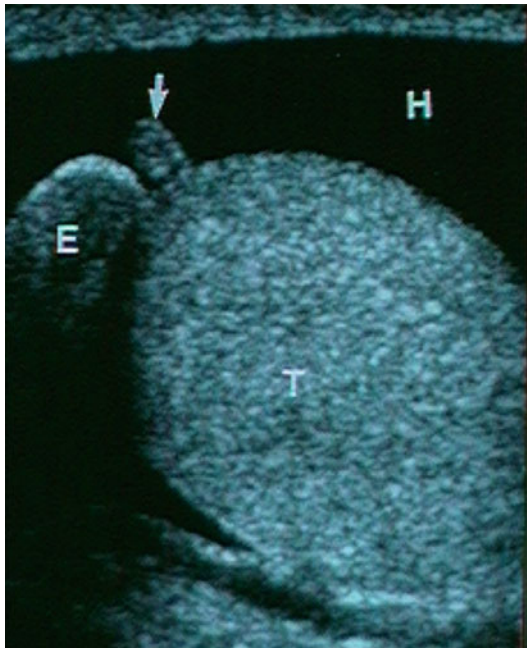

Fig. 6.21 Ultrasonic appearance of the appendix testis

vestigial remnant of the mesonephric ducts. Those tubules located cranial to the tubules that become the ductuli efferentia of the testis may protrude off the epididymis as a polypoid vestige called the appendix epididymis (Fig. 6.22). In addition, remnant mesonephric tubules can persist proximal to those draining the testicle as well. This remnant is known as the paradidymis (aka organ of Giraldés), a small collection of convoluted tubules lined by ciliated epithelium, that can be found anywhere along the epididymis or vas deferens.

Torsion of the appendix testis, appendix epididymis, and paradidymis are all in the differential diagnosis of the acute scrotum. The appendix testis, appendix epididymis, and ectasia of the rete tubules can be visualized during the scrotal ultrasound and their characteristic appearance should be kept in mind to avoid confusion of these structures with testicular and extratesticular masses.

Testicular Descent

The process of testicular descent begins prior to 7 or 8 weeks in development. At this time, the gonadal position in the dorsal abdominal wall is

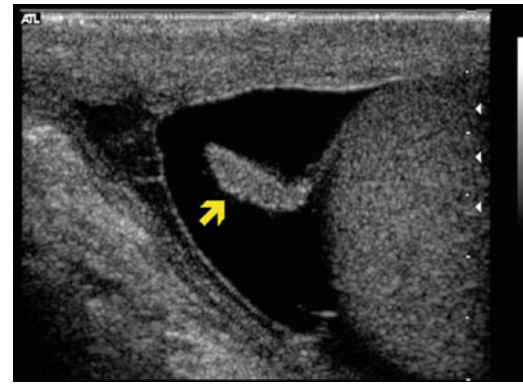

Fig. 6.22 Ultrasonic image of the caput epididymis with adjacent appendix epididymis

similar in both sexes. In males, the fetal testis begins to produce MIS from the Sertoli cells. In addition, androgens and an insulin-like hormone 3 (INSL3) are produced from the Leydig cells [22]. These hormones work in concert to control descent of the testis, which is held by a suspensory ligament at the upper pole, and, at the lower pole by the genito-inguinal ligament, or "gubernaculum."

During the initial phase of descent, the cranial suspensory ligament progresses and the gubernaculum thickens allowing the testis to be held near the inguinal region as the abdomen enlarges. The inguinal canal forms as the abdominal wall muscles develop around the thickened gubernaculum.

The subsequent phase of descent occurs several weeks later. At about 20–25 weeks an outpouching of the peritoneal membrane, which is known as the processus vaginalis, travels with the testis toward its final position in the scrotum. The processus vaginalis maintains a connection with both the epididymal tail and the lower pole of the testis. At about 25 weeks, testis and attached processus vaginalis begin to pass through the inguinal canal along with fascial coverings from the abdominal wall (Fig. 6.23). The processus vaginalis is continuous with the peritoneum and tunica vaginalis of the testis. Between 25 and 30 weeks the testis descends rapidly through the inguinal canal and then more slowly across the pubis into the scrotum. The fascial coverings from the abdominal wall that travel

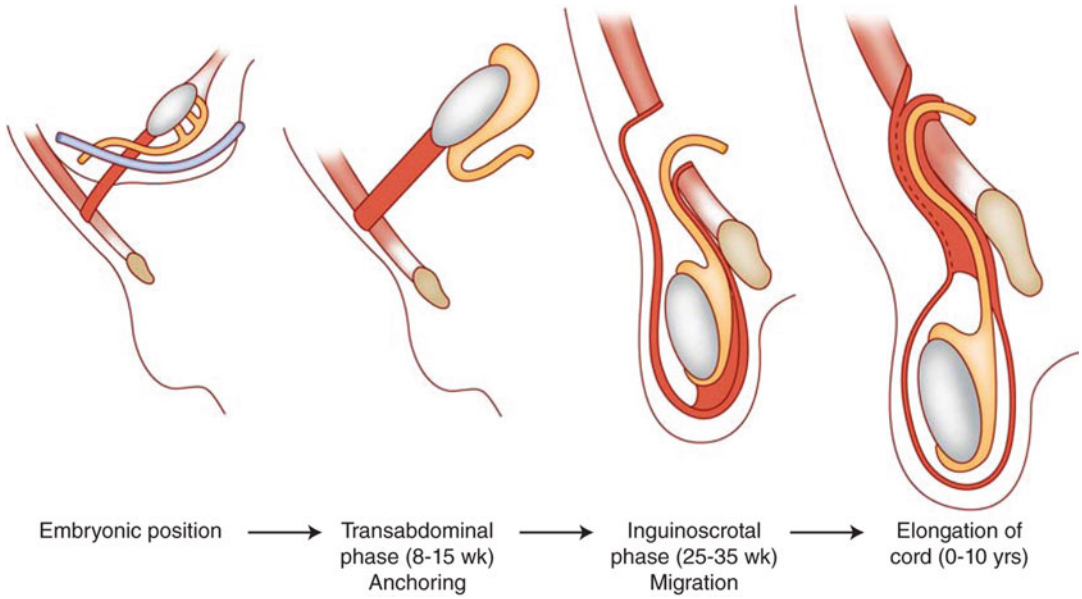

Fig. 6.23 The phases of testicular descent. At about 25 weeks, testis and attached processus vaginalis begin to pass through the inguinal canal along with fascial coverings from the abdominal wall

with the testis during its descent become the layers covering the spermatic cord and testis. This process is usually completed by 35 weeks of gestation and it is followed by the obliteration of the proximal portion of the processus vaginalis to close the connection between the scrotum and peritoneum. Closure may occur during prenatal development or in early infancy. The gubernaculum does not become anchored to the scrotum until descent is completed [23–25].

The embryology of testicular descent becomes important for the sonographer when evaluating the undescended or nonpalpable testis. A majority of undescended testes are found in the inguinal canal which is accessible to diagnostic ultrasound [26–29]. Ultrasound examination of the inguinal region is essential when a testis is not found on routine scrotal ultrasound.

Development of the Scrotum

The embryonic precursor to the scrotum is the labioscrotal folds. These structures originate as the embryonic cloaca develops and differentiates. The cloaca is a chamber shared by the allantois (which extends anteriorly from the cloaca into the umbilical cord) and the hindgut (Fig. 6.18a). The cloacal membrane makes up the ventral wall of the chamber and is located at the caudal end of the developing hindgut as a bilaminar apposition of ectoderm and endoderm located on the ventral midline. A septum develops as an ingrowth of folds from the lateral walls and a caudal extension of the intervening mesenchyme from the branch point of the allantois and hindgut, which ultimately divides the cloaca into the anterior/ventral urogenital sinus and the posterior/dorsal developing rectum. While the septum develops, mesodermal mesenchyme also encroaches between the two layers of the cloacal membrane. The septum also divides the membrane into a urogenital membrane and anal membrane. Both of these membranes ultimately rupture to create continuity between the ectoderm and both the urogenital sinus and rectum that will persist as the urethral meatus and anus. The mesenchymal tissues that have encroached around these orifices develop into the muscles and bones of the lower anterior abdomen and pubis.

The urethra prostate and bladder all develop from the urogenital sinus. The remnants of the caudal ends of the mesonephric ducts become incorporated into the urogenital sinus (Mullerian Tubercle, Fig. 6.19) and become aspects of the trigone and posterior urethra. The incorporated portions of the mesonephric ducts include the branch points of the metanephric ducts, which become the ureteral orifices. The unincorporated portions of the mesonephric ducts end up entering the urethra at the prostatic urethra as the ejaculatory ducts which channel the path of the testicular adnexal structures into the prostatic urethra.

The external male genitalia are indistinguishable from the female external genitalia until the eighth or ninth week of gestational. They both include the genital tubercles at the craniolateral edges of the cloacal membrane. The tubercles develop from mesoderm as it infiltrates the cloacal membrane. As the cloacal membrane divides to separate its anterior portion into the urogenital membrane, the tubercles fuse in the midline. The urogenital membranes and ultimately the urogenital sinus are flanked by collections of infiltrating mesoderm termed the urogenital folds with labioscrotal swellings located laterally on either side (Fig. 6.24). Masculinization of the indifferent external genitalia occurs under the endocrine influence of testosterone produced by the interstial Leydig cells of the fetal testis [30–32]. The tubercle becomes the future phallus and glans. The scrotum is formed by extension of the labioscrotal swellings between the pelvic portion and the anus. With testicular decent and migration of the gubernaculum into these labioscrotal swellings during the second phase of testicular descent, the scrotal sac takes shape around the testes and associated structures. The scrotal skin will ultimately become the point of contact with the ultrasonographer's transducer and the window into which clinical questions about the scrotal contents can be explored.

Pathologic Conditions and the Scrotal Ultrasound

Extratesticular Findings

Hydrocele

Hydrocele is the most common cause of painless scrotal swelling. A hydrocele is a serous fluid collection between the parietal and visceral layers of the tunica vaginalis. The tunica vaginalis is a mesothelium-lined sac that results from closure of the superior portion of the processus vaginalis. This fascial structure normally covers the entire testis except the posterior border. It has a visceral layer and an outer parietal layer that lines the internal spermatic fascia of the scrotal wall. Hydroceles can be congenital or acquired. The congenital hydrocele or communicating hydrocele occurs when a patent processus vaginalis allows fluid to pass from the peritoneal space into the scrotum [33]. The acquired hydrocele may be idiopathic with no identifiable cause. The incidence of hydroceles is about 1 % of adult males. Hydroceles are usually anechoic on ultrasonography (Fig. 6.25). They may contain echogenic cholesterol crystals. The presence of septations is often associated with infection, trauma, or metastatic disease. Hydrocele may develop secondary to venous or lymphatic obstruction caused by infection, trauma, torsion, or tumor. About 10 % of testicular tumors are accompanied by a hydrocele; clinical suspicion increases with new onset of hydrocele in men in their 30s or 40s [34]. Scrotal ultrasound is essential to rule out testicular pathology in these patients. The testis is often posteriorly displaced by the hydrocele. A massive hydrocele exerts a pressure effect that may compromise blood flow within the testis. Vascular resistance in intratesticular arteries is increased, and color Doppler ultrasound may demonstrate an increase in the caliber of capsular arteries. Fluid aspiration and surgical excision of hydrocele sac has been shown to restore normal blood flow to the testis [35].

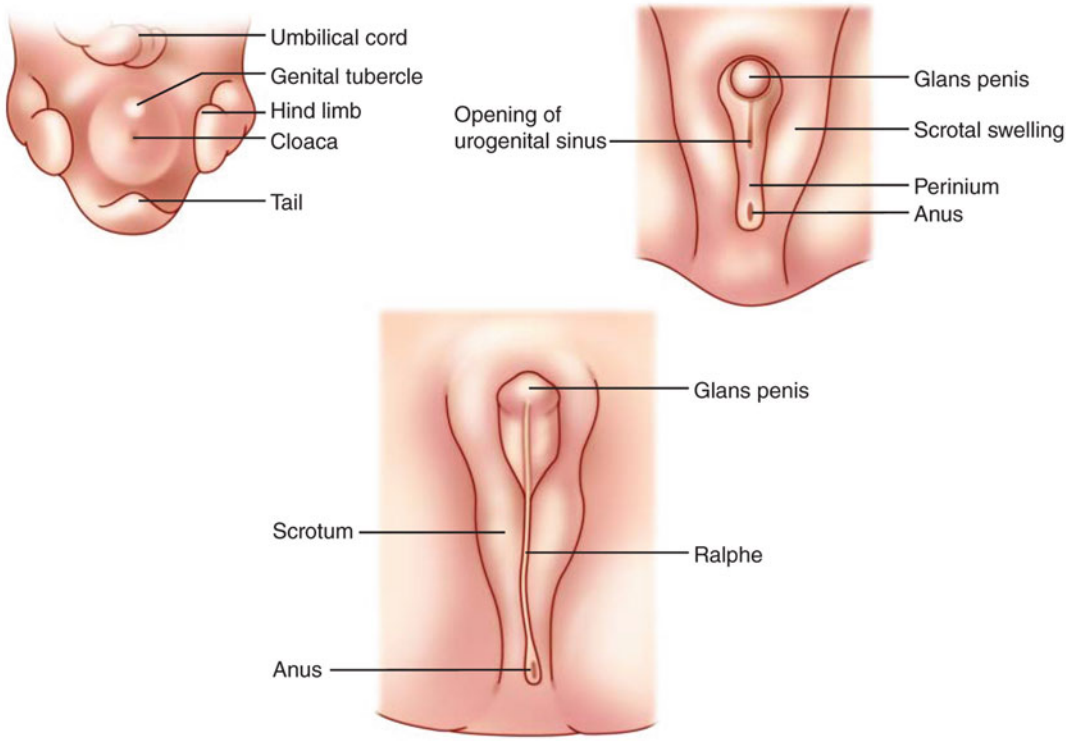

Fig. 6.24 The male external genital development progressing clockwise from the left. The genital tubercle develops into the glans penis. The *upper right panel* shows the urogenital sinus opening within the urogenital folds, which are between the scrotal swellings

Pyocele

Pyocele is an accumulation of purulent material within the tunica vaginalis and is most often occurring because of untreated epididymo-orchitis. Pyoceles present with acute scrotal pain and symptoms of sepsis. A pyocele also appears heterogeneous on the ultrasonogram, and gas may be identified, causing hyperechoic reflections and shadowing [36] (Fig. 6.26).

Scrotal Hernia

Congenital inguinal hernia is due to failure of the processus vaginalis to obliterate and result in passage of intestinal loops or omentum or peritoneal fluid in the scrotal sac [12, 37, 38]. Right inguinal hernias are more common as the right processus vaginalis closes later. Scrotal ultrasound can be helpful for inconclusive physical examination. Clinically occult contralateral hernia can also be assessed with the ultrasound [39]. Patients with a scrotal hernia usually present with mesenteric fat and/or bowel loops seen superior to the testis. Real-time imaging can identify peristaltic activity or intestinal gas bubbles with their characteristic echogenic interfaces. Ultrasound of an omental hernia will demonstrate highly echogenic fat [40] (Figs. 6.27a, b and 6.28).

Sperm Granuloma

Spermatazoa are highly antigenic, and an intense inflammatory reaction occurs when they exit the vas difference [40]. Sperm granulomas occur in at least 40 % of men following a vasectomy [41] (Fig. 6.29). Sperm granulomas are rarely symptomatic. However, 2–3 % of vasectomy patients will have pain attributed to sperm granulomas, usually occurring 2–3 weeks postoperatively [42].

Tumors of the Spermatic Cord

Lipomas of the spermatic cord are very common benign lesions of the spermatic card. They can be unilateral or bilateral, and often present as

asymptomatic fullness of the spermatic cord. Ultrasound of a lipoma demonstrates homogeneous echogenicity similar to subcutaneous fat without internal color flow. The echogenicity of lipomas may be variable, and MRI may be helpful to confirm diagnosis, showing nonenhancing, fat saturated areas [43]. It is also important to differentiate a lipoma from an inguinal hernia by noting the intact external inguinal ring on physical examination and assessing for the presence of a hernia on ultrasound.

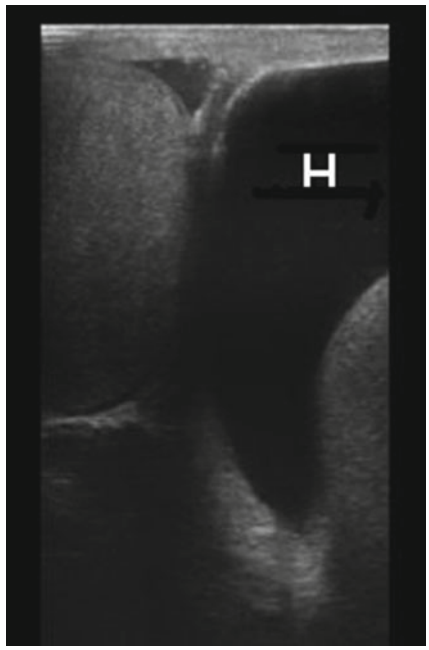

Fig. 6.25 Gray scale ultrasound showing a left hydrocele (H)

Rhabdomyosarcomas of the spermatic cord is a malignant lesion in children, and **liposarcoma** is the most common malignant tumor arising in the spermatic cord in adults, although both are rare. **Leiomyosarcomas** in the paratesticular space also have been reported. The ultrasound appearance of these lesions is an ill-defined solid mass with heterogeneous echotexture and increased vascular flow on Doppler color study (Fig. 6.30).

Epididymal Findings

Epididymo-Orchitis

Epididymitis is the most common cause of subacute unilateral scrotal pain in preadolescent and adolescent boys and adult men. On physical exam the epididymis can often be identified as an enlarged and tender structure posterolateral to the

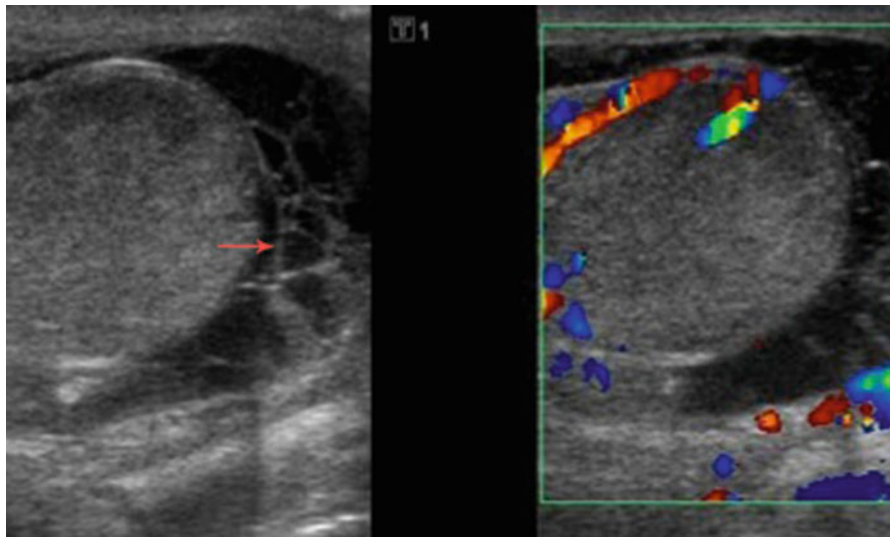

Fig. 6.26 A pyocele is seen as a complex heterogeneous fluid collection within the tunica vaginalis on gray scale ultrasound and without blood flow on Doppler study

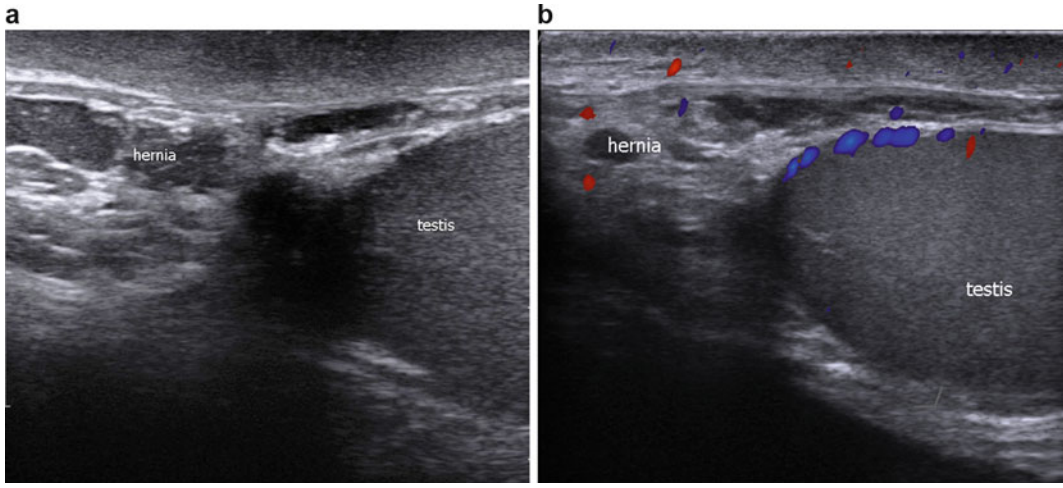

Fig. 6.27 (**a**) Gray scale ultrasound showing the highly echogenic omental fat of an omental hernia. (**b**) Color Doppler study showing no increased blood flow to the inguinal hernia

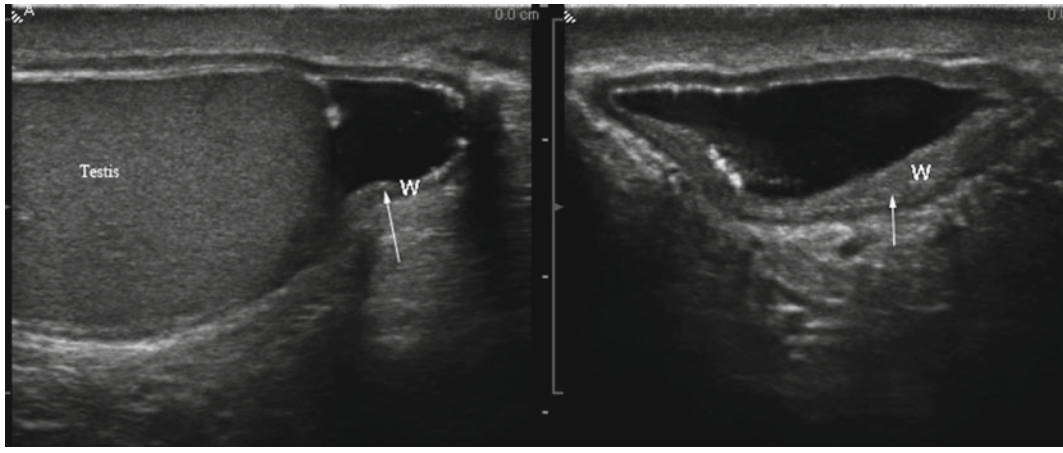

Fig. 6.28 Gray scale ultrasound showing thickened hernia sac (W) in chronic inguinal hernia (*arrows*)

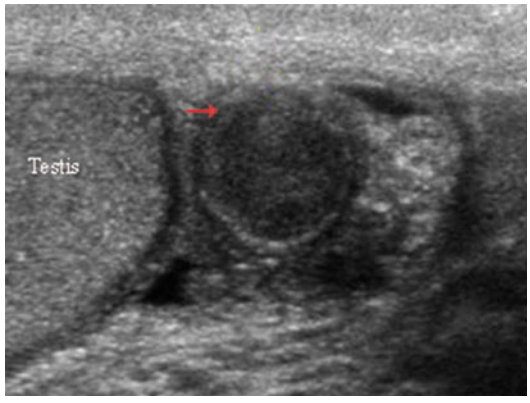

Fig. 6.29 Gray scale ultrasound showing a sperm granuloma (*red arrow*)

testis. The pain is often relieved with elevation of the testis over the symphysis pubis, known as Prehn's sign. Among sexually active men younger than 35 years old, epididymitis often results from sexually transmitted infections, particularly *Chlamydia trachomatis* and *Neisseria gonorrhoeae*. In older men, bacterial epididymitis can result from retrograde transit of bacteria from the vasa, and therefore the most common organisms are urinary pathogens: *Escherichia coli* and *Proteus mirabilis*. Rare infectious causes include brucellosis, tuberculosis, cryptococcus, syphilis, and mumps. Epididymitis in prepubertal boys normally has a benign course, and these boys

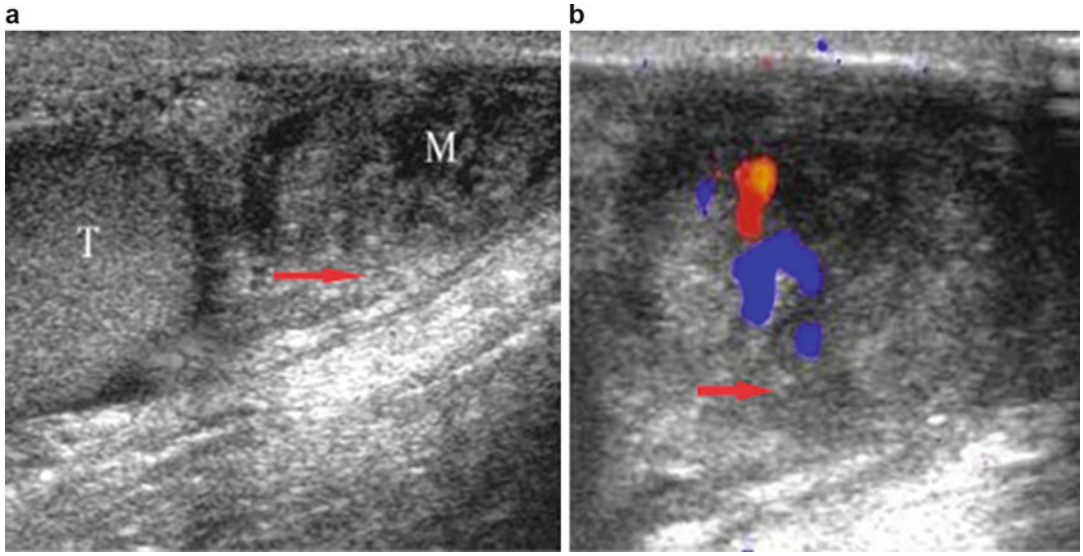

Fig. 6.30 Leiomyosarcoma of the scrotum: (**a**) Gray scale ultrasound appearance as an ill-defined solid mass with heterogeneous echotexture in the paratesticular space (*M* mass, *T* Testis). (**b**) Doppler color flow shows increased vascularity with in the mass

commonly are found to have positive titers for enteroviruses and adenoviruses and M. pneumonia. Rare noninfectious causes include sarcoidosis and amiodarone. Blunt trauma as well as congestion following vasectomy is potential cause of epididymal inflammation [44, 45].

In patients with acute epididymitis, the epididymis is enlarged with increased vascularity. Epididymitis may lead to focally or global enlargement and thickening of the epididymis. Gray scale ultrasound demonstrates a hypoechoic or heterogeneous enlarged epididymis (Fig. 6.31). The color flow Doppler shows increased vascularity with high-flow, low-resistance pattern (Fig. 6.32). A reactive hydrocele is often present. Complications of epididymitis include infectious spread to the testis resulting in epididymo-orchitis, testicular abscess formation, and testicular infarction due to obstruction of venous flow which may result in testicular atrophy. Patients with chronic epididymitis often present with persistent pain. In these men, ultrasound examination reveals an enlarged epididymis with increased echogenicity and possible areas of calcifications (Fig. 6.33).

Torsion of the Appendix Epididymis and Testis

Torsion of the appendix testis is important to differentiate from torsion of the spermatic cord (testicular torsion), as this condition is self-limiting and does not threaten testicular viability. Clinically, the cremasteric reflex is preserved and a palpable nodule with bluish discoloration (blue dot) is often detected [46]. Ultrasound shows a hyperechoic mass with central hypoechoic area adjacent to the testis or epididymis. Other associated findings include scrotal wall edema and epididymal enlargement. Blood flow in the peritesticular structures may be increased. Doppler ultrasound is helpful as blood flow within the testis is normal in torsion of the appendix testis.

Benign Epididymal Lesions

An **epidydimal cyst** is a nonpainful cystic structure that, when large, displaces the testis inferiorly. Cysts of the epididymis occur in up to 40 % of the men and contain lymphatic fluid. They are typically thin walled and well defined, usually with strong posterior acoustic enhancement and

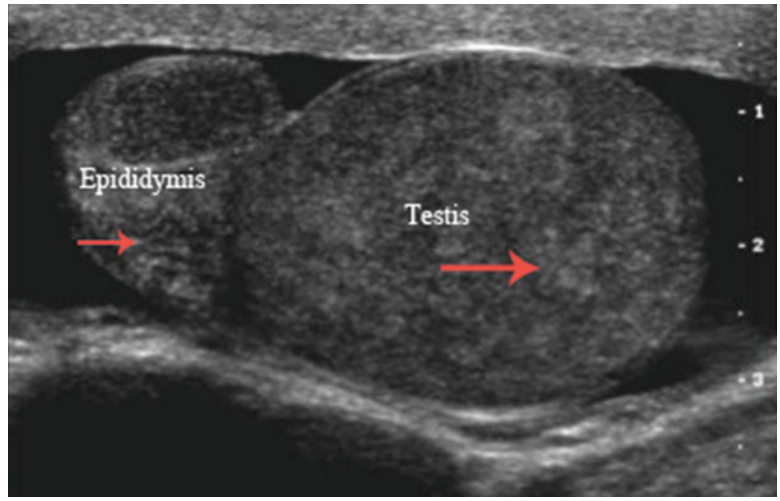

Fig. 6.31 Epididymo-orchitis: gray scale image demonstrates enlarged and heterogeneous epididymis and testis

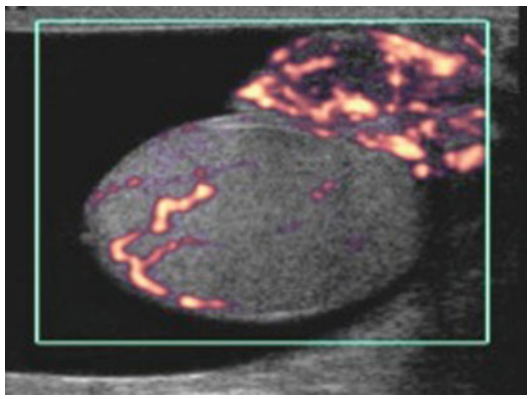

Fig. 6.32 Epididymo-orchitis: Power Doppler ultrasound showing increased vascularity of the epididymis and the testis

no internal echoes. These men will often have multiple cysts occurring present throughout the length of the epididymis.

Spermatoceles are benign cystic lesions, which contain spermatozoa, lymphocytes, and debris. Spermatoceles form as a result of efferent duct obstruction and usually located in the head of the epididymis. Ultrasonography cannot differentiate between epididymal cysts and spermatocele, but the spermatocele often has septations (Fig. 6.34).

Adenomatoid tumors are the most common tumors of the paratesticular tissues, accounting 30 % of these lesions and up to 77 % of the benign tumors arising from the epididymis. They are most commonly identified in men in their 20s to 40s. It has been suggested that they derive from vascular endothelium, the mesonephros, or müllerian epithelium, although most recent reports consider them to be mesothelial in origin [47]. They are round, firm, smooth, discrete masses measuring 0.5–5 cm in diameter that are usually asymptomatic and slow growing. Ultrasonography can confirm the extratesticular nature of these masses. Ultrasound of adenomatoid tumors reveals an isoechoic mass with increased vascularity (Fig. 6.35).

Papillary cystadenoma is a rare benign tumor of epithelial origin believed to arise from the efferent ductules of the head of the epididymis [48]. Papillary cystadenoma presents clinically as a firm, nontender palpable mass in the epididymis. Two-thirds of papillary cystadenomas occur in patients with von Hippel-Lindau (VHL) syndrome and are frequently bilateral [49]. Unilateral presentation is seen very rarely in sporadic cases. Sonographically, small papillary cystadenoma are usually solid and echogenic, but when large may appear vascular and cystic [49].

Leiomyomas are benign epididymal solid tumors. These lesions are most commonly seen in men over the age of 50. The ultrasound appearance is a well-defined solid mass with heterogeneous echotexture located in paratesticular space separate from the epididymis [50].

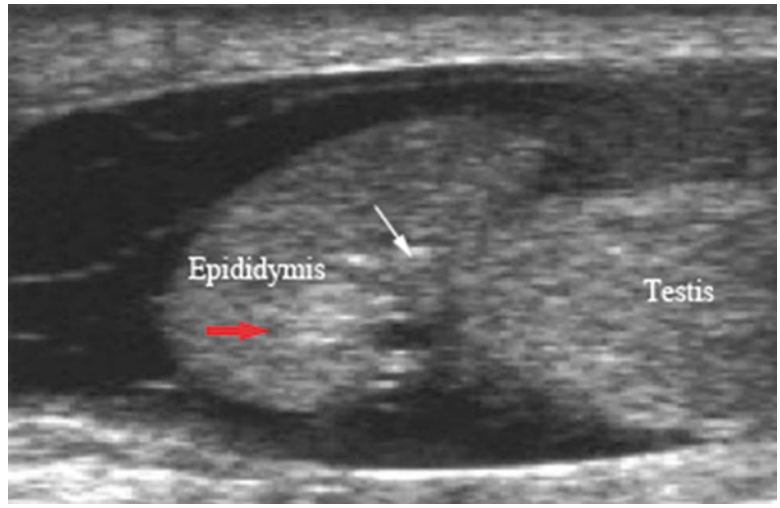

Fig. 6.33 Chronic epididymitis: Gray scale ultrasound showing increase of echogenicity and microcalcifications seen in the caput epididymis (*arrows*)

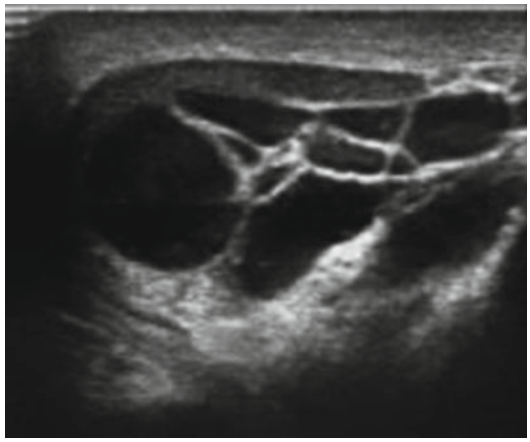

Fig. 6.34 Gray scale ultrasound showing multiple anechoic epididymal cysts

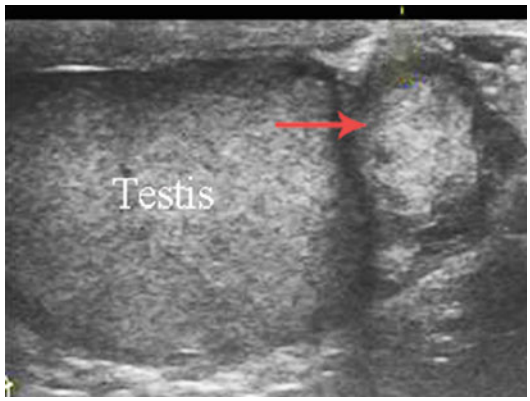

Fig. 6.35 Adenomatoid tumor seen on Gray scale imaging as an as isoechoic paratesticular mass

Malignant Epididymal Lesions

Malignant tumors arising from the epididymis are very rare, with the exact incidence of malignant tumors of the epididymis uncertain because of the small number of reported cases. **Sarcoma of the epididymis** comprises of more than half of the reported malignant neoplasms of the epididymis [51]. Fibrosarcoma of the epididymis has been reported in isolated case reports. Dowling et al. reported fibrosarcoma in a 60-year-old male confined to the epididymis on final pathology [52]. Leiomyosarcoma of the epididymis on ultrasound appears as a large hypoechoic mass (Fig. 6.36). **Clear Cell carcinoma of the Epididymis** is very rare and has been reported in individual case reports [53]. Ultrasound findings may include large cysts, necrosis, and invasive margins.

Scrotal Wall Lesions

Scrotal Infectious Findings

Patients who are diabetic or immunocompromised are more susceptible to infection and scrotal wall **cellulitis** or **abscess**. Ultrasonography demonstrates thickening of the subcutaneous tissue and heterogeneity with increased blood flow on color Doppler study. The scrotal wall abscess

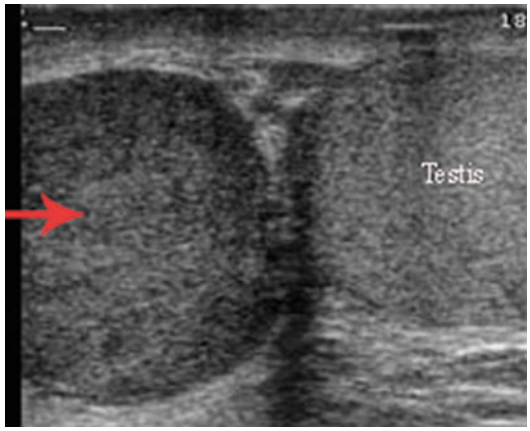

Fig. 6.36 Leiomyosarcoma of the epididymis. Gray scale ultrasound showing large hypoechoic mass in the epididymis with normal testis

appears on ultrasound as a well-defined hypoechoic lesion within the scrotal wall and no Doppler flow within the lesion [5].

Fournier's gangrene is a polymicrobial rapidly progressing necrotizing fasciitis commonly involves perineum and genital regions. Fournier's gangrene is a urologic emergency with mortality up to 50 % [54, 55]. Computer tomography remains the imaging modality of choice [56]. However, ultrasonography can provide valuable clues at the time of initial presentation. Ultrasonography shows marked thickening of the scrotal skin with multiple hyperechogenic foci associated with shadowing, which are consistent with the presence of subcutaneous gas, pathognomonic of Fournier's gangrene [57].

Benign Scrotal Lesions

Epidermoid Cysts of the Scrotal Wall

Epidermoid cysts or epidermal inclusion cysts are the most common cutaneous cysts of the scrotal wall. Epidermoid cysts result from the proliferation of epidermal cells within a circumscribed space of the dermis at the infundibulum of the hair follicle [58]. Epidermoid cysts may become infected and form scrotal wall abscess.

Henoch–Schonlein purpura (HSP) is a systemic vasculitis of unknown origin. It is characterized by a palpable skin rash, abdominal pain, and polyarthralgia. HSP has been reported to have scrotal wall swelling and ecchymosis in up to 38 % of cases [59].

Scrotal fibrous pseudotumors are uncommon and are thought to be reactive, benign lesions. The sonographic appearance of the fibrous pseudotumor of the scrotum is variable depending on the contributing fibrous tissue components, presence or absence of calcification, and the scrotal structure involved [60]. Pseudotumor of the scrotum is a benign condition and local excision of the mass is the treatment of choice; however, preoperative diagnosis is seldom made due to the nonspecific clinical and sonographic findings [61].

Acute idiopathic scrotal edema (AISE) is a self-limited disease of unknown origin. It presents with unilateral or bilateral scrotal swelling without pain and is associated with unilateral or bilateral inguinal lymphadenopathy. It is thought to be a variant of angioneurotic edema, often associated with eosinophilia. Physical examination findings include scrotal skin swelling and erythema that extends to the inguinal and perianal area. AISE is a diagnosis of exclusion. The characteristic ultrasound findings for AISE, include edema of the scrotal wall with hypervascularity and compressibility with enlargement of the inguinal lymph nodes, and normal testis and epididymis (Fig. 6.37) [62, 63].

The other noninflammatory causes of scrotal wall edema including congestive heart failure, renal failure, anasarca, hepatic failure, cirrhosis, nephrotic syndrome, and poor nutritional status. The scrotal wall appears thickened in chronic venous or lymphatic obstruction secondary to filariasis, radiation, and trauma or surgery. Ultrasound demonstrates scrotal wall thickness with layers of alternating hypo and hyperechogenicity [64, 65].

Malignant Scrotal Lesions

Squamous cell carcinoma (SCC) of the scrotum is an uncommon neoplasm. SCC is associated with occupational exposure to chemical or oil industries, radiation, chimney sweepers, human papilloma virus, chronic scar, and immune-related conditions such as psoriasis [66]. The literature concerning scrotal SCC is limited. Ultrasound evaluation of these lesions is not well defined.

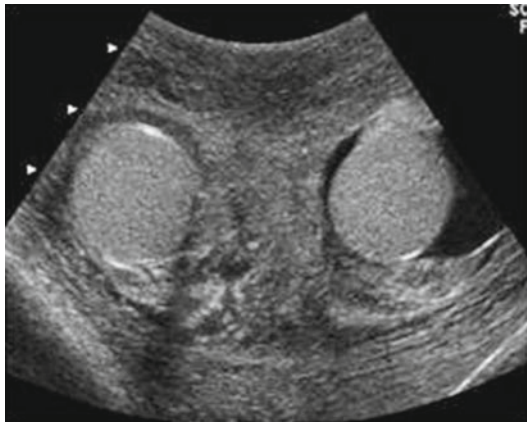

Fig. 6.37 Gray scale ultrasound showing diffuse scrotal wall thickening in a patient with scrotal wall edema

Testicular Pathology

Nonmalignant Abnormalities of the Testis

Torsion of the Spermatic Cord or Testicular Torsion

Ultrasound is often used to assess boys and adolescents with acute scrotal pain when the urologist is concerned for testicular torsion. Testicular torsion can be classified as extravaginal or intravaginal. The extravaginal form of torsion is found exclusively in newborn infants. Intravaginal torsion is more common and is due to a bell-and-clapper deformity in which the tunica vaginalis has an abnormally high insertion on the spermatic cord and completely encircles the testis, leaving the testis free to rotate within the tunica vaginalis. The deformity is bilateral in most cases. Intravaginal testicular torsion occurs most frequently in adolescent boys, with two-thirds of cases occurring between 12 and 18 years of age. Intravaginal torsion may occur in testes that are retractile or are not fully descended. Blunt trauma, sudden forceful rotation of the body, or sudden exertion also predispose to testicular torsion.

Ultrasound is very effective in differentiating testicular torsion from other causes of acute scrotal pain. The severity of torsion of the testis can range from 180° to 720°, but complete occlusion of blood flow is thought to occur after 450° of torsion [12]. Transient or intermittent torsion with spontaneous resolution sometimes occurs. Venous congestion or occlusion progresses to arterial occlusion, testicular ischemia, and infarction. The collateral blood flow is typically not adequate to provide viability to the testicle if the testicular artery is occluded. There is a 90 % chance of salvaging the testicle when ischemia has been present for less than 6 h, which decreases to 50 % at 12 h and 10 % at 24 h [67]. While irreversible testicular damage is presumed after 4 h of torsion, only 50 % of men who were detorsed less than 4 h after their symptoms began were noted to have normal semen quality [68].

On gray scale ultrasound, the affected testis usually appears hypoechoic (Fig. 6.38a) and Doppler color flow study shows decreased or no flow in the affected testis (Fig. 6.38b). Testicular size can vary from increased to decreased when compared to its counterpart depends upon the duration of the torsion. The sonographer should always compare the affected testis with the contralateral side using longitudinal, transverse, and coronal views. When the sonographer attempts to align the transducer parallel to flow, apical views can be particularly informative. In patients with acute torsion, the epididymis may appear hypoechoic and enlarged, similar to epididymitis. With testicular torsion ultrasound may also demonstrate that the spermatic cord immediately cranial to the testis and epididymis is twisted, which gives it a characteristic 'torsion knot' or 'whirlpool appearance' (Fig. 6.39a, b).

Acute unilateral scrotal pain may be of a nonemergent etiology, due to epididymitis or torsion of a testicular or epididymal appendage. Waldert et al. retrospectively reviewed the charts of 298 boys who presented with an acute scrotum and underwent color Doppler ultrasonography followed by exploratory surgery, regardless of the sonographic findings. Twenty percent were diagnosed with testicular torsion, 56 % with torsion of an appendage, 8 % with epididymitis, and 11 % with no definite diagnosis. Color Doppler sonography sensitivity, specificity, positive predictive value, and negative predictive value for testicular torsion were 96.8 %, 97.9 %, 92.1 %, and 99.1 %, respectively. The two boys in

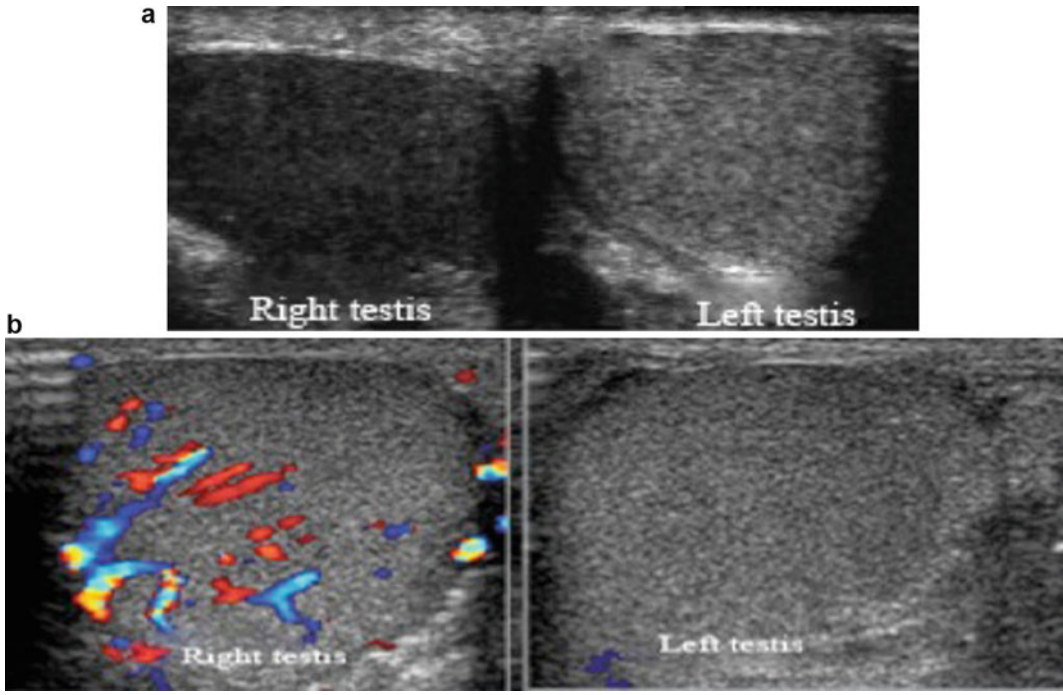

Fig. 6.38 (**a**) Right testicular torsion with normal left testis for comparison. The torsed testis has decreased echogenicity on gray scale ultrasonogram compared to the contralateral healthy testis. (**b**) Color Doppler ultrasound shows absent blood flow in the left testis with testicular torsion and normal flow in the healthy right testis

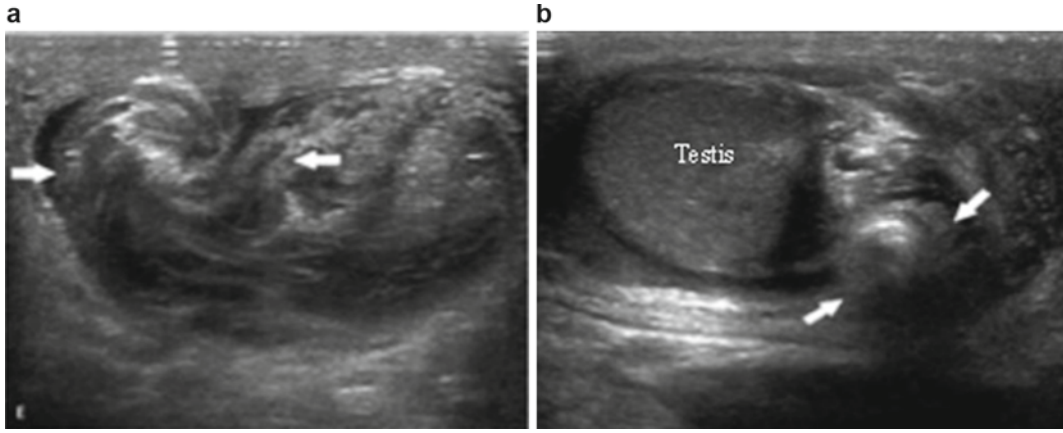

Fig. 6.39 (**a**, **b**) The spermatic cord immediately cranial to the testis and epididymis is twisted, which gives it a characteristic 'torsion knot' or 'whirlpool appearance' on gray scale ultrasound

this study misdiagnosed as epididymo-orchitis were both found to have 90° of torsion and no venous drainage but with residual arterial flow [69].

Despite the findings that color Doppler sonography has a high sensitivity and specificity, it is our feeling that torsion remains a clinical diagnosis proven only at surgery. Ultrasound should only be used to document findings. Many conditions including torsion–detorsion, intermittent torsion, persistent capsular flow, and color flow artifacts can suggest apparent flow in cases where none exists. Therefore, ultrasound does not diag-

nose or "rule out" torsion, only surgical exploration is indicated when the diagnosis of testicular torsion is suspected.

Primary Orchitis and Testicular Abscess

The ultrasound findings of patients with orchitis are often an enlarged testis with homogenous appearance. Orchitis may be diffuse or focal, with focal orchitis appearing as multiple hypoechoic lesions with increased testicular blood flow (Fig. 6.40a, b). Additionally, the RI of the epididymal and testicular artery has been shown to be significantly lower in patients with epididymo-orchitis than in control subjects [70]. If inflammation progresses, the pressure of intratesticular edema may compromise blood flow leading to infarction; the ultrasound will demonstrate absence of blood flow and surrounding reactive hyperemia [71].

A testicular abscess is seen in approximately 5 % of patients with orchitits and usually appears 1–7 weeks after orchitis, often as a result of ineffective treatment. The clinical hallmarks of a testicular abscess include persistent fever, scrotal pain, and swelling. These findings may resemble a tumor, yet evidence of inflammation and absence of Doppler flow will often differentiate an abscess from a tumor [72] (Fig. 6.41).

Nonpalpable Testis

When the testis is nonpalpable in the scrotum, a search is initiated to confirm its presence or absence. Ultrasound is often the initial diagnostic imaging modality because of its sensitivity in the inguinal canal where most undescended testes are found. If the absent testis is not identified within the inguinal canal, CT or MRI can be used in an attempt to locate an intra-abdominal testis. Surgical exploration, however, remains the "gold standard" for identifying an intra-abdominal testis. A cryptorchid testis in the inguinal canal, identified by the presence of the mediastinum testis, is usually small in size (hypotrophic). It can be differentiated from an inguinal hernia by the absence of peristalsis and highly reflective omental fat.

Testicular Microcalcification

The etiology of testicular microcalcification (TM) is unknown. It has been suggested that the calcified concretions within the lumen of seminiferous tubules originate from sloughing of degenerated intratubular cells and failure of the Sertoli cells to phagocyte the debris [73, 74]. TM has been defined as 5 or more microcalcifications within the testicular parenchyma. TM appears on ultrasound as hyperechogenic lesions measuring between 1 and

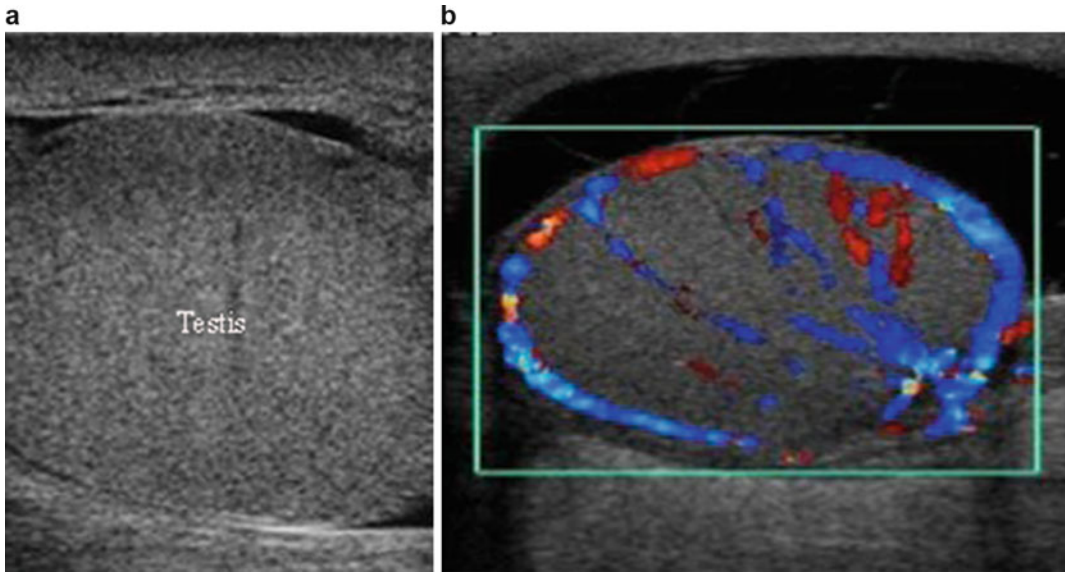

Fig. 6.40 (**a**) Gray scale ultrasound demonstrating orchitis with homogenous enlargement of the testis. (**b**) Color Doppler study shows increased blood flow to the testicle with prominent capsular vessels

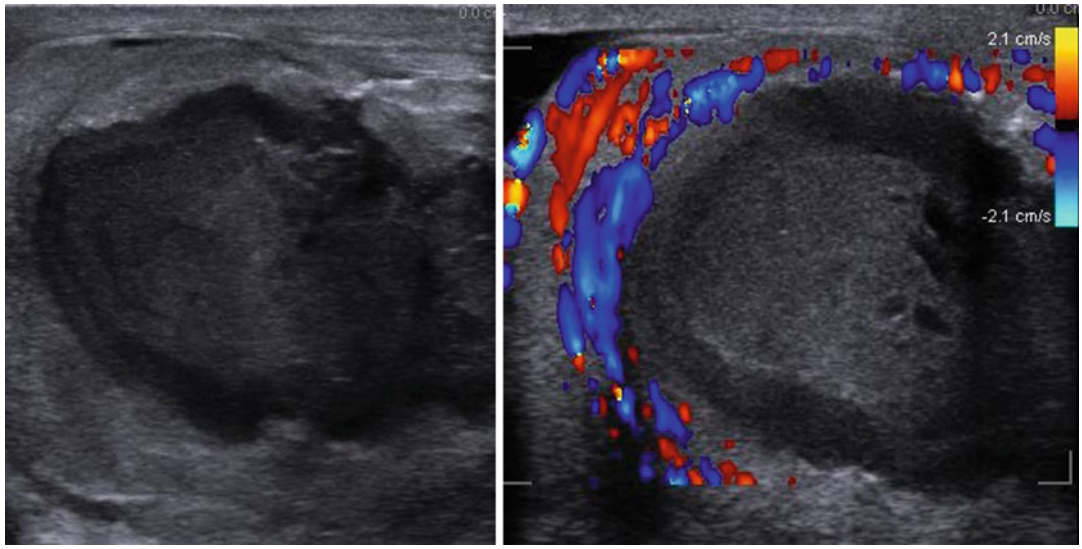

Fig. 6.41 Ultrasound findings show heterogeneous complex septate fluid collection. Color Doppler ultrasound shows no blood flow in the abscess and increased blood flow in the surrounding testicular parenchyma

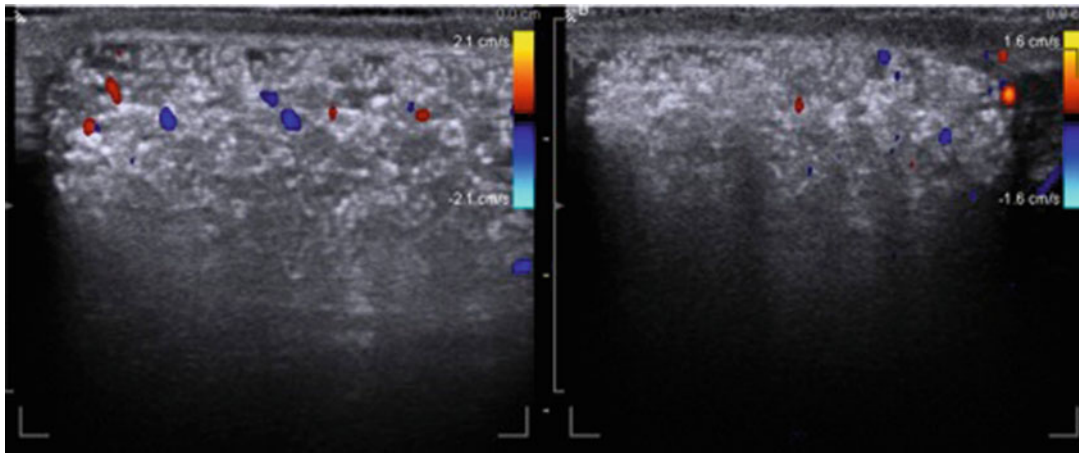

Figs. 6.42 Gray scale imaging demonstrating multiple bilateral microcalcifications of the testis. Note the lack of acoustic shadowing

3 mm sized multiple foci within the testicular parenchyma. The prevalence of TM varies from 1.5 to 5.6% of asymptomatic healthy men, compared with 0.8 to 20% in infertile men [75]. Acoustic shadowing on ultrasound is often absent, likely due to the small size of the calcifications [76, 77] (Figs. 6.42 and 6.43). They are usually bilateral, but occur unilaterally in 20% of the cases. Goede et al. reported 2.4% prevalence of TM in young asymptomatic boys [78]. TM is also described in association with various benign conditions including varicocele, cryptorchidism, male pseudo hermaphroditism, Klinefelter's syndrome, neurofibromatosis, and Down syndrome [79].

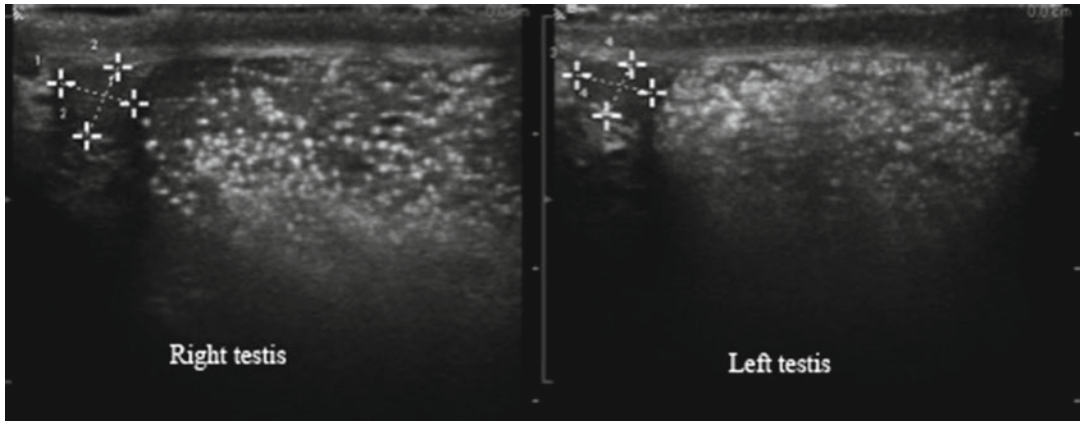

Fig. 6.43 Color Doppler study showing multiple microcalcifications

The risk of subsequent development of carcinoma in situ (CIS) and testicular germ cell tumor in patients presenting with TM is less clear [77, 80]. Data from several investigators suggest that TM is a benign, nonprogressive condition, at least when followed for up to 45 months [81, 82]. However, several recent case reports have documented the development of testicular tumors in patients with TM when follow up was extended for several years [82, 83].

In 2015, the European Society of Urogenital Radiology recommended against routine follow up of men with isolated TM in the absence of risk factors. Men with risk factors for malignancy are recommended to have an annual ultrasound until the age of 55, and if a mass is identified, the patient should be sent immediately for evaluation with a urologist. Risk factors include a history of testicular maldescent, history of orchiopexy, testis atrophy, and a personal or first degree relative with germ cell tumor [84].

Testicular Macrocalcification

Intratesticular macrocalcifications can be secondary to the presence of a germ cell tumor, a burnt out germ cell tumor, a Sertoli cell tumor, prior trauma, infection (TB), infarction, or inflammation (sarcoidosis) [85].

Extratesticular calcifications can be found with the tunica vaginalis space and can result from inflammation of the tunica vaginalis or from a sloughed testicular appendage. When these calcifications are freely mobile, they are known as scrotal pearls or scrotoliths.

Cystic Lesions

Intratesticular Cysts

Simple Testicular cysts occur in approximately 8–10 % of patients [86]. The common causes for the testicular cysts include trauma, surgery, and inflammation. Cysts most commonly are found at the mediastinum testis. Testicular cysts are usually simple cysts: on ultrasound they are anechoic, demonstrate an imperceptible wall and have through transmission. Testicular cysts normally have a size range from 2 mm to 2 cm in diameter [72] (Fig. 6.44).

Cystic teratoma appears on ultrasound as a cystic mass with solid components and should be considered whenever cystic testicular lesions are found. Cystic teratoma occurs in children and adults. In children, they behave as a benign tumor, whereas in adults and adolescents they are known to metastasize [87].

Cysts of the Tunica Albuginea

Tunica albuginea cysts arise from within the layers of the tunica albuginea. They are benign cysts and are clinically palpable by virtue of their location. These cysts meet the criteria for a simple cyst by ultrasound [88, 89] (Fig. 6.45).

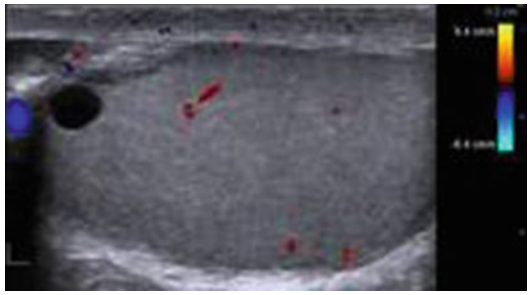

Fig. 6.44 Ultrasound demonstrating simple testicular cysts

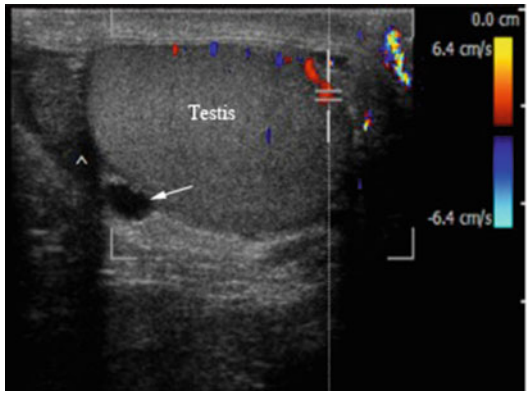

Fig. 6.45 Tunica albuginea cyst is found within the layers of the tunica. They appear as simple cysts on ultrasound (*arrow*)

Tubular Ectasia of Rete Testis

Tubular ectasia of the rete testis (TERT) is a benign clinical entity in which cystic dilation of rete testis results from partial or complete obstruction of the efferent ducts [90, 91]. Tubular ectasia of the rete testis often present an asymptomatic finding in men older than 50 years with unremarkable physical examination of the testes. On ultrasound, it is seen as multiple anechoic, avascular structures within the mediastinum (Fig. 6.46a, b). TERT is often associated with ipsilateral spermatoceles and usually found bilaterally. It is important to differentiate this benign cystic tumor from malignant cystic tumors of the testis and thus avoid unnecessary orchidectomy. Cystic malignant tumors, most commonly the cystic teratomas, can be distinguished sonographically by the presence of multiple cystic areas, often surrounded by a soft tissue. Tumors are almost always unilateral and are located anywhere in testicular parenchyma, not limited to the mediastinum [92].

Intratesticular Varicocele

Intratesticular varicocele has been defined as dilated veins radiating from the mediastinum testis into the testicular parenchyma [93, 94]. It is a clinically occult condition that may occur in association with extratesticular varicocele. The sonographic features of intratesticular varicoceles are similar to those of extratesticular varicoceles. Color flow Doppler sonography demonstrates tubular or serpentine vascular structures more than 2 mm in diameter with a positive Valsalva maneuver (Fig. 6.47a, b). Valsalva maneuver plays an important role in the diagnosis of intratesticular varicocele because in most cases the retrograde flow will not show up spontaneously on color flow Doppler sonography [95]. Approximately 40 % of intratesticular varicoceles are present bilaterally [96]. Patients with intratesticular varicocele may have testicular pain in up to 50 % of cases secondary to venous congestion, resulting in stretching of the tunica albuginea. Bucci et al. reported 2 % incidence of intratesticular varicocele in their series of 342 patients who were evaluated with color Doppler ultrasound for a fertility evaluation [94]. Color flow Doppler sonography helps to differentiate intratesticular varicocele from the tubular ectasia of rete testis adjacent to the mediastinum. Spectral Doppler yields the definitive diagnosis by confirming venous flow.

Congenital Testicular Adrenal Rests

Congenital adrenal hyperplasia (CAH) is an autosomal recessive disease characterized by deficiency of adrenocortical enzymes. More than 90 % of cases of congenital adrenal hyperplasia are caused by 21-hydroxylase deficiency [97, 98]. Congenital testicular adrenal rests are seen in about 29 % of patients with congenital adrenal hyperplasia [99]. An increase in adrenocorticotropic hormone (ACTH) levels causes hyperplasia of adrenal remnants in the testes in patients with CAH and results in the development of intratesticular masses. Sonographically, these masses

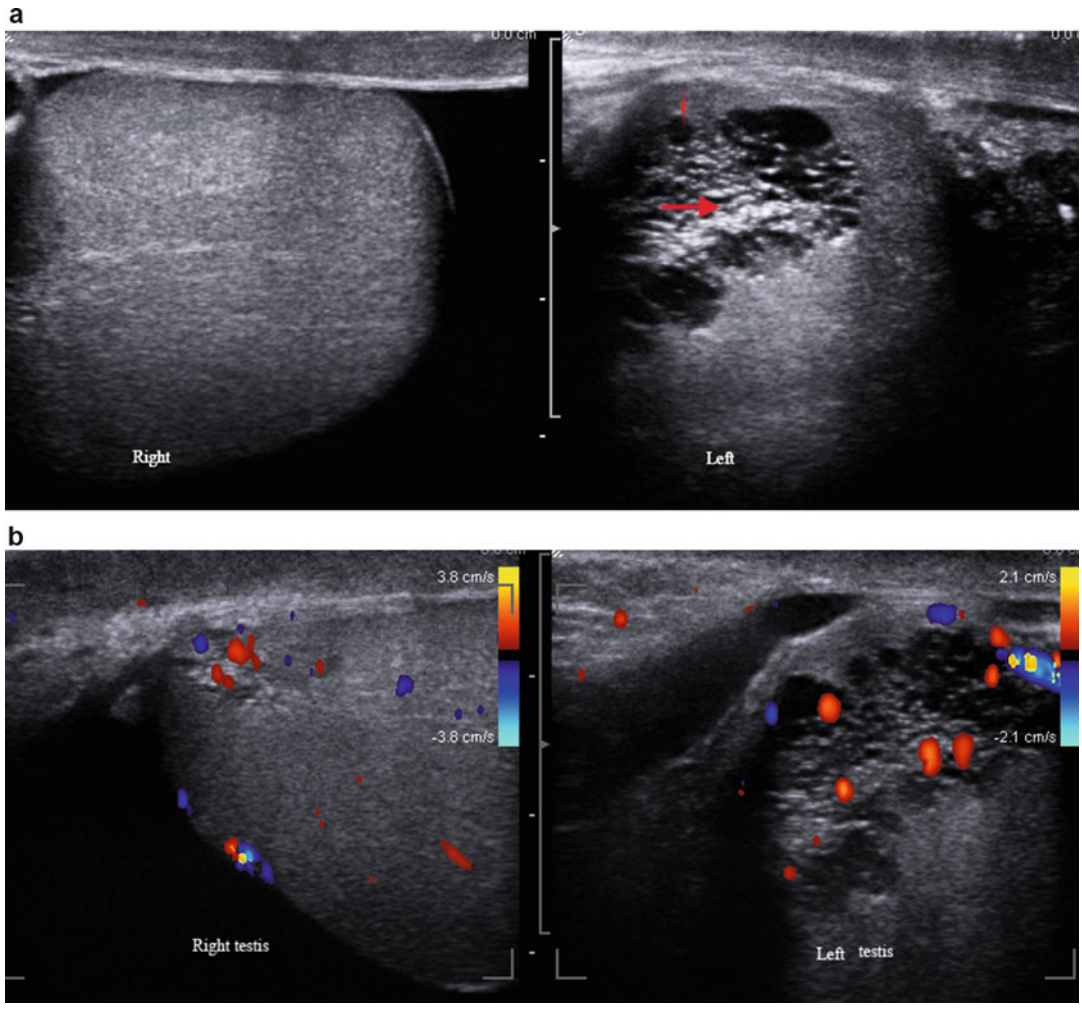

Fig. 6.46 (**a**) Left-sided tubular ectasia of the rete testis on gray scale ultrasound (*arrow*). (**b**) Doppler color flow study shows normal blood flow to the tubular ectasia of the rete testis

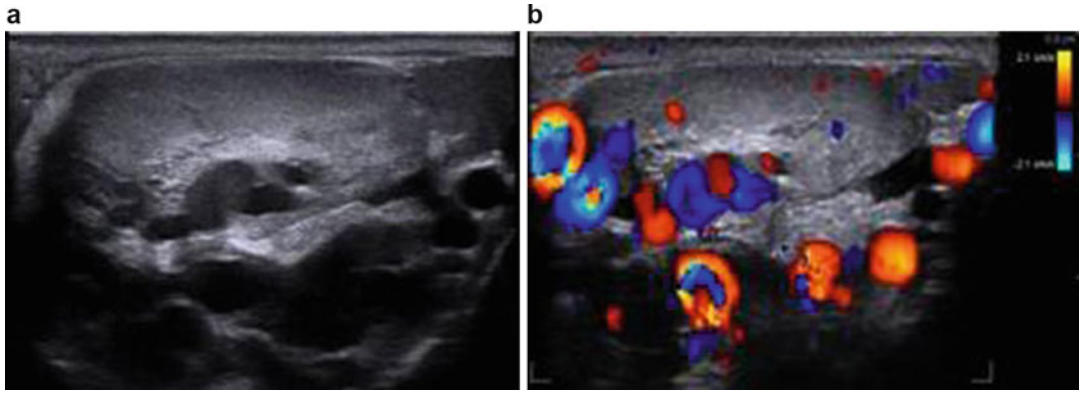

Fig. 6.47 (**a**) Gray scale ultrasound shows intratesticular varicoceles, dilated veins within the testicular parenchyma. (**b**) Color Doppler flow study confirms the venous nature of the intratesticular veins

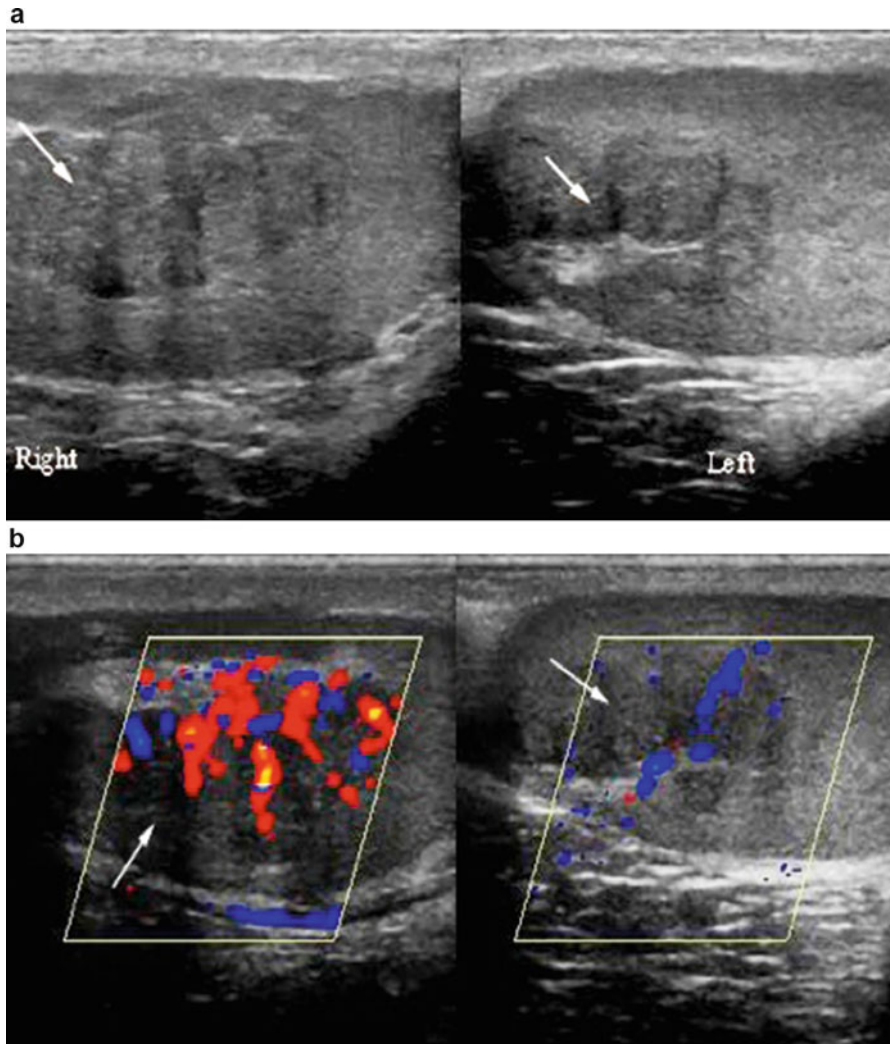

Fig. 6.48 (**a**) Ultrasound of testicular adrenal rests (*arrow*), located adjacent to the mediastinum testis and typically found bilaterally. (**b**) Doppler color flow study shows increased vascularity of testicular adrenal rests

appear as hypoechoic intratesticular masses in both testes and Doppler color flow shows increased vascularity located in the region of the mediastinum testis [99, 100] (Fig. 6.48a, b). Scrotal ultrasound is the diagnostic modality of choice for their diagnosis. Congenital testicular adrenal rests may have the appearance of other testicular tumors; however, the presence of bilateral lesions in patients with CAH should be considered congenital adrenal hyperplasia. The lesions should be followed by ultrasound and should regress with steroid replacement therapy [101].

Sarcoidosis

Involvement of the testis and epididymis with sarcoid is rare. Clinically it presents as a painless epididymal or testicular mass or as epididymitis. Sonographically the lesion is an irregular hypoechoic mass that may be calcified, multifocal, and bilateral [102].

Testicular Trauma

Testicular trauma accounts for less than 1 % of all trauma-related injuries with peak occurrence at ages 10–30 years [103, 104]. Common causes of trauma are motor vehicle accident and athletic injury. Blunt trauma accounts for 85 % of scrotal trauma and penetrating trauma for 15 % of total injuries [105]. Physical examination may be difficult in these patients with scrotal trauma due to tenderness and swelling of the scrotal contents. The scrotal ultrasound remains the standard imaging study to evaluate the testicular and epididymal integrity and assess the vascular status [104]. Findings after severe scrotal trauma include hematocele, testicular hematoma, and testicular rupture. Buckley and McAninch reported 100 % sensitivity and 93.5 % specificity when comparing ultrasound results of blunt trauma of the testes to the findings at surgical exploration [106]. Guichard et al. also reported sensitivity and specificity of ultrasound for testis rupture were 100 % and 65 %, respectively, when compared to surgical findings [107]. When ultrasound cannot be performed, magnetic resonance imaging (MRI) is a possible alternative, as MRI had 100 % diagnostic accuracy for the diagnosis of testicular rupture [108].

An intratesticular hematoma after trauma is diagnosed when images show an intact tunica albuginea and intratesticular hypoechoic areas with no blood flow on Doppler color flow study (Fig. 6.49). A discrete hypoechoic stripe in the testicular parenchyma and interruption of tunica albuginea are evidence of testicular rupture [109] (Figs. 6.50). A hematocele is an accumulation of blood within the tunica vaginalis. Hematoceles are usually secondary to trauma, yet may also be present after testicular torsion, presence of a tumor, and scrotal surgery. Ultrasonography of a hematocele reveals a complex heterogeneous appearance and may demonstrate mass effect with distortion of the testis [36].

The current management strategy for testicular rupture advocates early surgical intervention with the goal of preventing testicular loss. These recommendations are also applied in boys with a large hematocele since up to 80 % of significant hematoceles are due to testicular rupture [110]. The importance of early identification of testicular rupture is that 80 % of testis can be salvaged if surgical exploration is performed within 72 h of injury. Additionally, any abnormalities found on scrotal ultrasound at the time of trauma must be followed by ultrasound until resolution, as 10–15 % of testicular tumors manifest after trauma [105].

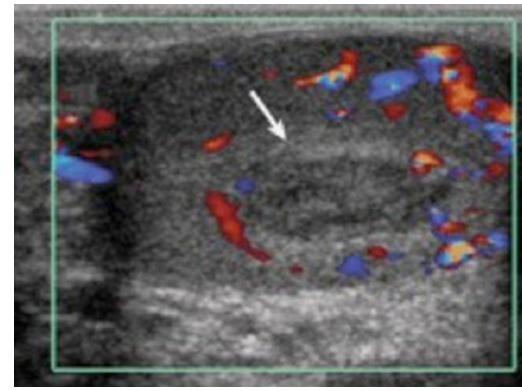

Fig. 6.49 Intratesticular hematoma (*arrow*) showing hypoechoic area without blood flow on Doppler color flow study

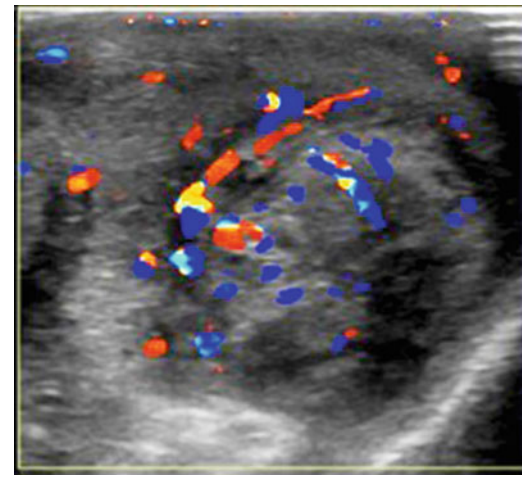

Fig. 6.50 Doppler color flow study showing testicular rupture following a blunt trauma scrotum. There is no increased blood flow noted in the testicular rupture

Malignant Lesions of the Testis

Ultrasound is a mandatory component in the evaluation of testicular cancer [111]. Testicular malignancies account for approximately 1 % of all the malignancies in men. The predicted 5-year survival rate is approximately 95 %, believed to be due to early detection as patient appreciation of abnormality in a superficially palpable organ and tumor sensitivity to chemotherapy and radiotherapy. The most common presentation is of a painless scrotal mass, with pain being reported in only 10 % of cases [112]. Ultrasonography is the gold standard imaging modality for diagnosis. Ultrasound characteristics differ significantly for malignant as compared to benign (Table 6.2) intratesticular masses.

Germ Cell Tumors

Germ cell tumors account for 95 % of testicular malignancies and can be divided into seminomatous and nonseminomatous germ cell tumors. The remaining minority of testis tumors are histologically sex cord stromal tumors, lymphomas, or metastases.

Table 6.2 Ultrasound characteristics of nonneoplastic intratesticular masses

Intratesticular lesion	Ultrasound findings
Simple testicular cyst	Well-circumscribed, anechoic, increased through-transmission
Epidermoid cyst	Classic appearance: an onion ring due to alternating layers of hypoechogenicity and hyperechogenicity
Tubular ectasia of the rete testis (TERT)	Avascular cystic dilations in the rete testis
Intratesticular varicocele	Anechoic, tortuous structure with a venous waveform on Doppler color flow study
Tunica albuginea cyst	Cyst at upper or lateral margin of testis; may be clinically palpable
Testicular hematoma	Avascular hyperechoic lesion within the testicular parenchyma
Congenital testicular adrenal rests	Bilateral hypoechoic or hyperechoic lesions with or without posterior acoustic shadowing

The most common germ cell tumor is **seminoma**, which comprises up to 50 % of all germ cell tumors. Seminoma occurs in men predominantly between the ages of 35 and 45. Bilateral seminomatous germ cell tumors are rare and are reported only in 2 % of the cases [113]. On gross pathology, they are lobulated and pale in color and may vary in size from small well-defined lesions to masses that completely replace normal testicular parenchyma [113]. The sonographic appearance of seminoma typically is a homogeneous well-defined hypoechoic lesion, with cystic areas found only in 10 % of cases [114]. Larger tumors tend to be more heterogeneous and may have poorly defined margins, are often diffusely infiltrative and multifocal (Fig. 6.51a, b).

Nonseminomatous germ cell tumors (NSGCT) generally occur in younger men between ages 25 and 35. NSGCT are mixed germ cell tumors comprised of embryonal carcinoma, yolksac tumor, choriocarcinoma, and teratoma. They can be locally aggressive with invasion of the tunica albuginea or the epididymis or the spermatic cord. The ultrasonographic findings reflect the diversity of the components and characteristically appear irregular with a heterogeneous parenchyma pattern, representing calcification, hemorrhage, or fibrosis and cystic lesions [115, 116] (Fig. 6.52a, b).

Pure **embryonal cell carcinoma** makes up 2–3 % of all germ cell tumors. An embryonal cell carcinoma is an aggressive tumor with ultrasonographic findings often demonstrating irregular and indistinct margins, with a heterogeneous echotexture. These tumors are characteristically smaller in size without enlargement of the testis [117]. **Yolk sac tumor**, also known as endodermal sinus tumor or infantile embryonal carcinoma, most commonly occurs in children younger than 2 years [117]. The sonographic appearance of yolk sac tumors of the testis is inhomogeneous and can have areas of hemorrhage; however, it is difficult to differentiate from other solid tumors of the testes based solely on ultrasonography [118]. **Choriocarcinoma** carries the worst prognosis of all germ cell tumors, with early metastatic spread to the lung, liver, gastrointestinal tract, and brain, and is associated

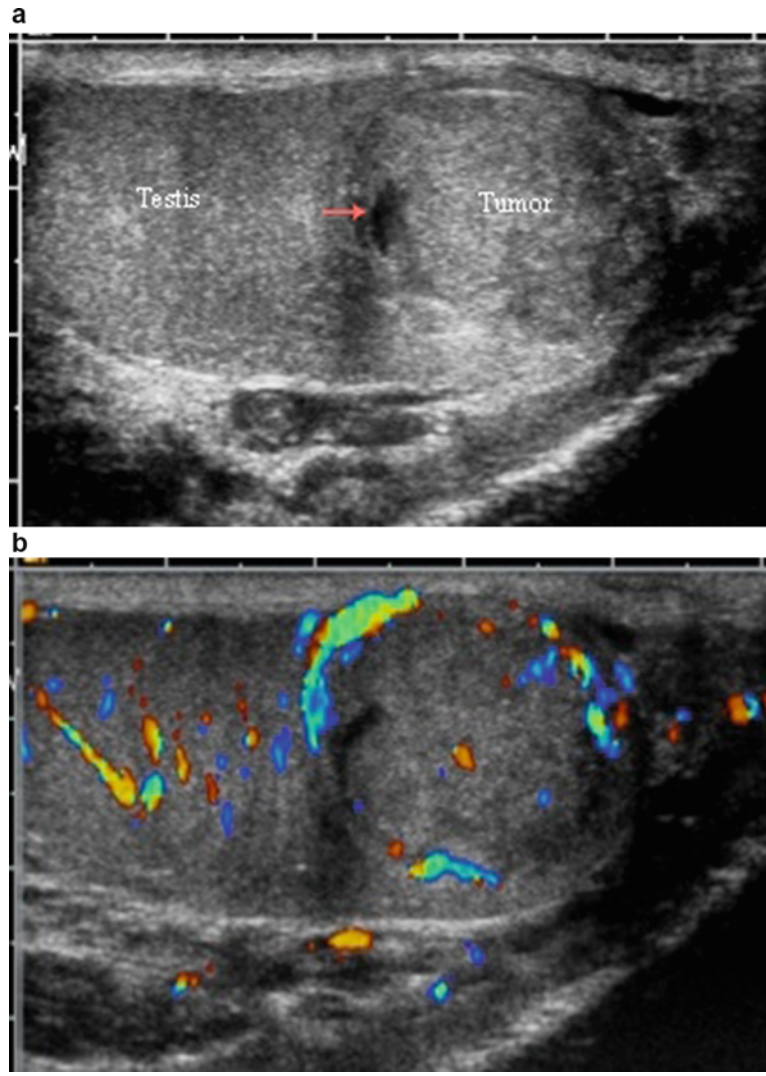

Fig. 6.51 (**a**) Testicular germ cell tumor showing heterogeneous appearance on gray scale ultrasound. (**b**) Color Doppler flow showing increased blood flow within the tumor

with an elevated human chorionic gonadotropin level. Ultrasound is characterized by cystic and solid areas, corresponding to areas of hemorrhagic necrosis [118].

Teratoma is the second most common pediatric testicular tumor, and a mature teratoma is often benign in children. A teratoma will demonstrate endodermal, mesodermal, and ectodermal components in a disorganized arrangement [115]. Echogenic foci in these tumors represent elements of its embryologic composition—immature bone, fat, and fibrosis.

Epidermoid cysts of the testis are rare benign germ cell tumors. Epidermoid cysts usually present between 20 and 40 years of age. They are normally unilateral; however, bilateral occurrence is rarely reported [119]. Epidermoid cysts are variable on sonographic appearance attributable to their contents with keratin and variable maturation. The characteristic "onion ring" sonographic appearance of the epidermoid cyst is due to alternating layers of hypo- and hyperechogenicity without internal flows [120–122] (Fig. 6.53a, b). An epidermoid cyst of less than 3 cm in size with negative tumor markers can be managed conservatively by enucleation provided that frozen sections are obtained to confirm the diagnosis [123].

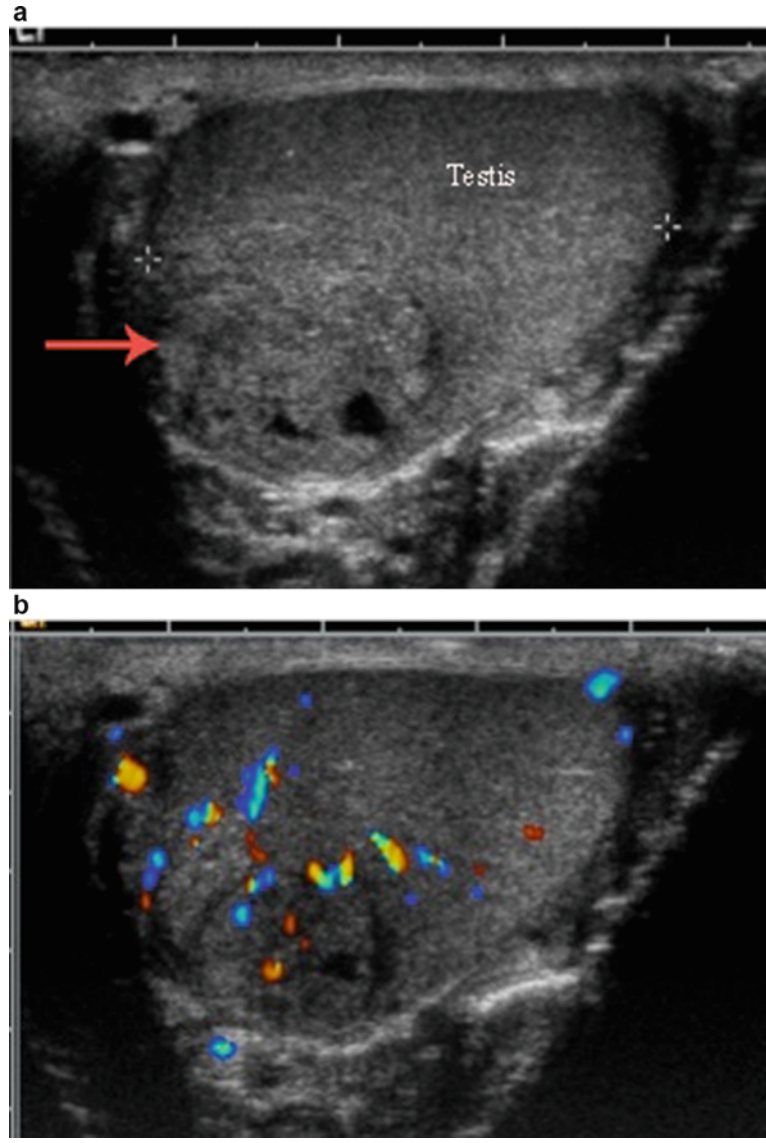

Fig. 6.52 (**a**) Nonseminomatous germ cell tumor showing heterogeneous appearance on gray scale ultrasound. (**b**) Color Doppler flow study demonstrating increased blood flow within the tumor

Nongerm Cell Tumors

Nongerm cell tumors are rare, but most commonly arise from Leydig or Sertoli cells. Leydig cells are the principal source of male testosterone. **Leydig cell tumors** represent fewer than 3 % of all testis tumors; they are usually benign but have malignant potential. Male patients have virilizing or feminizing characteristics due to androgen secretion. Ultrasound features are nonspecific, but if Leydig cell tumor is suspected, tumor enucleation may be performed. **Sertoli cell tumors** represent approximately 1 % of testicular tumors and can occur in children and adults. Sertoli cell tumors are usually found in patients younger than 40, do not secrete hormones, and can occur bilaterally in 20 % of patients [43]. Both Leydig cell and Sertoli cell tumors may be amenable to testis-sparing resection, where intraoperative ultrasonography is an essential component of the procedure.

Testicular Lymphoma

Primary testicular lypmhoma is the most common testicular malignancy in men over the age of 60 [124–126]. The most common histological type is large B-cell non-Hodgkins lymphoma.

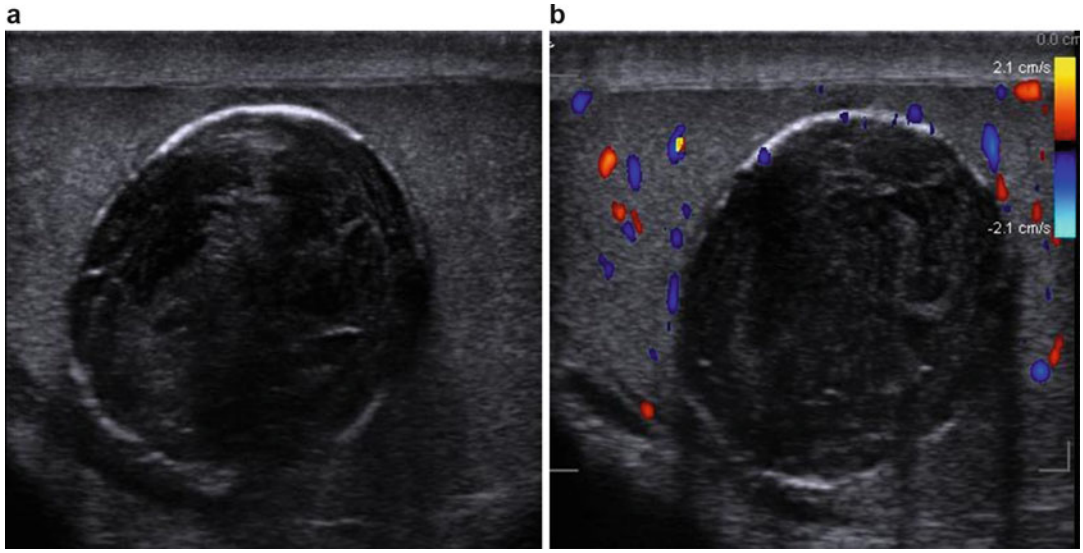

Fig. 6.53 (**a**) The Gray scale appearance of an epidermoid cyst with classic onion ring configuration. (**b**) Color Doppler flow study shows no blood flow

The ultrasound demonstrates diffuse enlargement of the testis with increased vascularity on Doppler color flow (Fig. 6.54a, b). Orchidectomy had been advocated as diagnostic and therapeutic procedure. The treatment recommendation was recently changed to a combined modality of systemic doxorubicin-based chemotherapy, prophylactic intrathecal chemotherapy, and orchidectomy or scrotal radiotherapy [125]. Lymphoma found in the testis may also be the initial site found with widespread disease or the site of recurrence for previously treated lymphoma as the testis a sanctuary organ due to the blood–gonad barrier that blocks accumulation of chemotherapy agents [118].

Metastasis

Ultrasonography cannot differentiate metastatic disease to the testicle from a primary testicular lesion. Metastasis to the testis is rare and usually occurs with advanced disease. The most common cancers to metastasize to the testis are melanoma, prostate, and lung [127, 128].

Regressed or Burnout Germ Cell Tumor

Some patients present with widespread metastatic disease, to the retroperitoneum or beyond, without identification of a primary tumor. Scrotal ultrasound performed for these patients may find an area of calcification in the testis, representing the "burnt-out" primary lesion. One theory to explain the genesis of the burned out tumor is that the tumor outgrows its blood supply and then subsequently involutes, resulting in fibrosis and calcification [129] (Fig. 6.55).

Incidentally Discovered Nonpalpable Testicular Lesions

Incidentally found solid testicular masses that are not palpable are usually benign. Significant risk factors for the presence of malignancy include size greater than 1 cm, ipsilateral atrophy, history of cryptorchidism, history of contralateral germ cell tumor, and severe oligospermia or azoospermia [130]. Previous work has shown that patients at low risk for malignancy can be managed with active ultrasound surveillance, proceeding with testis sparing excision biopsy or radical orchiectomy if the lesion size should increase in size [131, 132]. Patients at high risk for malignancy were managed with an ultrasound guided testis sparing excisional biopsy or radical orchiectomy [133].

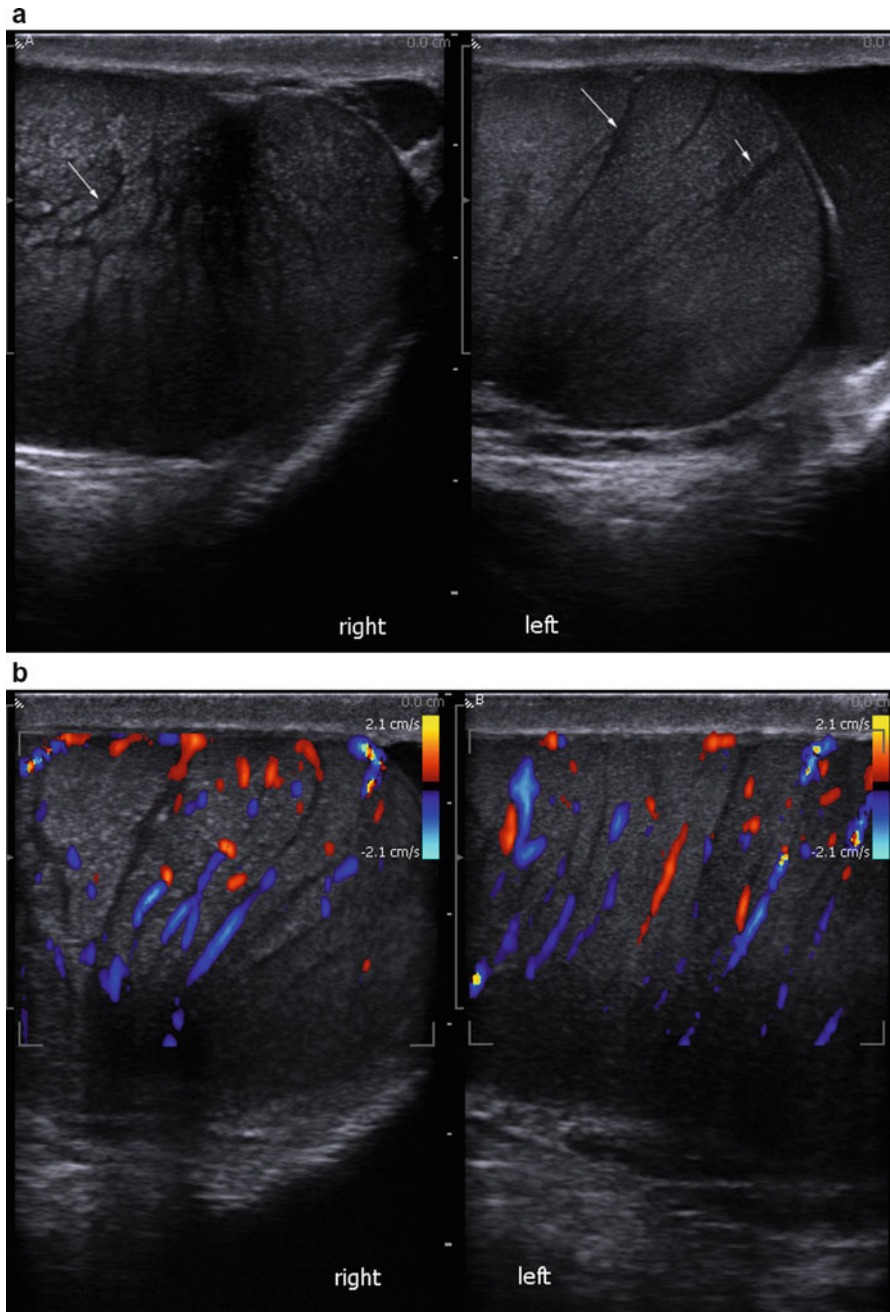

Fig. 6.54 (**a**) Gray scale ultrasound showing bilateral testicular lymphoma. *Arrows* showing dilated vascular markings. (**b**) Doppler color flow study showing increased vascularity in both the testes

Sonoelastography for Testis Lesions

Characterization of testicular masses classically includes palpation, which has been used to subjectively evaluate the firmness of tissue from time immemorial. An increase in tissue firmness is often associated with pathology while tissue without this increased firmness is generally considered healthy [134]. The physical exam is used to qualitatively evaluate a lesion's size and firmness. However, this evaluation is limited to lesions that are physically palpable. B-mode

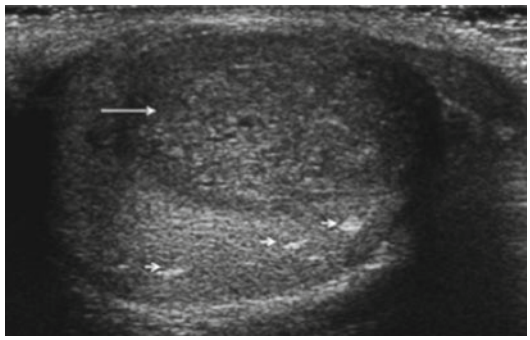

Fig. 6.55 Gray scale ultrasound showing a mixed germ cell tumor (*arrow*) and areas of burnt-out tumor (*small arrows*)

ultrasound has been used to quantitatively evaluate the size of testicular lesions, it also has the ability to extend this characterization to lesions that are not physically palpable, and it provides additional information about the acoustic qualities of the tissue. Color Doppler techniques add the ability to evaluate blood flow properties as well. In the early 1980s, groups began evaluating the compressibility of breast tissue with dynamic ultrasound images [135]. Over the past three decades, advancements in ultrasound technology have been combined with novel techniques that allow the characterization of tissue firmness in nonpalpable lesions and, with some of these techniques, in a quantitative fashion [136]. These techniques that use ultrasound to demonstrate tissue firmness are collectively called sonoelastography.

There are numerous terms that can be used to describe the palpable character of lesions (hard, soft, stiff, rigid, firm, etc.). As many of these terms are also used to describe a physical quantity in materials physics. The use of these terms by clinicians and the lay population does not always match with the definitions that describe the physical characteristics of materials. To minimize potential confusion, we use the term 'firm' and 'hard' for an increased elasticity or increase in elastic modulus (see next paragraph) and the term 'soft' for situations where the elasticity or elastic modulus is decreased.

Elasticity is the physical quantity used to express an object's firmness. The mechanical properties of that object (the manners by which the object deforms to various types of external forces) are governed by quantifiable elasticity

Box 6.1

$$E = \sigma / \varepsilon$$

descriptors called moduli. Biologic materials are also governed by these descriptors. By characterizing the tissue deformations to external forces we can demonstrate the elasticity of an object. There are several manners in which tissue deformations can be generated for this purpose [137]; however, we will focus on those that have been reported in the testicle to date: those employed in real-time sonoelastography (RTE) and shear wave sonoelastography (SWE).

Real-Time Sonoelastography

When a compressive force (known as stress) is placed on tissue, a degree of deformation in the same direction of the applied force (known as strain) occurs. The amount of deformation is inversely proportional to the firmness of the tissue. Furthermore, the amount of stress required to deform the tissue is directly proportional to the firmness of the tissue. Young's modulus (E) is the quotient of the relationship between the stress (σ) and the strain (ε) (Box 6.1).

Real-time sonoelastography (RTE) employs *manual compression* of the tissue with the ultrasound probe to produce a stress on the tissue [135]. If the tissue has a uniform firmness, then the strain is uniform. If there is a variable elasticity (Young's modulus) of the tissue, then there will be variations in the strain that can be detected using the ultrasound probe. Real-time sonoelastography takes advantage of variations in the tissue deformation in this way to demonstrate the relative differences in tissue firmness. These differences are displayed with a color scale overlying their location on the ultrasound.

Shear Wave Sonoelastography

Shear stress arises when a surface of a material is subjected to stress in a direction parallel to that surface and the opposite surface is held in place by an opposing force. A stress induced at a certain location in tissue will deform the tissue at that location and, since the tissue around it is held in place by the opposing force of friction

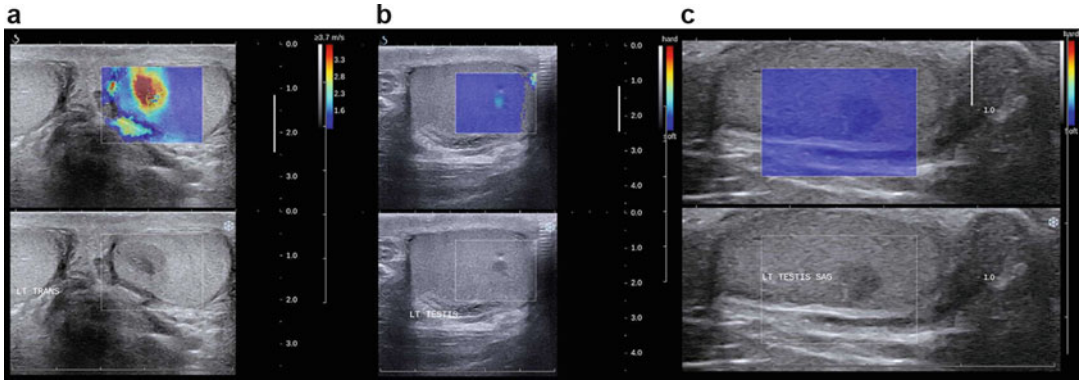

Fig. 6.56 Sonoelastograms of the testis. B-mode image on the bottom with elastogram box over the image on the top. A testicular lesion with minimal increased firmness (**a**), one with a markedly increased firmness (**b**), and one without increased firmness (**c**)

Box 6.2

$$v = \sqrt{G/\rho}$$

and normal forces of adjacent tissue structure, a shear stress is generated. One might imagine a block of gelatin sitting on a plate. When a finger is placed on the upper surface of the block and moved in any direction, the upper surface of the block is dragged and displaced in that direction. The lower surface remains in place on the plate. The whole block is subjected to torque across the length of the block that extends from the plate to the finger. The degree of resistance to this type of deformation a material exhibits is reflected in its shear modulus.

A shear stress may propagate radially from its source in a wave though the tissue in the same manner as the radial waves propagate away from the site where a pebble hits the surface of a body of water. These waves are shear waves and their motions through the tissue are governed by the shear modulus (G).

The speed (ν) at which shear waves propagate is inversely proportional to the square root of the medium's density (ρ) and directly proportional to the square root of its rigidity (expressed as the shear modulus) (Box 6.2).

Thus, the more firm the tissue (the greater the shear modulus), the faster the shear waves travel. It is this relationship and the notion that soft tissue density has little variability[1] that allow the firmness of tissue to be determined by calculation of the speed of shear wave propagation though the tissue.

The tissue deformations generated by these shear waves and thus the velocity of wave propagation can be detected by ultrasound receivers with very fast acquisition speeds. Shear wave sonoelastography (SWE) is a technique that employs the speed of these waves to determine the tissue elasticity [135, 136, 138]. The elasticity is displayed superimposed on the ultrasound images as a color scale (Fig. 6.56). The ultrasound transducer used for diagnostic ultrasound with this technique is specially constructed to generate these shear waves. Different lesions can be discriminated based on their firmness (Fig. 6.57). Be aware that the color given to hard lesions is determined by the manufacturer of the equipment as well as being able to be set by the user. Therefore, the user needs to look at the color bar to know which color represents a 'hard' and which color represents a 'soft' lesion just as one would need to look at the color bar on the color Doppler display to know the direction of blood flow.

[1]The density of soft tissues is roughly that of water 1.0 g/cc and ranges between 0.92 in adipose tissue and 1.06 in muscle (cortical bone density is 1.8 g/cc) which is miniscule variability compared to the three to four orders of magnitude variations in elasticity observed in tissues and thus differences in wave velocity can be nearly entirely attributed to differences in the elastic moduli [19].

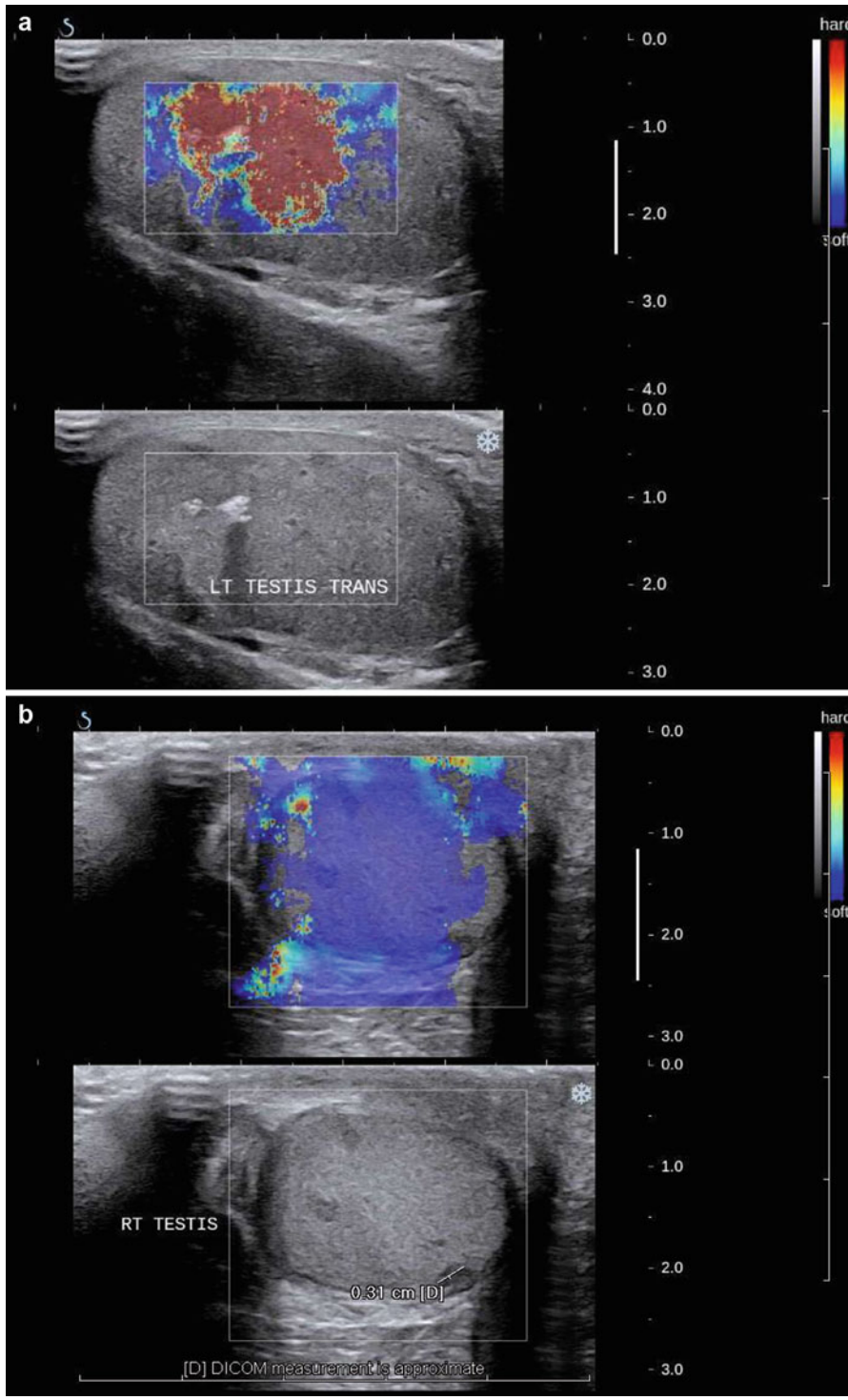

Fig. 6.57 (**a**) Sonoelastography and Gray scale images of a. a testicular nonseminomatous germ cell tumor. Note the "hardness" of the lesion based on color bar. (**b**) A Sertoli Cell nodule in a patient presenting with infertility. Note the "softness" of the lesion based on color bar. (**c**) The testis in a patient with testicular sarcoidosis. Note the "intermediate" elastography pattern of the lesion based on color bar

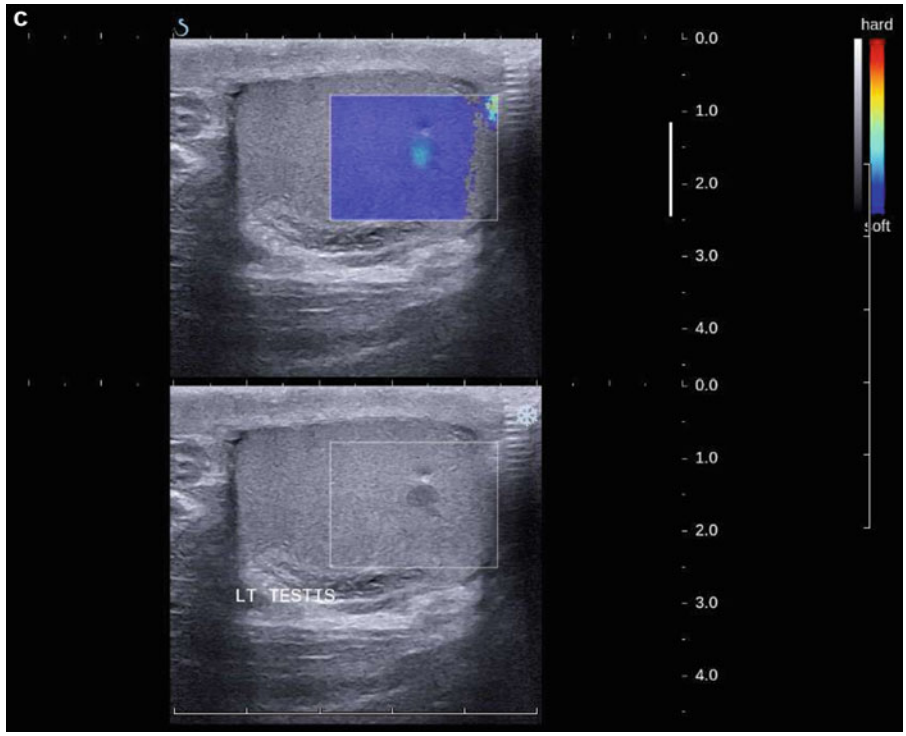

Fig. 6.57 (continued)

Differences Between the Technologies

Compressive forces generated by the ultrasonographer during RTE come with a degree of intersonographer variability, as the stress generated in this fashion cannot be consistently reproduced. It is dependent on how hard each sonographer compresses the tissue. Whereas the strain is measured from tissue changes on the ultrasound images, the stress is not determined. Thus, relative elasticity differences can be determined (as all the tissue examined is subjected to the same stress), but quantitative measurements of elasticity that can be compared between exams cannot be made with the current techniques used for RTE [136, 139].

Shear wave sonoelastography does not share this limitation [136, 139, 140]. It utilizes an alternative method for measuring tissue elasticity, which involves ultra-low frequency pulses that are rapidly transmitted into the tissue to induce a vibration in the tissue. The transducer that produces this low-frequency wave also sends the high frequency longitudinal waves that image the tissue in traditional B-mode fashion. These high frequency waves are able to capture the motion of the shear (transverse) wave generated by the mechanical reverberation, as it travels through the tissue. It is possible to follow the slow-moving (1–10 m/s) shear wave motion with established ultrasound and Doppler technology. With the faster modern imaging capabilities it is possible to create a map of the shear wave's motion, as the wave moves through the tissue. Shear wave propagation can be reproducibly generated by the transducer, imaged by its receiver, and then measured and calculated by the ultrasound software. Shear wave sonoelastography (SWE) has the advantage of being comparable over different exams and quantitative [139].

Shear waves are propagated in directions perpendicular to the direction of energy transfer and experience a far greater attenuation as they radiate out than the longitudinal ultrasound waves. The attenuation is many orders of magnitude greater than that the attenuation of ultrasound and increases as the frequency increases [141]. The FDA has limited the power intensity for ultrasound applications to 720 W/cm^2 [142]. As a result, the depths at which this technique can be used are

limited compared to RTE. Techniques generating waves that are timed and spaced to create multiple foci of shear wave generation (at different tissue depths) result in superposition at the overlapping wave fronts (like sound waves around a jet breaking the sound barrier and producing a sonic boom) and have expanded the depth of penetration without an increase in tissue heating.

Current Experience with Sonoelastography of Testicular Lesions

The first published experience with sonoelastograpy for the assessment of testicular lesions is a case series from 2009 using RTE by Grasso et al. [143]. Patients presenting with scrotal pain, infertility, scrotal enlargement, or testicular nodules (41 patients) underwent B mode and color Doppler ultrasound examination of the testes followed by RTE. In 38 of the patients, RTE findings correlated with B mode and color Doppler findings (no addition information is reported for this patient subset). The remaining three cases had distinct sonoelastography findings that provided useful, additional information to characterize the lesions. Two were homogenously hard on RTE and one was soft and heterogeneous. Inguinoscrotal exploration with testis sparing excision of the lesions was employed in the three cases. Histopathologic examination of the lesions demonstrated to be hard by RTE revealed a Sertoli cell tumor in one patient and an adenomatoid tumor in the other. The lesion characterized as heterogeneous and soft was an intratesticular hematoma. The authors concluded that sonoelastography could have a role in discriminating lesions for imaging follow-up from early testis sparing surgery based on the hardness profile [143].

Goddi et al. presented a series of 1617 patients who were referred for scrotal abnormalities and examined by B-mode ultrasound [144]. Those patients that had testicular lesions that could not be characterized as cysts or small calcifications by B-mode ultrasound underwent color Doppler ultrasound and RTE. A total of 88 testicles were examined with sonoelastography and 144 lesions were identified. The authors classified the lesions into one of five groups based on the firmness and distribution of firmness throughout the lesions and each group was designated with a score (previously described for evaluation of breast lesions [145]) two of which were considered to be high risk of malignancy and the remaining three scores, predictive of benign lesions. The lesions were managed under the care of a urologist. Lesions were considered benign if confirmed histologically or if a surveillance regimen revealed no lesion growth. Malignant lesions were confirmed histologically. They reported an overall sensitivity of 87.5 % and specificity of 98.2 % discriminating between malignant and benign lesions with RTE.

One hundred and twenty-one of the reported lesions fell into the subcentimeter size range (<1 cm). Among these, 101 were soft and 21 hard. There were two lesions that were hard on elastography, and followed, and found to have a benign course (in one, regression in size and resolution of firmness, the other no change in the lesion after 30 months follow-up). These were considered false positives. There was one soft lesion that was present in a patient with gynecomastia who underwent exploration and a Leydig tumor was found. This was considered a false negative. Thus, an overall sensitivity of 95 %, specificity of 98 %, PPV of 90 % (i.e., if it was hard on sonoelastograpy, 90 % of the time it was a tumor) and NPV of 99 % (i.e., if it was soft on sonoelastograpy, 99 % of the time it was benign) was demonstrated in subcentimeter lesions.

Aigner et al. [146] reported a series of 62 consecutive patients that were evaluated for clinical suspicion of testicular tumor using B-mode and color Doppler ultrasound as well as RTE. Those lesions suggestive of malignancy (by clinical findings and tissue firmness) had surgical evaluation and histopathologic examination of the lesions. Those not suggestive of malignancy (by clinical findings, small size of the lesion, and tissue firmness) were followed with an ultrasound-based surveillance regimen and confirmed benign by stability, decrease in size or vascularity, or resolution of the lesion and were defined as nontumorous (fibrous scar, cysts, partial infarction, or orchitis). Fifty patients had histologic diagnoses or sufficient follow-up to declare the lesions nontumorous. The soft lesions included four that were cysts by

B-mode criteria and thus benign. The lesions included to the tumor group included neoplasms that are both benign and malignant. There was an overall 100 % sensitivity and 81 % specificity for RTE hardness to discriminate lesions that were tumors. In the subset of patients with subcentimeter lesions, 14 had hard lesions 13 of which were tumors and the remaining hard lesion was not a tumor (Tobias De Zordo, personal communication, July 2013). The other four in this subset had lesions that were soft and determined to not be tumors based on the earlier criteria. Therefore, in this study, sonoelastography provides a sensitivity of 100 % and specificity of 80 % with a positive predictive value (PPV) of 93 % and negative predictive value (NPV) of 100 % in this subpopulation.

Clinical Role of Scrotal Sonoelastography

In clinical practice, testicular masses have been considered malignant until proven otherwise as 95 % of palpable intratesticular masses prove to be cancer [147]. The widespread use of ultrasonography to evaluate testicles has been associated with the recognition that certain subcategories of testicular lesions are associated with a lower likelihood of malignancy. These subcategories include small (with studies reporting size definitions from <25 to <5 mm) and nonpalpable lesions [130, 133, 148–156]. Smaller masses are associated with an increased likelihood of having a benign histology [156], but neither size nor nonpalpability palpability is sufficiently predictive to effectively guide management. The management of these populations with testicle sparing approaches using partial orchiectomy and rapid frozen section evaluation has gained popularity [151, 152, 155, 157–159]. These approaches allow excision of the lesion, preservation of the remaining testicle when benign pathology is encountered on frozen section analysis, and completion orchiectomy in cases where malignancy is confirmed. The management of these select populations has further evolved to include ultrasound surveillance, particularly when these small or nonpalpable masses are discovered in patients who are being evaluated for impaired fertility [133, 149, 152]. The ultrasound findings of lesion size and echogenicity have been used along with the assessment of the lesion's palpability on exam to select patients appropriate for surveillance strategies. Most strategies have employed a size threshold of 1 cm to discriminate those lesions that may be appropriate for surveillance [133, 150, 153].

In the current reported literature and in our experience, subcentimeter germ cell tumors that are soft on sonoelastography have yet to be encountered. The only tumor encountered in these reports without a firm sonoelastogram pattern was a Leydig cell tumor. This allows the sonoelastogram to be a powerful tool in justifying a decision to pursue imaging surveillance of a patient with a subcentimeter testicular lesion. We have incorporated the results of the current literature in a clinical decision tree (Fig. 6.58). A patient with a subcentimeter testicular lesion on ultrasound should have a history, physical examination, and tumor makers (alpha-fetoprotein, lactose dehydrogenase, and beta-human chorionic gonadotropin serum levels). Tumor makers and history can identify patients with high risk of malignancy, such as those with a previous germ cell tumor, or elevated markers. Those that are without those risk factors may be considered for surveillance and, at this point, sonoelastography can be used to discriminate those with firm lesions from those with minimal to no increase in firmness and direct the patient for surgical exploration rather than observation.

The reports of sonoelastography for the small testicular lesion are limited in number. The low risk of the examination and high negative predictive value so far warrant expansion of its use. There are a number of clinical questions that remain to be elucidated about the usefulness of this technology. First, all reports include histologic findings or clinical course of lesions on imaging to determine whether the lesions are malignant or indolent. There has yet to be a study that reports the pathologic findings for all lesions. Thus, there may exist a population of subcentimeter nodules with malignant pathology, but an indolent clinical course that are classified as benign with these technologies. Second, though this discussion focuses on the clinical question of the subcentimeter mass, it is unclear

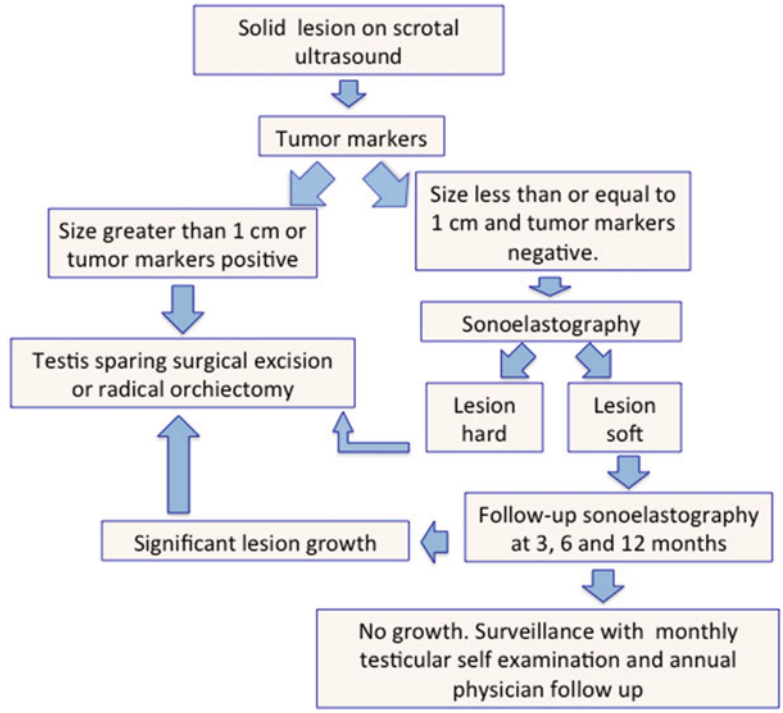

Fig. 6.58 Clinical decision tree for the management of lesions detected on ultrasound incorporating sonoelastography

at this time over what size ranges of lesions sonoelastography will offer the most useful information. Third, this modality also raises the possibility of the detection of sonoelastographic lesions that are not detected with ultrasound alone and the question of how to manage these scenarios. Finally, we have used shear wave sonoelastography for our sonoelastagrams and others have used real-time sonoelastography. It is unclear whether the modalities are equivalent or if one may offer an advantage for this clinical scenario. Thus, we await the reports of outcomes of others using sonoelastography for the subcentimeter testicular mass to help resolve the questions that remain and tailor the use of the modality with the perdurable fabric of a broader evidence base.

Intraoperative Testicular Ultrasound

Ultrasonography may be used to enhance the localization of intratesticular abnormalities at the time of surgery. Many of the lesions that are removed with the testis-sparing approach are nonpalpable and were diagnosed solely on ultrasound findings. In order to identify these lesion in the operating room, ultrasound is again used effectively to isolate the lesion for testis-sparing surgery. Hopps and Golstein described using intraoperative ultrasound prior to opening the tunica albuginea for needle localization of the mass removal of incidental testicular lesions found in infertile men [159]. De Stefani et al. describe use of intraoperative ultrasound in 20 cases of testis-sparing excision of lesion less than 2 cm in size. They found only two of the lesions to be malignant and all patients were disease free without hypogonadism at mean follow up of 1 year [160]. Use of ultrasound at the time of testis-sparing surgery is an extremely helpful tool to localize small lesions for testis-sparing surgery.

Male Infertility

In men with impaired fertility, ultrasound can provide diagnostic information and provide doc-

umentation prior to and after intervention. Ultrasound, being a noninvasive, real-time imaging modality, is often used in the comprehensive evaluation of men with impaired semen quality to document the presence or absence of pathology, especially when the physical exam is inconclusive or suggestive of intrascrotal pathology.

Varicocele

A varicocele is a dilatation of the testicular vein and the pampiniform venous plexus within the spermatic cord. With bilateral varicoceles, the larger varicocele is often on the left side, most likely related to the angle of insertion in to the left renal vein and the length of the left testicular vein [161, 162]. The left testicular vein is 8–10 cm longer than the right, with a proportional increase in pressure. Varicoceles have been found to be a bilateral condition in more than 80 % of cases in some series [162, 163]. Congenitally absent or incompetent venous valves have been thought to be the primary cause of varicocele [164–167].

The most common presentation of a varicocele is due to an investigation of male subfertility and infrequently due to scrotal pain. A varicocele is present in about 15 % of normally fertile men, yet present in 30–40 % of men with primary subfertility, and in as many as 80 % of men with secondary subfertility [168, 169]. Clinically detectable varicocele has been associated with testicular hypotrophy or atrophy, an abnormal gonadotropin axis, histologic changes in testis, abnormal spermatogenesis, and infertility [170]. Clinically significant varicoceles are associated with subfertility and impairments in semen quality [168]. After surgical varicocele ligation, semen analysis normally improves in approximately 70 % of the patients, with an increase in motility being the most common, but also improvements in sperm concentration, morphology percentage, and total motile sperm concentration [171–173].

Ultrasound characteristics of varicoceles include finding of multiple, low-reflective serpiginous tubular structures most commonly superior and posteriolateral to the testis. Veins larger than 2 mm in diameter are considered to be abnormal [118, 174]. Color flow Doppler is important in documenting the presence and size of a varicocele and should show reversal of flow during the Valsalva maneuver [43]. Color flow will also differentiate an intratesticular varicocele from a dilated rete testis (Fig. 6.59).

Importantly, a varicocele may also be a sign of pathology in the retroperitoneum causing compression of the gonadal veins leading to varicocele. Imaging of the retroperitoneum is therefore necessary in men with large varicoceles that do not decrease in the supine position and should also be considered in men with a predominately large right-sided varicocele. Patients who have sudden onset of a varicocele, whose varicocele persists in the supine position, or have an isolated right varicocele should be further evaluated with imaging of the retroperitoneum to assess for a renal vein thrombus, renal, or retroperitoneal mass [43].

Azoospermia and Oligospermia

In men with azoospermia, ultrasound as an initial modality of imaging study can often define the underlying etiology to determine whether there is an obstructive or nonobstructive cause of azoospermia [175]. The ultrasound, as well as physical exam, is useful in patients with congenital bilateral absence of the vas deferens (CBAVD) to assess for presence of the vas deferens as well as other mesonephric developmental structures, and associated conditions such as congenital renal agenesis [176, 177].

Ultrasound will also reveal testicular atrophy. Atrophy may be related to age, trauma, torsion, infection, or inflammation, or may occur secondary to hypothyroidism, drug therapy, or chronic disease. The appearance on ultrasound is variable, and while related to the underlying cause, is usually characterized by decreased echogenicity with a normal appearing epididymis.

Newer Ultrasound Technology to Assess Fertility

Recent literature supports the use of spectral Doppler ultrasound in providing information about intratesticular blood flow and function [70, 173, 178, 179] (Fig. 6.54). Biagiotti et al. provided data suggesting that Resistive Index (RI)

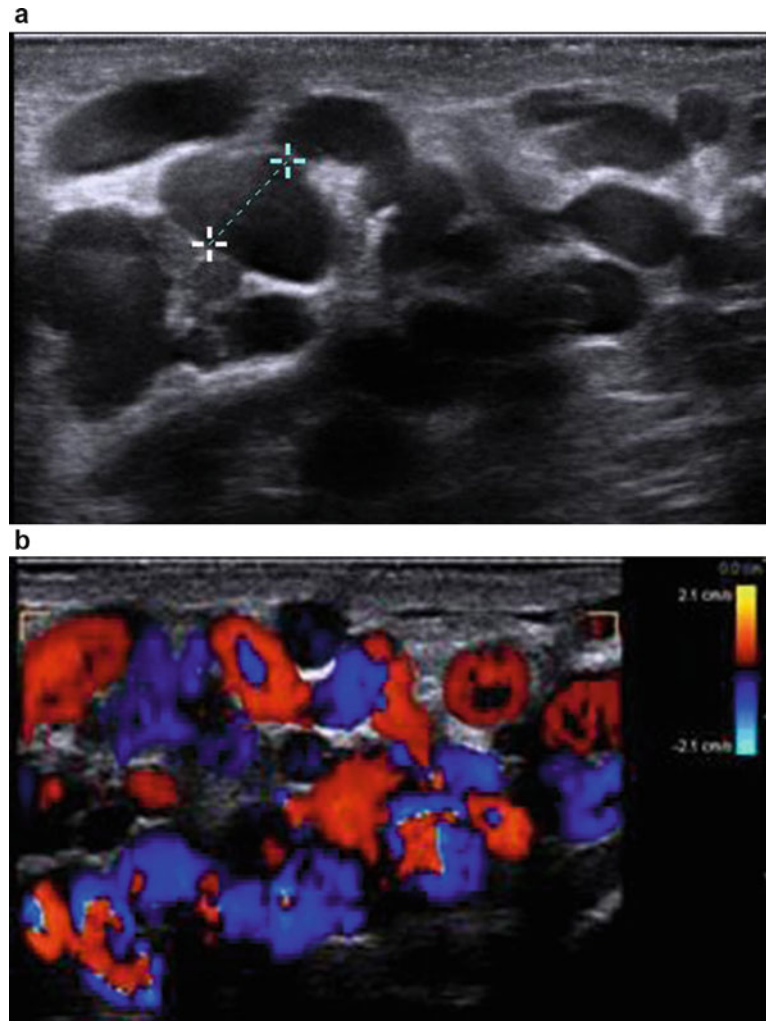

Fig. 6.59 Bilateral varicocele, (**a**) Doppler color flow study dilated veins on the superior aspect of the testis. (**b**) Doppler color flow study showing bilateral varicoceles

and PSV (Peak Systolic Velocity) of intratesticular vessels were better predictors of dyspermia than FSH and testicular volume [180]. Pinggera et al. [178] examined semen quality and the RI of intratesticular arteries in 160 men. In their study, the 80 men with a normal semen analysis had a RI of 0.54 ± 0.05 and the 80 men with impaired semen analysis had a statistically higher RI of 0.68 ± 0.06. This study concluded that an RI above the threshold of 0.60 was indicative of abnormal semen quality. This has also been confirmed by our group for subfertile men [181].

Additionally, sonoelastography has been studied in the infertile male (Fig. 6.60). Schurlich et al. reported that elastography could be used for structural analysis of the testicular tissue [182]. In another study, Li et al. used a five-point scoring system to describe the elastographic findings in azoospermic men. Patients with obstructive azoospermia (OA) and healthy controls with a normal semen analysis predominately had a high-strain score of 83 % and 85 %, respectively. Conversely, 82 % of men with nonobstructive azoospermia (NOA) had a score of 3 or higher, and therefore may assist in the diagnosis of NOA [183]. The initial data with elastography is intriguing and in the future this new modality may yield additional information on testicular function.

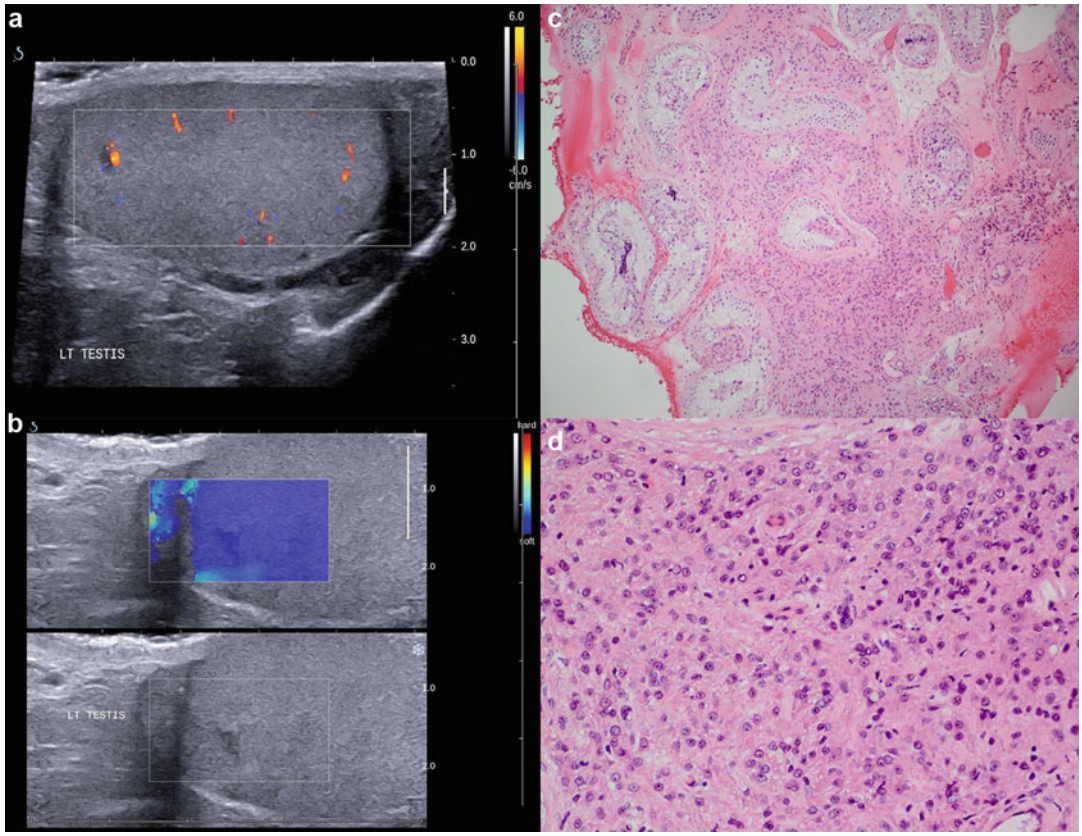

Fig. 6.60 Images and histology representative of lesions evaluated by biopsy. This is from patient 3 (Table 6.2). Color Doppler ultrasound image of left testis lesion with evidence of blood flow in lesion (**a**). Sonoelastography image demonstrating no increased firmness within the lesion (**b**). Photomicrographs of testicular biopsy of lesion at 10x (**c**) and 40x (**d**) revealing Leydig cell hyperplasia and tubules demonstrating hypospermatogenesis

Conclusions

Ultrasonography is the gold standard evaluation for abnormalities of the scrotum. The use of ultrasound enhances findings found on physical exam and can determine the diagnosis in many pathologic conditions of the scrotum. New technologic advances allow for improved visualization and novel diagnostic techniques, such as elastography. Overall, the ability to interpret ultrasonographic findings is a key component for any physician caring for patients with pathology of the scrotum, testis, epididymis, or infertility.

References

1. American Institute of Ultrasound in Medicine, American Urological Association. AIUM practice guideline for the performance of an ultrasound examination in the practice of urology. J Ultrasound Med. 2012;31(1):133–44.
2. American Institute in Medicine. AIUM practice guidelines for the performance of scrotal ultrasound examinations. J Ultrasound Med. 2015;34(8).
3. Nielsen ME. Use and misuse of imaging by urologists. J Urol. 2010;184(1):12–4.
4. Douglas PS. Improving imaging: our professional imperative. J Am Coll Cardiol. 2006;48(10):2152–5.
5. Dogra V, Bhatt S. Acute painful scrotum. Radiol Clin North Am. 2004;42(2):349–63.

6. Smart JM, et al. Ultrasound findings of masses of the paratesticular space. Clin Radiol. 2008;63(8):929–38.
7. Hadziselimovic F, et al. The importance of mini-puberty for fertility in cryptorchidism. J Urol. 2005;174(4 Pt 2):1536–9. Discussion 1538–9.
8. Raivio T, et al. Serum androgen bioactivity in cryptorchid and noncryptorchid boys during the postnatal reproductive hormone surge. J Clin Endocrinol Metab. 2003;88(6):2597–9.
9. Kuijper EA, et al. Ultrasonographically measured testicular volumes in 0- to 6-year-old boys. Hum Reprod. 2008;23(4):792–6.
10. Aso C, et al. Gray-scale and color Doppler sonography of scrotal disorders in children: an update. Radiographics. 2005;25(5):1197–214.
11. Wein AJ, Kavoussi LR, Campbell MF. Campbell-Walsh urology/editor-in-chief, Alan J. Wein. In: Kavoussi LR, et al., editors. 10th ed. Philadelphia: Elsevier Saunders; 2012.
12. Dogra VS, et al. Sonography of the scrotum. Radiology. 2003;227(1):18–36.
13. Thomas RD, Dewbury KC. Ultrasound appearances of the rete testis. Clin Radiol. 1993;47(2):121–4.
14. Pearl MS, Hill MC. Ultrasound of the scrotum. Semin Ultrasound CT MR. 2007;28(4):225–48.
15. Wishahi MM. Anatomy of the venous drainage of the human testis: testicular vein cast, microdissection and radiographic demonstration. A new anatomical concept. Eur Urol. 1991;20(2):154–60.
16. Black JA, Patel A. Sonography of the normal extratesticular space. AJR Am J Roentgenol. 1996;167(2):503–6.
17. Carlson BM. Human embryology and developmental biology. Elsevier Health Sciences; 2013.
18. Moore KL, Persaud TVN, Torchia MG. The developing human. Philadelphia: Saunders; 2011.
19. Bellinger MF. Embryology of the male external genitalia. Urol Clin North Am. 1981.
20. Sadler TW. Langman medical embryology. Int Ed. Auckland: Wolters Kluwer Health; 2011.
21. Kolettis PN, Sandlow JI. Clinical and genetic features of patients with congenital unilateral absence of the vas deferens. Urology. 2002;60(6):1073–6.
22. Hughes IA, Acernia CI. Factors controlling testis descent. Eur J Endocrinol. 2008;159 Suppl 1:S75–82.
23. Frey HL, Rajfer J. Role of the gubernaculum and intraabdominal pressure in the process of testicular descent. J Urol. 1984.
24. Heyns CF. The gubernaculum during testicular descent in the human fetus. J Anat. 1987.
25. Hutson JM, Southwell BR, Li R, et al. The regulation of testicular descent and the effects of cryptorchidism. Endocr Rev. 2013;34(5):725–52.
26. Malone PS, Guiney EJ. A comparison between ultrasonography and laparoscopy in localising the impalpable undescended testis. Br J Urol. 1985.
27. Madrazo BL, Klugo RC, Parks JA, DiLoreto R. Ultrasonographic demonstration of undescended testes. Radiology. 1979;133(1):181–3.
28. Cain MP, Garra B, Gibbons MD. Scrotal-inguinal ultrasonography: a technique for identifying the nonpalpable inguinal testis without laparoscopy. J Urol. 1996.
29. Weiss RM, Carter AR, Rosenfield AT. High resolution real-time ultrasonography in the localization of the undescended testis. J Urol. 1986.
30. Wilson JD, George FW, Griffin JE. The hormonal control of sexual development. Science. 1981;211(4488):1278–84.
31. Rey R, Picard JY. Embryology and endocrinology of genital development. Baillieres Clin Endocrinol Metab. 1998.
32. Wilson JD, Griffin JE, Leshin M, George FW. Role of gonadal hormones in development of the sexual phenotypes. Hum Genet. 1981.
33. Osifo OD, Osaigbovo EO. Congenital hydrocele: prevalence and outcome among male children who underwent neonatal circumcision in Benin City, Nigeria. J Pediatr Urol. 2008;4(3):178–82.
34. Wampler SM, Llanes M. Common scrotal and testicular problems. Prim Care. 2010;37(3):613–26, x.
35. Mihmanli I, et al. Testicular size and vascular resistance before and after hydrocelectomy. AJR Am J Roentgenol. 2004;183(5):1379–85.
36. Garriga V, et al. US of the tunica vaginalis testis: anatomic relationships and pathologic conditions. Radiographics. 2009;29(7):2017–32.
37. Jones ME, et al. Risk of congenital inguinal hernia in siblings: a record linkage study. Paediatr Perinat Epidemiol. 1998;12(3):288–96.
38. Rescorla FJ, et al. The "other side" of pediatric hernias: the role of laparoscopy. Am Surg. 1997;63(8):690–3.
39. Erez I, et al. Preoperative ultrasound and intraoperative findings of inguinal hernias in children: a prospective study of 642 children. J Pediatr Surg. 2002;37(6):865–8.
40. Adams CE, Wald M. Risks and complications of vasectomy. Urol Clin North Am. 2009;36(3):331–6.
41. Greek G. Vasectomy. A safe, effective, economical means of sterilization. Postgrad Med. 2000;108(2):173–6, 179.
42. Schwingl PJ, Guess HA. Safety and effectiveness of vasectomy. Fertil Steril. 2000;73(5):923–36.
43. Aganovic L, Cassidy F. Imaging of the scrotum. Radiol Clin North Am. 2012;50(6):1145–65.
44. Somekh E, Gorenstein A, Serour F. Acute epididymitis in boys: evidence of a post-infectious etiology. J Urol. 2004;171(1):391–4. Discussion 394.
45. Bohm MK, Gift TL, Tao G. Patterns of single and multiple claims of epididymitis among young privately-insured males in the United States, 2001 to 2004. Sex Transm Dis. 2009;36(8):490–2.
46. Drener ML. Torsed appendage. Diagnosis and management: blue dot sign. Urology. 1973;1(1):63–6.
47. Akbar SA, et al. Multimodality imaging of paratesticular neoplasms and their rare mimics. Radiographics. 2003;23(6):1461–76.
48. Aydin H, et al. Clear cell papillary cystadenoma of the epididymis and mesosalpinx: immunohistochemical differentiation from metastatic clear cell renal cell carcinoma. Am J Surg Pathol. 2005;29(4):520–3.

49. Alexander JA, Lichtman JB, Varma VA. Ultrasound demonstration of a papillary cystadenoma of the epididymis. J Clin Ultrasound. 1991;19(7):442–5.
50. Tchelepi H, et al. Sonography of spermatic cord leiomyoma: case report and review of the literature. J Ultrasound Med. 2004;23(4):569–71.
51. Salm R. Papillary sarcinoma of the epididymis. J Pathol. 1969;97(2):253–9.
52. Dowling KJ, Lieb HE. Fibrosarcoma of epididymis. Urology. 1985;26(3):307–8.
53. Kurihara K, et al. Papillary adenocarcinoma of the epididymis. Acta Pathol Jpn. 1993;43(7-8):440–3.
54. Malik AM, et al. The spectrum of presentation and management of Fournier's gangrene—an experience of 73 cases. J Pak Med Assoc. 2010;60(8):617–9.
55. Sorensen MD, et al. Fournier's gangrene: management and mortality predictors in a population based study. J Urol. 2009;182(6):2742–7.
56. Levenson RB, Singh AK, Novelline RA. Fournier gangrene: role of imaging. Radiographics. 2008;28(2):519–28.
57. Rajan DK, Scharer KA. Radiology of Fournier's gangrene. AJR Am J Roentgenol. 1998;170(1):163–8.
58. Swygert KE, et al. Melanoma in situ involving an epidermal inclusion (infundibular) cyst. Am J Dermatopathol. 2007;29(6):564–5.
59. Hara Y, et al. Acute scrotum caused by Henoch-Schonlein purpura. Int J Urol. 2004;11(7):578–80.
60. Germaine P, Simerman LP. Fibrous pseudotumor of the scrotum. J Ultrasound Med. 2007;26(1):133–8.
61. Seethala RR, et al. Diffuse fibrous pseudotumor of the testicular tunics associated with an inflamed hydrocele. Arch Pathol Lab Med. 2003;127(6):742–4.
62. Lee A, et al. Acute idiopathic scrotal edema: ultrasonographic findings at an emergency unit. Eur Radiol. 2009;19(8):2075–80.
63. Thomas AC, et al. Ultrasound findings of acute idiopathic scrotal edema. ScientificWorldJournal. 2004;4 Suppl 1:9–10.
64. Grainger AJ, Hide IG, Elliott ST. The ultrasound appearances of scrotal oedema. Eur J Ultrasound. 1998;8(1):33–7.
65. Sung EK, Setty BN, Castro-Aragon I. Sonography of the pediatric scrotum: emphasis on the Ts—torsion, trauma, and tumors. AJR Am J Roentgenol. 2012;198(5):996–1003.
66. Lowe FC. Squamous-cell carcinoma of the scrotum. Urol Clin North Am. 1992;19(2):397–405.
67. Ringdahl E, Teague L. Testicular torsion. Am Fam Physician. 2006;74(10):1739–43.
68. Bartsch G, et al. Testicular torsion: late results with special regard to fertility and endocrine function. J Urol. 1980;124(3):375–8.
69. Waldert M, et al. Color Doppler sonography reliably identifies testicular torsion in boys. Urology. 2010;75(5):1170–4.
70. Jee WH, et al. Resistive index of the intrascrotal artery in scrotal inflammatory disease. Acta Radiol. 1997;38(6):1026–30.
71. Yagil Y, et al. Role of Doppler ultrasonography in the triage of acute scrotum in the emergency department. J Ultrasound Med. 2010;29(1):11–21.
72. Dogra VS, et al. Benign intratesticular cystic lesions: US features. Radiographics. 2001;21 Spec No:S273–81.
73. Nakagawa A, et al. In vivo analysis of phagocytosis of apoptotic cells by testicular Sertoli cells. Mol Reprod Dev. 2005;71(2):166–77.
74. Drut R, Drut RM. Testicular microlithiasis: histologic and immunohistochemical findings in 11 pediatric cases. Pediatr Dev Pathol. 2002;5(6):544–50.
75. van Casteren NJ, Looijenga LH, Dohle GR. Testicular microlithiasis and carcinoma in situ overview and proposed clinical guideline. Int J Androl. 2009;32(4):279–87.
76. Dagash H, Mackinnon EA. Testicular microlithiasis: what does it mean clinically? BJU Int. 2007;99(1) :157–60.
77. Middleton WD, Teefey SA, Santillan CS. Testicular microlithiasis: prospective analysis of prevalence and associated tumor. Radiology. 2002;224(2):425–8.
78. Goede J, et al. Prevalence of testicular microlithiasis in asymptomatic males 0 to 19 years old. J Urol. 2009;182(4):1516–20.
79. Kocaoglu M, et al. Testicular microlithiasis in pediatric age group: ultrasonography findings and literature review. Diagn Interv Radiol. 2005;11(1):60–5.
80. von Eckardstein S, et al. Sonographic testicular microlithiasis as an indicator of premalignant conditions in normal and infertile men. J Androl. 2001;22(5):818–24.
81. Furness 3rd PD, et al. Multi-institutional study of testicular microlithiasis in childhood: a benign or premalignant condition? J Urol. 1998;160(3 Pt 2):1151–4. Discussion 1178.
82. DeCastro BJ, Peterson AC, Costabile RA. A 5-year followup study of asymptomatic men with testicular microlithiasis. J Urol. 2008;179(4):1420–3. Discussion 1423.
83. Frush DP, Kliewer MA, Madden JF. Testicular microlithiasis and subsequent development of metastatic germ cell tumor. AJR Am J Roentgenol. 1996;167(4):889–90.
84. Richenberg J, Belfield J, Ramchandani P, Rocher L, Freeman S, Tsili AC, Cuthbert F, Studniarek M, Bertolotto M, Turgut AT, Dogra V, Derchi LE. Testicular microlithiasis imaging and follow-up: guidelines of the ESUR scrotal imaging subcommittee. Eur Radiol. 2015;25(2):323–30.
85. Comiter CV, et al. Burned-out primary testicular cancer: sonographic and pathological characteristics. J Urol. 1996;156(1):85–8.
86. Gooding GA, Leonhardt W, Stein R. Testicular cysts: US findings. Radiology. 1987;163(2): 537–8.
87. Carver BS, Carver BS, Al-Ahmadie H, Sheinfeld J. Adult and pediatric testicular teratoma. Urol Clin North Am. 2007;34(2):245–51. abstract x.
88. Chou SJ, et al. Cysts of the tunica albuginea. Arch Androl. 2004;50(2):89–92.

89. Tammela TL, et al. Cysts of the tunica albuginea—more common testicular masses than previously thought? Br J Urol. 1991;68(3):280–4.
90. Nistal M, Mate A, Paniagua R. Cystic transformation of the rete testis. Am J Surg Pathol. 1996; 20(10):1231–9.
91. Nair R, et al. Tubular ectasia of the rete testis: a diagnostic dilemma. Ann R Coll Surg Engl. 2008;90(7): W1–3.
92. Bree RL, Hoang DT. Scrotal ultrasound. Radiol Clin North Am. 1996;34(6):1183–205.
93. Atasoy C, Fitoz S. Gray-scale and color Doppler sonographic findings in intratesticular varicocele. J Clin Ultrasound. 2001;29(7):369–73.
94. Bucci S, et al. Intratesticular varicocele: evaluation using grey scale and color Doppler ultrasound. World J Urol. 2008;26(1):87–9.
95. Kessler A, et al. Intratesticular varicocele: gray scale and color Doppler sonographic appearance. J Ultrasound Med. 2005;24(12):1711–6.
96. Das KM, et al. Intratesticular varicocele: evaluation using conventional and Doppler sonography. AJR Am J Roentgenol. 1999;173(4):1079–83.
97. Mouritsen A, et al. Testicular adrenal rest tumours in boys, adolescents and adult men with congenital adrenal hyperplasia may be associated with the CYP21A2 mutation. Int J Androl. 2010;33(3): 521–7.
98. Claahsen-van der Grinten HL, et al. Prevalence of testicular adrenal rest tumours in male children with congenital adrenal hyperplasia due to 21-hydroxylase deficiency. Eur J Endocrinol. 2007;157(3):339–44.
99. Dogra V, Nathan J, Bhatt S. Sonographic appearance of testicular adrenal rest tissue in congenital adrenal hyperplasia. J Ultrasound Med. 2004;23(7):979–81.
100. Proto G, et al. Bilateral testicular adrenal rest tissue in congenital adrenal hyperplasia: US and MR features. J Endocrinol Invest. 2001;24(7):529–31.
101. Dieckmann KP, et al. Bilateral testicular germ cell tumors. Report of nine cases and review of the literature. Cancer. 1986;57(6):1254–8.
102. Datta SN, et al. A case of scrotal sarcoidosis that mimicked tuberculosis. Nat Clin Pract Urol. 2007;4(4):227–30.
103. Deurdulian C, et al. US of acute scrotal trauma: optimal technique, imaging findings, and management. Radiographics. 2007;27(2):357–69.
104. Cubillos J, et al. A conservative approach to testicular rupture in adolescent boys. J Urol. 2010;184(4 Suppl):1733–8.
105. Wittenberg AF, et al. Sonography of the acute scrotum: the four T's of testicular imaging. Curr Probl Diagn Radiol. 2006;35(1):12–21.
106. Buckley JC, McAninch JW. Use of ultrasonography for the diagnosis of testicular injuries in blunt scrotal trauma. J Urol. 2006;175(1):175–8.
107. Guichard G, et al. Accuracy of ultrasonography in diagnosis of testicular rupture after blunt scrotal trauma. Urology. 2008;71(1):52–6.
108. Kim SH, et al. The efficacy of magnetic resonance imaging for the diagnosis of testicular rupture: a prospective preliminary study. J Trauma. 2009;66(1):239–42.
109. Bhatt S, Dogra VS. Role of US in testicular and scrotal trauma. Radiographics. 2008;28(6):1617–29.
110. Chandra RV, et al. Rational approach to diagnosis and management of blunt scrotal trauma. Urology. 2007;70(2):230–4.
111. Albers P, Albrecht W, Algaba f, Bokemeyer C, Cohn-Cedermark G, Fizazi K, Horwich A, Laguna MP, Nicolai N, Oldenburg NJ. Guidelines on testicular cancer. http://uroweb.org/wp-content/uploads/11-Testicular-Cancer_LR1.pdf
112. Metcalfe PD, et al. Pediatric testicular tumors: contemporary incidence and efficacy of testicular preserving surgery. J Urol. 2003;170(6 Pt 1):2412–5. Discussion 2415–6.
113. Horwich A, Shipley J, Huddart R. Testicular germ-cell cancer. Lancet. 2006;367(9512):754–65.
114. Schwerk WB, Schwerk WN, Rodeck G. Testicular tumors: prospective analysis of real-time US patterns and abdominal staging. Radiology. 1987;164(2):369–74.
115. Woodward PJ, et al. From the archives of the AFIP: tumors and tumorlike lesions of the testis: radiologic-pathologic correlation. Radiographics. 2002;22(1):189–216.
116. Shah A, et al. Re: new ultrasound techniques for imaging of the indeterminate testicular lesion may avoid surgery completely. Clin Radiol. 2010;65(6): 496–7.
117. Frush DP, Sheldon CA. Diagnostic imaging for pediatric scrotal disorders. Radiographics. 1998;18(4):969–85.
118. Mirochnik B, et al. Ultrasound evaluation of scrotal pathology. Radiol Clin North Am. 2012;50(2):317–32, vi.
119. Khalid M, et al. Concomitant bilateral testicular epidermoid cysts. Saudi Med J. 2008;29(6):907–9.
120. Bhatt S, et al. Imaging of non-neoplastic intratesticular masses. Diagn Interv Radiol. 2010; 17(1):52–63.
121. Dogra VS, et al. Testicular epidermoid cysts: sonographic features with histopathologic correlation. J Clin Ultrasound. 2001;29(3):192–6.
122. Malvica RP. Epidermoid cyst of the testicle: an unusual sonographic finding. AJR Am J Roentgenol. 1993;160(5):1047–8.
123. Loya AG, Said JW, Grant EG. Epidermoid cyst of the testis: radiologic-pathologic correlation. Radiographics. 2004;24 Suppl 1:S243–6.
124. Hasselblom S, et al. Testicular lymphoma—a retrospective, population-based, clinical and immunohistochemical study. Acta Oncol. 2004;43(8):758–65.
125. Vural F, et al. Primary testicular lymphoma. J Natl Med Assoc. 2007;99(11):1277–82.
126. Zucca E, et al. Patterns of outcome and prognostic factors in primary large-cell lymphoma of the testis in

a survey by the International Extranodal Lymphoma Study Group. J Clin Oncol. 2003;21(1):20–7.
127. Garcia-Gonzalez R, Pinto J, Val-Bernal JF. Testicular metastases from solid tumors: an autopsy study. Ann Diagn Pathol. 2000;4(2):59–64.
128. Tiltman AJ. Metastatic tumours in the testis. Histopathology. 1979;3(1):31–7.
129. Angulo JC, et al. Clinicopathological study of regressed testicular tumors (apparent extragonadal germ cell neoplasms). J Urol. 2009;182(5):2303–10.
130. Carmignani L, et al. High incidence of benign testicular neoplasms diagnosed by ultrasound. J Urol. 2003;170(5):1783–6.
131. Muller T, et al. Management of incidental impalpable intratesticular masses of < or = 5 mm in diameter. BJU Int. 2006;98(5):1001–4.
132. Hallak J, et al. Organ-sparing microsurgical resection of incidental testicular tumors plus microdissection for sperm extraction and cryopreservation in azoospermic patients: surgical aspects and technical refinements. Urology. 2009;73(4):887–91. Discussion 891–2.
133. Toren PJ, et al. Small incidentally discovered testicular masses in infertile men—is active surveillance the new standard of care? J Urol. 2010; 183(4):1373–7.
134. Bamber JC. Ultrasound elasticity imaging: definition and technology. Eur Radiol. 1999;9 Suppl 3:S327–30.
135. Wells PNT, Liang HD. Medical ultrasound: imaging of soft tissue strain and elasticity. J R Soc Interface. 2011;8(64):1521–49.
136. Arda K, Ciledag N, Aktas E, Arıbas BK, Köse K. Quantitative assessment of normal soft-tissue elasticity using shear-wave ultrasound elastography. Am J Roentgenol. 2011;197(3):532–6.
137. Greenleaf JF, Fatemi M, Insana M. Selected methods for imaging elastic properties of biological tissues. Annu Rev Biomed Eng. 2003;5(1):57–78.
138. Goddi A, Bonardi M, Alessi S. Breast elastography: a literature review. J Ultrasound. 2012;15(3):192–8.
139. Tanter M, Bercoff J, Athanasiou A, et al. Quantitative assessment of breast lesion viscoelasticity: initial clinical results using supersonic shear imaging. Ultrasound Med Biol. 2008;34(9):1373–86.
140. Sebag F, Vaillant-Lombard J, Berbis J, et al. Shear wave elastography: a new ultrasound imaging mode for the differential diagnosis of benign and malignant thyroid nodules. J Clin Endocrinol Metab. 2010;95(12):5281–8.
141. Madsen EL, Sathoff HJ, Zagzebski JA. Ultrasonic shear wave properties of soft tissues and tissuelike materials. J Acoust Soc Am. 1983;74(5):1346–55.
142. Nelson TR, Fowlkes JB, Abramowicz JS, Church CC. Ultrasound biosafety considerations for the practicing sonographer and sonologist. J Ultrasound Med. 2009;28(2):139–50.
143. Grasso M, Blanco S, Raber M, Nespoli L. Elastosonography of the testis: preliminary experience. Arch Ital Urol Androl. 2010;82(3):160–3.
144. Goddi A, Sacchi A, Magistretti G, Almolla J, Salvadore M. Real-time tissue elastography for testicular lesion assessment. Eur Radiol. 2011;22(4):721–30.
145. Itoh A, Ueno E, Tohno E, Kamma H, Takahashi H. Breast disease: clinical application of US elastography for diagnosis. Radiology. 2006;239(2):341–50.
146. Aigner F, De Zordo T, Pallwein-Prettner L, et al. Real-time sonoelastography for the evaluation of testicular lesions. Radiology. 2012;263(2):584–9.
147. Comiter CV, Benson CJ, Capelouto CC, et al. Nonpalpable intratesticular masses detected sonographically. J Urol. 1995;154(4):1367–9.
148. Subik MK, Gordetsky J, Yao JL, di Sant'Agnese PA, Miyamoto H. Frozen section assessment in testicular and paratesticular lesions suspicious for malignancy: its role in preventing unnecessary orchiectomy. Hum Pathol. 2012;43(9):1514–9.
149. Eifler Jr JB, King P, Schlegel PN. Incidental testicular lesions found during infertility evaluation are usually benign and may be managed conservatively. J Urol. 2008;180(1):261–5.
150. Mammen T, Costabile RA. Management of incidentally discovered non-palpable testicular lesions. AUA Update Series. Vol. 28, Lesson 2; 2009. p. 1-8.
151. Rolle L, Tamagnone A, Destefanis P, et al. Microsurgical "testis-sparing" surgery for nonpalpable hypoechoic testicular lesions. Urology. 2006;68(2):381–5.
152. Gentile G, Brunocilla E, Franceschelli A, et al. Can testis-sparing surgery for small testicular masses be considered a valid alternative to radical orchiectomy? A prospective single-center study. Clin Genitourin Cancer. 2013;11(4):522–6.
153. Connolly SS, D'Arcy FT, Gough N, McCarthy P, Bredin HC, Corcoran MO. Carefully selected intratesticular lesions can be safely managed with serial ultrasonography. BJU Int. 2006;98(5):1005–7.
154. Hindley RG, Chandra A, Saunders A, O'Brien TS. Impalpable testis cancer. BJU Int. 2003;92(6):572–4.
155. Kirkham APS, Kumar P, Minhas S, et al. Targeted testicular excision biopsy: when and how should we try to avoid radical orchidectomy? Clin Radiol. 2009;64(12):1158–65.
156. Shilo Y, Zisman A, Lindner A, et al. The predominance of benign histology in small testicular masses. Urol Oncol Semin Orig Invest. 2012;30(5):719–22.
157. Giannarini G, Dieckmann K-P, Albers P, Heidenreich A, Pizzocaro G. Organ-sparing surgery for adult testicular tumours: a systematic review of the literature. Eur Urol. 2010;57(5):780–90.
158. Powell TM, Tarter TH. Management of nonpalpable incidental testicular masses. J Urol. 2006;176(1):96–9.
159. Hopps CV, Goldstein M. Ultrasound guided needle localization and microsurgical exploration for incidental nonpalpable testicular tumors. J Urol. 2002;168(3):1084–7.
160. De Stefani S, et al. Microsurgical testis-sparing surgery in small testicular masses: seven years

retrospective management and results. Urology. 2012;79(4):858–62.
161. Shafik A, et al. Testicular veins: anatomy and role in varicocelogenesis and other pathologic conditions. Urology. 1990;35(2):175–82.
162. Gat Y, et al. Induction of spermatogenesis in azoospermic men after internal spermatic vein embolization for the treatment of varicocele. Hum Reprod. 2005;20(4):1013–7.
163. Gat Y, et al. Varicocele, hypoxia and male infertility. Fluid Mechanics analysis of the impaired testicular venous drainage system. Hum Reprod. 2005;20(9):2614–9.
164. Wishahi MM. Anatomy of the spermatic venous plexus (pampiniform plexus) in men with and without varicocele: intraoperative venographic study. J Urol. 1992;147(5):1285–9.
165. Braedel HU, et al. A possible ontogenic etiology for idiopathic left varicocele. J Urol. 1994;151(1):62–6.
166. Gorenstein A, Katz S, Schiller M. Varicocele in children: "to treat or not to treat"—venographic and manometric studies. J Pediatr Surg. 1986;21(12):1046–50.
167. Iafrate M, et al. Varicocele is associated with an increase of connective tissue of the pampiniform plexus vein wall. World J Urol. 2009;27(3):363–9.
168. The influence of varicocele on parameters of fertility in a large group of men presenting to infertility clinics. World Health Organization. Fertil Steril. 1992;57(6):1289–93.
169. Benoff S, Gilbert BR. Varicocele and male infertility: part I. Preface. Hum Reprod Update. 2001;7(1):47–54.
170. Robinson SP, Hampton LJ, Koo HP. Treatment strategy for the adolescent varicocele. Urol Clin North Am. 2010;37(2):269–78.
171. Sakamoto H, et al. Effects of varicocele repair in adults on ultrasonographically determined testicular volume and on semen profile. Urology. 2008;71(3):485–9.
172. Zucchi A, et al. Varicocele and fertility: relationship between testicular volume and seminal parameters before and after treatment. J Androl. 2006;27(4):548–51.
173. Tarhan S, et al. Long-term effect of microsurgical inguinal varicocelectomy on testicular blood flow. J Androl. 2011;32(1):33–9.
174. Cornud F, et al. Varicocele: strategies in diagnosis and treatment. Eur Radiol. 1999;9(3):536–45.
175. Donkol RH. Imaging in male-factor obstructive infertility. World J Radiol. 2010;2(5):172–9.
176. Honig SC, Lipshultz LI, Jarow J. Significant medical pathology uncovered by a comprehensive male infertility evaluation. Fertil Steril. 1994;62(5):1028–34.
177. McCallum T, et al. Unilateral renal agenesis associated with congenital bilateral absence of the vas deferens: phenotypic findings and genetic considerations. Hum Reprod. 2001;16(2):282–8.
178. Pinggera GM, et al. Assessment of the intratesticular resistive index by colour Doppler ultrasonography measurements as a predictor of spermatogenesis. BJU Int. 2008;101(6):722–6.
179. Lefort C, et al. Ischemic orchiditis: review of 5 cases diagnosed by color Doppler ultrasonography. J Radiol. 2001;82(7):839–42.
180. Biagiotti G, et al. Spermatogenesis and spectral echo-colour Doppler traces from the main testicular artery. BJU Int. 2002;90(9):903–8.
181. Hillelsohn JH, Chuang KW, Goldenberg E, Gilbert BR. Spectral Doppler sonography: a noninvasive method for predicting dyspermia. J Ultrasound Med. 2013;32(8):1427–32. doi:10.7863/ultra.32.8.1427.
182. Schurich M, et al. The role of ultrasound in assessment of male fertility. Eur J Obstet Gynecol Reprod Biol. 2009;144 Suppl 1:S192–8.
183. Li M, et al. The value of sonoelastography scores and the strain ratio in differential diagnosis of azoospermia. J Urol. 2012;188(5):1861–6.

Penile Ultrasound

7

Soroush Rais-Bahrami, Gideon Richards, and Bruce R. Gilbert

Introduction

Penile ultrasound is used commonly in the diagnostic workup of a patient with erectile dysfunction (ED), but also plays an important role by providing an anatomic and functional vascular assessment in a multitude of other conditions including Peyronie's disease, high-flow priapism, penile fracture, penile urethral strictures, urethral stones, urethral diverticulae, or masses involving deep tissues of the penis. As a component of the evaluation for ED, penile Doppler ultrasound (PDU) is performed to assess the quality of arterial blood flow and sufficiency of veno-occlusive mechanisms, both necessary for an adequate erection. This imaging modality, which incorporates real-time imaging of the vasculature, vessel wall compliance, and blood flow dynamics in an end organ small vessel arterial system, is playing a central role in the early detection and diagnosis of otherwise silent coronary artery disease (CAD). This is an important clinical finding in men who often present with ED as their initial symptom of underlying cardiovascular disease. PDU is also an essential component of the assessment of external genitalia in trauma situations where high-flow priapism or penile fracture is suspected. Penile ultrasound provides a readily available, minimally invasive diagnostic modality that evaluates both the structural anatomy and functional hemodynamics at a reasonable cost.

S. Rais-Bahrami, M.D. (✉)
Departments of Urology and Radiology, University of Alabama at Birmingham, Faculty Office Tower 1107, 510 20th Street South, Birmingham, AL 35294, USA
e-mail: sraisbahrami@uabmc.edu

G. Richards, M.D.
Arizona State Urological Institute, 1445 W. Chandler Blvd, Suite, A-5, Chandler, AZ 85224, USA
e-mail: gidrichards@gmail.com

B.R. Gilbert, M.D., Ph.D.
The Smith Institute for Urology, Northwell Health System, 450 Lakeville Road, Suite M41, New Hyde Park, NY 11040, USA
e-mail: bgilbert@gmail.com

Ultrasound Settings

Penile ultrasound is best performed with a high-frequency linear array transducer with an ultrasound frequency of 7.5–18 MHz which allows for high resolution images of the penis and internal vascular structures. Color and spectral Doppler are essential elements of penile ultrasonography in addition to B-mode ultrasound. 3D ultrasound is a developing technique that has the potential for better defining anatomic and vascular changes occurring with disease processes of the penis.

When available, split screen visualization allows for comparison of laterality very similar

P.F. Fulgham, B.R. Gilbert (eds.), *Practical Urological Ultrasound*, Current Clinical Urology,
DOI 10.1007/978-3-319-43868-9_7

to scrotal ultrasound discussed earlier. This is very important in penile ultrasound, but more specifically in PDU whereby the differences between vascular diameter, velocity of blood flow, and measurement of resistive index can be elegantly displayed in a single view for comparison of the right and left sides.

Scanning Technique

Scanning technique, as with any ultrasound examination, is operator dependent and hence may vary greatly. Nevertheless, it is essential for each practitioner to establish a routine protocol to which they fastidiously adhere. This allows for data to be comparable across serial examinations of the same patient and between studies performed on different patients with similar pathologies. Also, a routine protocol allows practitioners to provide anticipatory guidance to patients prior to beginning the study. A technique for patient preparation, routine survey scanning, and indication-specific scanning protocols for penile ultrasound are presented.

Importance of the Angle of Insonation

Knowledge of and correction for the angle of incidence is an essential to obtaining accurate data in PDU. The Doppler shift (FD) is a change in frequency between the transmitted sound wave F_T and received sound wave F_R resulting from the interaction between the frequency of the sound waves transmitted by the transducer (F_T), the velocity of blood (V_{BF}), the cosine of the angle of incidence (θ) between the vector of the transmitted sound wave from the transducer and the vector of blood flow as well as the speed of sound in tissue (c) as given by the equation:

$$\mathrm{FD} = F_R - F_T = \left(2 * F_T * V_{BF} * \cos\theta\right) / c$$

This concept of a Doppler shift is used to measure blood flow velocity whereby the shift in sound-wave frequency is detected by the ultrasound transducer after encountering active blood flow.

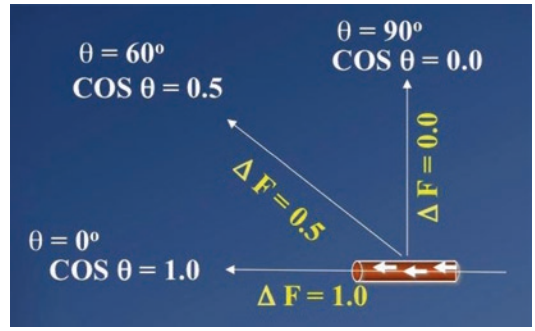

Fig. 7.1 Doppler angle: The change in Doppler frequency (ΔF) is directly related to the cosine of the angle of insonance (θ). The angle of insonance (the angle between the incident beam and the vector of blood flow) must be less than 60° for accurate measurements of blood flow velocity

However, several factors influence the resultant frequency shift and hence the measured velocity. These include the incident frequency of the ultrasound beam used, speed of sound in soft tissues, the velocity of the moving reflectors (i.e., blood in a vessel), and the angle between the incident beam and vector of blood flow (θ) called the angle of insonation.

The angle of insonation is inversely related to Doppler shift. Hence, as the angle of insonation increases, approaching 90°, the Doppler shift decreases and therefore the calculated blood flow velocity decreases to 0. The Doppler angle is therefore a significant technical consideration in performing duplex Doppler examinations, and an ideal angle of insonance between 0 and 60° is required (Fig. 7.1).

Clinical Pearl: Even if the angle of insonance is not corrected, the RI will be accurate. However, PSV and EDV will be inaccurate.

Patient Preparation

The patient should lie comfortably on the examination table in a supine position with legs together providing support for the external genitalia. An alternative position is dorsal lithotomy with the penis lying on the anterior abdominal wall.

Regardless of the patient position preferred, the area of interest should remain undraped for the duration of the examination. Care should be taken to cover the remainder of the patient as completely as possible including the abdomen, torso, and lower extremities. Ample amounts of ultrasonographic acoustic gel should be used between the transducer probe and the surface of the penis to allow uninterrupted transmission of sound waves, thus producing a high quality image without acoustic interruption.

Penile Ultrasound Protocol

As with other ultrasound exams, penile ultrasound uses specific scanning techniques and images targeting the clinical indication prompting the study. Irrespective of the indication for penile ultrasound, routine scanning during penile ultrasound should include both transverse and longitudinal views of the penis by placing the transducer probe on the dorsal or ventral aspect of the penis. The technique presented here uses a dorsal approach, which is easier for the flaccid phallus. However, the ventral approach, often with placement of legs in the lithotomy position, is often better with a fully erect phallus as well as allowing for better visualization of the proximal corpora cavernosa. The goal is to visualize the cross-sectional view of the two corpora cavernosa dorsally and the corpus spongiosum ventrally along the length of the penis from the base of the penile shaft through to the distal glans penis.

The corpora cavernosa appear dorsally, as two homogeneously hypoechoic circular structures, each surrounded by a thin (usually less than 2 mm) hyperechoic layer representing the tunica albuginea that envelops the corpora. The corpus spongiosum is a ventrally located circular structure with homogeneous echotexture, usually more echogenic than the corpora cavernosa [1]. It is best visualized by placing the ultrasound transducer probe on the ventral aspect of the penis; however, it is easily compressible so minimal pressure should be maintained while scanning. For routine anatomic scanning of the penis with ultrasound, all three corpora can be sufficiently viewed from a single dorsal approach to the penile shaft. A survey scan, with storage of a cine loop of this scan, is first performed prior to obtaining static images at the proximal (base), mid portion, and distal (tip) of the corpora cavernosal bodies for documentation (Figs. 7.2, 7.3, and 7.4). The value of the survey scan cannot be overstated. It often provides the prospective that is necessary to assure absence of coexisting pathology. A careful survey scan of the phallus will identify abnormalities of the cavernosal vessels, calcified plaques, and abnormalities of the spongiosa tissue.

Still images recommended as representative views of this initial surveying scan include one transverse view at the base of the penile shaft, one at the mid-shaft, and a third at the distal shaft just proximal to the corona of the glans penis (Fig. 7.2a, b). Each image should show transverse sections of all three corporal bodies. As noted in the labeled images, orientation by convention is for the right corporal body to be on the left side of the display (as viewed by the sonographer) while the left corporal body is located on the right side of the display on images obtained with the ultrasound probe on the dorsal aspect of the phallus. Figure 7.3 demonstrates a normal mid-shaft view with the transducer on the ventral aspect of the phallus. A longitudinal projection splitting the screen view helps to compare the right and left corporal bodies. Figure 7.4 demonstrates a dorsal approach with measurements of the cavernosal artery diameter, and peak systolic and end diastolic velocities. By convention, the orientation is constant, with the projection of the right corporal body on the left side of the display while the left corporal body is located on the right side of the display.

Embryology Relevant to Ultrasound Imaging of the Penis

A basic understanding of the embryologic development of the genitalia helps guide the interpretation of many abnormalities found on penile ultrasound. Presented in this section is the

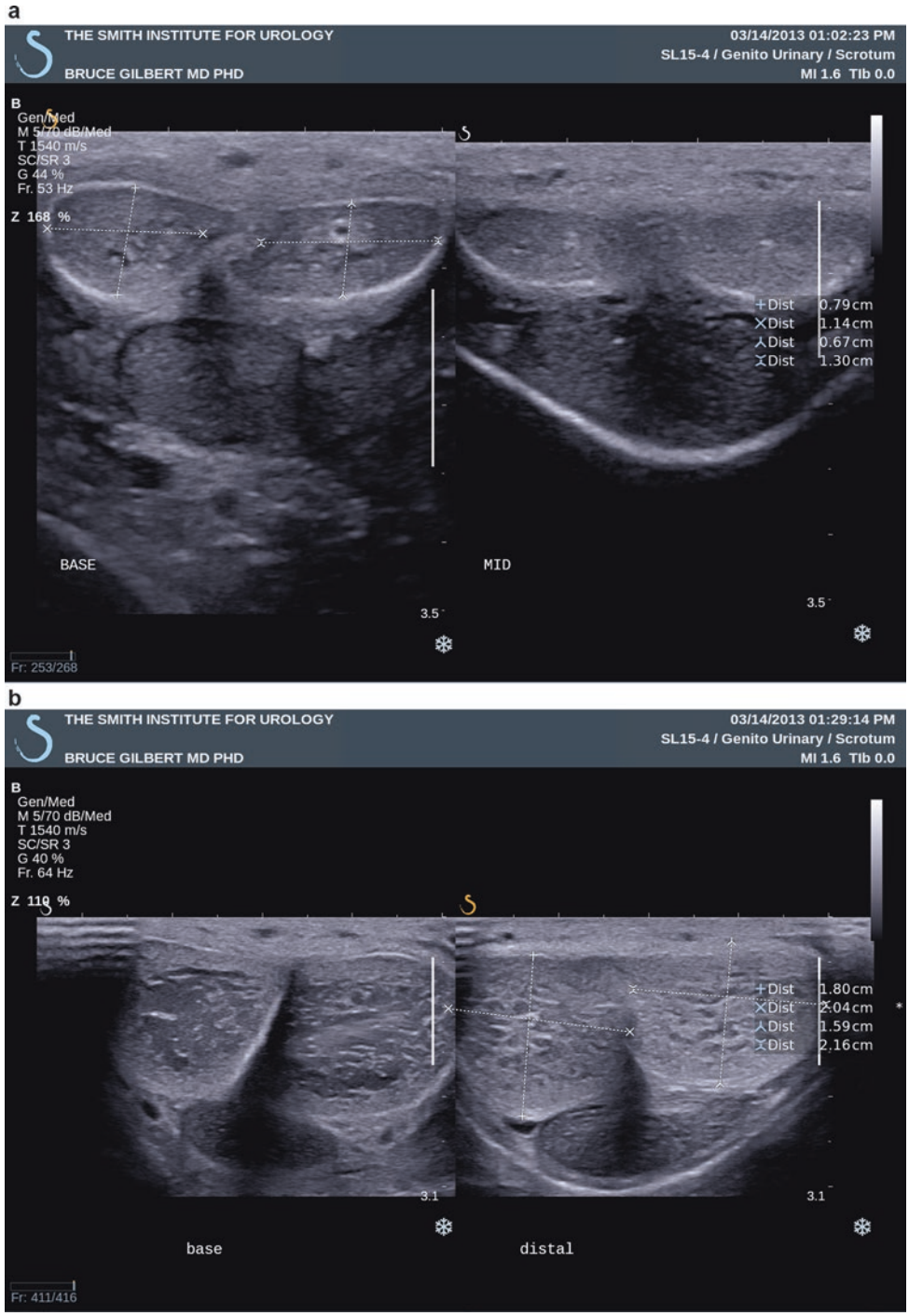

Fig. 7.2 (**a**) Survey scan with transverse views through the base (*left panel*) and mid-shaft (*right panel*) of the penis. In this image the transducer is on the dorsal penile surface and demonstrates the right and left corpora cavernosa nearer the ultrasound probe and corpus spongiosum in the midline ventrally, furthest from the ultrasound probe. (**b**) Survey scan with transverse views through the base (*left panel*) and distal shaft (*right panel*) regions of the penis. Similarly, in this image the transducer is on the dorsal penile surface and demonstrates the right and left corpora cavernosa dorsally (closest to the ultrasound probe) and urethra ventrally (away from the ultrasound probe)

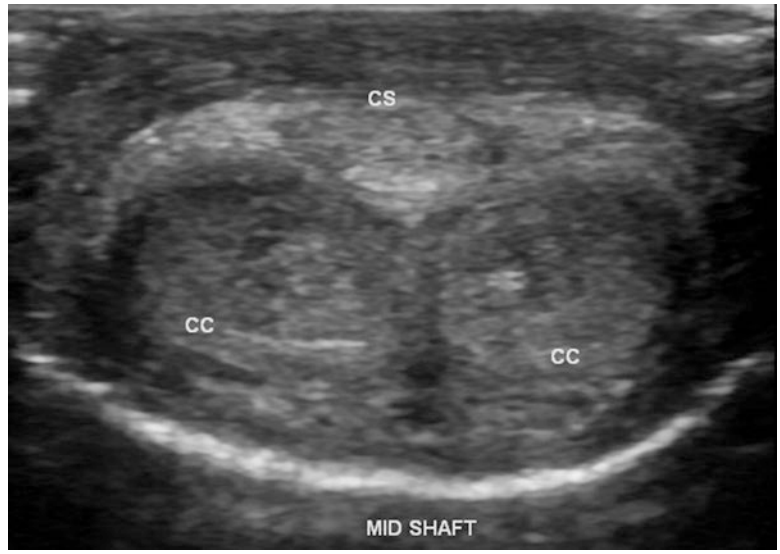

Fig. 7.3 Demonstrates normal mid-shaft view with the ultrasound transducer on the ventral surface of the phallus depicting the right and left corpora cavernosa (CC) and corpus spongiosum (CS)

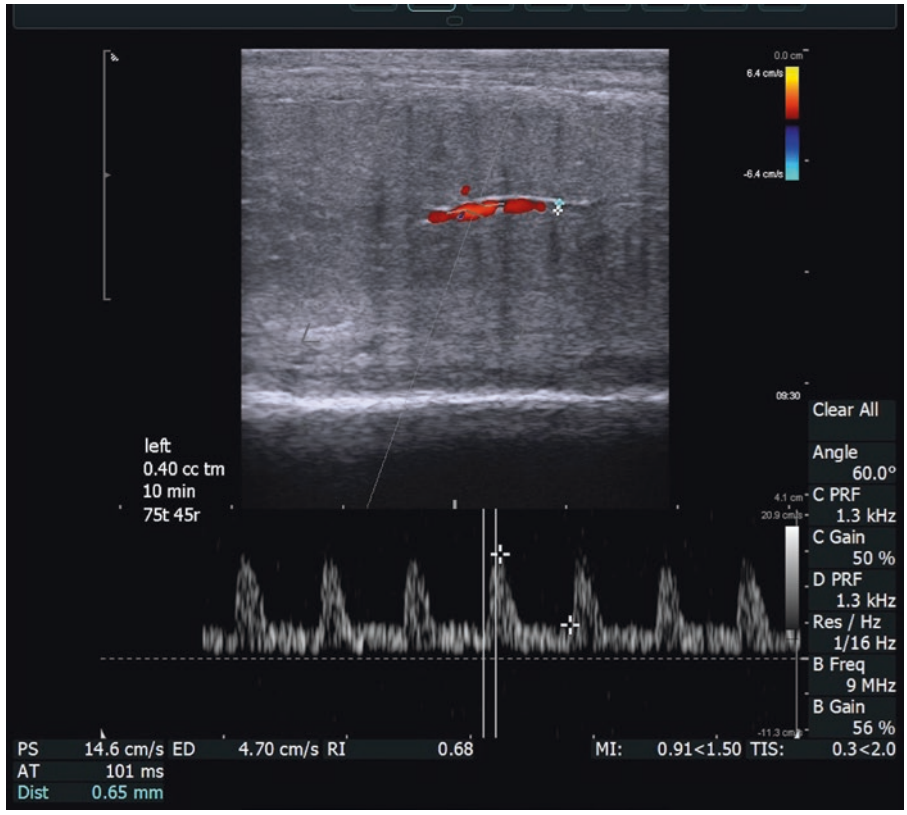

Fig. 7.4 Longitudinal view of (**a**) left corpora cavernosa taken 10 min after injection of 0.4 cc of a pharmacologic agent to induce an erection, displaying cavernosal artery diameter, PSV, and EDV

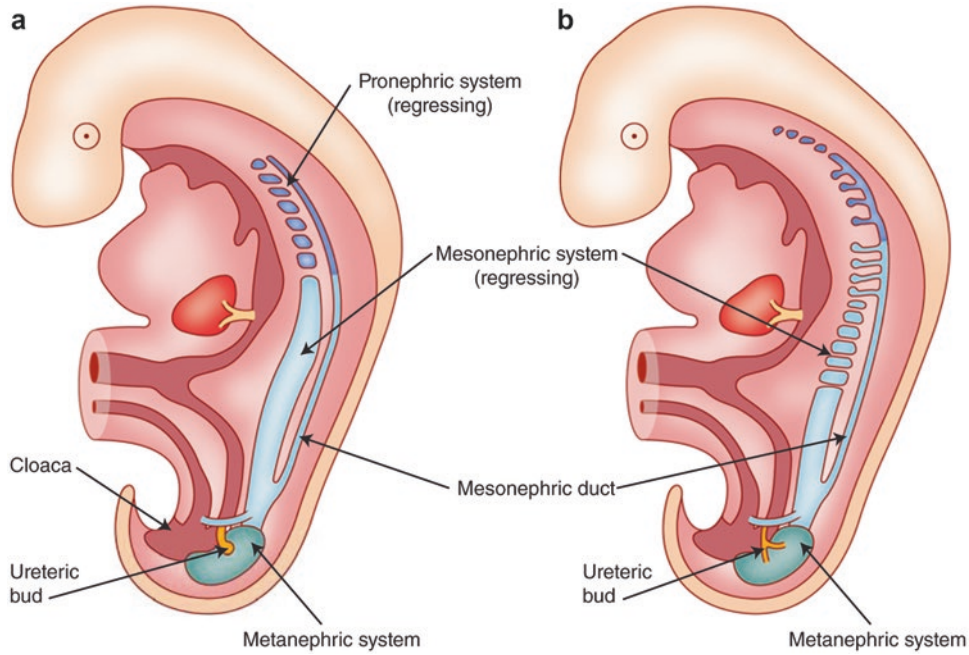

Fig. 7.5 Development of the early excretory system. Regression of the pronephros (**a**) and mesonephros (**b**) with the development of the metanephric system

embryology relevant to the ultrasound evaluation of the penis. The development of the phallus is in close association with the development of the scrotal structures. In addition, the development of the urinary and reproductive system takes place with the simultaneous development of all organ systems from the trilaminar embryo to those systems fully formed at the time of parturition. For a more detailed description of the interplay between these systems, there are several comprehensive texts to which the reader may be referred [2–5].

Development of the Urogenital Sinus

The penis serves as a conduit through which the most distal portion of the urinary tract passes. The lower urinary tract develops as a descendent of the endodermal hindgut, an offshoot that divides from the fledgling gastrointestinal system to interact with the mesonephros and metanephros and ultimately develop into a unique urinary system. In the early embryo, the cloacal membrane is located at the caudal end of the developing hindgut as a bilaminar apposition of ectoderm and endoderm located on the ventral midline (Fig. 7.5). The remainder of the cloaca is a chamber shared by the allantois (which extends anteriorly from the cloaca into the umbilical cord) and the hindgut. The cloacal membrane makes up the ventral wall of the chamber. A septum develops as an ingrowth of folds from the lateral walls and a caudal extension of the intervening mesenchyme from the branch point of the allantois and hindgut, which ultimately divides the cloaca into the anterior/ventral urogenital sinus and the posterior/dorsal developing rectum. While the septum develops, mesodermal mesenchyme also encroaches between the two layers of the cloacal membrane. The septum also divides the membrane into a urogenital membrane and anal membrane. These membranes ultimately rupture to create a continuity between the ectoderm and both the urogenital sinus and rectum. The mesenchymal tissues that have encroached develop into the muscles and bones of the lower anterior abdomen and pubis. An incompletely characterized

defect in this process results in the exstrophy-epispadias complex, a spectrum of abnormalities that can include continuities between the luminal surface of the bladder and the lower abdominal skin. If the defect occurs early enough in the process, specifically before the complete division of the cloaca, a cloacal exstrophy can occur which also includes a continuity of the intestinal lumen with the skin and bladder lumen. This is often found on prenatal ultrasound with an appearance that mimics the complete absence of a bladder in the fetus. These findings can also be found with penile anomalies.

The urethra, prostate, and bladder all develop from the urogenital sinus. The remnants of the caudal ends of the mesonephric ducts become incorporated into the urogenital sinus and become aspects of the trigone and posterior urethra. The incorporated portions of the mesonephric ducts include the branch points of the metanephric ducts, which become the ureteral orifices. The unincorporated portions of the mesonephric ducts end up entering the urethra at the prostatic urethra as the ejaculatory ducts. Ridges in the urethra, called plicae colliculi, remain along the path of the fusion of the mesonephric ducts as they become incorporated with the urogenital sinus and migrate while the sinus develops. It is hypothesized that abnormalities in this process result in the fusion of the plicae colliculi that is seen in the majority of posterior urethral valves. The remainder of posterior urethral valves is thought to result from an incomplete rupture of the urogenital membrane. Posterior urethral valves are associated with a dilated posterior urethra (Fig. 7.6) and thickened bladder wall on ultrasound, referred to as the keyhole sign. The bladder is often distended with marked hydroureteronephrosis also demonstrated on ultrasound examination.

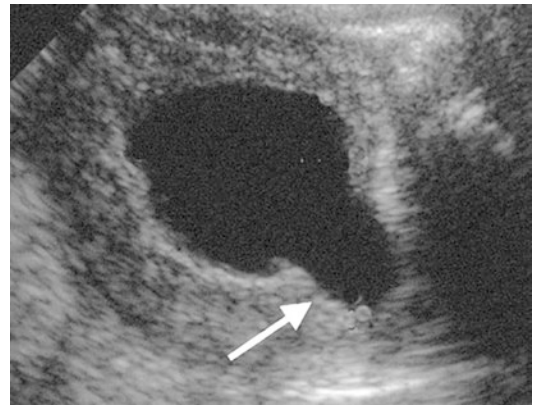

Fig. 7.6 Ultrasound of the bladder with the typical findings associated with posterior urethral valves including a thickened wall and dilated posterior urethra known as the keyhole sign

Development of the Male External Genitalia and Phallus

Up until the eighth or ninth week of gestational age the development of the external male genitalia is indistinguishable with that of the female genitalia. It is characterized in both genders by the development of the genital tubercles at the craniolateral edges of cloacal membrane. They develop from mesoderm as it infiltrates the cloacal membrane. As the cloaca membrane divides with the anterior portion becoming the urogenital membrane, the two tubercles fuse in the midline. This fusion can be disrupted and results in the bifid phallus that is sometimes seen in conjunction with bladder exstrophy. The urogenital membranes and ultimately the urogenital sinus are flanked by collections of infiltrating mesoderm termed the urogenital folds with labial scrotal swellings located laterally either side (Fig. 7.7). Masculinization of the indifferent external genitalia occurs under the influence of testosterone produced by the interstitial cells of the fetal testis [6–8]. The tubercle becomes the future phallus and glans. The terminal part of the phallus destined to be the glans becomes solid. The groove between the urogenital folds, which extend onto the underside and with the tubercle as the tubercle grows, is termed the urogenital groove. The urogenital sinus extends to the undersurface of the genital tubercle where it opens in this groove. Apical ridges of the urogenital folds grow towards each other and the walls of the phallic portion come together and fuse which creates a tubular extension of the urogenital sinus on the caudal aspect of the developing phallus. This opening is for a while the primitive uro-

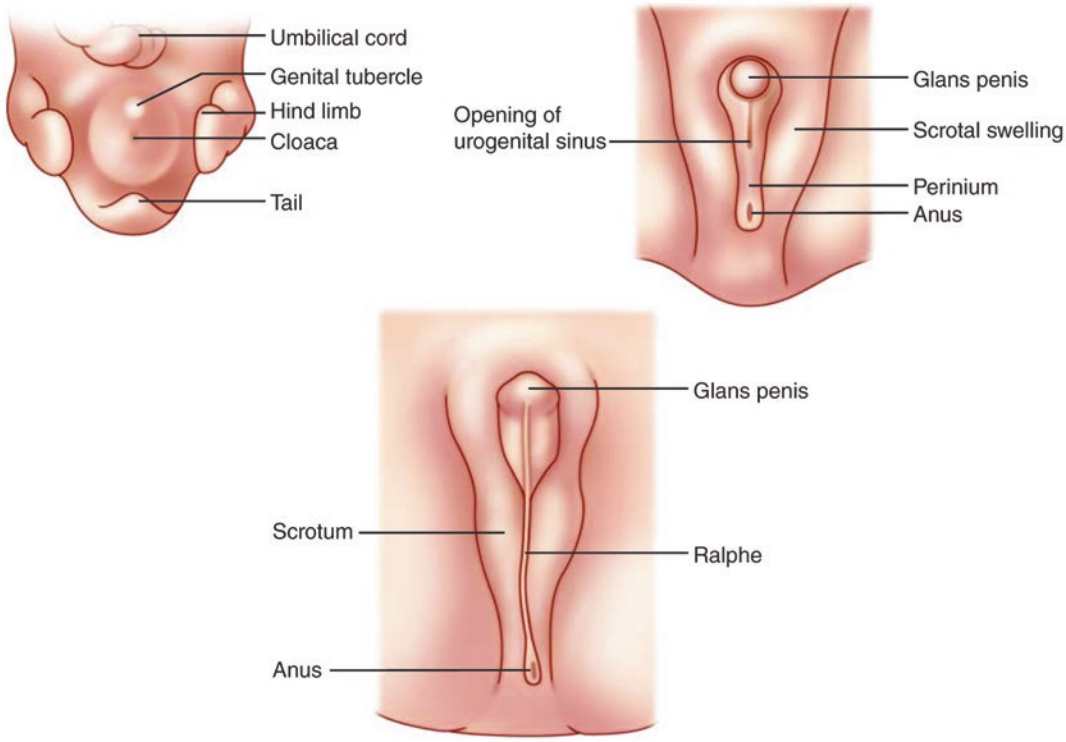

Fig. 7.7 The male external genital development progressing clockwise from the left. The genital tubercle develops into the glans penis. The *upper right panel* shows the urogenital sinus opening within the urogenital folds, which are between the scrotal swellings

genital opening, and it extends forward to the corona glandis (Fig. 7.7) and the final urethral meatus. Abnormalities in this process can result in the ectopic location of the urethral meatus along the ventral phallus or midline scrotum, penoscrotal junction, or scrotoperineal junction, termed hypospadias. This is often associated with a hypoplastic development of the corpus spongiosum which can be demonstrated ultrasonographically.

The corpora cavernosa of the penis as well as the spongiosum surrounding the urethra arises from the mesodermal tissue in the phallus. They are at first dense structures, but later vascular spaces appear in them, and they gradually become cavernous. A solid plate of ectoderm grows over the superficial part of the phallus. A bilayer tissue is formed by a breakdown of the more centrally situated cells forming the prepuce. The scrotum is formed by extension of the labioscrotal swellings between the pelvic portion and the anus. With testicular decent these labioscrotal swellings form the scrotal sacs (Fig. 7.7).

Penile Blood Supply

The anterior trunk of the internal iliac gives rise to the internal pudendal artery approximately at the level of the greater sciatic foramen (Fig. 7.8a and white circle in Fig. 7.8b). The internal pudendal artery then crosses behind the tip of the ischial spine and enters the peritoneum through the lesser sciatic foramen (Fig. 7.8b). It then enters then passes through Alcock's canal in the ischiorectal fossa to become the penile artery. It is at this point that the internal pudendal artery is most susceptible to injury (yellow circle in Fig. 7.8b). The penile artery passes through the urogenital diaphragm and along the medial aspect of the inferior limits of the pubic symphysis (Fig. 7.8c).

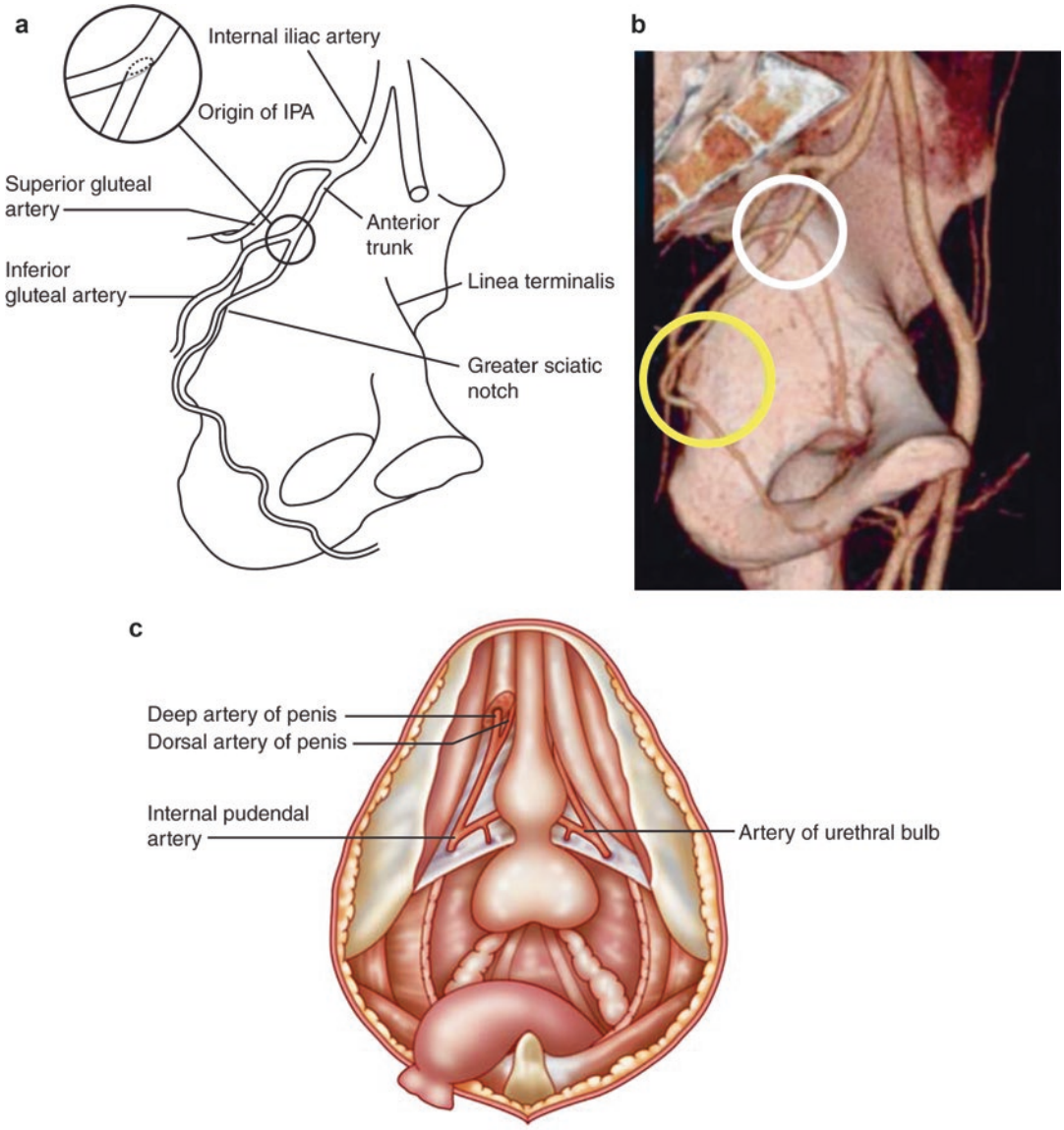

Fig. 7.8 Arterial blood supply to the penis and path through the pelvis in labeled schematic (**a**), in 3D imaging reconstruction (**b**). The *white circle* highlights to origin of the internal pudendal artery. The *yellow circle* highlights the path around the ischial spine and into Alcock's canal. The distal internal pudendal artery gives rise to the artery of the bulb (bulb-urethral artery) and the penile artery (**c**)

The penile artery then gives rise to branches including the bilateral urethral artery and another dorsal branch which gives rise in turn to the dorsal artery of the penis and the cavernosal artery (Fig. 7.9). The urethral artery travels within the spongiosal tissue and supplies the corpus spongiosa, urethra, and glans penis. The dorsal artery runs deep to Buck's fascia and just medial to the paired dorsal nerves and lateral to the single deep dorsal vein. The dorsolateral vessel gives rise to circumflex branches that pass around the corpus cavernosum and spongiosum. The cavernosal artery begins at the base of the penis and runs centrally through the corpus cavernosus. The caverno-

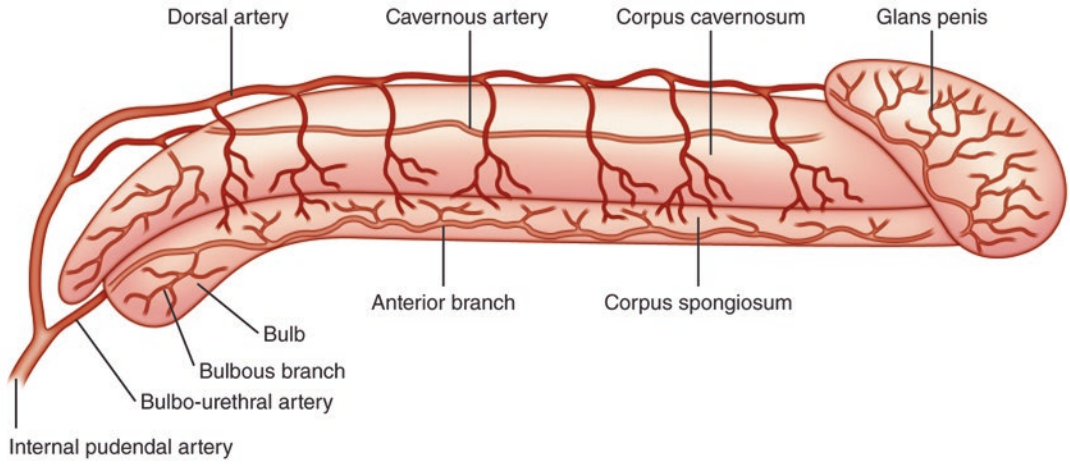

Fig. 7.9 Arterial supply within the penis. The distal internal pudendal artery gives rise to the artery of the bulb (bulbo-urethral artery) and the penile artery which in turn branches into the dorsal and cavernosal arteries of the penis

sal artery gives rise to two major branches one that supplies the smooth muscle and nerve fibers of the cavernosal trabecular tissue and the other which divides into a series of helicine arteries. The helicine arteries are unique in that they allow blood to pass directly into the cavernous sinusoids without first traversing a capillary bed. They also allow elongation and dilation of the penis without compromising the blood supply to the corpora [9].

There are three major venous drainage pathways in the penis [10, 11]. First the superficial receives drainage from the penile skin and layers superficial to Buck's fascia usually through a single vessel, the superficial dorsal vein, running the length of the dorsal aspect of the phallus. Secondly, the intermediate system deep to Buck's fascia and superficial to the tunica albuginea receives drainage from the glans, corpus spongiosum, and corpus cavernosum. Emissary veins, primarily from the dorsal and lateral corpora cavernosum, pierce the tunica albuginea and combine to become circumflex veins which enter into the deep dorsal vein. This usually single vein empties into the periprostatic plexus of Santorini. The third major venous drainage pathway is via a deep system that drains the proximal portion of the corpus spongiosum and a major portion of the corpora cavernosum. This drainage travels through the deep penile veins and exits through the pudendal plexus.

The location of penile vessels on ultrasound is dependent upon where the ultrasound probe is positioned on the phallus. Either the dorsal or ventral approach can be used. However, if the dorsal approach is used, the urethra is on opposite side of the cavernosal bodies as the transducer and if the ventral approach is used the urethra is between the transducer and the corpora cavernosa (Fig. 7.10). Note the corpora and urethral are usually more compressed in the ventral approach and therefore visualization of vessels is more difficult (Fig. 7.11). In addition, when the transducer is placed dorsally, the superficial and deep dorsal veins are found near the transducer. However, when the transducer is placed on the ventral aspect of the phallus, the urethral blood supply is closest to the transducer (Fig. 7.11).

The development of the male genitalia is a complex process. The understanding of this process and the abnormalities that correlate to embryologic processes and vestiges are crucial to aid the sonographer in identifying findings on the ultrasound evaluation of the phallus, scrotum, and male reproductive structures.

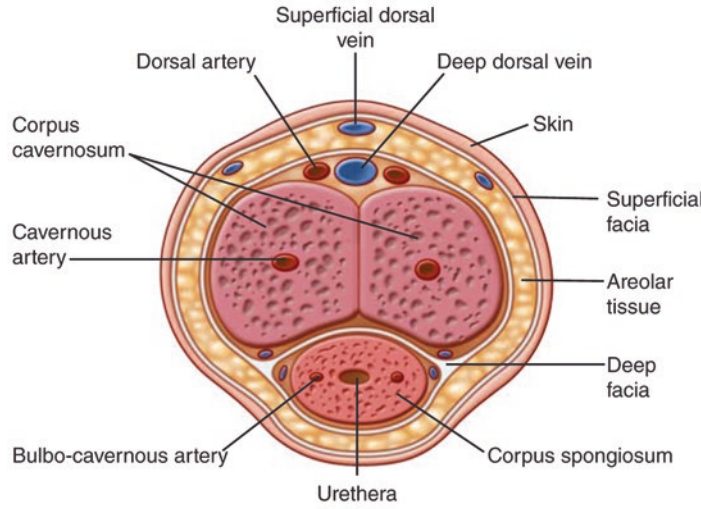

Fig. 7.10 Schematic of transverse view through penis with the distribution of major vessels. This view duplicates the transverse ultrasound view

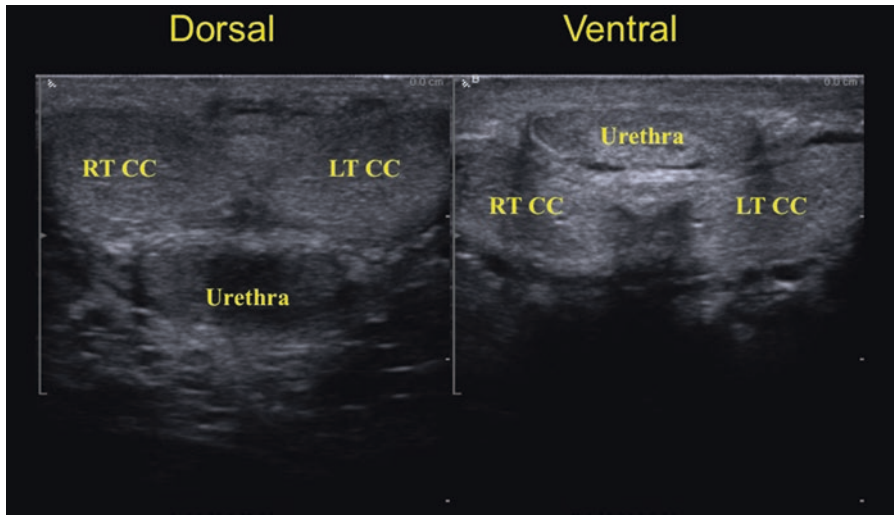

Fig. 7.11 Transverse B-mode ultrasound views of the phallus with the transducer on the dorsal and ventral aspects. *CC* corpus cavernosus, *RT* right, and *LT* left

Focused Penile Ultrasound by Indication

There are several accepted indications for penile ultrasound, each with specialized focus beyond the routine survey scan as previously described. General guidelines for the use of penile ultrasound are delineated by the "Consensus Statement of Urologic Ultrasound Utilization" put forth by the American Urologic Association [12] and the American Institute for Ultrasound in Medicine (AIUM). These indications can be further classified as either vascular, structural, or urethral pathology in nature (Table 7.1).

Erectile Dysfunction

PDU is an integral part of the assessment of patients with ED. Often practitioners use intra-

Table 7.1 Indications for penile and urethral ultrasound

Vascular pathology:
Erectile dysfunction (ED)
Cavernosal artery diameter
Flow velocity
Peak systolic velocity (PSV)
End diastolic velocity (EDV)
Resistive index (Ri)
Priapism
High-flow (arterial)
Low-flow (ischemic)
Penile trauma/fracture
Dorsal vein thrombosis
Structural pathology:
Penile fibrosis/Peyronie's disease
Plaque assessment (number, location, echogenicity, and size)
Perfusion abnormalities
Perfusion surrounding plaques
Penile mass
Primary penile tumors
Metastatic lesions to the penis
Penile foreign body (size, location, echogenicity)
Penile urethral disease:
Urethral stricture (location, size)
Perfusion surrounding plaques
Calculus/foreign body
Urethral diverticulum/cyst/abscess

cavernosal injection therapy with vasoactive agents in patients who have failed a course of oral phosphodiesterase-5 inhibitors. In this situation, PDU may be used as a diagnostic tool in conjunction with commencement of injection therapy. PDU allows for a baseline evaluation of the functional anatomy as well as providing a real-time assessment of the dynamic changes experienced in response to the dosing of vasoactive medications. In cases where intracavernosal injection of vasoactive substances does not prompt a penile erection, documentation provided by PDU will be a foundation for other management options including use of vacuum constriction devices or insertion of a penile prosthesis.

Possibly one of the most compelling reasons for the performance PDU in men presenting with ED is the finding that impaired penile vascular dynamics, as documented on PDU, may be associated with a generalized vessel disease that often predates cardiovascular disease by 5–10 years [13–15]. Significantly, early treatment of metabolic factors (e.g., hypertension, dyslipidemia, hyperglycemia) can delay and possibly prevent the development of cardiovascular disease [16, 17]. Therefore, the physician evaluating ED has a unique opportunity to diagnose vascular impairment at a time when lifestyle changes and possible medical intervention have the potential to change morbidity and mortality of cardiovascular disease. As suggested by Miner, there might be a "window of curability" which we like to refer to as a "window of opportunity" in which the significant risk of future cardiovascular events might be averted through early diagnosis and treatment [18–20].

In cases of diagnostic study for ED, emphasis is directed toward the cavernosal arteries. However, the initial survey scan is essential to evaluate for plaques, intracavernosal lesions, and urethral pathology as well as evaluation of the dorsal penile vessels. The cavernosal arteries are visualized within the corpora cavernosa, and the depth of these arteries can be easily defined within the corpora during transverse scanning to ensure a comprehensively represented assessment of diameter at different points along its course. Color Doppler examination of the penis should be performed in both transverse and longitudinal planes of view. Using the transverse views as a guide to cavernosal artery depth, turning the transducer probe 90° then provides longitudinal views of each corpus cavernosum separately, allowing for identification of the cavernosal arteries in longitudinal section (Fig. 7.4). The diameter of the cavernosal artery should be measured on each side. Color flow Doppler makes recognition of the location and direction of blood flow easy. Measurements of vessel diameter to assess the peak systolic flow velocity (PSV) as well as end diastolic flow velocity (EDV) allow for the assessment of a vascular resistive index (RI) (Fig. 7.12). The diameter of the cavernosal artery ranges from 0.2 to 1.0 mm in a flaccid penis [21, 22]. PSV varies at different points along the length of the cavernosal artery, typically with higher velocities occurs more proximally [23]. Hence, assessment of the PSV

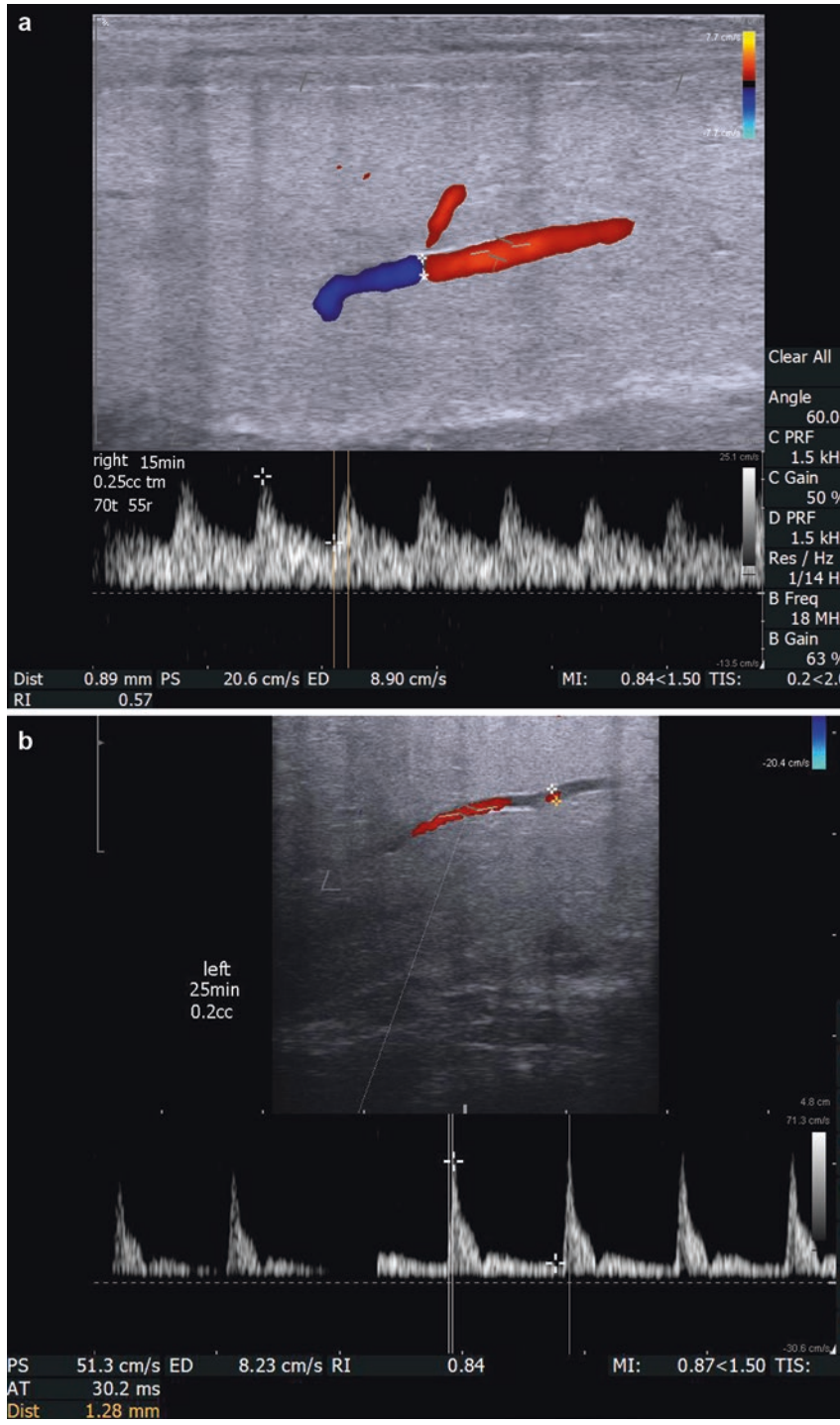

Fig. 7.12 (**a**) The right cavernosal artery is imaged 15 min after intracavernosal injection of 0.25 mL of trimix solution. The measured vessel diameter is 0.89 mm. The direction of flow and a dorsal branch of the cavernosal artery are easily appreciated with color Doppler. Also, documented on this image is measurement of arterial diameter (0.89 mm), PSV (20.6 cm/s), EDV (8.9 cm/s), and calculated RI (0.57) are shown. Please note that the angle of incidence is electronically made to be 60° by both electronic steering of the transducer and aligning the cursor to be parallel to the flow of blood through the artery. In addition the width of the caliper is adjusted to be approximately ¾ the width of the artery for best sampling. (**b**) The right cavernosal artery of another patient was imaged at 25 min after intracavernosal injection of 0.2 mL of trimix solution with a measured vascular diameter of 1.28 mm, PSV of 51.3 cm/s, EDV of 8.23 cm/s, and calculated RI of 0.84

and EDV should be recorded at the junction of the proximal one-third and the distal two-thirds of the penile shaft. In the flaccid state, cavernosal artery PSV normally measures 5–15 cm/s, at baseline. This should be assessed and compared to the pharmacostimulated state [24, 25].

The intracavernosal injection should then be given (Appendix 2). At regimented serial time points following the injection of vasoactive medication, cavernosal artery dimensions and flow velocities should be recorded to assess the response to pharmacologic stimulation. After prepping the lateral aspect of the penile shaft with an alcohol or providone-iodine prep pad, a finely measured volume of a vasoactive agent should be injected into one corpus cavernosum (in the distal two-thirds of the penile shaft) using a 29 or 30 gauge ½″ needle. Pressure should be held on the injection site for at least 2 min to prevent hematoma formation.

Vasoactive agents used for pharmacologic stimulation of erection include prostaglandin E1, papaverine, or trimix (combination of prostaglandin E1, papaverine, and phentolamine) [26]. As with every medication administration, the expiration date of the medication should be reviewed, patient allergies should be evaluated, and the dosage administered should be documented. We obtain an informed consent after the patient is counseled about the known risk for developing a low-flow priapism and appropriate follow-up if this were to arise [27]. This protocol requires the patient to stay in the office until penile detumescence occurs. A treatment protocol for low-flow priapism is given in Table 7.2. Of note, for patients in which we have given a vasoactive agent and have had to treat for low-flow priapism, aspiration, irrigation, and injection of intracorporal phenylephrine are usually successful to reverse the priapism state. In our experience, when required, corporal aspiration alone has been uniformly successful in the setting of pharmacologically induced priapism following diagnostic duplex penile ultrasonography.

Arteriogenic ED is a form of peripheral vascular disease, commonly associated with diabetes mellitus and/or coronary artery disease. PSV is the most accurate measure of arterial disease as the cause of ED. The average PSV after intracavernosal injection of vasoactive agents in healthy volunteers without ED ranges from 35 to 47 cm/s, with a PSV of 35 cm/s or greater signifying arterial sufficiency following pharmacostimulation [28–33]. Primary criteria for arteriogenic ED include a PSV less than 25 cm/s, cavernosal artery dilation less than 75 %, and acceleration time >110 ms. In cases of equivocal PSV measurements, particularly when PSV is between 25 and 35 cm/s, one should assess for asymmetry of greater than 10 cm/s in PSV between the two cavernosal arteries, focal stenosis of the cavernosal artery, and possible cavernosal artery to cavernosal-spongiosal flow reversal [34].

Veno-occlusive insufficiency, also referred to as venous leak, can only be diagnosed in cases of ED where the patient was confirmed to have appropriate arterial function as measured by PSV. PDU parameters to assess the presence of veno-occlusive insufficiency as the cause of ED are EDV and RI. Antegrade EDV greater than 5 cm/s in the cavernosal artery demonstrated throughout the study, especially at the most turgid level of erection achieved, is suggestive of a venous leak [35, 36]. This is only true if PSV is normal. Arteriogenic dysfunction by definition fails to produce a fully tumescent and rigid phallus. In the setting of venous leak, EDV is always greater than 0. The definitive test for venous leak is the DICC (dynamic infusion cavernosography and cavernosometry).

Table 7.2 Treatment protocol for low-flow priapism caused by pharmacologic induction by vasoactive agents

1. Observation: if no detumescence in 1 h, then
2. Aspiration: with a 19 or 21 gauge butterfly needle aspirate 30–60 cc corporal blood. A sample should be sent for diagnostic cavernosal blood gas to confirm low-flow, ischemic state. Repeat in ½ h if 100 % rigidity returns
3. Pharmacologic detumescence: (a) Phenylephrine 100–500 mcg injected in a volume of 0.3–1 cc every 3–5 min for a maximum of 1 h (b) Monitor for acute hypertension, headache, reflex bradycardia, tachycardia, palpitations, and cardiac arrhythmiã (c) Serial non-invasive blood pressure and continuous electrocardiogram monitoring are recommended

However, when both arteriogenic and venogenic dysfunction exists, interpretation of DICC is difficult. On PDU an RI of less than 0.75, measured 20 min following maximal pharmacostimulation, has been found to be associated with a venous leak in 95 % of patients [37]. In the absence of a venous leak, a fully erect penis should have an EDV nearing zero and hence the RI should approach or exceed (when reverse flow occurs) 1.0 (Fig. 7.13). In cases of diagnostic PDU with intracavernosal pharmacostimulation where a RI of 1.0 or greater is achieved, we recommend immediate treatment or prolonged observation to achieve detumescence because of the high specificity of absent diastolic flow for priapism [38].

In cases where arterial function and venous leak may be coexistent processes, indeterminate results may be yielded on PDU and a mixed vascular cause of ED may be assumed. However, venous competence cannot be accurately assessed in a patient with arterial insufficiency (Fig. 7.14).

As previously discussed, arteriogenic ED has been found to correlate directly with other systemic cardiovascular diseases, both coronary artery disease (CAD) and peripheral vascular disease (PVD), in a number of population studies [39, 40]. Researchers have postulated the common risk factor of atherosclerotic vascular disease and impaired endothelium-dependent vasodilation by way of the nitric oxide pathway as the underlying pathophysiologic explanation for the remarkable overlap between these disease processes [41–43]. Also, hypogonadism has been noted as a common etiology for organic erectile dysfunction and disorders leading to metabolic syndrome [44, 45]. Vessel compliance, particularly in small-caliber vessels, is compromised in arteriogenic ED as it is in CAD and PDU can identify systemic vascular compliance loss [46]. Patients with severe vascular etiology ED have an increased cavernosal artery diameter of less than 75 % (with overall luminal diameter rarely above 0.7 mm) following injection of vasoactive agents into the corpora cavernosa [32, 47].

Studies have demonstrated that vasculogenic ED may actually provide a lead time on otherwise

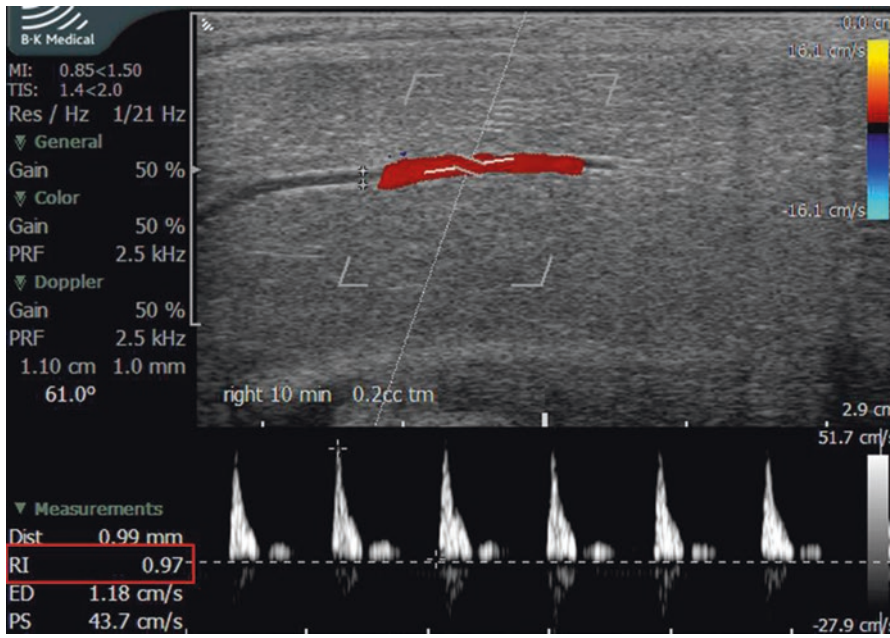

Fig. 7.13 In a fully erect phallus the RI should approach or exceed 1.0. If this condition persists, it is termed low-flow priapism. Color Doppler ultrasound findings in low-flow priapism demonstrate poor flow or absent flow in the cavernosal artery of the penis with moderate flow in the dorsal artery and vein. Also, there is no flow within the corpora cavernosa

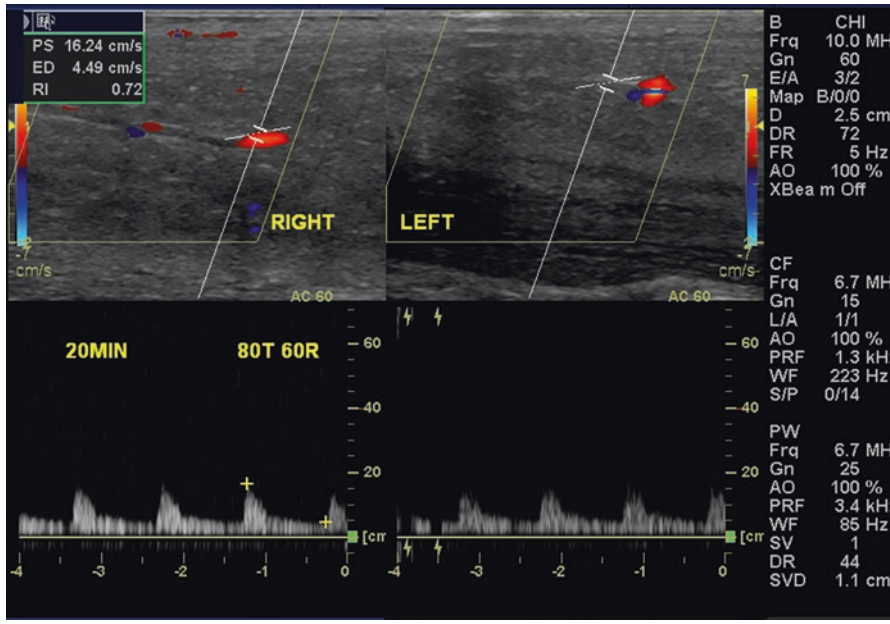

Fig. 7.14 With maximal stimulation, a PSV less than 25 cm/s suggests significant arteriogenic dysfunction. Referral for evaluation of cardiovascular disease is recommended

silent and undiagnosed cardiovascular disease [39, 48, 49]. ED has also been found to predict metabolic syndrome in men with normal body weight, as defined by body mass index (BMI) less than 25 kg/m^2, suggesting that the early diagnosis and intervention of vasculogenic ED might avert significant morbidity and provide a public health benefit by reducing the significant risk of cardiovascular and metabolic syndrome risk in men with ED [13, 15, 20, 50–53].

Priapism

Priapism can be differentiated as low-flow (ischemic) or high-flow (arterial) using PDU. Ultra sound plays an adjunct role to an illustrative history, which may commonly indicate the likely underlying mechanism of priapism. Like laboratory tests including a cavernosal blood gas, PDU provides documentable findings that may guide further treatment. High-flow priapism is commonly a result of pelvic or perineal trauma which results in arterial fistulization between the cavernosal artery and the lacunae of the corpus cavernosum. Unlike low-flow priapism, which is a medical emergency associated with severely compromised venous drainage from the corpora cavernosa, high-flow priapism does not result in venous stasis and rapid risk of tissue necrosis. Ultrasound used to aid in the definitive diagnosis and localization of the cause of high-flow priapism can expedite treatment with selective angioembolization [54]. In cases of high-flow priapism, PDU reveals normal or increased blood flow within the cavernosal arteries and irregular, turbulent flow pattern between the artery into the cavernosal body at the site of an arterial-lacunar fistula (Fig. 7.15). In contrast, a low-flow priapism on PDU would present with absent or very high-resistance flow within the cavernosal artery.

A transperineal approach should also be used in cases of suspected high-flow priapism to fully evaluate the proximal aspects of the corpora cavernosa. Ultrasonography of these deep structures may reveal ateriocavernosal fistula following perineal trauma, not evident by routine scanning of the penile shaft.

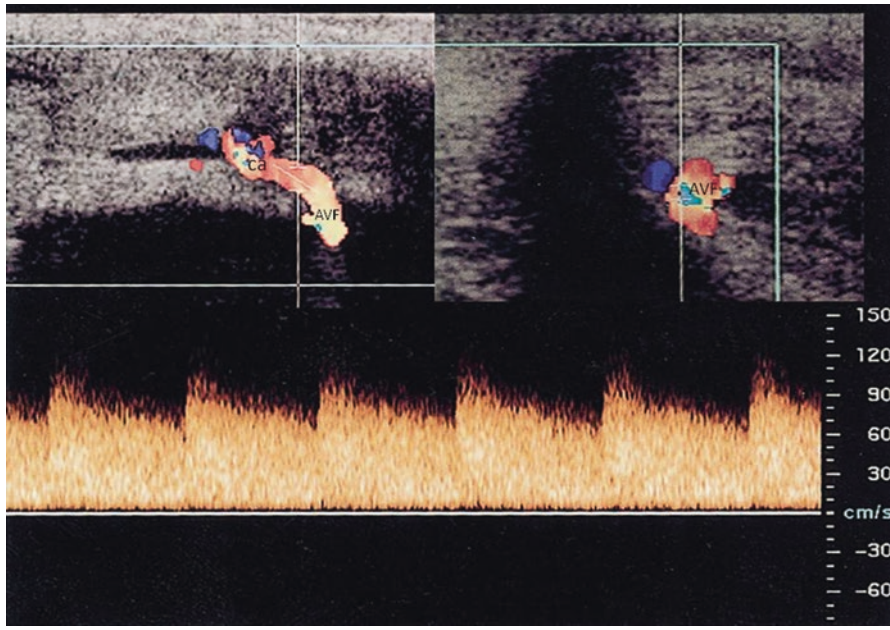

Fig. 7.15 Color Doppler ultrasound findings in a high-flow priapism demonstrating high-flow velocity in the cavernosal artery (ca) feeding the arteriovenous fistula (AVF)

Penile Fracture

Similar to priapism, the diagnosis of penile fracture is largely clinical, based upon the history gathered combined with the physical examination findings. However, PDU may play an important diagnostic role in more elusive cases, expediting a definitive diagnosis and early surgical management [55, 56]. Penile fracture can be seen on ultrasonography as a break point in the normally thin, hyperechoic tunica albuginea with altered echotexture in the adjacent area in the corpus cavernosum (Fig. 7.16a, b). This area of injury is also void of blood flow on color flow Doppler. Penile ultrasound can be used to measure the resultant hematoma that extrudes from the break point in the tunica albuginea (Fig. 7.16c).

In cases of both conservative management and postsurgical exploration and repair, PDU can be used as a minimally invasive follow-up study to ensure progressive healing, reabsorption of the hematoma, and intact blood flow on serial evaluations. Also, PDU allows for a dynamic anatomic assessment of erectile function following penile fracture in patients who have ED.

Dorsal Vein Thrombosis

Occasionally, dorsal vein thrombosis, often called Mondor's phlebitis, occurs with the triad of clinical symptoms of inflammation, pain, and fever resulting in patient consultation. There is often some induration and tenderness over the involved vein. The etiology has been variously ascribed to neoplasm, mechanical injury during intercourse, sickle cell disease, varicocele surgery, and herpes simplex infection. Occlusion of the vein can be visualized on ultrasound (Fig. 7.17) and followed with serial imaging as required to document resolution which usually occurs spontaneously as patency is reacquired in 6–8 weeks [57–61].

Peyronie's Disease

Penile ultrasonography can be used as an adjunct to a complete history and physical examination in the assessment of a patient with Peyronie's disease. Fibrotic plaques can be visualized as hyperechoic or hypoechoic areas of thickening of the

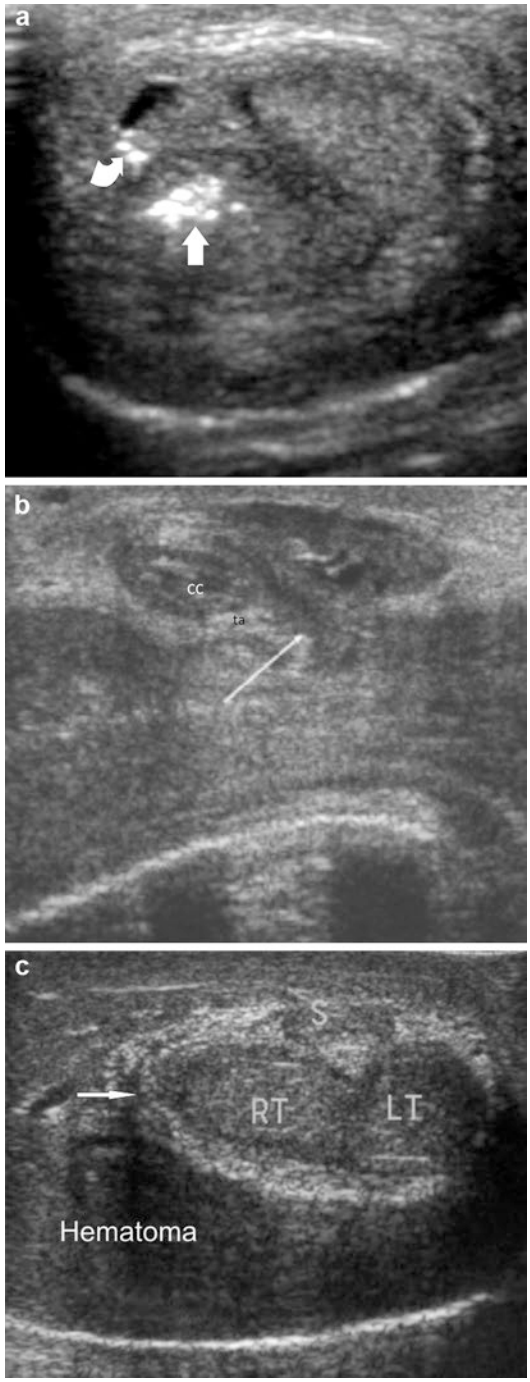

Fig. 7.16 Penile fracture depicted at the level of a tunica albugineal tear and presence of air spreading from urethral lumen through the corpus spongiosum (Fig. 7.16a, *curved arrow*) and right corpus cavernosum (Fig. 7.16a, *straight arrow*). In Fig. 7.16b the fracture is shown (*long arrow*) with tissue bulging above the tunica albuginea. Figure 7.16c depicts a ventral view penile ultrasound demonstrating a defect in the tunica albuginea enveloping the right corpus cavernosum (RT) with adjacent hematoma found typically on physical exam as an "eggplant deformity"

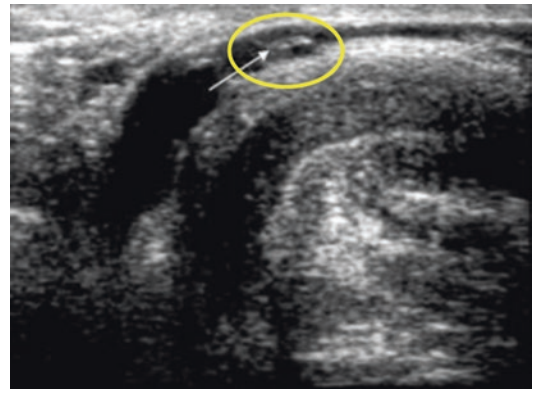

Fig. 7.17 Thrombosis of the dorsal penile vein (Mondors' phlebitis) is shown by the *arrow*

tunica albuginea [62, 63]. At times these plaques have elements of calcification, which cause a distinct hyperechoic focus with posterior shadowing on ultrasound (Fig. 7.18). Ultrasonography can aid to confirm the presence of plaques palpated on physical examination and allows for accurate measurement of these lesions. Whenever possible, measurement of the plaque length, width, and depth should be obtained and documented. PDU can be used to assess perfusion around the area of plaques. Hyperperfusion is suggestive of active inflammation.

Many men with Peyronie's disease have coexistent ED. Men with Peyronie's disease and ED most commonly have veno-occlusive insufficiency secondary to the fibrotic plaques present, but arterial insufficiency or mixed vascular abnormalities can also be implicated as the cause of ED [64]. Comprehensive assessment of the underlying cause of ED using PDU provides guidance for the most appropriate patient-specific, treatment course. In men with normal erectile function, plication or grafting procedures may be preferred. In men with concomitant Peyronie's disease and ED, reconstructive procedures may be undertaken with added care to define perforating collateral vasculature from the dorsal artery system. In more severe cases penile implant may be indicated.

Sonoelastography is an emerging technology that has been used as an adjunct to ultrasonography of the penis. Real-time sonoelastography has been used to complement B-mode ultrasound evaluation of Peyronie's plaques [65, 66].

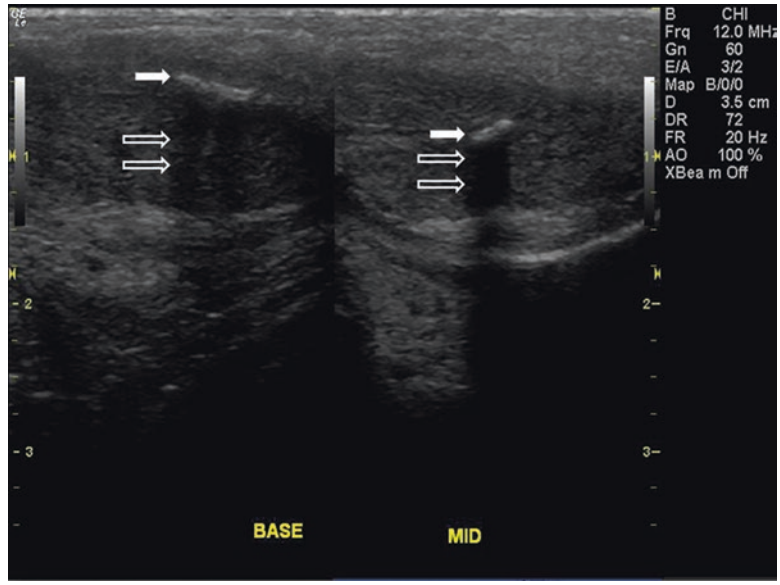

Fig. 7.18 Hyperechoic areas on the dorsal surface of the corpus cavernosum consistent with calcified plaque (*arrows*) at the base and mid portion of the phallus with posterior shadowing (*open arrows*)

Shearwave sonoelastography has been identified as technology to allow targeted intralesional therapy delivery to the locations of nonpalpable plaques that are also not visible on B-mode ultrasound [67]. Similarly, reports have emerged detailing the use of sonoelastography to evaluate the corpora cavernosal stiffness in those with [65, 67] and without [68] Peyronie's plaques. Sonoelastographic evaluation in these reports has provided evidence that the fibrosis of tunica albuginea plaques may also include fibrosis of the underlying cavernosal tissue as well (Fig. 7.19). The clinical role of evaluation of corporal tissue stiffness is as yet unclear; however, as this technique is more widely adopted we may see its role in aiding in our more robust understanding of Peyronie's disease and corporal fibrosis.

Penile Masses

Most commonly masses discovered on physical examination are benign entities such as Peyronie's plaques, subcutaneous hematomas, or cavernosal herniation through tunica albuginea defects.

Cancerous lesions of the penis are rare. Nevertheless, primary penile carcinomas with deep invasion and more rarely metastatic lesions may present as masses within the penile deep tissues. Penile carcinoma is usually identified by inspection as most arise as a superficial skin lesion. Ultrasound usually identifies these lesions as hypoechoic ill-defined lesions with increased blood flow relative to surrounding tissues. Although not indicated for staging purposes, ultrasound can aid in assessment of anatomic relationships of the mass to deep structures, at times identifying depth of penetration in cases where the tumor clearly invades the tunica albuginea and corporal bodies [69, 70].

Metastatic deposits within the penis are exceedingly rare, but appear on ultrasound similar to primary penile carcinomas as hypoechoic lesions with hyperperfusion. However, metastatic lesions in the penis are rarely contiguous with the skin surface and are more commonly well circumscribed compared to primary penile cancers (Fig. 7.20) [71].

Penile Urethral Pathologies

Penile ultrasound has been used as an adjunct to the physical examination to better diagnose and define specific urethral pathologies. Direct urethral visualization using a cystoscope is the preferred diagnostic test for many urologists. However, ultrasound can provide an economi-

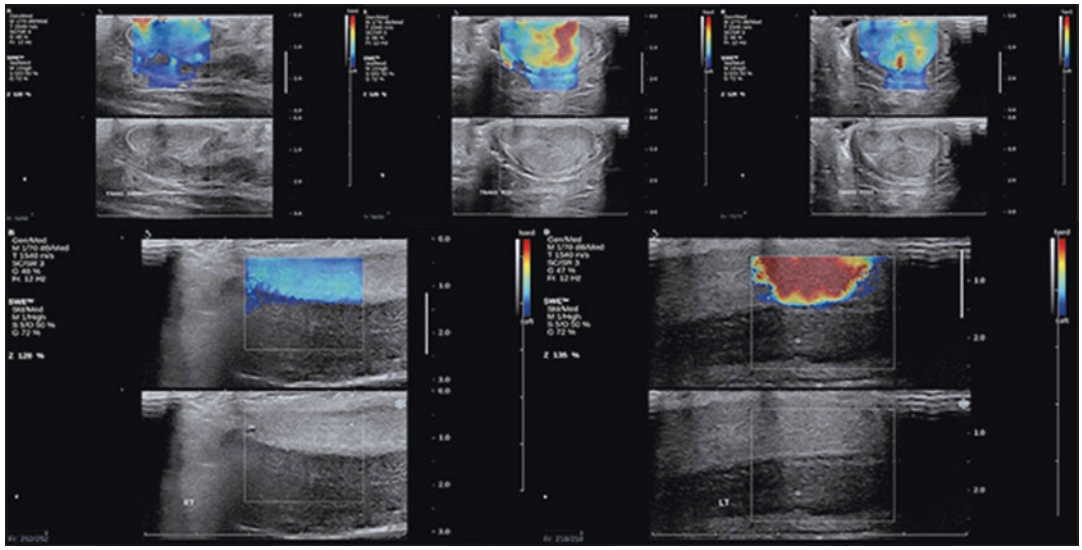

Fig. 7.19 A patient with penile curvature and without palpable plaque nor abnormalities visualized on the B-mode ultrasound. Sonoelastograms (scaled with *red* more firm and *blue* less firm) superimposed over transverse B-mode ultrasound images of the (**a**) proximal, (**b**) mid, and (**c**) distal phallus. Sonoelastograms superimposed over parasagittal views of the (**d**) right and (**e**) left cavernosal bodies. Notice the firm areas overlying the mid left cavernosal bodies demonstrated in the Peyronie's disease patient

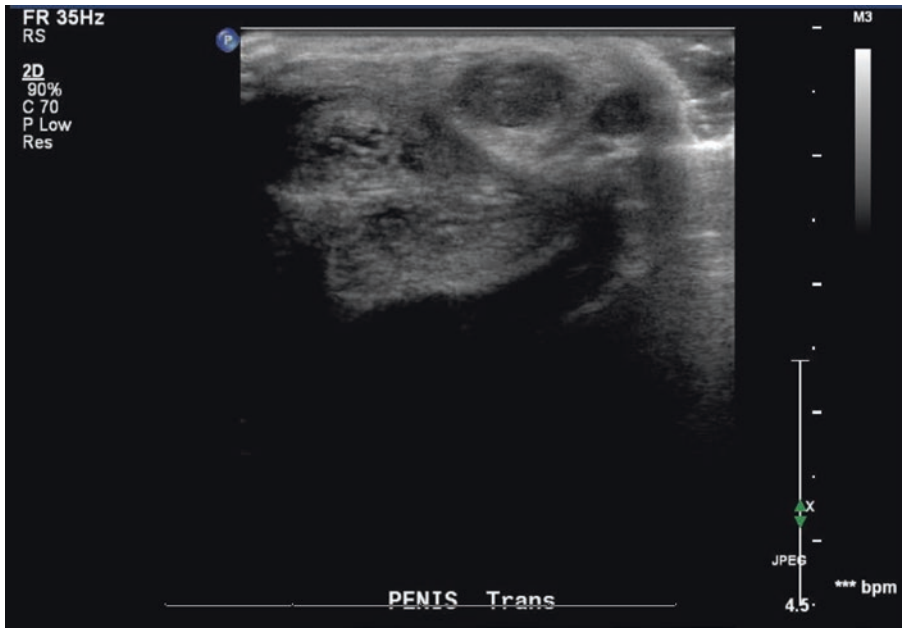

Fig. 7.20 Metastatic to the penile shaft, seen as subcutaneous soft-tissue mass, extrinsic to the corpora cavernosa

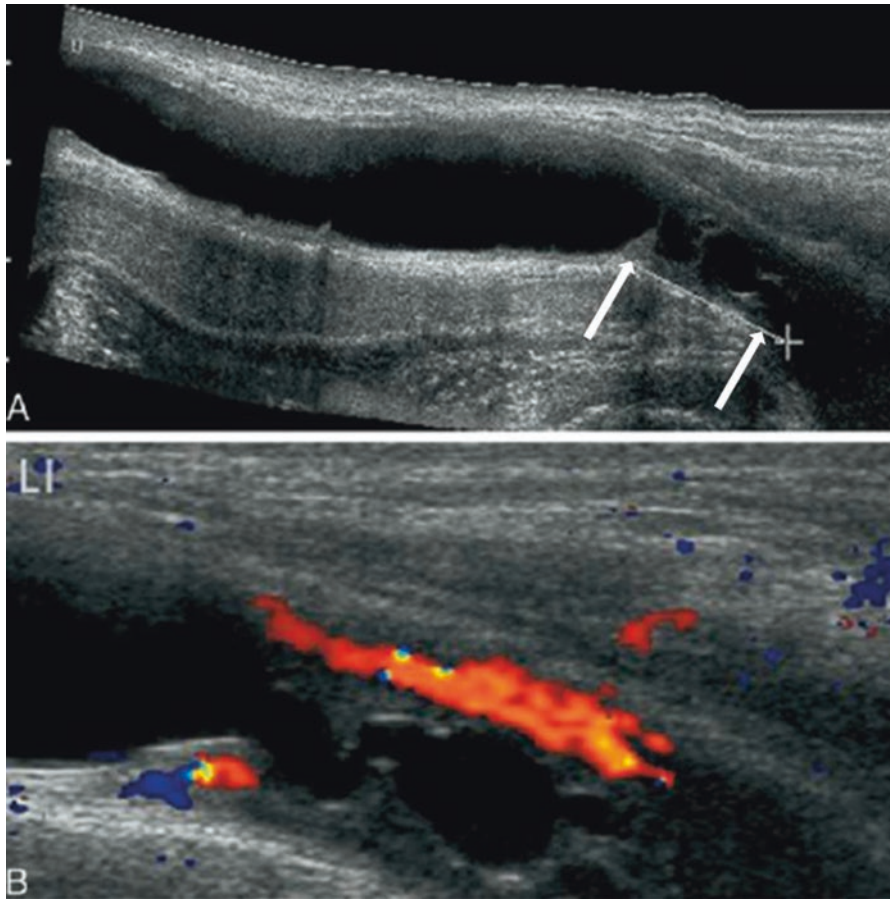

Fig. 7.21 Urethral stricture (*arrow*) with Sono-Urethrography and Sono-Urethrography with color doppler (*bottom*). Note the lumenal perfusion detail given by Sono-Urethrography

cally sound and noninvasive alternative for the assessment of urethral stricture, foreign bodies including urethral calculi, and urethral and periurethral diverticula, cysts, and abscesses.

Urethral stricturess are the result of fibrous scarring of the urethral mucosa and surrounding spongiosal tissues, which contract and narrow the luminal diameter of the urethral channel. Common causes of penile urethral strictures are infections, trauma, and congenital narrowing. Urethral trauma resulting in stricture disease includes, but is not limited to: straddle injury, passage of stones or foreign bodies, and iatrogenic instrumentation including catheterization and cystoscopy. Although retrograde urethrography is the standard imaging modality for urethral stricture disease (both anterior and posterior segments), penile ultrasound provides a more accurate assessment of stricture length and diameter in the anterior segment [72–74]. Furthermore, penile ultrasound allows for assessment of stricture involvement within the periurethral spongy tissue whereas a classic urethrogram only assesses the luminal component of the pathology (Fig. 7.21) [75]. On B-mode ultrasonography, strictures appear as hyperechoic areas surrounding the urethra without evidence of Doppler flow, consistent with findings of fibrosis. However, the fibrotic stricture segment may have surrounding Doppler flow demonstrating hyperemia from inflammation. With distension of the urethra with saline or lubricating jelly, areas of narrowing can be appreciated, corresponding to the location of a stricture (Fig. 7.21).

Urethral foreign bodies or calculi suspected based upon patient history and physical examination can be easily confirmed with penile ultrasound. Shape, size, and location of these obstructing bodies can be assessed and a therapeutic plan can be made based upon the data obtained [76].

Urethral and periurethral diverticula, cysts, and abscesses can be delineated with penile ultrasound with ease. A contrast medium such as normal saline or lubricating jelly is needed to provide a differential in ultrasound impedance to identify urethral or periurethral diverticula with the best sensitivity [77]. Cysts and abscesses around the urethra can be visualized using penile ultrasound without the insertion of contrast material. However, at times contrast material can be useful in identifying whether the structures noted are separate from the urethra once distended.

Role of Penile Ultrasound in Cardiovascular Health

Emerging data further supports that PDU can provide significant lead-time on the diagnosis of CAD and PVD. These telltale signs of underlying cardiovascular health can be seen on PDU prompted by the presenting clinical symptom of ED. Established work has demonstrated the association with arteriogenic ED predating recognized cardiovascular disease by several years [39, 47, 48]. ED has been associated with both atherosclerosis and endothelial dysfunction [78]. More recently, impaired parameters on PDU have been shown to be associated with the incidence of major adverse cardiovascular events, particularly in younger men who were otherwise considered low-risk of such cardiovascular disease events [79]. This has been corroborated as well as the role of the quantitative vascular assessment of ED on subsequent discovery of cardiovascular risk, particularly in unrecognized younger men in large cohort analyses and meta-analyses [19, 80].

PDU has not found a well-defined role in the realm of cardiovascular disease screening. However, in a man with no known cardiovascular disease, with or without recognized risk factors, arteriogenic ED as defined by PDU parameters should warrant counseling regarding potential underlying cardiovascular disease and referral for further systemic evaluation. This population may render a clinically significant benefit from early detection of otherwise occult vascular and cardiac disease found based upon erectile function evaluation and treatment.

Proper Documentation

Complete and meticulous documentation of every ultrasound examination is an element of a comprehensive study. Documentation often entails a series of representative static images or cine series (when electronic storage space and technology allows) that are archived with an associated report documenting pertinent findings and indicated measurements and calculations. The combination of images and a written document of findings allows for optimal diagnosis aiding in patient care, archival reference in the patient medical record, and appropriate billing of services provided.

Each report must include patient identification (i.e., name, medical record number, date of birth), date of the examination, type of examination performed, indications for the examination, and pertinent findings and diagnoses. It is mandatory to include complete identification of the patient and study. Each report should also be undersigned by the ultrasonographer and physician interpreter of the study to document who performed the study and who read the results in cases where a technician performs the study saving images for a physician's interpretation. Copies of the printed images should be attached to the report or electronically stored images and/or videos should be referenced in the written report. The ultrasound images should be labeled with the date and time of the study, patient identification, and applicable anatomic labeling,

Conclusion

With a proper understanding of penile anatomy and functional physiology, penile ultrasound provides a real-time imaging modality assessing the static anatomic features and vascular dynamics. As a diagnostic modality, penile Doppler ultrasound provides

urologists a vital tool in the office assessment of ED, Peyronie's disease, penile urethral strictures, and masses of the penis as well as an acute care setting evaluation of a penile trauma patient. It is essential that urologists maintain proficient PDU skills in their diagnostic armamentarium.

Appendix 1: A Sample Report Template for a Penile Doppler Ultrasound Performed as a Diagnostic Element in a Case of Erectile Dysfunction

Suggested protocol for evaluation of erectile dysfunction:

DORSAL view is primary, VENTRAL view as needed (indicate which view is used on image)

Pre-injection (also Images for non-injection penile ultrasound studies)

1. Longitudinal and transverse survey scan of the phallus with cine loops
2. Split screen base, mid, and distal view of phallus in transverse plane
3. Split screen longitudinal view of left and right corpora cavernosa
4. Flaccid phallus (image taken in mid 2/3 of exposed phallus):
   - (a) AP and width of each corpora
   - (b) Inner diameter measurements of left and right cavernosal artery at mid phallus
   - (c) Spectral Doppler waveform with PSV, EDV, and Ri
   - (d) Optional measurements: acceleration time, pulsatility index, velocity index

Post-injection

1. 5 and 10 min
   - (a) Spectral Doppler waveform with PSV, EDV, and Ri
   - (b) Inner diameter measurements of left and right cavernosal artery at mid phallus
   - (c) Optional measurements: acceleration time, pulsatility index, velocity index
   - (d) Subjective evaluation of tumescence and rigidity
2. 15 and 20 min (second injection if indicated, document total dose)
   - (a) Spectral Doppler waveform with PSV, EDV, and Ri
   - (b) Inner diameter measurements of left and right cavernosal artery at mid phallus
   - (c) Optional measurements: acceleration time, pulsatility index, velocity index
   - (d) Subjective evaluation of tumescence and rigidity
3. 25 and 30 min (third injection if indicated, document total dose)
   - (a) Spectral Doppler waveform with PSV, EDV, and Ri
   - (b) Inner diameter measurements of left and right cavernosal artery at mid phallus
   - (c) Optional measurements: acceleration time, pulsatility index, velocity index
   - (d) Subjective evaluation of tumescence and rigidity
4. End of study
   - (a) Inner diameter measurements of left and right cavernosal artery and mid phallus

Appendix 2: Patient Instructions for Penile Injection Therapy

Preparation for Injection

Items You Will Need

- *Alcohol sponges or swaps.*
- *One milliliter insulin syringe with #28 or #30 gauge needle.* These are disposable and not to be reused for a second injection. Disposal should be performed with the cap on the needle so as not to injure anyone disposing of trash.
- *Papaverine/Phentolamine combination, Prostaglandin E1 or Papaverine/Phentolamine/Prostaglandin combination* either pre-drawn by the physician a pharmacist in the syringe, or in a vial to be drawn into the syringe by the patient in the appropriate volume as prescribed by the physician. *The medication must be refrigerated and away from light exposure.*

Filling the Syringe

1. Check the expiration date of medication. Hold the medication bottle so that your fingers do not touch the rub or stopper (Fig. 7.22).
2. Using a circular motion, wipe off the top of the bottle with alcohol swab (Fig. 7.23).
3. Remove the needle cover. Do not allow the needle to touch anything before drawing the medication or before injecting the medication (Fig. 7.24).
4. Draw a small amount of the air into the syringe to be injected into the medication vial. The

Fig. 7.22

Fig. 7.23

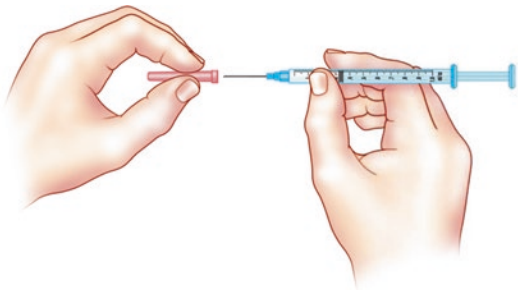

Fig. 7.24

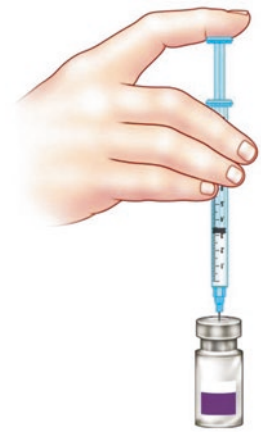

Fig. 7.25

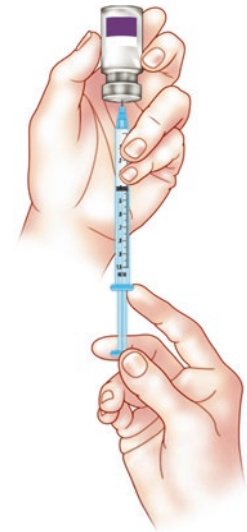

Fig. 7.26

syringe needle should be inserted into the center of the rubber stopper of the medication vial. Push the air into the bottle (Fig. 7.25).

5. Turn the bottle and syringe upside down. Solely draw the medication into the syringe. Tap the syringe gently to remove the bubbles (Fig. 7.26).
6. Move the plunger in and out several times while gently tapping the syringe, just removing all air bubbles (Fig. 7.27).
7. Gently remove the syringe from the medication vial and replace the needle cap over the needle. Keep the protected needle on the filled syringe within easy reach prior to injection (Fig. 7.28).

Self-Injection Technique

Step 1: Grasp the head of the penis, not the skin, and hold upwards toward the trunk. Position the penis along your inner thigh. Choose the injection site on the side of the penis. Avoid injecting into any visible veins. The crossed hatched areas in the figure below represent the ideal locations to inject into (Fig. 7.29).

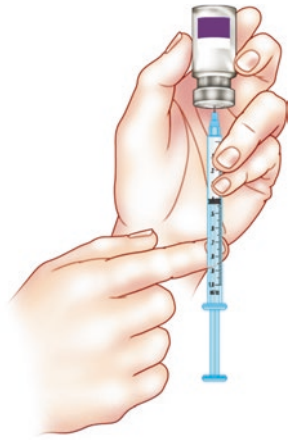

Fig. 7.27

Fig. 7.28

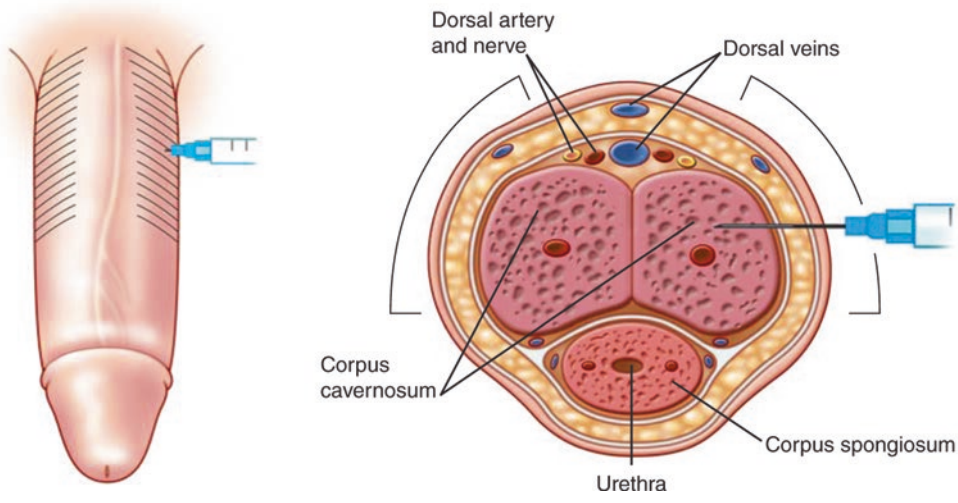

Fig. 7.29

Step 2: Wipe the skin with an alcohol swab (Fig. 7.30).

Step 3: Pick up the syringe between the thumb and middle finger, like a pen, and push the needle gently but firmly through the skin until the entire needle is buried inside the penis (Fig. 7.31).

Step 4: Holding the syringe, use your thumb to slowly (8–10 s) inject the entire amount of medication. Then remove the needle from your penis (Fig. 7.32).

Step 5: Immediately apply pressure on the injection site with another alcohol wipe for at least 2 min. Make sure there is no bleeding (Fig. 7.33).

Step 6: Dispose of the syringe unit into the puncture-proof receptacle provided.

Step 7: Stand up to allow your erection to develop quickly. You are now ready to start sexual foreplay. You will have a full or action within a few minutes.

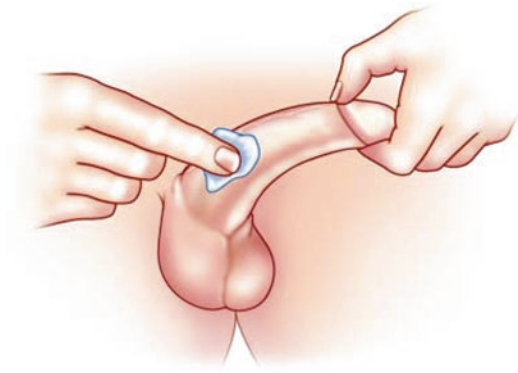

Fig. 7.30

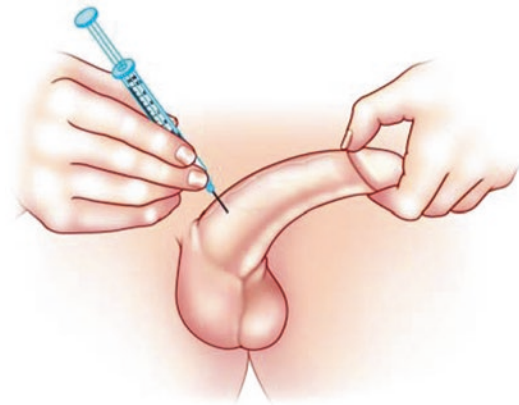

Fig. 7.31

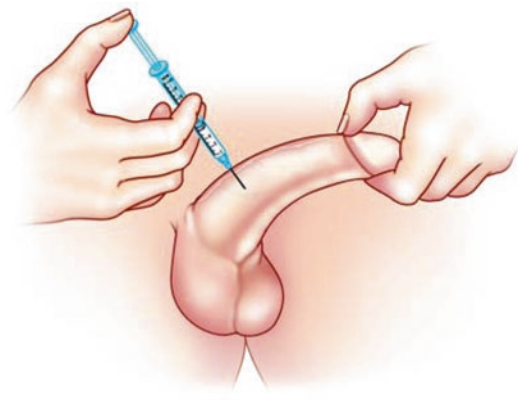

Fig. 7.32

Normally, the erection will last anywhere from 30 to 120 min. If your erection lasts longer than 3 h, you should seek immediate medical attention.

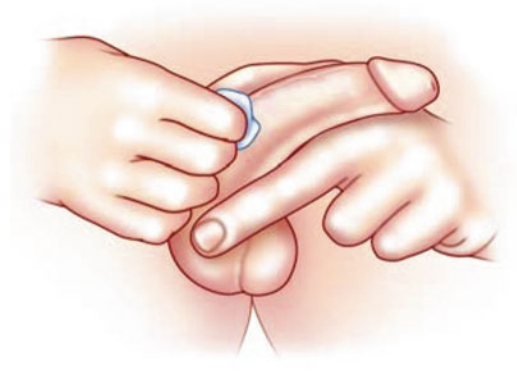

Fig. 7.33

References

1. Doubilet PM, Benson CB, Silverman SG, et al. The penis. Semin Ultrasound CT MR. 1991;12:157.
2. Carlson BM. Human embryology and developmental biology. Philadelphia: Elsevier Health Sciences; 2013.
3. Moore KL, Persaud TVN, Torchia MG. The developing human. Philadelphia: Saunders; 2011.
4. Bellinger MF. Embryology of the male external genitalia. Urol Clin North Am. 1981;8(3):375–82.
5. Sadler TW. Langman medical embryology (international ed). Auckland: Wolters Kluwer Health; 2011.
6. Wilson JD, George FW, Griffin JE. The hormonal control of sexual development. Science. 1981;211:1278.
7. Rey R, Picard JY. Embryology and endocrinology of genital development. Baillieres Clin Endocrinol Metab. 1998;12:17.
8. Wilson JD, Griffin JE, Leshin M, George FW. Role of gonadal hormones in development of the sexual phenotypes. Hum Genet. 1981;58:78.
9. Newman HF, Northup JD. Mechanism of human penile erection: an overview. Urology. 1981;17:399.
10. Fuchs AM, Mehringer CM, Rajfer J. Anatomy of penile venous drainage in potent and impotent men during cavernosography. J Urol. 1989;141:1353.
11. Hsu GL, Hsieh CH, Wen HS, Chen YC, Chen SC, Mok MS. Penile venous anatomy: an additional description and its clinical implication. J Androl. 2003;24:921.
12. AUA Guidelines. http://www.auanet.org/content/guidelines-and-quality-care/policy-statements.cfm. Spring 2016
13. Shin D, Pregenzer Jr G, Gardin JM. Erectile dysfunction: a disease marker for cardiovascular disease. Cardiol Rev. 2011;19:5.
14. Tomada N, Tomada I, Botelho F, et al. Are all metabolic syndrome components responsible for penile hemodynamics impairment in patients with erectile dysfunction? The role of body fat mass assessment. J Sex Med. 2011;8:831.
15. Corona G, Monami M, Boddi V, et al. Male sexuality and cardiovascular risk. A cohort study in patients with erectile dysfunction. J Sex Med. 1918;7:2010.

16. Wing RR. Long-term effects of a lifestyle intervention on weight and cardiovascular risk factors in individuals with type 2 diabetes mellitus: four-year results of the Look AHEAD trial. Arch Intern Med. 2010;170:1566.
17. Hayashi T, Farrell MA, Chaput LA, et al. Lifestyle intervention, behavioral changes, and improvement in cardiovascular risk profiles in the California WISEWOMAN project. J Womens Health (Larchmt). 2010;19:1129.
18. Miner MM. Erectile dysfunction: a harbinger or consequence: does its detection lead to a "window of curability?". J Androl. 2011;32:125.
19. Inman BA, Sauver JL, Jacobson DJ, et al. A population-based, longitudinal study of erectile dysfunction and future coronary artery disease. Mayo Clin Proc. 2009;84:108.
20. Billups KL, Bank AJ, Padma-Nathan H, et al. Erectile dysfunction as a harbinger for increased cardiometabolic risk. Int J Impot Res. 2008;20:236.
21. Patel U, Lees WR. Penile sonography. In: Solibiati L, Rizzatto G, editors. Ultrasound of superficial structures. London: Churchill Livingstone; 1995. p. 229–42.
22. Wilkins CJ, Sriprasad S, Sidhu PS. Colour Doppler ultrasound of the penis. Clin Radiol. 2003;58:514.
23. Kim SH, Paick JS, Lee SE, et al. Doppler sonography of deep cavernosal artery of the penis: variation of peak systolic velocity according to sampling location. J Ultrasound Med. 1994;13:591.
24. Roy C, Saussine C, Tuchmann C, et al. Duplex Doppler sonography of the flaccid penis: potential role in the evaluation of impotence. J Clin Ultrasound. 2000;28:290.
25. Mancini M, Bartolini M, Maggi M, et al. Duplex ultrasound evaluation of cavernosal peak systolic velocity and waveform acceleration in the penile flaccid state: clinical significance in the assessment of the arterial supply in patients with erectile dysfunction. Int J Androl. 2000;23:199.
26. van Ahlen H, Peskar BA, Sticht G, et al. Pharmacokinetics of vasoactive substances administered into the human corpus cavernosum. J Urol. 1994;151:1227.
27. Patel U, Amin Z, Friedman E, et al. Colour flow and spectral Doppler imaging after papaverine-induced penile erection in 220 impotent men: study of temporal patterns and the importance of repeated sampling, velocity asymmetry and vascular anomalies. Clin Radiol. 1993;48:18.
28. Broderick GA, Lue TF. The penile blood flow study: evaluation of vasculogenic impotence. In: Jonas U, Thon WF, Stief CG, editors. Erectile dysfunction. Berlin: Springer; 1991.
29. Shabsigh R, Fishman IJ, Shotland Y, et al. Comparison of penile duplex ultrasonography with nocturnal penile tumescence monitoring for the evaluation of erectile impotence. J Urol. 1990;143:924.
30. Benson CB, Vickers MA. Sexual impotence caused by vascular disease: diagnosis with duplex sonography. AJR Am J Roentgenol. 1989;153:1149.
31. Lue TF, Hricak H, Marich KW, et al. Vasculogenic impotence evaluated by high-resolution ultrasonography and pulsed Doppler spectrum analysis. Radiology. 1985;155:777.
32. Mueller SC, Lue TF. Evaluation of vasculogenic impotence. Urol Clin North Am. 1988;15:65.
33. Pescatori ES, Hatzichristou DG, Namburi S, et al. A positive intracavernous injection test implies normal veno-occlusive but not necessarily normal arterial function: a hemodynamic study. J Urol. 1994;151:1209.
34. Benson CB, Aruny JE, Vickers Jr MA. Correlation of duplex sonography with arteriography in patients with erectile dysfunction. AJR Am J Roentgenol. 1993;160:71.
35. Bassiouny HS, Levine LA. Penile duplex sonography in the diagnosis of venogenic impotence. J Vasc Surg. 1991;13:75.
36. Quam JP, King BF, James EM, et al. Duplex and color Doppler sonographic evaluation of vasculogenic impotence. AJR Am J Roentgenol. 1989;153:1141.
37. Naroda T, Yamanaka M, Matsushita K, et al. [Clinical studies for venogenic impotence with color Doppler ultrasonography—evaluation of resistance index of the cavernous artery]. Nippon Hinyokika Gakkai Zasshi. 1996;87:1231.
38. Cormio L, Bettocchi C, Ricapito V, et al. Resistance index as a prognostic factor for prolonged erection after penile dynamic colour Doppler ultrasonography. Eur Urol. 1998;33:94.
39. Feldman HA, Johannes CB, Derby CA, et al. Erectile dysfunction and coronary risk factors: prospective results from the Massachusetts male aging study. Prev Med. 2000;30:328.
40. Blumentals WA, Gomez-Caminero A, Joo S, et al. Should erectile dysfunction be considered as a marker for acute myocardial infarction? Results from a retrospective cohort study. Int J Impot Res. 2004;16:350.
41. Sullivan ME, Thompson CS, Dashwood MR, et al. Nitric oxide and penile erection: is erectile dysfunction another manifestation of vascular disease? Cardiovasc Res. 1999;43:658.
42. Solomon H, Man JW, Jackson G. Erectile dysfunction and the cardiovascular patient: endothelial dysfunction is the common denominator. Heart. 2003;89:251.
43. Montorsi P, Montorsi F, Schulman CC. Is erectile dysfunction the "tip of the iceberg" of a systemic vascular disorder? Eur Urol. 2003;44:352.
44. Guay AT. The emerging link between hypogonadism and metabolic syndrome. J Androl. 2009;30:370.
45. Traish AM, Guay AT. Are androgens critical for penile erections in humans? Examining the clinical and preclinical evidence. J Sex Med. 2006;3:382.
46. Kaya C, Ergelen M, Ilktac A, Karaman MI. Impaired elasticity of aorta in patients with erectile dysfunction. Urology. 2007;70:558.
47. Lue TF, Tanagho EA. Physiology of erection and pharmacological management of impotence. J Urol. 1987;137:829.
48. O"Kane PD, Jackson G. Erectile dysfunction: is there silent obstructive coronary artery disease? Int J Clin Pract. 2001;55:219.
49. Mulhall J, Teloken P, Barnas J. Vasculogenic erectile dysfunction is a predictor of abnormal stress echocardiography. J Sex Med. 2009;6:820.

50. Zambon JP, Mendonca RR, Wroclawski ML, et al. Cardiovascular and metabolic syndrome risk among men with and without erectile dysfunction: case-control study. Sao Paulo Med J. 2010;128:137.
51. Mottillo S, Filion KB, Genest J, et al. The metabolic syndrome and cardiovascular risk a systematic review and meta-analysis. J Am Coll Cardiol. 2010;56:1113.
52. Bohm M, Baumhakel M, Teo K, et al. Erectile dysfunction predicts cardiovascular events in high-risk patients receiving telmisartan, ramipril, or both: the ONgoing Telmisartan Alone and in combination with Ramipril Global Endpoint Trial/Telmisartan Randomized AssessmeNt Study in ACE iNtolerant subjects with cardiovascular Disease (ONTARGET/TRANSCEND) Trials. Circulation. 2010;121:1439.
53. Batty GD, Li Q, Czernichow S, et al. Erectile dysfunction and later cardiovascular disease in men with type 2 diabetes: prospective cohort study based on the ADVANCE (Action in Diabetes and Vascular Disease: Preterax and Diamicron Modified-Release Controlled Evaluation) trial. J Am Coll Cardiol. 2010;56:1908.
54. Kang BC, Lee DY, Byun JY, et al. Post-traumatic arterial priapism: colour Doppler examination and superselective arterial embolization. Clin Radiol. 1998;53:830.
55. Asgari MA, Hosseini SY, Safarinejad MR, et al. Penile fractures: evaluation, therapeutic approaches and long-term results. J Urol. 1996;155:148.
56. El-Bahnasawy MS, Gomha MA. Penile fractures: the successful outcome of immediate surgical intervention. Int J Impot Res. 2000;12:273.
57. Atan A, Gungor S, Ozergin O, et al. Idiopathic penile mondors' disease: a case report. Int Urol Nephrol. 2002;34:97.
58. Dicuio M, Pomara G, Ales V, et al. Doppler ultrasonography in a young patient with penile Mondor's disease. Arch Ital Urol Androl. 2005;77:58.
59. Sasso F, Gulino G, Basar M, et al. Penile Mondors' disease: an underestimated pathology. Br J Urol. 1996;77:729.
60. Nachmann MM, Jaffe JS, Ginsberg PC, et al. Sickle cell episode manifesting as superficial thrombophlebitis of the penis. J Am Osteopath Assoc. 2003;103:102.
61. Luzzi GA, Pattinson J, Wathen CG. Penile Mondor's disease and inherited thrombophilia. Int J STD AIDS. 2006;17:70.
62. Brock G, Hsu GL, Nunes L, et al. The anatomy of the tunica albuginea in the normal penis and Peyronie's disease. J Urol. 1997;157:276.
63. Chou YH, Tiu CM, Pan HB, et al. High-resolution real-time ultrasound in Peyronie's disease. J Ultrasound Med. 1987;6:67.
64. Kadioglu A, Tefekli A, Erol H, et al. Color Doppler ultrasound assessment of penile vascular system in men with Peyronie's disease. Int J Impot Res. 2000;12:263.
65. Morana C, Loiero G, Sangiorgio A, Zani T, Catalano G. Elastosonography in the Peyronie's disease: our preliminary experience. Arch Ital Urol Androl. 2010;82:269–70.
66. Riversi V, Tallis V, Trovatelli S, et al. Realtime-elastosonography of the penis in patients with Peyronie's disease. Arch Ital Urol Androl. 2012;84:174.
67. Richards G, Goldenberg E, Pek H, Gilbert BR. Penile sonoelastography for the localization of a non-palpable, non-sonographically visualized lesion in a patient with penile curvature from Peyronie's disease. J Sex Med. 2014;11:516.
68. Zhang J, Qiao X, Gao F, et al. A new method of measuring the stiffness of corpus cavernosum penis with ShearWave™ Elastography. Br J Radiol. 2015;88:1048.
69. Horenblas S, Kroger R, Gallee MP, et al. Ultrasound in squamous cell carcinoma of the penis; a useful addition to clinical staging? A comparison of ultrasound with histopathology. Urology. 1994;43:702.
70. Lont AP, Besnard AP, Gallee MP, et al. A comparison of physical examination and imaging in determining the extent of primary penile carcinoma. BJU Int. 2003;91:493.
71. Lan SK, Lin CW, Ho HC, et al. Penile metastasis secondary to nasal NK/T-cell lymphoma. Urology. 2008;72:1014.
72. Gallentine ML, Morey AF. Imaging of the male urethra for stricture disease. Urol Clin North Am. 2002;29:361.
73. Morey AF, McAninch JW. Role of preoperative sonourethrography in bulbar urethral reconstruction. J Urol. 1997;158:1376.
74. Choudhary S, Singh P, Sundar E, et al. A comparison of sonourethrography and retrograde urethrography in evaluation of anterior urethral strictures. Clin Radiol. 2004;59:736.
75. Morey AF, McAninch JW. Sonographic staging of anterior urethral strictures. J Urol. 2000;163:1070.
76. Kim B, Kawashima A, LeRoy AJ. Imaging of the male urethra. Semin Ultrasound CT MR. 2007;28:258.
77. Bearcroft PW, Berman LH. Sonography in the evaluation of the male anterior urethra. Clin Radiol. 1994;49:621.
78. Rastrelli G, Corona G, Mannucci E, Maggi M. Vascular and chronological age in men with erectile dysfunction: a longitudinal study. J Sex Med. 2016;13:200.
79. Rastrelli G, Corona G, Lotti F, et al. Flaccid penile acceleration as a marker of cardiovascular risk in men without classical risk factors. J Sex Med. 2014;11:173.
80. Vlachopoulos CV, Terentes-Printzios DG, Ioakeimidis NK, et al. Prediction of cardiovascular events and all-cause mortality with erectile dysfunction: a systematic review and metaanalysis of cohort studies. Circ Cardiovasc Qual Outcomes. 2013;6:99.

Transabdominal Pelvic Ultrasound

8

R. Ernest Sosa and Pat F. Fulgham

Introduction

Transabdominal pelvic ultrasound provides instant noninvasive imagery of the lower urinary tract for the assessment of urologic conditions. It is useful in evaluating patients with lower urinary tract symptoms. The examining physician gains valuable information about the anatomy and function of a patient's bladder and prostate. In the female patient, bladder hypermobility can be assessed. Urologists performing and interpreting bladder ultrasound will have a specific clinical question in mind as a reason for performing the scan. In order to obtain a good-quality diagnostic image and render an interpretation of the ultrasound findings, it is important to have an understanding of ultrasound machine settings, patient positioning, probe manipulation, normal ultrasound anatomy, and common artifacts.

Indications

Ultrasound of the bladder is performed for a variety of clinical indications (Table 8.1). When the bladder is full, it provides information about bladder capacity as well as bladder wall thickness. The presence of bladder wall pathology such as tumors, trabeculations, and diverticula and the presence of bladder stones or of a foreign body can also be ascertained. Imaging of the ureteral orifices using Doppler can confirm the presence of ureteral efflux of urine. The presence of a ureterocele or a stone in the distal ureter or the presence of distal ureteral dilation may also be appreciated. In the male patient, prostate size and morphology may be evaluated. In the female patient, bladder hypermobility can be assessed. In male and female patients, the proper position of a urethral catheter in the bladder can be confirmed (Fig. 8.1). The presence of blood clot and tumor in the bladder can also be determined (Fig. 8.2).

Pelvic ultrasound may also be useful to guide procedures such as deflation of a retained catheter balloon or for guiding the placement of a suprapubic catheter [1].

R.E. Sosa, M.D.
Division of Urology, Veterans Administration Healthcare System, New York Harbor, Manhattan, New York, NY, USA
e-mail: ernie.sosa@gmail.com

P.F. Fulgham, M.D., F.A.C.S. (✉)
Department of Urology, Texas Health Presbyterian Hospital of Dallas, 8210 Walnut Hill Lane Suite 014, Dallas, TX 75231, USA
e-mail: pfulgham@airmail.net; patfulgham@yahoo.com

P.F. Fulgham, B.R. Gilbert (eds.), *Practical Urological Ultrasound*, Current Clinical Urology,
DOI 10.1007/978-3-319-43868-9_8

Table 8.1 Indications for bladder ultrasound

1.	Measurement of bladder volume
2.	Measurement of post-void residual
3.	Measurement of prostate size and morphology
4.	Assessment of anatomic changes associated with bladder outlet obstruction
	(a) Bladder wall thickness
	(b) Bladder wall trabeculation
	(c) Bladder wall diverticula
	(d) Bladder stones
5.	Documentation of efflux of urine from the ureteral orifices
6.	Evaluation of pediatric posterior urethral valves
7.	Assessment of correct position of a urethral catheter
8.	Guidance for placement of a suprapubic tube
9.	Assessment for completeness of the evacuation of bladder clots
10.	Evaluation of hematuria
11.	Evaluation for bladder tumors
12.	Evaluation for distal ureteral dilation
13.	Evaluation for foreign body in bladder
14.	Evaluation for distal ureteral stone
15.	Evaluation for ureterocele
16.	Evaluation for complete bladder emptying
17.	Assessment for bladder neck hypermobility in women
18.	Evaluation of pelvic fluid collections
19.	Guidance for transperineal prostate biopsy
20.	Imaging of prostate when the rectum is absent or obstructed

Patient Preparation and Positioning

The patient should have a full bladder but should not be uncomfortably distended. A bladder volume of approximately 150 cc is optimal. The patient is placed in the supine position on the examining table. The abdomen is exposed from the xiphoid process to just below the pubic bone. The patient may place their arms up above their head or by their side on the table. The room should be at a comfortable temperature. The lights are dimmed. A paper drape placed over the pelvic area and tucked into the patient's clothing will protect the clothing and allow for easy cleanup after the procedure. The examiner assumes a comfortable position to the patient's right.

Equipment and Techniques

The appropriate mode for performing pelvic ultrasound is selected on the ultrasound equipment, and the patient's demographics are entered into demographic fields. A curved-array transducer is utilized for the pelvic ultrasound study (Fig. 8.3). The advantage of the curved-array transducer is that it requires a small skin surface for contact and produces a wider field of view.

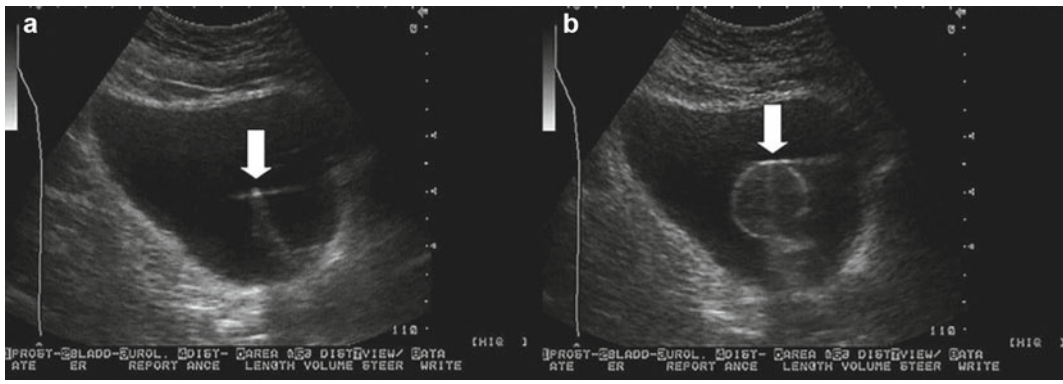

Fig. 8.1 (**a**) The tip of the balloon catheter is seen in the bladder (*arrow*). (**b**) Image of the inflated balloon in the bladder (*arrow*)

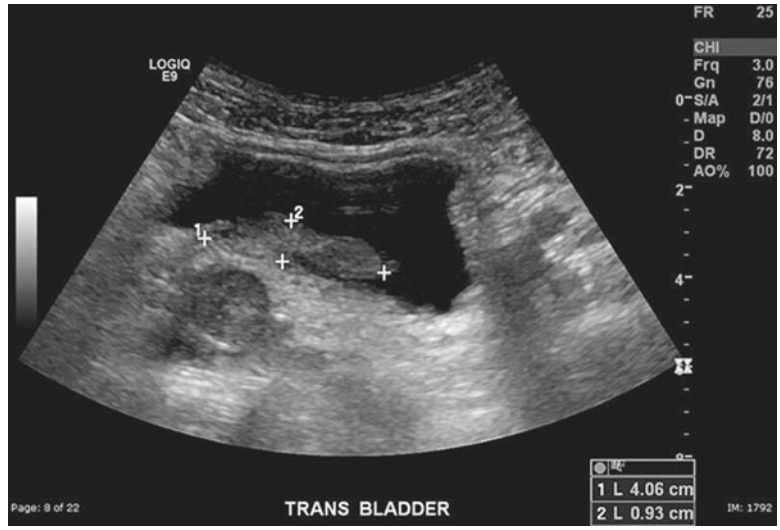

Fig. 8.2 Residual blood clot in the bladder after irrigation for clot retention

Fig. 8.3 Curved-array transducer with orienting notch (*arrow*). The notch is, by convention, oriented to the patient's head during longitudinal scanning and to the patient's right during transverse scanning

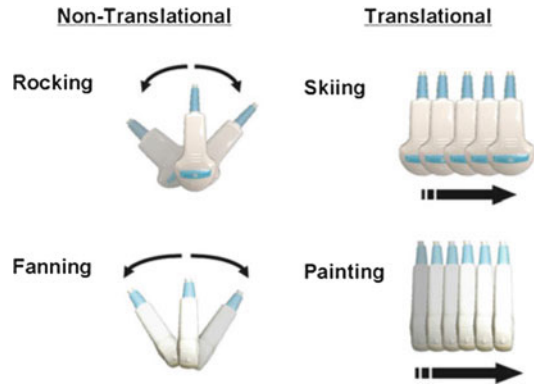

Fig. 8.4 Various techniques for probe manipulation

In the adult patient, a 3.5–5.0 MHz transducer is utilized to examine the bladder. For the pediatric patient, particularly for a small, young child, a higher frequency transducer is desirable, particularly for a small, young child.

An even coating of warm conducting gel is placed on the skin of the lower abdominal wall or on the probe face. Prior to beginning the ultrasound examination the transducer is most often held in the examiner's right hand. The orienting notch on the transducer is identified (Fig. 8.3). The orientation of the transducer may be confirmed by placing a finger on the contact surface near the notch. The image produced by contact with the finger should appear on the left side of the screen indicating the patient's right side in the transverse plane and the cephalad direction in the sagittal plane.

Various techniques for probe manipulation are useful in ultrasound (Fig. 8.4). The techniques of rocking and fanning are non-translational, meaning the probe face stays in place while the probe body is rocked or fanned to evaluate the area of interest. The techniques of painting and skiing are translational, meaning the probe face is moved along the surface of the skin to evaluate the area of interest. All four techniques are useful for avoiding obstacles like the pubic bone or bowel gas and for performing a survey scan.

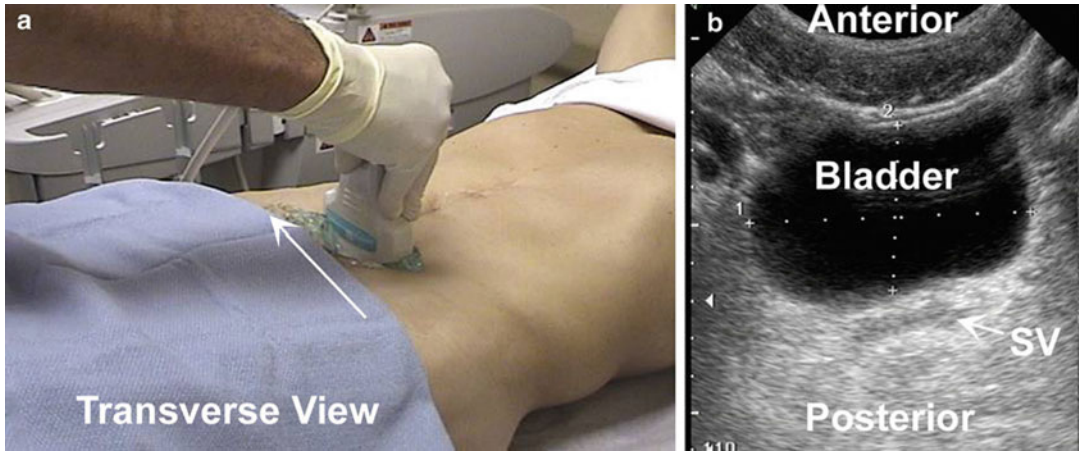

Fig. 8.5 (**a**) Position of transducer for obtaining a transverse image. Notch (*arrow*) is directed toward patient's right. (**b**) Transverse image of the bladder with measurements of the width (1) and height (2) of the bladder. *SV* seminal vesicles

Ultrasound of the bladder may be started in the transverse view with the notch on the transducer to the patient's right (Fig. 8.5). The transducer is placed on the lower abdominal wall with secure but gentle pressure. If the pubic bone is in the field of view, the bladder may not be fully visualized. The pubic bone will reflect the sound waves resulting in acoustic shadowing which obscures the bladder. The pubic bone may be avoided by varying the angle of insonation using the fanning technique until a full transverse image is obtained. In the transverse view of the bladder, the right side of the bladder should appear on the left side of the screen. The machine settings may be adjusted until the best-quality image is obtained.

Survey Scan of the Bladder

A survey scan should be conducted prior to addressing specific clinical conditions to determine if any additional or incidental pathology is present. The survey scan is performed in the transverse view then the sagittal view. When starting with a transverse view, the sagittal view is obtained by rotating the transducer 90° clockwise with the probe notch pointing toward the patient's head (Fig. 8.6). The rocking technique may be used to facilitate viewing the bladder in the sagittal view.

Measurement of Bladder Volume

The bladder volume is obtained by first locating the largest transverse diameter in the mid-transverse view (Fig. 8.7). The width and the height are measured. The transducer is then rotated 90° clockwise to obtain the sagittal view. In the midsagittal view, the length of the bladder is measured using the dome and the bladder neck as the landmarks. These measurements may be made using a split screen so that both measurements are on the same screen. These images are printed or saved electronically. The bladder volume is calculated by multiplying the width, height, and length measurements by 0.625. When the specified measurements are obtained, the calculated bladder volume will usually be automatically displayed. When measuring urine volume in the bladder, the report should indicate whether the volume is a bladder volume measurement or a post-void residual urine volume measurement.

Measurement of Bladder Wall Thickness

Measurement of bladder wall thickness is taken, by convention, when the bladder is filled to at least 150 cc. Bladder wall thickness may be measured at a number of different locations. In this

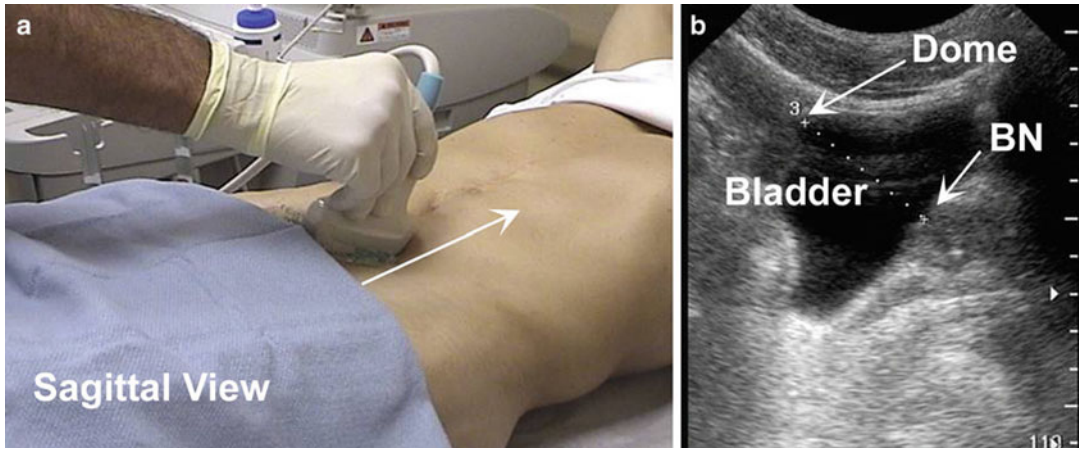

Fig. 8.6 (**a**) Position of the transducer with the notch to the patient's head. (**b**) Sagittal image of the bladder with length of the bladder (3) from the dome on the *left* to the bladder neck (BN) at the *right*

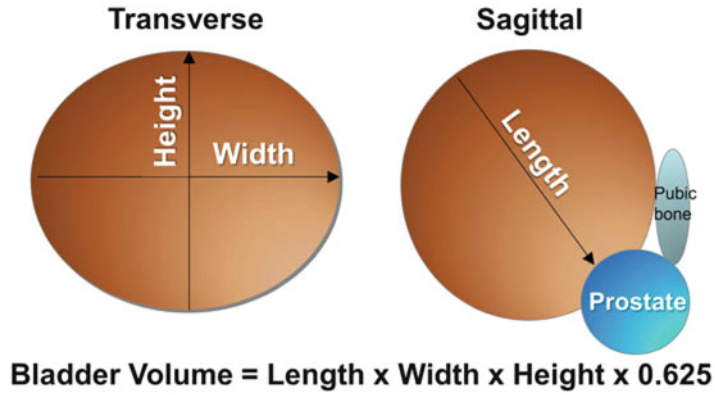

Fig. 8.7 The formula for calculating bladder volume = width (1) × height (2) × length (3) × 0.625

case, the bladder wall thickness is measured along the posterior wall on the sagittal view (Fig. 8.8). If the bladder wall thickness is less than 5 mm when the bladder is filled to 150 cc, there is a 63 % probability that the bladder is not obstructed. However, if the bladder wall thickness is over 5 mm at this volume, there is an 87 % probability that there is bladder outlet obstruction. Nomograms are available to calculate the likelihood of urodynamically demonstrated bladder outlet for bladder wall thickness at various bladder volumes [2].

Evaluation of Ureteral Efflux

The efflux of urine from the distal ureters can be appreciated using power or color Doppler. By positioning the probe in the sagittal view (orienting notch toward the patient's head) and then twisting the probe approximately 15° to one side or the other, the probe is aligned with the direction of urine efflux from the ureteral orifice. This will often demonstrate efflux. Ureteral "jets" of urine can be seen on gray scale but are more easily seen using Doppler. These jets are seen as a yellow/orange streak when power Doppler is used (Fig. 8.9). These jets would appear red on color Doppler.

Common Abnormalities

Bladder Stones

Many of the abnormalities appreciated on bladder ultrasound are the result of bladder outlet obstruction or urethral obstruction. Bladder stones may be easily visualized on ultrasound (Fig. 8.10). A stone will reflect sound waves

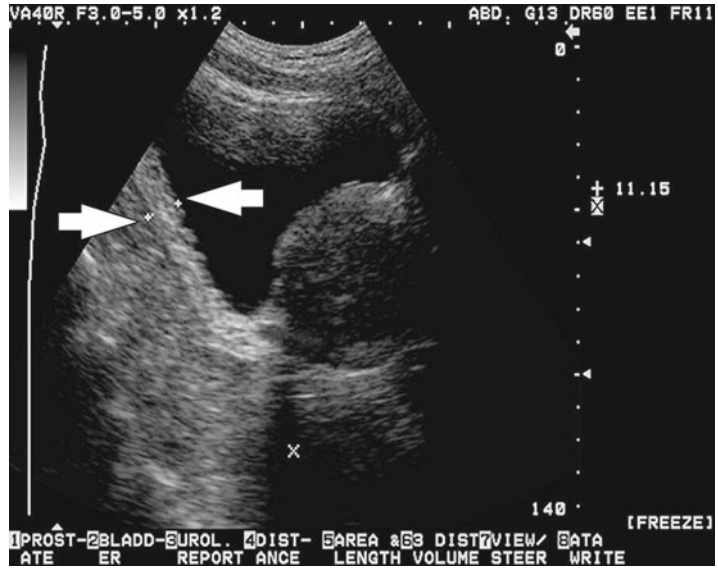

Fig. 8.8 Bladder wall thickness, in this case, is measured (*arrows*) along the posterior wall. In this image the wall measures 11.15 mm in thickness

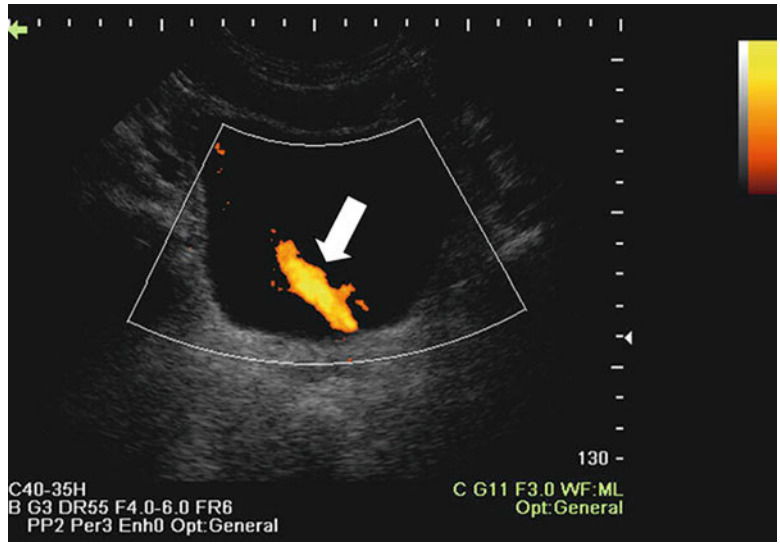

Fig. 8.9 Ureteral jet (*arrow*) demonstrated using power Doppler

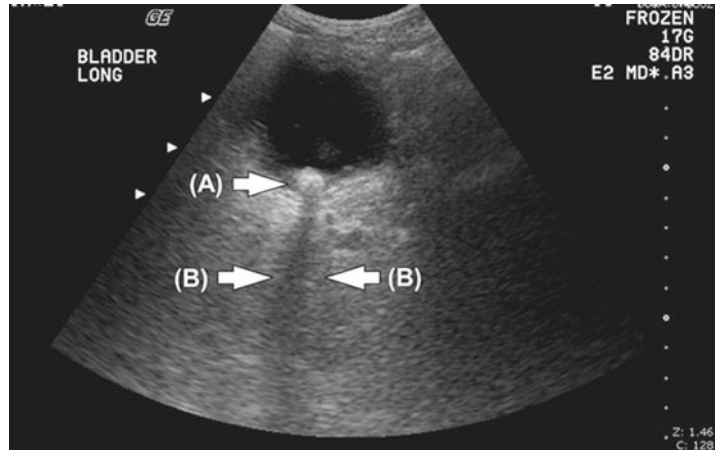

Fig. 8.10 A hyperechoic bladder calculus (**A**) is seen in this image along with the posterior acoustic shadowing from the calculus (**B**)

resulting in a shadow posterior to the stone. A technique of having the patient turn on their side will cause the stone to move thus proving it to be a stone and not a fixed bladder wall lesion such as a bladder tumor with dystrophic calcification.

Trabeculation and Diverticula

Trabeculation of the bladder wall may be seen in response to distal obstruction. This finding is often best observed on the sagittal view (Fig. 8.11). **Bladder diverticula** may be demonstrated on ultrasound (Fig. 8.12). Using the Doppler mode, the flow of urine in and out of the diverticulum may be seen (Fig. 8.12b).

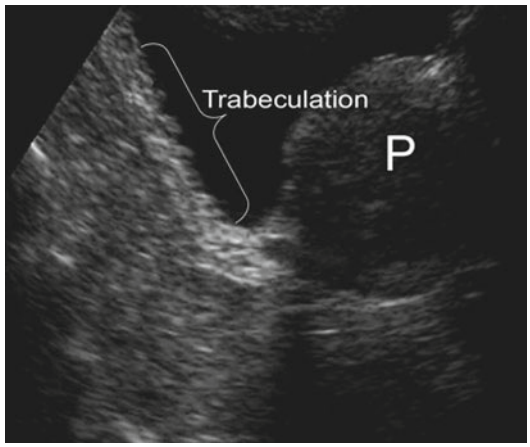

Fig. 8.11 Trabeculation of the bladder is demonstrated in this sagittal image. (P) represents the prostate

Ureteral Dilation

The distal ureters may be examined sonographically for the presence of distal ureteral dilation (Fig. 8.13). Ureteral dilation is a nonspecific finding with multiple possible causes including primary congenital dilation, reflux, obstruction at the bladder neck from prostatic enlargement or at the urethra from posterior urethral valves, or urethral stricture disease. In some cases, the obstruction may be caused by distal ureteral scar tissue, a tumor, or a distal ureteral stone (Fig. 8.14). The ureters are also evaluated in the sagittal view and are located in the bladder base. **Ureteroceles** may be well seen as rounded fluid-filled membranes (Fig. 8.15). Associated congenital abnormalities, such as duplication or ectopy, may also be detected.

Neoplasms

Ultrasound of the bladder can determine the presence of focal lesions, such as bladder tumors (Fig. 8.16). The sensitivity of ultrasound for bladder tumor detection is dependent on the location and size of the tumor. Tumors located in the anterior region of the bladder will have the lowest detection rate on ultrasound (47 %) whereas tumors located in the lateral side walls of the bladder have the highest detection rates [3]. The diameter of the bladder tumor also affects detection rate. Detection is most reliable for tumors >5 mm in diameter. In one study, the detection

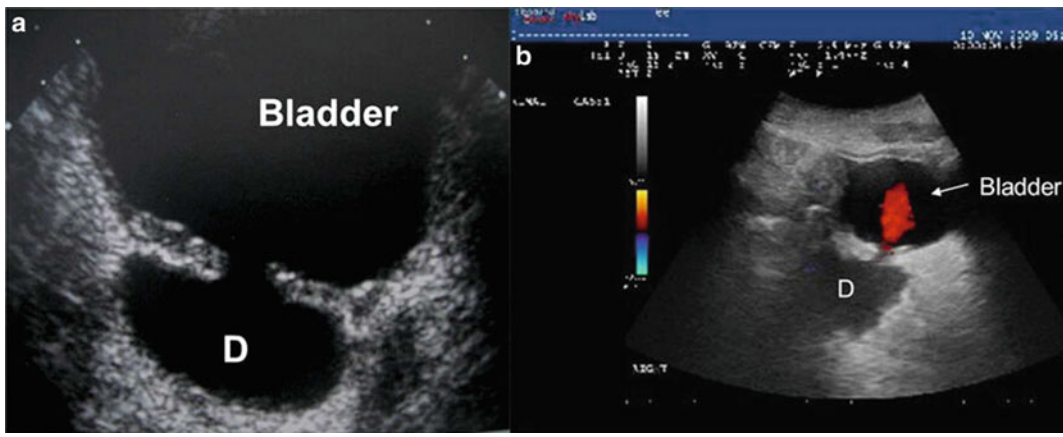

Fig. 8.12 (**a**, **b**) Bladder diverticula (D) are seen. (**b**) The color Doppler mode is used to demonstrate the flow of urine out of the diverticula (D). The flow of urine is from the diverticula into the bladder as indicated by the *red* color. The flow is toward the transducer and is assigned the color *red* in this case

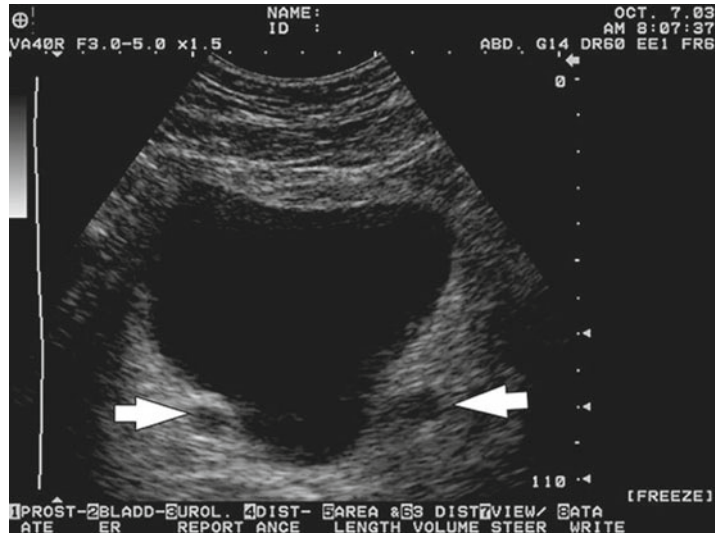

Fig. 8.13 Dilated distal ureters (*arrows*) on this transverse view of the bladder. The cause of the dilation in this case was bladder outlet obstruction

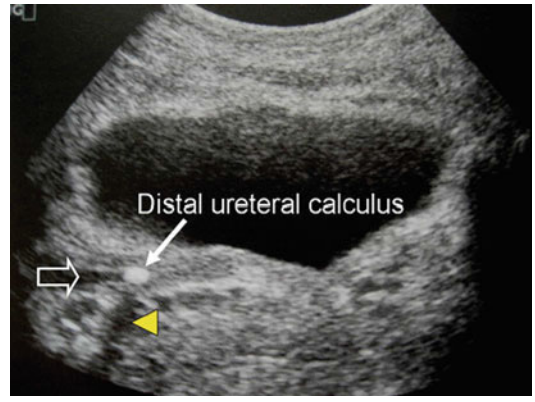

Fig. 8.14 Dilated distal ureter seen on this transverse view of the bladder is a hypoechoic structure (*open arrow*) parallel to the floor of the bladder. Shadowing (*yellow arrowhead*) is seen posterior to a distal ureteral calculus (*white arrow*)

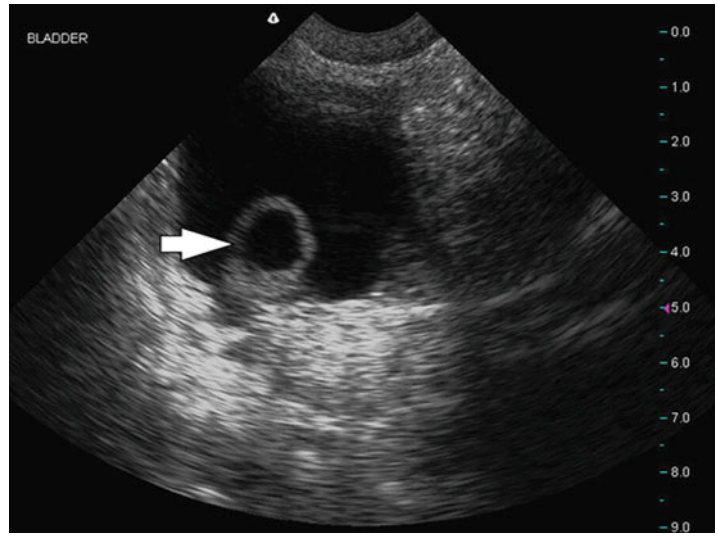

Fig. 8.15 Ureterocele (*arrow*) is seen as a hyperechoic structure surrounding anechoic fluid. This ureterocele is thickened. Many ureteroceles appear as a thin hyperechoic membrane on ultrasound

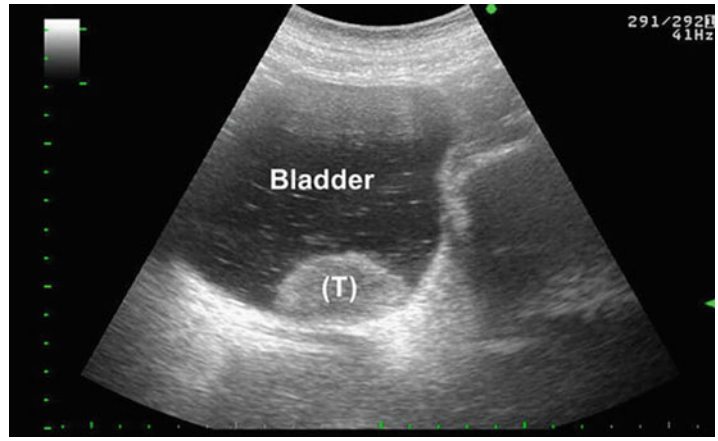

Fig. 8.16 A bladder wall lesion (T) consistent with transitional cell carcinoma. The lack of shadowing suggests a soft tissue abnormality

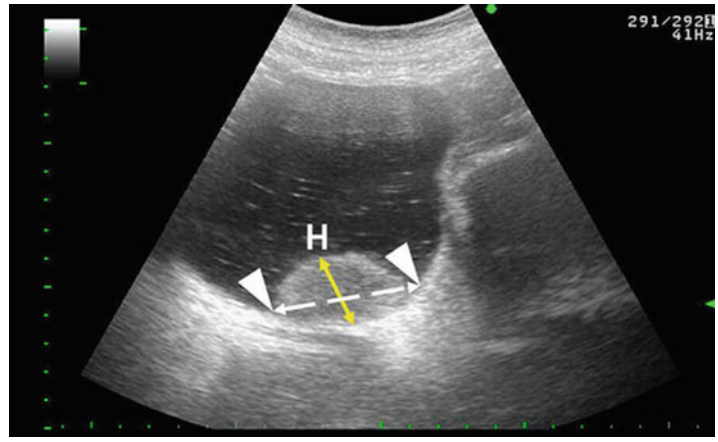

Fig. 8.17 Contact length (*arrowheads*) is the width of a tumor that is in contact with the bladder wall. The tumor height (*H*) is obtained by measuring the distance from the base to the luminal margin of the tumor (*yellow arrow*)

rate for tumors >5 mm was the highest for tumors located in the right lateral wall (100 %) and lowest in the anterior wall (61 %) [4].

Ultrasound may be helpful in the **staging of bladder carcinoma**. Although direct observation of the depth of bladder wall invasion is difficult, some predictions of invasiveness may be obtained by measuring ***contact length*** (length of the base of the tumor that is in contact with the distended bladder wall) and ***height*** (distance from the base of the tumor to the luminal margin of the tumor). A ***height-to-contact length ratio*** may be calculated. This ratio is correlated with the likelihood of muscle invasion (Fig. 8.17). In a study by Ozden et al., it was determined that a contact length of greater than 41.5 mm and a height-to-contact length ratio of less than 0.605 were the cutoff values for differentiating superficial from invasive tumors with a sensitivity rate of 81 % [5]. Tumors smaller than 0.5 cm that are flat and/or near the bladder neck may be missed [4].

Foreign Bodies and Perivesical Processes

Transabdominal ultrasound of the pelvis may be very useful in identifying foreign bodies in the bladder or in assessing perivesical pathology. Perivesical neoplasms and fluid collections are best appreciated when the bladder is full.

Evaluation of the Prostate Gland

Once examination of the bladder has been concluded, attention is given to the prostate gland. The prostate is evaluated in both the transverse and sagittal views. To view the prostate, however, the ultrasound probe may need to be angled more steeply behind the pubic bone. It may be necessary to apply more pressure to the probe in cases where the abdomen is protuberant. The height and width of the prostate are measured in the transverse view (Fig. 8.18). The length of the prostate is measured by rotating the transducer 90° clockwise into the sagittal position, making sure to maintain the indicator on the probe toward the patient's head (Fig. 8.19). The volume of the prostate is automatically determined by most ultrasound equipment but may also be calculated using the formula: length × width × height × 0.523.

Intravesical prostatic protrusion (IPP) is measured on the sagittal view. IPP is present when the middle lobe extends into the bladder lumen (Fig. 8.20). IPP has been shown to correlate with bladder outlet obstruction as demonstrated by urodynamic evaluation [6–8]. The prostate should be carefully evaluated for calcifications in the parenchyma, lucent lesions, cysts, and solid mass effects. Further characterization of pros-

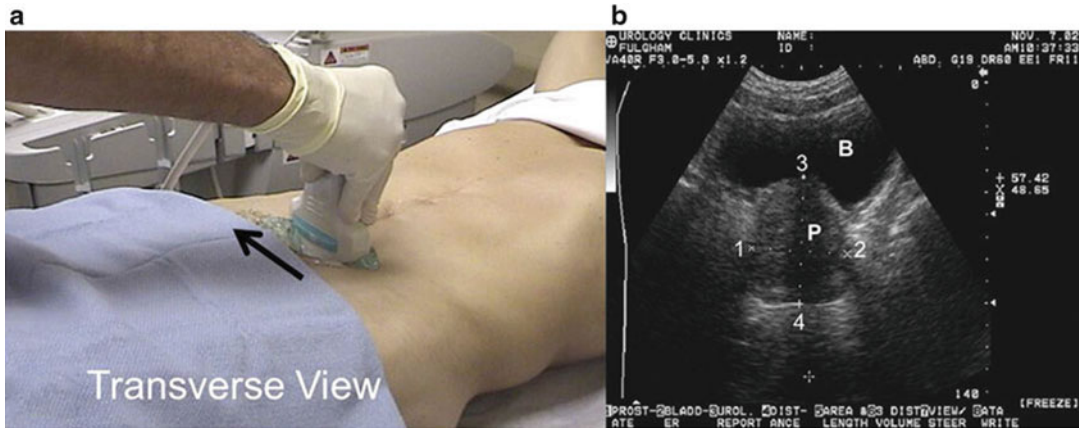

Fig. 8.18 (**a**) The probe is positioned for evaluating the prostate in the transverse view. The orienting notch on the transdcuer is to the patient's right side (*black arrow*). In image (**b**) a full bladder (B) is helpful for visualizing the prostate (P). The width (1–2) and the height (3–4) are obtained

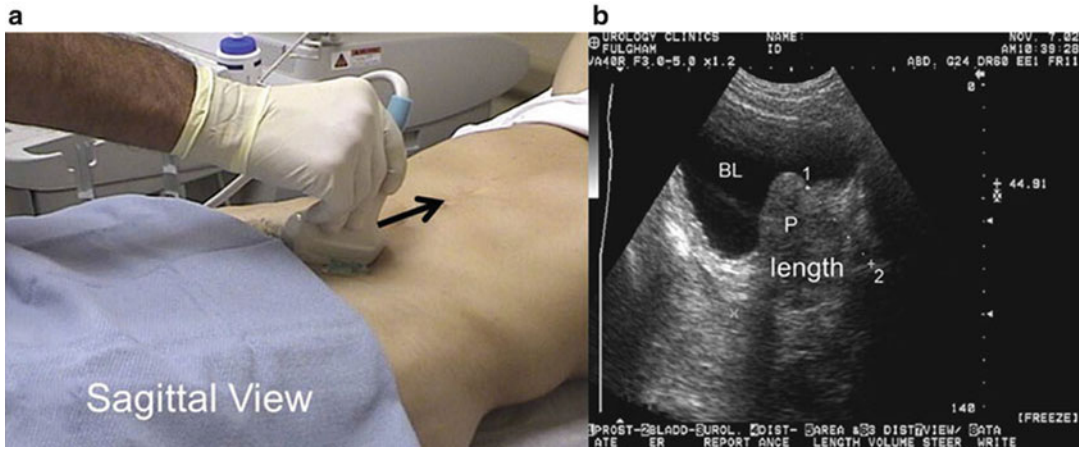

Fig. 8.19 (**a**) The probe is positioned for measuring prostate length. The notch is directed toward the patient's head (*black arrow*). (**b**) The length of the prostate (P) is measured as indicated by calipers 1–2 in this sagittal view

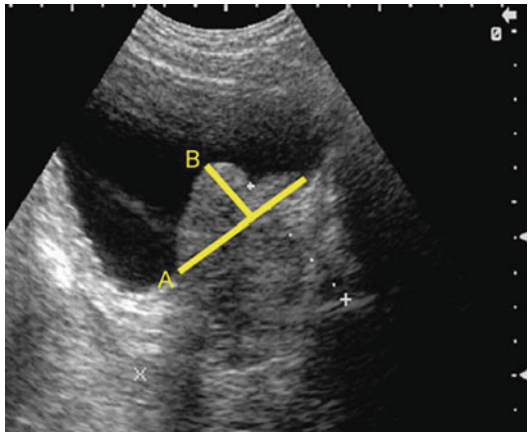

Fig. 8.20 The IPP is measured by first drawing a line (*A*) across the bladder neck. The protrusion of the prostate is determined by measuring the perpendicular length from line *A* to the luminal tip of the prostate, line (*B*)

tatic abnormalities can be made with digital rectal examination, transrectal ultrasound, and computerized tomography and multiparametric magnetic resonance imaging (mpMRI) if necessary. Other structures which may be evaluated include the seminal vesicles and ejaculatory ducts though they are typically better seen on transrectal ultrasound of the prostate.

Documentation

Proper documentation is imperative to creating a permanent record of the study. The images obtained should be of sufficient and uniform quality with appropriate labeling of structures. It is important that the report of the study states the indications for the study, description of findings, measurements, impression/assessment, and the signature and name of the interpreting physician.

Image Documentation

- Measurement of bladder volume, if indicated (this may be performed using a split screen)
  - Midsagittal view length measurement from dome of the bladder to the bladder neck
  - Mid-transverse view with height and width measurements
- Measurement of bladder wall thickness, if indicated
- Documentation of the presence of ureteral jets, if indicated
- Documentation of any abnormalities
- Calculated bladder volume or post-void residual, if indicated
- Measurement of prostate volume (this may be performed using a split screen)
  - Midsagittal view with height measurement
  - Mid-transverse view with measurement of width and length
- Seminal vesicles: transverse and longitudinal views for length and width measurements, if indicated
- Measurement of IPP, if appropriate

Ultrasound Report

- Patient identification (name, date of birth, other facility identifiers)
- Date of study
- Facility name, location
- Ordering physician
- Indication
- Findings: bladder measurements, prostate measurements, bladder wall thickness, and abnormalities
- Impression/assessment
- Name of interpreting physician and signature

Automated Bladder Scanning

A handheld device to obtain a bladder volume or a post-void residual is an important piece of equipment for the urologist's office. It allows for a quick measurement of post-void residual and can be performed by office staff. However, this is not a diagnostic ultrasound study and is only performed if the intent of the study is to determine the bladder volume or post-void residual (Fig. 8.21). A diagnostic ultrasound machine may also be used to determine post-void residual. Automated bladder ultrasound may be useful for determining if a patient has an adequate pre-void bladder volume (>150 mL) prior to executing a urinary flow rate determination.

Fig. 8.21 An example of an automated bladder scanner. The automated bladder scan is useful for obtaining a post-void residual but is not considered a diagnostic ultrasound study

Table 8.2 Potential causes of inaccuracy by automated scanning devices

1. Obesity
2. Ascites
3. Clot retention
4. Bladder diverticulum
5. Perivesical fluid collection
(a) Urinoma
(b) Hematoma
(c) Lymphocele
(d) Ovarian cyst
6. Distortion or compression of bladder by perivesical mass

Automated bladder scanners may be inaccurate in a number of clinical circumstances (Table 8.2). The presence of ascites, urinomas, or bladder diverticula may result in inaccurate determinations of residual urine. Tumor, blood clots, or distortion of the bladder by extrinsic mass may also produce inaccurate results. Findings on automated scans which seem inappropriate to the clinical findings should be verified by manually performed transabdominal pelvic ultrasound.

Conclusion

Transabdominal pelvic ultrasound is a valuable tool in the practice of urology. It allows for the immediate assessment of many urologic conditions and assists the urologist in immediate diagnosis and treatment.

References

1. Jacob P, Rai BP, Todd AW. Suprapubic catheter insertion using an ultrasound-guided technique and literature review. BJU Int. 2012;110(6):779–84.
2. Manieri C, Carter S, Romano G, Trucchi A, Valenti M, Tubaro A. The diagnosis of bladder outlet obstruction in men by ultrasound measurement of bladder wall thickness. J Urol. 1998;159:761–5.
3. Ozden E, Turgut AT, Turkolmez K, Resorlu B, Safak M. Effect of bladder carcinoma location on detection rates by ultrasonography and computed tomography. Urology. 2007;69(5):889–92.
4. Itzchak Y, Singer D, Fischelovitch Y. Ultrasonographic assessment of bladder tumors. I. Tumor detection. J Urol. 1981;126(1):31–3.
5. Ozden E, Turgut AT, Yesil M, Gogus C, Gogus O. A new parameter for staging bladder carcinoma: ultrasonographic contact length and height-to-length ratio. J Ultrasound Med. 2007;26:1137–42.
6. Franco G, De Nunzio C, Costantino L, Tubaro A, Ciccariello M, et al. Ultrasound assessment of intravesical prostatic protrusion and detrusor wall thickness—new standards for noninvasive bladder outlet obstruction diagnosis? J Urol. 2010;183:2270–4.
7. Chia SJ, Heng CT, Chan SP, Foo KT. Correlation of intravesical prostatic protrusion with bladder outlet obstruction. BJU Int. 2003;914(4):371–4.
8. Lieber MM, Jacobson DJ, McGree ME, et al. Intravesical prostatic protrusion in men in Olmsted County, Minnesota. J Urol. 2004;182(6):2819–24.

Suggested Reading

Hoffer M, editor. Ultrasound teaching manual: the basics of performing and interpreting ultrasound scans. Stutgart: Georg Thieme; 2005.
Middleton W. General and vascular ultrasound. 2nd ed. Philadelphia: Mosby; 2007.
Block B. The practice of ultrasound: a step by step guide to abdominal scanning. Stutgart: Georg Thieme; 2004.

Pelvic Floor Ultrasound

9

Ricardo Palmerola, Farzeen Firoozi, and Chad Baxter

Introduction

Pelvic ultrasound is increasingly used to evaluate pelvic floor disorders and has several advantages in contrast to other imaging modalities such as magnetic resonance imaging (MRI) and cystourethrography. Ultrasound is relatively inexpensive, widely available, and offers real-time, dynamic imaging of the pelvic anatomy without radiation. Most urologists are trained in transrectal ultrasonography. However, those skills are easily translated to translabial pelvic ultrasonography. This chapter focuses on 2D ultrasound imaging and technique, as it is the most widely available and familiar to urologists. However, the expanding prevalence of 3D/4D ultrasound reconstruction of the pelvic anatomy and the future application of elastography will likely advance the understanding of pelvic floor pathology and our appreciation and use of pelvic ultrasound [1].

R. Palmerola, M.D. • F. Firoozi, M.D., F.A.C.S. (✉)
Department of Urology, Hofstra Northwell Health System School of Medicine, The Arthur Smith Institute for Urology, Center of Pelvic Health and Reconstructive Surgery, Northwell Health System, 450 Lakeville Road, Lake Success, NY 11042, USA
e-mail: ffiroozi@northwell.edu

C. Baxter, M.D.
Department of Urology, David Geffen School of Medicine at UCLA, 1260 15th Street, Suite 1200, Santa Monica, CA 90404, USA
e-mail: cbaxter@mednet.ucla.edu

This chapter describes translabial pelvic ultrasound examination by anatomic compartments. Normal and commonly encountered aberrant findings of the anterior, central, and posterior compartments are described. Imaging of surgically placed materials including transvaginal mesh and urethral bulking agents concludes the chapter.

Anterior Compartment

The anterior compartment includes the urethra, bladder neck, bladder, and retropubic space of Retzius, as well as the surrounding supportive muscular and connective tissue.

Indications for Anterior Compartment Ultrasound

The indications for anterior compartment ultrasound are urinary incontinence, urinary retention, urethral diverticulum, urethral stricture, urethral hypermobility, vaginal cyst, cystocele, mesh extrusion, mesh erosion, and pelvic pain.

Technique

Ultrasonographic examination of the anterior compartment is most commonly performed translabially with a 5–8 cm, 3.5–5 MHz, curved array transducer. Alternatively, the ultrasonographer may select a 7.5 MHz linear array transducer. For

P.F. Fulgham, B.R. Gilbert (eds.), *Practical Urological Ultrasound*, Current Clinical Urology,
DOI 10.1007/978-3-319-43868-9_9

3D translabial ultrasonography, a 4–8 MHz curved array transducer can be used. In contrast to a transvaginal technique, translabial ultrasound examination is noninvasive and does not distort the pelvic anatomy. We typically perform the exam with the patient in the dorsal lithotomy position; however, the exam can be performed in the standing position. After covering the probe with a condom and applying a small amount of gel, the probe is placed against the labia minora and the urethral meatus. Firm contact with the tissue should be ensured and one may ask the patient to cough to help part the labia and expel air between the skin and transducer (Fig. 9.1). Conventional ultrasonography orients the 2D image in the midsagittal line with the pubic symphysis in the upper-left portion of the image (Fig. 9.2). This orientation has also been applied for 3D and 4D systems. By rotating the transducer 90° to the right or left, a coronal image can be attained. Furthermore, imaging can be performed at rest, during Valsalva maneuver, and during pelvic floor contraction.

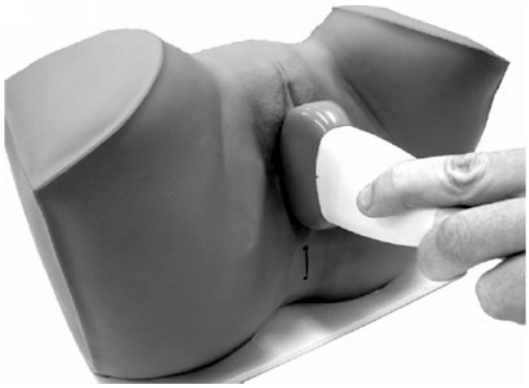

Fig. 9.1 Curved array transducer position

Normal Ultrasound Anatomy

Urethra

The urethral complex appears immediately caudal to the pubic symphysis and includes the urethral mucosa, smooth muscle, and surrounding vasculature (Fig. 9.3). The normally oriented urethra is parallel to the incident ultrasound beam and appears hypoechoic. With increasing degrees of urethral hypermobility (as with Valsalva maneuver), the proximal urethra will begin to rotate in the posteroinferior direction, more perpendicular to the ultrasound beam, and the urethral complex progressively appears less hypoechoic.

The fibers of the rhabdosphincter are oriented transversely to the incident beam in the normally oriented urethra, and the rhabdosphincter thus appears hyperechoic. With progressive urethral

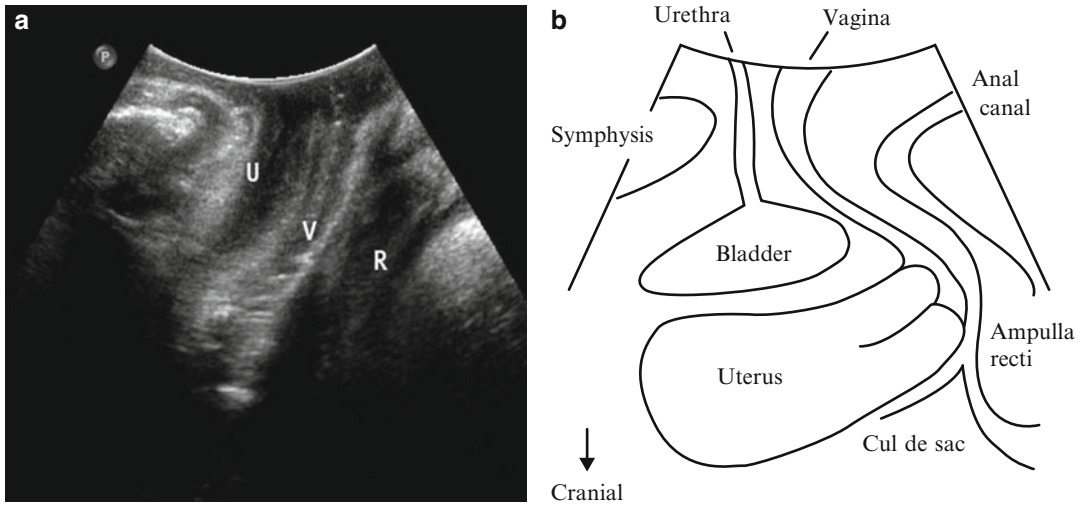

Fig. 9.2 (**a**) Two-dimensional orientation of translabial ultrasound image in midsagittal line. *U* urethra, *V* vagina, *R* rectum (**b**) Illustration demonstrating pertinent anatomy in midsagittal plane

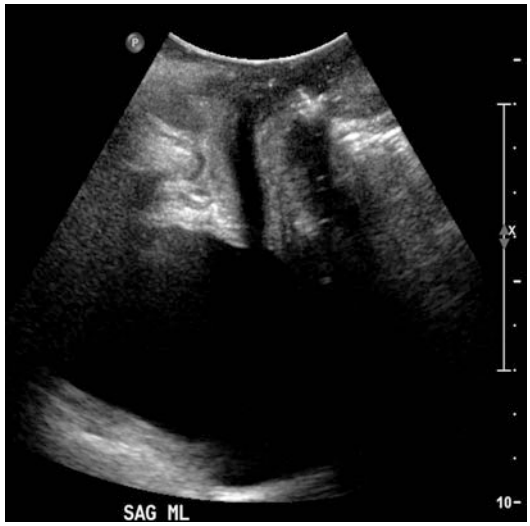

Fig. 9.3 Hypoechoic urethra

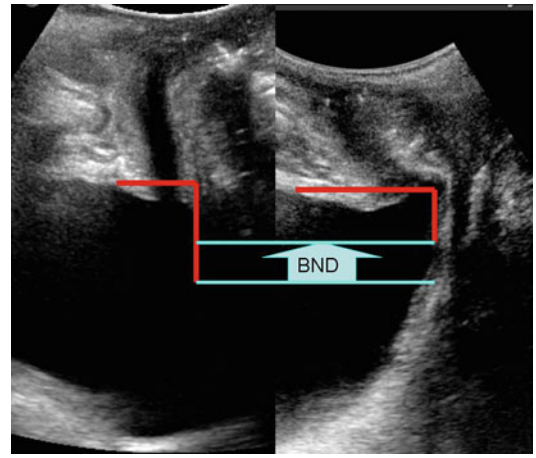

Fig. 9.4 Bladder neck descent. *Left side* image without Valsalva maneuver, *right side* image with Valsalva

hypermobility, rhabdosphincter orientation shifts in relation to the ultrasound energy and may become less hyperechoic [2]. Periurethral connective tissue appears hyperechoic relative to the urethral complex, though clearly less echogenic than the adjacent inferoposterior margin of the pubis. Frequently observed punctate echogenicities within the urethra that are likely calcified periurethral glands appear to be of no clinical significance [3].

Bladder Neck

Multiple techniques are described, but the position of the bladder neck may be the most reliably described relative to the inferoposterior margin of the symphysis pubis [4]. Though bladder fullness influences examination findings, volumes have not been standardized. A full bladder may reduce sensitivity in demonstrating the degree of bladder neck mobility, and an empty bladder makes it more difficult to identify the location of the bladder neck [5].

Bladder neck descent (BND) is conventionally determined by measuring the displacement of the bladder neck from rest to maximum Valsalva relative to the inferoposterior symphysis pubis margin (Fig. 9.4). The normal amount of BND has yet to be defined with numerous proposed cutoffs ranging between 15 and 30 mm. It does appear that the greater the BND, the more likely the patient is to have stress urinary incontinence. Many variables confound the measurement of BND, including Valsalva maneuver effort, bladder fullness, parity, and recruitment of levator ani contraction at the time of Valsalva [6]. Alternatively, bladder neck mobility may be measured by retrovesical angle (RVA), defined as the angle formed by the proximal urethra and the bladder trigone. This angle measures urethral rotation around the urethral axis as demonstrated (Fig. 9.5). Normal RVA values, as commonly observed in continent patients, range from 90° to 120° [7]. RVA can be used to radiographically classify cystoceles using the criteria proposed by Green et al., which has been shown to have moderate to good correlation with clinical examination [8].

Abnormal funneling of the bladder neck and proximal urethra may also be observed both at rest and with Valsalva maneuver and with or without significant BND or enlarged RVA. Furthermore, bladder neck funneling is related to urethral hypermobility, greater rotation of the bladder neck, low Valsalva leak point pressures, and low urethral closing pressures [9].

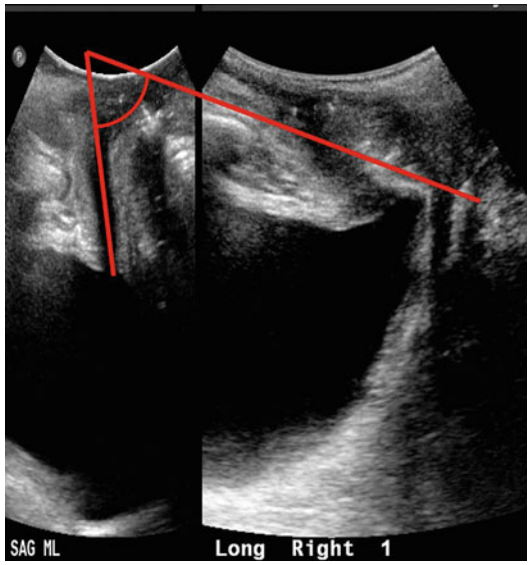

Fig. 9.5 Retrovesical angle measurement describing urethral rotation

Bladder

The bladder is examined for position, wall thickness, intravesical volume, intravesical lesions, and adjacent ureterectasis of the distal ureters. In patients without prolapse, the bladder is positioned above the inferior margin of the symphysis pubis. Cystocele may be understaged if the bladder is examined only when fully distended, particularly in patients with stenosis of the vaginal introitus, as this will prevent the bladder from descending during Valsalva maneuvers. If the bladder is examined while partially or completely distended, the luminal surface of the posterior wall in a partially filled bladder appears hyperechoic due to through transmission of the incident beam. The bladder lumen should be examined for echogenic material such as debris secondary to infection, or urolithiasis. While bladder ultrasound is inadequate for complete oncologic screening, the urothelial surface should be examined for neoplasm. The inter-ureteric ridge is also commonly apparent. The distal ureter may be visualized posterior to the ridge with lateral movement of the transducer. Inspection of the ureter at this level may reveal ureterectasis, possibly indicative of vesicoureteral reflux, ureteric obstruction, or normal physiology. Doppler flow ultrasonography may reveal the presence of a ureteral urine jet. The absence of a ureteral jet does not establish ureteral obstruction; thus the clinical utility of a ureteral jet is debated [10].

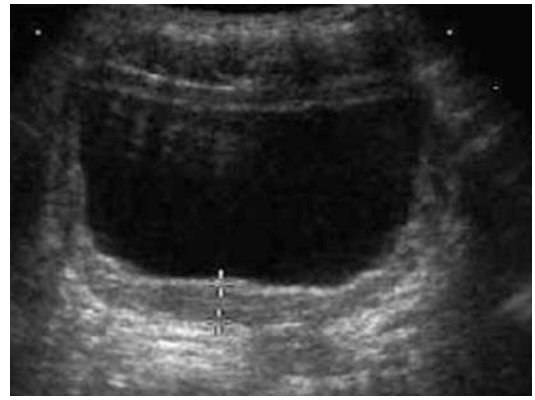

Fig. 9.6 Bladder wall thickness

Much has been made of detrusor wall thickness (DWT). Association between DWT and the presence of urodynamically proven detrusor overactivity, obstruction, stress incontinence, and p_{det}/Q_{max} has been described [11]. Likewise, DWT has been investigated as a predictor of de novo detrusor overactivity following anti-incontinence surgery [12]. In a compliant bladder, DWT lessens with increased bladder filling. No consensus exists regarding bladder volume at which DWT is calculated. DWT is calculated most commonly by measuring the wall thickness at three discreet locations: posterior wall, dome, and anterior wall (Fig. 9.6). Some authors consider normal DWT to be 5 mm or less [13], but this is controversial [14].

3D/4D Assessment of Levator Ani Complex

With the adoption of 3D/4D ultrasound, practitioners now have an alternative to magnetic resonance imaging in the evaluation of the levator ani complex in the axial plane. Advantages of 3D ultrasound in comparison to MRI include low cost, reproducibility, and real-time imaging where imaging planes can be modified for optimal visibility of anatomic structures. One recent multi-institutional

study has found a sensitivity of 0.078 and specificity of 0.86 in detecting levator ani defects detected on MRI; however, because of interobserver disagreement the authors concluded widespread implementation may be limited [15]. The technique is similar to 2D imaging, with orientation set in the midsagittal plane. To obtain volumes, an acquisition angle between 70° and 85° is needed to capture pertinent anatomy (levator hiatus, vagina, paravaginal tissue, urethra, puborectalis muscle, anorectal angle). Higher acquisition angles may be needed in women with significant prolapse, as displacement of lateral structures may occur. Display modes for 3D ultrasound are best depicted in three cross-sectional planes including the axial, coronal, and midsagittal plane (Fig. 9.7) [16]. A thorough assessment of the pelvis can be conducted in real time, assessing for musculofascial defects, measuring downward displacement of pelvic organs, and the assessment of the levator hiatus with Valsalva maneuver. Special attention should be placed to the inferomedial aspect of the puborectalis muscle which can account for delivery-related trauma predisposing women to pelvic organ prolapse. The levator hiatus lies between the two muscle bellies of the puborectalis muscle's attachment to the pubic bone. Within this space the urethra can be found anteriorly, the rectum posteriorly, and the vaginal canal medially. Measurements are taken at the midsagittal plane, measuring the anteroposterior distance, then an axial plane is used to obtain the anteroposterior and transverse diameter. Levator hiatus area measuring >25 cm^2 has been defined as abnormal on Valsalva maneuver [17]. Defects in the levator ani complex can be quantified using tomographic ultrasound imaging (TUI), which displays an axial multislice image. This modality is performed while the patient is performing a pelvic contraction and begins at 5 mm below to 12 mm above the plane of minimal hiatal dimensions [18]. The slices are obtained in 2.5 mm intervals and eight images are produced. A score of zero is used if there are no defects graded with 16 being consistent with bilateral avulsion. Imaging in the 4D mode allows a real-time dynamic investigation of the pelvic floor. Valsalva maneuver can be done

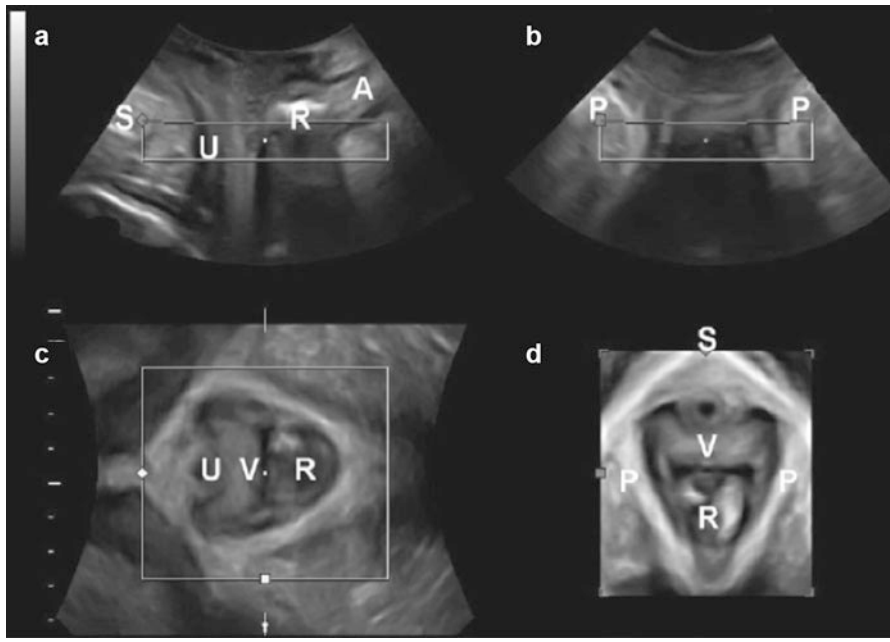

Fig. 9.7 3D pelvic floor ultrasound. (**a**) midsagittal plane; (**b**) coronal plane; (**c**) axial planes; (**d**) rendered axial plane. **A* anal canal, *P* puborectalis muscle, *R* Rectal ampulla, *S* symphysis pubis, *U* urethra, *V* vagina. *Source*: *American Journal of Obstetrics and Gynecology*, *Pelvic floor ultrasound*: *a review*, *Dietz HP*, *April 2010*, *Vol 202*, *Issue 4*, *Fig 2*, *with permission from Elsevier*

in real time to assess defects in the rectovaginal septum and detachment of the puborectalis from the pubis can be appreciated during voluntary levator contraction (as with Kegel exercise). Pelvic floor muscle contractility can be assessed in the midsagittal view and measured by the displacement of the bladder neck and reduction of levator hiatus anteroposterior diameter. Although pelvic floor muscle tone is important for continence, one recent study did not show a strong association with contractility measured on ultrasound or physical exam and urinary continence [19]. However, defects in the pubovisceral musculature delineated by 3D/4D ultrasound are associated with larger levator hiatus dimensions, and severity of pelvic organ prolapse [20]. Despite this clinical relation, one recent study found no association between pubovisceral muscle avulsion in cadavers undergoing translabial ultrasound and pubovisceral muscle avulsion at dissection [21]. Thus, further investigation is necessary to correlate sonographic findings with functional and anatomical pelvic floor disorders.

Common Abnormal Findings

Urethra

As mentioned above urethral hypermobility may be suspected by static ultrasound imaging and confirmed with dynamic ultrasonography with Valsalva maneuvering. Periurethral tissues should be homogenous and without hypoechoic, cystic-appearing lesions. Periurethral lesions may include urethral diverticulum as well as nearby Gartner's duct cysts. Large urethral diverticula are readily imaged with ultrasound. Typically, urethral diverticula arise from the dorsal aspect of the urethra. Less frequently, they arise ventrally from the urethra. Ultrasound is not as sensitive as MRI for small diverticula, but ultrasound can confirm an otherwise palpable suburethral fluctuance suggestive of diverticulum [22, 23].

Gartner's duct cysts and Bartholin's gland lesions may be readily distinguished from urethral diverticula. The former lesions are stationary on Valsalva maneuver while the diverticula are affixed to the urethra and thus commonly mobile on Valsalva. Diverticula of the urethra are commonly septated and contain heterogeneously echogenic material. Bartholin's and Gartner's cysts are typically homogenous in appearance [24]. Urethral ultrasonography may also reveal the presence and extent of periurethral fibrosis. This may be important in patients with urethral stricture desiring reconstruction, or in planning extent of urethrolysis, or anti-incontinence surgery.

Bladder

Bladder ultrasonography may reveal bladder diverticula as well. These may appear as periureteral cystic lesions near the trigone and inter-ureteric ridge or along the posterolateral walls and dome. Ureteroceles may also be visualized, particularly with ureterectasis. Bladder calculi may also be identified as hyperechoic intravesical filling defects with posterior shadowing. Papillary bladder lesions may be identified as intravesical echogenic foci attached to the bladder wall. These lesions are best imaged with a full bladder and may easily be missed without bladder distension. Bladder ultrasound may reveal significant detrusor fibrosis and thinning of the wall, perhaps suggestive of patients at risk for bladder rupture during planned hydrodistension. Ultrasonography may also be valuable in office-based imaging of vesicovaginal fistulae. Particularly in radiation-induced fistula where physical exam is often precluded by patient discomfort and distal vaginal stenosis, office-based ultrasound may prove useful in identifying extent of fibrosis and ischemia. With increasing use of mesh in vaginal reconstruction, hyperechoic mesh is increasingly encountered. With 3D reconstruction, the lattice structure of the mesh is visible. This is more thoroughly explored later in the chapter.

Apical and Posterior Compartments

Basics of Apical and Posterior Prolapse Assessment

Translabial ultrasound can be used for the assessment of apical and posterior wall prolapse [25, 26]. A full sonographic assessment of the apical

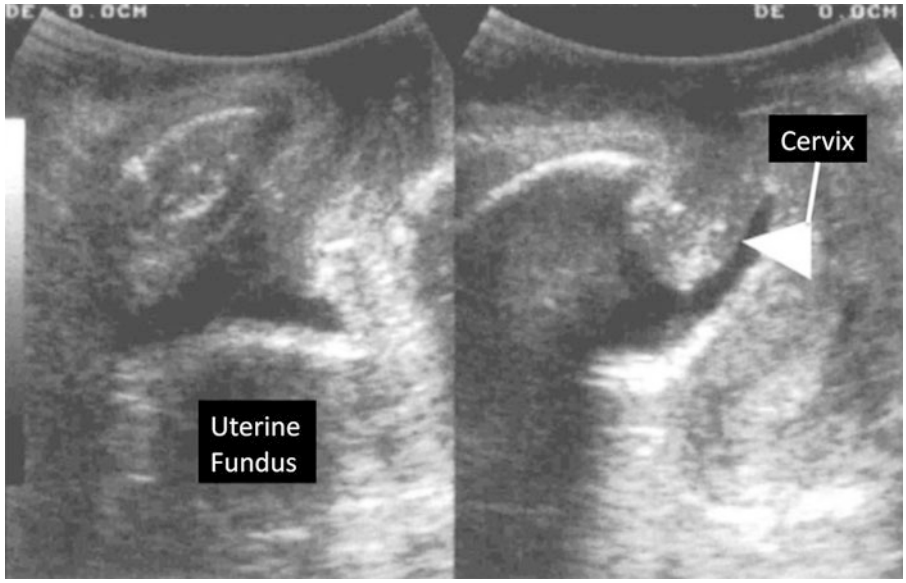

Fig. 9.8 Uterine fundus is easily visualized in image to the *left*. Prolapse of the cervix and uterus is noted with Valsalva maneuver

portion of the vagina includes the uterus. The uterus can be difficult to visualize due to a few factors: it is iso- to hypoechoic making it similar and difficult to discern from vaginal tissues, a retroverted position can be obscured by a rectocele or hidden by rectal contents, and overall it is small in size in postmenopausal women. There are some clues that can be used to localize the uterus. The cervix is typically seen as a specular echo which represents its leading edge. A specular reflector reflects sound waves with minimal scatter usually producing a bright linear echo. The uterus can also be identified by locating nabothian follicles which are oftentimes seen within the cervix. Translabial ultrasound can be readily used to locate the cervix, especially in patients with prolapse (Fig. 9.8). The same can be said for identifying a prolapsed vault posthysterectomy.

Quantification of apical prolapse is performed using the cervix or pouch of Douglas and the posterior wall using the leading edge of the rectocele. We use the inferior margin of the pubic symphysis as a line of reference for measuring the degree of descent. Translabial ultrasound measurement of apical and posterior compartment prolapse has been shown to correlate well with validated prolapse quantification systems, with correlations of $r = 0.77$ for uterine prolapse and $r = 0.53$ for posterior prolapse [27]. Furthermore, in a contemporary series using 3D/4D ultrasound, the authors compared POP-Q coordinate measurements and ultrasound measurements to allow direct comparison of the two modalities. They found a near linear relationship between POP-Q measurements and previously established sonographic cutoffs for significant prolapse, with the strongest correlation for points Ba, C, and Bp. Radiographic cutoffs for significant prolapse symptoms include cystocele ≥ 10 mm below the pubic symphysis and posterior compartment descent ≥ 15 mm below the pubic symphysis [28, 29].

Although correlations between clinical prolapse staging and translabial ultrasound for posterior compartment prolapse are not as strong when compared to anterior or apical compartment prolapse, we are able to use this form of imaging to separate a true or false rectocele. That is to say we can distinguish a rectocele sonographically from other findings such as a rectovaginal septum defect or perineal hypermobility without any actual fascial defects (Fig. 9.9). True rectoceles, which occur as a result of fascial defects, are located consistently very close to the anorectal junction, typically transversely oriented (Fig. 9.10).

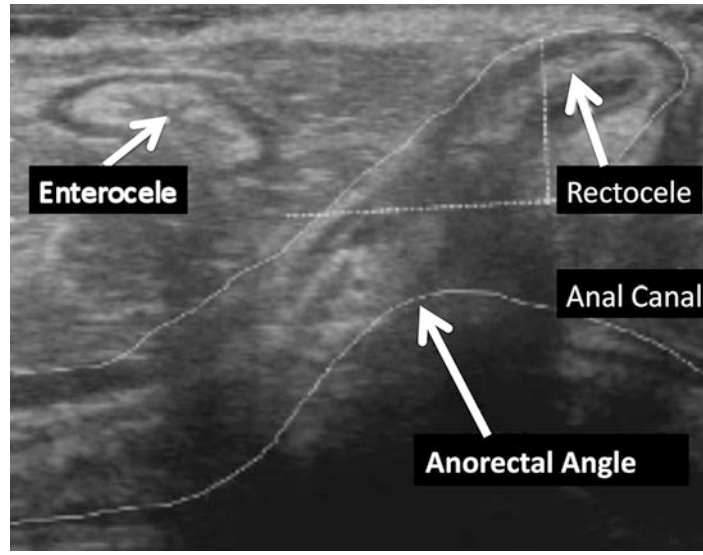

Fig. 9.9 The inferior margin of the pubic symphysis is used as a line of reference. Perineal hypermobility is noted with descent of the rectal ampulla

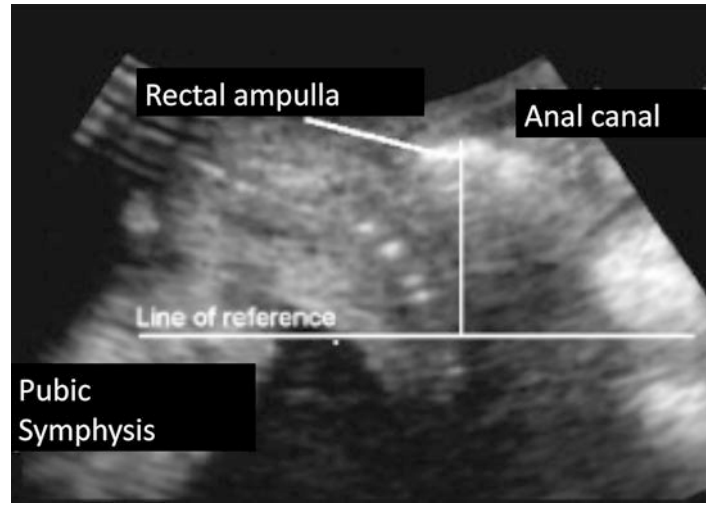

Fig. 9.10 Normal position of the posterior vaginal wall is delineated with the *oblique white line*. A rectocele is noted with prolapse of the true posterior vaginal wall into the vagina

Enterocele

A major strength of translabial ultrasound for apical and posterior compartment assessment of prolapse is the ability to distinguish rectocele from enterocele [30]. An enterocele is readily diagnosed sonographically by visualizing within the herniation small bowel, fluid containing peritoneum, omentum, or sigmoid anterior to the anorectal junction (Figs. 9.11 and 9.12). While MRI is very sensitive for radiographically mapping all vaginal compartment prolapse, it can be cost-prohibitive. Although not expensive, a defecogram can show an enterocele easily, but not before exposing the patient to a significant amount of radiation. Translabial ultrasound can be used easily and inexpensively to diagnose an enterocele with no radiation exposure. From a surgical planning standpoint, ultrasound identification of herniated contents can apprise the surgeon of what to expect during repair of the prolapse.

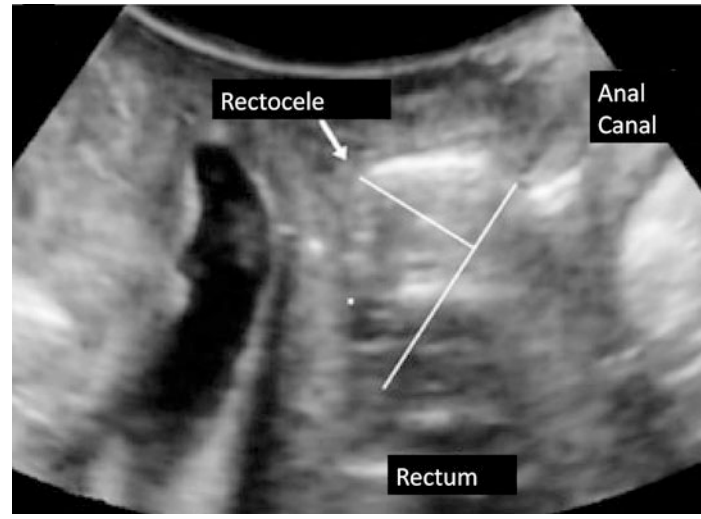

Fig. 9.11 An enterocele is noted in the *left upper* portion of the ultrasound image. In addition, a rectocele is also noted in the *upper-right* portion of the image

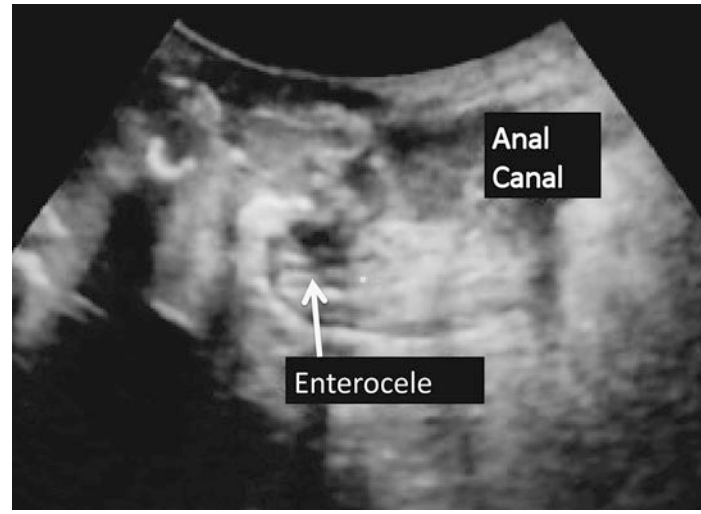

Fig. 9.12 The *white arrow* points to the vault prolapse which contains small bowel (enterocele)

Imaging Implant Materials

Midurethral Slings

One of the unique aspects of sonography of the pelvic floor is the ability to detect synthetic materials, namely mesh, that can be difficult if not impossible to localize with computed tomography, MRI, or X-ray imaging [31]. This has proven very useful in the last decade, as the popularity of midurethral synthetic slings has risen exponentially due to relative ease of procedure and overall high success rates [32]. Sonographic imaging adds to the overall information on postoperative assessment of outcome, specifically by elucidating in vivo biomechanical characteristics. From a clinical standpoint, ultrasonography can shed light on assessment of complications after sling placement, which may include erosion, voiding dysfunction, and recurrence of stress incontinence. In addition, ultrasound can confirm the presence of a sling in patients unsure of previous anti-incontinence procedures performed in the past as well as examination of patients with partially removed mesh.

Both xenografts and allografts are difficult to visualize due to the iso-echoic nature of these

implants. Synthetic slings, on the other hand, are hyperechoic and much more visible on ultrasound (Fig. 9.13). Using translabial ultrasound the entire intrapelvic contents can be visualized, from the pubic rami to anterior to the urethra and back through the contralateral side [33]. With the use of 3D reconstructions, others have achieved success in diagnosing sling erosions into the periurethral fascia in symptomatic patients when cystoscopy was noncontributory [34]. Another advantage of translabial ultrasound for synthetic slings is the ability to characterize orientation of the sling, which includes asymmetry, varying width, tape twisting, and effect of tape division. With the use of rendered volumes of 2D imaging, TVT (transvaginal taping) and TOT (transobturator taping) slings can be easily distinguished from one another. One of the techniques utilized to discern a TVT from TOT is to follow the tape with oblique parasagittal views until the levator ani insertion is reached—TOT slings typically traverse the muscle (Fig. 9.14). Varying echogenicity can be characteristic of some types of slings (e.g.,

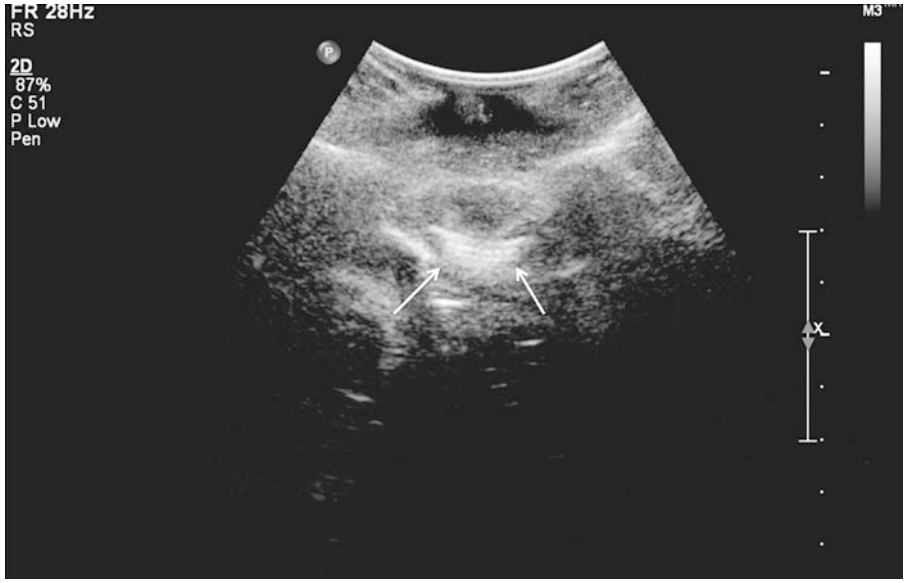

Fig. 9.13 Mesh is delineated by the two *white arrows*. The orientation can be seen hugging the urethra in a hammock fashion

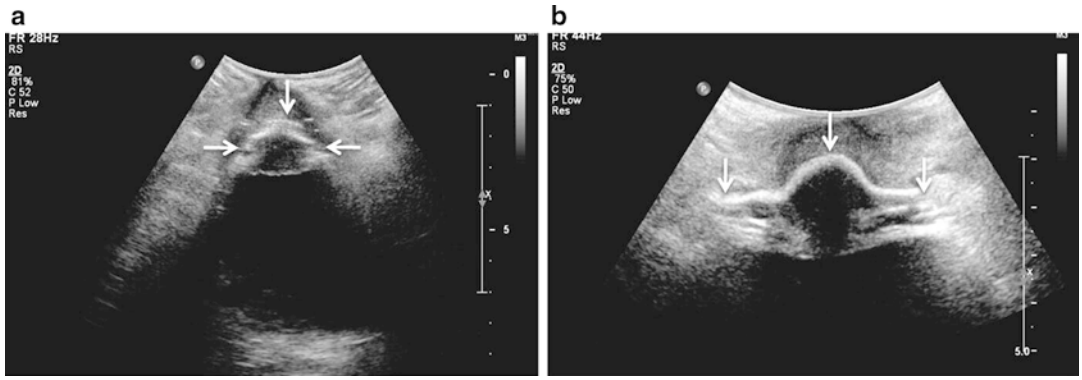

Fig. 9.14 (**a**) This image demonstrates the mesh sling pointed to by three *white arrows*, with a retropubic course which is a TVT sling. (**b**) This image reveals the three *white arrows* pointing to the mesh sling in a horizontal orientation denoting a TOT sling

relatively less echogenic IVS when compared to a TVT™ or Sparc™, when trying to determine sling type when imaging patients). The typical c-shape of all retropubic slings is pretty consistent, seen most clearly during a Valsalva maneuver. The tighter the c-shape, the more tensioned the tape tends to be in patients. With regard to positioning, even though a midurethral location for a sling is thought by most to be the ideal position, some studies have shown that this is not necessarily the case [35], thus translabial ultrasound can assist in surgical planning by identifying the location of the sling [34].

Prolapse Mesh Kits

The majority of the commercial mesh kits currently available are polypropylene, which is highly echogenic and easily seen on ultrasound. Commercial mesh kits utilize mesh arms that traverse the obturator foramen, levator sidewall, and pararectal space by the use of external trocars. Alternatively, trocarless systems have mesh arms that anchor internally to the same fixed structures.

One of the uses of ultrasound in evaluation of prolapse mesh kits is the evaluation of their anatomical success. A study done by Shek at al. used ultrasound to assess the outcomes of using mesh for repair of large and/or recurrent cystoceles [36]. The implant material was able to be imaged in all patients. In 10% of the patients, the authors were able to note cystocele recurrence dorsal to the mesh, with 8% of the patients demonstrating significant descent ventral to the mesh. Interestingly, they were also able to demonstrate dislodgement of the superior anterior arms by showing mesh axis alteration of more than 90° of rotation of the cranial margin in the ventrocaudal direction; this occurred in 10% of their patients. This study is an example of the potential future role of ultrasound in assessing outcomes of prolapse surgery.

Although the use of mesh kits for pelvic organ prolapse delivers excellent anatomical and functional outcomes, their routine use has been limited by concerns over postoperative complications made public by FDA (Food and Drug Administration) warnings [37]. Prior to these warnings there was a surge in complications related to the use of mesh for prolapse surgery [38]. Mesh erosion involving the vaginal wall and other pelvic structures such as the bladder and bowel has been reported [39]. Involvement of pelvic structures such as the bladder and bowel can be easily delineated with the use of ultrasound (Fig. 9.15). Ultrasound certainly plays a

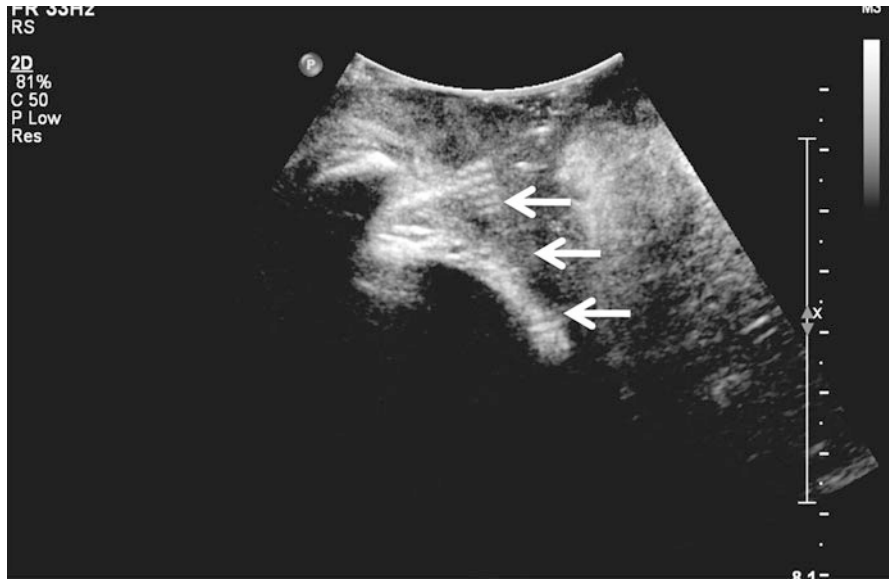

Fig. 9.15 The three *white arrows* map the anterior position of this anterior Prolift™ mesh

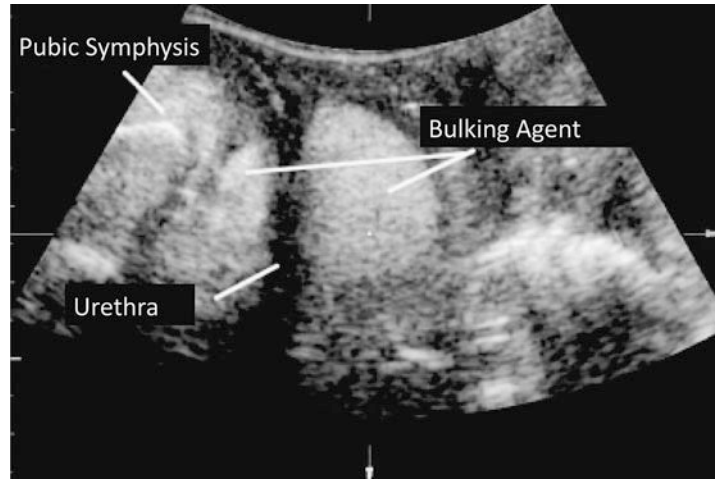

Fig. 9.16 This view reveals a periurethral bulking agent (Macroplastique™), which is echogenic and seen circumferentially around the urethra

role in mapping the location of mesh in order to plan surgical removal of the mesh (Fig. 9.15). Other mesh complications such as dyspareunia and vaginal/pelvic pain have been described [40]. Ultrasound can be used to assess the need for any further resection of mesh if the patient remains symptomatic. As the role of mesh in prolapse surgery becomes better defined, ultrasonography will become increasingly important in assessing outcomes, improving surgical technique, and aiding in the management of complications.

Periurethral Bulking Agents

Most injectables used as periurethral bulking agents for the management of stress incontinence are highly echogenic (Fig. 9.16). A popular injectable, Microplastique™, can be easily seen as a hyperechoic donut shape encircling the urethra. Even though useful in locating injectables, translabial ultrasound has not been shown in any studies to correlate well with treatment success.

References

1. Xie M, Zhang X, Liu J. Evaluation of levator ani with no defect on elastography in women with POP. Int J Clin Exp Med. 2015;8(6):10204–12.
2. Mitterberger M, Pingerra GM, Mueller T, et al. Dynamic transurethral sonography and 3D reconstruction of the rhabdosphincter and urethra. J Ultrasound Med. 2006;25:315–20.
3. Yang JM, Huang WC. The significance of urethral hyperechogenicity in female lower urinary tract symptoms. Ultrasound Obstet Gynecol. 2004;24(1):67–71.
4. Dietz HP, Eldridge A, Grace M, Clarke B. Test-retest reliability of the ultrasound assessment of bladder neck mobility. Int Urogynecol J. 2003;14 Suppl 1:S57–8.
5. Dietz HP, Wilson PD. The influence of bladder volume on the position and mobility of the urethrovesical junction. Int Urogynecol J. 1999;10(1):3–6.
6. Oerno A, Dietz HP. Levator co-activation is an important confounder of pelvic organ descent on Valsalva maneuver. Ultrasound Obstet Gynecol. 2007;30:346–50.
7. Alper T, Cetinkaya M, Okutgen S, Kokcu A, Lu E. Evaluation of the urethrovesical angle by ultrasound in women with and without urinary stress incontinence. Int Urogynecol J. 2001;12(5):308–11.
8. Chantarasorn V, Dietz HP. Diagnosis of cystocele type by clinical examination and pelvic floor ultrasound. Ultrasound Obstet Gynecol. 2012;39:710–4.
9. Huang WC, Yang JM. Bladder neck funneling on ultrasound cystourethrography in primary stress urinary incontinence: a sign associated with urethral hypermobility and intrinsic sphincter deficiency. Urology. 2003;61(5):936–41.
10. Delair SM, Kurzrock EA. Clinical utility of ureteral jets: disparate opinions. J Endourol. 2006;20(2):111–4.
11. Kuhn A, Genoud S, Robinson D, et al. Sonographic transvaginal bladder wall thickness: does the measurement discriminate between urodynamic diagnoses? Neurourol Urodyn. 2011;30(3):325–8.
12. Robinson D, Khullar V, Cardozo L. Can bladder wall thickness predict postoperative detrusor overactivity? Int Urogynecol J Pelvic Floor Dysfunct. 2005;16:S106.
13. Lekskulchai O, Dietz HP. Normal values for detrusor wall thickness in young Caucasian women. In: International continence society annual scientific meeting (abstract), Montreal; 2005.

14. Blatt AH, Titus J, Chan L. Ultrasound measurement of bladder wall thickness in the assessment of voiding dysfunction. J Urol. 2003;169(4):1395–7.
15. Notten KJB, Kluivers KB, Futterer JJ, et al. Translabial three-dimensional ultrasonography compared with magnetic resonance imaging in detecting levator ani defects. Obstet Gynecol. 2014;124(6):1190–7.
16. Dietz HP. Pelvic floor ultrasound: a review. Am J Obstet Gynecol. 2010;202(4):321–4.
17. Dietz HP, Shek K, Clarke B. Biometry of the pubovisceral muscle and levator hiatus by three-dimensional pelvic floor ultrasound. Ultrasound Obstet Gynecol. 2005;25:580–5.
18. Adisuroso T, Shek KL, Dietz HP. Tomographic ultrasound imaging of the pelvic floor in nulliparous pregnant women: limits of normality. Ultrasound Obstet Gynecol. 2012;39:698–703.
19. Oversand S, Kamisan AI, Shek KL, et al. The association of urinary and anal incontinence with measures of pelvic floor contractility. Ultrasound Obstet Gynecol. 2015;47(5):642–5. doi:10.1002/uog.14902.
20. Memona M, Braekken IH, Bo K, et al. Levator hiatus dimensions and pelvic floor function in women with and without major defects of the pubovisceral muscle. Int Urogynecol J. 2012;23:707–14.
21. Da Silva AS, Digesu GA, Dell'Utri C, et al. Do ultrasound findings of levator ani "avulsion" correlate with anatomical findings: a multicenter cadaveric study. Neurourol Urodyn. 2015;35(6):683–8. doi:10.1002/nau.22781.
22. Gerrard ER, Lloyd LK, Kubricht WS, et al. Transvaginal ultrasound for the diagnosis of urethral diverticulum. J Urol. 2003;169(4):1395–7.
23. Ockrim JL, Allen DJ, Shah PJ, et al. A tertiary experience of urethral diverticulectomy: diagnosis, imaging, and surgical outcomes. BJU Int. 2009;103(11):1550–4.
24. Tunn R, Petri E. Introital and transvaginal ultrasound as the main tool in assessment of urogenital and pelvic floor dysfunction: an imaging panel and practical approach. Ultrasound Obstet Gynecol. 2003;22(2):205–13.
25. Creigton SM, Pearce JM, Stanton SL. Perineal video-utrasonography in the assessment of vaginal prolapse: early observations. Br J Obstet Gynaecol. 1992;99(4):310–3.
26. Dietz HP, Haylen BT, Broome J. Ultrasound in the quantification of female pelvic organ prolapse. Ultrasound Obstet Gynecol. 2001;18(5):511–4.
27. Bump RC, Mattiason A, Bo K, et al. The standardization of terminology of female pelvic organ prolapse and pelvic floor dysfunction. Am J Obstet Gynecol. 1996;175(1):10–7.
28. Dietz HP. What's "normal" pelvic organ descent, and what's prolapse? In: ICS Annual Scientific Meeting 2006, Christchurch; 2006.
29. Dietz HP, Kamisan Atan I, Salita A. The association between ICS POPQ coordinates and translabial ultrasound findings: implications for the definition of 'normal pelvic organ support'. Ultrasound Obstet Gynecol. 2015;47(3):363–8. doi:10.1002/uog.14872.
30. Dietz HP, Steensma AB. Posterior compartment prolapse on two-dimensional and three-dimensional pelvic floor ultrasound: the distinction between true rectocele, perineal hypermobility and enterocele. Ultrasound Obstet Gynecol. 2005;26:73–7.
31. Halsaka M, Otcenasek M, Martam A, et al. Pelvic anatomy changes after TVT procedure assessed by MRI. Int Urogynecol J. 1999;10(S1):S87–8.
32. Kaum HJ, Wolff F. TVT: on midurethral tape positioning and its influence on continence. Int Urogynecol J. 2002;13(2):110–5.
33. Dietz HP, Wilson PD. The "iris effect": how two-dimensional and three-dimensional ultrasound can help us understand anti-incontinence procedures. Ultrasound Obstet Gynecol. 2004;23(3):267–71.
34. Staack A, Vitale J, Ragavendra N, et al. Translabial ultrasonography for evaluation of synthetic mesh in the vagina. Urology. 2014;83(1):68–74.
35. Ng CC, Lee LC, Han WH. Use of three-dimensional ultrasound to assess the clinical importance of midurethral placement of the tension-free vaginal tape (TVT) for the treatment of incontinence. Int Urogynecol J. 2005;16(3):220–5.
36. Shek K, Dietz HP, Rane A. Transobturator mesh mesh anchoring for the repair of large or recurrent cystocele. In: ICS Annual Scientific Meeting 2006, Christchurch; 2006.
37. Altman D, Vayrynen T, Engh ME, et al. Anterior colporrhaphy versus transvaginal mesh for pelvic-organ prolapse. N Engl J Med. 2011;364:1826.
38. Achtari OA, O'Reilly B, Schierlitz L, et al. Mesh erosion following vaginal repair: is I avoidable? Int Urogynecol J. 2003;14(S1):S65.
39. Firoozi F, Goldman HB. Transvaginal excision of mesh erosion involving the bladder after mesh placement using a prolapse kit: a novel technique. Urology. 2010;75(1):203–6.
40. Ridgeway B, Walters M, Paraisa MF, et al. Early experience with mesh excision for adverse outcomes after transvaginal mesh placement using prolapse kits. Am J Obstet Gynecol. 2008;199:703–7.

Transrectal Ultrasound

10

Edouard J. Trabulsi, Xialong S. Liu,
Whitney R. Smith, and Akhil K. Das

Definition and Scope

Transrectal ultrasound (TRUS), first described by Watanabe and colleagues in the 1960s, is an essential tool for the diagnosis of prostate cancer as well as for image-guided prostate interventions [1]. By the 1970s, TRUS imaging had achieved wide use in clinical practice. Most commonly, TRUS is used to guide core needle biopsy for prostate cancer diagnosis. This was first described by Hodge in 1989 when he advocated the systematic biopsy of the prostate gland [2]. Further treatment modalities including brachytherapy, cryotherapy, and high intensity focus ultrasound (HIFU) also rely on TRUS to appropriately treat prostate cancer patients [3]. In addition, TRUS provides valuable information for follow-up and treatment of benign prostatic hyperplasia (BPH) and may be helpful in the evaluation of patients with idiopathic infertility [4–8]. The anatomy of the prostate, indications and techniques for TRUS, proper documentation, and new ultrasonographic technologies will be discussed in this chapter. The topic of TRUS with prostate biopsy is covered under a separate chapter in this book.

Anatomy of the Prostate

The prostate gland lies beneath the pubis between the bladder neck and the urogenital diaphragm just anterior to the rectum in an ideal position to be imaged via TRUS. Traditionally, the prostate gland is described using pathological zonal architecture [9]. These divisions consist of the anterior fibromuscular stroma (AFS), which is devoid of glandular tissue, transition zone (TZ), central zone (CZ), and peripheral zone (PZ). Typically, the prostate on TRUS is divided into the inner gland, consisting of the AFS, TZ, periurethral tissue, and CZ, and the outer gland that is the PZ. The TZ comprises 5–10 % of normal prostate volume where approximately 20 % of prostate cancers originate. The CZ surrounds the ejaculatory ducts and accounts for a minority of cancers. Finally, the PZ makes up 75 % of the prostate volume and is the source of the great majority of prostate carcinoma. Unfortunately, these zonal regions are difficult to distinguish using sonographic imaging.

E.J. Trabulsi, M.D. (✉) • W.R. Smith, M.D.
A.K. Das, M.D.
Department of Urology, Sidney Kimmel Medical College at Thomas Jefferson University,
1015 Walnut Street, Suite 1102, Philadelphia,
PA 19107, USA
E-mail: Edouard.trabulsi@jefferson.edu;
whitney.smith@jefferson.edu;
Akhil.Das@jefferson.edu

X.S. Liu, M.D.
Department of Urology, Tufts Medical Center,
800 Washington St. Box #389, Boston,
MA 02111, USA
E-mail: xliu4@tuftsmedicalcenter.org

P.F. Fulgham, B.R. Gilbert (eds.), *Practical Urological Ultrasound*, Current Clinical Urology,
DOI 10.1007/978-3-319-43868-9_10

The prostatic inner gland has a more heterogeneous appearance whereas the outer gland has a more homogenous appearance. Frequently, hyaline concretions known as *corpora amylacea* [10] highlight the plane between the outer gland and the inner gland [11]. These are noted to be small multiple diffuse hyaline concretions which appear hyperechoic on TRUS (Fig. 10.1b). They are normal and often an incidental ultrasonographic finding of the prostate. Generally, these represent a common, normal ultrasound finding rather than a pathological entity [12]. Larger prostatic calculi may be associated with symptoms and can be related to underlying inflammation. These larger calculi may require further evaluation and treatment.

The prostatic urethra traverses the length of the gland in the midline and thus must be imaged in the sagittal plane to be viewed in its entirety along its course. Generally, the distended urethral lumen is hypoechoic in appearance, where as periurethral calcifications may produce a thin echogenic outline. Smooth muscle of the internal sphincter extends from the bladder neck encircling the urethra to the level of the verumontanum. These muscle fibers may be visualized sonographically as a hypoechoic ring around the upper prostatic urethra providing a funnel-like appearance proximally. The urethra angles anteriorly and runs the remainder of the gland to the exit at the apex of the prostate. This angle gives the prostatic urethra an anterior concave appearance when viewed along the entire course of the sagittal plane.

The seminal vesicles (SV) are positioned posteriorly to the base of the prostate. They have a smooth saccular appearance that should be symmetrical. The normal SV measures approximately 4.5–5.5 cm in length and 2.2 cm in width. Solid lesions in the SV can be concerning for malignancy, where cystic masses of the SV are generally benign [13, 14]. Solid lesions are even more worrisome if there is a history of primary neoplasm elsewhere. Infectious etiologies such as schistosomiasis should be considered in patients with solid SV masses who have lived in areas of endemic infestation [15]. The vas deferentia can be visualized in a transverse plane just above the ipsilateral SV before diving caudally towards the prostate near the midline. Each vas lies just medial to the tapering ipsilateral SV before the two structures fuse to form the ejaculatory duct. The ejaculatory ducts enter the gland posteriorly and empty into the urethra at the level of verumontanum. These ducts are occasionally seen as hypoechoic structures on TRUS. Their course parallels the prostatic urethra proximal to the verumontanum.

Indications

The list of potential indications for TRUS evaluation is lengthy, but fall into the following general categories: prostate cancer diagnosis and treatment, BPH management and work-up, infertility evaluation, and non-oncologic interventions such as prostatic abscess drainage or aspiration of prostatic or ejaculatory ducts cysts.

The evaluation of a patient with an elevated serum prostate-specific antigen (PSA) commonly includes a TRUS evaluation with ultrasound-guided prostate biopsy (see Chap. 11). To be facile with TRUS evaluation of the prostate the urologist must have expertise in recognizing normal and abnormal anatomy. Hypoechoic areas of the prostate should be recognized and specifically targeted for biopsy as the likelihood that these areas harbor cancer is higher [16] Absence of hypoechoic lesions does not preclude biopsy, and the clinical significance of hypoechoic areas of the prostate has been questioned in the modern era; a large study of nearly 4000 patients from Wayne State University demonstrated that the prostate cancer detection rate of targeted biopsies of hypoechoic lesions was the same as biopsies from isoechoic regions [17]. Other TRUS findings which may suggest prostate cancer include lobar asymmetry, capsular bulging, deflection of the junction between the TZ and PZ, and any area of increased vascularity (Fig. 10.1a, b). A systematic evaluation of the entire prostate and seminal vesicles should be performed together with three-dimensional volume measurement prior to performing any prostate biopsy.

TRUS is used to define the anatomy and calculate the volume of the prostate in symptomatic BPH prior to surgical therapy or minimally invasive therapy (MIT) for BPH [18, 19]. The size or

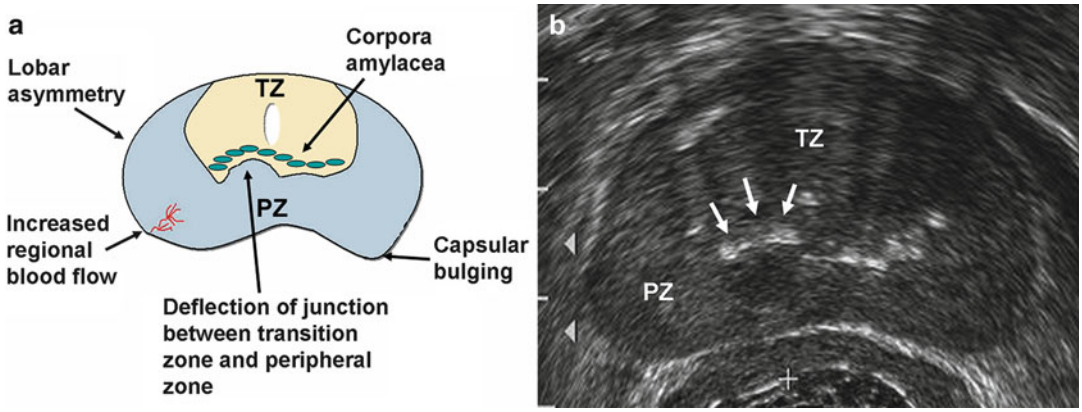

Fig. 10.1 TRUS findings suspicious for prostate cancer. (**a**) Lobar asymmetry, capsular bulging, increased blood flow, and deflection of the junction between the TZ and PZ can all be indicators for prostate cancer on TRUS. (**b**) Transverse image of the prostate demonstrating upward deflection of the junction between the TZ and PZ. The *corpora amylacea* (*arrows*) indicate this junction and also demarcate the border between the inner and outer gland

anatomy of the prostate can recommend or exclude certain MIT procedures for patients. Specific volume limits are used to stratify patients for transurethral resection of the prostate (TURP), MITs such as transurethral microwave therapy (TUMT) or transurethral radiofrequency needle ablation (TUNA) or open simple prostatectomy. In addition to prostate volume measurements, the presence or absence of a large intravesical median lobe of the prostate visualized on TRUS may also help guide the optimal technique for surgical treatment of BPH.

Minimally invasive prostate cancer treatment options are dependent on TRUS technology to accurately monitor and guide treatment planning and delivery [20]. TRUS provides the clinician the anatomy and specifically an accurate volume assessment of the prostate prior to any procedure. Certain patients may be excluded from some treatment options for prostate cancer or may require hormonal downsizing prior to treatment based on TRUS findings. For cryotherapy, real-time TRUS is vital to accurately place probes and monitor the freezing area during the procedure [21]. Similarly, in brachytherapy, real-time TRUS is used to volume the prostate and construct the plan for seed implantation. Continuous real-time TRUS is also used during high intensity focused ultrasound (HIFU) treatment of the prostate [22, 23]. As part of image-guided radiotherapy for prostate cancer, TRUS is used to accurately place prostate markers such as fiducial gold seeds within the prostate for daily monitoring of prostate position and accurate imaged-guided treatment planning, as shown in Fig. 10.2 [24, 25].

In patients with azoospermia or ejaculatory dysfunction, TRUS may also help diagnose cysts of the SV or ejaculatory ducts as well as obstruction of the vas deferentia. Accurate diagnosis of these rare conditions can change the management strategy of infertility patients [6–8]. Another rare but useful application of TRUS is for the treatment of prostatic abscesses which can be associated with prostatitis or epididymitis [26, 27]. These abscesses can then be surgically unroofed during transurethral or transrectal procedures.

Techniques

A complete TRUS evaluation of the prostate includes scanning in both the sagittal and transverse planes to obtain a volume calculation. The CZ and the PZs are evaluated for hypoechoic lesions and contour abnormalities. The SVs and the vas deferentia are also visualized during the ultrasound procedure. Any abnormalities or ectasia are measured and documented. Additionally,

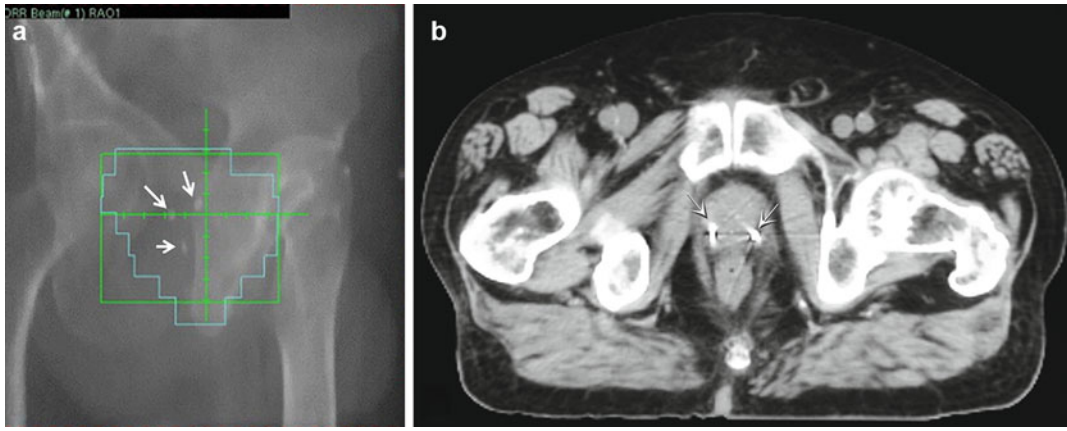

Fig. 10.2 Port film after fiducial marker placement for prostate cancer. Three markers are visible on plain film within the prostate and are used for daily position adjustments during radiotherapy treatment

the rectal wall is examined for abnormal thickening or focal lesions as occasional rectal tumors can be encountered on TRUS.

Prior to the transrectal ultrasound procedure, patients are typically asked to do a cleansing enema at home before the procedure. The enema helps decrease the amount of stool in the rectum, thereby producing a superior acoustic window for prostate imaging. Although an enema is not absolutely mandatory, it is helpful in obtaining optimal images during TRUS. In patients undergoing real-time imaging for cryotherapy, brachytherapy or HIFU, preoperative or intra-operative enema is integral for adequate real-time imaging and image guidance during the procedure. If any invasive procedure is planned, antiplatelet and anti-coagulation medications such as ASA, NSAIDs, clopidogrel, warfarin, vitamin E, and fish oil should be stopped at least 1 week prior to the procedure reducing bleeding risk associated with the procedure. Oral antibiotics should also be given to reduce the risk of bacterial septicemia. This should be given prior to the procedure as well as continued post-procedurally.

Patients are positioned either in the left lateral decubitus or the lithotomy position. Most clinicians would prefer the left lateral decubitus position, especially for a straightforward TRUS. In this position, an arm board is usually placed parallel to the table and a pillow is placed between the knees to help maintain the position. The buttocks should be flushed with the end of the table to allow manipulation of the probe. Next, a digital rectal exam should be performed prior to insertion of the TRUS probe. Any palpable contour abnormalities should be documented including descriptive identifiers and their location on the gland. The lithotomy position is used with patients who are undergoing brachytherapy, cryotherapy for external beam radiation. In addition, the lithotomy position is used for patients in whom color flow and power Doppler imaging of the prostate is planned [28]. Because the vascularity pattern of the prostate is dependent on patient positioning and gravity, the lithotomy position is preferred to help accurately identify areas of hyperemia for targeted biopsies of the prostate.

Gray-scale TRUS has been the most common imaging modality of the prostate. Although Doppler imaging with color flow, power Doppler, and harmonic imaging have been advocated in the diagnosis of prostate cancer, their exact role for other treatment modalities such as cryotherapy or brachytherapy is still under investigation. These techniques will be further discussed in a separate section of this chapter.

There are two different types of probes available for TRUS, with either side or end firing models, based on surgeon preference and experience. Either type of probe transmits mid-level frequencies between 6 and 10 megahertz (MHz). Models with new biplane probe technology provide a

simultaneous image of both sagittal and transverse images during the transmission period. By increasing the frequency used, the spatial resolution is improved. As the frequency of the probe is increased, however, the depth of tissue penetration declines, and the portion of the image that has adequate returning echo amplitude is closer to the transducer [29]. Increased resolution may be helpful in patients who have peripheral zone cancers which may be identified as a hypoechoic nodule with TRUS, but the anterior portions of the prostate furthest from the probe may suffer from poorer resolution, especially for marked BPH. Lower frequency transducers, such as the 4 MHz transducers, have a greater depth of penetration (between 2 and 8 cm) but with much lower resolution. Lower frequency transducers improve the anterior delineation of larger glands with deeper tissue penetration, thus increasing the accuracy of volume measurements but provide poorer resolution.

A coupling medium, which is usually sonographic jelly or a lubricant, is usually placed between the probe and the rectal surface. This is essential since ultrasound waves propagate inefficiently through air and are completely reflected when they strike tissues of a significant impedance difference. Most probes are also covered with a protective condom. A coupling medium is placed between the probe and the condom as well as the condom and rectal mucosa.

Any TRUS scanning protocol must involve the prostate and should be performed in both the transverse and the sagittal planes. By advancing the probe in a cephalad direction in the rectum, images of the prostate base, seminal vesicles and the bladder neck are obtained. By pulling the probe caudally towards the anal sphincter, the prostatic apex and proximal urethra are visualized. Transverse imaging with end fire, side fire, and some biplane probes is accomplished by angling the handle of the probe, right or left using the anal sphincter as a fulcrum. Angling the probe towards the scrotum produces more cephalad images while angling the probe towards the sacrum produces more caudal images. There are also two approaches to probe manipulation for sagittal imaging. One method is rotation of the probe either clockwise or counterclockwise. Clockwise rotation visualizes the left side of the prostate and counterclockwise rotation yields images of the right side. Alternatively, sagittal images can also be viewed by angling the probe up or down the anal sphincter which functions as a fulcrum. If the patient is placed in the left lateral decubitus position, angling the probe up or towards the ceiling images the left side of the prostate while angling the handle of the probe down or towards the floor images the right side. Prostate volume is usually calculated after complete scanning of the prostate is accomplished. Volume calculation requires measurement in three dimensions. The transverse and anterior posterior (A-P) dimensions are measured at the point of the widest diameter in the axial plane. The longitudinal dimension is measured in the sagittal plane just off the midline as sometimes the bladder neck may obscure the cephalad extent of the gland. Most formulas to assess prostate volumes assume an ideal geometric shape of the gland. These shapes can include an ellipse ($\pi/6 \times$transverse diameter$\times$A-P diameter$\times$longitudinal diameter), a sphere ($\pi/6 \times$the transverse diameter^3), or an egg-shaped spheroid ($\pi/6 \times$transverse diameter$^2 \times$the A-P diameter). Despite the inherent inaccuracies that arise from these geometric hypotheses, these formulas reliably estimate the gland volume and weight with correlation coefficients greater than 0.90 when compared to prostatectomy specimen weights (based on the assumption that 1 cm^3 equals 1 g of prostate tissue) [30]. By calculating the prostate volume, one can then derive the PSA density (PSAD) which is the ratio of serum PSA to prostate volume. The PSAD can help improve prostate cancer detection specificity and has been shown to be higher in patients diagnosed with cancer on initial and repeat prostate biopsies [31].

In patients undergoing brachytherapy, more accurate gland volume may be required. This is accomplished by a technique called planimetry. With the patient in the lithotomy position, the probe is mounted to a stepping device and transverse images are obtained at set intervals. This is done throughout the length of the gland. The surface area of each serial image is determined and the sum of these measurements is multiplied by the total gland length to obtain the prostate volume.

TRUS imaging of the prostate alone is a relatively benign procedure. Other than patient discomfort due to the physical presence of an ultrasound probe in the rectum, there is little patient risk in receiving a stand-alone TRUS. However, complications can result after TRUS coupled with penetration of the rectal wall (e.g., fiducial marker placement). These include hematuria, hematospermia, rectal bleeding, and urinary retention. Hematuria after needle biopsy occurs in roughly 47 % of patients and typically resolves after 5–7 days [32]. Hematospermia can be observed in up to 36 % of biopsies and small traces of blood may even persist up to several months [33]. Rectal bleeding is usually mild and controllable with digital or TRUS probe pressure. Bleeding requiring transfusion, bacteremia requiring IV antibiotics, and other more major complications are uncommon, but antibiotic resistant organisms are becoming more common and troublesome, raising questions about the appropriate antibiotic prophylactic coverage for these procedures [34]. Fortunately, most complications are generally minor and usually self-limiting.

Documentation

A standard protocol or a standard template should be used in documenting a transrectal ultrasound procedure. The template should state the indication, PSA, if appropriate, and the findings on digital rectal exam. The technique should be described and the position of the patient should be documented. The machine and the probes used in the procedure should be described. The anatomy and the calculated volume of the prostate should be annotated. Any abnormal findings should be noted. A sample TRUS documentation sheet is shown in Fig. 10.3a, a sample prostate biopsy documentation template is shown in Fig. 10.3b.

Multiparametric Ultrasound and Emerging Technologies

Despite the most meticulous and systematic approach to TRUS, the sensitivity of prostate biopsy remains disappointingly low, with false negative rates of 25 % or higher in multiple studies [35, 36]. In an attempt to make the biopsy procedure less random and more targeted, enhanced ultrasonographic techniques have been utilized to better identify areas of the prostate more suspicious for cancer to allow targeted biopsies. Similar to multiparametric MRI, multiparametric ultrasound has emerged. Various ultrasound modalities include: color Doppler ultrasound, dynamic contrast-enhanced ultrasound, power Doppler ultrasound, computerized transrectal ultrasound, and elastography [37]. Neoplastic prostate tissue is histologically distinct from normal prostate tissue, differentiated by a loss of glandular architecture, increased cellular density and increased microvascularity [38]. The loss of glandular architecture reduces the content of reflective interfaces causing a hypoechoic appearance on TRUS [38]. Increased cellular density may change the normal elasticity of prostate tissue which may be measurable by real-time elastography [39]. These characteristics can be used as potential targets in advanced ultrasound imaging.

Color and power Doppler have both been used to enhance TRUS biopsy detection of prostate cancer [40, 41]. Color Doppler measures the frequency shift in ultrasound waves as a function of the velocity and direction of vascular flow. Increased blood flow as a result of increased microvascularity to cancerous tissue forms the theory behind use of color and power Doppler sonography [38]. Amplified flow patterns to areas of tumor, which harbor increased number and size of blood vessels, is the hallmark of prostate cancer detection using color Doppler imaging (Fig. 10.4a–c). Targeted biopsies of the prostate can then be performed where there is enhanced flow. Power Doppler reflects the integrated amplitude or power of the Doppler signal. This technique is more sensitive to low velocity flow than color Doppler (Fig. 10.4c) can detect vessels as small as 1 mm allowing for visualization of prostate tumor feeding vessels. Several studies have shown an increased sensitivity of power Doppler to detect cancer [42, 43]. Unfortunately, when looking at the overall picture, the use of color and power Doppler has yielded mixed results. Sensitivity for tumor detection lies anywhere from 13 to 49 % in recent studies and ultrasound

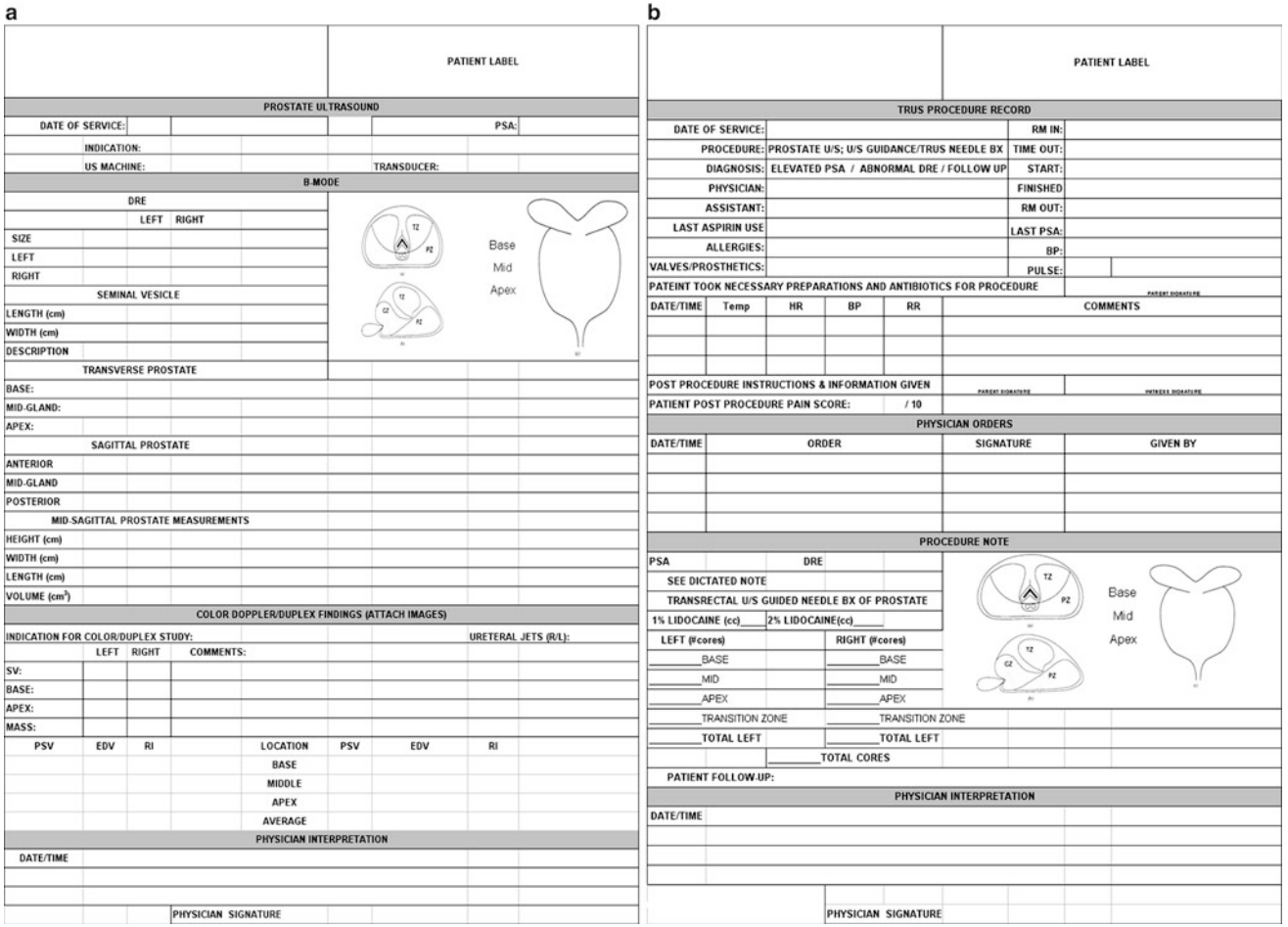

Fig. 10.3 Sample TRUS documentation sheets are shown. (**a**) Patient unique identifiers need to be appropriately labeled. Date of exam, indication for procedure, pre-evaluation PSA, and specific TRUS machine/probe models should also be documented. A DRE should be performed and any findings acknowledged. All features of the TRUS findings should be completely documented. These include (1) all lengths necessary for volume measurements, (2) the volume of the gland, (3) any areas suspicious for neoplasm, and (4) any other interesting or concerning findings. The presence or absence of urethral jets can also be commented on if visualization of the bladder is desired. Color or power Doppler findings can also be noted. *PZ* peripheral zone, *CZ* central zone, *TZ* transition zone, *SV* seminal vesicle, *PSV* peak systolic velocity, *EDV* end diastolic velocity, *RI* resistive index. (**b**) Documentation for prostate biopsy with TRUS. Akin to standard operative documents, all necessary components such as physician/assistant names, time in/out, allergies, and pre-procedural antibiotics should be written. The number of biopsies at each prostate site should be documented and correlated to eventual pathology reports

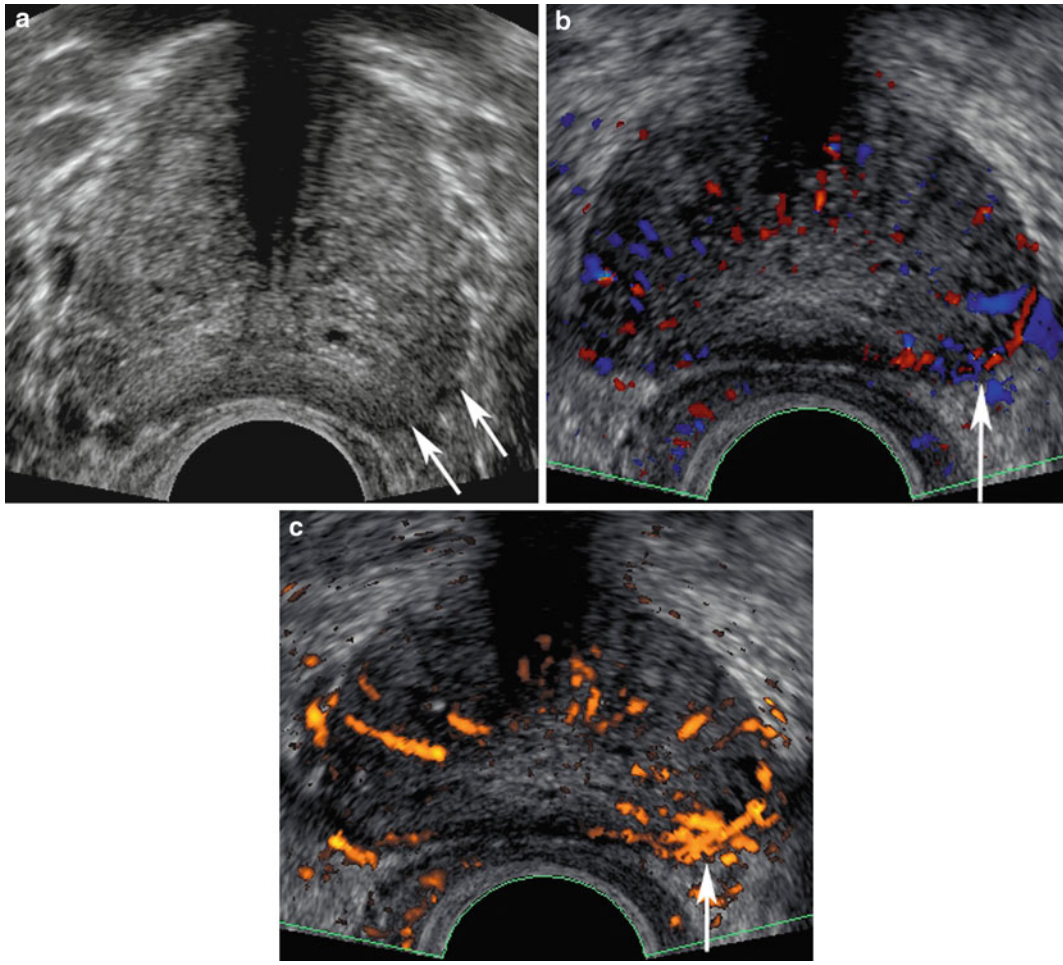

Fig. 10.4 Gleason 3+3=6 prostate adenocarcinoma. Several transverse images through the midgland of the prostate. (**a**) Conventional gray-scale imaging demonstrates a slightly hypoechoic lesion along the left midgland *(arrow)*. (**b**) Color Doppler demonstrates increased vascular flow to this area, corresponding to area of probable cancer. (**c**) Power Doppler shows increased flow to the same left midgland area, confirming hypervascularity

abnormalities has been shown in many patients with subsequently demonstrated benign pathology [40, 41, 44, 45]. These findings may be due to the presence of benign conditions, such as prostatitis, that result in increased blood flow to the prostate thereby clouding the picture for targeted cancer biopsies using this technique. In a study by Eisenberg et al., pathology from radical prostatectomy specimens from men between 2002 and 2007 were compared to preoperative TRUS and power Doppler ultrasound findings. When a hypoechoic lesion visualized on TRUS was combined with the finding of a hypervascular lesion on Power Doppler imaging, the specificity improved from 47 to 74 % [46]. However, the sensitivity decreased from 59 to 47 % [46]. Several studies have attempted to use power Doppler ultrasound in predicting tumor stage and grading, but, so far, results have been inconsistent [46].

Microbubble contrast agents for use in contrast-enhanced TRUS were first developed in the 1980s [45]. They are composed of tiny bubbles of injectable gas contained within a supporting shell such as a lipid or a surfactant microsphere. Contrast microbubbles are on the order of 1–10 μm in size and thus able to penetrate even the smallest microvessels. These contrast agents support microbubbles of gas which irregularly reflect the

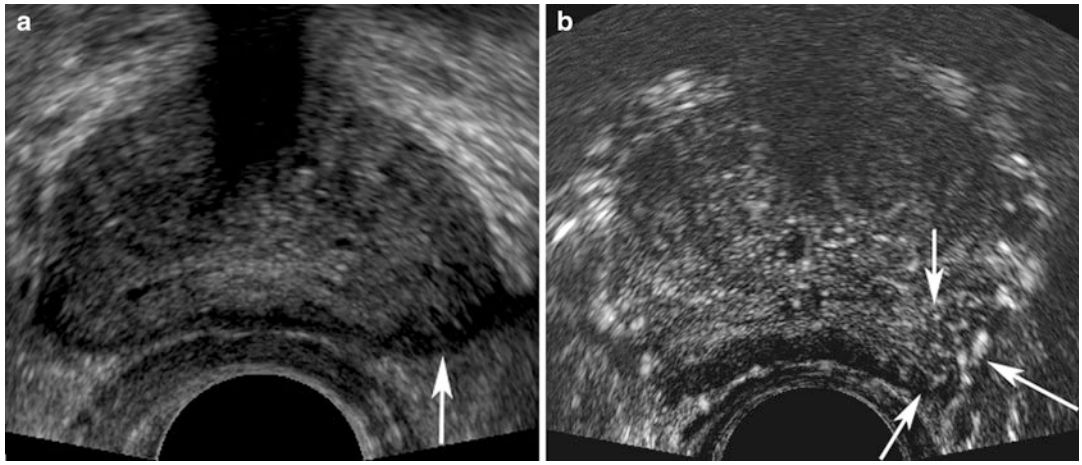

Fig. 10.5 Transverse image through the midgland of the prostate. (**a**) Gray-scale imaging demonstrates a hypoechoic contour bulge of the left midgland suspicious for prostate cancer (*arrows*). (**b**) After microbubble contrast injection, gray-scale imaging reveals a slightly larger area of parenchymal enhancement with visualization of hypervascularity (*arrows*). After biopsy, this area revealed (Gleason 4 + 4 = 8) prostate adenocarcinoma

ultrasound signal and are thereby able to show the increased microvascularity and vascular density correlated to prostate cancer (Fig. 10.5a, b) [47]. *Dynamic contrast-enhanced ultrasound* utilizes a suspension of gas-filled microbubbles as an ultrasound contrast agent that can be used to visualize microvascular flow patterns [48]. Findings on dynamic contrast-enhanced ultrasound associated with malignancy include asymmetrical rapid inflow, increased focal enhancement, and asymmetry of intraprostatic vessels [37]. Dynamic contrast-enhanced ultrasonography of the prostate alone is very operator dependent. However, techniques are emerging that can distinguish benign from malignant tissue to display this data in the form of a parametric map [48]. A study by Postema et al. showed that when dynamic contrast-enhanced ultrasound is combined with parametric maps, the sensitivity, specificity, positive predictive value, and negative predictive value were 91, 56, 57, and 90 % [48].

Advanced imaging strategies can be applied to contrast-enhanced ultrasound including: color and power Doppler, flash replenishment techniques, and maximum intensity projection to guide prostate imaging and improve detection of cancer with directed biopsies. Studies comparing systematic biopsy versus contrast-enhanced color-flow Doppler sonography using microspheres to target areas of increased neovascularity for directed biopsies was twice as likely to yield positive results and higher Gleason grades [49–51] when compared to systematic biopsies. Flash replenishment technology takes advantage of the ability of ultrasound waves to periodically "destroy" the microbubbles and provide a clean viewing field on the monitor. Low energy pulses show blood vessels refilling with contrast permitting optimal visualization of vascular flow to cancerous cells. Increased positive core rates for targeted biopsies over systematic biopsy have been reported in the literature utilizing this flash replenishment technique [52].

Computerized transrectal ultrasound was initially described in 2004 by Loch [53]. This technology now exists as a stand-alone "network-compatible" module where the user is able to securely transmit TRUS images to an Artificial Neural Network (ANNA) analysis center using their own ultrasound device [54]. The images with areas suspicious for cancer are color marked, and then retransmitted to the user's system to allow for the user to perform targeted prostate biopsies. In a study performed in 2011, 57 different urologists transmitted 1545 images to the analysis center (median number of images per

patient were 6) and were able to diagnose prostate cancer in 91 patients [54]. In a group of 75 patients who have never been biopsied, C-TRUS was able to detect prostate cancer in 31 patients (41 %) [54].

Prostate cancer typically results in both glandular architecture loss and increased cellular density. Decreased tissue elasticity is a product of these changes. Decreased tissue elasticity may be measurable using ultrasound elastography. Ultrasound elastography, also called strain imaging, is a method of signal processing using a special ultrasound probe that generates an elastogram. Lower density tissues allow higher displacement when compressed with the ultrasound probe while higher density tissues allow for less displacement (Fig. 10.6a–c). The elastogram is created by compression and decompression of the

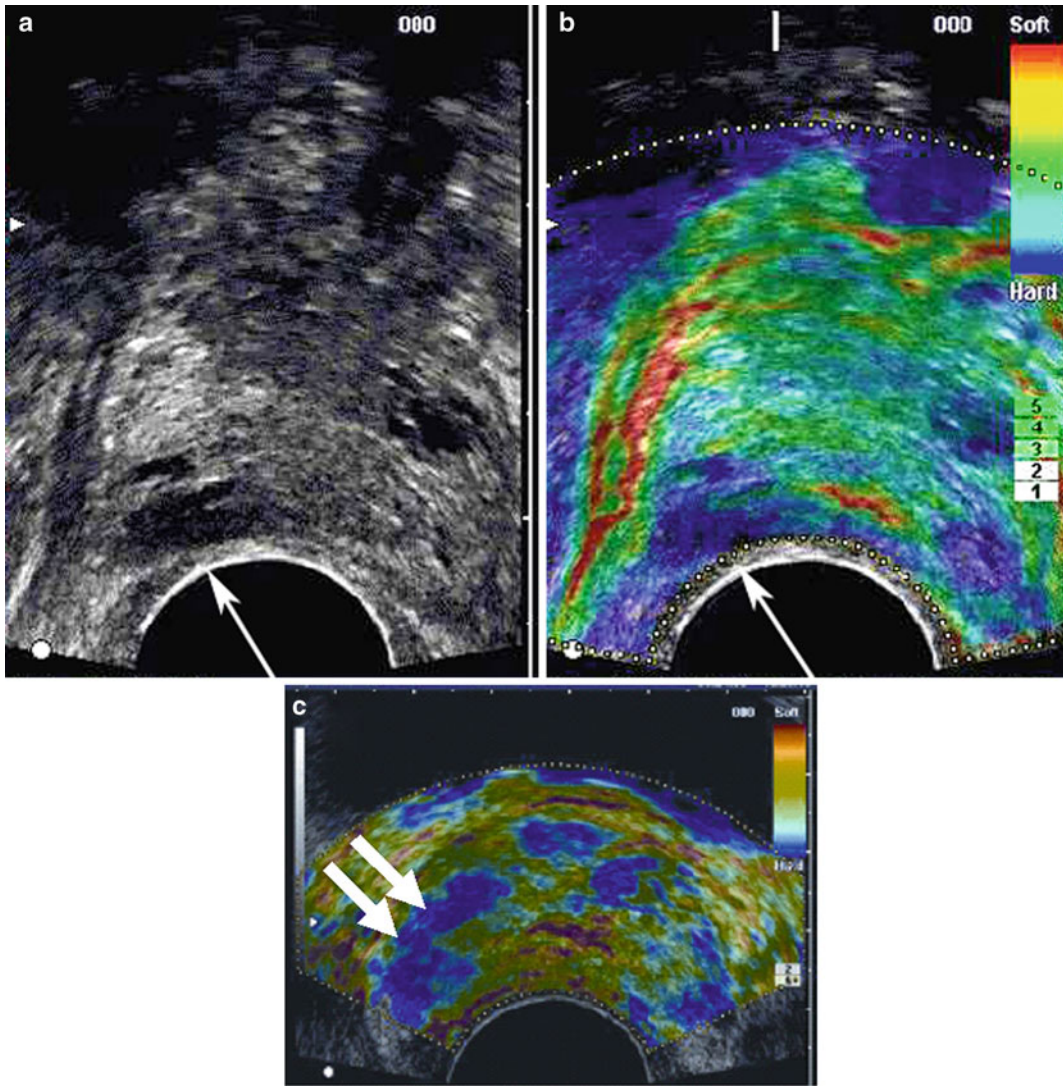

Fig. 10.6 Transverse images through the midgland of two different prostates. (**a**) Gray-scale imaging reveals a hypoechoic lesion in right midgland (*arrow*). (**b**) This lesion corresponds to an area of increased tissue stiffness (*dark blue*) on the corresponding elastogram. Note color scale in *upper right corner* indicating relative tissue "firmness." Targeted biopsy of this region revealed prostate adenocarcinoma. (**c**) Another elastogram depicting an area of increased firmness (*arrow*) concerning for neoplasm

prostate by the TRUS operator using the probe. This difference in compressibility allows for the use of elastography in targeted prostate biopsy [55]. A study published in 2008 reported a sensitivity of 86 % and specificity of 72 % in detecting prostate cancer with a negative predictive value of 91.4 % using ultrasound elastography [56]. In contrast to microbubble enhancement or flow-based imaging techniques (e.g., Doppler) elastograms provide a less subjective target and thus shows promise in the future of TRUS-guided prostate biopsy. Two variations of elastography are *Strain Elastography* and *Shear Wave Elastography*. In strain elastography, the variation in the amount of deformation (or strain) is displayed in color over the ultrasound image [56]. This relies on an endorectal probe that applies cyclical compression to the prostate. In the literature, per patient sensitivity and specificity was 62 % and 79 %, respectively, and per prostate biopsy core, the sensitivity and specificity was 34 % and 93 % [56]. Shear wave elastography works by measuring the speed at which a shear wave, generated by a focused ultrasound beam, propagates through the prostate tissue. The shear wave will propagate faster through stiffer tissue (such as in prostate cancer tissue). This is based on Young's modulus which relates the ratio of stress applied to the tissue to the resulting deformation of the tissue [56]. The advantage of shear wave elastography over strain elastography is that cyclical compression with a rectal probe is not needed, and quantification is possible since shear wave and Young's modulus are absolute values [56]. In a study by Ahmad et al., in patients with a PSA <20 μg/L the sensitivity and specificity of shear wave elastography to detect prostate cancer was 90 % and 88 %, respectively [57]. For patients with a PSA >20 μg/L, the sensitivity and specificity were both 93 %.

As mentioned previously, these ultrasound modalities utilize different characteristics of the prostate and tumor, and the thought is that by combining one or more of these modalities, one could improve the ability of detecting prostate cancer. There are studies that show, crudely, that by combining these modalities, there is improved sensitivity by 10–59 % [56]. However, these studies have insufficient data to calculate the specificity of these combinations [56].

Experience with three-dimensional (3D) ultrasound of the prostate has been limited. Currently, the use of specialized ultrasound probes is required for 3D visualization of the prostate. In addition to the standard axial and sagittal planes, 3D ultrasound provides an additional coronal plane. The use of 3D ultrasound for prostate biopsy has demonstrated mixed results. In a study by Hamper et al., 16 patients underwent both 2D and 3D TRUS-guided biopsy of the prostate [58]. The authors noted only a subjective improvement in the ability to identify hypoechoic areas of the prostate while using 3D. Further studies utilizing 3D need to be performed to better elucidate its role in TRUS of the prostate.

Although gray-scale TRUS imaging is the current gold standard for prostate imaging, new technologies have emerged in the field of ultrasonography to better guide the urologist in prostate cancer imaging and detection. With more patients undergoing evaluation for elevated PSA each year and thus likely receiving a TRUS with needle biopsy of the prostate, it is crucial that we develop new technologies to more accurately and efficiently identify suspicious areas concerning for malignancy. Reliable techniques showing no suspicious areas might obviate a biopsy. No current advanced ultrasound technique has been shown to be capable of replacing standard systematic biopsy. However, with continued research and improvement we may be able to one day reduce the number of specimens needed for prostate cancer detection or altogether eliminate the need for biopsy in those patients without cancer.

Conclusion

Transrectal ultrasound imaging plays a crucial role in the evaluation and management of both benign and malignant pathologies of the prostate. The development and use of TRUS has greatly enhanced the armamentarium of the urologist. With future research, newer technologies can hopefully further refine the use of TRUS in the diagnosis and treatment of prostatic conditions.

References

1. Watanabe H, et al. [Diagnostic application of ultrasonotomography to the prostate]. Nihon Hinyokika Gakkai Zasshi. 1968;59(4):273–9.
2. Hodge KK, et al. Random systematic versus directed ultrasound guided transrectal core biopsies of the prostate. J Urol. 1989;142(1):71–4. Discussion 74–5.
3. Beerlage HP. Alternative therapies for localized prostate cancer. Curr Urol Rep. 2003;4(3):216–20.
4. Wasserman NF. Benign prostatic hyperplasia: a review and ultrasound classification. Radiol Clin North Am. 2006;44(5):689–710, viii.
5. Stravodimos KG, et al. TRUS versus transabdominal ultrasound as a predictor of enucleated adenoma weight in patients with BPH: a tool for standard preoperative work-up? Int Urol Nephrol. 2009;41(4):767–71.
6. Smith JF, Walsh TJ, Turek PJ. Ejaculatory duct obstruction. Urol Clin North Am. 2008;35(2):221–7, viii.
7. Raviv G, et al. Role of transrectal ultrasonography in the evaluation of azoospermic men with low-volume ejaculate. J Ultrasound Med. 2006;25(7):825–9.
8. Zahalsky M, Nagler HM. Ultrasound and infertility: diagnostic and therapeutic uses. Curr Urol Rep. 2001;2(6):437–42.
9. McNeal JE. The zonal anatomy of the prostate. Prostate. 1981;2(1):35–49.
10. Christian JD, et al. Corpora amylacea in adenocarcinoma of the prostate: incidence and histology within needle core biopsies. Mod Pathol. 2005;18(1):36–9.
11. Halpern E. Anatomy of the prostate gland. In: Halpern E, Cochlin D, Goldberg B, editors. Imaging of the prostate. London: Martin Dunitz; 2002. p. 3–15.
12. Geramoutsos I, et al. Clinical correlation of prostatic lithiasis with chronic pelvic pain syndromes in young adults. Eur Urol. 2004;45(3):333–7. Discussion 337–8.
13. Sheih CP, et al. Seminal vesicle cyst associated with ipsilateral renal malformation and hemivertebra: report of 2 cases. J Urol. 1993;150(4):1214–5.
14. Narayana A. Tumors of the epididymis, seminal vesicles, and vas deferens (spermatic cord). In: Culp D, Loening S, editors. Genitourinary oncology. Philadelphia: Lea & Febiger; 1985. p. 385–98.
15. Al-Saeed O, et al. Seminal vesicle masses detected incidentally during transrectal sonographic examination of the prostate. J Clin Ultrasound. 2003;31(4):201–6.
16. Frauscher F, Klauser A, Halpern EJ. Advances in ultrasound for the detection of prostate cancer. Ultrasound Q. 2002;18(2):135–42.
17. Onur R, et al. Contemporary impact of transrectal ultrasound lesions for prostate cancer detection. J Urol. 2004;172(2):512–4.
18. Issa M, Oesterling J. Radiofrequency thermal therapy for benign prostatic hyperplasia by transurethral needle ablation of the prostate. In: Narayan P, editor. Benign prostatic hyperplasia. London: Churchill Livingstone; 2000. p. 269–80.
19. Wheelahan J, et al. Minimally invasive non-laser thermal techniques for prostatectomy: a systematic review. The ASERNIP-S review group. BJU Int. 2000;86(9):977–88.
20. Eggener SE, et al. Focal therapy for localized prostate cancer: a critical appraisal of rationale and modalities. J Urol. 2007;178(6):2260–7.
21. Aus G. Current status of HIFU and cryotherapy in prostate cancer—a review. Eur Urol. 2006;50(5):927–34. Discussion 934.
22. Marberger M, et al. New treatments for localized prostate cancer. Urology. 2008;72(6 Suppl):S36–43.
23. Polascik TJ, Mouraviev V. Focal therapy for prostate cancer. Curr Opin Urol. 2008;18(3):269–74.
24. Dehnad H, et al. Clinical feasibility study for the use of implanted gold seeds in the prostate as reliable positioning markers during megavoltage irradiation. Radiother Oncol. 2003;67(3):295–302.
25. Linden RA, et al. Technique of outpatient placement of intraprostatic fiducial markers before external beam radiotherapy. Urology. 2009;73(4):881–6.
26. Oliveira P, et al. Diagnosis and treatment of prostatic abscess. Int Braz J Urol. 2003;29(1):30–4.
27. Lim JW, et al. Treatment of prostatic abscess: value of transrectal ultrasonographically guided needle aspiration. J Ultrasound Med. 2000;19(9):609–17.
28. Halpern EJ, et al. High-frequency Doppler US of the prostate: effect of patient position. Radiology. 2002;222(3):634–9.
29. Kossoff G. Basic physics and imaging characteristics of ultrasound. World J Surg. 2000;24(2):134–42.
30. Terris MK, Stamey TA. Determination of prostate volume by transrectal ultrasound. J Urol. 1991;145(5):984–7.
31. Djavan B, et al. Optimal predictors of prostate cancer on repeat prostate biopsy: a prospective study of 1,051 men. J Urol. 2000;163(4):1144–8. Discussion 1148–9.
32. Rodriguez LV, Terris MK. Risks and complications of transrectal ultrasound guided prostate needle biopsy: a prospective study and review of the literature. J Urol. 1998;160(6 Pt 1):2115–20.
33. Goldenberg SL, et al. Sonographic characteristics of the urethrovesical anastomosis in the early post-radical prostatectomy patient. J Urol. 1992;147(5):1307–9.
34. Batura D, et al. Adding amikacin to fluoroquinolone-based antimicrobial prophylaxis reduces prostate biopsy infection rates. BJU Int. 2011;107(5):760–4.
35. Chen ME, et al. Optimization of prostate biopsy strategy using computer based analysis. J Urol. 1997;158(6):2168–75.
36. Daneshgari F, et al. Computer simulation of the probability of detecting low volume carcinoma of the prostate with six random systematic core biopsies. Urology. 1995;45(4):604–9.
37. Postema A, Mischi M, de la Rosette J, Wijkstra H. Multiparametric ultrasound in the detection of prostate cancer: a systematic review. World J Urol. 2015;33(11):1651–9. doi:10.1007/s00345-015-1523-6.
38. Bigler SA, Deering RE, Brawer MK. Comparison of microscopic vascularity in benign and malignant prostate tissue. Hum Pathol. 1993;24(2):220–6.
39. Taylor LS, et al. Three-dimensional sonoelastography: principles and practices. Phys Med Biol. 2000;45(6):1477–94.

40. Newman JS, Bree RL, Rubin JM. Prostate cancer: diagnosis with color Doppler sonography with histologic correlation of each biopsy site. Radiology. 1995;195(1):86–90.
41. Halpern EJ, Strup SE. Using gray-scale and color and power Doppler sonography to detect prostatic cancer. AJR Am J Roentgenol. 2000;174(3):623–7.
42. Cho JY, Kim SH, Lee SE. Diffuse prostatic lesions: role of color Doppler and power Doppler ultrasonography. J Ultrasound Med. 1998;17(5):283–7.
43. Okihara K, et al. Ultrasonic power Doppler imaging for prostatic cancer: a preliminary report. Tohoku J Exp Med. 1997;182(4):277–81.
44. Nelson ED, et al. Targeted biopsy of the prostate: the impact of color Doppler imaging and elastography on prostate cancer detection and Gleason score. Urology. 2007;70(6):1136–40.
45. Furlow B. Contrast-enhanced ultrasound. Radiol Technol. 2009;80(6):547S–61.
46. Eisenberg ML, Cowan JE, Carroll PR, Shinohara K. The adjunctive use of power Doppler imaging in the preoperative assessment of prostate cancer. BJU Int. 2010;105:1237–41. doi:10.1111/j.1464-410X.2009.08958.x.
47. Brawer MK, et al. Predictors of pathologic stage in prostatic carcinoma. The role of neovascularity. Cancer. 1994;73(3):678–87.
48. Postema AW, Frinking PJA, Smeenge M, De Reijke TM, De la Rosette JJMCH, Tranquart F, Wijkstra H. Dynamic contrast-enhanced ultrasound parametric imaging for the detection of prostate cancer. BJU Int. 2016;117:598–603. doi:10.1111/bju.13116.
49. Frauscher F, et al. Detection of prostate cancer with a microbubble ultrasound contrast agent. Lancet. 2001;357(9271):1849–50.
50. Frauscher F, et al. Comparison of contrast enhanced color Doppler targeted biopsy with conventional systematic biopsy: impact on prostate cancer detection. J Urol. 2002;167(4):1648–52.
51. Mitterberger M, et al. Comparison of contrast enhanced color Doppler targeted biopsy to conventional systematic biopsy: impact on Gleason score. J Urol. 2007;178(2):464–8. Discussion 468.
52. Linden RA, et al. Contrast enhanced ultrasound flash replenishment method for directed prostate biopsies. J Urol. 2007;178(6):2354–8.
53. Loch T. Computerized supported transrectal ultrasound (C-TRUS) in the diagnosis of prostate cancer. Urologe A. 2004;43:1377–84.
54. Grabski B, Baeurle L, Loch A, et al. Computerized transrectal ultrasound of the prostate in a multicenter setup (C-TRUS-MS): detection of cancer after multiple negative systematic random and in primary biopsies. World J Urol. 2011;29:573–9. doi:10.1007/s00345-011-0713-0.
55. Krouskop TA, et al. Elastic moduli of breast and prostate tissues under compression. Ultrason Imaging. 1998;20(4):260–74.
56. Pallwein L, et al. Sonoelastography of the prostate: comparison with systematic biopsy findings in 492 patients. Eur J Radiol. 2008;65(2):304–10.
57. Ahmad S, Cao R, Varghese T, Bidaut L, Nabi G. Transrectal quantitative shear wave elastography in the detection and characterisation of prostate cancer. Surg Endosc. 2013;27:3280–7.
58. Hamper UM, et al. Three-dimensional US of the prostate: early experience. Radiology. 1999;212(3):719–23.

Ultrasound for Prostate Biopsy

11

Christopher R. Porter and John S. Banerji

Introduction

The urologists' application of transrectal ultrasound (TRUS) is ubiquitous: virtually all urologists' offices, whether they are in a private small group setting or in the academic setting, have one or more ultrasound units with probes appropriate for transrectal imaging.

This chapter will focus on TRUS-guided prostate biopsy, in addition to transperineal saturation biopsy techniques, with an added focus on MRI/Ultrasound fusion-guided targeted biopsy. The chapter will encompass the initial evaluation of the gland, the techniques used to perform prostate biopsy, and the references for documenting the exam and patient safety.

History

TRUS-guided prostatic biopsy is the standard method for early detection of adenocarcinoma of the prostate. Prostate biopsy was first described in 1930 using a transperineal approach [1]. Seven years later the first transrectal biopsy was performed by Astraldi [2]. TRUS was first described in 1955 [3] and was widely used in practice by the 1970s [4]. Hodge described the first systematic biopsy template (sextant) in 1989 [5]. Further refinements have included an extended-core biopsy scheme as well as refinements to pain control strategies.

Anatomy

Grossly the prostate is situated anterior to the rectum and beneath the pubic arch. Laterally the prostate is bordered by the levator ani and inferiorly by the bladder neck. Prostatic glandular anatomy is typically described in terms of zonal architecture. The anterior fibromuscular stroma (AFS) is devoid of glandular tissue. The transition zone (TZ), which makes up 5–10 % of normal prostate volume, gives rise to benign prostatic hyperplasia (BPH) and is the zone or origin for 20 % of prostate cancers. The central zone (CZ) surrounds the ejaculatory ducts, makes up 20 % of the prostate volume, and gives rise to a minority of prostate cancers (5 %). The peripheral zone (PZ) makes up to 75 % of the normal prostate volume and is the source of the majority of prostate cancers. These zonal distinctions are not always evident on ultrasound examination; however, in the presence of BPH, the PZ may be

C.R. Porter, M.D., F.A.C.S. (✉)
J.S. Banerji, M.D., M.Ch. (Urology), D.N.B. (Urology)
Section of Urology and Renal Transplantation,
Virginia Mason, 1100 9th Ave, C7 URO, Seattle,
WA 98101, USA
e-mail: Christopher.Porter@vmmc.org;
johnsbanerji2002@gmail.com

P.F. Fulgham, B.R. Gilbert (eds.), *Practical Urological Ultrasound*, Current Clinical Urology,
DOI 10.1007/978-3-319-43868-9_11

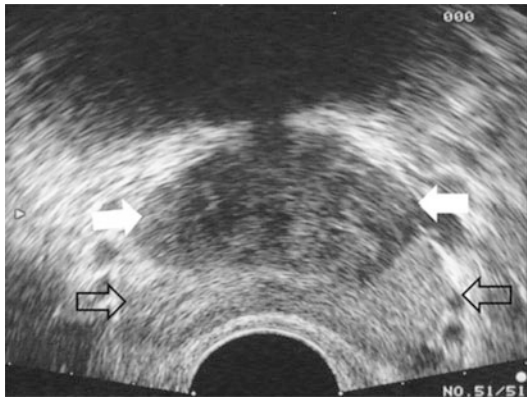

Fig. 11.1 Transrectal ultrasound image (7.5 MHz) of the prostate. Hypoechoic region anteriorly corresponds to transition zone (*white arrows*). Peripheral zone (relatively more hyperechoic) lies posteriorly (*open arrows*)

differentiated from the CZ. The paired seminal vesicles (SV), which are generally symmetrical in appearance, are located posteriorly (Fig. 11.1).

Technique Preparation

Patients undergoing a prostate needle biopsy should refrain from taking antiplatelet/anticoagulation medications (i.e., ASA/NSAIDs/clopidogrel/warfarin) 7 days prior to the procedure. Other medications including over-the-counter medications and herbal products which may affect clotting time should also be avoided. A list of medications which should be avoided prior to biopsy is included in the Appendix.

Crawford et al. [6] have demonstrated that antibiotics 24 h prior to and continuing 24–48 h postprocedure reduce bacterial septicemia. Recently, there has been a rise in septicemia rates from the modern-day prophylaxis rate of less than 1 % [7]. This has been due in part to an increased incidence of extended-spectrum beta-lactamase-producing (ESBL) *Escherichia coli* that tend to be resistant to ciprofloxacin, ceftriaxone, sulbactam/ampicillin, and cefazolin. Generally imipenem and piperacillin–tazobactam are the effective agents against ESBL-producing *E. coli* [8, 9]. Prophylaxis against infective endocarditis, with appropriate antibiotics—usually gentamicin and ampicillin [10]—is recommended by the American Heart Association for patients at high risk for infective endocarditis. This includes patients (1) with prosthetic cardiac valves or prosthetic material used for cardiac valve repair, (2) those with previous infective endocarditis, (3) patients with congenital heart defects, and (4) cardiac transplant recipients with valve regurgitation [11]. The American Academy of Orthopedic Surgeons (AAOS) guidelines [12] state that clinicians should consider antibiotic prophylaxis for all total joint replacement patients prior to any invasive procedure that may cause bacteremia. For genitourinary procedures, the AAOS recommends ciprofloxacin 60 min prior to the biopsy. Prophylactic antibiotic use may need to be modified based on local patterns of bacterial resistance.

An enema may be given the night prior to and the morning of the procedure. Reduced rectal contents will increase visibility by reducing interference and have been demonstrated to reduce the rate of bacteremia [13].

Anesthesia

It is accepted that transrectal ultrasound prostate biopsy can be painful [14, 15]. Patient perception of this procedure is a major source of anxiety and a deterrent for undergoing biopsy. Nijs demonstrated 18 % of patients in a population-based screening program refused biopsy due to anticipated pain [16]. Nash first conducted randomized, double-blind studies evaluating the effect of infiltration of 1 % lidocaine in the vascular pedicles of 64 patients undergoing PNB [17]. The mean pain scores on the side injected with drug were significantly lower than the control side. Numerous investigators have demonstrated decreased pain with various preprocedural periprostatic local anesthetic strategies (including a meta-analysis of 14 studies examining 994 procedures) [17–20]. Conversely, a small number of studies have shown no benefit [21–23]. There have been several different periprostatic injection techniques described. The most common strategy involves injection of local anesthetic between the base of the prostate and the seminal vesicles, causing a wheal between the corresponding

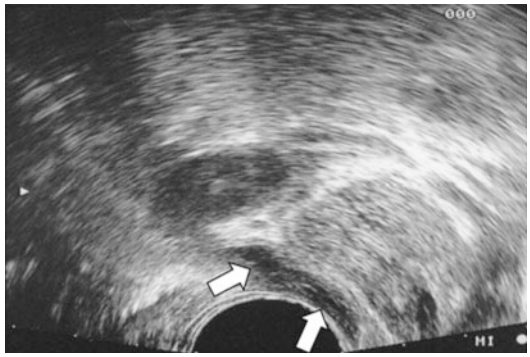

Fig. 11.2 Transrectal ultrasound image (7.5 MHz) of the prostate—sagittal view. Hypoechoic region posterior to the gland represents local anesthetic injection site (*arrows*)

seminal vesicle and the prostate gland from the rectal wall [24–26]. Other authors have described injecting the prostatic plexus in the area of the apex of the prostate [18, 27]. A majority of studies advocate bilateral injections [19, 24–26]. The administered anesthetic described varies from 1 to 2% lidocaine [17, 18, 22, 25] with a meta-analysis showing cumulative anesthetic dose varying from 2.5 to 20 mL [20] (Fig. 11.2).

Transrectal Biopsy Technique

Patients are typically placed in the left lateral decubitus position. Digital rectal exam is performed, and any palpable lesions are noted with respect to their location in the gland. Usually a 7.5 MHz probe is used. The probe is activated and placed using the ultrasound image to guide the probe gently beyond the anal sphincter and adjacent to the prostate. It is recommended to perform this slowly and carefully to minimize patient discomfort. TRUS should be performed in the sagittal and the transverse planes using gray-scale ultrasound. The gland is then inspected using color and power Doppler in both planes for the presence of lesions demonstrating increased flow with respect to other PZ areas of the gland. Abnormalities are recorded by image-saving mechanisms (either paper hard copy or electronic). Localization of all lesions is performed in real time with image documentation. Following instillation of local anesthesia, prostate volume calculations should be carried out. These volumes can be calculated through a variety of formulas that assume the prostate to be that of a geometric shape. These formulas estimate weight as well as volume, as 1 cm^3 equals 1 g of prostatic tissue [28]. The specific gravity of prostate tissue is approximately 1.02 g/cm^3.

Formulas for estimated weight and volume of the prostate gland:

(a) Ellipse: ($\pi/6 \times$ transverse diameter $\times$ AP diameter $\times$ longitudinal diameter)
(b) Sphere: ($\pi/6 \times$ transverse diameter^3)
(c) Prolate (egg shaped): ($\pi/6 \times$ transverse $\text{diameter}^2 \times$ AP diameter)

Volume measurements of the TZ and bladder volume may be carried out and recorded depending on the preference of the physician. The integrity of the surrounding structures should be evaluated which include examination of the bladder wall, seminal vesicles, and anal canal up to the level of the prostate.

PSA Density

Calculating prostate volume allows the use of PSA density (PSAD) defined as the ratio of serum PSA-to-prostate volume. PSAD is thought to improve cancer detection (sensitivity) and reduce the number of unnecessary prostate needle biopsies (PNB) (specificity). Djavan and colleagues demonstrated that PSAD and TZ PSAD were significantly higher in subjects diagnosed with prostate cancer on initial and repeat biopsies [29]. The authors routinely calculate PSAD and record it in real time; however, their data do not support basing the decision to perform prostate biopsy solely on this parameter.

Prostatic and Paraprostatic Cysts

As the prostate is examined focal cystic areas can often be noted. These cysts can vary in size and, when associated with BPH, are due to cystic dilatation of TZ glands. Other common cysts

include acquired prostatic retention cysts which represent dilatation of glandular acini. Acquired prostatic retention cysts may occur in any zone and are not associated with BPH. Other cysts are less common but have important associations or implications. Utricular and Mullerian duct cysts are congenital midline or paramedian cysts. Utricular cysts are intraprostatic in nature. Arising from a dilated utricle originating at the verumontanum, these communicate with the urethra and can be associated with cryptorchidism and hypospadias [30]. Mullerian duct cysts are located retrovesically and originate from Mullerian remnants. They have no communication with the urethra and can be associated with calculi and renal agenesis [31]. Ejaculatory cysts, arising from an obstructed ejaculatory duct, can be located in a midline or paramedian position. These can be associated with seminal vesicle obstruction and may contain calculi. Seminal vesicle cysts are found lateral to the prostate and are secondary to congenital hypoplasia of the ejaculatory duct [32]. Unilateral in nature, they may contain calculi and are associated with renal agenesis and epididymitis. Prostatic abscesses can be associated with surgery, prostatitis, or epididymitis [33].

Hypoechoic Lesions

The gland should be examined for hypoechoic lesions. The classic appearance of prostate cancer is a round/oval hypoechoic lesion located in the PZ. Contemporary series have noted that the presence of these lesions is a less sensitive sign for prostate cancer than once thought, with hypoechoic lesions being malignant at a rate of 17–57 % [34]. However, a continued valuable asset of TRUS is directed biopsy of these lesions. Absence of hypoechoic lesions is not a contraindication to biopsy as 39 % and 1 % of prostate cancer are isoechoic and hyperechoic, respectively [35]. TRUS has a known poor specificity in regard to the presence of a hypoechoic lesion. Entities which also have a hypoechoic appearance on TRUS include granulomatous prostatitis [36], prostatic infarction [37], lymphoma [38], and TZ BPH [39] (Fig. 11.3).

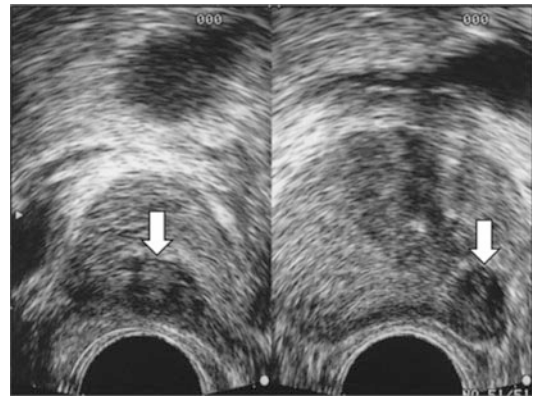

Fig. 11.3 Transrectal ultrasound image (7.5 MHz) of the prostate—transverse view (*left*) and sagittal view (*right*). Hypoechoic lesion in the peripheral zone posterolaterally represents an area of increased suspicion for malignancy (*arrows*)

Color Doppler

Color Doppler (CD) is a tool that attempts to allow TRUS to differentiate benign from malignant tissue. CD measures the frequency shift in sound waves as a measurement of the velocity of blood flow. This capitalizes on the hypervascular appearance of prostate cancer due to increased microvessel density secondary to increased angiogenesis versus benign tissue [40]. Cornud et al. [41] noted that in patients with clinical T1c disease, high-risk pathologic features (ECE, pT3b) were present more often in tumors visualized with CD versus those with the absence of a positive CD signal. Another study demonstrated a 2.6 times increased detection of prostate cancer versus conventional gray-scale ultrasound [34]. Halpern and Strup [42] demonstrated CD sensitivity and specificity to diagnose prostate cancer at 27.3 and 83.9 %, respectively. This is an improvement in specificity with respect to gray-scale imaging (sensitivity 44.4 %, specificity 70.5 %). However, 45 % of cancers still went undetected by any ultrasound modality. Arger [43] has suggested that pathologic groups based on Gleason scores, high (8–10), intermediate (5–7), and low (2–4), were not separable by vascular measurement. While several studies [41, 44, 45] have demonstrated increased cancer detection

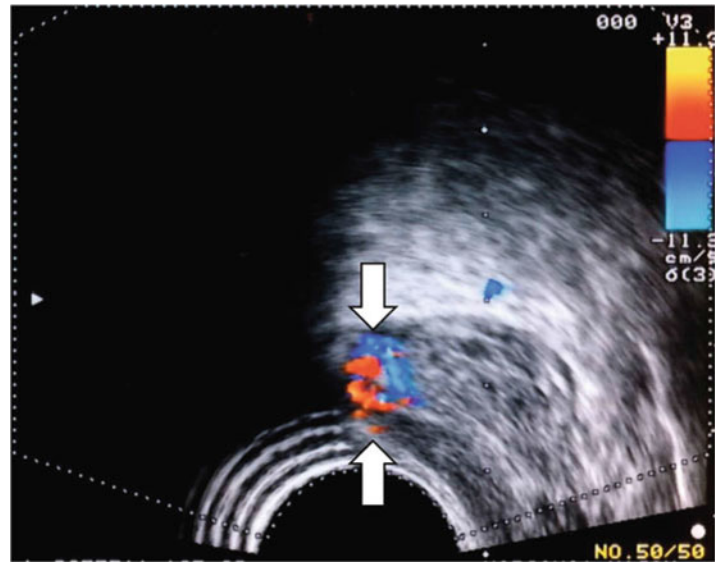

Fig. 11.4 Transrectal ultrasound image, color Doppler, of the prostate—sagittal view. Colored area (*arrows*) in the posterior lateral aspect of the gland represents an area of increased vascular flow relative to the surrounding parenchyma

using CD-targeted focal biopsy strategies, there remain enough questions to preclude replacement of a systemic biopsy approach [46] (Fig. 11.4).

Biopsy Strategies

The advent of the sextant biopsy technique, that is, systematic biopsy of the apex, mid, and base of the prostate on each side of the gland, represented an improvement in prostate cancer detection over site-specific biopsies of hypoechoic lesions or palpable abnormalities [5]. With this limited template, there is still concern for a high false-negative rate, with Levine et al. [47] demonstrating in a repeat biopsy series a false-negative rate of 30 % of men with an abnormal digital rectal examination (DRE) and/or elevated serum PSA. Refinements have focused on the importance of increased number of cores, as well as including laterally directed biopsies. Many groups have reported series (Table 11.1) in which improved cancer detection rates are achieved by including additional laterally directed cores and/or increasing the cores taken from 6 to as many as 13 [47–51].

Investigators [52, 53] have demonstrated a lack of usefulness for TZ and SV sampling on initial biopsy with only 2.1 and 3.7 %, respectively, of biopsies being positive. The spatial distribution of cancer foci of prostate cancers with negative initial biopsies or with a gland volume larger than 50 cc may vary compared to that of prostate carcinomas diagnosed on initial biopsy. In these cases special emphasis on the apico-dorsal peripheral and transitional zones should be considered [54, 55]. Biopsy of the SV is not recommended unless a palpable abnormality is appreciated.

It is generally recommended that 10–12 biopsies of the gland be obtained with attention to the anterior horns. Technique is important in obtaining laterally directed biopsies. It should be recalled that the tru-cut needle travels between 17 and 24 mm depending on the manufacturer's

Table 11.1 Prostate cancer detection rates with extended-core biopsy

Study	Number of cores/ biopsy	Prostate cancer detection %
Eskew [48]	6	26.1
	13	40.3
Babian [49]	6	20
	11	30
Presti [50]	6	33.5
	8	39.7
	10	40.2
Naughton [51]	6	26
	12	27

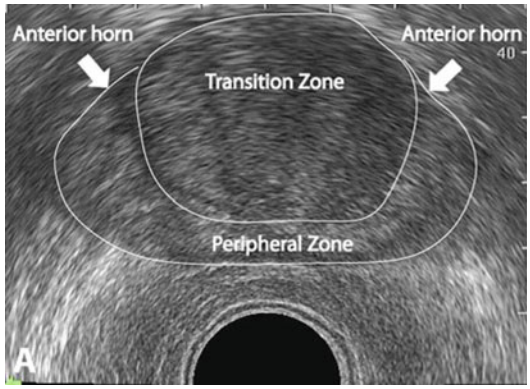

Fig. 11.5 Transrectal ultrasound image (7.5 MHz) of the prostate—transverse view. *White arrow* depicts the anterior horns of the prostate

standard. The user must appropriately guide the angle of the biopsy to maximize its position laterally on the gland, particularly when the anterior horns are approached (Fig. 11.5).

Repeat Biopsy

For the patient who has had a previous negative biopsy but has a persistent PSA elevation or abnormal DRE, an additional biopsy may be considered. During repeat biopsy the standard extended-core biopsy protocol should be carried out. Additionally any sites of ultrasound abnormality and any sites of high-grade prostatic intraepithelial neoplasia (HGPIN) or ASAP should be sampled [56]. The aforementioned strategy of apico-dorsal peripheral and TZ biopsies should be included. It is well established that as successive biopsies are obtained, a decreased rate of prostate cancer detection will be observed with each additional biopsy [57]. A large series of over 1100 men undergoing biopsy as directed by PSA screening found an initial prostate cancer detection rate of 34 % [58]. This declined to 19, 8, and 7 % on biopsies 2–4, respectively. This was echoed by Djavan in the European Prostate Cancer Detection Study [59]. Thousand and fifty-one men with a PSA value of 4–10 ng/mL had a detection rate of 22 % on primary biopsy. This declined to 10, 5, and 4 % on subsequent biopsies 2, 3, and 4. The use of free and total PSA, along with prostate cancer antigen-3 (PCA3), may allow risk stratification of patients for additional prostate biopsy. Catalona et al. [60] proposed the use of the percentage of free PSA to reduce unnecessary biopsies in patients with PSA values between 4.0 and 10.0 ng/mL and a palpably benign gland. In this study Catalona suggested that patients with a free PSA of less than 25 % were significantly more likely to have a positive biopsy. PCA3 encodes a prostate-specific messenger ribonucleic acid (mRNA) that serves as the target for a novel urinary molecular assay for prostate cancer detection [61]. It has also shown promise as an aid in prostate cancer diagnosis in identifying men with a high probability of a positive (repeat) biopsy. Urine is collected after DRE, and PCA3 mRNA concentration is measured. Haese et al. [62] compared PCA3 to percent-free PSA and biopsy results in 463 men undergoing repeat biopsy. The overall positive repeat biopsy was 28 %. The probability of a positive repeat biopsy increased with rising PCA3 scores. The PCA3 score (cut point of 35) was superior to percent-free PSA (cut point of 25 %) for predicting repeat prostate biopsy outcomes.

Saturation Biopsy

Saturation biopsy has a role in maximizing prostate cancer detection rates in select patients at high risk for prostate cancer in the setting of a negative biopsy. Protocols have been described using both transrectal and transperineal approaches [63]. Various series have shown detection rates of 30–34 % [64–67]. A drawback to this procedure is the need for the biopsies to be performed under sedation in a hospital setting. However, there are circumstances that warrant more extensive gland sampling. These include (1) a persistent rise in serum PSA, with prior negative biopsies and (2) new DRE abnormalities and low volume cancers for which a surveillance approach is being considered.

The importance of saturation biopsies lies in the fact that as high as 35 % of cancers might be upgraded with the saturation biopsy technique [68, 69].

In addition, about a third of patients have exclusively anteriorly located tumors, which can best be sampled with transperineal saturation biopsies [70, 71]. The standard transrectal approach has a theoretical disadvantage due to its limited ability to obtain anterior prostatic tissue particularly at the apex. The technique described later focuses on the transperineal approach with glandular mapping.

Transrectal Ultrasound-Guided Transperineal Prostate Biopsy Using the Brachytherapy Template

Indications for transrectal ultrasound-guided/transperineal prostate biopsy (TRUS/TPB) include men with further worrisome serum PSA changes or DRE abnormalities after one or more negative standard biopsies or those considering active surveillance for prostate cancer. The TRUS/TPB includes stereotactic TPB using a standard brachytherapy template and the ultrasound device together with a brachytherapy stepper device [72].

Patients are appropriately counseled on the risks and benefits of the procedure, and surgical consent is obtained. Similar prebiopsy precautions are taken as per those outlined for the transrectal technique.

Under general anesthesia, patients are placed in the lithotomy position. Intravenous antibiotics are administered. A DRE is again performed and any lesions noted. As in the case of transrectal biopsies the prostate is scanned in gray scale and color Doppler, and any abnormalities are recorded. The transrectal probe is placed in a brachytherapy stepper device and synchronized with the ultrasound device. Prostate volumes are again obtained and recorded. The prostate is divided into 12 sections: four quadrants at the base, mid-gland and apex, respectively. Tissue cores are harvested using a biopsy gun beginning at the apical quadrants. Twenty-four core samples are targeted in both the sagittal and axial views. Specimens are placed in individual jars and reported accordingly. Patients are discharged with oral antibiotics and analgesics.

MRI/Ultrasound Fusion-Guided Biopsy for Targeted Diagnosis of Prostate Cancer

The overwhelming need in the evaluation of prostate cancer is the ability to differentiate significant cancer from indolent cancer. Routine gray scale and color Doppler imaging and conventional biopsy is unable to differentiate clinically significant cancer, thus leading to the problem of overdetection. While the conventional biopsy might be "blind" systematic biopsies, the MRI TRUS fusion biopsies truly map, track, and target suspicious lesions, thus increasing yield. Gray-scale Doppler ultrasound is able to recognize up to 80 % of suspicious lesions detected by MRI [73]. Taking systematic biopsies is responsible for the incidental detection of low-grade disease in both MRI-directed and conventional sono-directed biopsies.

This relatively newer technology utilizes MRI to initially detect "targetable lesions" in the prostate. Multiparametric MRI (mp-MRI) (using T2 weighted images, Diffusion-weighted images which uses movement of water molecules into and out of tumor cells, and dynamic contrast enhanced imaging) in conjunction with a powerful 3T magnetic field is initially used to classify "suspicious lesions" based on the Prostate Imaging Reporting and Data System-(PI-RADS) score.

The MRI is performed prior to the TRUS, and is read by a specialist uro-radiologist, who identifies a "targetable" lesion, and assigns a PI-RADS score to it. These images are stored on the software. There are currently five FDA approved fusion devices (Artemis, Eigen CA; Philips Percunav, Koelis Urostation,Hitachi/HI-RVS and Biojet). At the time of the biopsy, transrectal ultrasound is used to visualize the prostate in the usual manner, with the MRI images which highlight the tumor can be superimposed over the ultrasound in real time. This "fusion" with real-time ultrasound is done using a mechanism called digital overlay. The fusion thus results in the formation of a three-dimensional image of the prostate, enabling accurate and easy biopsy of the "targets."

Recently, there have been claims of mp-MRI and fusion biopsies to have a good negative predictive value (NPV), thus being accurate enough to rule out indolent prostate cancer, while detecting clinically significant prostate cancer [74, 75]. It is yet to be determined whether the transperineal approach or the MRI-based approach is more accurate in determining the presence of aggressive disease in patients originally thought to be candidates for surveillance.

TRUS Biopsy After Definitive Treatment and Hormonal Ablative Therapy

External beam radiotherapy (EBRT) decreases the size of the prostate gland. Small areas of cancer which have moderate or severe radiation effects tend to appear isoechoic while large (greater than 4 mm) foci of cancer usually show little radiation effect, and these foci typically appear hypoechoic [76]. In situations that are worrisome for biochemical relapse and where the urologist and patient are seeking proof of local relapse, prostate needle biopsy is usually performed as described in the transrectal ultrasound-guided manner.

With the exception of the presence of well-distributed foreign bodies, long-term changes after brachytherapy resemble EBRT [77]. Biopsies of the gland are obtained in the same fashion as described earlier.

Whittington [77] described the effect of LHRH analogs on prostate tissue. The median decrease in prostate volume as a result of androgen deprivation was 33 %. The reduction in volume was greatest in men with the largest initial gland volume (59 %) and least in men with the smallest glands (10 %). It is rare that further biopsies will be required after hormonal ablation; however, if biopsies are required, it is very important to notify the pathologist as to the presence of hormonal ablation given the histologic changes that usually occur in these situations.

After radical prostatectomy, the presence of lesions (hyper or hypoechoic) interrupting the tapering of the bladder to the urethra, representing the anastomotic plane, is considered worrisome for recurrence [78]. One notable exception is nodules anterior to the anastomosis which may be the ligated dorsal venous complex [79]. Biopsies of the bladder neck–urethral anastomosis are possible. The target for biopsy is usually small, and care is required to accurately map the anatomy prior to biopsy. The typical area of concern is between the bladder neck and the external sphincter. The urologist is reminded to exhibit extreme caution around the sphincter.

Complications

Transrectal ultrasound-guided needle biopsy is safe for diagnosing prostate cancer. Complications do arise after a prostate needle biopsy with few major but frequent minor self-limiting complications (Table 11.2).

Vagal response, secondary to pain/anxiety, occurs in 1.4–5.3 % of patients [67]. Vagal response is generally responsive to hydration and placing the patient in the Trendelenburg position. Hematuria is quite common immediately following biopsy (71 %), with 47 % of patients having limited hematuria resolving over 3–7 days [74]. Hematospermia is observed in 9–36 % of biopsies and may persist for several months [7, 72]. Rectal bleeding is observed in 2–8 % of biopsies [7, 74]. Frequently, the bleeding is mild and can be controlled with digital pressure. In severe cases where bleeding is not controlled with conservative approaches, bleeding may be managed with rectal packing [75, 80], using a tampon or gauze, or can be addressed with endoscopic injection of vasoconstrictive agents or ligation of bleeding vessels during colonoscopy [76]. Acute

Table 11.2 Complication rates in TRUS biopsies

Complication	Incidence
Vagal response secondary to pain/anxiety	1.4–5.3 % [67]
Hematuria	71 %
	47 % resolved over 3–7 days [81]
Hematospermia	9–36 % [7, 79]
Rectal bleeding	2–8 % [7, 79]
Acute urinary retention	0.4 % [112]
Bacteremia (with enema)	44 % [83]
Bacteriuria (with enema)	16 % [83]

urinary retention requiring catheter drainage occurs up to 0.4 % of the time [76]. Men with enlarged prostates or with severe baseline lower urinary tract symptoms are at an increased risk [81, 82]. In the preprophylaxis era, Thompson [83] demonstrated a bacteremia rate of 100 % with a bacteriuria rate of 87 %. This decreased to 44 % and 16 %, respectively, with enema alone [83]. Crawford et al. [6] administered 48 h of carbenicillin and noted bacteriuria to decrease from 36 to 9 % versus the control group. The treatment group's incidence of fever was 17 % compared to a rate of 48 % in the control group. Antibiotic prophylaxis is now standard of care. Berger demonstrated fever (>38.5 °C) in 0.8 % of 4303 patients receiving a 5-day course of ciprofloxacin [7]. Similarly, a study administering 1–3 days of ciprofloxacin noted a fever incidence of 0.6 % [84]. Seeding of prostate cancer in the needle tract is rare but is reported in the literature. It is seen more commonly in the form of perineal recurrences after transperineal biopsy [85, 86] but has been reported after TRUS biopsy [87]. Perineal recurrence has a poor prognosis [86], while rectal seeding has been shown to be responsive to hormonal therapy as well as EBRT [88]. Hara demonstrated increased circulating PSA mRNA in men following positive biopsy; [89] however, the risk of developing metastatic disease is thought to be low [56].

Pathologic Findings

HGPIN and ASAP

High-grade intraepithelial neoplasia (HGPIN) is detected on needle biopsy in 1–25 % of patients [90]. HGPIN was thought to be a precursor lesion for adenocarcinoma, and historically, its presence prompted rebiopsy at 3–6 months in the absence of prostate cancer in the biopsy specimen [91–93]. Lefkowitz et al. noted that with extended 12-core biopsy technique, the repeat biopsy cancer detection rate was 2.3 % and recommended repeat biopsy was not indicated for HGPIN in the absence of any other findings [94]. Atypical small acinar proliferation (ASAP) demonstrates proliferation of gland without atypia [95, 96] and has an incidence of 5 % of men undergoing biopsy. The association of ASAP with prostate cancer is stronger than with HGPIN [97, 98], with the cancer detection rates on subsequent biopsies ranging from 51 to 75 % [99, 100].

Predicting Outcomes Following Local Treatment

The pathologic elements obtained during needle biopsy including the number of cores positive, the percent involvement of each core, and the location of positive cores may contribute to important prognostic information. Clinical understaging by TRUS needle biopsy occurs [101] but is reduced in the era of extended-core strategies [102]. Studies have demonstrated the number of cores positive and/or the percent of cores positive, to have a correlation to prostate cancer extracapsular extension (ECE), surgical margin status, tumor volume and stage, seminal vesicle involvement, and the presence of lymph node metastasis [103–106]. Length of tumor tissue involved in each core can be measured. Longer tumor lengths, or higher percentage of core positivity, have been strongly associated with the presence of ECE, SV involvement, and biochemical recurrence following treatment [107–110]. Biopsy site-specific percent cores positivity is predictive of sextant site of extension [111], which can aid in identification of appropriate candidates for nerve-sparing surgery.

Summary

Transrectal biopsy technique using prophylactic antibiotics, local analgesia, and an extended-core technique is safe and allows detection of prostate cancer while providing important prognostic information. Transperineal saturation techniques improve detection especially in anterior tumors of the prostate. MRI/USG fusion techniques offer an important means of "targeted" biopsies, with the theoretical advantage of precise identification of clinically significant prostate cancer.

Appendix: List of Medications to be Avoided Prior to Biopsy

Aminosalicylic acid (*Paser*)	*Topical medication* (*cream*, *gel*, *ointment*, etc.)
Aspirin (***numerous***, e.g., *Bayer*, *Bufferin*, *Ecotrin*, *Fiorinal*, *Aspergum*, *Alka-Seltzer*, *Percodan*, *Anacin*, *Goody's*, *Zorprin*)	**Diclofenac** (*Flector*, *Solaraze*, *Voltaren*)
Celecoxib (*Celebrex*)	**Trolamine** (e.g., *Aspercreme*, *Mobisyl*, *Myoflex*)
Choline magnesium trisalicylate	**Methyl salicylate** (e.g., *Salonpas*, *Icy Hot*)
Clopidogrel (*Plavix*)	*Ophthalmic medication*
Cilostazol (*Pletal*)	**Bromfenac** (*Xibrom*)
Diclofenac (*Cataflam*, *Voltaren*, *Arthrotec*)	**Diclofenac** (*Voltaren*)
Diflunisal	**Flurbiprofen** (*Ocufen*)
Dipyridamole (*Aggrenox*, *Persantine*)	**Ketorolac** (*Acular*)
Etodolac (*Lodine*)	**Nepafenac** (*Nevanac*)
Fenoprofen	*Injectable medication*
Flurbiprofen	**Enoxaparin** (*Lovenox*)
Ibuprofen (e.g., *Advil*, *Midol*, *Motrin*)	**Dalteparin** (*Fragmin*)
Indomethacin (*Indocin*)	**Fondaparinux** (*Arixtra*)
Ketoprofen (*Orudis*)	**Heparin** (*HepFlush*, *Hep-Lock*)
Ketorolac (*Toradol*)	**Tinzaparin** (*Innohep*)
Magnesium salicylate (e.g., *Doan's*, *Momentum*)	**Ketorolac** (*Toradol*)
Meclofenamate	*Herbals/natural products*[a]
Mefenamic acid (*Ponstel*)	**Aloe**
Meloxicam (*Mobic*)	**Bilberry**
Nabumetone (*Relafen*)	**Cayenne**
Naproxen (e.g., *Aleve*, *Naprosyn*, *Pamprin*, *Treximet*)	**Dong quai**
Oxaprozin (*Daypro*)	**Feverfew**
Piroxicam (*Feldene*)	**Fish oil**
Salicylamide (e.g., *BC Fast Pain Relief*, *Lobac*)	**Flaxseed oil**
Salsalate	**Garlic**
Sulindac (*Clinoril*)	**Ginger**
Ticlopidine (*Ticlid*)	**Ginkgo biloba**
Tolmetin	**Ginseng**
Warfarin (*Coumadin*, *Jantoven*)	**Glucosamine**, **chondroitin**
– Many OTC headache, allergy, and cough and cold products also contain aspirin, ibuprofen, or naproxen	**Golden seal**
– Tylenol is okay. Take as instructed	**Supplement oils**
	Vitamin E

Prior to surgery it is important to review *all medications* you are taking with your physician as some products may increase your risk of bleeding. These include prescription, over-the-counter (OTC), and herbal products. Please notify your physician if you are taking any of the following medications. *Medications are listed by their generic name, with some common brand names in parentheses.
Always consult your healthcare provider if you are unsure if you are taking a medication that may increase your bleeding risk.
[a]Includes pills, liquids, teas, etc.

References

1. Ferguson R. Prostatic neoplasms; their diagnosis by needle puncture and aspiration. Am J Surg. 1930;9:507.
2. Astraldi A. Diagnosis of cancer of the prostate; biopsy by rectal route. Urol Cutaneous Rev. 1937;41:421.
3. Wild J, Reid J. Fourth annual conference in ultrasound therapy. Philadelphia; 1955
4. Wantanabe H, Kato H, Kato T. Diagnostic application of ultrasonotomography to the prostate. Nippon Hinyokika Gakkai Zasshi. 1968;59:273.
5. Hodge KK, McNeal JE, Terris MK, et al. Random systematic versus directed ultrasound guided transrectal core biopsies of the prostate. J Urol. 1989;142:71.
6. Crawford ED, Haynes Jr AL, Story MW, et al. Prevention of urinary tract infection and sepsis following transrectal prostatic biopsy. J Urol. 1982; 127:449.
7. Berger AP, Gozzi C, Steiner H, et al. Complication rate of transrectal ultrasound guided prostate biopsy: a comparison among 3 protocols with 6, 10 and 15 cores. J Urol. 2004;171:1478.
8. Cannon Jr GM, Smaldone MC, Paterson DL. Extended-spectrum beta-lactamase gram-negative sepsis following prostate biopsy: implications for use of fluoroquinolone prophylaxis. Can J Urol. 2007;14:3653.
9. Ozden E, Bostanci Y, Yakupoglu KY, et al. Incidence of acute prostatitis caused by extended-spectrum beta-lactamase-producing Escherichia coli after transrectal prostate biopsy. Urology. 2009;74(1): 119–23.

10. Dajani AS, Taubert KA, Wilson W, et al. Prevention of bacterial endocarditis: recommendations by the American Heart Association. Clin Infect Dis. 1997;25:1448.
11. Nishimura RA, Carabello BA, Faxon DP, et al. ACC/AHA 2008 guideline update on valvular heart disease: focused update on infective endocarditis: a report of the American College of Cardiology/American Heart Association Task Force on Practice Guidelines: endorsed by the Society of Cardiovascular Anesthesiologists, Society for Cardiovascular Angiography and Interventions, and Society of Thoracic Surgeons. Circulation. 2008;118:887.
12. Bratzler DW, Houck PM. Antimicrobial prophylaxis for surgery: an advisory statement from the National Surgical Infection Prevention Project. Clin Infect Dis. 2004;38:1706.
13. Lindert KA, Kabalin JN, Terris MK. Bacteremia and bacteriuria after transrectal ultrasound guided prostate biopsy. J Urol. 2000;164:76.
14. De Sio M, D'Armiento M, Di Lorenzo G, et al. The need to reduce patient discomfort during transrectal ultrasonography-guided prostate biopsy: what do we know? BJU Int. 2005;96:977.
15. Soloway MS. Do unto others—why I would want anesthesia for my prostate biopsy. Urology. 2003;62:973.
16. Nijs HG, Essink-Bot ML, DeKoning HJ, et al. Why do men refuse or attend population-based screening for prostate cancer? J Public Health Med. 2000;22:312.
17. Nash PA, Bruce JE, Indudhara R, et al. Transrectal ultrasound guided prostatic nerve blockade eases systematic needle biopsy of the prostate. J Urol. 1996;155:607.
18. Schostak M, Christoph F, Muller M, et al. Optimizing local anesthesia during 10-core biopsy of the prostate. Urology. 2002;60:253.
19. Trucchi A, De Nunzio C, Mariani S, et al. Local anesthesia reduces pain associated with transrectal prostatic biopsy. A prospective randomized study. Urol Int. 2005;74:209.
20. Hergan L, Kashefi C, Parsons JK. Local anesthetic reduces pain associated with transrectal ultrasound-guided prostate biopsy: a meta-analysis. Urology. 2007;69:520.
21. Bozlu M, Atici S, Ulusoy E, et al. Periprostatic lidocaine infiltration and/or synthetic opioid (meperidine or tramadol) administration have no analgesic benefit during prostate biopsy. A prospective randomized double-blind placebo-controlled study comparing different methods. Urol Int. 2004;72:308.
22. Vanni AP, Schaal CH, Costa RP, et al. Is the periprostatic anesthetic blockade advantageous in ultrasound-guided prostate biopsy? Int Braz J Urol. 2004;30:114.
23. Walsh K, O'Brien T, Salemmi A, et al. A randomised trial of periprostatic local anaesthetic for transrectal biopsy. Prostate Cancer Prostatic Dis. 2003;6:242.
24. Adamakis I, Mitropoulos D, Haritopoulos K, et al. Pain during transrectal ultrasonography guided prostate biopsy: a randomized prospective trial comparing periprostatic infiltration with lidocaine with the intrarectal instillation of lidocaine-prilocaine cream. World J Urol. 2004;22:281.
25. Obek C, Ozkan B, Tunc B, et al. Comparison of 3 different methods of anesthesia before transrectal prostate biopsy: a prospective randomized trial. J Urol. 2004;172:502.
26. Rabets JC, Jones JS, Patel AR, et al. Bupivacaine provides rapid, effective periprostatic anesthesia for transrectal prostate biopsy. BJU Int. 2004;93:1216.
27. Nambirajan T, Woolsey S, Mahendra V, et al. Efficacy and safety peri-prostatic local anesthetic injection in trans-rectal biopsy of the prostrate: a prospective randomized study. Surgeon. 2004;2:221.
28. Terris MK, Stamey TA. Determination of prostate volume by transrectal ultrasound. J Urol. 1991;145:984.
29. Djavan B, Zlotta A, Remzi M, et al. Optimal predictors of prostate cancer on repeat prostate biopsy: a prospective study of 1,051 men. J Urol. 2000;163:1144.
30. Zagoria RJ. Genitourinary radiology. In: Thrall JH, editor. The requisites. 2nd ed. Philadelphia: Mosby; 2004. p. 335–8.
31. Gregg DC, Sty JR. Sonographic diagnosis of enlarged prostatic utricle. J Ultrasound Med. 1989;8:51.
32. McDermott V, Orr JD, Wild SR. Duplicated Mullerian duct remnants associated with unilateral renal agenesis. Abdom Imaging. 1993;18:193.
33. King BF, Hattery RR, Lieber MM, et al. Congenital cystic disease of the seminal vesicle. Radiology. 1991;178:207.
34. Frauscher F, Klauser A, Volgger H, et al. Comparison of contrast enhanced color Doppler targeted biopsy with conventional systematic biopsy: impact on prostate cancer detection. J Urol. 2002;167:1648.
35. Shinohara K, Scardino PT, Carter SS, et al. Pathologic basis of the sonographic appearance of the normal and malignant prostate. Urol Clin North Am. 1989;16:675.
36. Terris MK, Macy M, Freiha FS. Transrectal ultrasound appearance of prostatic granulomas secondary to bacillus Calmette-Guerin instillation. J Urol. 1997;158:126.
37. Purohit RS, Shinohara K, Meng MV, et al. Imaging clinically localized prostate cancer. Urol Clin North Am. 2003;30:279.
38. Varghese SL, Grossfeld GD. The prostatic gland: malignancies other than adenocarcinomas. Radiol Clin North Am. 2000;38:179.
39. Ramey JR, Halpern EJ, Gomella LG. Ultrasonography and biopsy of the prostate. In: Wein AJ, editor. Campbell-Walsh urology, vol. 3. 9th ed. Philadelphia: Saunders; 2007. p. 2883–95.
40. Bigler SA, Deering RE, Brawer MK. Comparison of microscopic vascularity in benign and malignant prostate tissue. Hum Pathol. 1993;24:220.
41. Cornud F, Hamida K, Flam T, et al. Endorectal color Doppler sonography and endorectal MR imaging features of nonpalpable prostate cancer: correlation with radical prostatectomy findings. AJR Am J Roentgenol. 2000;175:1161.

42. Halpern EJ, Strup SE. Using gray-scale and color and power Doppler sonography to detect prostatic cancer. AJR Am J Roentgenol. 2000;174:623.
43. Arger PH, Malkowicz SB, VanArsdalen KN, et al. Color and power Doppler sonography in the diagnosis of prostate cancer: comparison between vascular density and total vascularity. J Ultrasound Med. 2004;23:623.
44. Okihara K, Kojima M, Nakanouchi T, et al. Transrectal power Doppler imaging in the detection of prostate cancer. BJU Int. 2000;85:1053.
45. Kelly IM, Lees WR, Rickards D. Prostate cancer and the role of color Doppler US. Radiology. 1993; 189:153.
46. Halpern EJ, Frauscher F, Strup SE, et al. Prostate: high-frequency Doppler US imaging for cancer detection. Radiology. 2002;225:71.
47. Levine MA, Ittman M, Melamed J, et al. Two consecutive sets of transrectal ultrasound guided sextant biopsies of the prostate for the detection of prostate cancer. J Urol. 1998;159:471.
48. Eskew LA, Bare RL, McCullough DL. Systematic 5 region prostate biopsy is superior to sextant method for diagnosing carcinoma of the prostate. J Urol. 1997;157:199.
49. Babaian RJ, Toi A, Kamoi K, et al. A comparative analysis of sextant and an extended 11-core multisite directed biopsy strategy. J Urol. 2000;163:152.
50. Presti Jr JC, Chang JJ, Bhargava V, et al. The optimal systematic prostate biopsy scheme should include 8 rather than 6 biopsies: results of a prospective clinical trial. J Urol. 2000;163:163.
51. Naughton CK, Miller DC, Mager DE, et al. A prospective randomized trial comparing 6 versus 12 prostate biopsy cores: impact on cancer detection. J Urol. 2000;164:388.
52. Terris MK, Pham TQ, Issa MM, et al. Routine transition zone and seminal vesicle biopsies in all patients undergoing transrectal ultrasound guided prostate biopsies are not indicated. J Urol. 1997;157:204.
53. Epstein JI, Walsh PC, Sauvageot J, et al. Use of repeat sextant and transition zone biopsies for assessing extent of prostate cancer. J Urol. 1997; 158:1886.
54. Mazal PR, Haitel A, Windischberger C, et al. Spatial distribution of prostate cancers undetected on initial needle biopsies. Eur Urol. 2001;39:662.
55. Chang JJ, Shinohara K, Hovey RM, et al. Prospective evaluation of systematic sextant transition zone biopsies in large prostates for cancer detection. Urology. 1998;52:89.
56. Katsuto Shinohara VM, Chi T, Carroll P. Prostate needle biopsy techniques and interpretation. In: Voegelzang S, Shipley D, Linehan, editors. Genitourinary oncology. 3rd ed. Philadelphia: Lippincott; 2006. p. 111–9.
57. Djavan B, Remzi M, Marberger M. When to biopsy and when to stop biopsying. Urol Clin North Am. 2003;30:253.
58. Keetch DW, Catalona WJ, Smith DS. Serial prostatic biopsies in men with persistently elevated serum prostate specific antigen values. J Urol. 1994;151:1571.
59. Djavan B, Ravery V, Zlotta A, et al. Prospective evaluation of prostate cancer detected on biopsies 1, 2, 3 and 4: when should we stop? J Urol. 2001;166:1679.
60. Catalona WJ, Partin AW, Slawin KM, et al. Use of the percentage of free prostate-specific antigen to enhance differentiation of prostate cancer from benign prostatic disease: a prospective multicenter clinical trial. JAMA. 1998;279:1542.
61. Wang R, Chinnaiyan AM, Dunn RL, et al. Rational approach to implementation of prostate cancer antigen 3 into clinical care. Cancer. 2009;115(17): 3879–86.
62. Haese A, de la Taille A, van Poppel H, et al. Clinical utility of the PCA3 urine assay in European men scheduled for repeat biopsy. Eur Urol. 2008;54:1081.
63. Bott SR, Henderson A, McLarty E, et al. A brachytherapy template approach to standardize saturation prostatic biopsy. BJU Int. 2004;93:629.
64. Lane BR, Zippe CD, Abouassaly R, et al. Saturation technique does not decrease cancer detection during follow up after initial prostate biopsy. J Urol. 2008;179:1746.
65. Borboroglu PG, Comer SW, Riffenburgh RH, et al. Extensive repeat transrectal ultrasound guided prostate biopsy in patients with previous benign sextant biopsies. J Urol. 2000;163:158.
66. Stewart CS, Leibovich BC, Weaver AL, et al. Prostate cancer diagnosis using a saturation needle biopsy technique after previous negative sextant biopsies. J Urol. 2001;166:86.
67. Fleshner N, Klotz L. Role of "saturation biopsy" in the detection of prostate cancer among difficult diagnostic cases. Urology. 2002;60:93.
68. Pham KN, Porter CR, Odem-Davis K, et al. Transperineal template guided prostate biopsy selects candidates for active surveillance—how many cores are enough? J Urol. 2015;194(3):674–9.
69. Seles M, Gutschi T, Mayrhofer K, et al. Sampling of the anterior apical region results in increased cancer detection and upgrading in transrectal repeat saturation biopsy of the prostate. BJU Int. 2016;117(4): 592–7.
70. Mabjeesh NJ, Lidawi G, Chen J, et al. High detection rate of significant prostate tumours in anterior zones using transperineal ultrasound-guided template saturation biopsy. BJU Int. 2012;110(7): 993–7.
71. Magers MJ, Zhan T, Udager AM, et al. Clinicopathologic characteristics of anterior prostate cancer (APC), including correlation with previous biopsy pathology. Med Oncol. 2015;32(11):249.
72. Moran BJ, et al. Re-biopsy of the prostate with stereotactic transperineal technique. J Urol. 2006;176: 1376–81.
73. Ukimura O, Coleman JA, de la Taille A, et al. Contemporary role of systematic prostate biopsies:

indications, techniques, and implications for patient care. Eur Urol. 2013 Feb;63(2):214–30.
74. Ouzzane A, Puech P, Lemaitre L, et al. Combined multiparametric MRI and targeted biopsies improve anterior prostate cancer detection, staging, and grading. Urology. 2011;78:1356–62.
75. Pinto PA, Chung PH, Rastinehad AR, et al. Magnetic resonance imaging/ultrasound fusion guided prostate biopsy improves cancer detection following transrectal ultrasound biopsy and correlates with multiparametric magnetic resonance imaging. J Urol. 2011;186:1281–5.
76. Egawa S, Wheeler TM, Scardino PT. The sonographic appearance of irradiated prostate cancer. Br J Urol. 1991;68:172.
77. Whittington R, Broderick GA, Arger P, et al. The effect of androgen deprivation on the early changes in prostate volume following transperineal ultrasound guided interstitial therapy for localized carcinoma of the prostate. Int J Radiat Oncol Biol Phys. 1999;44:1107.
78. Kapoor DA, Wasserman NF, Zhang G, et al. Value of transrectal ultrasound in identifying local disease after radical prostatectomy. Urology. 1993;41:594.
79. Goldenberg SL, Carter M, Dashefsky S, et al. Sonographic characteristics of the urethrovesical anastomosis in the early post-radical prostatectomy patient. J Urol. 1992;147:1307.
80. Maatman TJ, Bigham D, Stirling B. Simplified management of post-prostate biopsy rectal bleeding. Urology. 2002;60:508.
81. Rodriguez LV, Terris MK. Risks and complications of transrectal ultrasound guided prostate needle biopsy: a prospective study and review of the literature. J Urol. 1998;160:2115.
82. Raaijmakers R, Kirkels WJ, Roobol MJ, et al. Complication rates and risk factors of 5802 transrectal ultrasound-guided sextant biopsies of the prostate within a population-based screening program. Urology. 2002;60:826.
83. Thompson PM, Pryor JP, Williams JP, et al. The problem of infection after prostatic biopsy: the case for the transperineal approach. Br J Urol. 1982;54:736.
84. Desmond PM, Clark J, Thompson IM, et al. Morbidity with contemporary prostate biopsy. J Urol. 1993;150:1425.
85. Moul JW, Bauer JJ, Srivastava S, et al. Perineal seeding of prostate cancer as the only evidence of clinical recurrence 14 years after needle biopsy and radical prostatectomy: molecular correlation. Urology. 1998;51:158.
86. Moul JW, Miles BJ, Skoog SJ, et al. Risk factors for perineal seeding of prostate cancer after needle biopsy. J Urol. 1989;142:86.
87. Bastacky SS, Walsh PC, Epstein JI. Needle biopsy associated tumor tracking of adenocarcinoma of the prostate. J Urol. 1991;145:1003.
88. Koppie TM, Grady BP, Shinohara K. Rectal wall recurrence of prostatic adenocarcinoma. J Urol. 2002;168:2120.
89. Hara N, Kasahara T, Kawasaki T, et al. Frequency of PSA-mRNA-bearing cells in the peripheral blood of patients after prostate biopsy. Br J Cancer. 2001;85:557.
90. Meng MV, Shinohara K, Grossfeld GD. Significance of high-grade prostatic intraepithelial neoplasia on prostate biopsy. Urol Oncol. 2003;21:145.
91. Oyasu R, Bahnson RR, Nowels K, et al. Cytological atypia in the prostate gland: frequency, distribution and possible relevance to carcinoma. J Urol. 1986;135:959.
92. Prange W, Erbersdobler A, Hammerer P, et al. Significance of high-grade prostatic intraepithelial neoplasia in needle biopsy specimens. Urology. 2001;57:486.
93. Davidson D, Bostwick DG, Qian J, et al. Prostatic intraepithelial neoplasia is a risk factor for adenocarcinoma: predictive accuracy in needle biopsies. J Urol. 1995;154:1295.
94. Lefkowitz GK, Sidhu GS, Torre P, et al. Is repeat prostate biopsy for high-grade prostatic intraepithelial neoplasia necessary after routine 12-core sampling? Urology. 2001;58:999.
95. Helpap BG, Bostwick DG, Montironi R. The significance of atypical adenomatous hyperplasia and prostatic intraepithelial neoplasia for the development of prostate carcinoma. An update. Virchows Arch. 1995;426:425.
96. Helpap B, Bonkhoff H, Cockett A, et al. Relationship between atypical adenomatous hyperplasia (AAH), prostatic intraepithelial neoplasia (PIN) and prostatic adenocarcinoma. Pathologica. 1997;89:288.
97. Iczkowski KA, Chen HM, Yang XJ, et al. Prostate cancer diagnosed after initial biopsy with atypical small acinar proliferation suspicious for malignancy is similar to cancer found on initial biopsy. Urology. 2002;60:851.
98. Iczkowski KA, MacLennan GT, Bostwick DG. Atypical small acinar proliferation suspicious for malignancy in prostate needle biopsies: clinical significance in 33 cases. Am J Surg Pathol. 1997;21:1489.
99. Alsikafi NF, Brendler CB, Gerber GS, et al. High-grade prostatic intraepithelial neoplasia with adjacent atypia is associated with a higher incidence of cancer on subsequent needle biopsy than high-grade prostatic intraepithelial neoplasia alone. Urology. 2001;57:296.
100. Park S, Shinohara K, Grossfeld GD, et al. Prostate cancer detection in men with prior high grade prostatic intraepithelial neoplasia or atypical prostate biopsy. J Urol. 2001;165:1409.
101. Javidan J, Wood DP. Clinical interpretation of the prostate biopsy. Urol Oncol. 2003;21:141.
102. Makhlouf AA, Krupski TL, Kunkle D, et al. The effect of sampling more cores on the predictive accuracy of pathological grade and tumour distribution in the prostate biopsy. BJU Int. 2004;93:271.
103. Wills ML, Sauvageot J, Partin AW, et al. Ability of sextant biopsies to predict radical prostatectomy stage. Urology. 1998;51:759.

104. Ravery V, Boccon-Gibod LA, Dauge-Geffroy MC, et al. Systematic biopsies accurately predict extracapsular extension of prostate cancer and persistent/recurrent detectable PSA after radical prostatectomy. Urology. 1994;44:371.
105. Badalament RA, Miller MC, Peller PA, et al. An algorithm for predicting nonorgan confined prostate cancer using the results obtained from sextant core biopsies with prostate specific antigen level. J Urol. 1996;156:1375.
106. D'Amico AV, Whittington R, Malkowicz SB, et al. Clinical utility of percent-positive prostate biopsies in predicting biochemical outcome after radical prostatectomy or external-beam radiation therapy for patients with clinically localized prostate cancer. Mol Urol. 2000;4:171.
107. Naya Y, Slaton JW, Troncoso P, et al. Tumor length and location of cancer on biopsy predict for side specific extraprostatic cancer extension. J Urol. 2004;171:1093.
108. Freedland SJ, Aronson WJ, Terris MK, et al. Percent of prostate needle biopsy cores with cancer is significant independent predictor of prostate specific antigen recurrence following radical prostatectomy: results from SEARCH database. J Urol. 2003; 169:2136.
109. Freedland SJ, Csathy GS, Dorey F, et al. Percent prostate needle biopsy tissue with cancer is more predictive of biochemical failure or adverse pathology after radical prostatectomy than prostate specific antigen or Gleason score. J Urol. 2002; 167:516.
110. Freedland SJ, Csathy GS, Dorey F, et al. Clinical utility of percent prostate needle biopsy tissue with cancer cutpoints to risk stratify patients before radical prostatectomy. Urology. 2002;60:84.
111. Elliott SP, Shinohara K, Logan SL, et al. Sextant prostate biopsies predict side and sextant site of extracapsular extension of prostate cancer. J Urol. 2002;168:105.
112. Brullet E, Guevara MC, Campo R, et al. Massive rectal bleeding following transrectal ultrasound-guided prostate biopsy. Endoscopy. 2000;32:792.

Pediatric Urologic Ultrasound

12

Lane S. Palmer and Adam Howe

Introduction

Ultrasound maintains its position as the primary imaging study of the genitourinary tract in children despite technological advances in computerized tomography (CT) and magnetic resonance imaging (MR). Some of the attributes of ultrasound that help to maintain this position include its ease and rapidity to perform, noninvasive nature, reproducibility, and its avoidance of ionizing radiation and sedation/general anesthesia. These are all important, particularly in the small child whose behavior may preclude a second chance to properly image the abnormality. The commonplace performance of prenatal ultrasound leads to the need for postnatal sonographic confirmation of possible urologic pathology. The other commonly ordered studies, voiding cystourethrography (VCUG), diuretic renography, CT, and MR are ordered mainly based upon the results of the ultrasound.

L.S. Palmer, M.D., F.A.C.S. (✉) • A. Howe, M.D.
Division of Pediatric Urology, Hofstra Northwell School of Medicine, Cohen Children's Medical Center of New York of the Northwell Health System, 1999 Marcus Avenue, M18, Lake Success, NY 11042, USA
e-mail: lpalmer@northwell.edu; adamo.howe@gmail.com

Ultrasound Performance in Children

Definitions and Scope

The kidney is just one component to be evaluated in sonogram of the retroperitoneum in children or in adults; the other components include adrenals, ureters (when visible), and any masses. Similarly, the bladder is one component of a pelvic ultrasound which also includes the surrounding organs such as the rectum, ovaries, and uterus. The scrotal ultrasound examination includes images of the testis, epididymis, and the spermatic cord.

The definitions of the complete and limited examinations are the same regardless of the age of the patient. The complete ultrasound of the retroperitoneum consists of a B-mode scan of the kidneys, abdominal aorta, common iliac artery origins, and inferior vena cava, including any abnormalities. The components of the complete ultrasound examination of the pelvis are gender specific and include uterus and adnexal structures, endometrium in girls, prostate and seminal in boys, and the bladder and any pelvic pathology in both sexes. In contrast, the limited examination assesses one or more elements but not all of the components of the complete examination or the reevaluation of one or more previously demonstrated abnormalities. An examination performed simply to determine a post-void volume is not considered a limited study and is often

P.F. Fulgham, B.R. Gilbert (eds.), *Practical Urological Ultrasound*, Current Clinical Urology,
DOI 10.1007/978-3-319-43868-9_12

performed with automated equipment for that specific purpose.

Indications

Ultrasound is the most common imaging study performed in the pediatric urinary tract. There are several indications for performing renal and bladder sonograms in children that can be further divided into investigative, screening, and surveillance indications (Table 12.1). Most commonly, ultrasound is the first imaging study of the child with a febrile UTI [1] or one with an abnormality noted on prenatal sonogram or in the boy with scrotal pain.

Table 12.1 Indications for ultrasound in children

Renal and bladder
• Urinary tract infection—febrile or recurrent nonfebrile
• Prenatal GU abnormality
• Voiding dysfunction
• Renal colic
• Palpable abdominal mass
• Single umbilical artery
• Hypertension
• Hematuria
• Proteinuria
• Azotemia
• Family history polycystic kidney disease
• Hemihypertrophy
• Urinary retention
• Syndrome associated with renal involvement (e.g., Tuberous sclerosis, CHARGE, VACTERL, WAGR)
• Surveillance of:
– Vesicoureteral reflux
– Nephrolithiasis
– Hydronephrosis
– Cystic renal disease
– Neurogenic bladder dysfunction (e.g., myelodysplasia)
– Obstructive uropathy (e.g., Posterior urethral valves)
Scrotal
• Palpable intrascrotal mass
• Acute scrotal pain
• Acute scrotal swelling
• Varicocele
• Testicular asymmetry

Technique

Kidneys: The kidneys are imaged in both longitudinal and transverse planes with the child primarily in the supine position. If the child is able to follow commands, the kidneys are best imaged with the child making a deep inspiration pushing the kidney caudally below the ribs. If the child cannot follow commands, the images might be better obtained with a bolster placed under the flank or with the child turned on the side and the arm raised above the head to open up the space between the ribs and the iliac crest allowing better access to the kidney. Images must be taken with the child in the prone position for better visualization of the kidney between the ribs. The right kidney is imaged along the anterior axillary line using the liver as an acoustic window while the left kidney is imaged along the posterior axillary line using the spleen as an acoustic window. Imaging is done with a curved linear array probe. For children under age 18 months or so, a 6–12 MHz probe is used while older children are better imaged using a 3.5–5 MHz probe.

Bladder: The bladder is imaged with the child in the supine position using a curved array probe (7.7–11 MHz for children under 18 months or 3.5–5 mHz for older children) which makes small skin contact and is easy to angle to gather the most information. The sonographer performs the study in both the transverse and longitudinal directions with the bladder at least partially filled looking for a normal bladder and surrounding organs and documenting any luminal, intraluminal, or extraluminal abnormalities. The transverse images are taken moving from the pubis to the umbilicus in 1–2 cm intervals while the longitudinal images are taken moving from the midline in either direction in 1–2 cm intervals. Measurements are made in the transverse plane measuring the height and width of the urine within the bladder and then the length in the sagittal plane. These three measurements are multiplied together and then multiplied by 0.65 [2] to calculate the bladder volume. Efflux of urine from the ureteral orifices can be demonstrated by applying the Doppler mode over the appropriate location on the bladder floor.

Scrotum: Ultrasound imaging of the scrotum is performed with the child supine and the scrotum supported by a folded towel placed between the thighs. In older children and adolescents, the penis position is maintained suprapubically with a second towel or held in position by the patient. Scanning should be performed with 7–18 MHz high-frequency linear array transducer. Both testes and epididymides should be compared for size, echogenicity, masses, and vascularity and imaged in both the transverse and longitudinal axes. Spectral Doppler analysis of the intratesticular vasculature of both testes is performed when indicated. In patients presenting with acute scrotum, the asymptomatic side should be scanned first so that grayscale and color Doppler gain settings are set optimally to obtain a baseline for comparison with the affected side. In the presence of a suspected varicocele, having the child perform the Valsalva maneuver or placing the child in the upright position can improve the evaluation of venous distention.

Documentation

The documentation of the ultrasound examination should be as complete and systematic as the examination itself. Mention should be made of normal and abnormal findings. All measurements that were taken should be documented. An example of some components of documentation of the kidneys, bladder, and scrotum is shown in Table 12.2.

Table 12.2 Documentation of ultrasound examination

Kidneys:						
Size:	_____ x_____x_____					
Abnormal location	No	Pelvic	Horseshoe			
Hydronephrosis	No	Grade	1	2	3	4
Malrotated	No	Yes				
Duplication	No	Yes				
Proximal ureteral dilation	No	Yes				
Cortical thinning	No	Yes				
Abnormal cortical echotexture	No	Yes				
Cortical cyst	No	Size____mm UP___MP___LP___				
Stones	No	Size____mm UP___MP___LP___				
Mass	No	Yes				
Bladder:						
Pre-void volume	_____cc	Post-void volume		_____cc		
Thickened bladder		No	Yes			
Distal ureteral dilation		No	Yes			
Bladder mass		No	Yes			
Pelvic mass		No	Yes			
Bladder stones		No	Yes			
Scrotal:						
Right Left						
Testis size: _____ x_____x_____						
Testis mass	No	Yes	____ mm Location_____			
Microcalcifications	No	Yes				
Varicocele	No	Yes	_____mm			
Epididymal cyst	No	Yes	_____mm			
Hernia	No	Yes				
Hydrocele	No	Yes				

Kidney

Normal Anatomy

The proper evaluation of kidney assesses the location, orientation, axis, size, echogenicity of the parenchyma and the integrity of its contour, the nature of the central echogenic focus, and the absence of a visible proximal ureter (Fig. 12.1).

Normal kidneys lie in the retroperitoneum along the psoas, orientated parallel to it; both are oblique such that the upper pole of the kidney is posterior to the lower pole. The size of the kidney is age-dependent and is determined by measuring the distance between the two poles and compared to published nomograms [3]. From a sonographic perspective, the most important neighbor is the anterior relationship to the liver on the right side and the spleen on the left side. During the first several months of life, the echogenicity of the renal parenchyma may be isoechoic or hyperechoic in comparison to the adjacent liver or spleen and then becomes hypoechoic in comparison.

The renal cortex can be distinguished from the medulla by the presence of a line, reflecting the subtle differences in echogenicity. The presence of this corticomedullary differentiation is an indicator of normal architecture and a marker of parenchymal integrity.

The contour of the pediatric kidney can be smooth but is often lobulated. The lobes of parenchyma consist of a central pyramid covered by cortical parenchyma and the Columns of Bertin are located between these pyramids. The lobulated appearance regresses with time and the contour becomes smooth.

The renal pyramids are seen as hypoechoic areas radially distributed surrounding the central echogenic focus (CEF) that are most commonly seen in infants and also regress with time. The CEF consists of the renal pelvis, hilar vasculature and lymphatics, and sinus fat (accounting for its hyperechoic appearance). In the sagittal plane, there is ordinarily a single CEF surrounded by a symmetric thickness of parenchyma. The CEF should be collapsed upon itself unless it is distended with urine and the walls of the renal pelvis separate. The proximal ureter should ***not*** normally be visible on sonogram.

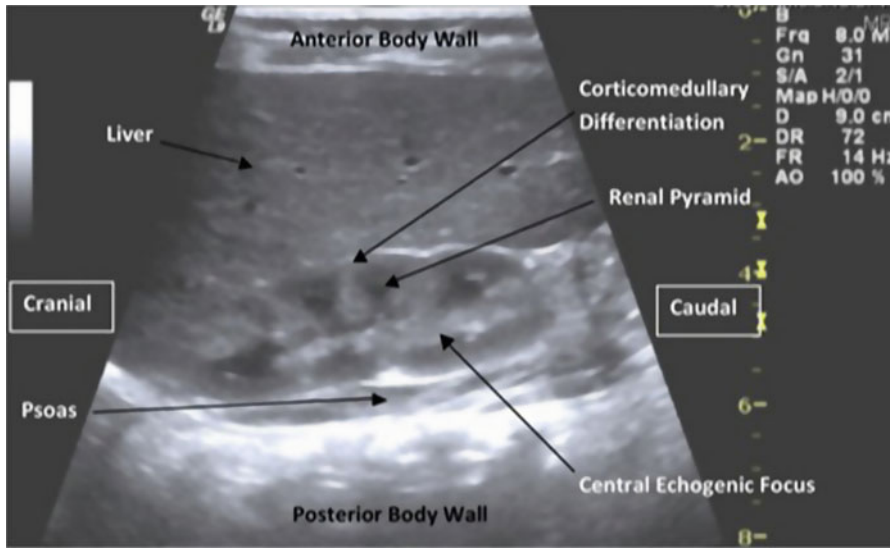

Fig. 12.1 Sagittal view of a normal kidney demonstrating a normal position in the flank and a normal axis, with good corticomedullary differentiation, a collapsed central echogenic focus, and hypoechoic pyramids oriented radially about the perimeter

Renal Anomalies

Anomalies or abnormalities of the kidneys in children can be described developmentally as either congenital or acquired and then again anatomically by number, location, vascular, parenchymal, and collecting system.

Unilateral Renal Agenesis (Fig. 12.2)

Unilateral renal agenesis is most commonly detected in children during imaging performed (1) prenatally, (2) for a urinary complaint, (3) during screening for associated anomalies, or (4) incidentally during evaluation of unrelated conditions. On ultrasound, the renal fossa is empty of a reniform structure and may instead be occupied by bowel. Otherwise the surrounding organs are normal in appearance. It is important that the person performing the study then scans the pelvis to determine if the kidney is ectopic in position. In infants, the adrenal will be prominent and in the normal anatomical position. The remaining kidney will be large reflecting compensatory hypertrophy. The diagnosis can be confined by nuclear scintigraphy (DMSA), MR, or CT; although Krill et al. found that measuring the polar size of the kidney on ultrasound offers sufficient accuracy in predicting a solitary kidney [4]. VCUG is indicated because of the significant incidence of vesicoureteral reflux in the remaining renal unit [5].

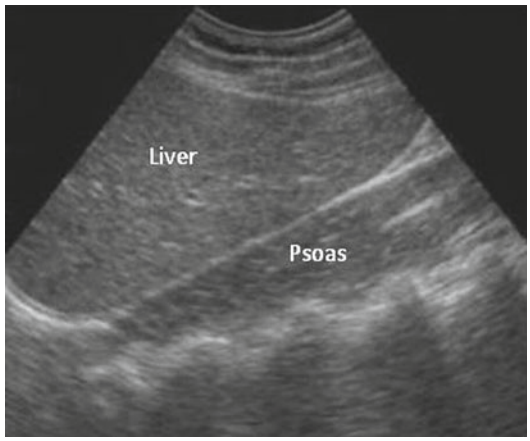

Fig. 12.2 An empty renal fossa demonstrating the psoas muscle posterior and the normal liver anterior and superior

Renal Ectopia

Kidneys begin their embryologic journey in the bony pelvis with the renal pelvis oriented anteriorly and then reach the renal fossa and finish their medial rotation by the ninth week of gestation. However, this process may abort anywhere along the course of ascent. Similarly, the metanephric blastema may cross over to the contralateral side and may attach to the other metanephric blastema (crossed-fused ectopia).

A normal appearing reniform kidney may be seen in the pelvis behind the bladder (Fig. 12.3). However, because of the associated malrotation of a pelvic or crossed (fused, non-fused) kidney, the cortex may appear variable in echogenicity and in corticomedullary differentiation. Also, or for the same reason, measurement of polar length may be artificially small.

The horseshoe kidney is the most common fusion anomaly in children (Fig. 12.4). This may be suspected when both malrotated kidneys are positioned caudal to their usual position. Horseshoe kidneys are at risk for UPJ obstruction and Wilms' tumor and these may be detected easily by ultrasound. The isthmus between the two kidneys may be thick on ultrasound; function of the isthmus can be evaluated by nuclear scintigraphy.

Renal Vein Thrombosis

Ultrasound is well suited for evaluating the kidney with suspected renal vein thrombosis. Risk factors for renal vein thrombosis include dehydration, traumatic delivery, and sepsis. During the acute phase, during which there is considerable edema, ultrasound will demonstrate an enlarged kidney with loss of corticomedullary differentiation (Fig. 12.5). The parenchyma is hypoechoic early in the process due to edema but

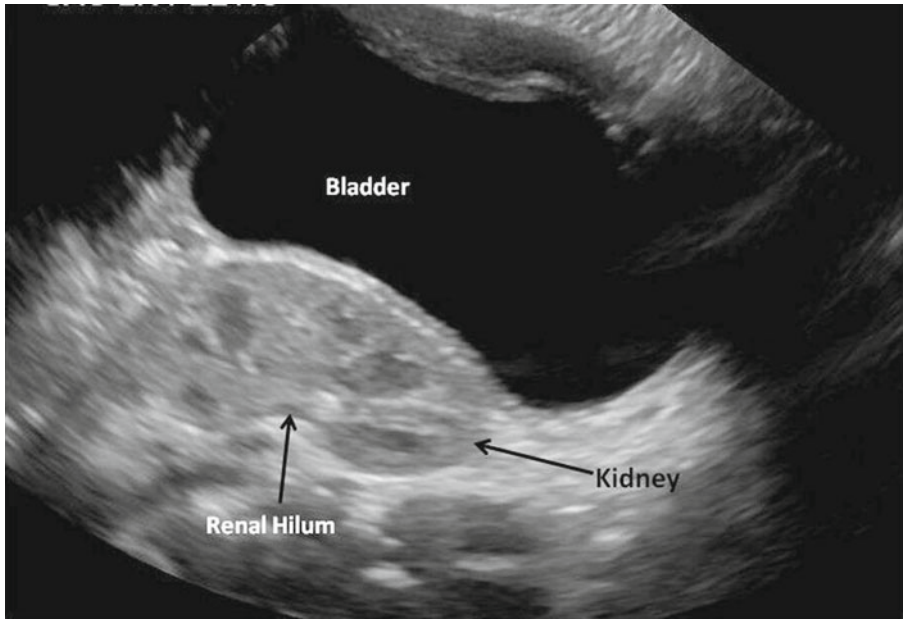

Fig. 12.3 The presence of an ectopic kidney in the pelvis situated posterior to the urinary bladder. The kidney has normal contour and echogenicity but is malrotated due to incomplete medial rotation during ascent

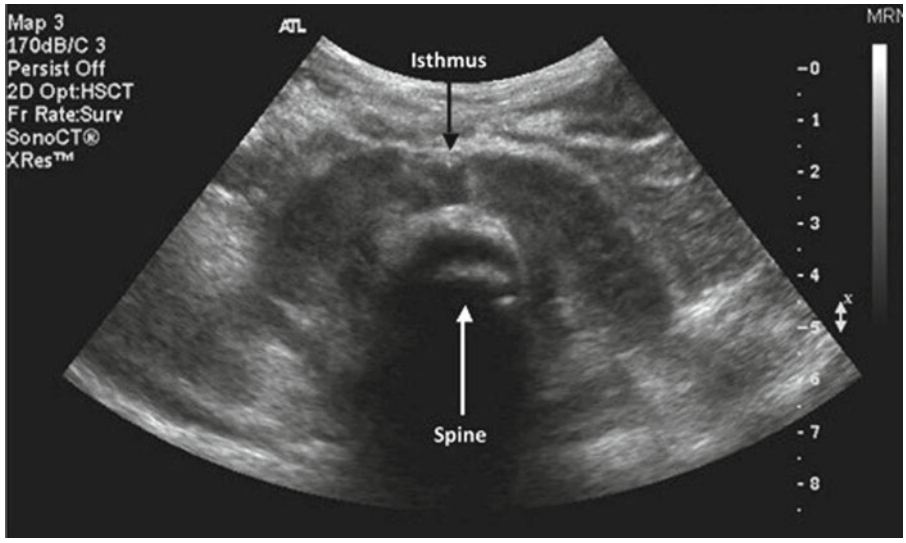

Fig. 12.4 Transverse view demonstrating the caudal location of malrotated and fused kidneys, i.e., a horseshoe kidney. The isthmus is identified in the midportion of the kidney and the spine located posteriorly

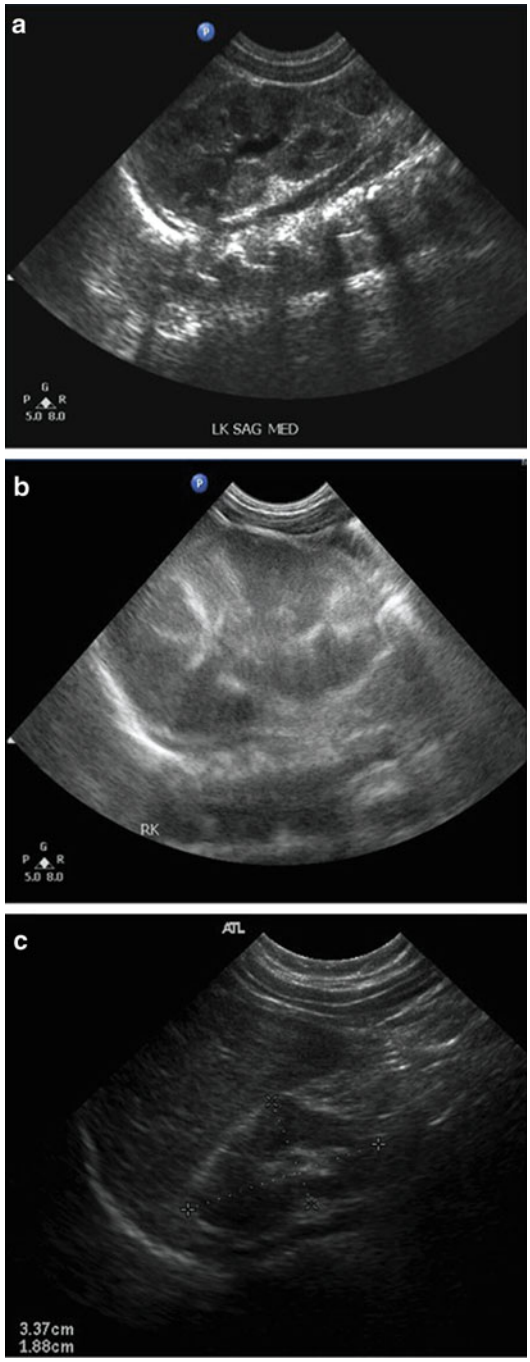

Fig. 12.5 Sequence of renal sonograms from a neonate with renal vein thrombosis. (**a**) Sagittal view of the left kidney demonstrating normal echogenicity and pyramids with grade 1 hydronephrosis. (**b**) Sagittal view of the right kidney taken at the same time as (**a**) demonstrates a larger kidney with poor corticomedullary differentiation. (**c**) Six months later, the left kidney has become atrophic and continues to have poor corticomedullary differentiation

becomes hyperechoic as fibrosis sets in. Thrombi in smaller vessels are seen as radiating linear echogenic bands in the parenchyma. At later phases, atrophy will be seen as well as calcifications in the area of the thrombi. Venous flow is absent when Doppler is applied.

Infection and Scarring (Fig. 12.6)

Urinary tract infections are a leading indication for ordering renal ultrasound in children. The spectrum of the clinical presentation of UTIs is variable and often matches the ultrasound findings. In many cases, the sonogram of the kidneys and bladder are completely normal. In some cases, all is normal except for some self-limited mild hydronephrosis or hydroureter as a result of the dilating effect of bacteria-released endotoxins. When there is diffuse pyelonephritis, the kidney will be enlarged and hypoechoic (either diffusely or multifocal) with loss of corticomedullary differentiation.

Following a pyelonephritic episode, particularly when associated with vesicoureteral reflux, the healing parenchyma may leave a scar. The scar needs to be large to be detected on ultrasound: the indented contour in the area(s) of scar reflecting cortical loss. This contraction of parenchyma may be focal or in severe cases involves the entire kidney. In such cases, the size of the kidney will also contract. One needs to avoid confusing these scars with persistent fetal lobulations. Scarring typically occurs *over* calyces (the point of retrograde entry of bacteria to the parenchyma) while the contour indentations associated with fetal lobulations are *between* the calyces (reflecting the adjacent lobes of renal development) (Fig. 12.7).

Renal Cystic Diseases

There are several conditions in which renal cysts are prominent. The more important ones in children are Multicystic Dysplastic Kidney, and Polycystic Kidney Disease (both autosomal recessive and autosomal dominant).

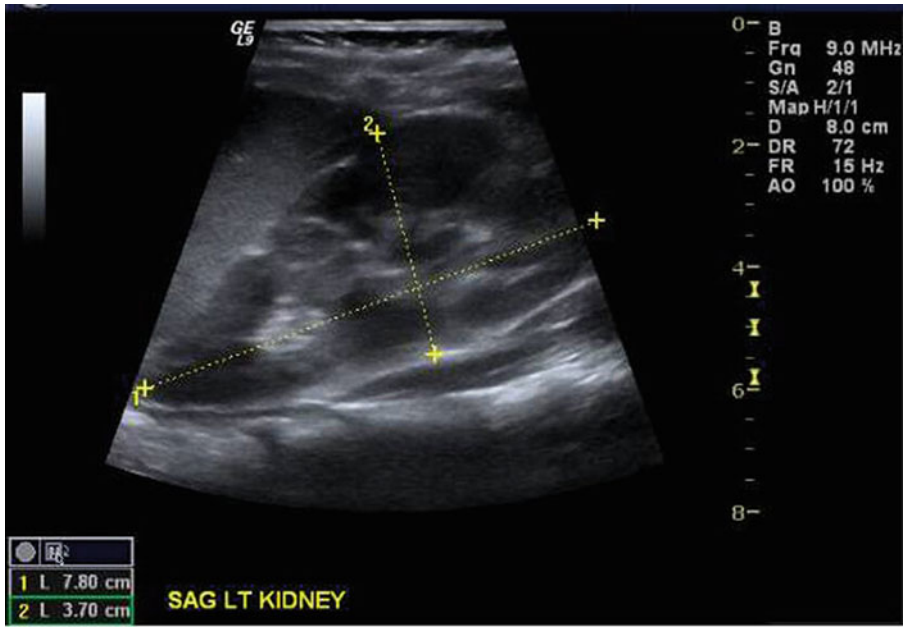

Fig. 12.6 Sagittal view of the kidney of a hospitalized, febrile (103.4 °F), 3-year-old girl whose catheterized urine culture grew 100,000 E. Coli. The kidney is enlarged (7.8 cm) and has disturbed echogenicity due to edema and inflammation

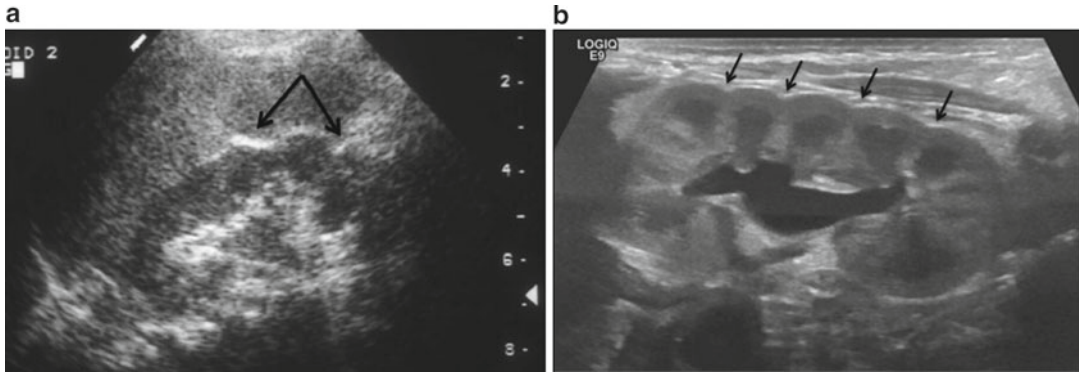

Fig. 12.7 (**a**) Sagittal view of the right kidney of a child with a history of febrile urinary tract infections. Scarring is identified in the upper pole of the kidney (*black arrows*). (**b**) Comparison sonogram demonstrating indentations of the renal contour (*black arrows*) that represent fetal lobulations positioned between the pyramids and not over the calyces

Multicystic Dysplastic Kidney (MCDK): The classic ultrasound findings are those of multiple noncommunicating cysts of variable size (Fig. 12.8). The largest cysts are located in the periphery of the kidney thus helping to distinguish this from severe hydronephrosis where the larger hypoechoic areas are located centrally. However, despite this difference, it may be very difficult to distinguish between the two entities. There is a paucity of renal parenchyma in the MCDK which has minimal to no function as documented by nuclear scintigraphy. The natural history of a MCDK is involution with subsequent contraction or even disappearance of the kidney as followed by ultrasound. Associated contralateral renal abnormalities may be seen in about 40 % of the cases and vesicoureteral reflux may be present in the stump of the MCDK or in the contralateral kidney; therefore, VCUG is indicated [6].

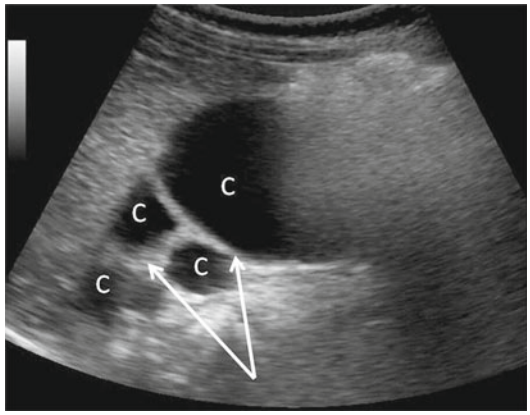

Fig. 12.8 Multicystic dysplastic kidney with multiple sized anechoic areas of variable sizes without identifiable parenchyma in the periphery and hyperechoic parenchyma (*arrows*) between the cysts (C)

Polycystic Kidney Disease (Fig. 12.9)

The genetics of the two diseases are self-evident in their names and their clinical courses are different. The ultrasound features of autosomal recessive polycystic kidney disease (ARPCKD) type include extremely large, reniform kidneys that are homogeneous and hyperechoic. The multiple reflective interfaces of the ectatic dilated renal tubules cause the characteristic hyperechoic appearance. Autosomal dominant polycystic kidney disease (ADPCKD) demonstrates bilateral multiple renal cysts of variable size. At the youngest ages, the cysts are fewer in number and the renal parenchyma relatively normal with respect to corticomedullary differentiation and echogenicity. However, with time, the cysts grow in size and number leading to compression of the renal parenchyma and possible distortion of the renal pelvis.

Renal Tumors

Mesoblastic nephroma and Wilms' tumor (Fig. 12.10) are the more important solid renal masses in children. The benign mesoblastic nephroma is the most common solid renal mass in children under 3 months while the malignant Wilms' tumor is the most common solid renal mass in childhood. They commonly present as abdominal or flank masses and their ultrasound features are similar. These are heterogeneous intrarenal masses of variable size that are mainly solid and hyperechoic but areas of necrosis and hemorrhage lead to areas that are hypoechoic. Cystic variants of Wilms' tumor will demonstrate anechoic areas. Hydronephrosis may be present with either mass. The contralateral kidney may demonstrate involvement in Wilms tumor. Tumor thrombus may be present in the renal vein.

Stones

Urolithiasis is not unique to children and has the same features as in adults. Stones are detected as hyperechoic foci with posterior shadowing; the shadowing distinguishes the stone from fat or blood vessels. The axial resolution of ultrasound allows for its detection of medium sized or large stones; sometimes an apparently single stone is actually 2 or more smaller stones in close proximity. Hydronephrosis proximal to the stone can be seen.

Hydronephrosis

Dilation of the renal pelvis goes by a variety of monikers: pyelectasis, pelviectasis, pelvis dilation, and hydronephrosis. Regardless of the name, renal pelvic dilation is the most common ultrasound abnormality of the kidney seen prenatally or postnatally [7]. Prenatally, dilation of the renal pelvis is measured in millimeters in the anteroposterior dimension; the risk of a significant uropathy increases with the age of gestation [8] or size of the pelvis [9]. Postnatally, hydronephrosis is divided into grades using systems such as that outlined by the Society for Fetal Urology (Fig. 12.11). By the SFU system, the lowest grade of hydronephrosis refers to slight pelvic dilation and the highest grade refers to extension of the dilatation into the calyces and the presence of renal parenchymal thinning [10].

Hydronephrosis may be primary or secondary and either obstructive or nonobstructive. VCUG and/or diuretic renography help to define the nature of the hydronephrosis. In contrast to higher grades of hydronephrosis, milder grades (1-2) are unlikely to be obstructive. The most

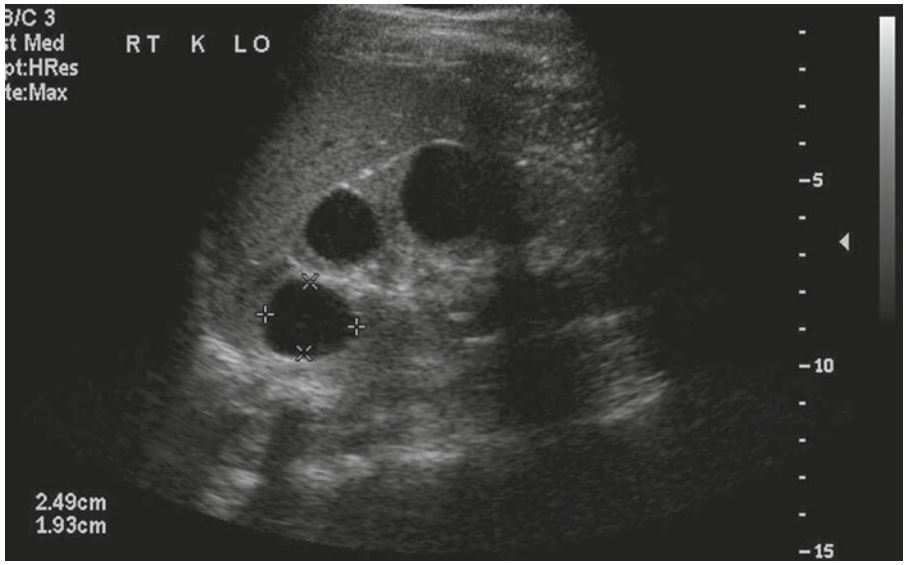

Fig. 12.9 Sagittal view of a renal ultrasound of a teenager with ADPCK demonstrating replacement of the renal parenchyma with several cysts of variable size

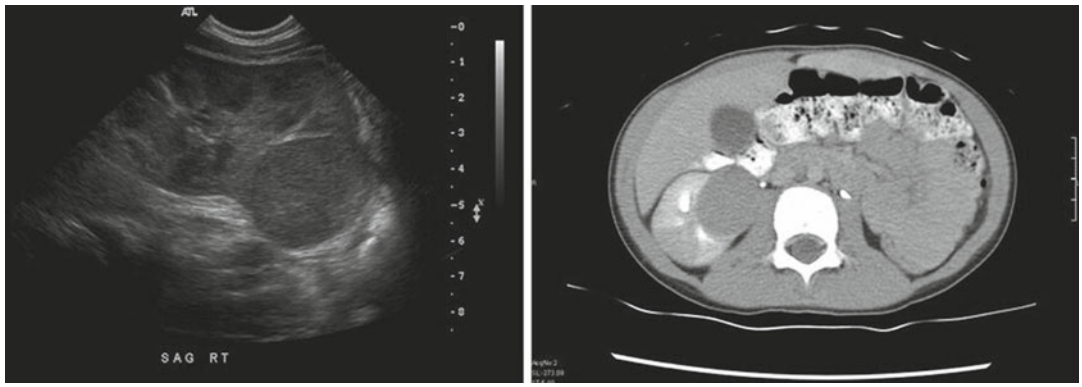

Fig. 12.10 Sonogram and corresponding CT of a 2-year-old child with a right sided Wilms' tumor. The lower pole exophytic mass is seen as a homogeneous mass in this case. However, other cases may demonstrate a heterogeneous mass reflecting bleeding and necrosis replacing the majority of the renal parenchyma

common cause of obstruction is at the ureteropelvic junction either due to a congenital intrinsic narrowing or from a lower pole vessel crossing anterior to the ureter. When UPJ obstruction is suspected, the ultrasound will demonstrate a large centrally located hypoechoic area (renal pelvis) extending into and blunting the calyces (grade III). As mentioned above, if the renal parenchyma is compressed and thinned compared with the contralateral kidney, this constitutes grade IV hydronephrosis and is likely due to obstruction. In cases of intermittent obstruction, the SFU grade of hydronephrosis may be lower than expected [11]. The diagnosis of obstruction is only suspected by ultrasound but not made without the adjuvant use of other provocative studies such as furosemide nuclear scintigraphy, magnetic urography, or even retrograde pyelogram or excretory urography (Case Study 1).

The invasive nature of these provocative studies has led to a search for ultrasound features that may imply or define obstruction. The presence of

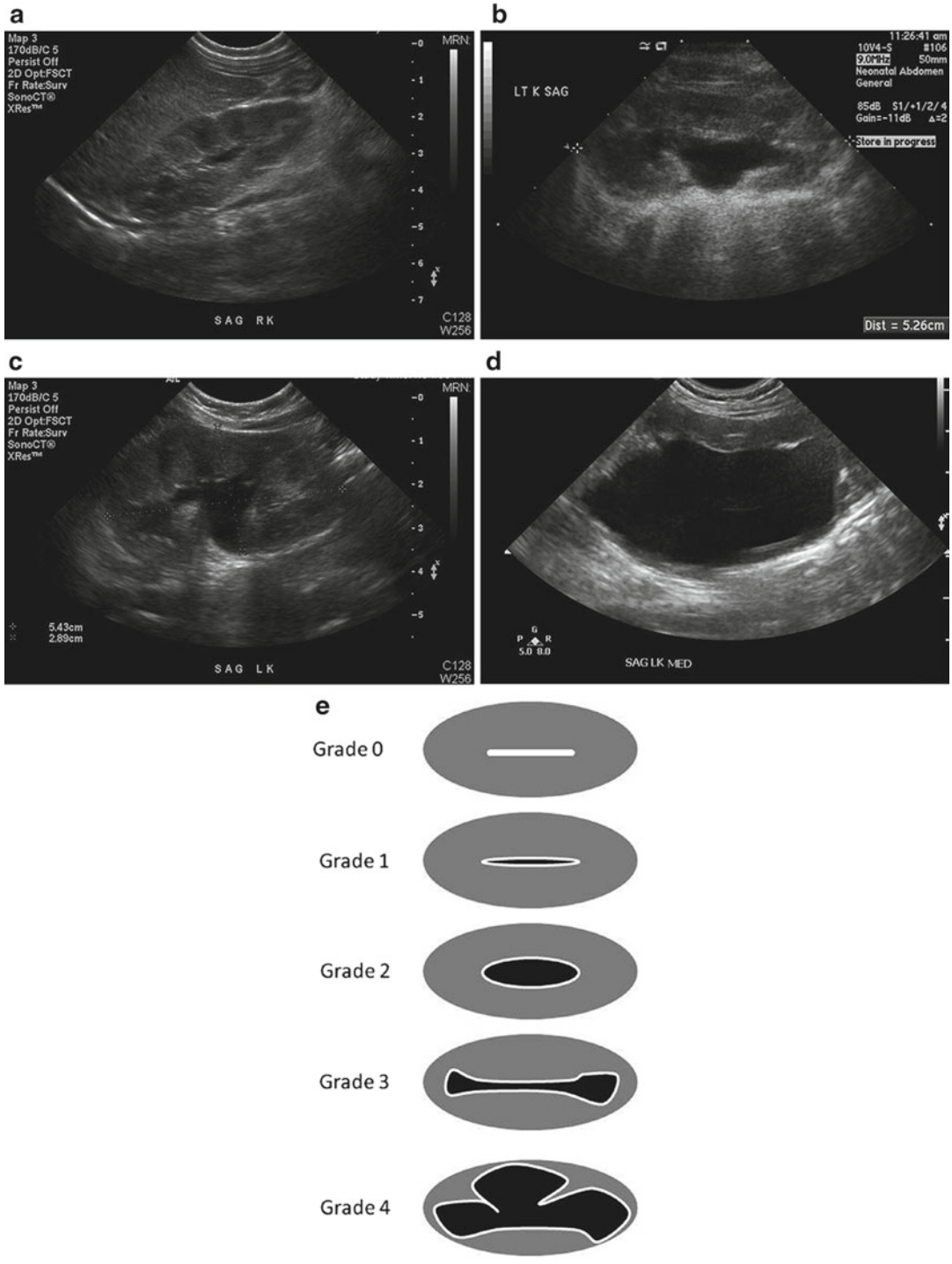

Fig. 12.11 Society for Fetal Urology grading system: (**a**) 1—mild pelvic dilation, (**b**) 2—moderate pelvic dilation, (**c**) 3—dilation extending into the calyces and normal parenchyma; (**d**) 4—calyceal dilation and thinning of the parenchyma compared to the contralateral kidney; (**e**) a schematic representation of these grades is depicted for comparison with the images above

ureteral jets seen during Doppler ultrasound of the bladder may aid in ruling out complete obstruction [12]; however, ureteral jets are not always identified during studies of even normal kidneys. Measuring the intrarenal impedance of the arcuate and interlobar arteries on Doppler ultrasound has been studied for differentiating renal obstruction from nonobstruction. The resistive index (RI) is calculated as (peak systolic velocity − peak diastolic velocity)/peak systolic velocity. Technically, this is measured after adequate hydration, and is calculated as the mean of at least three measurements [13]; most ultrasound units contain software to calculate this automatically [12]. Some authors advocate an RI ≥ 0.70 as obstructive [12, 14] while other have found significant variation of RI ranges (0.34–0.94) in children with normal kidneys, leaving this finding of questionable clinical utility [15]. RI can also vary with age leading to the use of the resistive index ratio (RIR), comparing RI in the right and left kidneys with a cutoff of 1.10 (sensitivity >90 %, specificity >80 %), which can be more helpful in cases of suspected unilateral obstruction [13, 14]. However, RIR was also noted to be variable in non-hydronephrotic kidneys [15] and not helpful in differentiating acute (calculus) from chronic obstruction (ureteropelvic junction obstruction), or ruling out intravascular disorders [12, 13].

Acoustic radiation for impulse (AFRI) elastography is an ultrasound-based technology that evaluates wave dispersion and tissue stiffness. The pulse generates shear waves within the kidney aimed at the central renal parenchyma between the capsular surface and collecting system. Shear wave velocities (SWV) are measured in at least the upper, middle, and lower poles and the mean is calculated [16, 17]. Most studies fail to demonstrate a relationship between the AFRI and obstructive hydronephrosis, as well as mixed results seen when assessing for renal damage (i.e., tissue stiffness from fibrosis from scarring) with vesicoureteral reflux disease [16–18]. One study found hydronephrotic kidneys to have high SWV compared to non-hydronephrotic kidneys; however, there was no difference in etiologies of obstruction vs. nonobstruction [19]. Therefore, ARFI elastography still needs maturation refining before it can be considered a useful clinical modality.

Collecting System Duplication

The presence of a duplicated collecting system is very common [20]. Most duplication anomalies are inconsequential and are discovered incidentally on prenatal ultrasound or later when ultrasound is performed for urologic or non-urologic reasons. However, some duplication anomalies can be clinically significant such as in cases of ureterocele and ectopic ureters that are associated with the upper pole moiety and ureteropelvic junction obstruction and reflux that are associated with the lower pole moiety. These significant duplications may be detected prenatally or after their clinical presentation leads to the performance of an ultrasound.

The ultrasound must include the kidney and the bladder to best document the nature of the duplication. In the simplest case, there are two central echogenic foci separated by a bar of renal parenchyma isoechoic to the rest of the normal parenchyma, no hydronephrosis, and the proximal ureters are not identifiable (Fig. 12.12). The bladder is normal in thickness and contour without any defects within it and the distal ureters are not visible. In the more complex cases, ultrasound identifies hydronephrosis in either upper or lower pole moieties, dilation and possible tortuosity of the proximal and/or distal ureters, upper pole scarring or dysplasia (shrunken hyperechoic

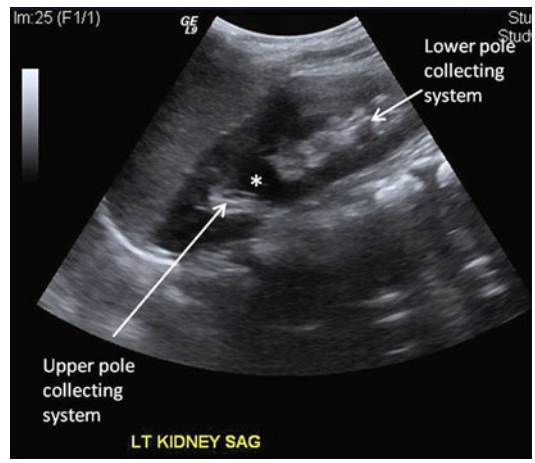

Fig. 12.12 Renal duplication. Sagittal ultrasound demonstrating two central echogenic foci separated by a bar of normal renal parenchyma (*)

region), or ureterocele. VCUG and diuretic renogram supplement the ultrasound in better defining the complete anomaly.

Bladder

Normal Bladder

The bladder should be smooth in contour and thin walled. In general, thickened bladders reflect bladder outlet obstruction as seen in neurogenic states or posterior urethral valves; however, bladder wall thickness is of arguable clinical value. The urine will be hypoechoic and there should be an absence of debris, masses, or significant postvoid residual urine. The area inferior to the bladder contains the rectum and the presence of stool should be noted (Fig. 12.13a–c).

Bladder Anomalies

Ureterocele

Ureteroceles have a variable effect on the urinary tract and thus on the findings at ultrasound. Bladder ultrasound is most effective in making the radiographic diagnosis of ureterocele [21]: a round thin-walled cystic structure at the bladder base perhaps with the dilated ureter leading into it. An everting ureteroceles may be confused for bladder diverticulum [22]. Hydroureter is present when the ureterocele delays the passage of urine or is associated with reflux. The contralateral ureter may also be dilated when the ureterocele encroaches upon the contralateral orifice retarding the passage of urine, or undermines the antireflux mechanism, or causes obstruction of the bladder neck. The renal ultrasound may demonstrate a single system (males more likely) or a duplicated system (females more likely). Hydronephrosis of variable grade may be seen ipsilateral and/or contralateral to the kidney with the ureterocele (Case Study 2).

Vesicoureteral Reflux

Vesicoureteral reflux is the most common anomaly detected following abnormal prenatal renal ultrasound or after a urinary tract infection. Ultrasound may demonstrate variable degree of hydronephrosis or hydroureteronephrosis. However, the grade of hydronephrosis does not necessarily correlate with the grade of vesicoureteral reflux (Fig. 12.14) [23]. Notwithstanding this fact, renal ultrasound is often used to screen older siblings of probands with reflux. When reflux is associated with renal scarring, ultrasound can document advanced scarring where irregular renal contour, loss of corticomedullary differentiation, or a shrunken kidney. Scarring is best documented by areas of decreased uptake during nuclear scintigraphy (DMSA). Ultrasound may be useful as a postoperative study to document that the kidneys appear the same as the preoperative images [24].

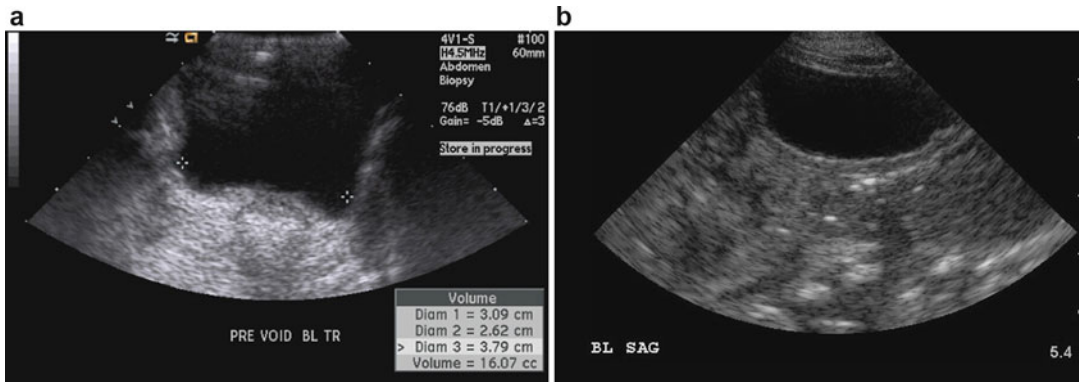

Fig. 12.13 Pre- and post-void images of a normal bladder. (**a**) Demonstrates transverse and sagittal images of a thin-walled bladder without debris, intraluminal or extraluminal abnormalities. (**b**) The bladder empties its volume to completion and stool is seen in the rectal vault

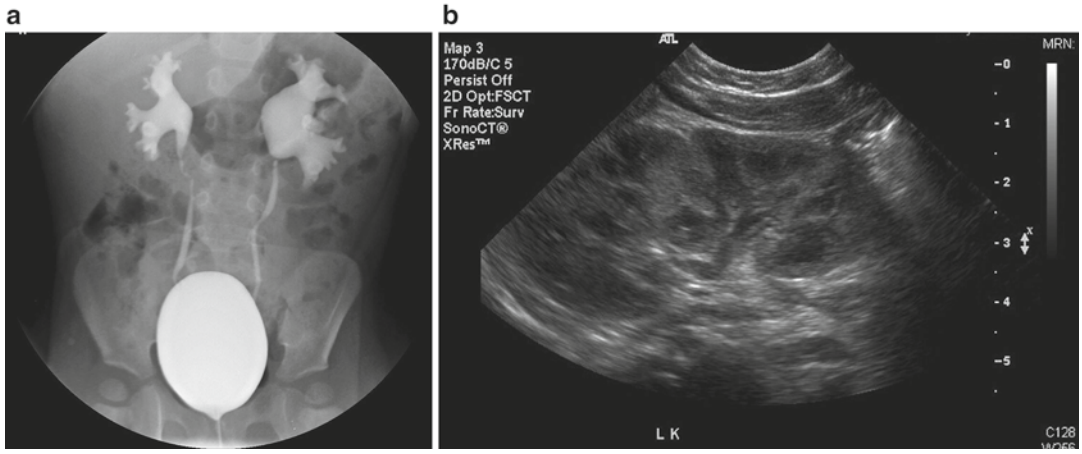

Fig. 12.14 VCUG from a young child with bilateral vesicoureteral reflux, Grade 3 on the *right* and grade 4 on the *left* (**a**). The sonogram of the kidneys was completely normal as seen here of the left side, the side with the higher grade of reflux (**b**)

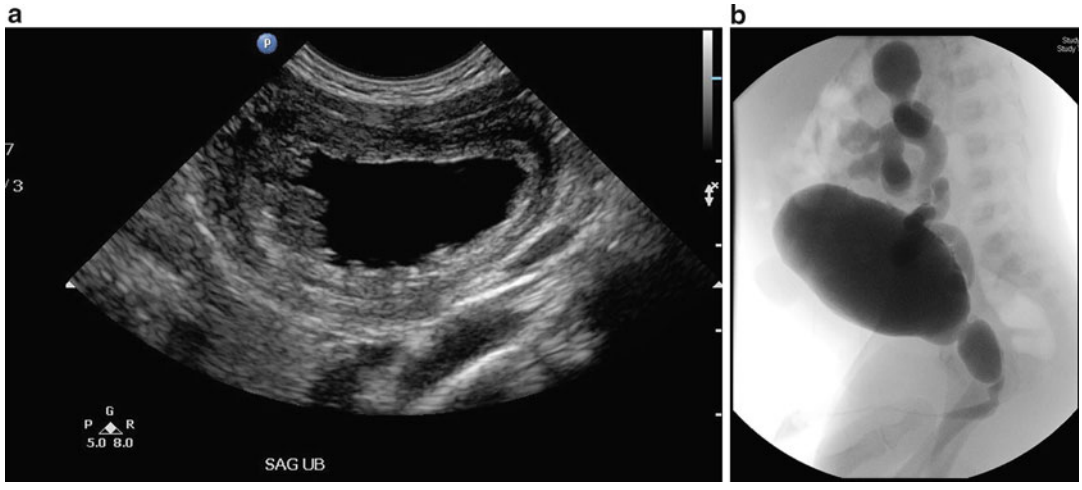

Fig. 12.15 Neonate with posterior urethral valves confirmed and treated cystoscopically. This transverse sonographic image of the bladder highlights the much thickened muscular wall (**a**). Other features included a dilated posterior urethra and bilateral hydroureteronephrosis. The VCUG shown demonstrates irregular shaped bladder with dilated posterior urethra and sudden change in caliber at the location of the valve and high grade vesicoureteral reflux (**b**)

Posterior Urethral Valves

Posterior urethral valves are not diagnosed by ultrasound but the effect of the valves on the bladder, ureters, and kidneys can be detected and can be profound. Bladder wall thickening may be seen reflecting detrusor hypertrophy. Dilation of the ureters is variable and may be present due to the obstructive phenomena and/or vesicoureteral reflux. When present, hydroureters may be seen distally as hypoechoic areas posterior to the bladder and may be traced proximally, in severe cases, to the ureteropelvic junction. At the level of the kidney, hydronephrosis of all grades may be seen. In the presence of renal damage, the parenchyma may be hyperechoic and thinned with the loss of corticomedullary differentiation, or cystic changes. When suspected on prenatal ultrasound, oligohydramnios and a dilated prostatic urethra may be present in addition to the above findings [25] (Fig. 12.15a, b).

Neurogenic Bladder

The sonographic images of urinary tract of children with neurogenic bladders are similar to those seen in posterior urethral valves. Ultrasound will often demonstrate bladder wall thickening, associated hydronephrosis or hydroureteronephrosis due to reflux or high bladder pressures. Ultrasound studies in both conditions will provide information regarding the post-void residual and thus the bladder's ability to empty. As in posterior urethral valves, there is spectrum of effect on the urinary tract and the findings outlined above may be seen to varying degrees.

Scrotum

The details of scrotal ultrasound and varicoceles will be discussed in greater detail in Chap. 8. However, it is important to outline the findings associated with the more common scrotal pathologies in children.

Undescended Testis

Ultrasound is of limited utility for the evaluation of cryptorchidism. Since a majority of undescended testes are located in the inguinal canal, high-frequency (18 mHz) linear array transducers are often able to identify gonads in this location. The presence or absence of a testis on sonogram should only confirm the findings at physical examination. The features of the testis would be similar to that of the normally descended testis unless atrophy has occurred. In these cases, the testis size is smaller and the parenchyma is hyperechoic.

Hydrocele

Hydroceles in children are commonly communicating with the abdomen via a patent processus vaginalis; otherwise they are isolated from the abdomen and surround the testes. The diagnosis is typically one based on history and physical examination. However, ultrasound can be a useful adjunct in which there is an anechoic fluid collection located in the anterolateral position of the affected hemiscrotum (Fig. 12.16). Long-standing hydroceles may become septated and proteinaceous debris found in the hydrocele fluid. Septations appear on sonogram as hyperechoic linear or curvilinear areas separating the hypoechoic or anechoic fluid while the debris appears as scattered punctuate hyperechoic structures within the fluid. Large communications with the abdomen may be seen as the probe is moved proximally within the inguinal canal as a fluid-filled anechoic tubular structure.

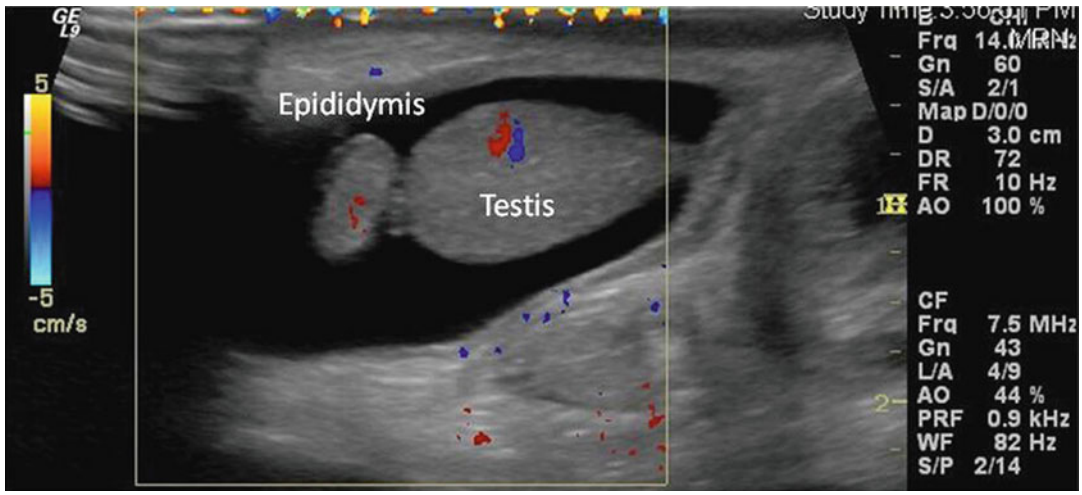

Fig. 12.16 Sagittal view of a scrotal ultrasound from a neonate with a nonpalpable right testis. The testis was identified in the scrotum with adequate blood flow documented by Doppler. The difficulty in palpating the testis stemmed from the large surrounding hydrocele (anechoic area surrounding the testis)

Disorders of Sexual Differentiation

In the child with ambiguous genitalia, the goal of imaging is to identify gonads and Müllerian structures. Ultrasound may distinguish testicle from ovary in the case of a palpable gonad by its oval shape, larger size, and the presence of an epididymis. Ovaries are more echogenic and follicular cysts may be identified (Fig. 12.17). Ultrasound is less reliable than MR to assess an intra-abdominal gonad. Pelvic ultrasound may be useful in identifying a well-developed uterus otherwise it is a difficult structure to properly identify when it is rudimentary.

Acute Testicular Pain (Case Study 3)

Ultrasound is an excellent modality to help define the nature of acute scrotal pain and swelling, i.e., distinguish between torsion of the spermatic cord or an inflammatory process (epididymo-orchitis or torsion of the appendix testis). Its rapidity and excellent sensitivity and specificity make it the first line of imaging in many institutions [26]. The unaffected testis/epididymis should be imaged first and compared to the affected side with respect to symmetry, architecture, and perfusion.

The sonographic findings of testicular torsion evolve with time. The study should start with the evaluation of the unaffected side. Early in the time course, the affected testis will have normal size and echogenicity. Sometimes, the point of torsion on the cord can be identified [27]. This is followed by an increase in testis and epididymal size and a decrease in echogenicity. The extent of hypoechogenicity increases with time. Reactive hydroceles and thickening of the overlying scrotal skin may be present. The non-salvageable testis appears heterogeneous as infarction and necrosis ensues [28] and Doppler flow may be detected due to hyperemia of the skin and surrounding soft tissue. Ultimately, the testis will contract. While the sine qua non of testicular torsion is the unilateral absence of Doppler flow on the affected side, decreased flow may be seen in cases of partial torsion or may reflect technical limitations of documenting flow in the normal testes.

Inflammation of the epididymis and/or testis in children may be infectious in nature or secondary to trauma or torsion of an appendage. Sonographically, the epididymis (more commonly at the caput) and/or testis may be enlarged and hypoechoic. Color Doppler will demonstrate increased flow to these structures or only to the epididymis. As in cases of spermatic cord torsion, comparison to the unaffected contralateral hemiscrotum is imperative. The actual torsed appendage (Fig. 12.18) may be seen as a hypoechoic structure at the junction of the epididymis and testis [29]. Reactive hydroceles and scrotal skin thickening may be present on the sonogram.

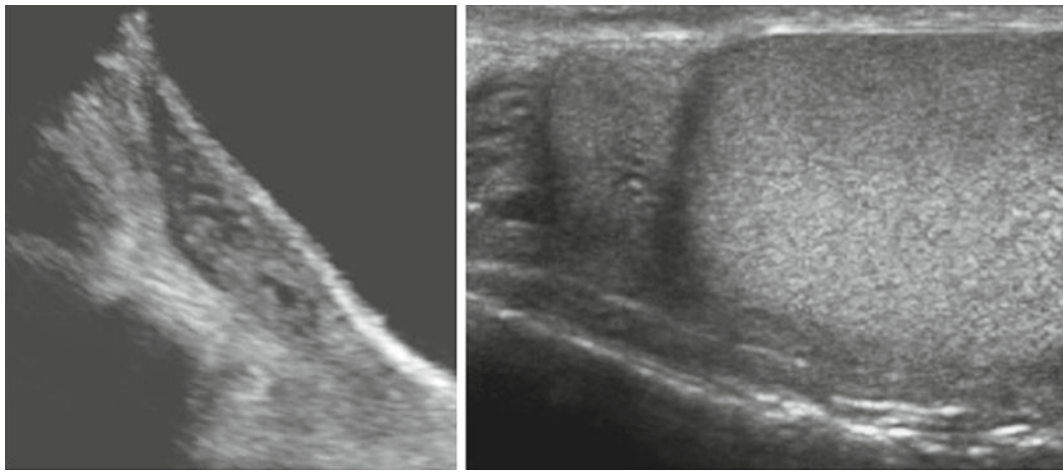

Fig. 12.17 Comparative images of an ovary (*left*) and testis (*right*). Ovaries tend to be oblong and follicles are sometimes present. The testis is oval and the presence of the epididymis helps to make the distinction

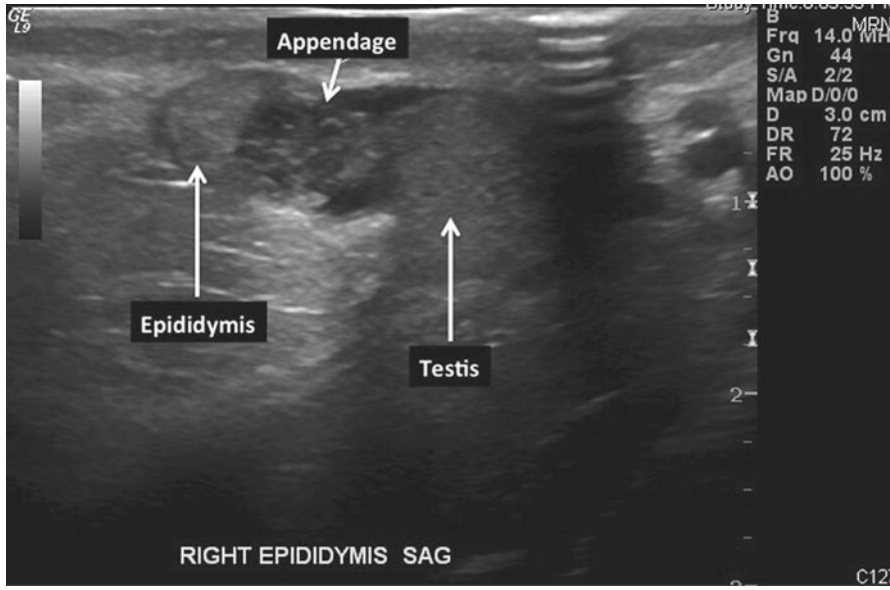

Fig. 12.18 Sagittal view of the testis in an adolescent male with acute onset of scrotal pain. A hypoechoic lesion is found superior to the testis and inferior or overlying the epididymis consistent with an appendage. Blood flow was present to tall structures except to the torsed appendage

Conclusion

Ultrasound continues to have a pivotal role in managing children with urologic conditions. The practicing urologist needs to understand the nuances in performing and interpreting these studies in children. It is imperative for urologists to know the ultrasound findings associated with the more common urologic conditions in childhood of the kidney, bladder, and scrotum.

Appendix

Case Study 1. Child with ureteropelvic junction obstruction. (a) Preoperative sagittal view of a left renal ultrasound demonstrates S.F.U. grade 4 hydronephrosis—extension into the calyces with parenchymal thinning (arrow). (b) The diuretic MAG 3 renogram demonstrates a right kidney with rapid uptake and drainage while the left one (*) shows persistent tracer. The drainage curve of the left kidney remains flat, even after furosemide injection while the right kidney drained before injection. (c) Intraoperative retrograde pyelogram demonstrates a dilated renal pelvis and narrowing at the ureteropelvic junction (arrow). (d) Postoperative ultrasound image of the left kidney showing resolution of the hydronephrosis and minimal residual calyceal dilation (*).

Case Study 2. This 3-month-old female was born with prenatally detected left hydronephrosis. The postnatal imaging included (a) sagittal image of the kidney that reveals a duplicated left collecting system with hydronephrosis isolated to the upper pole. (b) The bladder sonogram demonstrates a very large ureterocele (*) presumed to be from the left side (this was confirmed cystoscopically). (c) The VCUG demonstrates vesicoureteral reflux into the lower pole moiety only with displacement of the lower pole by the dilated upper pole segment. The area of the upper pole system is marked as *.

Case Study 3. Sonographic images from two adolescent boys presenting to the Emergency Department with acute scrotal pain and swelling. (a) Longitudinal views of the testes of a 13-year-old male presenting with 4 h of acute scrotal pain and swelling of the right side. The ultrasound

demonstrates similar echogenicity of the two sides. However, Doppler signal is present within the left testis while there is no signal identified within the right testis, only in the surrounding tissue; this is consistent with torsion. (b) Color flow study of the spermatic cord demonstrates point at which flow is no longer detected. (c) Longitudinal view of the testis of a 16-year-old male with 1 day of acute right sided scrotal pain. There is significant increased Doppler signal in the testis and in the epididymis which is consistent with an inflammatory process such as epididymo-orchitis.

References

1. Giorgi Jr LJ, Bratslavsky G, Kogan BA. Febrile urinary tract infections in infants: renal ultrasound remains necessary. J Urol. 2005;173(2):568–70.
2. Li-Ing B, et al. Bladder shape impact on the accuracy of ultrasonic estimation of bladder volume. Arch Phys Med Rehabil. 1998;79:1553–6.
3. Rosenbaum DM, Korngold E, Teele RL. Sonographic assessment of renal length in normal children. AJR Am J Roentgenol. 1984;142(3):467–9.
4. Krill A, Salami S, Rosen L, Friedman SC, Gitlin J, Palmer LS. Evaluating compensatory hypertrophy: a growth curve specific for solitary functioning kidneys. J Urol. 2012;188(4 Suppl):1613–7.
5. Cascio S, Paran S, Puri P. Associated urological anomalies in children with unilateral renal agenesis. J Urol. 1999;162(3 Pt 2):1081–3.
6. Damen-Elias HA, Stoutenbeek PH, Visser GH, Nikkels PG, de Jong TP. Concomitant anomalies in 100 children with unilateral multicystic kidney. Ultrasound Obstet Gynecol. 2005;25(4):384–8.
7. Mandell J, Blyth BR, Peters CA, Retik AB, Estroff JA, Benacerraf BR. Structural genitourinary defects detected in utero. Radiology. 1991;178(1):193–6.
8. Ismaili K, Hall M, Donner C, Thomas D, Vermeylen D, Avni FE, Brussels Free University Perinatal Nephrology study group. Results of systematic screening for minor degrees of fetal renal pelvis dilatation in an unselected population. Am J Obstet Gynecol. 2003;188(1):242–6.
9. Odibo AO, Raab E, Elovitz M, Merrill JD, Macones GA. Prenatal mild pyelectasis: evaluating the thresholds of renal pelvic diameter associated with normal postnatal renal function. J Ultrasound Med. 2004; 23(4):513–7.
10. Fernbach SK, Maizels M, Conway JJ. Ultrasound grading of hydronephrosis: introduction to the system used by the Society for Fetal Urology. Pediatr Radiol. 1993;23(6):478–80.
11. Rooks VJ, Lebowitz RL. Extrinsic ureteropelvic junction obstruction from a crossing renal vessel: demography and imaging. Pediatr Radiol. 2001; 31(2):120–4.
12. Mostbeck GH, Zontsich T, Turetschek K. Ultrasound of the kidney: obstruction and medical disease. Eur Radiol. 2001;11(10):1878–89.
13. Lim GT, et al. Utility of the resistive index ratio in differentiating obstructive from nonobstructive hydronephrosis in children. J Clin Ultrasound. 1999;27(4):187–93.
14. Brkljacic B, Kuzmic AC, Dmitrovic R, Rados M, Vidjak V. Doppler sonographic renal resistance index and resistance index ratio in children and adolescents with unilateral hydronephrosis. Eur Radiol. 2002;12(11):2747–51.
15. Gill B, Palmer LS, Koenigsberg M, Laor E. Distribution and variability of resistive index values in undilated kidneys in children. Urology. 1994;44(6):897–901.
16. Dillman JR, et al. Can shear-wave elastography be used to discriminate obstructive hydronephrosis from nonobstructive hydronephrosis in children? Radiology. 2015;277(1):259–67.
17. Goya C, et al. Acoustic radiation force impulse (ARFI) elastography for detection of renal damage in children. Pediatr Radiol. 2015;45(1):55–61.
18. Bruno C, et al. Acoustic radiation force impulse (AFRI) in the evaluation of the renal parenchymal stiffness in pediatric patients with vesicoureteral reflux: preliminary results. Eur Radiol. 2013;23(12):3477–84.
19. Sohn B, Kim MJ, Han SW, Im YJ, Lee MJ. Shear wave velocity measurements using acoustic radiation force impulse in young children with normal kidneys versus hydronephrotic kidneys. Ultrasonography. 2014;33(2):116–21.
20. Campbell MF. Anomalies of the ureter. In: Campbell MF, Harrison JH, editors. Urology. 3rd ed. Philadelphia: WB Saunders Company; 1970. p. 1512.
21. Cremin BJ. A review of the ultrasonic appearances of posterior urethral valve and ureteroceles. Pediatr Radiol. 1986;16:357.
22. Zerin JM, Baker DR, Casale JA. Single-system ureteroceles in infants and children: imaging features. Pediatr Radiol. 2000;30:139–46.
23. Blane CE, DiPietro MA, Zeim JM, et al. Renal sonography is not a reliable screening examination for vesicoureteral reflux. J Urol. 1993;150:752–5.
24. Grossklaus DJ, Pope JC, Adams MC, Brock JW. Is postoperative cystography necessary after ureteral reimplantation? Urology. 2001;58(6):1041–5.
25. Dinneen MD, Dhillon HK, Ward HC, Duffy PG, Ransley PG. Antenatal diagnosis of posterior urethral valves. Br J Urol. 1993;72(3):364–9.
26. Siegel MJ. The acute scrotum. Radiol Clin North Am. 1997;35(4):959–76.
27. Baud C, Veyrac C, Couture A, et al. Spiral twist of the spermatic cord: a reliable sign of testicular torsion. Pediatr Radiol. 1998;28:950–4.
28. Kaye JD, Levitt SB, Gitlin JS, Friedman SC, Freyle J, Palmer LS. Parenchymal echo texture predicts testicular salvage after torsion—a new paradigm to determine the need for emergent exploration. J Urol. 2008;180(4, 2 of 2):1733–36.
29. Strauss S, Faingold R, Manor H. Torsion of the testicular appendages: sonographic appearance. J Ultrasound Med. 1997;16:189–92.

Applications of Urologic Ultrasound During Pregnancy

13

Majid Eshghi

Ultrasound Evaluation During Pregnancy

The hormonal changes during pregnancy caused by estrogen, progestational, and prostaglandin-like agents are considered to be a contributing factors toward hydronephrosis and ureterectasis. Additionally, the anatomic location of the sigmoid colon on the left side provides a buffering effect on the left ureter and typically leads to less hydronephrosis. The growing size of the uterus in a limited pelvic space is considered to be the primary reason for dilation of the ureters and hydronephrosis. It is also thought that increasing gestational age and the growth of the uterus out of the pelvis contribute to a decrease in the pressure exerted on the ureters. This stabilization of the hydronephrosis results in a decrease in flank pain experienced during the late stage of pregnancy.

The pregnancy-induced hormonal and associated physiological changes result in a decrease in renal vascular resistance, and an increase in cardiac output which in turn leads to increased renal plasma flow. Along with these changes, there is also an approximate 30 % increase in the size of the kidneys and glomerular surface area under the influence of prolactin and its growth hormone-type effect. Another physiologic outcome is hypercalciuria, secondary to approximately 30–50 % increased GFR and reduction of creatine. The calcium filtration and intestinal calcium absorption are related to the high levels of placenta calcitriol. During the pregnancy, there is also an increase in inhibitors of stone formation, such as citrate, magnesium, and glycosaminoglycans. In spite of hypercalciuria and dilation of the upper tract, gravid and nongravid patients are at equal risk for development of urolithiasis with similar stone composition [1–7]. A review of renal volume in 150 healthy pregnancies revealed a mean left renal volume of 163.44 cm^3 and 141.85 cm^3 on the right side [8]. There is about 1–1.3 cm cranial displacement of kidney by growing fetus.

The hydronephrosis of pregnancy usually begins in the second trimester and affects 90 % of pregnancies by the 26–28th weeks. Dilatation increases up to the 30th week of gestation and remains stable for the remaining 8–10 weeks. The incidence of dilation is greatest in nulliparous patients [9, 10]. The hydronephrosis subsides within the 6 weeks after parturition, but sometimes it may persist longer. As a rule, there is more dilation on the right (85 %) than the left (15 %). The ureteral dilation does not occur below the pelvic brim in physiologic

M. Eshghi, M.D., F.A.C.S., M.B.A. (✉)
Department of Urology, New York Medical College, Westchester Medical Center, 100 Woods Road, Bldg 19 Skyline Drive 1S-B48, Valhalla, New York, NY 10595, USA
e-mail: Majid_Eshghi@nymc.edu

P.F. Fulgham, B.R. Gilbert (eds.), *Practical Urological Ultrasound*, Current Clinical Urology,
DOI 10.1007/978-3-319-43868-9_13

hydronephrosis versus distal ureteral obstruction where the dilation can extend to the uretero-vesical junction [11]. It is also believed that the gravid uterus compresses the ureters at the pelvic brim. Other potential contributory factors are dextrorotation of the uterus and ureteral compression by the uterine and gonadal vessels, which become quite engorged during pregnancy (ovarian vein syndrome). The elevated baseline or resting ureteral pressures recorded above the pelvic brim decrease in prone position—and ureteral contractile pressures recorded during pregnancies argue against ureteral atony caused by progesterone. It has been observed that ureters that do not cross the pelvic brim such as those connected to pelvic kidneys or in an ileal conduit urinary diversion do not develop hydronephrosis, nor does it occur in quadrupeds [12]. These findings also argue against the role that hormones play during the early stages of gestation. Finally, the hydronephrosis can be considered to be the result of a combination of the above factors. Increased hydration has been shown to increase the degree of hydronephrosis. There are some conditions that can simulate urolithiasis symptoms during pregnancy, namely, acute pyelonephritis, renal vein thrombosis (RVT), and renal rupture [13–16]. Twin pregnancy, uterine rotation, passage of sloughed papilla, or blood clot can cause standing or transient hydronephrosis during pregnancy as well.

The indications for ultrasonography of the kidney include bilateral or unilateral flank pain, unilateral colicky pain, and less frequently, hematuria. Ultrasound evaluation helps in differentiating physiologic hydronephrosis from obstruction secondary to calculus disease. There are occasional situations where the colicky pain may be caused by papillary necrosis and in rare cases of HELLP syndrome (Hemolysis, Elevated Liver Enzymes, and Low Platelets). The sole placental condition responsible for hematuria is placenta percreta that involves the bladder or ureter. Placenta accreta and increta do not extend beyond the uterus. Other general indications for ultrasonography during pregnancy include oliguria, anuria, urinary tract infection, pyelonephritis, and urinary retention which is more commonly seen postpartum) [17–24]. Additionally there is new data that the fetal sonography during pregnancy with measurement of fetal kidney, renal pelvis, and adrenal gland may be useful in diagnosis and assessment of pathologies of the kidney and adrenal gland [25]. Several clinical investigations have documented measurement of fetal renal length as a reliable parameter in determining gestational age [26]. A report from 2005 described screening sonography in 101 pregnant patients with blunt abdominal trauma. Five injuries required surgical intervention four out of five diagnosed injuries requiring surgery including one renal trauma were identified on ultrasound [27]. There is a rare report of hydronephrosis of pregnancy in ectopic kidney [28].

Resistive Index (RI) is a useful tool for the assessment of obstruction either in gravid or nongravid kidneys. RI measures intrarenal impedance. This is a measure of pulsatile blood flow reflecting the resistance to blood flow caused by microvascular bed distal to the site of measurement. RI was developed by French physician Leandre Pourcelot and it is calculated from the following formula and has gained great significance in assessment of placental blood flow during pregnancy.

$$\text{Resistive index}\left(\text{RI}\right) = \frac{\text{Peak systolic velocity}\left(\text{PSV}\right) - \text{End diastolic velocity}\left(\text{EDV}\right)}{\text{Peak systolic velocity}\left(\text{PSV}\right)}$$

$$\text{RI} = \frac{\text{PSV} \quad \text{EDV}}{\text{PSV}}$$

The resistive index (RI) is the peak systolic velocity (PSV) minus the end diastolic velocity (EDV) divided by the PSV. The proper location of measuring RI is at the corticomedullary junction where renal arcuate arteries and/or interlobar arteries along the medullary pyramids are assessed usually at an angle of 50–60° [29]. The normal RI is equal to or more than 0.7, and typically, an RI of more than 0.9 indicates renal dysfunction. RI increases with decreasing diastolic flow. Therefore in a hypothetical situation of absence of flow in diastole, the resistive index equals 1.0. In normal pregnancy there is no appreciable change in RI. In the early stages of obstruction, RI is often elevated and usually occurs within 6 h after clinical acute obstruction [8]. From a technical point of view, compression of the kidney can cause elevation of RI, and this is typically noted in transplanted pelvic kidneys that are superficially located (Fig. 13.1) [30–33]. In one study, duplex ultrasound in a nonpregnant population detected acute renal obstruction with an approximate 77 % sensitivity [34].

$$\text{Pulsatility Index}\left(\text{PI}\right):\text{PI}=\frac{\left(\text{PSV}-\text{MDV}\right)}{\text{MV}}$$

Several vascular studies use the pulsatility index parameter which is a measure of variability of blood velocity in a vessel. It represents the difference between peak systolic and minimum (end) diastolic velocities divided by the mean arterial velocity during a cardiac cycle. Assessment of RI and PI in patients with renal disease can identify patients with slow and fast progression of renal failure [35].

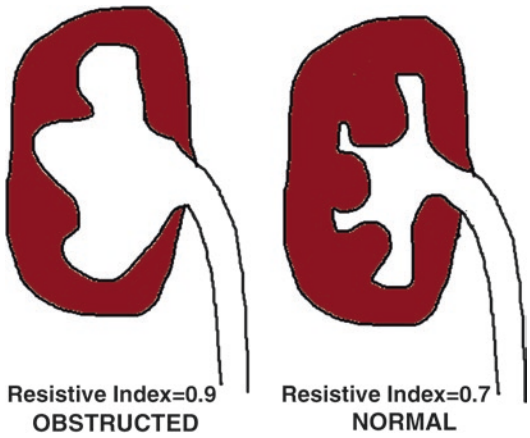

Fig. 13.1 Schematic diagram indicating an obstructed right kidney with associated elevated resistive index

Diuretic Doppler ultrasound is a modification of conventional Doppler sonography to assess physiological responses of obstructed and nonobstructed kidneys to diuretic stimulation. Furosemide-enhanced diuresis leads to significant increases in the RI of obstructed kidneys, while having no effect on that of nonobstructed kidneys in adults or children. Saline loading followed by furosemide results in a divergent response with an increased RI in obstructed and a decreased RI in nonobstructed kidneys. Other factors causing elevated RI are medical renal disease, diabetic nephropathy, and external factors such as fasting and exsanguination. Recent studies documented decrease in RI with increasing heart rate and stable blood pressure and increasing RI with pulse pressure widening [36–39].

Contrast Enhanced ultrasound (CEUS) of kidneys during pregnancy has been reported only before scheduled termination of pregnancy. It may be a good tool for assessment of placental vascular insufficiency. Laboratory animal studies in pregnant rats has also shown value of this modality in evaluation of placenta [40, 41].

Resistive index is usually normal in a pregnant patient. The elevation of obstruction-related RI is thought to be due to increased renal vascular resistance secondary to elevated prostaglandins. It is recommended that, for the assessment of RI, patients should avoid the use of NSAIDs prior to ultrasound imaging. NSAIDs may interfere with interpretation which may be due to blocking prostacyclin synthesis resulting in decreased renal blood flow and mask the expected changes in RI [42]. Several NSAIDs (e.g., ketorolac, indomethacin) have been shown, in animal models, to reverse both the early vasodilation and subsequent vasoconstriction of acute ureteric obstruction [43, 44]. Measurement of RI is usually most evident during the first 6–48 h of obstruction. A difference of more than 0.1 from side to side is suggestive of obstruction. The overall sensitivity of RI for the assessment of obstruction is 42–100 %, and it is less sensitive for partial versus complete obstruction.

Anteroposterior Diameter (APD) is another method for assessing obstruction in a gravid kidney. APD is the measurement of renal pelvic dilation. Pathological obstruction is suspected if the cross-sectional measurement of the renal pelvis exceeds 27 mm on the right or 18 mm on the left during the second and third trimester. It is therefore imperative to obtain both sagital and cross-sectional images of the gravid kidney. Pathological obstruction is suspected if the *APD* measurement exceeds 18 mm on the right and 15 mm on the left side during the first trimester. The cross-section measurement of the renal pelvis should be in the midpole where the maximum dilation can best be assessed [45] (Figs. 13.2 and 13.3). The frequency of developing hydronephrosis is not related to the number of pregnancies [15, 46]. These changes should be interpreted in correlation with subjective and objective clinical manifestations (Table 13.1). Predominately left renal pelvic dilation with left flank pain suggests obstruction. Right flank pain with minimal to no pelvic dilation suggests no pathological obstruction (Figs. 13.4).

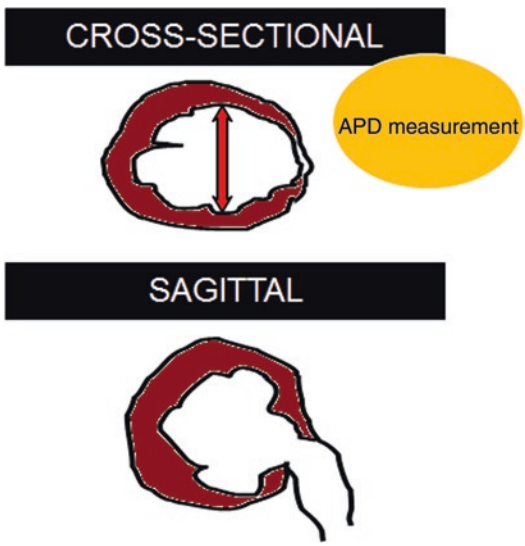

Fig. 13.2 Diagram depicting renal pelvic measurements

Renal Pelvic *APD* and Calyceal Measurements Suggesting Obstruction

In early pregnancy, there is no significant difference in calyceal dilation. With the increase of gestational age, the degree of hydronephrosis increases on the right side and decreases on the left [47] (Table 13.2).

Example: Grade 1 hydronephrosis is detected bilaterally in 53 % of patients. For grade 2, the ratio changes to 35 % on the right and 14 % on the left. The following graph shows the mean calyceal diameter of the right and the left kidneys as plotted against gestational age (Table 13.3). Similar to measurement of mother's kidneys, the obstetric ultrasound protocol requires assessment of fetal hydronephrosis. Ante Natal Hydronephrosis (ANH) is also classified based on APD. The values indicating obstruction are obviously significantly smaller due to the smaller size of fetal kidney. Table 13.4 presents a modified current classification and measurements [48].

Ureteral Jets: One of the more recent applications of Doppler is imaging of the base of the bladder and trigone for detection of pulsatile (peristaltic) egress of urine from the ureteral orifices (Fig. 13.5). Ureteral jets can be well documented even after placement of double pigtail ureteral stent (Fig. 13.6a, b). This application is quite useful in assessing the patency of the ureter. Ureteral jets can be assessed during the follow-up and observation period of medical expulsive therapy, in anticipation of spontaneous stone passage. This application is very valuable in management of pregnant patients with renal colic as it eliminates radiation exposure. Presence, clinical utility, value, and accuracy of ureteral jets, at times, remain controversial. This is due to the significant variability of ureteral jets frequency in normal volunteers [49–53]. Presence of stones in the distal ureter can easily be documented with grayscale ultrasound and Doppler showing twinkle artifact. From a clinical point of view if there is adequate ureteral jets and patient is not in severe pain or septic, observation, pain management and Alpha blockers

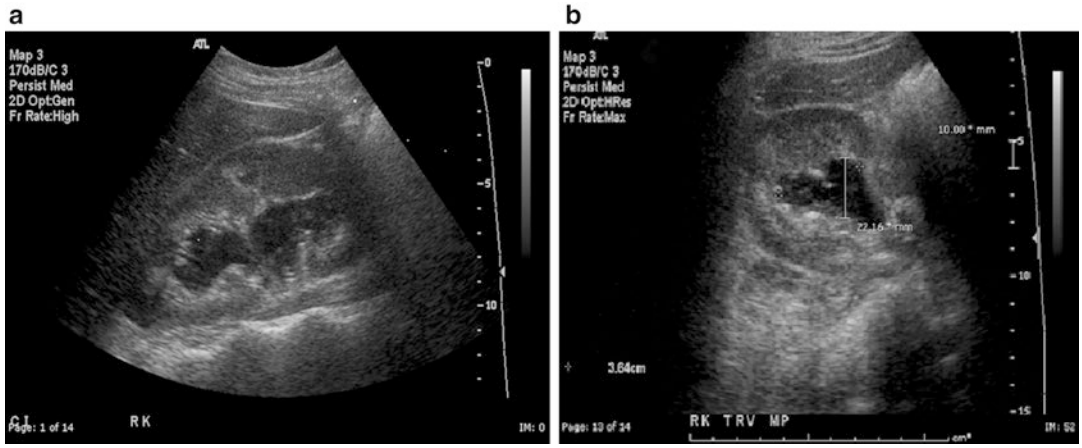

Fig. 13.3 Sagittal (**a**) and transverse (**b**) midpole ultrasound images of a pregnant patient with right flank pain, APD measurement of 27 mm is indicative of obstruction

Table 13.1 The grading of hydronephrosis during pregnancy

Grading	
Grade 0	Hydronephrosis 0–5 mm, minimal separation of central echo complex
Grade 1	Hydronephrosis 6–10 mm
Grade 2	Hydronephrosis 11–15 mm
Grade 3	Hydronephrosis equal or more than 16 mm. A large sonolucent sac occupies a major portion of the kidney

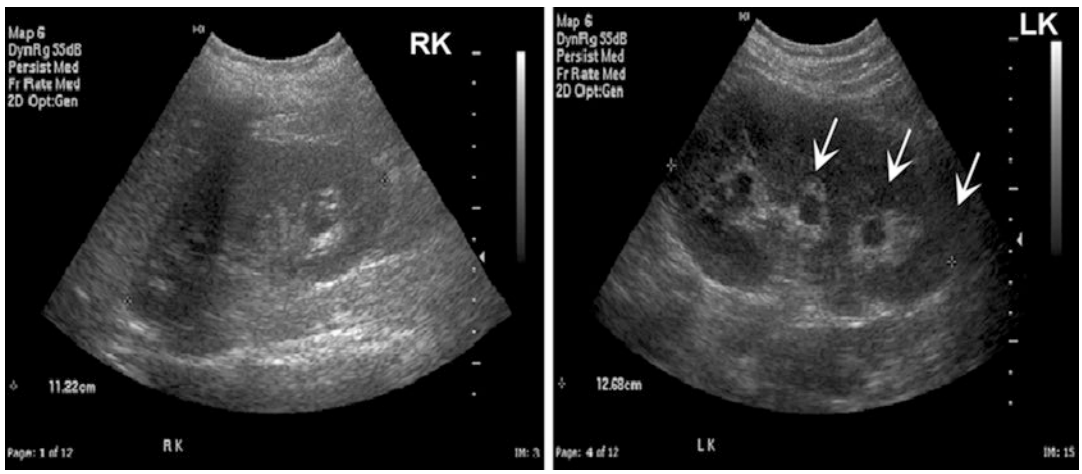

Fig. 13.4 Thirty-year-old female, G2P1, at 28 weeks of gestation, presenting with left flank pain. The right kidney (RK) shows no hydronephrosis, whereas the left kidney (LK) demonstrates calyceal dilation (*arrows*)

Table 13.2 AP renal pelvic and calyceal measurements suggesting obstruction

	Right kidney (mm)	Left kidney (mm)	Calyceal diameter (mm)
First trimester	>18	>15	>10
Second and third trimester	>27	>18	>10

Table 13.3 This table describes renal calyceal dilation as it relates to gestational age

Gestational age (week)	Observed percentiles				Adjusted percentiles			
	Right		Left		Right		Left	
	50th	70th	90th	90th	50th	75th	90th	90th
4–6	0.0	3.0	5.0	2.1	1.4	2.4	3.4	0.1
7–8	0.0	0.0	5.0	0.0	0.3	3.2	4.5	2.2
9–10	0.0	0.0	4.0	0.0	1.2	4.0	5.7	3.5
11–12	0.0	5.0	7.0	6.0	2.0	4.9	7.0	4.5
13–14	0.0	5.8	8.0	6.9	2.7	5.7	8.4	5.3
15–16	0.0	1.0	8.9	4.9	3.0	6.7	9.8	6.0
17–18	5.0	9.5	12.0	8.8	3.7	7.6	11.2	6.6
19–20	0.0	8.0	11.0	7.7	4.2	8.6	2.6	7.1
21–22	5.0	9.0	13.8	6.8	4.6	9.6	13.9	7.1
23–24	8.0	12.0	15.0	8.2	4.9	10.5	15.1	7.9
25–26	7.0	13.0	16.7	8.0	5.3	11.4	16.2	8.2
27–28	7.0	13.0	21.0	9.0	5.6	12.2	17.2	8.4
29–30	7.0	11.0	16.0	9.0	5.9	13.0	18.0	8.6
31–32	8.0	15.5	19.4	8.2	6.1	13.7	18.7	8.7
33–34	4.5	13.0	20.5	8.5	6.4	14.3	19.3	8.8
35–36	6.0	15.0	19.0	8.0	6.6	14.8	19.7	8.9
37–38	5.0	14.0	20.4	8.0	6.8	15.2	19.8	8.9
39–42	7.0	14.0	17.0	9.2	7.1	15.5	19.8	8.7

Table 13.4 Classification of ANH using APD measurement

	Second trimester (mm)	Third trimester (mm)
1-mild	≤7	≤9
3-moderate	7–10	9–15
5-severe	≥10	≥15

(Medical Expulsive Therapy) can be considered. A recent study indicated that an Alpha blocker was safely used in 28 pregnant women with renal colic as part of medical expulsive therapy (MET) [54] (Fig. 13.7a, b).

The drawback to the assessment of ureteral jets is that it may add significant scanning time to a standard renal bladder study, but in the case of a pregnant patient this is the most viable option. In well-hydrated patients ureteral jets can often be documented within a few minutes of scanning the bladder. To indicate that there is an absence of ureteral jets, adequate scanning time needs to be allowed. Usually a minimum of 10 min is recommended to adequately document absence of ureteral jets [53]. Thirty minutes may be required to document asymmetry of jet frequency in order for it to be a true finding. The patients must be adequately hydrated. The urine density differences contribute to visualization of ureteral jets [51]. Some of the other theories discussed in relation to ureteral jets include that frequency decreases during normal pregnancy. Findings suggestive of ureteral obstructions are asymmetry of ureteral jets and absence or sluggish continuous flow from the affected side. Lack of ureteral jets suggesting obstruction is after 10 min of observation with no obvious flow in a well-hydrated patient whereas in partial obstruction, there is sluggish trickling along the trigone versus strong upward jet toward opposite bladder wall.

Some of the above-mentioned signs that are indicative of obstruction can be seen in asymptomatic pregnant women. They may be attributed

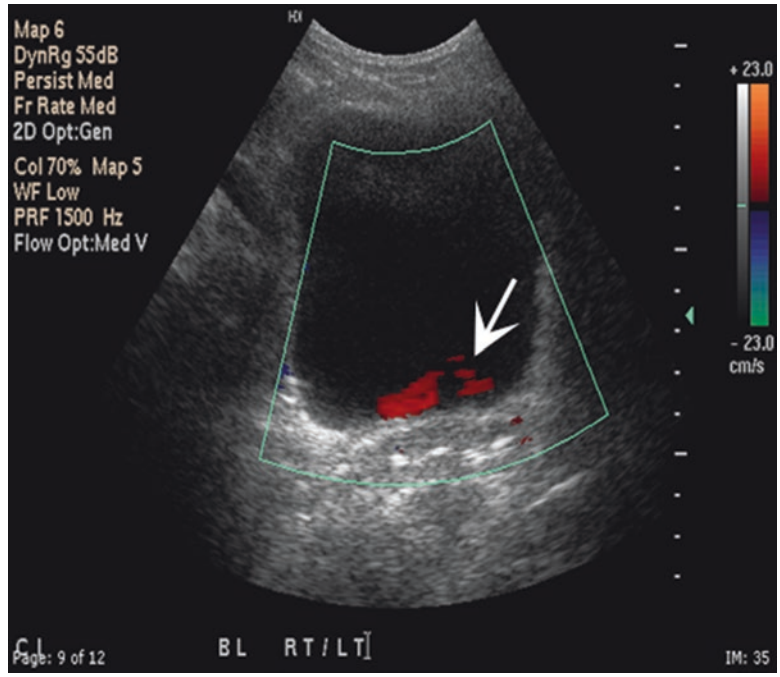

Fig. 13.5 Ureteral jets in the previous patient, note sluggish jet from the *left* side (*arrow*)

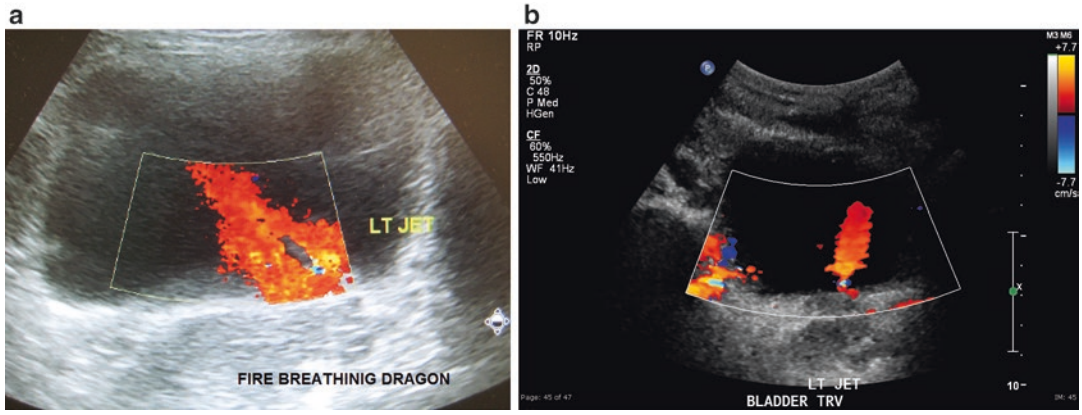

Fig. 13.6 (**a**) A strong left ureteral jet: pulsatile egress of urine into bladder gives the appearance of a dragon-breathing fire. (**b**) A strong left ureteral jet (*arrows*) in a patient with a left double pigtail ureteral stent. Note that the direction of the jet is slightly toward left of bladder and vertical secondary to changes in the orientation of the orifice with the stent in place

to diminished ureteral smooth muscle tone and extrinsic ureteral compression by the gravid uterus. There is no correlation between the degree of hydronephrosis and mean jet frequency [53] (Fig. 13.8). Transvaginal sonography demonstrating a dilated distal ureter or presence of a stone can further document obstruction specifically if combined with Doppler showing twinkling artifact [55–57] (Fig. 13.9). Transvaginal ultrasound orientation is not a single orientation. The intracavitary transducer is end fire and can create images in different orientations: Upward (similar to transrectal) or downward (transabdominal) views of the bladder. The operator should provide orientation of images for radiologist's interpretation.

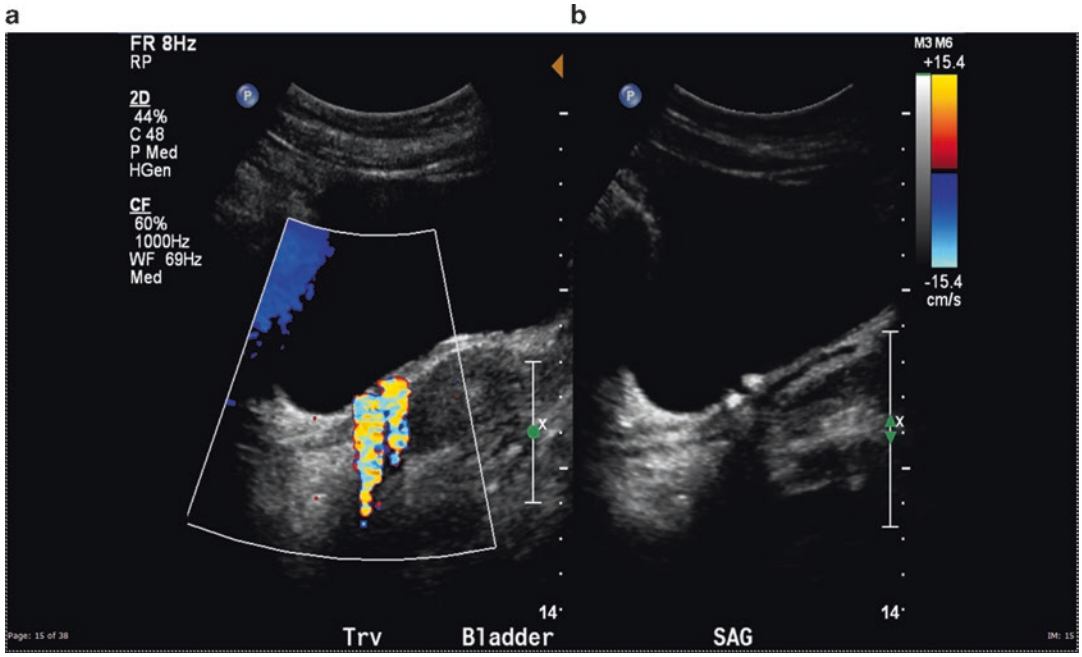

Fig. 13.7 Patient with history of right flank pain managed with MET. The *right* shows twinkle artifact arising from two distal ureteral stones. Continued Doppler evaluation reveals strong right ureteral jet ruling out significant obstruction

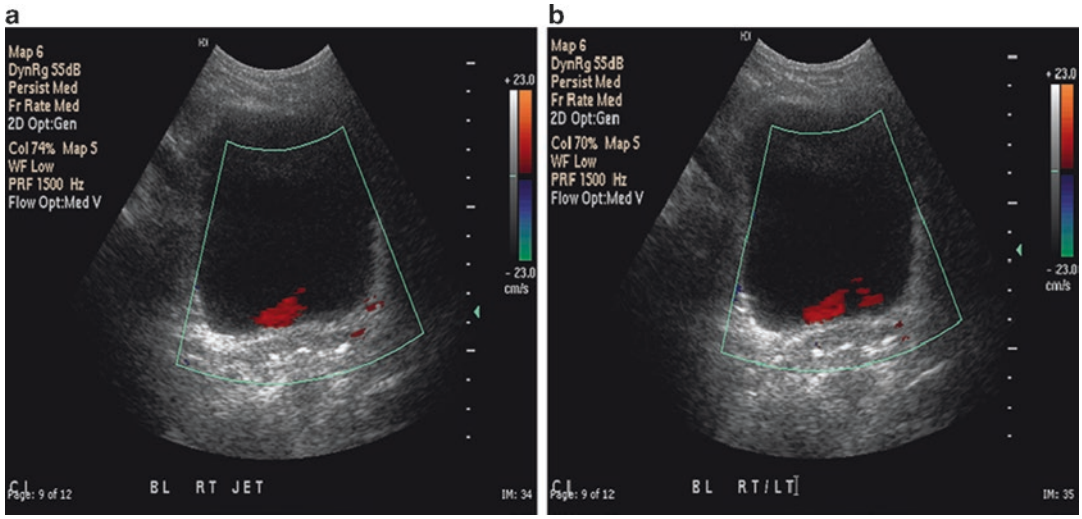

Fig. 13.8 (**a**) Presence of right ureteral jet from an unobstructed right gravid kidney. (**b**) Very sluggish left ureteral jet in an unobstructed left gravid kidney

Absence of ureteral jets is reported in 33.2–50 % of asymptomatic pregnant women.

The absence of ureteral jets may be attributed to the patient's **supine position** and ureteral compression, which can be alleviated by placing the patient in the **contralateral decubitus position** [58]. True obstruction of the ureter would not respond to a change in patient position (Figs. 13.10a, b).

Patients with a previous UPJ obstruction or reflux may show a discrepancy of dilation spe-

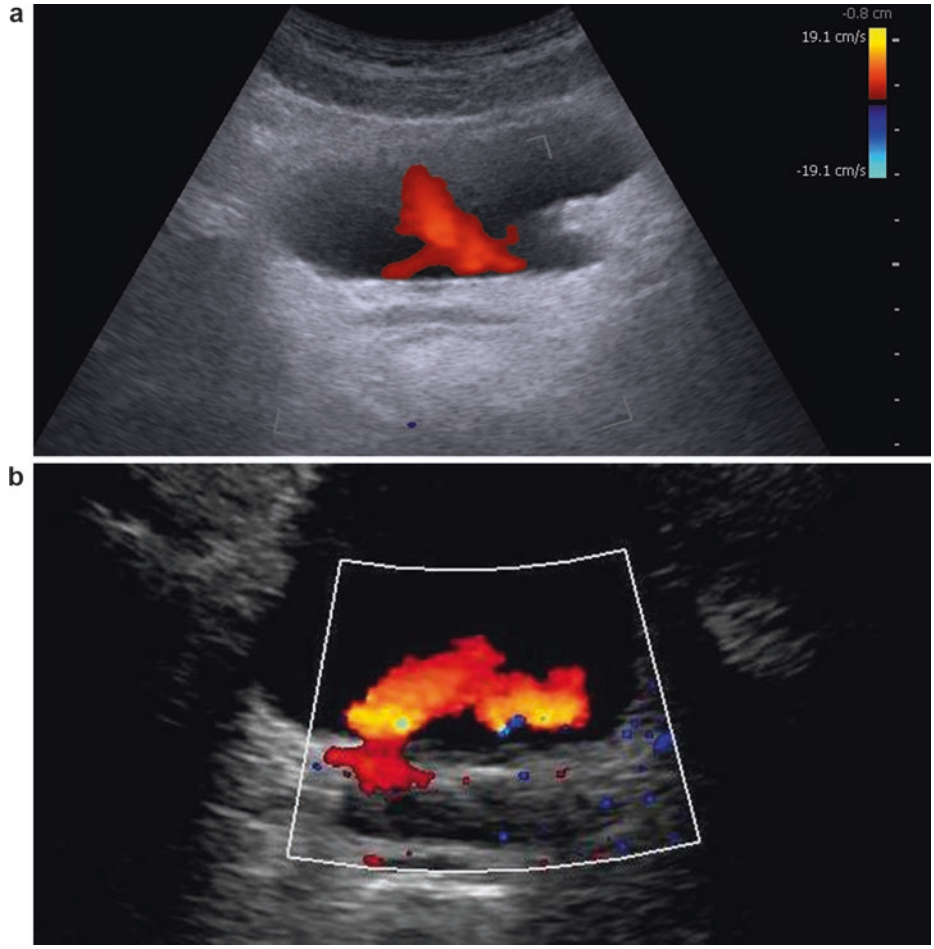

Fig 13.9 (**a**) Simultaneous bilateral ureteral jets with a crossing X pattern (**b**) or merging ARCH pattern

cially on the left side which may show a more dilated renal pelvis without true or symptomatic obstruction. Renal ultrasound imaging for assessment of pregnant women with horseshoe kidneys is technically challenging due to the orientation of the kidneys: nonobstructed dilated pelvis situated anteriorly, more central position and malrotation. Ultrasound imaging becomes even more difficult in advanced stages of gestation due to the cephalad growth of the gravid uterus. These patients need to be continuously monitored with frequent imaging and clinical correlation if they become symptomatic (Fig. 13.11a–g).

Ultrasound-Guided Ureteroscopy During Pregnancy

Symptomatic pregnant patients may require ureteroscopy or stenting for relief of obstruction. It is best to avoid radiation during pregnancy [59]. Thus, ultrasound-guided ureteroscopy is more widely used now [60]. The following steps are recommended to help the physician achieve this goal:

Fetal monitoring, pre, intra, and postoperatively are performed according to the obstetric protocol and recommendations of the obstetric team depending on the gestational status, stability,

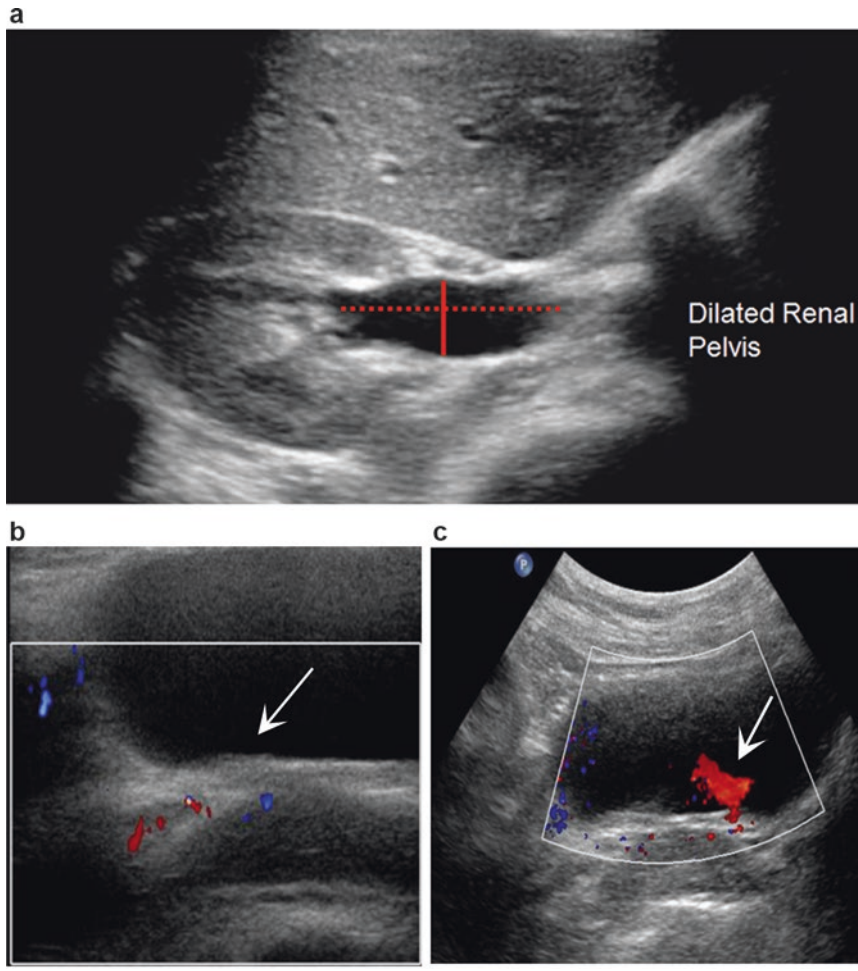

Fig. 13.10 (**a**) Hydronephrosis on the right side with dilation of the renal pelvis due to acute ureteral obstruction. (**b**) Absence of Rt. ureteral jet (*arrow*). (c) Presence of a strong Lt ureteral jet (*arrow*)

or risk factors involved. Patient and family should be counseled about perioperative risks such as premature contracture, fever, sepsis, or cardiopulmonary complications. Standard lab tests and preoperative urine culture and sensitivity should be done unless due to a very emergent condition there is not enough time to allow for culture and sensitivity assessment. Intravenous antibiotic is administered in consultation with obstetric and infectious disease teams based on the classification of safety. This can be continued per orally post op as needed. Penicillins, Cephalosporin, Erythromycin, and Nitrofurantoin (possible hemolytic anemia) are usually considered safe.

Preoperative ultrasound may be repeated if there has been a time lag of 24–48 hours since the original imaging assessment especially if the patient has become asymptomatic.

Ultrasound-guided percutaneous nephrostomy should be considered in patients with severe hydronephrosis and signs of sepsis. Online or sideloaded needle guide will allow for placement of initial puncture into the collecting system. Limited fluoroscopy may be needed to confirm the nephrostomy tube location. Anesthesia evaluation should be done with consideration of regional versus general anesthesia [61].

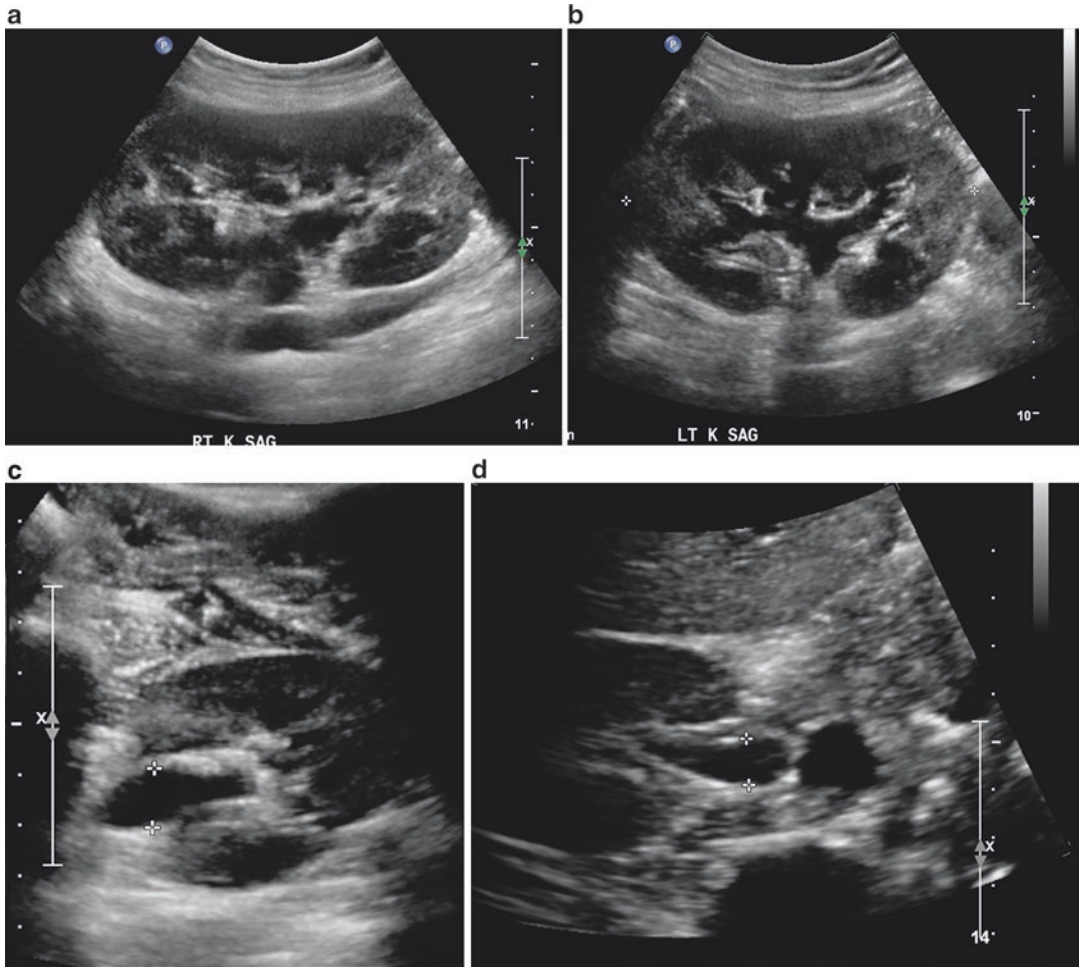

Fig. 13.11 (**a**) Nineteen-year-old female with history of horseshoe kidney and left vesico-ureteral reflux, sagittal image of right kidney shows dilation of collecting system appropriate for 30 weeks gestation. (**b**) Left renal image shows more significant hydronephrosis secondary to previous history of reflux. Patient was asymptomatic. (**c**) APD Measurement (1.5 cm) of midtransverse view of left kidney. (**d**) APD (1 cm) of midtransverse view of right kidney. There is more dilation on the left side. (**e**) Patient at 14 weeks of gestation with horseshoe kidney this is area showing the isthmus of the kidney (**f**) the left moiety is much smaller due to a previous history of reflux. Patient is status post deflux injection. (**g**) The right moiety is much larger. Note the malrotation of the kidney which makes the assessment of true hydronephrosis difficult. The right upper ureter is seen in the front

Room Setup and Patient Positioning

- The patient is placed on the dedicated cystoscopy operating table in a dorsolithotomy position with a lead apron under the patient and wrapped around the abdomen only exposing the upper portion of the affected kidney. This is for possible emergency use of C-arm fluoroscopy to assess the renal area while protecting the fetus. In recent years, we do not or rarely bring in the C-Arm in the field for ureteroscopy during pregnancy. A 3.5/5 MgH transducer is used for scanning the flank area as well as the right or left lower quadrant for assessment of distal ureter and bladder.

In a typical case, assuming a right ureteroscopy is being performed, the surgeon's assistant or sonographer stands on the patient's right side with a 3.5–5 MgH probe. The ultrasound monitor

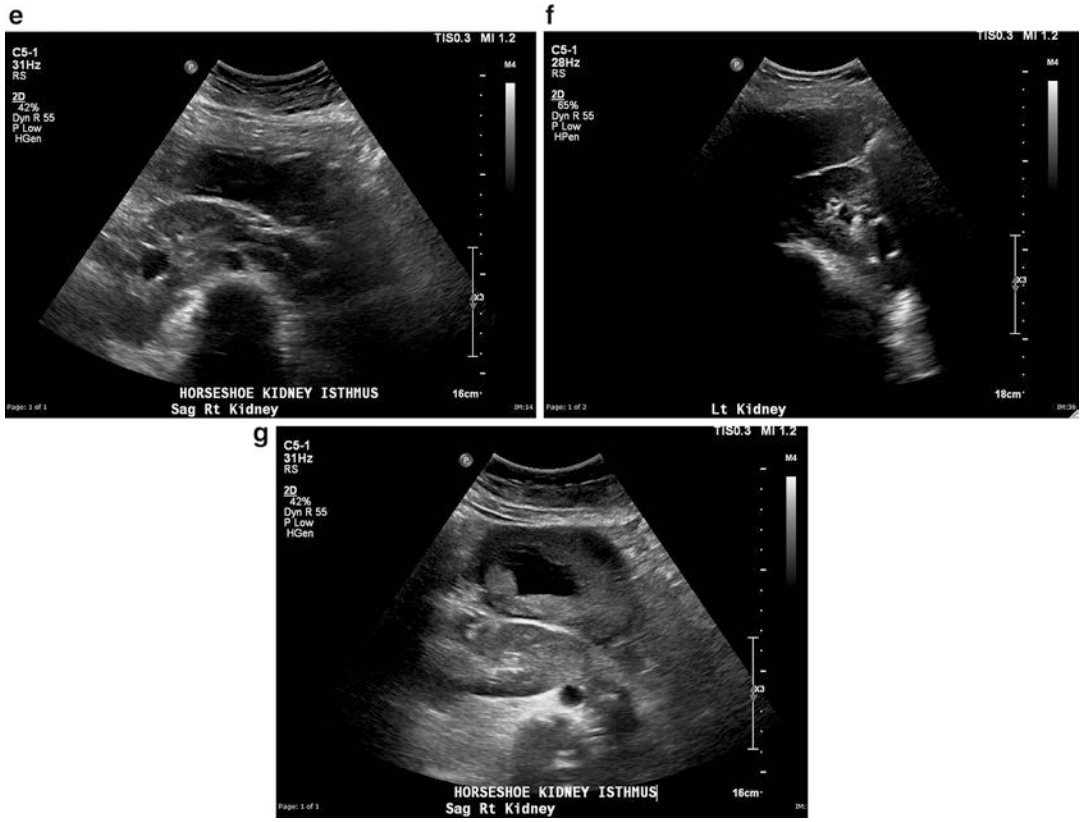

Fig. 13.11 (continued)

is placed across on the patient's left side with about 15–20° angle toward the feet to allow direct viewing for both the sonographer and the endoscopist who is at the feet of the patient. If there is a need for C-Arm for emergency use that will be placed in the same location to the left of the ultrasound monitor. The fluoroscopy monitor can be placed either on the right or left side of the patient as per the surgeon's preference. The video monitor for a right-sided procedure is best to be situated on the left side of the patient so all members of the surgical team can view the procedure. Modern video equipment with a swiveling arm will allow the monitor to be in the middle right over the body thus allowing for all members of the surgical team to view the procedure (Fig. 13.12a, b).

An initial sonography of the kidney will be done to confirm continued hydronephrosis (Fig. 13.13). Transvaginal sonography can be helpful in assessing the distal ureter if transabdominal ultrasound is inadequate. Ureteroscopy and laser lithotripsy can be performed safely in patients with stable pregnancy. In case initial placement of guidewire or ureteral catheter results in purulent egress of urine from the kidney it is best for the patient to be temporarily stented. Alternatively an open-ended or single pigtail catheter can be placed under ultrasound control and anchored to a Foley catheter. The patient will undergo definitive procedure after the results of urine culture and sensitivity from renal pelvis is available, proper antibiotic is administered, and patient is stable physiologically and obstetrically. If a ureteral catheter is advanced to the renal pelvis, injection of a few milliliters of air will create a bubbling effect, thus confirming the proper location of the catheter. This procedure is helpful for locating the ureteral catheter (Fig. 13.14).

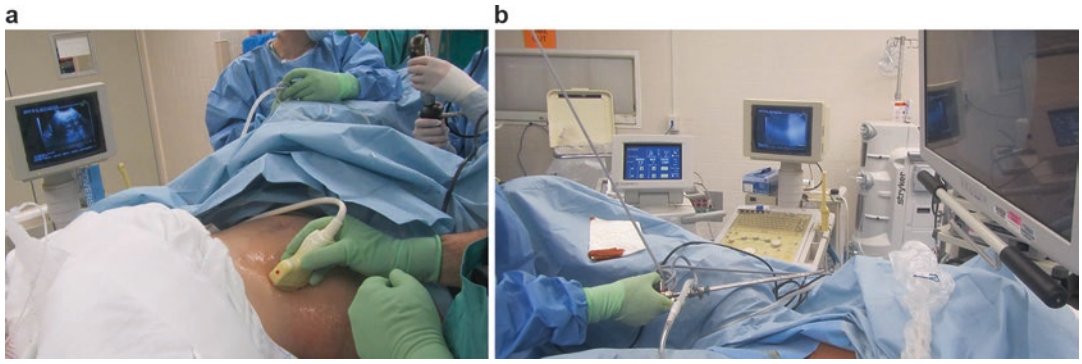

Fig. 13.12 (**a**) Right sided ureteroscopy: the sonographer member of the team stands at the right side of patient with endoscopy members at the foot of table (**b**) Left sided ureteroscopy: Ultrasound monitor and laser placed across the patient on right side and video monitor over the patient's upper body

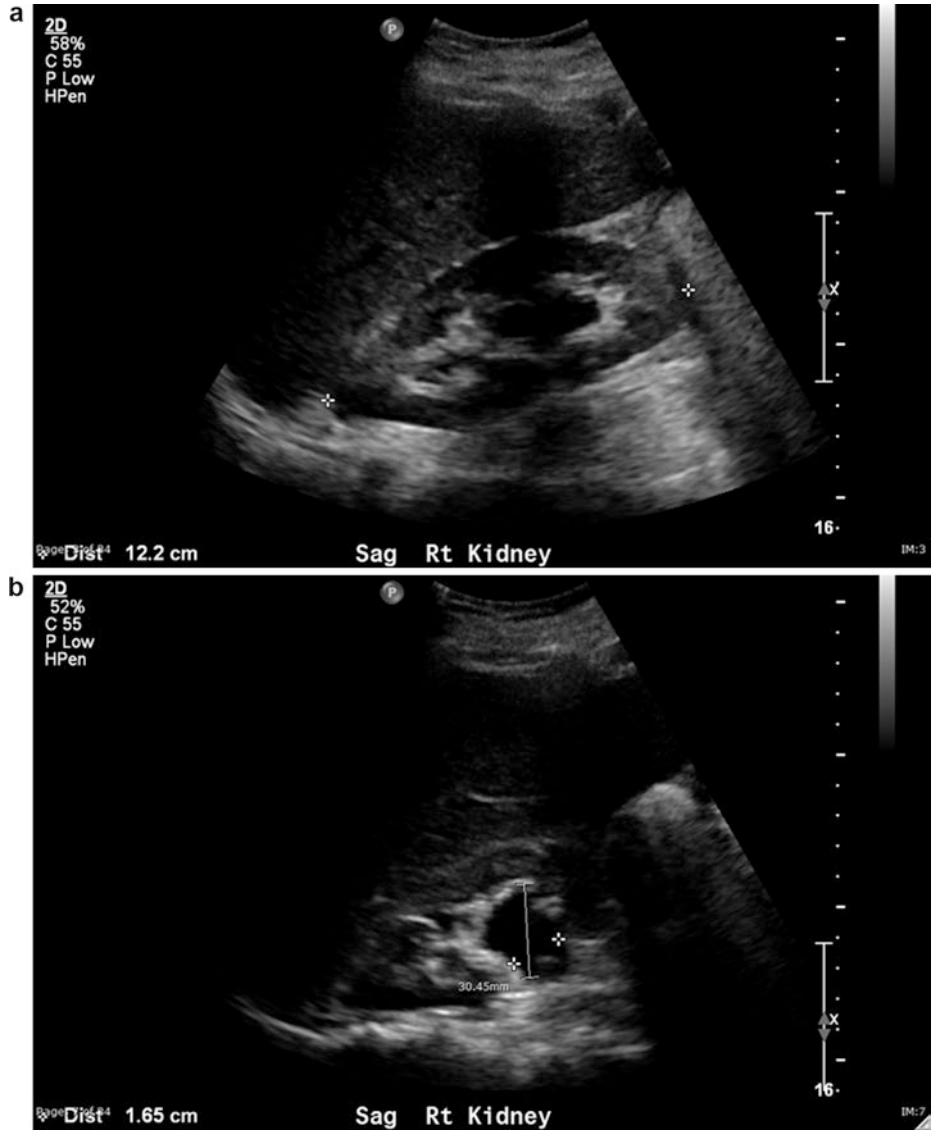

Fig. 13.13 (**a**) Obvious dilated collecting system on sagittal view (**b**) transverse view shows a APD of 30.45 mm

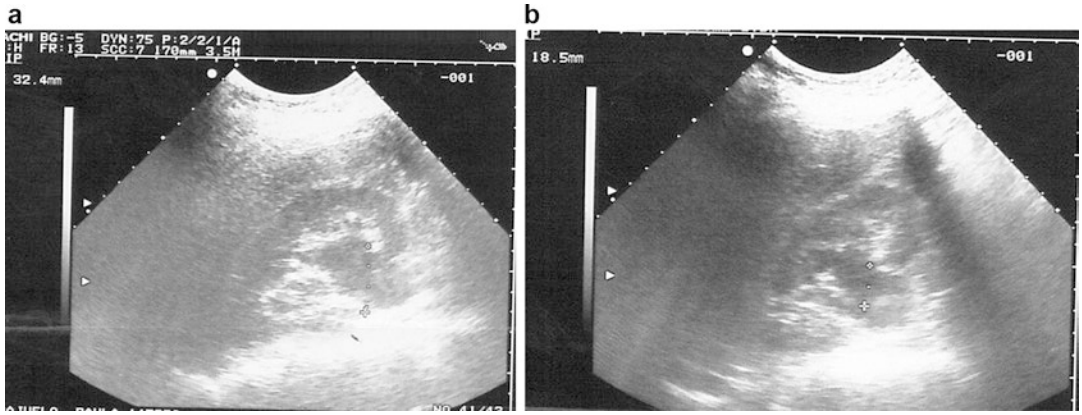

Fig. 13.14 (**a**, **b**) Intra op preprocedure sonogram shows a measurement of 32.4 mm (**a**) immediate postprocedure and stent placement shows APD has decreased to 18.5 mm (**b**)

Depending on the surgeon's preference and location of stone, if identified, a semirigid or flexible ureteroscope can be used to perform the operation. Distal ureteral stones can easily be managed with a semirigid ureteroscope. If necessary distal ureteral stones can be monitored with lower quadrant ultrasound imaging at the time of ureteroscopy. The use of a semirigid ureteroscope in the mid and upper ureter during pregnancy depends on the urologist's experience and level of comfort. The ureter is usually dilated and accommodates the ureteroscope with rare conditions that may require dilation of the distal ureter. Flexible ureteroscopy especially with digital imaging is ideal for evaluation of mid, upper ureter, and renal pelvis. After the placement of the guidewire, the ultrasound imaging of the kidney can show motion of the wire, indicating the proper location of the guidewire. If intra-op ultrasound cannot identify the wire in kidney, there is no egress and hydronephrosis is unchanged it is usually due to tortuosity of the upper ureter or UPJ area. With a flexible ureteroscope a guidewire can be inserted under vision to help negotiate the tortuosities and bedside ultrasound can confirm final position in the renal pelvis. It is our practice to aspirate the renal pelvis and send a sample of pelvic urine by placing a syringe at the irrigation port of the ureteroscope. This should be sent separately from the bladder urine. Initial decompression of the renal pelvis is always recommended to decrease pyelovenous or pyelotubular backflow. Bedside ultrasound confirms a decrease in hydronephrosis after aspiration (Fig. 13.15a, b).

Ureteral stones are managed using holmium laser. In the past, semirigid ureteroscopy with ultrasonic lithotripsy has been used safely. There were theoretical concerns about the possible ill effects of ultrasound due to high frequency energy and auditory damage to the fetus. Electrohydraulic lithotripsy generates high peak pressure and is not generally recommended during pregnancy. Holmium laser lithotripsy has been used for several years without obvious complication. The short thermal penetration range of 0.5–1 mm has very little effect beyond the ureteral wall. Laser lithotripsy of uric acid stones produces cyanide which is washed out with irrigant and there is a theoretical concern about poisoning but with no reported cases [62].

- **Parallel Stenting—Intraluminal Stenting**: We had described the technique of renal pelvis decompression and stent placement through the larger diameter rigid ureteroscope several years ago [63, 64]. The larger diameter ureteroscopes would allow a 5Fr stent to be placed through their lumen, while drawing

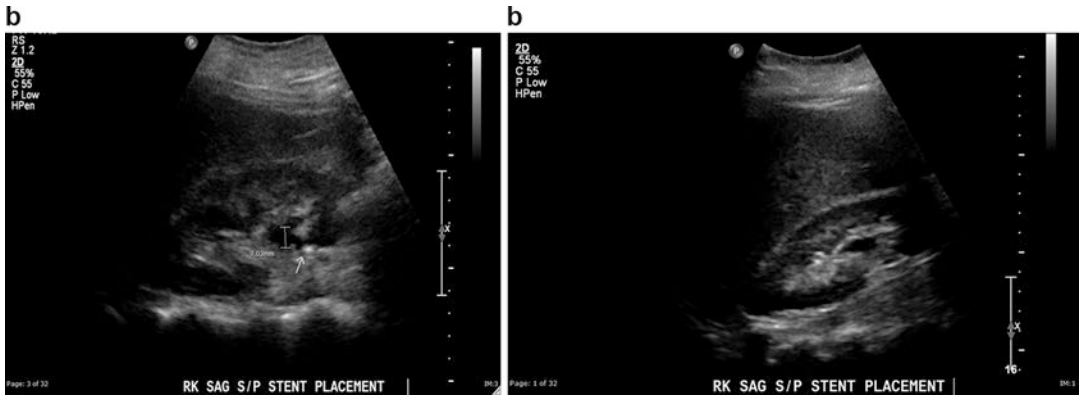

Fig. 13.15 Ultrasound post op day one APD is decreased to 9.03 mm. *Arrow* points to stent

back the scope with a pusher or a 5Fr ureteral catheter keeping the stent in place. The wire is removed when the ureteroscope is in the bladder and ultrasound also confirms the location of proximal position in the pelvis. In recent years with flexible ureteroscopy we use "Parallel technique." After ureteroscopy is completed a 4.8Fr pigtail stent is advanced over the guidewire parallel to the flexible ureteroscope while the tip of the scope is at the UPJ area. Once an adequate length of stent to allow a pigtail formation enters the renal pelvis the flexible scope is withdrawn while the stent is kept in place by the pusher, until the ureteroscope is inside the bladder and ideally at the bladder neck. At this point the wire is removed and the pusher is released and position is confirmed by ureteroscope. This "parallel stenting" technique eliminates need for fluoroscopy, change of scope, and is less traumatic (Fig. 13.16). We also use this technique in many of our regular ureteroscopy cases. Some of the modern semirigid ureteroscopes with outer diameter of 8.5–9 F and lumen size of 5 F allow for "intraluminal stenting" technique. A guidewire is inserted into the lumen of the semirigid ureteroscope and a 4.8 F-stent is advanced over the wire into the pelvis while withdrawing the ureteroscope to the bladder neck area. Due to the length of the ureteroscope the standard pusher is not long enough for this technique, instead a 5 F open-ended catheter is used to function as a pusher. The color differentiation, markings on the stent, and the open-ended catheter still helps identify the end of the stent (Fig. 13.17a, b). Proper location of the stent may also be confirmed using sonography. We routinely order a follow-up renal ultrasound at the radiology department for the next day as a formal documentation to be compared with pre-procedure images. If the urologists do not feel comfortable or have not had enough experience to perform the intraoperative sonography, they should consider requesting a radiologist or a sonographer imaging technician, as per the regulation of the institution, to be present for acquisition and interpretation of images.

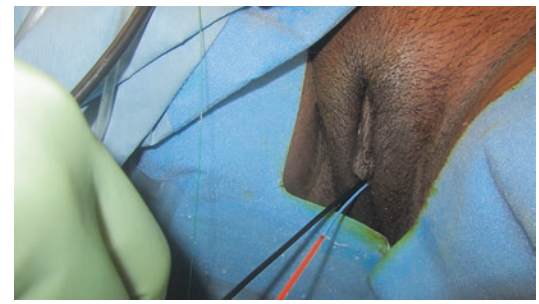

Fig. 13.16 Parallel stenting—the proximal end of ureteroscope (*black*) on the left side is at the ureteropelvic junction. The stent (*blue*) is being advanced by the pusher (*orange*) parallel to the ureteroscope

Case Studies: 1

Sonography of the lower pelvis on the right side in a pregnant patient with right flank pain shows echo and shadowing, which is suggestive of the

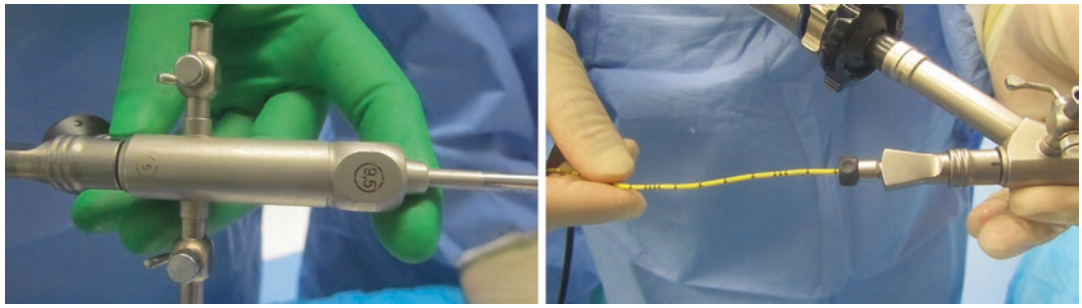

Fig. 13.17 Intraluminal Stenting —(**a**) the 9.5 F semirigid ureteroscope with a 5 F channel allows for insertion of the stent through the lumen of the ureteroscope. (**b**) a 5 Fr open ended catheter used as a pusher

presence of ureteral stone (9c). This patient had undiagnosed, complete duplication of the right collecting system, with two stones obstructing both ureters. After ureteroscopy and stone removal of one stone, intraoperative ultrasound continued to show persistence of an echogenic area. Further evaluation of the trigone revealed a second orifice and ureter with an obstructing stone (Fig. 13.18a–f).

Case Study 2

Thirty-nine year old woman at 12 weeks of gestation of her first pregnancy with twins was evaluated for left flank pain. One week earlier she was evaluated elsewhere and after pain had subsided she was discharged with the diagnosis of spontaneous stone passage. At the time of her evaluation renal ultrasound showed significant left hydronephrosis with APD of 23.3 mm, left distal stone, and presence of not a strong ureteral jet (Fig. 13.18g–k).

At the time of ureteroscopy a 1 cm distal stone was removed. The ultrasound performed on the first post op day revealed resolution of left hydronephrosis with excellent Lt. ureteral jet, no twinkle artifact (Fig. 13.18l–n).

The most common concern during perioperative time is preterm labor and delivery. A review of 46 ureteroscopies performed during pregnancy at five tertiary centers showed two (4.3 %) obstetric complications which were preterm labor, one was managed conservatively and the other resulted in preterm delivery [65]. In a 5-year period, 117 pregnant women underwent rigid and flexible ureteroscopies for renal colic with gestational age of 9–36 weeks. Ultrasound was the imaging study in all of the patients. One patient (1.2 %) in the stone group of 86 developed sepsis. Out of these 86 patients 62 (72.1 %) were diagnosed on pre-ureteroscopy ultrasound. Twelve patients developed uterine contraction, all of the complications were managed conservatively [60]. In a smaller group of seven patients, ultrasound guided ureteroscopy was performed at the mean gestation age of 28 weeks. All patients had undergone preoperative stent placement. One patient developed premature labor [66].

Our data regarding endoscopic manipulation at New York Medical College, Westchester Medical Center over 30 years more than 50 high-risk pregnancies did not result in any fetal or maternal demise due to the urologic intervention. Procedures performed included: stent placement, rigid-flexible ureteroscopy, laser lithotripsy and percutaneous nephrostomy and stone extractions. One patient with close to term pregnancy and severe obstructive symptoms causing contraction developed labor postprocedure with normal delivery the next day. One patient had documented fetal demise on admission and prior to the urologic procedure for obstruction.

Acknowledgement The author would like to thank A. Arsanjani, MD, D. Lankford, MD and M. Degen, MD for assistance in preparing these manuscripts.

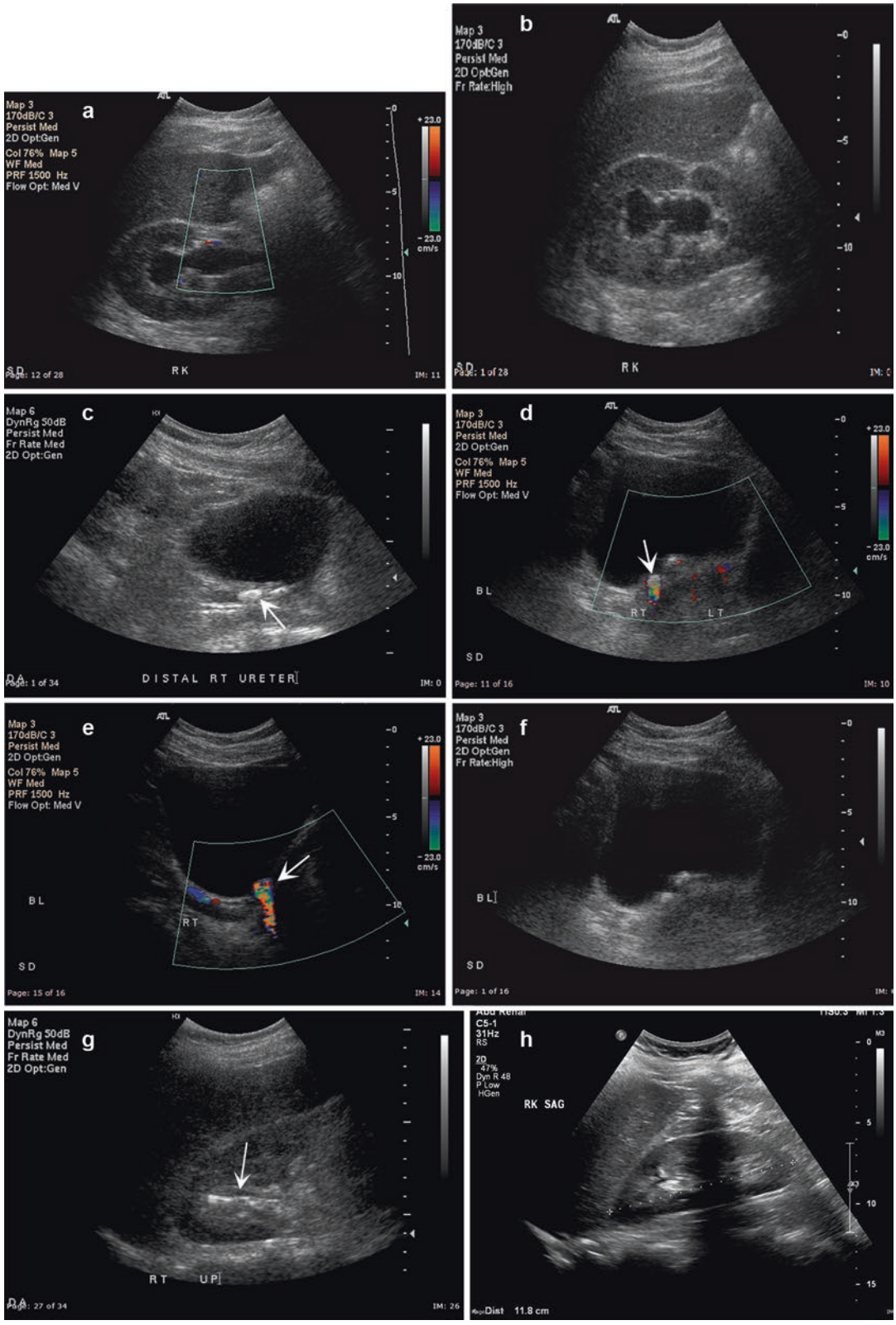

Fig. 13.18 (**a**) Ultrasound reveals dilated upper pole. (**b**) Hydronephrotic mid- and lower pole. (**c**) Pelvic ultrasound detecting two stones in the vicinity of the distal ureter(s). (**d**) Twinkle artifact confirming the first stone (*arrow*). (**e**) Twinkle artifact confirming the second stone (*arrow*). (**f**) AP view of bladder showing separation of two orifices with stone in each. (**g**) Stent in upper pole (*arrow*) (**h**) 39-year-old pregnant patient at 12 weeks of gestation

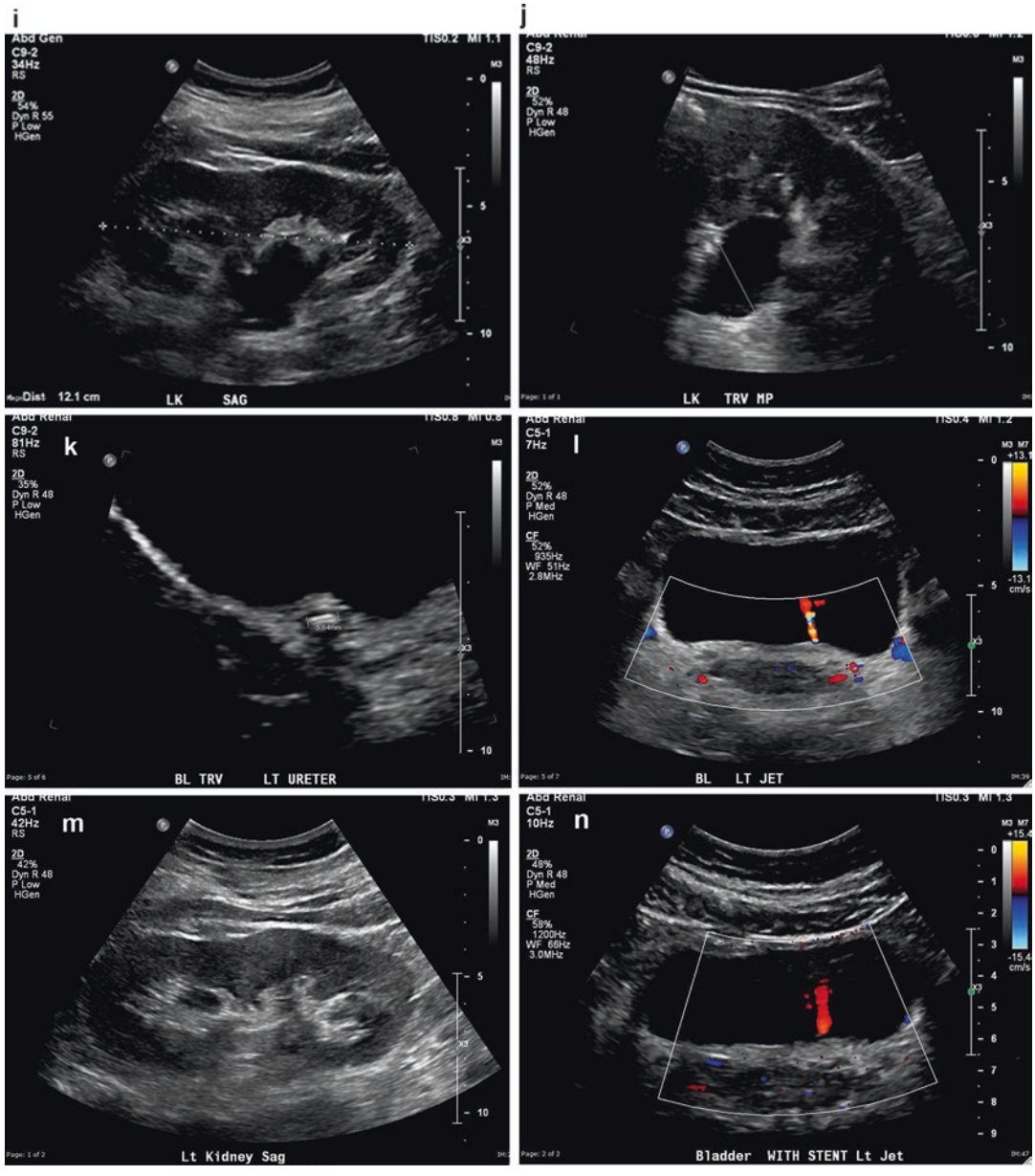

Fig. 13.18 (continued) with twin pregnancy was evaluated for second episode of left flank pain. Sagittal view of the right kidney reveals no hydronephrosis. (**i**) Sagittal images of the left kidney shows significant hydronephrosis. (**j**) Transverse mid left renal APD measurement of 23.3 mm is consistent with nonphysiologic hydronephrosis (**k**) ultrasound imaging of left distal ureter shows a 5.6 mm calculus. (**l**) Doppler imaging shows presence of ureteral jet (**m**) sagittal image of left kidney after ureteroscopy and laser lithotripsy. (**n**) Strong left ureteral jet after relief of obstruction

References

1. Moore CL, Scoutt L. Sonography first for acute flank pain? J Ultrasound Med. 2012;31:1703–11.
2. Schaeffer AJ, Schaeffer EM. Infections of the urinary tract. In: Kavoussi L, Novick A, Partin A, Peters C, editors. Campbell-Walsh urology, vol. 1. 10th ed. Philadelphia: Elsevier Saunders; 2011. p. 257–326.
3. Coe FL, Parks JH, Lindhemer MD. Nephrolithiasis during pregnancy. N Engl J Med. 1978;298:324–6.
4. Pearle M, Lotan Y. Urinary lithiasis: etiology, epidemiology, and pathogenesis. In: Kavoussi L, Novick A, Partin A, Peters C, editors. Campbell-Walsh urology, vol. 2. 10th ed. Philadelphia: Elsevier Saunders; 2011. p. 1257–86.
5. Ferrandino M, Pietrow P, Preminger G. Evaluation and medical management of urinary lithiasis. In: Kavoussi L, Novick A, Partin A, Peters C, editors. Campbell-Walsh urology, vol. 2. 10th ed. Philadelphia: Elsevier Saunders; 2011. p. 1287–323.
6. Fulgham P, Bishoff J. Urinary tract imaging: basic principles. In: Kavoussi L, Novick A, Partin A, Peters C, editors. Campbell-Walsh urology, vol. 1. 10th ed. Philadelphia: Elsevier Saunders; 2011. p. 99–139.
7. Korkes F, Rauen EC, Heilberg IP. Urolithiasis and pregnancy. J Bras Nefrol. 2014;36(3):389–95.
8. Ugboma E, Ugboma H, Nwankwo N, Okpani A. Sonographic evaluation of the renal volume in normal pregnancy at the University of Port Harcourt teaching hospital: a pilot study. J Clin Diagn Res. 2012;6(2):234–8.
9. Fried AM, Woodring JH, Thompson DJ. Hydronephrosis of pregnancy: a prospective sequential study of the course of dilation. J Ultrasound Med. 1983;2(6):255–9.
10. Rasmussen PE, Nielsen FR. Hydronephrosis during pregnancy: a literature survey. Eur J Obstet Gynecol Reprod Biol. 1988;27(3):249.
11. Schulman A, Herlinger H. Urinary tract dilation in pregnancy. Br J Radiol. 1975;48:638–45.
12. MacNeily AE, Goldenberg SL, Allen GJ, et al. Sonographic visualization of the ureter in pregnancy. J Urol. 1991;146:298–301.
13. Park SJ, Yi BH, Lee HK, et al. Evaluation of patients with suspected ureteral calculi using sonography as an initial diagnostic tool. J Ultrasound Med. 2008;27:1441–50.
14. Singh I, Strandhoy JW, Assimos DG. Pathophysiology of urinary tract obstruction. In: Wein AJ, editor. Campbell-Walsh urology. 10th ed. Philadelphia: Elsevier Saunders; 2011. p. 1087–121.
15. Peake SL, Roxburgh HB, Langlois SL. Ultrasonic assessment of hydronephrosis of pregnancy. Radiology. 1983;146:167–70.
16. Nyholm JL, Brost BC, Watson WJ. Maternal hydration status affects pelvic calyceal diameter in pregnancy. Am J Perinatol. 2008;25(3):157–9.
17. Ellenbogen PH, Scheible FW, Tainer LB, et al. Sensitivity of gray scale ultrasound in detecting urinary tract obstruction. AJR Am J Roentgenol. 1978;130:731–3.
18. Boridy I, Maklad N, Sandler C. Suspected urolithiasis in pregnant women: imaging algorithm and literature review. AJR Am J Roentgenol. 1996;167:869–75.
19. Deyoe LA, Cronan JJ, Breslaw BH, et al. New techniques of ultrasound and color Doppler in the prospective evaluation of acute renal obstruction: do they replace the intravenous urogram? Abdom Imaging. 1995;20:58–63.
20. Tublin ME, Dodd GE, Verdile VP. Acute renal colic: diagnosis with duplex Doppler ultrasound. Radiology. 1994;193:697–701.
21. Platt JF, Rubin JM, Ellis JH, et al. Distinction between obstructive and non obstructive pyelocaliectasis with duplex Doppler sonography. AJR Am J Roentgenol. 1989;153:997–1000.
22. Calenoff L, Lin PJ, Ward WF. Radiology in obstetrical practice. In: Silvio A, editor. Obstetric practice. St. Louis: CV Mosby; 1980. p. 242.
23. Hill MC, Rich JI, Mardiat JG, Finder CA. Sonography vs. excretory urography in acute flank pain. AJR Am J Roentgenol. 1985;144:1235–8.
24. Shokeir AA, Abdulmaaboud M. Prospective comparison of nonenhanced helical computerized tomography and Doppler ultrasonography for the diagnosis of renal colic. J Urol. 2001;165:1082–4.
25. Van Vuuran S, et al. Size and volume charts of fetal kidney, renal pelvis and adrenal gland. Ultrasound Obstet Gynecol. 2012;40:659–64.
26. Shivalingaiah N, et al. Fetal kidney length as a parameter for determination of gestational age in pregnancy. Int J Repro Contracept Obstet Gynecol. 2014;3(2):424–7.
27. Brown MA, et al. Screening sonography in pregnant patients with blunt abdominal trauma. J Ultrasound Med. 2005;24:175–81.
28. Talpfer NI. Hydronephrosis of pregnancy in an ectopic kidney. BJUI. 2012.
29. Olin JW, Piedmonte MR, Young JR, et al. The utility of duplex ultrasound scanning of the renal arteries for diagnosing significant renal artery stenosis. Ann Intern Med. 1995;122:833–8.
30. Tublin ME, Buda RO, Platt JI. The resistive index in renal Doppler sonography: where do we stand? AJR Am J Roentgenol. 2003;180:885–92.
31. Hertzberg BS, Carroll BA, Bowie JP, et al. Doppler US assessment of maternal kidneys: analysis of intrarenal resistivity indexes in normal pregnancy and physiologic pelvicaliectasis. Radiology. 1993;186:689–92.
32. Soria Gálvez F. Usefulness of renal resistive index in the diagnosis and evolution of the obstructive uropathy. Experimental study. Actas Urol Esp. 2007;31(1):38–42.
33. Shokeir AA. Renal colic in pregnant women: role of renal resistive index. J Urol. 2000;55(3):344–7.
34. Azam A, Ul-Hag A, Beg M. Role of renal arterial resistive index (RI) in obstructive uropathy. J Pak Med Assoc. 2013;63:1511–5.

35. Peterson J, et al. The pulsatility index and the resistive index in renal arteries. Associations with long-term progression in chronic renal failure. Nephrol Dial Transplant. 1997;12:1376–80.
36. Renowden SA, Cochlin DC. The effect of intravenous furosemide on Doppler wave form in normal kidneys. J Ultrasound Med. 1992;11:65.
37. Shokeir AA, Provost AP, El Azab M, et al. Renal Doppler ultrasound in children with obstructive uropathy: effect of intravenous normal saline fluid load and furosemide. J Urol. 1996;156:1455.
38. Farmakides G, Schulmand H, Schneider E. Surveillance of pregnant hypertensive patient with Doppler flow velocimetry. Clin Obstet Gynecol. 1992;35:387–94.
39. Mallek R, Bankier AA, Etele-Hainz A, et al. Distinction between obstructive and non obstructive hydronephrosis: value of diuresis duplex Doppler sonography. AJR Am J Roentgenol. 1996;166:113–7.
40. Roberts VH, et al. Quantitative assessment of placental perfusion by contrast-enhanced ultrasound in macaques and human subjects. Am J Obstet Gynecol. 2016;214(3):369.e1–8.
41. Zhou YJ, et al. Real-time placental perfusion on contrast-enhanced ultrasound and parametric imaging analysis in rats at different gestation time and different portions of placenta. PLoS One. 2013;8(4):e58986. doi:10.1371/journal.pone.0058986.
42. Jerde TJ, Calamon-Dixon JL, Bjorling DE, et al. Celecoxib inhibits ureteral contractility and prostanoid release. Urology. 2005;65:185.
43. Pozniak MA, Kelcz F, Stratta RJ, Oberley TD. Extraneous factors affecting resistive index. Invest Radiol. 1988;23:899–904.
44. Sjodin JG. Clinical experience of indomethacin in pain from ureteral stone. Scand J Urol Nephrol. 1983;75:35–6.
45. N'Guyen Tand Lung R, Cirarci-Vigneron N, Rabbe A, et al. Interet de l'echographie du rein maternel pendant la grassesse. Annu Radiol (Paris). 1986;20:381–3.
46. Grenier NL, Parient JL, Trillaud H, et al. Dilatation of the collecting system during pregnancy: physiologic vs obstructive dilatation. Eur Radiol. 2000;10(2):271–9.
47. Faudes A, Bricola-Rilho M, Pinto E, et al. Dilatation of urinary tract during pregnancy: proposal of a curve of maximal caliceal diameter by gestational age. Am J Obstet Gynecol. 1998;178:1082–8.
48. Lee RS, et al. Antenatal hydronephrosis as a predictor of postnatal outcome: a meta-analysis. Pediatrics. 2006;118(2):586–93.
49. Burge HL, Middleton WB, McClennan BL, et al. Ureteral jets in healthy patients and in patients with unilateral ureteral calculi: comparison with color Doppler ultrasound. Radiology. 1991;180:437–42.
50. Cox IH, Erickson SJ, Foley WD, et al. Ureteral jets: evaluation of normal flow dynamics with color Doppler sonography. AJR Am J Roentgenol. 1992;158:1051–5.
51. Baker SM, Middleton WD. Color Doppler sonography of ureteral jets in normal volunteers: importance of the relative specific gravity of urine in the ureter and bladder. AJR Am J Roentgenol. 1992;159:773–5.
52. Dubbins PA, Kurtz AB, Darby J, Goldberg B. Ureteric jet effect: the echographic appearance of urine entering the bladder. Radiology. 1981;140:513–5.
53. Delair SM, Kurzrock EA. Clinical utility of ureteral jets: disparate opinions. J Endourol. 2006;20(2):111–4.
54. Bailey G, et al. Perinatal outcomes with Tamsulosin therapy for symptomatic urolithiasis. J Urol. 2016;195:99–103.
55. Laing FC, Benson CB, DiSalvo DN, et al. Distal ureteral calculi: detection with vaginal ultrasound. Radiology. 1994;192:545–8.
56. Damani N, Wilson SR. Non gynecologic application of transvaginal US. Radiographics. 1999;19:S179–200.
57. Lee JY, Kim SH, Cho JY, et al. Color and power Doppler twinkling artifacts from urinary stones: clinical observation and phantom studies. AJR Am J Roentgenol. 1992;159:773–5.
58. Karabulut N, Karabulut A. Color Doppler evaluation of ureteral jets in normal second and third trimester pregnancy: effect of patient position. Br J Radiol. 2002;75(892):351–5.
59. Swartz HM, Reichling BA. Hazards of radiation exposure for pregnant women. JAMA. 1978;239:1907–8.
60. Zhang S, et al. Application of ureteroscope in emergency treatment with persistent renal colic patients during pregnancy. PLoS One. 2016;11(1):e1046597. doi:10.1371/journal.pone.0146597.
61. Abdel-Kader M, et al. Management of symptomatic ureteral calculi during pregnancy: experience of 23 cases. Urol Ann. 2013;5(4):241–4.
62. Tan A, et al. Endourologic technique: surgery during pregnancy. In: Smith textbook of endourology. 2nd ed. Hamilton: DC Becker; 2007. p. 877–82.
63. Eshghi M, Addonizio J. Renal pelvis decompression during ureteroscopy. Urology. 1987;29:398–9.
64. Eshghi M. Pressure controlled hydraulic dilation of ureter: a new approach to one-step ureteroscopy. AUA Annual meeting 1988. Karl Storz Film library; 1988.
65. Johnson E, et al. Obstetric complications of ureteroscopy during pregnancy. J Urol. 2012;188(1):151–4.
66. Deters L, et al. Ultrasound guided ureteroscopy in pregnancy. Clin Nephrol. 2013;79:118–23.

Application of Urologic Ultrasound in Pelvic and Transplant Kidneys

14

Majid Eshghi

Ultrasound Evaluation of Pelvic Kidneys

Pelvic kidneys are either congenital or transplanted. The transplant kidney can be either autotransplant, deceased donor, living-related, or living unrelated in anephric or end-stage renal disease patients requiring dialysis.

The anatomy of the congenital pelvic kidneys is different from the surgically implanted pelvic kidneys. Congenital kidneys are located centrally and like cross-fused ectopia have normal ureteral orifices (Fig. 14.1). Renal ultrasound can reveal common problems with pelvic kidneys, such as stone formation and hydronephrosis due to malrotation and poor drainage. Sonography of the congenital pelvic kidneys can sometimes be difficult or impossible because it is superimposed by the bowel, but the assessment of ureteral jets is simple due to the normal location of orifices.

On the other hand, transplant kidneys are commonly placed extraperitoneally in the right or left lower quadrants. This anatomic arrangement provides for an easy imaging target since the distance between the skin and the kidney is short, without bowel interposition. The transplant kidney ureters are implanted into the bladder, commonly in the anterior lateral location using a modified Lich-Gregoir technique. Depending on the technique of anastomosis, there may be a **nipple artifact** in the bladder, which can be detected via ultrasound. Stones can be formed at this site which produces an echo during imaging. Doppler application reveals significant twinkle artifact [1] (Figs. 14.2 and 14.3).

Post surgery, the hilar anatomy of a transplant kidney differs from the native kidney. In these kidneys, the pelvis is more anterior, whereas the artery and vein are situated more posteriorly. Ultrasound imaging of the transplant kidneys is performed from the anterior abdominal wall with the patient in the supine position. In the post-transplant kidney, the renal artery and vein have a different orientation. The renal artery is anastomosed to either the internal iliac end to end or external iliac artery end to side. The renal vein is anastomosed to the external iliac vein end to side. The knowledge of this altered anatomy is critical for ultrasonographer. A basic allograft ultrasound evaluation is usually performed 24–48 h post transplant unless indicated sooner due to clinical findings. A detailed examination protocol usually includes renal size, assessment of echogenicity, collecting system, ureter, and evaluation of fluid collections. Doppler imaging should assess flow in the renal and iliac vessels. Intrarenal vessels are also assessed along with flow quantification, RI, PI, and systolic to diastolic ratio [2].

M. Eshghi, M.D., F.A.C.S., M.B.A. (✉)
Department of Urology, New York Medical College, Westchester Medical Center, 100 Woods Road, Bldg 19 Skyline Drive 1S-B48, Valhalla, New York, NY 10595, USA
e-mail: Majid_Eshghi@nymc.edu

P.F. Fulgham, B.R. Gilbert (eds.), *Practical Urological Ultrasound*, Current Clinical Urology,
DOI 10.1007/978-3-319-43868-9_14

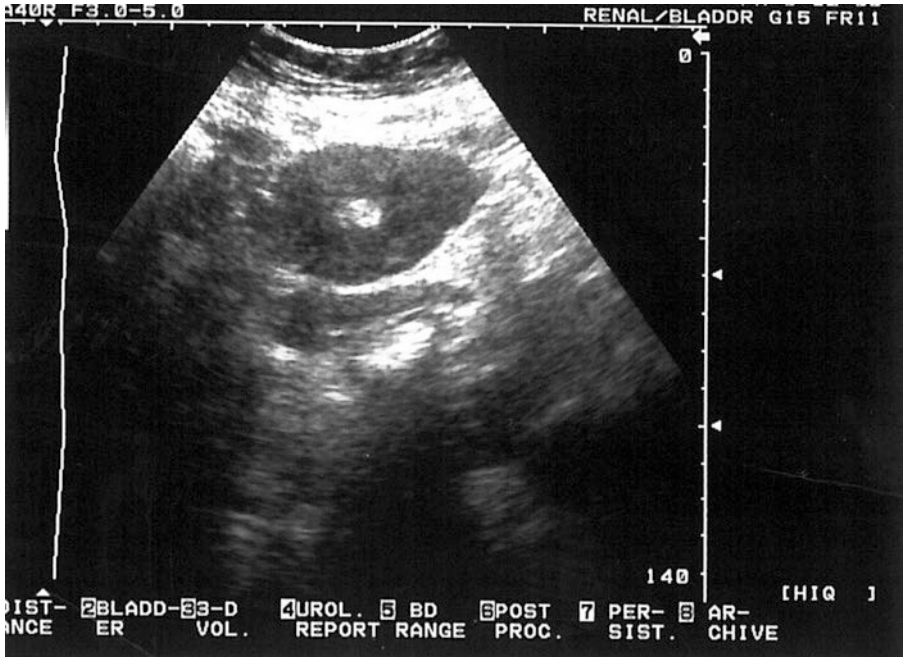

Fig. 14.1 A 48-year-old female with a right congenital pelvic kidney and 1 cm stone. Note that there are no usual boundaries such as liver or spleen

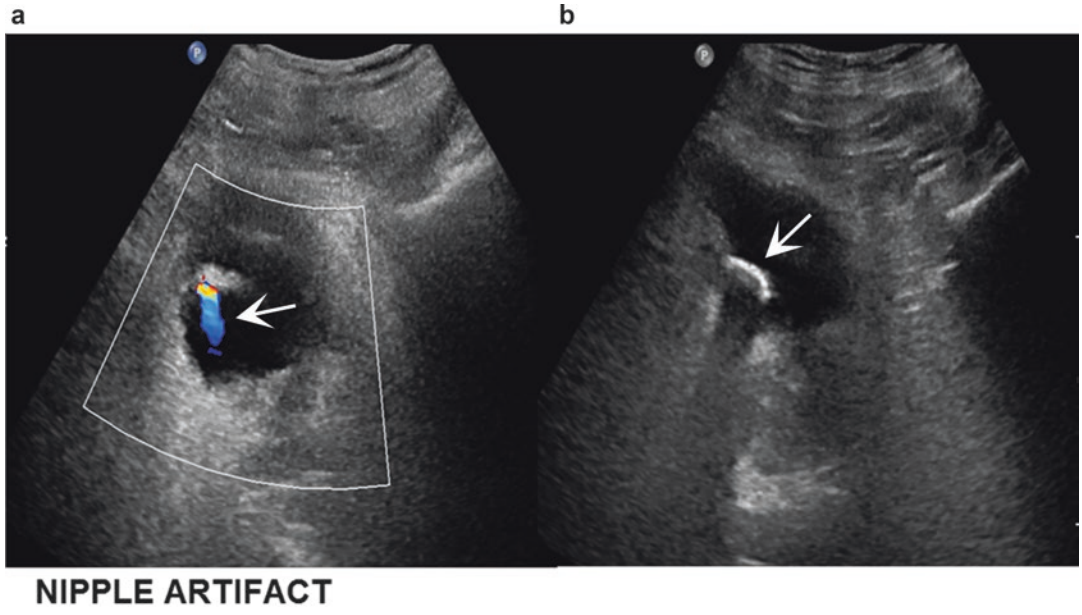

Fig. 14.2 Stone at the stump of a ureteral implant (**b**) with echo and posterior shadowing (*arrow*). Note the "twinkling" artifact with the Doppler wave (**a**)

Renal transplant sizes are similar to native kidneys; however, gradual increase of its dimensions can be seen over the first few weeks by up to 32 % of the initial length by the fourth week [3].

Doppler evaluation of the transplant kidney and renal vasculature is usually the first method for studying the kidney during the postoperative period for routine follow-up or when there is

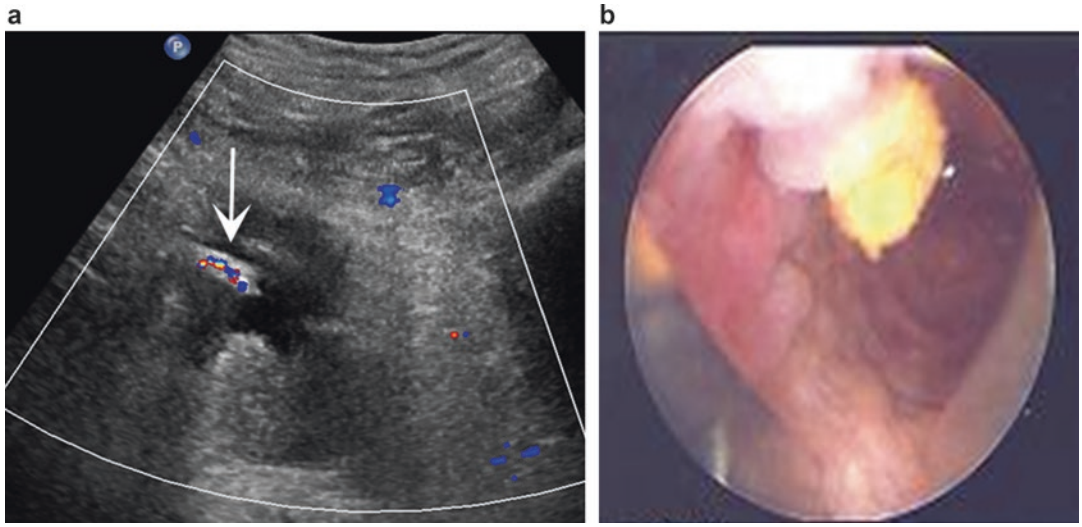

Fig. 14.3 A nipple artifact (**a**) at the anterolateral aspect of the bladder on sonography (*arrow*) represents the location of an implanted ureter. Endoscopic view of stone (*arrow*) formation at implant (**b**) site

dysfunction noted in the graft. These applications include the assessment for rejection, renal artery stenosis, and thrombosis of the renal artery or vein. Obviously some of the drainage complications in a transplant kidney such as ureteral obstruction, leakage, urinoma, and lymphocele can also be identified with ultrasound imaging [4].

Peak systolic velocity (**PSV**) in transplant kidneys is usually 100 ± 25 cm/s. In cases of renal artery stenosis (RAS), the PSV is between 180 and 200 cm/s.

Renal aortic ratio (**RAR**) is another tool to assess the degree of renal artery stenosis, and it is calculated from the following equation:

$$\frac{\text{Renal peak systolic velocity}\left(\text{RPSV}\right)}{\text{Aortic peak systolic velocity}\left(\text{APSV}\right)}$$

RAR is considered normal up to 3.0, but **a ratio of more than 3.5 generally indicates renal artery stenosis** [5].

RI: A resistive index of more than 0.9 usually indicates renal transplant dysfunction. Causes of elevated RI in renal transplants are shown in (Fig. 14.4).

Power Doppler (**PD**), also known as nondirectional Doppler, is useful for assessing low flow states, or when optimal Doppler angles cannot be obtained. PD is 3–5 times more sensitive in depicting flow than the color Doppler imaging in all arteries (CDI) [6, 7]. Unlike CDI, PD does not provide information relative to velocity or direction of the blood flow. In transplant kidneys, PD is an invaluable tool for the evaluation of vascular thrombosis, occlusion of vessels, and evaluation of the parenchymal flow. Unlike the CDI red and blue color scheme, PD typically has a single salmon color appearance (Fig. 14.5a, b). The color schema can be changed by the sonographer. Color red is customarily assigned to arterial and color blue to venous flow. Newer versions of some of the ultrasound machines have the capability of performing directional power doppler (eFLOW) (Fig. 14.7e).

Contrast-Enhanced Ultrasound (**CEUS**): Gray scale with color Doppler imaging remains the initial basic diagnostic procedure of transplant kidneys. Although color Doppler can assess renal arterial and venous flow, it cannot display subtle microvascular tissue perfusion which is crucial for evaluation of acute and chronic allograft dysfunction. Real-time contrast-enhanced ultrasound using gas-filled microbubbles can visualize and also quantify renal blood flow and perfusion in small arterioles and capillaries [8]. Microbubbles act as a contrast agent by creating surface between the fluid phase in blood at the outside and gaseous phase at the inside. This change of

Causes of elevated RI	
Parenchymal	Acute rejection Acute tubular necrosis pyelonephritis
Vascular	Renal vein thrombosis Hypotension
Urological	Ureteral obstruction
Technical	Graft compression

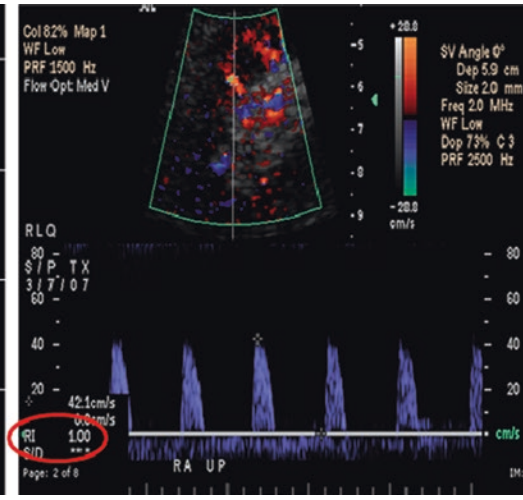

Fig. 14.4 Table showing causes of elevated RI. Doppler evaluation showing RI of 1.00 indicated a lack of diastolic blood flow: a classic finding in renal vein thrombosis (*right image*)

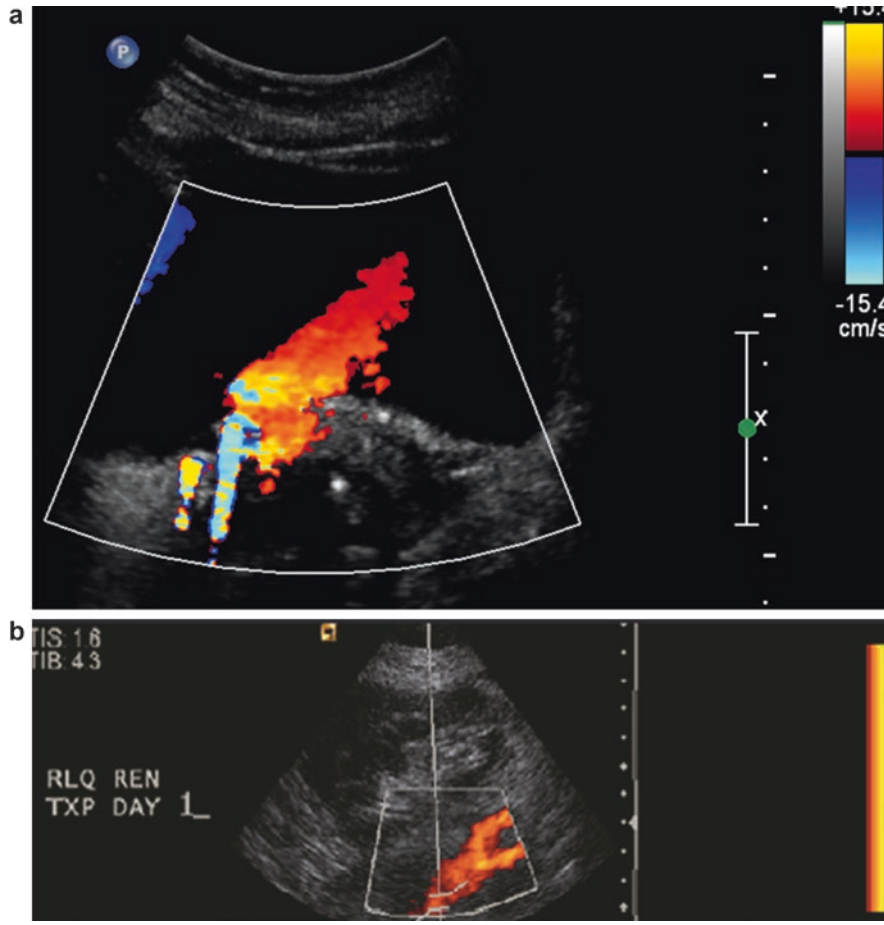

Fig. 14.5 (**a**) Color Doppler with *red* and *blue bar* indicating the flow towards (*red*) in this case egress of urine towards transducer and (*blue*) away. (**b**) Due to lack of flow on color power Doppler (*salmon*) color is used to assess the flow to a transplant kidney

impedance and reflection enhances echogenicity of blood by a factor of 500–1000. This modality is not yet used widely in the United States. The gas is exhaled through the lungs within 20–30 min and the shell is metabolized in the liver [9]. This agent is not excreted in the urinary tract and thus cannot provide excretory urography and should not be used in patients with severe cardiopulmonary disease where as impaired renal function is not a contraindication. Impaired renal function is not a contraindication. Indications for CEUS in renal transplant include assessment of renal blood flow, vasculopathy, small peripheral infarcts, and necrosis. CEUS proved to be helpful in patients with acute rejection by showing delayed parenchymal perfusion. CEUS also has some values in prognosticating allograft function. Finally this modality also has some applications in space occupying and inflammatory lesions.

In one study 91 patients were evaluated after living renal transplant within the first week and 6 months of transplant. Resistive Index (RI), Pulsatility Index (PI), End Diastolic Velocity (EDV), graft length, and parenchymal volume were measured. It was concluded that lower RI, PI and higher EDV at 1 week predicted a better graft function at 6 months post transplantation [10]. A recent retrospective study reviewed 575 renal transplant ultrasound obtained within 4 h of surgery. The authors examined major vascular abnormalities: lack of renal artery or vein flow, elevated PSV >300 cm/s, parvus tardus waveforms, and markedly decreased or no color parenchymal flow identified the cases most likely to benefit from immediate reoperation [10].

Shear Wave Elastography (SWE): Shear Wave Elastography (SWE) and its variants referred to as Real Time Sonoelastography (RTS), Super Sonic Shear Imaging (SSI), Time Stress Imaging (TSI) Transient Elastography (TE) and Shear Wave Dispersion Ultrasound Vibrometry (SDUV) are the latest additions to ultrasound imaging. This is an emerging sonographic technique that permits noninvasive measurement of tissue stiffness. SWE uses focused acoustic energy pulses to produce microscopic tissue displacement which includes perpendicular shear waves that are sonographically tracked as they travel through tissue. Harder and stiffer tissues have been shown to have increased shear wave velocities. Estimates of tissue Young's module (YM) which is expressed in Kilopascals (kPa) are derived from shear wave velocity. The ultrasound monitor has vertical color bar similar to Doppler indicating soft (benign) versus stiff (hard) tissue (tumor, fibrosis). Elastography has been shown to be a good tool for identifying fibrosis. There is a dynamic display of pressure distribution as well. In a different model of this technology, the pulses are delivered mechanically by the operator which requires a learning curve. SWE is approved in the USA for assessment of liver fibrosis in cirrhosis and outside the USA it has already been used extensively in imaging of breast and thyroid and is being evaluated for other clinical uses as well. SWE has been used for assessment of chronic kidney disease as well as renal transplants. In urology, it also has potential value in testicular and prostate imaging. Transrectal sonography with doppler and grayscale elastography can be considered a multiparametric prostate ultrasound. Patients with CKD show higher tissue stiffness with renal fibrosis as a plausible explanation. In native kidneys, the shortest distance to the kidney should be chosen to provide better images with several variables. BMI and kidney depth are the main variants. **Renal allograph due to their superficial position in pelvis allows to eliminate the above variants thus rendering SWE as a valuable tool for assessment of chronic allograft dysfunction secondary to progressive interstitial fibrosis and tubular atrophy**. In another study SWE results of allografts cortical stiffness was performed along with renal biopsy. This quantitative measurement showed to be promising as a noninvasive tool to evaluate global histological deterioration. In another study elastography could identify stages of renal graft damage. One study showed 94.5% success in assessing kidney stiffness and with newer studies there appear to be adequate data to use elastography as a noninvasive method to evaluate renal allograft fibrosis, one of the first signs of graft dysfunction [11–19].

Ultrasonic Findings in Transplant Complications

Renal Cell Carcinoma: This is not a common finding in transplanted kidneys (Fig. 14.6a–d). The incidence of RCC in atrophic native kidneys is 1.1–1.55% versus 0.22–0.25% in transplanted kidneys [20] (Fig. 14.7a–e).

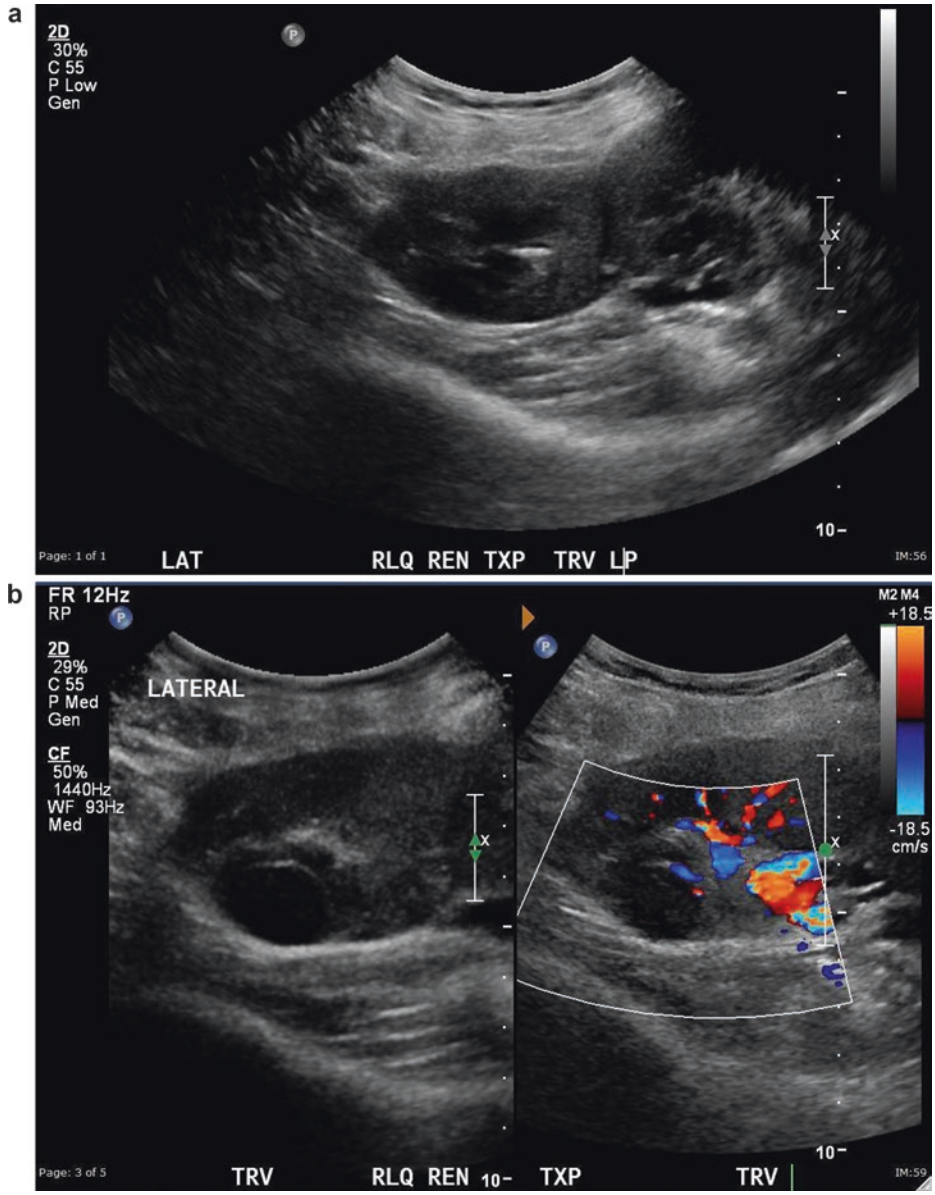

Fig. 14.6 (**a**) A 64-year-old female with a double pediatric kidney allograph in RLQ. (**b**) The lateral superior component shows a solid mass. (**c**) Image of the lateral kidney after microwave ablation of renal cell carcinoma. (**d**) Elastography of the medial noninvolved kidney shows homogenous parenchyma. The center of the kidney with the fluid represents a softer image

Transitional Cell Carcinoma: This is a very rare finding in transplanted kidneys except in southeast Asia where consumption of Chinese herbs containing aristolochic acid shows a high incidence of this disease [21]. Special follow-up attention should be given to recipients who had a high-risk donor such as history of smoking, diagnosis of urothelial carcinoma after donating a kidney and if the recipient has been exposed to such risk factors.

- **Acute tubular necrosis (ATN)**: In this condition, the kidney is grossly edematous, echo poor, with a lack of corticomedullary differen-

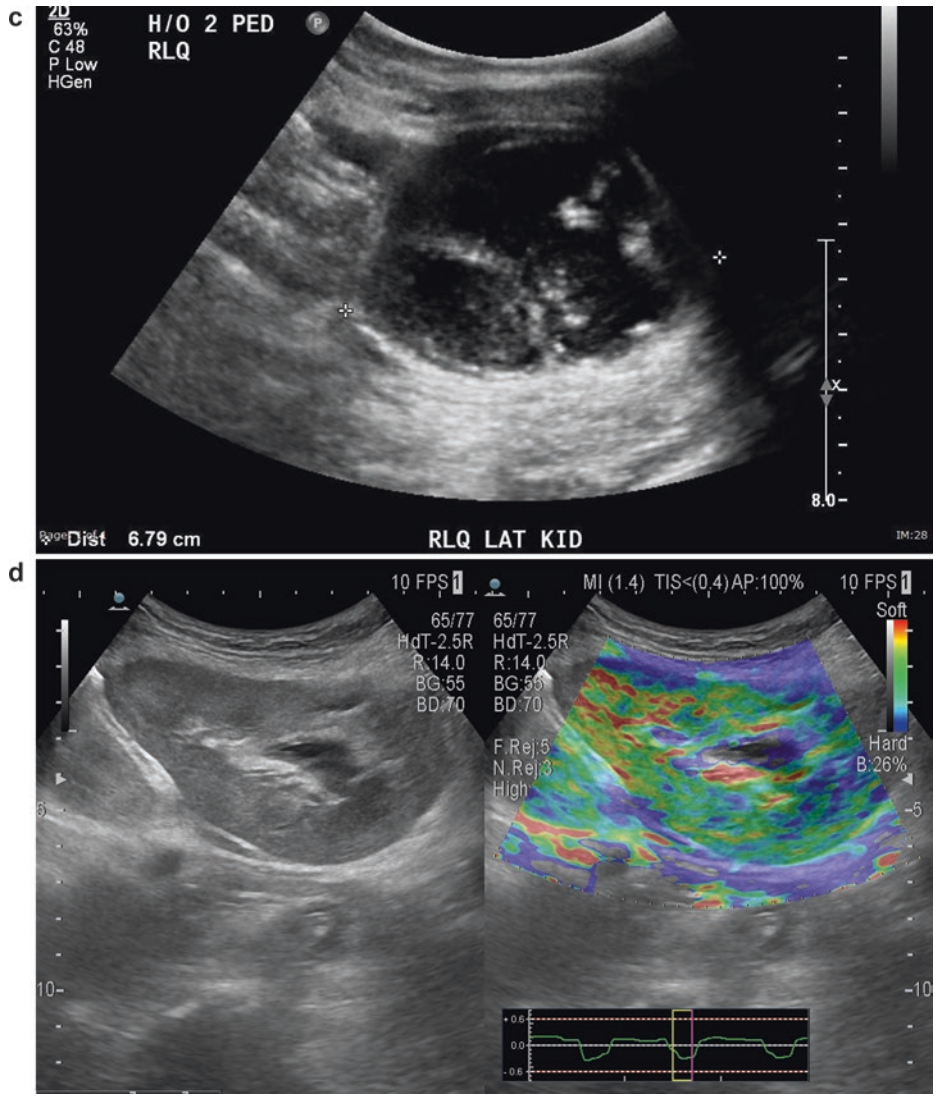

Fig. 14.6 (continued)

tiation. RI is elevated to over 0.8 (Fig. 14.8). Nuclear scan is the primary imaging modality for ATN assessment.

- **Acute rejection**: Grayscale and spectral ultrasound imaging typically reveals graft enlargement due to edema, decreased cortical echogenicity, and swelling of the medullary pyramids resulting in loss of corticomedullary differentiation. The renal sinus fat may show edema as well on spectral Doppler imaging.
- **Chronic rejection**: Imaging of a chronically rejected kidney shows a small graft, thin, echogenic renal cortex, and relative sparing of medullary pyramids. In chronic rejection RI is typically normal or slightly elevated [4].
- **Fungas ball and Foreign body**: Chronically infected and obstructed kidneys can develop organized amorphous intrarenal debris or fungus balls. This can be a rapid process due to the patient's immunocompromised state. Sonography can detect these lesions readily. Broken stents in the collecting system and fragments of stones dislodged into the paren-

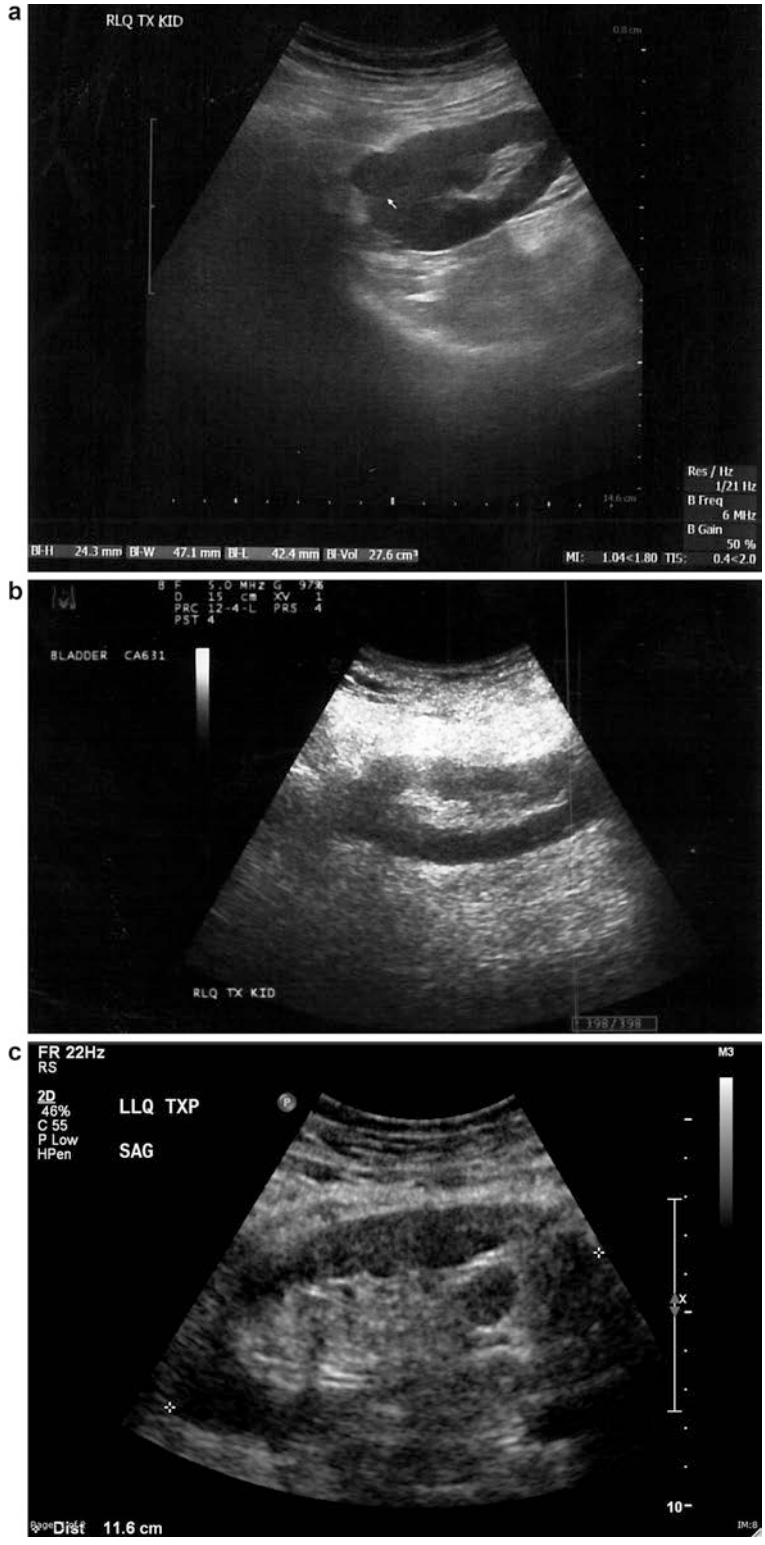

Fig. 14.7 (**a**) An 83-year-old male s/p bilateral autotransplantation for bilateral renal cell carcinoma at age 72 there was a recurrence in the RLQ which was resected. (**b**) At age 82 appearance of the RLQ kidney after partial nephrectomy. (**c**) At age 82 patient developed another recurrence in LLQ-transplanted kidney saggital view. (**d**) LLQ-transplanted kidney cross section view showing measurement. (**e**) eFLOW (sensitive power Doppler) shows presence of central flow in

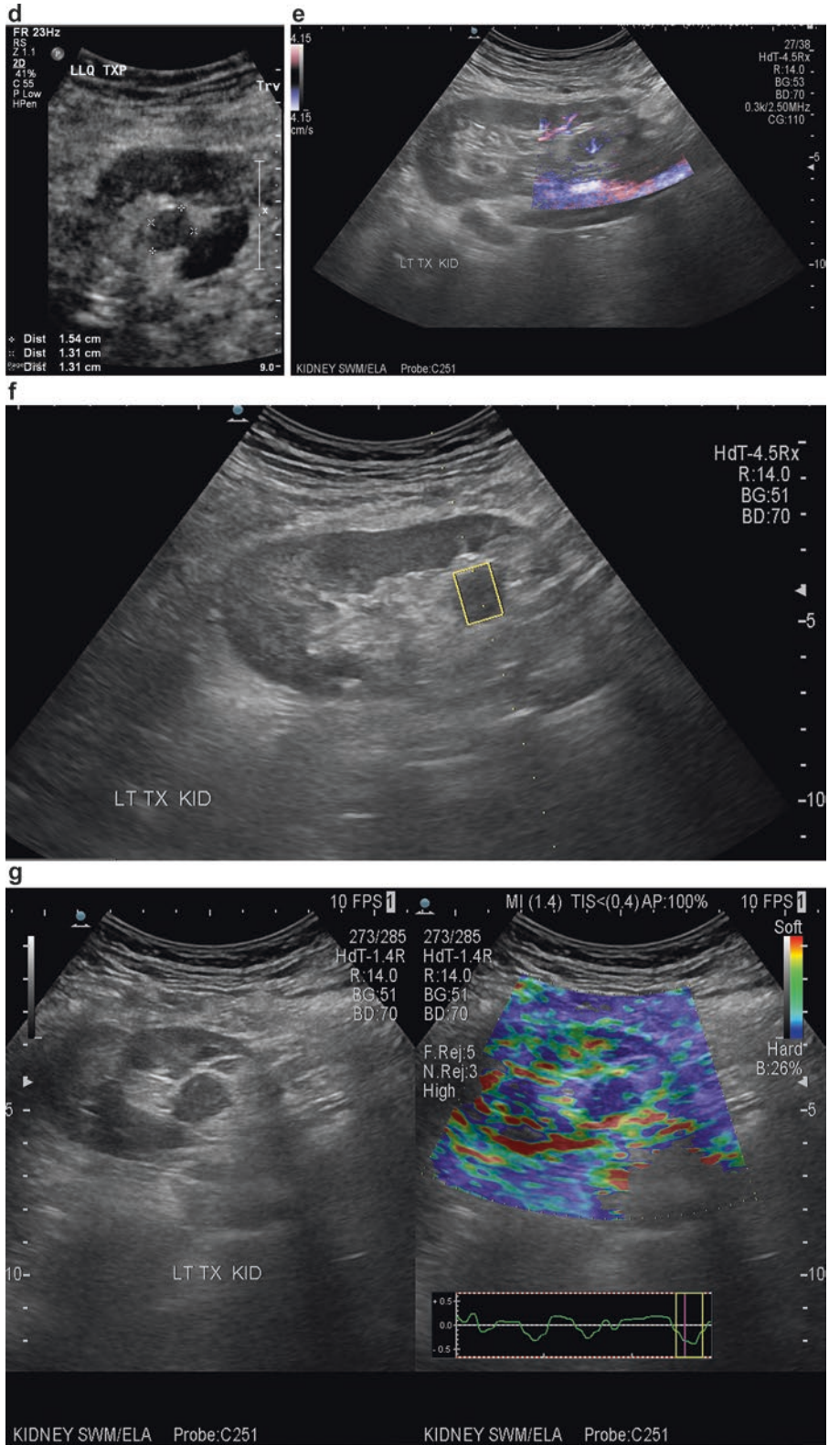

Fig. 14.7 (continued) the lesion. (**f**) Shear wave measurement of the lesion. (**g**) Shear wave elastography of the LLQ allograft shows "tissue hardness" discrepancy. The suspected lesion is dominantly blue suggestive of tumor versus the normal parenchyma showing softer color

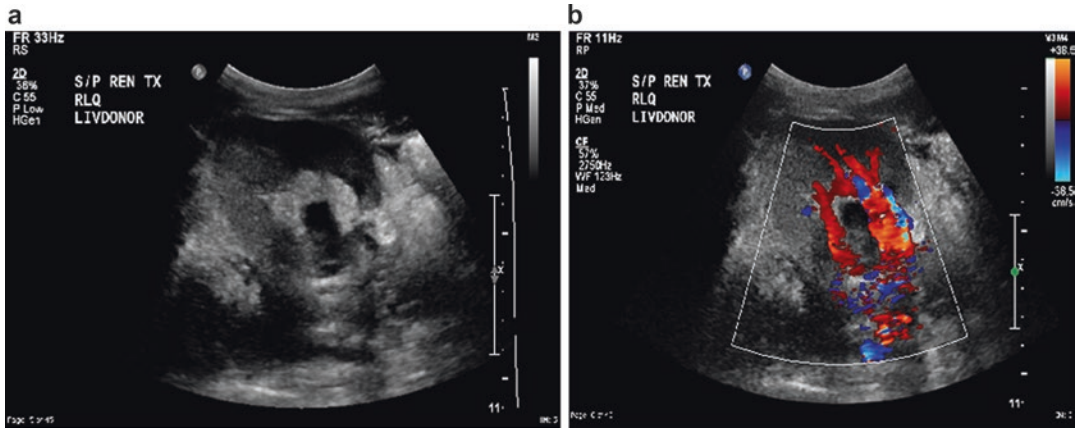

Fig. 14.8 Transverse grayscale image of a kidney 2 days post transplant with decreased urine output secondary to acute tubular necrosis (**a**). Note that the renal vascular supply is intact (**b**)

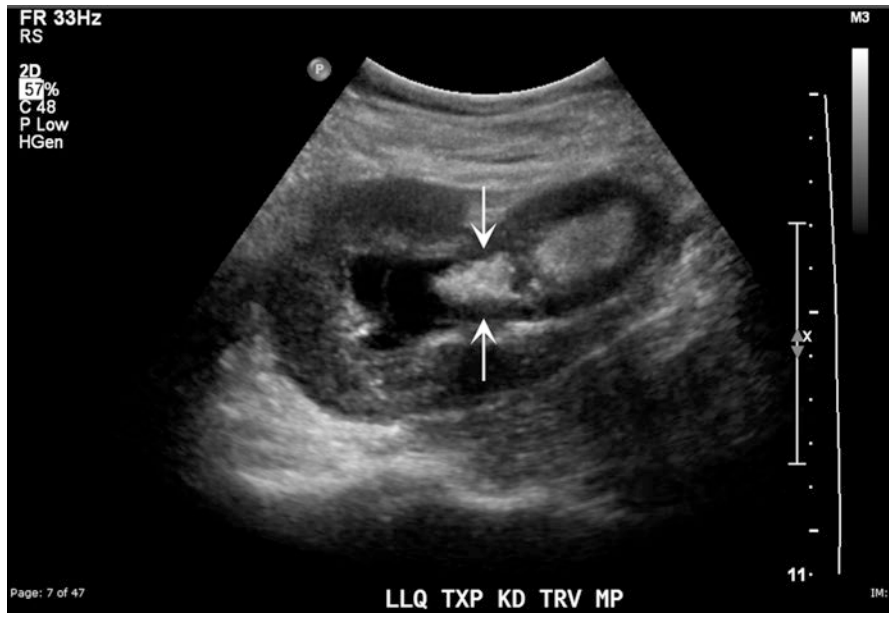

Fig. 14.9 A left lower quadrant transplant kidney obstructed with infectious amorphous debris. Filling defects in the center and the pelvic portion of the collection system are readily visible (*arrows*)

chyma are some examples of foreign bodies. (Fig. 14.9).

- **Renal vein thrombosis**: This is a surgical emergency and occurs in less than 1–2 % of cases. Early detection of RVT is critical because it requires immediate surgical exploration. Doppler evaluation is diagnostic in these cases, since there are no collateral pathways in transplanted kidneys. The findings include enlarged kidney with absent venous flow on color Doppler or power Doppler and distended and thrombus-filled main renal vein. On arterial Doppler, wave will be prolonged, and in a U-shape or plateau-like pattern, due to a diagnostic reversal of arterial flow in diastole (Fig. 14.10a, b) [22–24].
- **Renal artery thrombosis (RAT)**: A rare condition occurring in less than 1 %, usually due

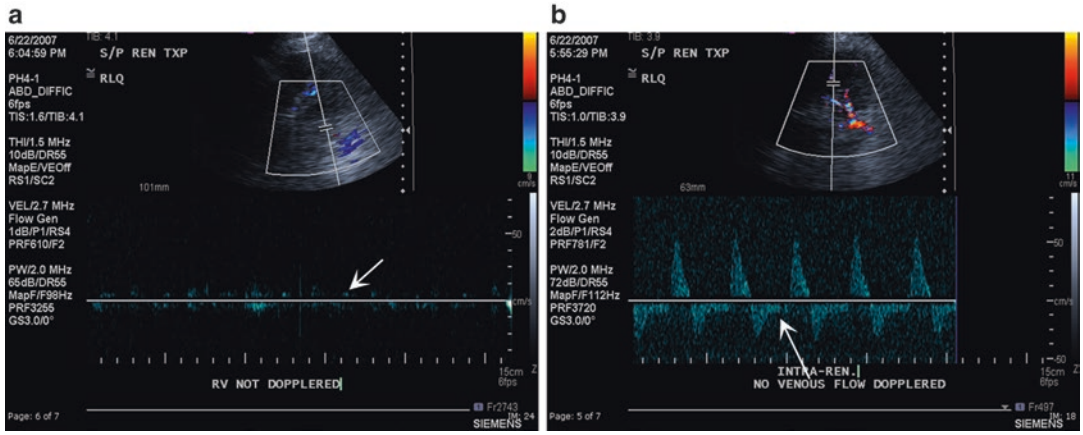

Fig. 14.10 (**a**, **b**) Renal vein thrombosis. Doppler imaging of the renal hilum in a patient with renal vein thrombosis showing the absence of venous flow (*arrow*) (**a**) and spectral Doppler shows reversal of arterial flow (below the line) in diastole (*arrow*): classic sign of RVT (**b**)

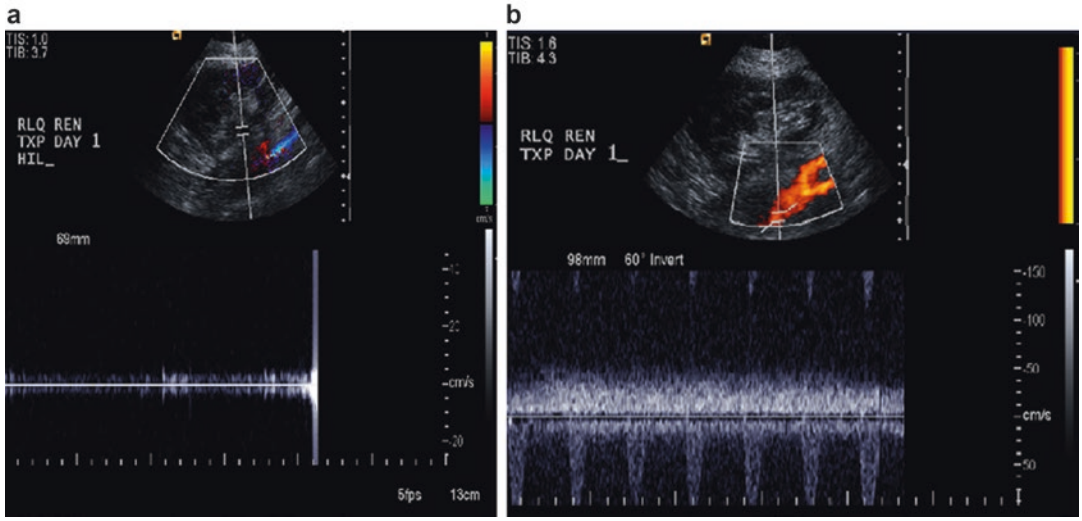

Fig. 14.11 (**a**, **b**) Patient with acute drop of urine output on the first day post renal transplantation (**a**). Doppler imaging of the renal hilum reveals the absence of flow in the transplanted renal artery (**b**). Power Doppler (*salmon color*) shows good flow in the iliac vessels. Renal artery thrombosis was confirmed at the time of surgical exploration

to technical reasons. The patients are anuric and hypertensive and Doppler ultrasound imaging reveals the absence of arterial flow (Fig. 14.11) [4].

- **Renal artery stenosis**: This condition is usually accompanied by a rise in serum creatinine, hypertension, and a bruit over the graft can be auscultated. Grayscale ultrasound findings suggest the appearance of a structurally normal kidney, whereas the CDI of renal artery displays a high-velocity jet exceeding peak flow in the iliac artery (distalstenotic jet effect). A pathologically low RI within the graft equal to or less than 0.6 may be highly specific for stenosis of over 50 % since the actual flow is low within the kidney. **Parvus Tardus**, which is a small amplitude waveform with a prolonged systolic rise (slow upstroke),

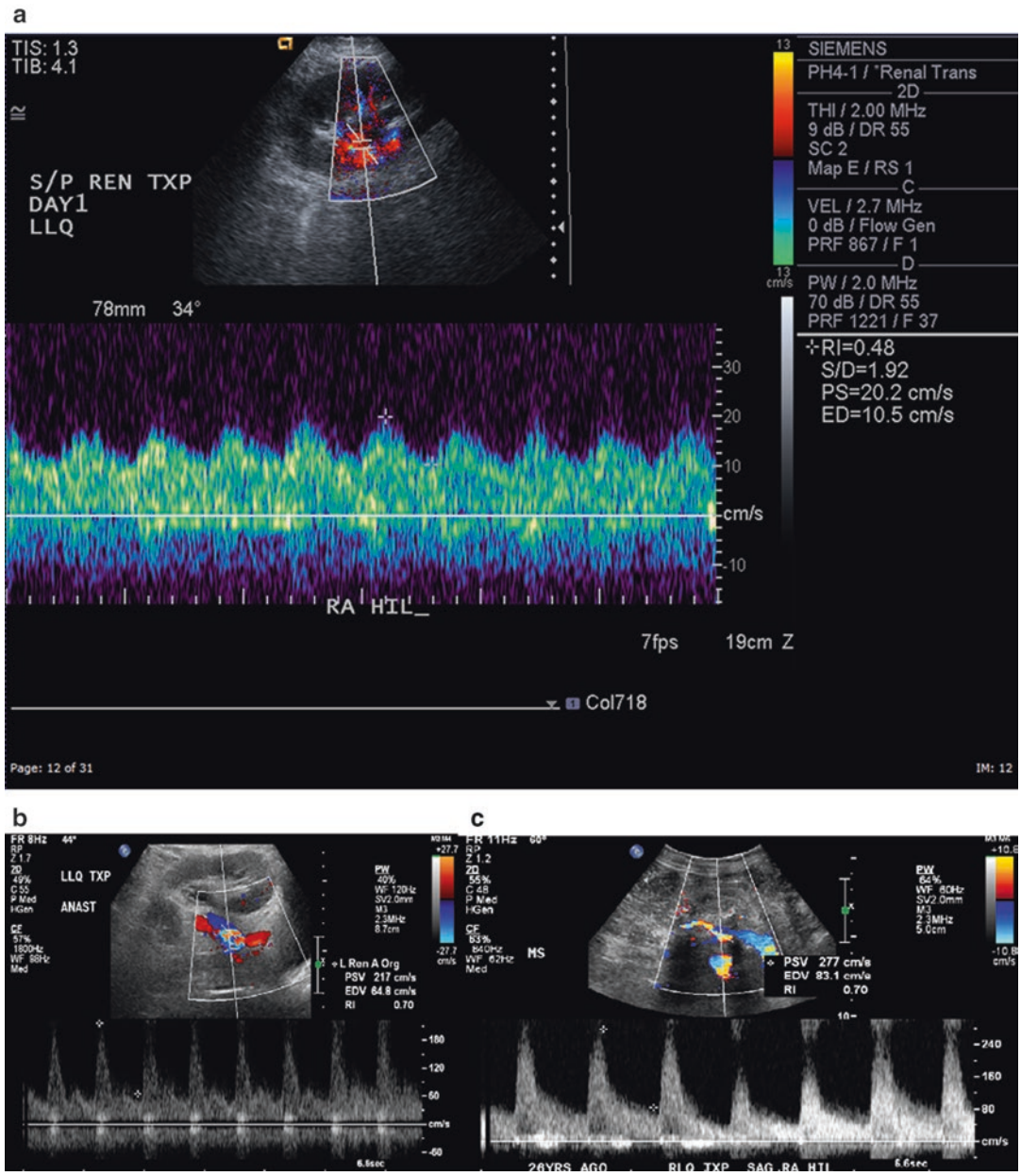

Fig. 14.12 (**a**) Spectral Doppler in a transplant patient with RAS showing a prolonged systolic rise or Parvus Tardus (slow upstroke). (**b**) Arterial anastomotic stenosis PSV = 217 cm/s past anastomosis. (**c**) Main renal arterial stenosis PSV = 277 cm/s measurement distal to stenosis

is indicative of proximal renal artery stenosis. Parvus Tardus is usually identified within the renal parenchyma downstream from significant stenosis [22–28] (Fig. 14.12).

- **Ureteral obstruction**: Ureterovesical anastomotic stricture is the most common type usually secondary to a tight anastomosis (early) or ischemia (late) (Fig. 14.13). In the acute phase of obstruction, RI is elevated whereas in the late phase it is usually normal. Stone disease, upper ureteral ischemic stricture, and lymphocele causing extraluminal compression occur less commonly. With rotation of the transplant kidney, some patients

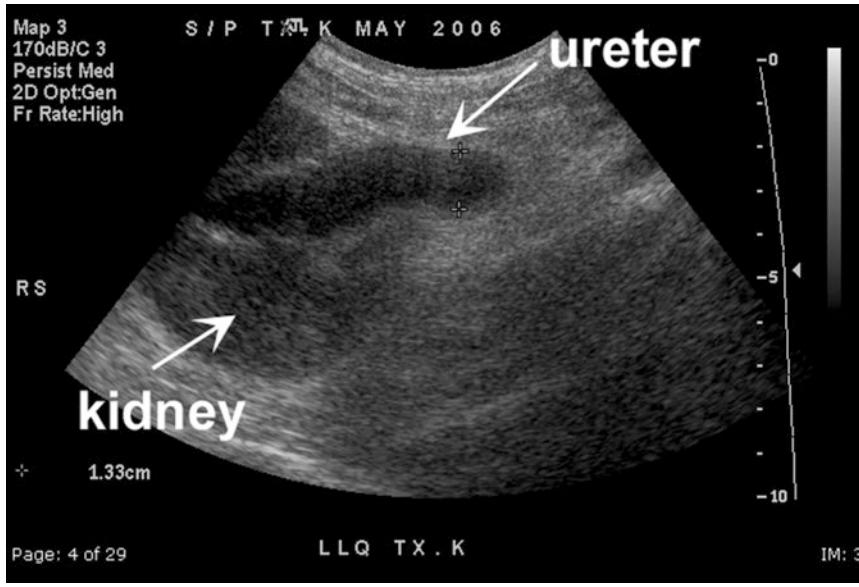

Fig. 14.13 Ultrasound image of a left lower quadrant kidney showing hydronephrosis and dilation (1.33 cm diameter) of the ureter due to ureterovesical anastomotic stricture

develop ureteral obstruction at the level of the ureteropelvic junction. Even in normal circumstances, due to tilted retroperitoneal lie of the graft, it is not unusual to find a mild degree of hydronephrosis or calyceal dilation in either pole of a transplanted kidney without clinical evidence of obstruction or changes in serum creatinine (Fig. 14.14).

- **UPJ obstruction**: Hydronephrosis due to UPJ obstruction has been diagnosed in patients after transplant, even in the absence of preoperative obstruction in donor. The clinical and ultrasound findings are similar to congenital or secondary UPJ obstruction in native kidneys (Fig. 14.15).
- **Lymphocele**: This is the most common fluid collection in transplant patients (5–15 %), which can cause hydronephrosis or a pelvic collection. Lymphocele can cause graft dysfunction, extraluminal ureteral obstruction, lower extremity edema, pelvic discomfort, and bladder displacement—mimicking symptoms suggestive of LUTS or prostatic outlet obstruction. Pelvic ultrasound shows a collection, usually between the transplant kidney and a displaced bladder. It may also cause hydronephrosis (Fig. 14.16a–c). Lymphocele in other locations may not cause similar findings.
- **Renal transplant stones**: The localization of the stone in the transplant kidney is similar to congenital kidneys, which shows an echogenic area with posterior shadowing and twinkle artifact. A ureteral jet can be documented by aiming the Doppler at lateral and anterior aspect of the bladder at the site of ureteroneocystostomy (Fig. 14.17).
- **AV fistula**: Percutaneous renal biopsy of the transplant kidneys is commonly performed to rule out possible rejection versus nephrotoxicity. The most significant complications of percutaneous needle biopsy are acute bleeding and AV fistula formation. Doppler ultrasound findings of AV fistula include high-velocity, whirling flow pattern, mosaic color pattern due to AV shunting, spectral broadening, and turbulent flow with mirror-imaging. The shunting will result in increased diastolic flow velocities (80 cm/s) due to abnormal arteriovenous communications (Fig. 14.18) [4]. The incidence of fistula post biopsy is reported at 5–10 % [29].

Acute pyelonephritis/Emphysematous pyelonephritis: Acute and chronic infections can occur in transplant kidneys with similar image findings as native kidneys, which include graft enlargement, changes in echogenicity, and loss of corticomedul-

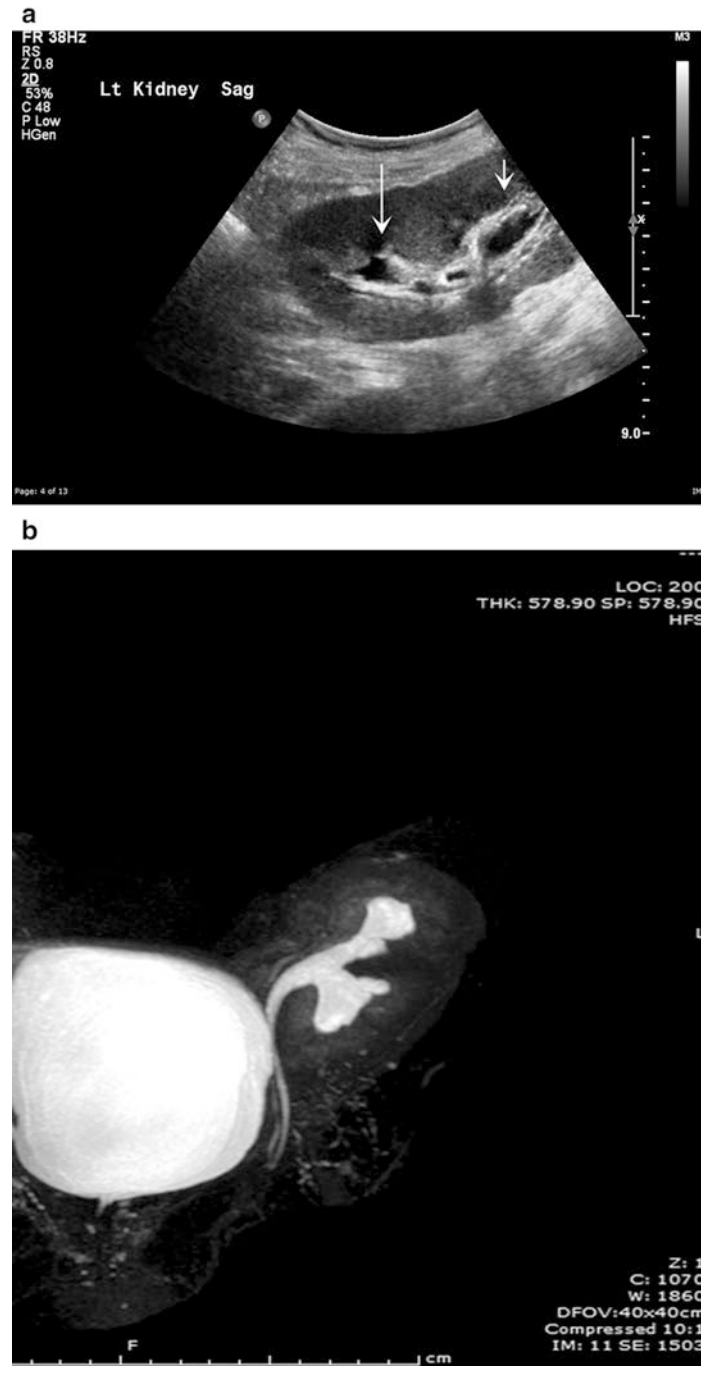

Fig. 14.14 Nonobstructed left lower quadrant renal transplant with mild hydronephrosis. (**a**) Grayscale sonogram showing calyceal dilation (*arrows*). (**b**) Non-contrast MR urogram with hydration rules out obstruction

lary junction. Additional further progression can lead to pyleonephrosis and emphysematous pyelonephritis with acute necrotizing infection involving the renal parenchyma and surrounding tissue caused by gas forming organisms. The risk factors are diabetes mellitus, urinary obstruction secondary to stones or strictures. Untreated UTI in an immunosuppressed patient can progress into such condition. An ultrasound in addition to the above findings may identify areas with significant air pockets in the kidney (Fig. 14.19a, b). Emergency nephrectomy is usually indicated in these cases [30].

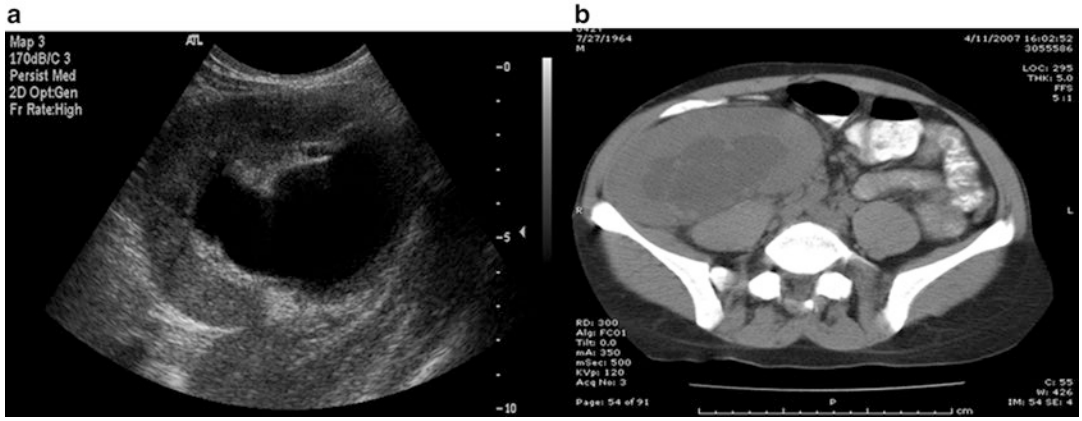

Fig. 14.15 Renal ultrasound and CT scan of a right lower quadrant transplant kidney (**a**) with UPJ obstruction. Corresponding CT scan of the same kidney (**b**)

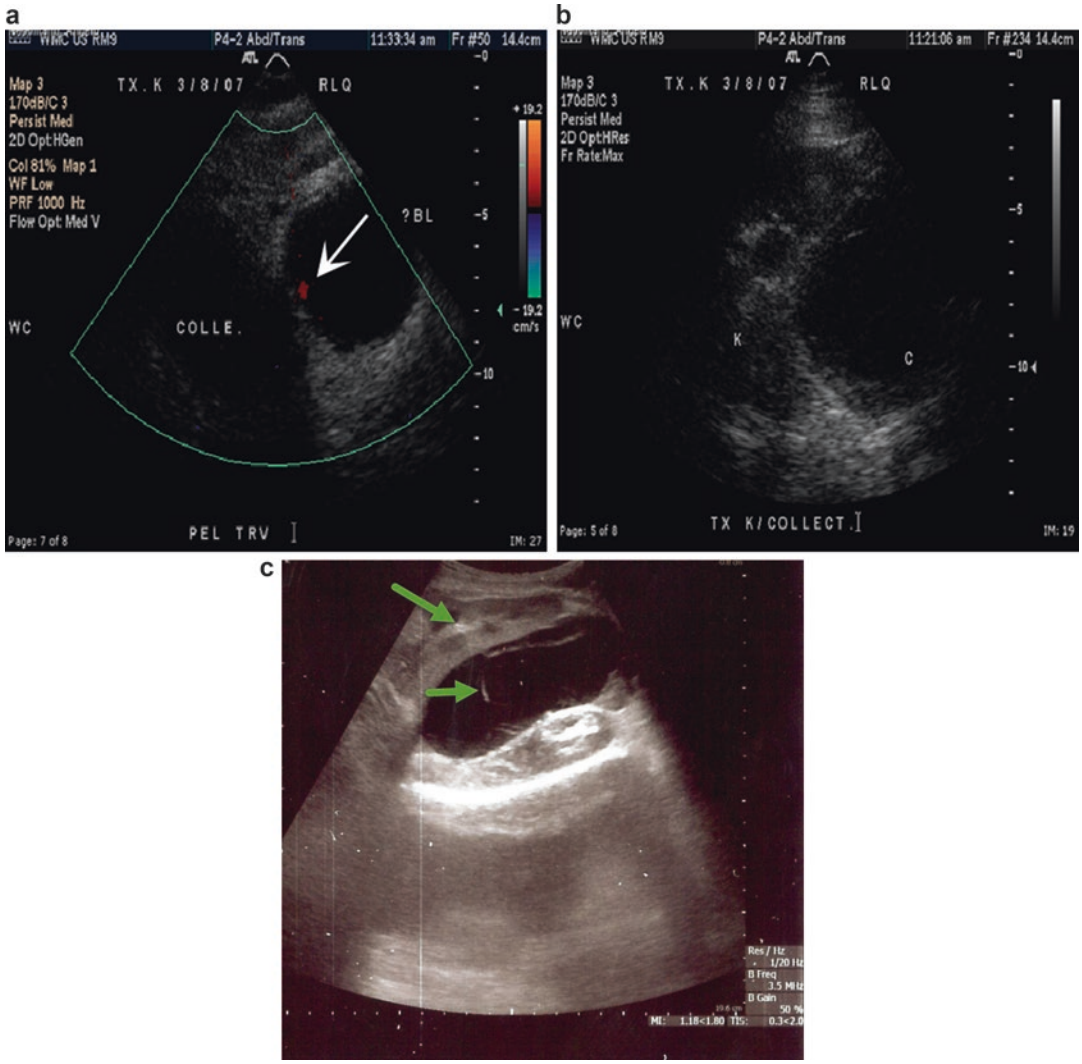

Fig. 14.16 (**b**) Right lymphocele (C) collection next to the RLQ transplant kidney (K) and the bladder (**a**). Note a sluggish ureteral jet from the transplant ureter (*arrow*) (**c**) patient post RLQ transplant with loculated lymphocele (septation). Note the kidney being displayed laterally and cephalad

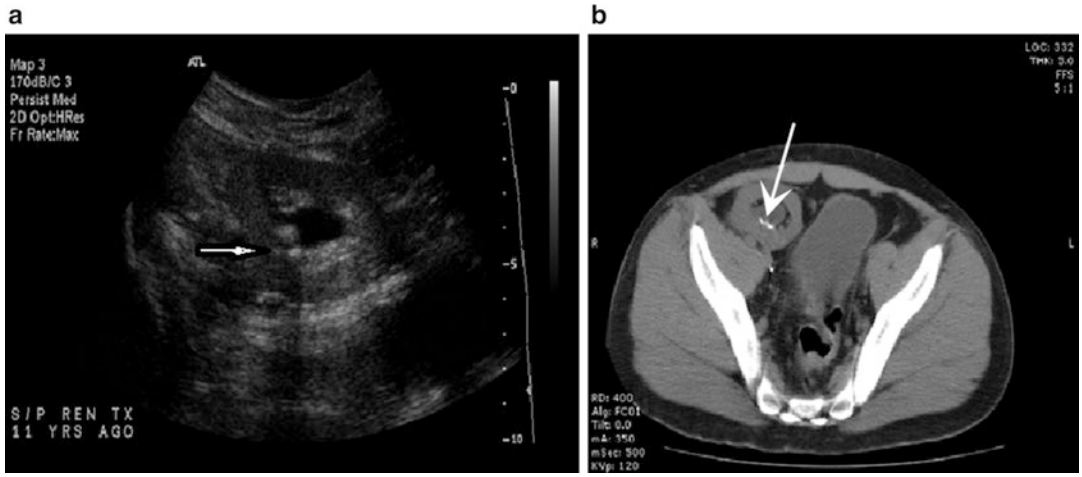

Fig. 14.17 Ultrasound (**a**) and (**b**) CT image comparison of transplant renal stone (*arrows*)

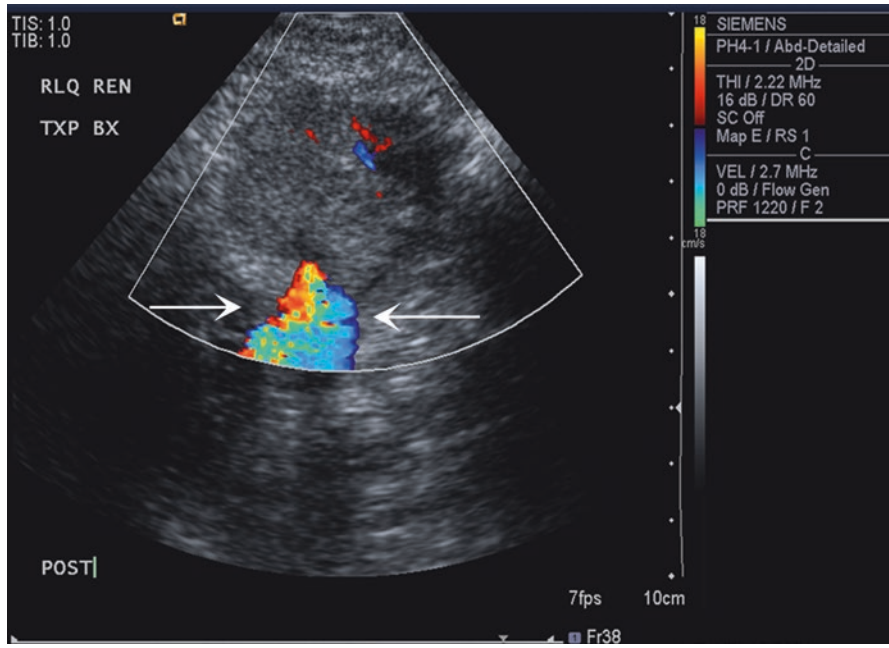

Fig. 14.18 Doppler imaging of a right lower quadrant renal transplant kidney demonstrating arteriovenous fistula, secondary to percutaneous renal needle biopsy. Note the mosaic pattern due to AV shunting and high-velocity whirling flow pattern (*arrows*)

Drug Toxicity: cyclosporine and tacrolimus which are key immunosuppressive agents used to fight rejection are potentially nephrotoxic. They can cause vasoconstriction of the afferent glomerular arteries and interstitial fibrosis with long-term use. Polyoma (BK) virus nephropathy is indistinguishable from rejection or ATN. Allograft ultrasound can be either normal or nonspecific such as possible elevated RI.

Ultrasound-guided percutaneous renal allograft biopsy: Ultrasound-guided renal biopsy is now considered standard in most institutions. This is true of both native and transplant kidneys. In a

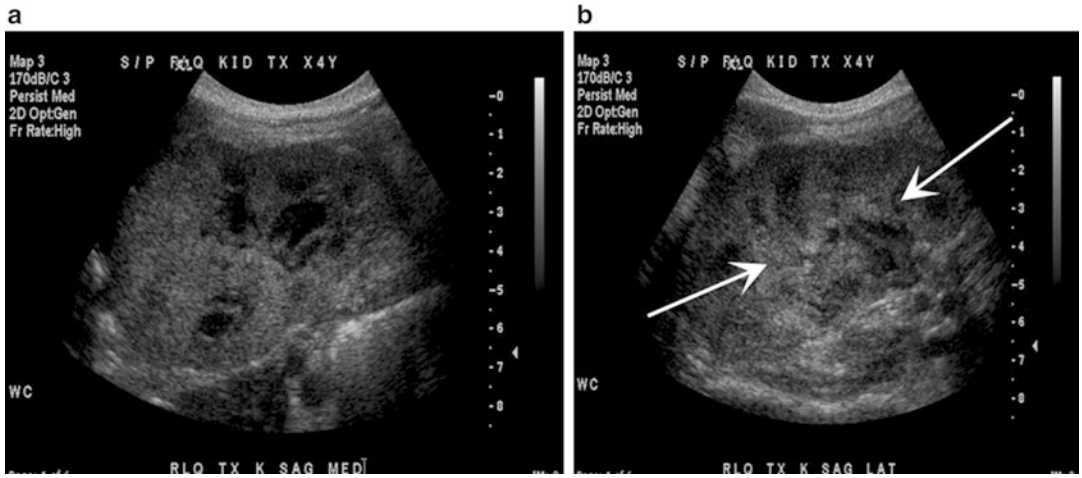

Fig. 14.19 Classic findings of chronic pyelonephritis (**a**). Note the loss of corticomedullary junction which should normally be seen at location arrows (**b**)

14-year period, 438 ultrasound-guided renal transplant biopsies were performed with 169 children and adolescents in this group. The success rate was 99 % with 4.1 % complication rate and all except for one case were diagnosed on post-biopsy ultrasound [30]. In another study, 345 ultrasound-guided biopsy of transplant and native kidneys were performed with 8.7 % complication rate. A comparative study of manual technique compared to 82 ultrasound-guided biopsies of transplant kidneys revealed higher diagnostic yield and fewer complications in the latter group. In summary, ultrasound allows for ideal localization of proper areas of transplant kidneys to be biopsied in order to avoid injury to vital vascular structure. Ultrasound guidance will minimize injury to the collecting system with proper skin to parenchyma measurement and knowledge of the core length of the biopsy gun to limit the biopsy core to cortex. The ideal approach is aiming at the lateral cortex and avoiding medial and central punctures. Immediate Doppler evaluation post biopsy will also identify potential arteriovenous complication and significant bleeding. In spite of all these precautions it is not unusual to find asymptomatic AVMs in patients who have undergone renal biopsy. Some of the small AVMs resolve spontaneously with time. Although ultrasound-guided compression treatment has been described for management of pseudoaneurysm in structures like femoral artery, it has not been widely reported for renal transplant. There is concern that high pressure compression over a long period of time can result in ischemic changes. In cases that the immediate post biopsy Doppler evaluation detects a small AVF or AVM, ultrasound-guided compression under Doppler control to assure there is continuous flow to the transplant kidney can be tried at short intervals with reassessment of size of AVF or AVM [29, 31–35]. Over an approximate period of 12 years this approach was used in several transplant patients post biopsy with good success rate in closing small fistulas without any ill effect on the graft [36].

Acknowledgement The author would like to thank A. Arsanjani, MD, D. Lankford, MD, and M. Degen, MD for assistance in preparing these manuscripts.

References

1. Lee JY, Kim SH, Cho JY, et al. Color and power Doppler twinkling artifacts from urinary stones: clinical observation and phantom studies. AJR Am J Radiol. 1992;159:773–5.
2. Kolofousi C, et al. Ultrasonographic feature of kidney transplants and their complications: an imaging review. ISRN Radiol. 2012;2013:12. Article ID 480862.
3. Lachance SL, et al. Ultrasonically determined kidney transplant hypertrophy. J Urol. 1988;139(3):497–8.

4. Dudd III GD, Tublin ME, Shah A, et al. Imaging vascular complications associated with renal transplants. AJR Am J Radiol. 1991;157:449–59.
5. Rasmussen PE, Nielsen FR. Hydronephrosis during pregnancy: a literature survey. Eur J Obstet Gynecol Reprod Biol. 1988;27(3):249.
6. Fulgham P, Bishoff J. Urinary tract imaging: basic principles. In: Kavoussi L, Novick A, Partin A, Peters C, editors. Campbell-Walsh urology, vol. 1. 10th ed. Philadelphia: Elsevier Saunders; 2011. p. 99–139.
7. Schwaighafer B, Kainberger F, Fruehwald F, et al. Duplex sonography of normal renal allografts. Acta Radiol. 1989;30:35.
8. Zeisbrich M, et al. When is contrast-enhanced sonography preferable over conventional ultrasound combined with Doppler imaging in renal transplantation. Clin Kidney J. 2015;8(5):606–14.
9. Morel DR, et al. Human pharmacokinetic and safety evaluation of SonoVue, a new contrast agent for ultrasound imaging. Invest Radiol. 2000;35:80–5.
10. Enhesari A. Early ultrasound assessment of renal transplantation as the valuable biomarker of long lasting graft survival: a cross-sectional study. Iran J Radiol. 2014;11(1):e11492.
11. Horrow M, et al. Immediate postoperative sonography of renal transplants: vascular findings and outcomes. Am J Roentgenol. 2013;201:W479–86.
12. Tatar IG, et al. Real time sonoelastographic evaluation of renal allografts in correlation with clinical prognostic parameters: comparison of linear and convex transducers according to segmental anatomy. Med Ultrason. 2014;16(3):229–35.
13. Gilbert B, Fulghan P. Urinary tract imaging: basic principles of urologic ultrasonography. In: Wein AJ, Kavoussi LR, Partin AW, Peters CA, editors. Campbell-Walsh urology, vol. 1. 11th ed. Philadelphia: Elsevier Saunders; 2016. p. 63–84.
14. Samir A, et al. Shear wave elastography in chronic kidney disease: a pilot experience in native kidneys. BMC Nephrol. 2015;16:119.
15. Grenier N, et al. Quantitative elastography of renal transplants using supersonic shear imaging: a pilot study. Eur Radiol. 2012;22(10):2138–46. doi:10.1007/s00330-012-2471-9.
16. Kahn J, et al. TSI ultrasound elastography for the disgnosis of chronic allograft nephropathy in kidney transplanted patients. J Ultrason. 2013;13(54):253–62.
17. Oriacchio A, et al. Kidney transplant: usefulness of real-time elastography (RTE) in the diagnosis of graft interstitial fibrosis. Ultrasound Med Biol. 2014;40(11):2564–72.
18. Sommerer C, et al. Assessment of renal allograft by transient elastography. Transpl Int. 2013;26(5):545–51.
19. Brocchi S, et al. Shearwave elastography in kidney transplantation: a new diagnostic tool to assess chronic allograft fibrosis. EPOS. 2014. doi:10.1594/ecr2014/c-1199.
20. Althaf M, et al. Chromophobe renal cell carcinoma occurring in the renal allograft of a transplant recipient presenting with weight loss. Saudi J Kidney Dis Transpl. 2016;27(1):139–43.
21. Li XB, et al. Transitional cell carcinoma in renal transplant recipients: a single center experience. Int J Urol. 2008;15(1):53–7.
22. Braun B, Weilemann LS, Weigand W. Ultrasonographic demonstration of renal vein thrombosis. AJR Am J Radiol. 1989;138:157–8.
23. Kaveggia LP, Parrella RR, Grant EG, et al. Duplex Doppler sonography in renal allograph: the significance of reversed flow in diastole. AJR Am J Radiol. 1990;155:295–8.
24. Reuther G, Wanjura D, Bauer H. Acute renal vein thrombosis in renal allografts: detection with duplex Doppler ultrasound. AJR Am J Radiol. 1989;170:557–8.
25. Kohler TR, Zierler RE, Martin RL, et al. Non invasive diagnosis of renal artery stenosis by ultrasonic duplex scanning. Vasc Surg. 1986;4:450–6.
26. Gottlieb RH, Lieberman JL, Paico RC, et al. Diagnosis of renal artery stenosis in transplanted kidneys: value of Doppler waveform analysis of the intrarenal arteries. AJR Am J Radiol. 1995;165:1441–6.
27. Nazzal MM, Hoballah JJ, Miller EV, et al. Renal hilar Doppler analysis is of value in the management of patients with renovascular disease. Am J Surg. 1997;174:164–8.
28. House MK, Dowling RJ, King P. Using Doppler sonography to reveal renal artery stenosis. An evaluation of optimal imaging parameters. AJR Am J Radiol. 1999;173:761–5.
29. Preda A, et al. Complication rate and diagnostic yield of 515 consecutive ultrasound-guided biopsies of renal allografts and native kidneys using a 14-guage Biopty gun. Eur Radiol. 2003;13(3):527–30.
30. Piracha K, et al. Emphysematous pyelonephritis in a renal transplant patient. Open J Nephrol. 2014;4:86–91.
31. Franke M, et al. Ultrasound-guided percutaneous renal biopsy in 295 children and adolescents: role of ultrasound and analysis of complications. PLoS One. 2014;9(12):e114737. doi:10.1371/journal.pone.0114737.
32. Nyman RS, et al. Yield and complications in percutaneous renal biopsy. A comparison between ultrasound-guided gun-biopsy and manual techniques in native and transplant kidneys. Acta Radiol. 1997;38(3):431–6.
33. Manno C, et al. Predictors of bleeding complications in percutaneous ultrasound-guided renal biopsy. Kidney Int. 2004;66:1570–7.
34. LaBerge J. Interventional management of renal transplant arteriovenous fistula. Semin Intervent Radiol. 2004;21(4):239–46.
35. Saad N, et al. Pseudoaneurysms and the role of minimally invasive techniques in their management. Radiographics. 2005;25((Suppl 1)):S173–89.
36. Rachlin S. New York Medical college; department of radiology, Personal communication.

Intraoperative Urologic Ultrasound

15

Fernando J. Kim and Rodrigo R. Pessoa

Types of Transducers (Fig. 15.1)

Linear: The linear array scanners produce sound waves parallel to each other which generate a rectangular image. The width of the image and number of scan lines are the same at all tissue levels. Thus coupled with high-frequency settings, this probe has great near-field resolution. The linear transducer can be used for viewing surface texture of the liver. The disadvantage of this probe is the tendency for artifacts when applied to a curved part of the body which generate air gaps between skin and transducer.

Sector/vector: It produces a fanlike image that is narrow near the transducer and increases in width with deeper penetration. It is useful when scanning between the ribs as it fits in the intercostal space. The disadvantage is poor near-field resolution.

Curved: The curved probe is a compromise of the linear and sector scanners. The density of the scan lines decreases with greater distance from the transducer, but not to the level as sector scanners. Often imaging requires greater depth of the acoustic waves, so lower frequencies (3–5 MHz) are used. This lower frequency also allows scanning for patients with various body habitus. The curved probe may be difficult to use in curved regions of the body, e.g., the spleen behind the left costal margin.

Laparoscopic ultrasound (*LUS*): Laparoscopy with the assistance of ultrasound avoids unnecessary open surgery and improves selection of patients for renal and adrenal tumor resection. The diameter is less than 10 mm to allow introduction through a 10–11-mm laparoscopic port. The length is typically 35–50 cm and with articulating tips to allow imaging to any location in the abdominal cavity. LUS enables direct contact of the probe with the target tissue thus enabling the use of high-frequency (6–10 MHz) waves to improve resolution with a depth of 4–10 cm. LUS may be used to identify and characterize tumors, guide biopsy needles and probes, and monitor the freezing zone during cryoablation. Challenges of LUS include limitations of the small working space resulting in images from oblique planes.

Transrectal ultrasound: (a) *End fire* is a linear array whose direction of maximum radiation is along the axis of the array; it may be either unidirectional or bidirectional; the elements of the

F.J. Kim, M.D., M.B.A., F.A.C.S. (✉)
R.R. Pessoa, M.D.
Division of Urology, Denver Health Medical Center and University of Colorado Denver, 777 Bannock Street MC 0206, Denver, CO 80204, USA
e-mail: Fernando.kim@dhha.org; rodrigo.pessoa@dhha.org

P.F. Fulgham, B.R. Gilbert (eds.), *Practical Urological Ultrasound*, Current Clinical Urology,
DOI 10.1007/978-3-319-43868-9_15

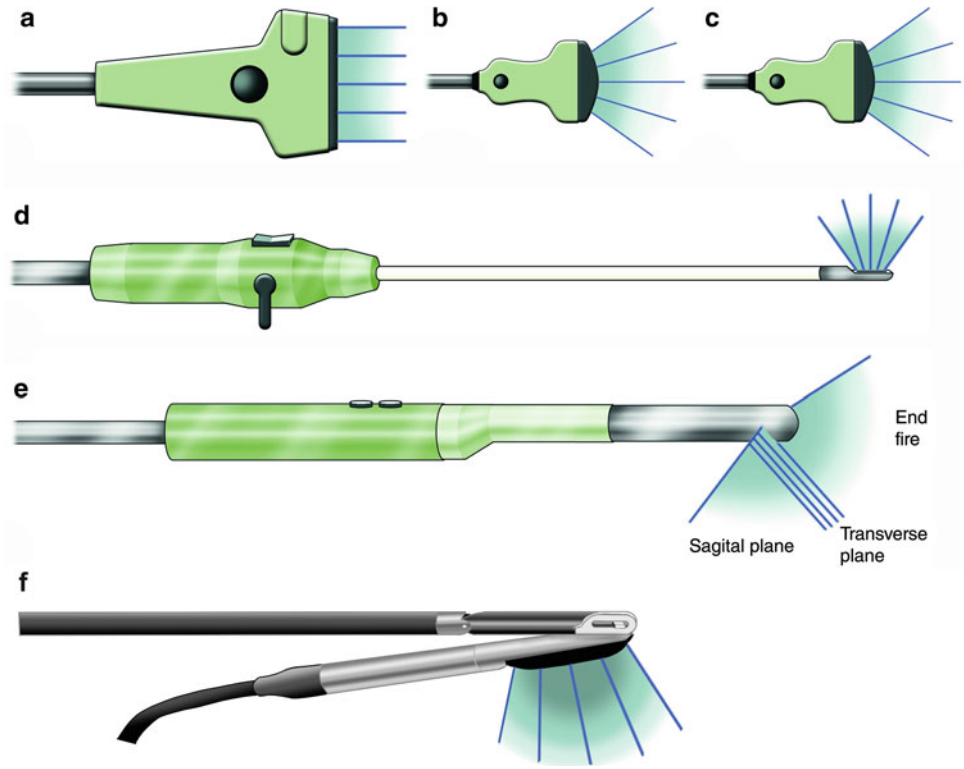

Fig. 15.1 Ultrasound probes used in urology. (**a**) Linear array (**b**) section/vector (**c**) curved array (**d**) laparoscopic (**e**) transrectal biplane (**f**) robotic ultrasound probe

array are parallel and in the same plane, as in a fishbone antenna. (b) *Biplane is* composed of two arrays: one linear for imaging of the longitudinal plane and a highly curved one to image the transverse plane. These two planes allow simultaneous visualization of perpendicular planes in real time.

The Kidneys

The same principles and techniques to perform renal procedures guided by ultrasonography apply to interventional techniques.

Percutaneous Nephrostomy and Percutaneous Nephrolithotomy

Percutaneous access to the renal collecting system was first described in 1955 by Goodwin et al. as a means to either drain or stent an obstructed urinary system [1]. Beyond the usual indications for an obstructed urinary system, percutaneous nephrostomy (PCN) can be used to access the collecting system in an antegrade manner for definitive treatment of nephrolithiasis, commonly performed by laser lithotripsy [2]. Generally, for percutaneous approach the left kidney is more challenging than the right due to the rib cage as described previously during the Kidney US chapter. Reports show that only 11 % of urologists perform their own PCN access and majority uses fluoroscopic guidance, but given appropriate training and use of ultrasound guidance, this technique still remains well within the realm of the urologist as seen in some European and Asian countries [3–5].

Ultrasound probe: For adult abdominal scanning, a curved-array transducer 3–5 MHz is used. For pediatric patients, a higher-frequency transducer may be utilized. The use of color Doppler

provides good visualization of vascular structures within the kidney, and the probes usually allow attachments that can display the path of the needle towards the target (calyx or stone).

Technique: Hydronephrosis on ultrasound will demonstrate enlarged renal calyces and pelvis that appear black (hypoechoic), indicating the presence of fluid. While acute hydronephrosis generally does not affect renal parenchyma, chronic obstruction of the urinary tract can result in thinning of the renal cortex (atrophy) and blunting of the renal papillae. Renal stones are identified as hyperechoic structure on US with shadowing, and color Doppler can identify vascular structures (Fig. 15.2). Presence of these findings on ultrasound examination should be noted. Additionally, the operator should attempt to visualize the ureter, which may be dilated depending on etiology.

There are several described techniques, but the two most common are a one-stab technique and the Seldinger technique for placement of a PCN tube. The one-stab technique is usually reserved for moderately to severely dilated collecting systems. Meanwhile the Seldinger technique can be applied with or without dilation of the tract [6]. Both techniques are performed with the patient in a prone or prone-oblique position (Fig. 15.3). Recently, the supine position has been popularized for percutaneous nephrolithotomy (PCNL) [7]. The one-punch technique involves the use of ultrasound imaging to guide placement of a hollow 18-gauge needle with a sharp, beveled edge mounted to a pigtail catheter. Once inserted into the hydronephrotic collecting system and a flash of urine is obtained, the catheter can be slid over the needle and the needle subsequently removed. Real-time ultrasound is used at all times to monitor the target and ensure that the needle, wire, and dilators enter the calyx and do not violate other structures (Fig. 15.4). If only drainage is needed, a 12-French PCN tube can then be inserted over the wire with curl confirmation on ultrasound imaging. Imaging can be enhanced by injecting sterile saline to identify the collecting system under US guidance. Further serial dilation or inflating balloon dilators can be performed with dilators up to the size of the instrument sheath (24 °F), ensuring that the wire

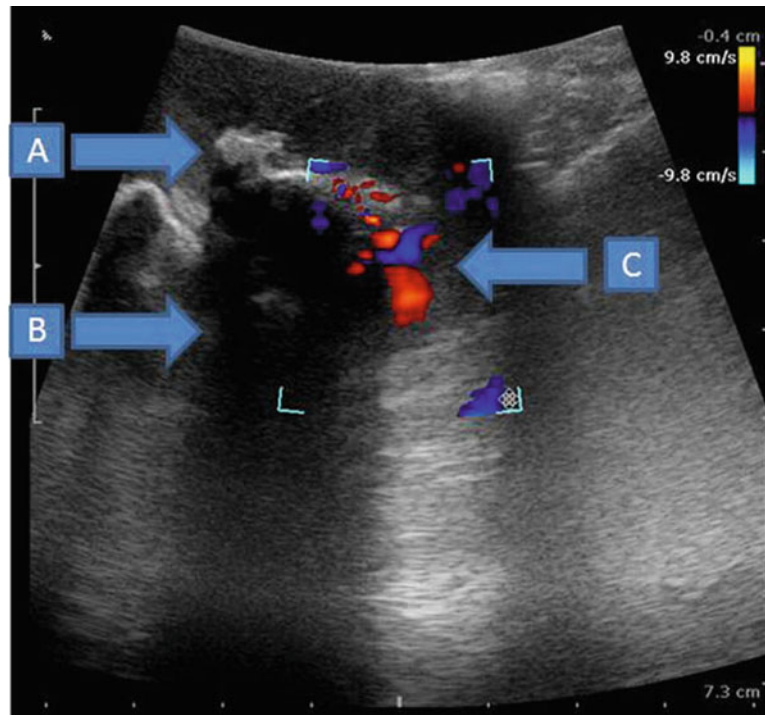

Fig. 15.2 Large hyperechoic renal stone with acoustic shadowing and color Doppler of vessels. (**a**) Large renal stone (**b**) acoustic shadowing (**c**) vessels on color Doppler

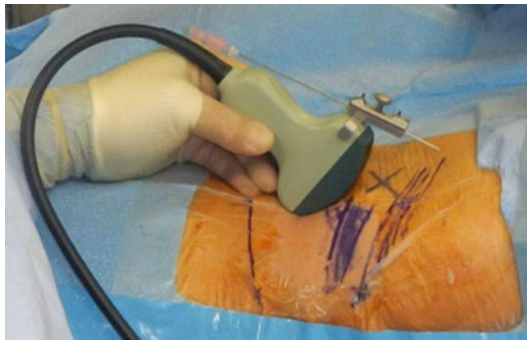

Fig. 15.3 Percutaneous nephrolithotomy with needle-probe attachment. *Blue* marking of ribs

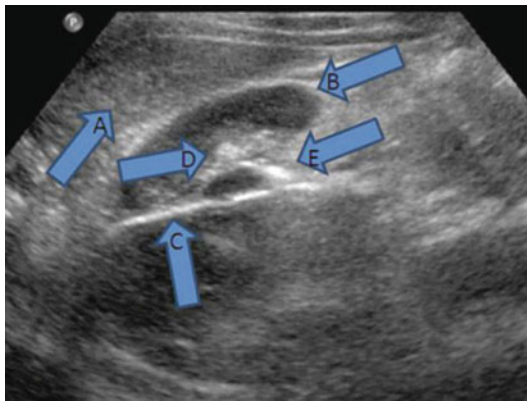

Fig. 15.4 Transverse view of the right kidney. (**a**) Liver (**b**) right kidney (**c**) percutaneous needle (**d**) collecting system (**e**) stone

remains in place for access purposes throughout the operation. In case of staghorn calculi, ultrasound guidance towards the stone or puncture of an alternate calyx may be required. The patient in a prone position allows the US probe to examine from the most lateral side of the abdomen under the rib cage and scan medially to enable a global view of the anatomy. The serious limitation of the ultrasound probe is the two-dimensional view of the kidney, calices, and the path which the needle may traverse injuring a viscera. The risk factors for colonic perforation are the following: the presence of colonic distension due to previous intestinal bypass surgery, female sex, elderly, thin patients, the presence of a horseshoe kidney, and previous renal surgery placing the colon in a more retroperitoneal position. The incidence of colonic injury is also greater on the left side, with a lower caliceal puncture, and with an extreme lateral origin of the percutaneous puncture [8]. Nevertheless, no statistically significant evidence has shown the implication of these factors in the development of colonic injury. Moreover, injuries to the spleen may occur on the left and liver on the right PCNL or PCN.

Clinical data: There has been one randomized trial that compared ultrasound-guided PCNL access to traditional fluoroscopic access and found comparable results with less exposure to ionizing radiation but longer access time (11.0 min vs. 5.5 min) [9]. In a large series of ultrasound-guided PCN by urologists, complications included urinary tract infection (1.1 %), hemorrhage (1.9 %), sepsis (0.76 %), inferior vena cava injury (0.15 %), gall bladder injury (0.15 %), and death (0.3 %). Overall, major complications occurred in 3.3 % of patients (3–6.7 % in various series) and minor complications in 5 % (5–38 % in various series) [10–12]. Successful PCN has been reported in these series as 90–95 %. PCN and PCNL under ultrasound guidance are safe and highly successful techniques in the hands of a trained urologist.

Percutaneous Renal Biopsy

Renal biopsy can be divided in two groups of patients: (1) patients with an abnormal mass to rule out malignancy or (2) patients with medical renal disease that requires histologic diagnosis. In both groups of patients, ultrasound imaging aids significantly to identify the suspected area. As discussed in other chapters of this book, the left renal US is often more challenging than the contralateral side due to the anatomic position.

Ultrasound probe: The use of curved-array 3.5–5-MHz probes with or without color Doppler provides good visualization and allows attachments that can display the path of the needle placement towards the target.

Technique: The technique is similar to PCNL. The target is different: (a) solid mass to rule out malignancy or (b) renal cortex to evaluate medical renal disease. As a general rule, percutaneous renal biopsy can be easily performed in nonobese patients and also transplanted kidneys since they are placed in the iliac fossa. The technique is similar to percutaneous renal procedures. If the colon is causing visual obstruction, rotate the patient and scan the kidney from posterior to anterior until the target is visualized. Preparation of the patient by fasting the night prior to the procedure may further improve visualization.

Clinical data: In the analysis of 623 renal biopsies guided by real-time ultrasound, the effectiveness was 97.6% with 110 complications. Fourteen (2.24%) were major complications (Clavien ≥3): nine cases of renal hematoma, two cases with macroscopic hematuria (which required blood transfusion), one case of intestinal perforation (which required exploratory laparotomy), one nephrectomy, and one case of a dissecting hematoma. The author concluded that the risk factors for developing major complications were the following: diastolic blood pressure ≥90 mmHg, RR 7.6 (95% CI 1.35–43); platelet count ≤120 × 103/μL; RR 7.0 (95% CI 1.9–26.2); and blood urea nitrogen (BUN) ≥60 mg/dL, RR 9.27 (95% CI 2.8–30.7) [13].

Laparoscopic Ablative and Partial Nephrectomy

Historically, radical nephrectomy has been the treatment of choice for patients with renal masses, but our understanding and appreciation of nephron-sparing surgery for small renal masses ≤4 cm (and more recently, ≤7 cm in select patients) with regard to cancer control and preservation of renal function has increased dramatically in recent years [14–16]. There has been a recent migration towards nephron-sparing approaches as innovations with minimally invasive techniques continue [17]. The application of probe ablation therapies such as cryoablation and radio-frequency ablation, although promising, is currently not the treatment option of choice when compared to partial nephrectomy due to the lack of long-term outcome data. Although the percutaneous approach of the kidney for ablative procedures is feasible, the preferred imaging modality used to treat the renal masses by interventional radiologists has been CT scan. However amongst urologists, a laparoscopic approach using ultrasonography is more commonly implemented. Therefore, we will describe the use of laparoscopic ultrasonography for these procedures.

In the early 1990s, cryotherapy was reintroduced for the treatment of prostate cancer after study in animals and human trials in the 1970s and 1980s. On the basis of these experimental and clinical studies, an optimal drop in temperature of −40 °C is required to achieve total cell death [18]. Although many theories were suggested for the underlying mechanism of the cryoablative tissue effect, the vascular component of initial vasoconstriction followed by reperfusion injury (increased capillary permeability) triggered by the thawing phase is considered to be the primary mechanism of tissue damage. However, intracellular crystallization and subsequent water shifting during the thawing phase also contribute significantly to the rupture of the cell membrane and irreversible cellular death [19].

Ultrasound probe: Laparoscopic renal ultrasound will often be performed with a 6–10-MHz linear array transducer. Endoluminal probes of 10–12 MHz may be used for transurethral evaluations. The 7.5-MHz flexible side-viewing laparoscopic transducer offers distinct capability to contour the organ. The rigid 7.5-MHz linear side-viewing laparoscopic transducer is easier to operate and is preferred by surgeons. Both types of transducers use a 10-mm laparoscopic port for introduction to the abdominal cavity (Fig. 15.5).

Technique: LUS imaging and orientation may not be intuitive and easy to understand the exact position of the lesion or particular regions of the target. The universal orientation left/cephalad also applies to LUS, but prior to the scan one should tip the end of the LUS to visualize the left side of the monitor and run along the crystals of the probe to translate the images of the US with

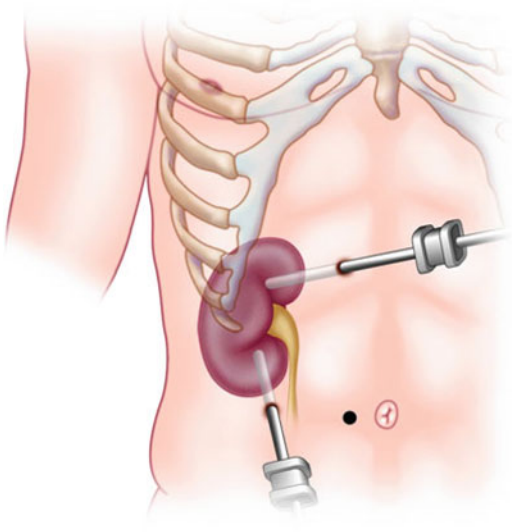

Fig. 15.5 Laparoscopic ultrasonic probe placement through a 10-mm trocar

the location in the monitor. For example, if only the tip of the LUS probe is touching the lesion, the image will be displayed only on the right side of the monitor. As the probe travels from the tip to the base of the probe, the image will be displayed in the entirety of the monitor (Fig. 15.6).

Indications for ultrasound-guided ablative therapy include small tumors (≤4 cm in diameter), older age, higher-risk patient, solitary kidney, and surgically scarred abdomen. Larger tumors and proximity to hilar vessels may be relative contraindications to ablative kidney surgery.

The size and optimal port placement are pivotal for LUS evaluation of renal lesions. The port size must be at least 10 mm. Generally, the posterior lesions are more challenging to be scanned. Either right or left side upper pole posterior lesions are best evaluated through an ipsilateral midclavicular or subxiphoid port. Anterior lesions can be evaluated almost through any port position. For a renal lesion biopsy and ablation, the needle or ablation probes are passed percutaneously through the abdominal wall. In general, multiple core biopsies (between 3 and 5) are taken with a 14- or 18-gauge needle under visual and ultrasonic guidance. Equally, the "rocking" maneuver allows the identification of the hyperechoic needle/probes and visualization of ablated tissue (Fig. 15.7).

Clinical data: A cryosystem consisting of argon (freezing phase) and helium (thawing phase) gases (Joule–Thomson effect) was used. Ultrasonic evaluation of the kidney should reveal suspect lesions. Simple cysts are generally spherical or ovoid, lack internal echoes, have a smooth, thin wall, and should show enhancement of the posterior wall indicating the presence of water. Lesions of suspect nature can include those with multiple septae, calcifications, or heterogeneous appearance that differentiates the lesion from healthy renal parenchyma [20]. The cryoneedles are introduced under real-time ultrasound guidance and will appear as hyperechoic structures with resultant shadowing. The borders of the ice ball can be readily identified on ultrasound as a hyperechoic rim (Fig. 15.8) which is generated by the interface between frozen and unfrozen tissues. The ice ball should be extended 1 cm beyond the visible border of treated lesions circumferentially to ensure negative margins. When thawed, the lesion will continue to remain hyperechoic compared with the surrounding kidney parenchyma [21]. All lesions should undergo two cycles of freezing and thawing.

Robotic Partial Nephrectomy

Recently, ultrasound probes have been developed for robotic procedures including partial nephrectomies. Rogers et al. described the use of intraoperative ultrasonography for tumor identification during robotic partial nephrectomies (RPN) [22]. A major drawback of laparoscopic ultrasonography during RPN is that the surgeon may rely on the assistant's ultrasound skills, limiting the surgeons' autonomy and precision. Due to these limitations, a robotic ultrasound probe controlled directly by the surgeon was developed [23]. The ProArt, a robotic transducer with doppler capability, was created by BK Medical in Herlev, Denmark [24]. It has a unique fin over the array which can be grasped by robotic instruments, giving the surgeon total autonomy over the probe. It can be maneuvered independently by the surgeon, achieving difficult angles while maintaining perpendicular contact of the probe with the kidney surface. Similarly, another fully articulated transducer by Hitachi-Aloka has been

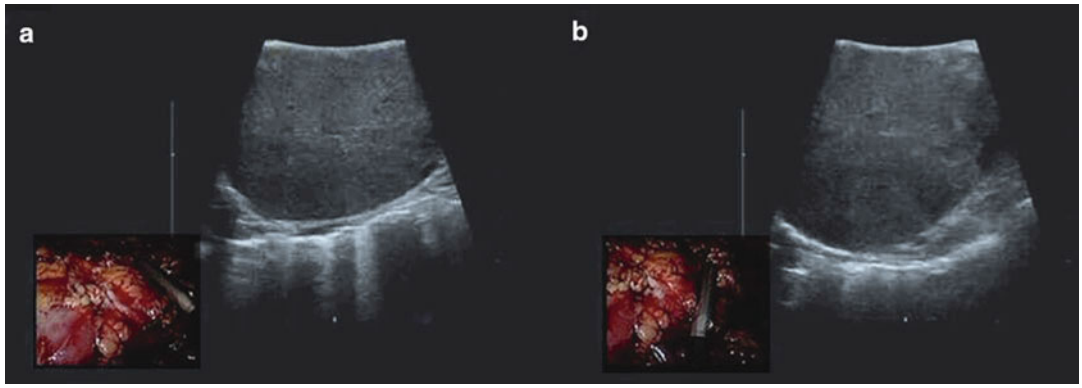

Fig. 15.6 Picture-in-picture of laparoscopic US during partial nephrectomy evaluates tumor size and depth to ascertain safe surgical margins. (**a**) lateral aspect of the renal tumor (**b**) medial aspect of the renal tumor

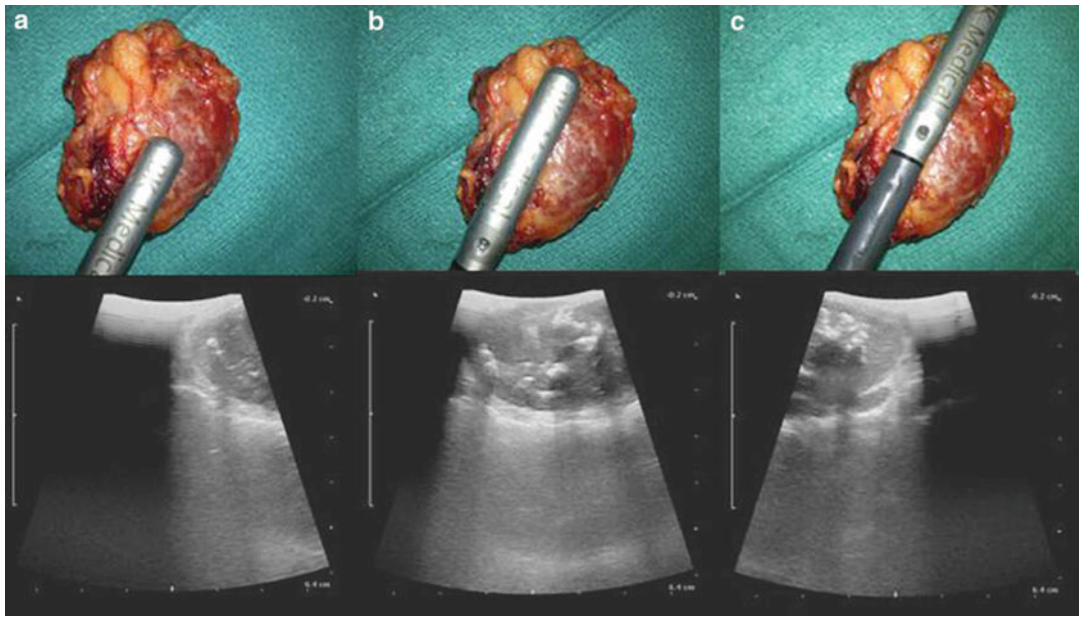

Fig. 15.7 Using the skiing technique across renal mass. The universal orientation of the laparoscopic probe is as follows: tip of the transducer is left and cephalad; therefore in (**a**) the distal end of the probe will demonstrate the adrenal mass on the right side of the monitor. When the transducer allows larger surface area contact, the image will show in the monitor (**b**) until only the base of the transducer is touching the adrenal mass and displaying the image on the left corner of the monitor (**c**) proximal end will demonstrate the adrenal mass on the left side of the monitor

developed to achieve complex angles [24]. The DaVinci surgeon console has a software imaging program (Tilepro) that allows up to two adjunctive imaging inputs to be viewed by the surgeon simultaneously with the regular 3D camera field view. It has been recently demonstrated that robotic ultrasound probes for tumor identification during RPN had comparable perioperative outcomes and surgical margin rates to a laparoscopic ultrasound probe [25].

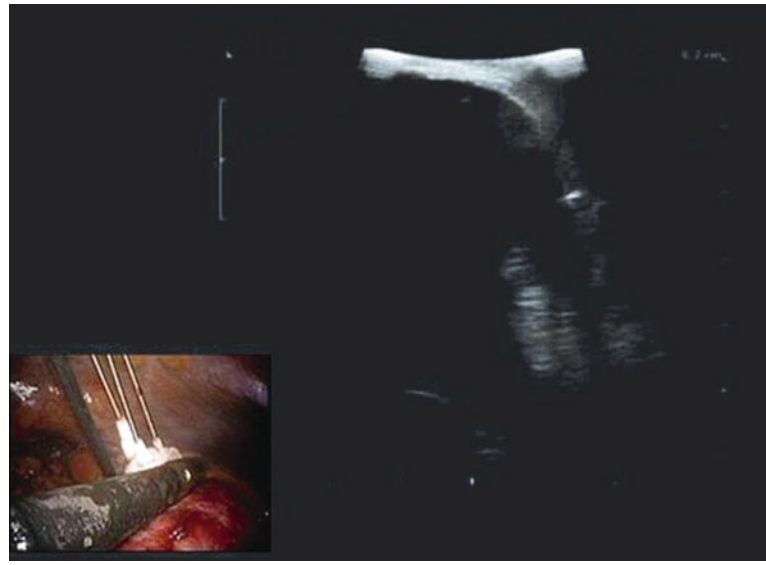

Fig. 15.8 Hyperechoic rim represents the outer layer of the ice ball. The homogeneous hypoechoic image is the ice ball that can be appreciated as the probes move towards the normal renal parenchyma

The Adrenal Gland

Ultrasonography of the adrenal gland is technically difficult and is better evaluated by other imaging studies, i.e., CT scan and MRI [26]. LUS is a valuable adjunct to laparoscopic adrenalectomy facilitating tumor localization and identification of adjacent structures to direct the dissection particularly for partial adrenalectomies. Although large lesions on either side are easily identified, laparoscopic US may facilitate identification of small tumors in obese patients and right-sided lesions that are usually partially retrocaval.

Ultrasound probe: Although the flexible side-viewing 7.5-MHz rigid laparoscopic transducer offers distinct capability to contour the organ, often surgeons find the rigid, linear side-viewing transducer the simplest and most convenient to use in adrenal surgery.

Technique: In the transabdominal technique, the patient is placed in the modified flank position with 3–4 trocars inserted subcostally on the right and three trocars on the left, on an axis between the midclavicular and the midaxillary lines. After the dissection along the gutter to deviate the liver or the spleen medially to expose the suprarenal retroperitoneum, the laparoscopic transducer is inserted through the 10- or 12-mm port on the anterior axillary line or subxiphoid port. If the adrenal gland has not been identified, the upper pole of the kidney should be scanned demonstrating characteristic appearance of its parenchyma with the cortex and the collecting system. Then the transducer is advanced cephalad in the longitudinal plane until the adrenal gland is identified. Large tumors are easily identified and the value of intraoperative sonography in these cases is in elucidating their relationship with the kidney, aorta, spleen, and the tail of the pancreas on the left and the kidney, inferior vena cava, and the liver on the right side, respectively. The use of flow color Doppler also helps to identify the aorta and the inferior vena cava. Nonsecreting and secreting adenomas have a similar ultrasonographic appearance. They are usually less than 3 cm and have a very low echodensity. They sometimes contain cystic and calcified areas. Pheochromocytomas may appear as solid or cystic or may have both solid and cystic components. Hypoechoic areas represent necrosis and hyperechoic areas indicate hemorrhage. The ultrasound appearance of adrenal hyperplasia is of smooth enlargement with a normal echo pattern. Adrenal cortical carcinoma of 3–6 cm shows a homogeneous echo pattern similar to

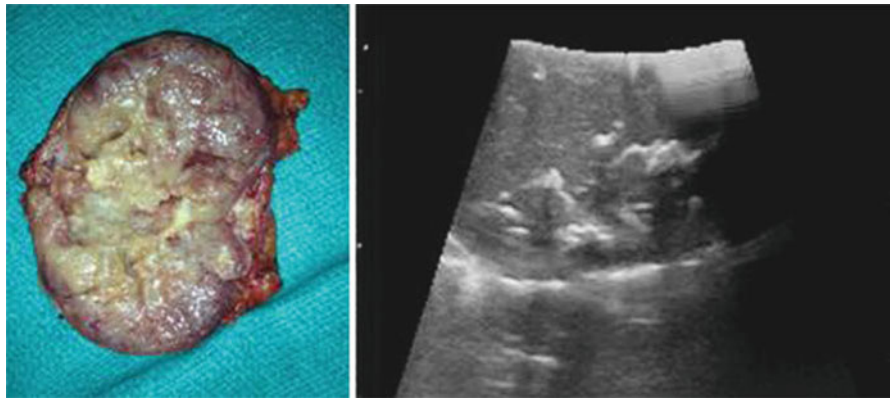

Fig. 15.9 An adrenal gland with ovarian metastasis. Gross anatomy with internal calcifications identified during laparoscopic adrenalectomy and use of LUS

renal cortical tissue. Larger lesions vary in ultrasonographic appearance, having a heterogeneous appearance with focal or scattered hypoechoic or hyperechoic zones representing areas of tumor necrosis, hemorrhage, or, rarely, calcification. Metastatic adrenal tumors usually have an ovoid shape and variable echogenicity (Fig. 15.9). Adrenal cysts appear as anechoic masses with enhanced posterior sound transmission, whereas myelolipomas are highly echogenic because of their fat content. Although the use of LUS facilitates tumor evaluation and identification of adjacent structures, especially large vessels, in cases of pheochromocytoma and adrenal cortical carcinomas, compression of the adrenal gland may have very harmful effects either triggering catecholamine release or rupture of the malignant tumor causing spread of cancer.

Clinical experience: Contrast-enhanced ultrasonography has been employed in Europe and other countries to evaluate hypervascularity and correlate with malignancy. Hijioka et al. reported their experience on contrast-enhanced endoscopic ultrasonography (CE-EUS) to identify adrenal mass hypervascular lesions and perform EUS-guided fine needle aspiration (EUS-FNA). They concluded that this imaging modality can assist in the diagnosis of metastatic lesions, i.e., clear cell carcinoma leading to adrenalectomy and confirmation of metastatic clear cell carcinoma of the kidney [27]. Additional reports of ultrasound and/or CT scan-guided percutaneous cryoablation of adrenal masses have shown encouraging cost-effective outcomes. This procedure was associated with very low morbidity and local tumor recurrence rates and increased overall survival. Even as an adjunct to systemic therapies, it seems that percutaneous cryoablation of adrenal masses appeared cost-effective for palliation [28].

The Bladder

Suprapubic Tube Placement or Suprapubic Aspiration

Aspiration or trocar suprapubic tube placement (SPT) or "punch" suprapubic tube, as they are commonly referred, can offer quick drainage of the urinary bladder. The clinical scenario that necessitates SPT placement is the inability of the patient to void (posterior urethral disruption, urethral stricture) or when invasive urethral procedure may trigger sepsis (acute prostatitis) or autonomic dysreflexia (spinal cord injury patients) [29]. The primary risk associated with this technique is perforation of bowel overlying the urinary bladder and open SPT approach must be applied in these patients.

Ultrasound probe: The use of curved-array 3.5–5-MHz probes with or without color Doppler provides good visualization and allows attachments

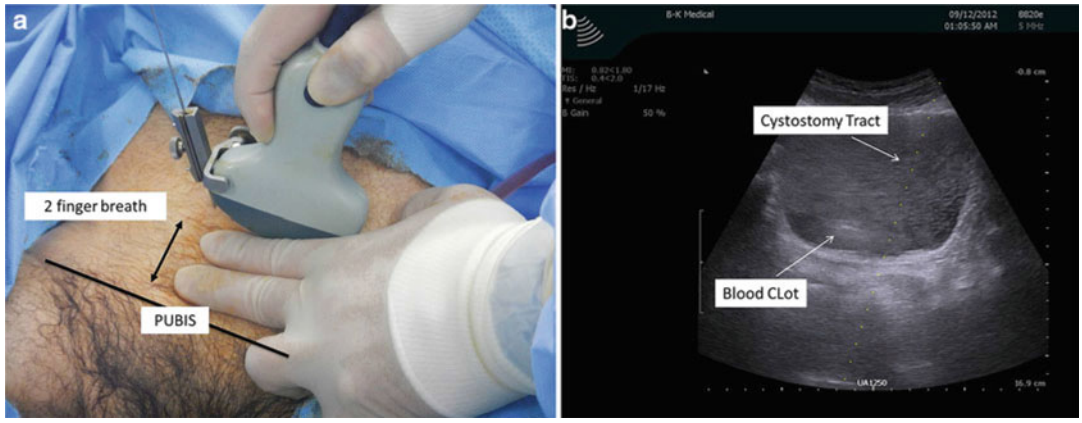

Fig. 15.10 (**a**) Placement of a suprapubic catheter. (**b**) The clear visualization of the full bladder demonstrates no interposing bowel

that can display the path of the introducing needle towards the bladder. In the absence of this type of probe, a linear array can be used to rule out bowel interposition between the skin and the bladder.

Technique: For ultrasound-guided trocar (SPT) placement or aspiration, the urologist should inquire the past surgical history of the patient, as prior abdominal operations could signify increased risk for bowel overlying the urinary bladder. On exam, the patient should have a distended bladder prior to the procedure and no scars that include the lower abdomen. Typical ultrasonography findings should include a variable-thickness bladder wall and dark homogeneous fluid content representing urine. One may survey the infraumbilical area and detect bowel contents represented by dark dynamic shadowing images representing peristalsis with gas content or any intervening tissue planes or heterogeneous echogenicity between the abdominal wall and urinary bladder. Presence of large blood clots also interferes with the hypoechoic characteristic of a full bladder. Further ruptured bladders will be difficult visualizing since the bladder may be empty. "Rocking" of the US probe will verify needle and catheter placement in a full bladder, and immediate urine drainage should be observed after initial puncture. The US probe follows the universal left/cephalad position and it should be positioned approximately three fingerbreadths above the pubic bone allowing the SPT needle to be placed between the US probe and the pubic bone (Fig. 15.10).

However some cases may require exploratory laparotomy, thus allowing for direct visual placement of suprapubic cystotomy tube. In instances where surgery is not needed, however, percutaneous SPT may be desirable. Trocar SPT or "punch" suprapubic tube, as they are commonly referred, can offer quick drainage of the urinary bladder. The primary risk associated with placement is perforation of bowel overlying the urinary bladder. While blind techniques have certainly been described in the past, modern access to ultrasonography can assist the urologist in an outpatient, operative, or emergency room setting in mitigating risk. Alternatives to straight ultrasound-guided placement include optional cystoscopic visualization and the previously mentioned open cystotomy and SPT.

For ultrasound-guided trocar SPT, the urologist or proceduralist should inquire as to the patient's past surgical history, as prior abdominal operations could signify increased risk for adhesions, particularly with respect to bowel overlying the urinary bladder. On exam, the patient should have a distended bladder prior to beginning the procedure. Typical ultrasonography findings should include a variable-thickness abdominal wall and dark, fluid-filled urinary bladder.

Clinical data: A total of 140 pediatric patients less than 2 years old that required suprapubic aspiration (SPA) were randomized to either an ultrasound-guided or ultrasound-unguided (control) protocol. The aspirations under ultrasound guidance were performed under ultrasound examination during insertion of the needle. SPA had an overall success rate in 90 % of attempts (63/70) in the ultrasound-guidance group compared with 64 % (45/70) in the no-ultrasound group ($p < 0.05$). There were fewer passes made in those patients who had the procedure done under ultrasound guidance ($p < 0.05$). Ozkan et al. demonstrated the use of ultrasonography as an assistant tool for SPA in centers where portable ultrasound guidance is available, in particular, for infants more than 1 month old [30]. There are several clinical scenarios for SPT including traumatic injury (posterior urethral disruption, intraperitoneal bladder perforation), short-term use for neurogenic bladder, and urinary retention (as in setting of stricture or other bladder outlet obstruction) [29].

The Prostate

Transrectal Ultrasound

The advent of US technology has improved visualization, and 3D reconstruction of the prostate via transrectal US is under development. The transrectal probes are slimmer and offer a real-time simultaneous sagittal and transverse view of the prostate. Moreover, the prostate can be visualized by either a suprapubic or transrectal approach. The former does not offer complete evaluation of the prostate but may assist to define the presence of an intravesical prostate. We have recently demonstrated the correlation of US anatomical findings and comparative cadaveric anatomy of the external urethral sphincter. The rhabdosphincter can be appreciated in the US images as a hyperechoic triangle at the apex of the prostate (Fig. 15.11), and the cadaveric models demonstrated a significant amount of muscle fibers overlapping the prostatic apex [31].

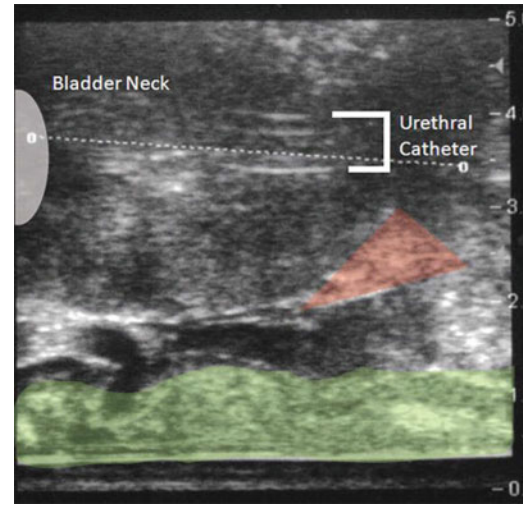

Fig. 15.11 Measurement of prostatic urethral length from the bladder neck to the prostate apex. The external sphincter is highlighted in *red*, the bladder neck in *white*, and the rectal wall in *green*

Ultrasound probe: A biplane or end-fire transrectal ultrasound probe with frequency range of 6.0–9.0 MHz should be used to evaluate the prostate and surrounding structures. Prostate size and morphology may also be evaluated using a transabdominal approach with a curved linear array probe. The transrectal probe should be able to accommodate a needle guide for transrectal ultrasound-guided biopsy. The needle guide may be a single-use or a reusable device.

Technique: For optimal evaluation during transrectal ultrasound imaging, one must prepare the patient, giving instructions to clean the rectal vault. Presence of stool and gas compromises visualization. Fleet enema is recommended the night prior and the morning of the study. Slow introduction of the transrectal probe with lubrication in the rectum should be performed by gentle rotation and forward movement until the prostate is visualized. When a stepper is used, one may verify the correct model to use with different probes. Different techniques will be dependent on patient's position from lateral decubitus to lithotomy. The surgeon has to adjust and standardize images to transverse and sagittal views.

Transperineal Prostate Biopsies

The transperineal needle biopsy of the prostate is popular in Europe more than in the United States. While transperineal needle biopsy of the prostate was described as early as 1963, a grid-based, systematic, ultrasound-guided approach was not described until 2001 by Igal et al. Present biopsies involve the simultaneous use of image guidance via transrectal ultrasound with systematic sampling by either the standard sextant or whole gland mapping biopsies [32, 33]. Moreover, Barzell et al. describe extended biopsy technique with transrectal ultrasonography as an option for men with low-volume, low-grade, histologically proven prostate cancer who may be considering experimental targeted focal therapy. Prior to biopsy, the patient should undergo TRUS measurements of the prostate to ensure that the gland is not too large (<65 cm^3) and is not obstructed by the pubic arch. If the gland is too large or perineal access is partially obstructed, the patient can be started on 5α-reductase inhibitors and reevaluated every 3 months until the prostate is fully accessible. The procedure is generally performed in the clinic under local anesthesia with the patient in high lithotomy and use of a standard 5-mm interval brachytherapy perineal grid and a standard 18-gauge prostate needle biopsy gun. Five millimeter was determined to be the optimal grid size to ensure very few lesions are missed [34]. Cross-sectional ultrasound images are captured using a standard transrectal ultrasound probe, and these images are used to reconstruct the prostate in three dimensions by denoting borders of the gland. During the procedure, the urologist should note position of the urethra to avoid perforation with the biopsy gun. Care must be taken to ensure complete gland coverage by taking deeper (base) and shallow (apex) passes at the same grid position, as the length of the gland may be longer than a single pass of a standard 18-gauge biopsy needle. Each biopsy is labeled with *x*–*y*–*z* coordinates and placed in separate jars for histological analysis. Specialized software can then be used to combine pathology results (i.e., cancerous foci) with 3D model of the prostate generated from transrectal ultrasound images.

Cryotherapy

Cryotherapy was first proposed and used as a treatment for cancer in the nineteenth century. Using a combination of salt and ice applied to cervical and breast tumors, patients experienced less pain and decreased tumor size. Ultimately, conversion of air (oxygen and nitrogen) to their liquid forms and the ability to store them in adequate quantities for regular use brought about a resurgence in use in the early twentieth century. The first cryoprobe was built by Cooper and Lee in 1961 and circulated liquid nitrogen, allowing them to freeze tissues that were in contact with the probe, and the first use in the prostate was in 1964 [35]. The advent of ultrasound as a monitoring tool made cryotherapy as an ablative tool more attractive for the treatment of prostate cancer. The AUA recognized cryotherapy for localized prostate cancer as a standard treatment option in 1996. Current devices are labeled third generation and use urethral warmers, a combination of argon (cooling) and helium (warming) gases taking advantage of the Joule–Thomson effect, and TRUS guidance.

Technique: With the patient in exaggerated lithotomy position, a brachytherapy template guide is placed on the perineum. A multifrequency biplanar transrectal ultrasound probe on a stepper is used for visualization of the prostate, urethra, bladder neck, and rectum. Temperature monitors are placed near Denonvilliers' fascia, external urinary sphincter, and neurovascular bundles to monitor for appropriate level of freezing and avoid thermal damage to these sensitive structures. Current recommendations state that temperature of these structures should remain above 15 °C. Cryoneedles are inserted under TRUS visualization into the grid to encompass either the entire gland or, in cases where focal therapy is desired, in the area of concern, identified by prior transperineal mapping biopsies (Fig. 15.12). Lastly, the urethral warmer is placed under cystoscopic guidance. For full-gland treatment, 2–4 mm of periprostatic tissues should be included in the treatment zone to ensure adequate cancer control. At the time of cystoscopy, the urethra is

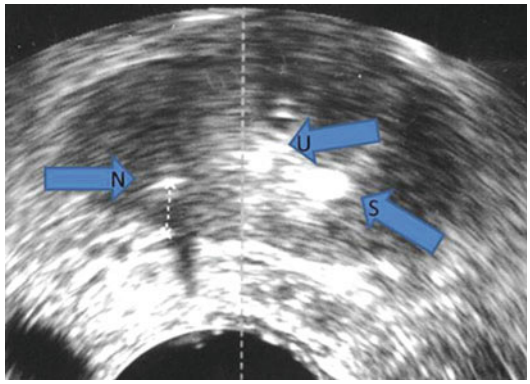

Fig. 15.12 Hyperechoic cryoablation needle (*N*) is observed and the distance to the prostate capsule may be measured. Additional left prostate stone (*S*) is visualized as well as the Foley catheter in the urethra (*U*)

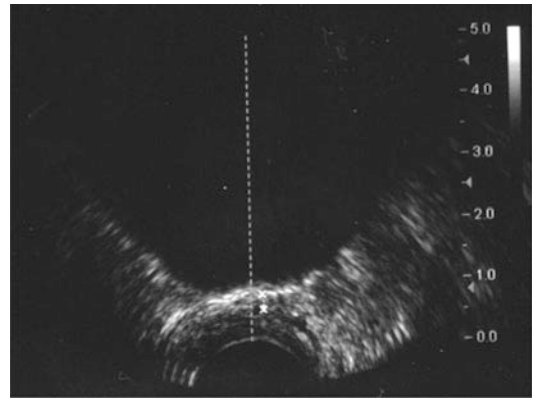

Fig. 15.13 Hyperechoic rim features of the external aspect of the ice ball during cryoablation of the prostate and the hypoechoic lesion representing the ice ball

inspected for possible perforation of the needles or thermocouples, so that they can be moved prior to starting the freezing cycles. Freezing is carried out in an anterior-to-posterior direction to maintain TRUS visibility down to −40 °C for two freeze–thaw cycles. Visual guidance with ultrasound, though, has limitations that should be acknowledged prior to use [36, 37]. Ultrasound imaging cannot capture tissue temperature information during the procedure and changes visible in these images do not reliably correspond to specific temperature regions. Therefore, the temperature probes are placed before the cryoprobes. The identification of the external urinary sphincter must be well recognized by the surgeon to ensure proper probe placement to prevent urinary incontinence due to sphincter damage. We described the US findings and correlated with the studies in human cadaveric external urethral sphincter. The hyperechoic triangle distal to the apex of the prostate is the rhabdosphincter that has an important segment in the prostatic apex. The sphincter can be well demonstrated by pressing with the thumb over the base of the scrotum under the pubic arch [31]. Constant changes of views from sagittal to transverse and vice versa are required to evaluate the real-time progression of the ice ball to prevent rectal and urinary sphincter injury. The typical cryolesion is described as a well-marginated, hyperechoic rim with acoustic shadowing in the middle (Fig. 15.13). This hyperechoic rim obstructs the leading edge of frozen tissue, obscuring the true extent of affected area. Color Doppler may be useful to monitor blood flow around the rectum; however, this is not thought to be an objective monitoring tool. Complete thaw of the ice ball allows the visualization of the prostate as the beginning of the procedure.

Brachytherapy

Brachytherapy, or the placement of radioactive materials or seeds within the prostate, was first suggested by Alexander Graham Bell in 1908 [38–41]. Introduction of transrectal ultrasound-guided imaging offered the possibility of uniform distribution of the radioactive seeds for either permanent low-dose therapy (iodine-125, palladium-103) or temporary high-dose therapy (iridium-192) deposited into the prostate gland through a perineal template grid [42–44]. The introduction of image guidance also ensures seeds are not placed in close proximity to the urethra, nerves, or rectum, limiting side effects like lower urinary tract symptoms, erectile dysfunction, and fecal urgency. Ultrasound imaging during or at time of seed placement will generally reveal the hyperechoic needle and resultant shadowing. Similarly, seeds appear as small hyperechoic points. Assuring adequate dosimetry through appropriate placement of seeds remains paramount and

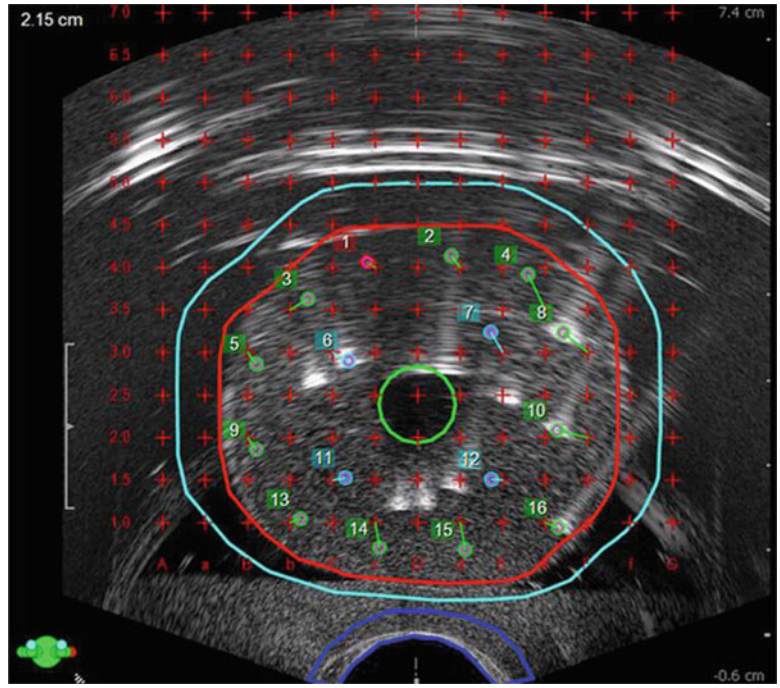

Fig. 15.14 Brachytherapy planning grid with positions of the brachy seeds. Seeds are visualized as hyperechoic objects

has been shown to highly operator-dependent. However, computer-based planning systems coupled with TRUS imaging have allowed for precise and predictable seed placement that is reproducible (Fig. 15.14) [45]. Intraoperative preplanning replaces the need for an office visit with a planning session just prior to implantation in the operating room [46]. Because the exact number of required seeds is unknown prior to entering the OR, an approximate number is ordered according to a nomogram of gland volume derived from prior TRUS (at time of prostate biopsy) or CT. Biplanar TRUS imaging is performed in the exaggerated lithotomy position in the operating room and is fed to the treatment planning system. Transperineal implantation is then performed according to this plan. Biplanar TRUS imaging via US probe on a stepper is used to guide the needles throughout the procedure with confirmation of placement via fluoroscopy, since TRUS routinely cannot visualize anywhere from 2 to 45 % of seeds during or after placement [47]. There are newer technologies that are under investigation looking at TRUS-fluoroscopy fusion imaging to verify seed placement and accurately verify dosimetry results during brachytherapy.

High-Intensity Focused Ultrasound

High-intensity focused ultrasound (HIFU) was first used over 15 years ago for the treatment of benign prostatic hypertrophy, and subsequently in 1996, Gelet et al. used this new technology for the treatment of patients with localized, low-grade adenocarcinoma of the prostate [48, 49]. HIFU is one such technique that can be used to focally ablate cancerous lesions using ultrasound energy to cause mechanical and thermal injury to the targeted tissue. HIFU, when used for the treatment of localized prostate cancer, uses a multifrequency ultrasound transducer placed in the rectum to generate acoustical energy that is focused on the tissue target, creating high temperatures and irreversible coagulative necrosis. HIFU utilizes a "trackless" principle, whereby tissue outside the focal plane is not damaged; the transrectal probe sits on the rectal mucosa and sends acoustical energy through the intervening tissues, only heating the tissue volume targeted by the probe [50]. The probe is repositioned mechanically as needed to target the prostate in its entirety. HIFU is performed with the patient placed under spinal or general anesthesia with

prostate volumes greater than 40 cm^3 [51]. (Notably, study protocols of US trials do not permit the use of TURP prior to HIFU.) The prostate is visualized using real-time diagnostic images generated by the probe using lower, nondestructive acoustical energies (0.1–100 mW/cm^2). Once the target areas are identified, the prostate tissue is ablated with high energies (1300–2200 W/cm^2) focused in a small 1–3-mm-wide by 5–26-mm-long focal plane. Each pulse heats the tissue to 80–98 °C over a 3-s period. The gland is revisualized with lower ultrasound energies between ablative pulses. The probe is then moved and rotated in a semiautomated manner (device-dependent) using lower-energy diagnostic images to target adjacent prostate tissue. The end goal is to create overlapping lesions until the whole gland is treated. HIFU destroys target tissue through the thermal and mechanical effects of nonionizing, acoustical radiation (i.e., sound waves) delivered to target tissues after focusing by an acoustic lens, bowl-shaped transducer, or electronic phased array. Although not shown, the ablated area will become hyperechoic on lower-energy imaging. Because HIFU utilizes nonionizing radiation, it can be repeated one or more times during multiple sessions. The thermal effects are achieved by heating tissues to 60 °C or higher, resulting in near-instantaneous coagulative necrosis and cell death [52]. By focusing the energy, more destruction occurs within the focal plane, but tissues outside the target area are spared of damage as energy intensities are far lower.

Laparoscopic Radical Prostatectomy

Ukimura, Gill, and colleagues recently described the use of real-time TRUS imaging of the prostate during laparoscopic prostatectomy, allowing for visualization of key structures such as the neurovascular bundles, bladder neck, and apex of the prostate, thus aiding in dissection [53].

Their report on intraoperative use of TRUS imaging for 25 consecutive patients notes the use of high-frequency 2D ultrasound imaging, power Doppler imaging, and 3D ultrasound imaging to aid in the identification of these key structures. In particular, the authors note that intraoperative use of ultrasound aided in three primary aspects of the laparoscopic prostatectomy. Ultrasound aided in identification of the correct plane between the posterior bladder neck and base of the prostate, thus allowing for laparoscopic visualization of seminal vesicles and vasa deferentia. Secondly, the authors described the ability to identify the distal protrusion of the prostate apex posterior to the membranous urethra in difficult cases, thus enhancing apical dissection to ensure negative margins. Finally, the authors note that intraoperative ultrasound offered the ability to identify hypoechoic nodules abutting the prostate capsule, allowing the surgeon to perform a wide dissection around these locations.

The Testis

Traditionally, patients with palpable or suspicious testicular masses would undergo radical orchiectomy, but investigators began to explore partial orchiectomy after intraoperative biopsy to confirm a lesion as benign or malignant, thus preserving testicular function in those where radical surgery is deemed unnecessary. Two recently published series show that the most common type of testicular tumor in prepubertal children is teratoma, a benign germ cell tumor (GCT).

Ultrasound probe: A high-frequency broadband linear transducer (4–12 MHz) can perform both power and spectral Doppler ultrasonography. Imaging of the scrotum, penis, and urethra is performed with a 7–12-MHz linear array transducer. The length of the transducer may vary from 4 to 8 cm. Equipment with Doppler capabilities is required for demonstrating blood flow in the evaluation of testicular torsion.

Technique: Technique and ultrasound probe for testis evaluation is described in detail in an earlier chapter. The linear array US is used intraoperatively after the testis is delivered via inguinal approach if malignancy is suspected. The cord is temporarily clamped and the testicle may be placed on ice (to minimize ischemia reperfusion

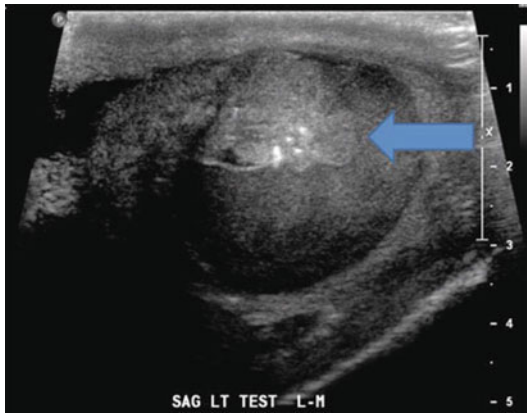

Fig. 15.15 *Blue arrow* depicts heterogeneous hyperechoic lesion of intratesticular mass (non-seminomatous germ cell tumor) with calcification

injury) while the evaluation of the lesion is done. The goal is to delineate and determine respectability of the abnormal mass (hypoechoic/hyperechoic lesion compared to healthy parenchyma) (Fig. 15.15) that can be round or irregular and intratesticular. Dissection through the tunica albuginea and enucleation of the lesion with 2–5-mm margins should be carried out. The lesion should be sent for frozen section analysis by surgical pathology, and a determination of whether radical or partial orchiectomy is appropriately made. In the case of benign pathology, the tunica should be inspected for hemostasis and the incision closed. Finally, ultrasound may be used to inspect the affected area to ensure adequate resection of the lesion.

Clinical data: Organ-sparing approaches generally remain an option for a highly selected group of patients with testicular GCT only—men with bilateral testicular cancer or GCT in a solitary testis. Partial orchiectomy should be performed in such patients if the size and location of the mass are amenable to surgery. Partial orchiectomy of GCT provides a number of potential benefits over radical surgery: reduced need for androgen substitution, less psychological stress, preservation of fertility, and a durable cure rate. Partial orchiectomy of benign testicular lesions reduces the proportion of patients who are overtreated with radical orchiectomy. CIS detected in the testes remaining after partial orchiectomy can be treated with radiation therapy. Up to 40 % of patients will need hormonal replacement after this treatment. It should be emphasized that bilateral orchiectomy remains the best chance of cure in men with a solitary testis but comes at the cost of morbidity. Men should only undergo partial orchiectomy if one is certain that the lesion is benign. In this regard, size is important as masses larger than 2 cm in diameter are extremely suspicious for malignancy. Also, the lack of blood flow, serial growth, risk factors for GCT, and being impalpable all favor this approach [54].

The Renal Pelvis and Ureters

Stent Placement During Pregnancy and Patients in the ICU

Urolithiasis during pregnancy remains relatively common, affecting about 1 in 200 pregnancies [55]. While a majority of stones can be successfully managed conservatively with hydration, pain control, and antibiotics if necessary (70–80 % will pass spontaneously owing mostly to physiologic dilatation of the ureters during pregnancy), the rest may require urologic intervention. Intravenous hydration may be necessary in cases of prolonged nausea and vomiting, and pain control should consist of acetaminophen with narcotic. Nonsteroidal anti-inflammatory medications should be avoided as they interfere with prostaglandin synthesis, which is required to maintain a patent ductus arteriosus until birth. In a portion of cases, renal colic and not urolithiasis may be the underlying cause of pain and necessitate urologic intervention [56]. Stent placement remains the most common of modern urologic interventions with various types of lithotripsy or PCN comprising the remainder. The urologist should note that stones and intervention may each increase the risk of preterm premature rupture of membranes and preterm labor. Minimally invasive techniques for managing patients who fail conservative treatment fall into two categories: temporary urinary drainage for obstructed urinary systems and procedures that

facilitate stone removal. Stent placement has been performed using ultrasound guidance negating the need for ionizing radiation from intraoperative fluoroscopy and the concomitant risk to a fetus, particularly during the first trimester. When deciding on appropriate intervention for stones, diversion is usually recommended for stones that reside proximally in the collecting system [57]. Additionally, in cases of infected hydronephrosis or urosepsis, diversion is the mainstay of treatment. Cystoscopy for retrograde placement or PCN for antegrade placement of stents can be performed under local or regional anesthesia, thus minimizing the risk to the mother and fetus. Ureteral stents are placed at the time of cystoscopy, and ultrasound has been described as a valid tool for image guidance and confirmation of final stent position within the renal pelvis and bladder. This procedure can be performed using ultrasound guidance negating the need for ionizing radiation from intraoperative fluoroscopy and the concomitant risk to a fetus, particularly during the first trimester.

Ultrasound probe: The use of a curved-array 3.5–5-MHz probe with or without color Doppler provides good visualization of the hydronephrosis calyx and or stone.

Technique: The technique, ultrasound probe, and limitations are similar to any renal ultrasound evaluation, with the special attention to the well-being of two instead of one patient. Fetal monitoring must be performed during the procedure with the assistance of the obstetric team. On renal ultrasound, stents appear as hyperechoic structures, and final placement with curls in the renal pelvis and bladder can be easily visualized as the cystoscope operator introduces and advances the ureteral stent up to the kidney. Additionally, one can evaluate the ureteral orifices with Doppler ultrasound of the bladder to confirm the presence of ureteral jets. Visualization of ureteral jets is an acceptable method of confirming the patency of the urinary tract. Patient can be awake or lightly sedated for the procedure with the assistance of the anesthesiologist and obstetric team to monitor the fetus. While one operator performs the cystoscopy, the radiologist or a second surgeon should perform the renal ultrasonography. The sonographer will detect the hydronephrotic kidney and visualize the guide wire and stent placement in real time (Fig. 15.16). Patients that are extremely unstable with septic shock due to impacted stone may have a stent placement using flexible cystoscopy and US guidance. In this case, a single-J ureteral stent is preferable due to the stiffness and easier manipulation. Notably, stents should be changed every 4–6 weeks during pregnancy, as there is an increased propensity during pregnancy for stents to encrust.

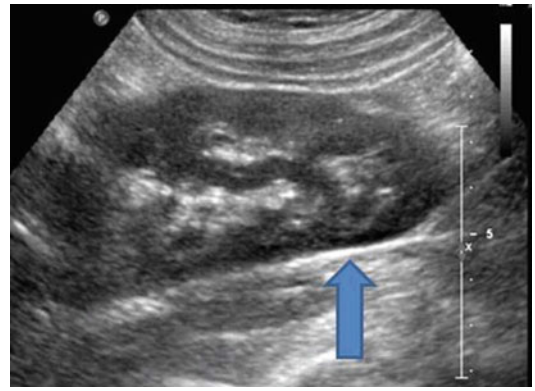

Fig. 15.16 Right ureteral stent placement under ultrasound guidance (*blue arrow*)

Clinical data: One series of 300 pregnant women with renal colic, of whom 44 ultimately underwent ureteral stenting for symptomatic control or urinary obstruction, showed that stents placed during the second trimester were tolerated more (13/15 or 86.7 %) as compared to those placed during the third trimester (14/26 or 53.8 %) [56]. Our unpublished series includes five patients requiring ureteral stent placement in the intensive care unit. Three patients had a right-sided upper tract impacted stones, and two were left-sided (distal and mid ureter) stones. All patients were intubated and unstable. The use of flexible cystoscopy and single-J ureteral stents allowed prompt drainage of purulent urine and resolution of the septic shock. Placement of the left stents was more challenging due to the inability to move the patient to different positions and due to

their high body mass index, but visualization of stent and flow during collection of intrarenal urine for culture was identified by color Doppler US. Moreover, the single-J stent allows repositioning that can be verified with simple abdominal X-ray (KUB).

Conclusion

Intraoperative use of ultrasound imaging has become standard in many different urologic interventions. Understanding its role in urologic surgery and interpreting key findings on ultrasound are essential to the successful use of this adjunct imaging technology. As newer devices, probes, and software are developed, we feel that use of ultrasound in the operating room will continue to expand into new areas.

References

1. Goodwin WE, Casey WC, Woolf W. Percutaneous trocar (needle) nephrostomy in hydronephrosis. J Am Med Assoc. 1955;157(11):891–4.
2. Gu Z, et al. Percutaneous nephroscopic with holmium laser and ultrasound lithotripsy for complicated renal calculi. Lasers Med Sci. 2010;25(4):577–80.
3. Gupta S, et al. Percutaneous nephrostomy with real-time sonographic guidance. Acta Radiol. 1997;38(3): 454–7.
4. Bird VG, Fallon B, Winfield HN. Practice patterns in the treatment of large renal stones. J Endourol. 2003;17(6):355–63.
5. Skolarikos A, et al. Ultrasound-guided percutaneous nephrostomy performed by urologists: 10-year experience. Urology. 2006;68(3):495–9.
6. Alken P, Hutschenreiter G, Günther R. Percutaneous kidney stone removal. Eur Urol. 1982;8(5):304–11.
7. Miano R, et al. Position: prone or supine is the issue of percutaneous nephrolithotomy. J Endourol. 2010;24(6):931–8.
8. El-Nahas AR, et al. Colonic perforation during percutaneous nephrolithotomy: study of risk factors. Urology. 2006;67(5):937–41.
9. Basiri A, et al. Ultrasonographic versus fluoroscopic access for percutaneous nephrolithotomy: a randomized clinical trial. J Endourol. 2008;22(2):281–4.
10. Radecka E, Magnusson A. Complications associated with percutaneous nephrostomies. A retrospective study. Acta Radiol. 2004;45(2):184–8.
11. von der Recke P, Nielsen MB, Pedersen JF. Complications of ultrasound-guided nephrostomy. A 5-year experience. Acta Radiol. 1994;35(5):452–4.
12. Lewis S, Patel U. Major complications after percutaneous nephrostomy-lessons from a department audit. Clin Radiol. 2004;59(2):171–9.
13. Torres Muñoz A, et al. Percutaneous renal biopsy of native kidneys: efficiency, safety and risk factors associated with major complications. Arch Med Sci. 2011;7(5):823–31.
14. Fergany AF, Hafez KS, Novick AC. Long-term results of nephron sparing surgery for localized renal cell carcinoma: 10-year followup. J Urol. 2000;163(2):442–5.
15. Lau WK, et al. Matched comparison of radical nephrectomy vs nephron-sparing surgery in patients with unilateral renal cell carcinoma and a normal contralateral kidney. Mayo Clin Proc. 2000;75(12):1236–42.
16. Huang WC, et al. Chronic kidney disease after nephrectomy in patients with renal cortical tumours: a retrospective cohort study. Lancet Oncol. 2006;7(9): 735–40.
17. Lee CT, et al. Surgical management of renal tumors 4 cm. or less in a contemporary cohort. J Urol. 2000;163(3):730–6.
18. Baust JG, et al. Cryosurgery—a putative approach to molecular-based optimization. Cryobiology. 2004;48(2):190–204.
19. Baust JG, Gage AA. The molecular basis of cryosurgery. BJU Int. 2005;95(9):1187–91.
20. Curry NS, Bissada NK. Radiologic evaluation of small and indeterminant renal masses. Urol Clin North Am. 1997;24(3):493–505.
21. Onik GM, et al. Ultrasound characteristics of renal cryosurgery. Urology. 1993;42(2):212–5.
22. Kaczmarek BF, et al. Robotic ultrasound probe for tumor identification in robotic partial nephrectomy: initial series and outcomes. Int J Urol. 2013;20(2):172–6.
23. Rogers CG, et al. Maximizing console surgeon independence during robot-assisted renal surgery by using the Fourth Arm and TilePro. J Endourol. 2009;23(1): 115–21.
24. Liao JC, Su L-M. Advances in image-guided urologic surgery. New York: Springer; 2015.
25. Kaczmarek BF, et al. Comparison of robotic and laparoscopic ultrasound probes for robotic partial nephrectomy. J Endourol. 2013;27(9):1137–40.
26. Lockhart ME, Smith JK, Kenney PJ. Imaging of adrenal masses. Eur J Radiol. 2002;41(2):95–112.
27. Hijioka S, et al. Contrast-enhanced endoscopic ultrasonography (CE-EUS) findings in adrenal metastasis from renal cell carcinoma. J Med Ultrason. 2011;38(2):89–92.
28. Bang HJ, et al. Percutaneous cryoablation of metastatic renal cell carcinoma for local tumor control: feasibility, outcomes, and estimated cost-effectiveness for palliation. J Vasc Interv Radiol. 2012;23(6):770–7.
29. Rosenstein D, McAninch JW. Urologic emergencies. Med Clin North Am. 2004;88(2):495–518.
30. Ozkan B, et al. Suprapubic bladder aspiration with or without ultrasound guidance. Clin Pediatr (Phila). 2000;39(10):625–6.
31. Miano R, et al. Morphological evaluation of the male external urethral sphincter complex by transrectal ultrasound: feasibility study and potential clinical applications. Urol Int. 2012;89(3):275–82.

32. Coppola R. Diagnosis of prostatic carcinoma by means of transperineal needle biopsy. Riforma Med. 1963;77:1282–4.
33. Igel TC, et al. Systematic transperineal ultrasound guided template biopsy of the prostate in patients at high risk. J Urol. 2001;165(5):1575–9.
34. Crawford ED, et al. Clinical staging of prostate cancer: a computer-simulated study of transperineal prostate biopsy. BJU Int. 2005;96(7):999–1004.
35. Gonder MJ, Soanes WA, Smith V. Experimental prostate cryosurgery. Invest Urol. 1964;1:610–9.
36. Onik G, et al. US characteristics of frozen prostate. Radiology. 1988;168(3):629–31.
37. Littrup PJ, et al. Prostatic cryotherapy: ultrasonographic and pathologic correlation in the canine model. Urology. 1994;44(2):175–83. Discussion 183–4.
38. Scardino P, Carlton C. Combined interstitial and external irradiation for prostatic cancer. In: Javadpour N, editor. Principles and management of urologic cancer. Baltimore: Williams & Wilkins; 1983. p. 392–408.
39. Whitmore WF, Hilaris B, Grabstald H. Retropubic implantation of iodine 125 in the treatment of prostatic cancer. 1972. J Urol. 2002;167(2 Pt 2):981–3. Discussion 984.
40. DeLaney TF, et al. Preoperative irradiation, lymphadenectomy, and 125iodine implantation for patients with localized carcinoma of the prostate. Int J Radiat Oncol Biol Phys. 1986;12(10):1779–85.
41. Aronowitz JN. Dawn of prostate brachytherapy: 1915–1930. Int J Radiat Oncol Biol Phys. 2002;54(3):712–8.
42. Holm HH, et al. Transperineal 125iodine seed implantation in prostatic cancer guided by transrectal ultrasonography. J Urol. 1983;130(2):283–6.
43. Ho AY, et al. Radiation dose predicts for biochemical control in intermediate-risk prostate cancer patients treated with low-dose-rate brachytherapy. Int J Radiat Oncol Biol Phys. 2009;75(1):16–22.
44. Potters L, et al. Postoperative nomogram predicting the 9-year probability of prostate cancer recurrence after permanent prostate brachytherapy using radiation dose as a prognostic variable. Int J Radiat Oncol Biol Phys. 2010;76(4):1061–5.
45. Hinnen KA, et al. Long-term biochemical and survival outcome of 921 patients treated with I-125 permanent prostate brachytherapy. Int J Radiat Oncol Biol Phys. 2010;76(5):1433–8.
46. Nag S, et al. Intraoperative planning and evaluation of permanent prostate brachytherapy: report of the American Brachytherapy Society. Int J Radiat Oncol Biol Phys. 2001;51(5):1422–30.
47. Han BH, et al. Prostate brachytherapy seed identification on post-implant TRUS images. Med Phys. 2003;30(5):898–900.
48. Rove KO, Sullivan KF, Crawford ED. High-intensity focused ultrasound: ready for primetime. Urol Clin North Am. 2010;37(1):27–35. Table of Contents.
49. Gelet A, et al. Local control of prostate cancer by transrectal high intensity focused ultrasound therapy: preliminary results. J Urol. 1999;161(1):156–62.
50. Warwick R, Pond J. Trackless lesions in nervous tissues produced by high intensity focused ultrasound (high-frequency mechanical waves). J Anat. 1968;102(Pt 3):387–405.
51. Chaussy C, Thüroff S. The status of high-intensity focused ultrasound in the treatment of localized prostate cancer and the impact of a combined resection. Curr Urol Rep. 2003;4(3):248–52.
52. Dewhirst MW, et al. Basic principles of thermal dosimetry and thermal thresholds for tissue damage from hyperthermia. Int J Hyperthermia. 2003;19(3):267–94.
53. Ukimura O, et al. Real-time transrectal ultrasonography during laparoscopic radical prostatectomy. J Urol. 2004;172(1):112–8.
54. Zuniga A, Lawrentschuk N, Jewett MA. Organ-sparing approaches for testicular masses. Nat Rev Urol. 2010;7(8):454–64.
55. Cormier CM, et al. Urolithiasis in pregnancy: current diagnosis, treatment, and pregnancy complications. Obstet Gynecol Surv. 2006;61(11):733–41.
56. Andreoiu M, MacMahon R. Renal colic in pregnancy: lithiasis or physiological hydronephrosis? Urology. 2009;74(4):757–61.
57. Loughlin KR, Ker LA. The current management of urolithiasis during pregnancy. Urol Clin North Am. 2002;29(3):701–4.

Urologic Ultrasound Protocols

16

Bruce Gilbert

Introduction

This chapter describes one Urologist's view of what a complete ultrasound evaluation of the primary organs of interest for the Urologist (i.e., Kidney, Bladder, Prostate, Testis, Perineum, and Phallus) should include. As a Urologist I find myself striving to improve diagnostic accuracy and the management of patient's pathology. Ultrasound, being an accurate, safe, noninvasive, and low cost modality has become the primary modality of diagnosing as well as guiding treatment of urologic diseases. However, having taught many Urologists how to perform the ultrasound exam, the question kept being asked "What images do I need for a complete ultrasound examination." Although I was tempted to answer "as many as it takes to document the presence or absence of disease" I knew the student of ultrasound was in need of a protocol they could start with and change as their proficiency increased. In addition, quality involves consistency which in the context of ultrasound is the need to assure that all required images are documented. This is especially important in large practices and institutions in which the multiple of sonographers employed different levels of training and experience. As a Physician Director of a large urology ultrasound practice I find it essential to assure that each exam contains specified images, with consistent labeling and that images are documented in a specific order. This has helped assuring that a quality study has been performed and that reviewers of these images know exactly where to locate the images of interest. It also helps with assuring that all required images are documented.

I am also a stickler for detail. Not only do I require of my studies for the images to be in a specified order but the quality of each and every image must be 'ready for publication,' as I often refer to my obsession for image quality. The seven user adjustable settings of gain, time-gain compensation, frequency, focal zone, depth, field of view must be optimized. Labeling should be of either upper or lower case and neatly organized on the image.

I was therefore motivated to include this chapter which describes a precise protocol for performing and documenting the Urologic ultrasound examination. My expectation is that as the Urologist becomes an expert sonographer, changes to the protocol will occur. I have incorporated the requirements of the American Institute of Ultrasound in Medicine (AIUM) to assure those interested in AIUM Urology Practice Accreditation as well as meeting the ever escalating requirements of third-party payers, that use of these protocols will meet their requirements.

B. Gilbert, M.D., Ph.D. (✉)
The Smith Institute for Urology, Northwell Health System, 450 Lakeville Road, Suite M41, New Hyde Park, NY 11040, USA
e-mail: bgilbert@gmail.com

P.F. Fulgham, B.R. Gilbert (eds.), *Practical Urological Ultrasound*, Current Clinical Urology,
DOI 10.1007/978-3-319-43868-9_16

I would also hope that this chapter can serve as a training tool for new and seasoned sonographers. Nonetheless, it is my hope that use of these protocols will add to the quality of patient care that we provide.

Documentation

Documentation of ultrasound images and the written report is essential for insuring high-quality patient care. Proper documentation includes the production of a permanent record of the ultrasound examination and the interpretation of the examination [1]. In addition, documentation should be easily retrievable and storage and access to this documentation should comply with local, State, and Federal requirements.

Components of Proper Documentation

Written Report

The report should include specific identifiers including the patient identification, the date of the examination, and the measurement parameters as well as a description of the atypical findings of the examination. Ideally the report should also include specifics on how the evaluation was performed including details on the transducer used and machine settings employed. Most of the important machine settings are often already included on the recorded image. The report must be signed by the physician who ordered and interpreted the ultrasound examination. The Final report must be signed by the interpreting physician within 24 h. If the ordering physician is not the interpreting physician then the ordering physician must sign the report within 48 h. Prominently displayed at the top of the report should be the indications for performing the examination. The Appendix contains a set of templates that offer a structure for the report. These templates were designed for direct entry into an electronic database; however, they can be easily formatted by the user for a printable report.

Report Essentials:

1. Indication for Procedure: This should be first and foremost on any report. The diagnosis code is often included with the description of the indication to document medical necessity.
2. Transducer: Frequency and type of transducer (e.g., linear array, curved array, endorectal, biplane, etc.). If possible, specify the size of the footprint.
3. Report signed and dated by Physician. This should be done within 24 h of the time of the exam.
4. Report Includes facility contact information. This is essential information for anyone reviewing the report and needing additional information.
5. Report is appropriate for the examination.

Please note: if all components of the exam are not seen then the report should document that component was “Not Seen” and reasons why.

Images

Images should include patient identification, the date and time of each image, clear image orientation, measurements clearly identified, and labeling of anatomy and any abnormalities. If appropriately documented the image should be able to be viewed by any trained sonographer. The image should provide a clear, unimpeded ultrasound representation of the anatomy of interest. Gain, acoustic output, Time-Gain Compensation, Transducer frequency, Focal zone, Depth size, Image contrast, Image brightness, and Field of view must be set to be of ‘publishable’ quality. No images should be stored in which the settings are not optimized. Images should always be attached to the report or be easily accessible from the report. Images must also be technically adequate to provide diagnostic information.

Image quality must be of ‘publishable’ quality and have/be (Fig. 16.1):

1. Sufficient and uniform brightness
2. Sharp and in focus

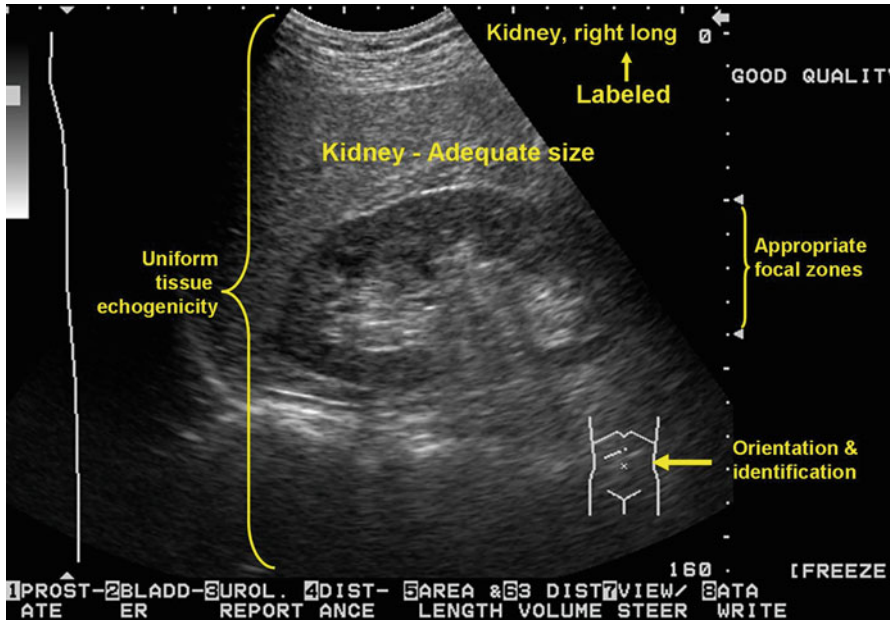

Fig. 16.1 The image should provide a clear, unimpeded ultrasound representation of the anatomy of interest. Gain, acoustic output, Time-Gain Compensation, Transducer frequency, Focal zone, Depth size, Image contrast, Image brightness, and Field of view must be set to be of 'publishable' quality

3. Adequate size
4. Proper image orientation
5. Proper labeling which should be of uniform case and esthetically positioned

The use of electronic medical records has made the documentation of ultrasound examinations somewhat easier. However, it has also created challenges in managing the archives of images and assuring the accessibility of these records to only authorized personnel. Regulatory requirements for documentation have been promulgated by the American College of Radiology (ACR) and the American Institute of Ultrasound in Medicine (AIUM). In addition, Federal and state regulations governing electronic data storage of patient information also apply and need to be adhered to.

The AIUM PRACTICE GUIDELINES and in particular for Ultrasound in the Practice of Urology [2]. These guidelines discuss Qualifications and responsibilities of personnel as well as specifications for individual examinations.

Considerations regarding the documentation and storage of ultrasound studies include:

- Providing a mechanism for the retrieval and storage of images and reports of all studies performed.
- Storing ultrasound images and the report on a secure recording media.
- The report and the information included on the images should meet or exceed the standards promulgated by accreditation organizations such as the AIUM.
- Ultrasound images and a report from the interpreting physician must be maintained in a readily accessible fashion for comparison and consultation.
- Recording media must have a shelf life compatible with the minimum number of years, required by law, for the maintenance of patient records. In most states, this will be for at least 7 years after the patient's last examination was performed; however, these requirements vary from state to state. For pediatric patients, the

recommended period is until the patient reaches the age of 21.
- Images and the reports pertaining to them are considered protected health information and are subject to the regulations of the Health Insurance Portability and Accountability Act of 1996. **Federal and State Regulatory Requirements for Document Storage**.

Federal and State regulatory requirements must be implemented for storage of patient studies. These include the Health Insurance Portability and Accountability Act of 1996 (HIPAA) [3], HiTech Act of 2009 [4], possibly FDA regulations Title 21 CFR Part 1270 if human tissue is also being stored as part of the procedure, Subpart C [5], plus State regulations usually written and enforced by the State's Department of Health.

Specific Ultrasound Protocols

To assist the urologic sonographer to develop a systematic way to scan a particular organ system I present the following set of ultrasound protocols. There is no "correct" way to perform a scan. Many alternative approaches exist. However, I strongly believe that having an organized approach will allow the sonographer to perform a comprehensive and expeditious exam that will provide optimum patient care. What follows represents one Urologist's approach and should be used as a guideline for the novice and as a point of reference for the more experienced sonographer. Protocols for quick reference and templates for data entry are provided (Appendix). Many practices incorporate the templates as part of their electronic medical record.

Color and Spectral Doppler

The use of color Doppler imaging should be considered an integral part of all ultrasound exams. Many inflammatory, neoplastic, and benign conditions have characteristic flow patterns that can assist in diagnosis. Each examination requires images that document the blood flow in that organ and if a paired organ system is present then comparison of blood flow between the organs interrogated is required.

Spectral Doppler is evolving as an invaluable component of the several urologic ultrasound exams. There is an expanding literature suggesting that these modalities might be a noninvasive indicator of testicular function. Biagiotti et al. [6] provided data suggesting that resistive index (RI) and peak systolic velocity (PSV) were better predictors of dyspermia than FSH and testicular volume. In a companion study they demonstrated that Ri and PSV can differentiate obstructive azoospermia (OA) from nonobstructive azoospermia (NOA).

It is often difficult to interrogate intratesticular vessels when the intratesticular microcirculation is impaired. Unsal et al. [7] provided data supporting interrogation of the capsular vessel and capsular branches in lieu of the intratesticular vessels (Fig. 16.2).

They found that RI of both capsular vessel and capsular branches could serve as indicators of impaired testicular microcirculation. Pinggera et al. [8] examined semen quality and the RI of intratesticular arteries in 160 men. Of interest, their study indicated that 80 with a normal sperm count had a Ri of $0.54 + 0.05$ while the 80 with impaired sperm counts had a statistically higher Ri of $0.68 + 0.06$. In addition, Balci et al. [9] demonstrated that a decrease in Ri, suggestive of an improved testicular microcirculation, was found after varicocele repair in patients with improvements in semen quality. More recently, we found (Hillelsohn et al. [10]) that an Ri greater than 0.6 was associated with dyspermia and as well as correlating with impaired spermatogenesis on testicular biopsy [11].

In the kidney and Ri of approximately 0.7 is considered normal. An elevated Ri is found in acute renal failure [12] and several other types of renal dysfunction including obstruction [13].

It is therefore our protocol to include Spectral Doppler measurements when examining the testis and kidney with ultrasound.

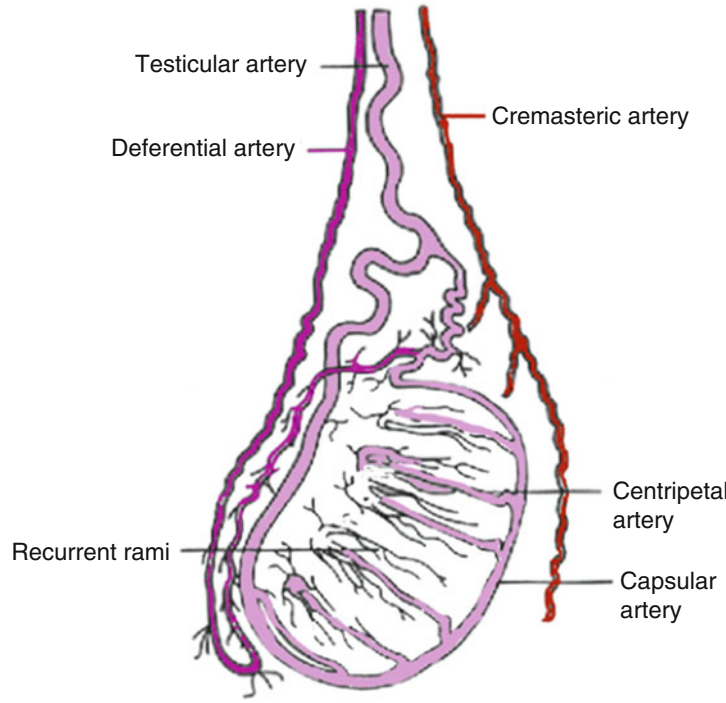

Fig. 16.2 Intratesticular arterial circulation consists of the centripetal and recurrent rami arteries which are branches off the capsular artery which is formed, in turn, from anastomosis of the testicular, deferential and cremasteric arteries

Sonoelastography

The ability to access pathology by palpation has long been a key part of the Physician's physical examination. Hard lesions are often a sign of pathology. Sonoelastography (tissue elasticity imaging) is an evolving ultrasound modality which adds the ability to evaluate the elasticity of biological tissues. Essentially, it gives a representation, using color, of the softness or hardness of the tissue of interest.

But how do we use ultrasound to 'palpate' an organ? To do so requires a mechanical wave to be produced in the tissue of interest. There are two ways to produce this mechanical wave.

1. A Compression Wave travels quickly in tissue (1500 m/s). The echoes produced by these waves successively compressing tissue layers produce scatter which is then received and processed by the ultrasound equipment. Since the Stress produced by the compression wave cannot be measured only a relative elasticity can be determined.
2. A Shear Wave travels much slower (1–10 m/s) and propagates by creating a tangential 'sliding' force between tissue layers. The elasticity (E), density of the tissue (p, kg/m^2), and shear wave propagation speed (c) are directly related through the equation $E = 3pc^2$. Therefore, by measuring the shear wave propagation speed the elasticity of the tissue can be directly determined.

Several approaches for elastography have been introduced. All of them have three common steps:

1. Generate a low frequency vibration in tissue to induce shear stress.
2. Image the tissue with the goal of analyzing the resulting stress.
3. Define a parameter related to tissue stiffness.

The principle of elastography is based on the concept that a given force applied to softer tissue results in a larger displacement than the same force applied to harder tissue. By measuring the

tissue displacement induced by compression, it is possible to estimate the tissue hardness and to differentiate benign (soft) from malignant (hard) lesions. This relationship between stress (s) and strain (e) is given by Young's Modulus or Elasticity (E),

$$E = s / e$$

E is larger in hard tissues and lower in soft tissues.

Visually, the elasticity of a tissue is represented by color spectrum. Be aware that the color given to hard lesions is determined by the manufacturer of the equipment as well as being able to be set by the user. Therefore, just as in using color Doppler, the user needs to look at the color bar (see Figs. 16.3 and 16.4) to know what color represents a 'hard' and 'soft' lesion.

The three methods commonly used for sonoelastography are as follows:

1. Quasi-Static ultrasound or Real Time Elastography (RTE) and Fig. 16.3 In which the deformation is induced by manually pressing on the anatomy with the transducer, and measured using ultrasound. RTE is a qualitative technique. Due to the requirement of manual displacement, RTE is not able to measure absolute tissue stiffness as currently employed. Its major benefits are that it has a high spatial resolution, is a real time measurement, and does not require any modifications to conventional ultrasound hardware. Companies utilizing this technique including Siemens Healthcare, Toshiba Medical, Medison, GE Healthcare, and Philips Healthcare.
2. Dynamic Elastography: A continuous Low-frequency vibration induces stationary waves which are evaluated to determine elasticity. This approach is used more often with MR since they require manipulation of two devices simultaneously.
3. Shear wave elastography (Fig. 16.4) relies on the observation of the propagation of a transient pulsed (shear) wave to determine the viscoelastic properties of the tissues. This method allows rapid scanning of the organ of interest. A limitation of the generated shear waves is that they are very weak resulting in only a few

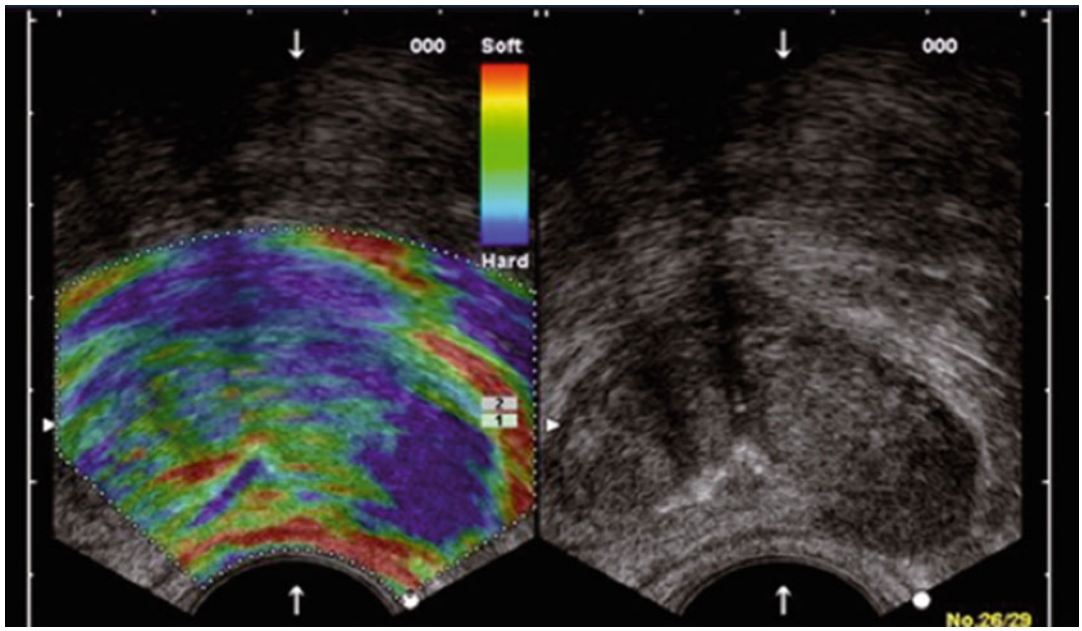

Fig. 16.3 Real-Time elastography of prostate (*left image*) and gray scale image on the *right*. In this set of images the harder/firmer tissue is *blue* while the softer tissue is *red*

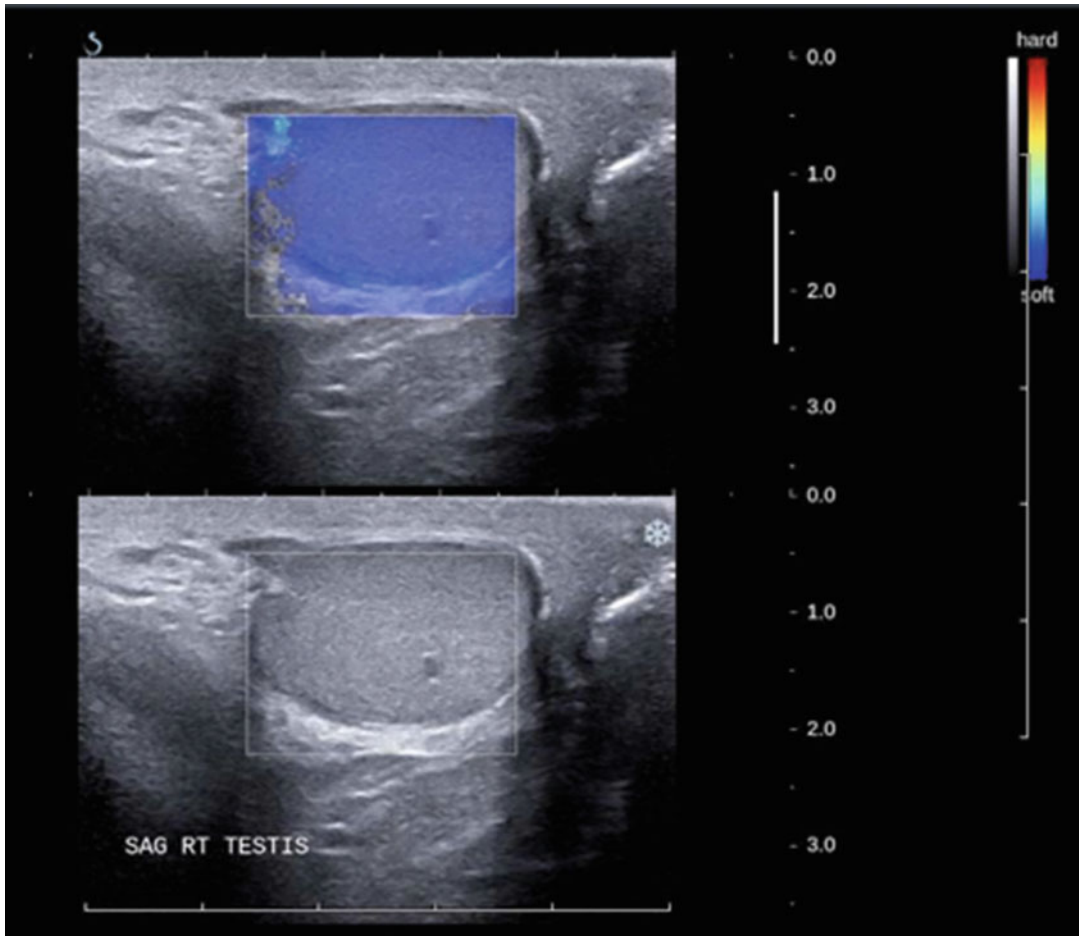

Fig. 16.4 Shear wave elastography of the testis (*top image*) with B-mode (grey scale) image on the *bottom*. In this set of images the softer tissue is *blue*

millimeters of propagation. To compensate for this various electronic innovations have been developed to limit the ultrasound power and overheating that would occur with larger perturbations. Supersonic Imagine is the primary company using this technology.

Two recent studies have used real-time elastography to differentiate benign from malignant testicular lesions, as it is postulated that malignant lesions have an increased stiffness due to a higher concentration of vessels and cells compared to surrounding tissues. Goddi et al. assessed 88 testis with 144 lesions and found a 93 % positive predictive value, 96 % negative predictive value, and 96 % accuracy, and similarly Algner et al. assessed 50 lesions and found a 92 % positive predictive value, 100 % negative predictive value, and 94 % accuracy in differentiating malignant from benign lesions. Additionally, Li et al. have found that men with nonobstructive azoospermia had a significantly different elasticity compared to patients with obstructive azoospermia and healthy controls with a normal semen analysis. Real-time tissue elastography is an exciting new innovation in assessing abnormalities on scrotal examination; however, more data is necessary prior to avoiding surgical intervention based on the findings.

In the kidney, renal masses [14, 15] as well as the viability of renal transplants [16] have been assessed.

When compared with fusion MRI, sonoelastography of the Prostate has similar sensitivity and specificity [17]. The use of various ultrasound modalities, including sonoelastography, has been described as multiparametric ultrasound and appears to significantly improve diagnostic accuracy of ultrasound [18].

If your equipment has Sonoelastography enabled I would encourage you to use this burgeoning modality on all abnormal lesions detected in any organ system interrogated by ultrasound.

Specific Protocol for Scrotal Ultrasound

Specifics to be documented on report:

Indication for Procedure: For example, testicular pain, palpable mass, and thickened skin/contracted scrotum make physical exam difficult. Diagnosis code can also be included to document medical necessity.

Transducer: 12–18 MHz linear array transducer with a footprint that is greater than the testicular length.

Please note: if all components of the exam are not seen then the report should document that component was "Not Seen" and why.

Scanning Technique

The patient is examined in the supine position. There are several different techniques to support the scrotum. The easiest is to use the patient's legs for support. Other approaches use towels placed across the patient's thighs or under the scrotum. The phallus is positioned up on the pubis held by the patient and/or covered by a towel.

Transducer Selection

High frequency (12–18 MHz) linear array transducers are most often used for scrotal scanning. Broad bandwidth transducers allow for multiple focal zones, eliminating the need for adjustment during the examination. Multiple frequency transducers allow the transducer to be set at one of several distinct frequencies. A linear array probe with a "footprint" able to measure the longitudinal length of testis is ideal. A curved array probe can be used when there is a thickened scrotal wall or in the presence of scrotal edema or for large testis. The curved array transducer is also useful to compare echogenicity of the testes. However, the frequency is usually lower, resulting in a less detailed image. Color and spectral Doppler are becoming essential elements of scrotal ultrasound because they provide documentation of normal testicular blood flow and paratesticular findings.

Survey Scan

Evaluation of the scrotal contents begins with a longitudinal survey scan, progressing medial to lateral to get an overall impression of the testis and paratesticular structures. The standard orientation of the image should be with the superior pole to the left and the inferior pole to the right on the monitor screen (Fig. 16.5 Top). If the testis is larger than the footprint of the transducer it is difficult to visualize the entire midsagittal testis in a

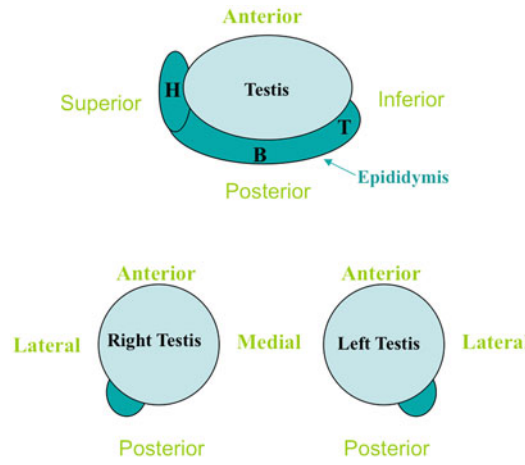

Fig. 16.5 The standard orientation for the right testis is to have the lateral aspect to the left and the medial aspect to the right. Conversely, for the left testis, the lateral aspect should be to the right and the medial aspect to the left. With a view demonstrating both testes the right testis is on the left side of the screen and the left testis is on the right

single image. It separately documents views of the superior and inferior portions of the testis including the epididymis in these regions. At least one image should visualize both testes to document the presence of two testes. In addition, a lateral and medial view of each testis should be documented.

The transverse view is obtained by rotating the transducer 90° counterclockwise. The standard orientation for the right testis is to have the lateral aspect to the left and the medial aspect to the right. Conversely, for the left testis, the lateral aspect should be to the right and the medial aspect to the left (Fig. 16.5).

Using the mid-testis as a starting point of the survey scan, proceed first toward the superior pole and then back to the mid-testis before scanning to the inferior pole. Measurements of width and AP dimensions are taken and documented at the mid-testis. A measurement should also be made of the long axis at the mid-testis together with the mid-transverse AP measurement. Testicular volume is than calculated from these measurements. If the equipment being used has split screen capabilities, comparative views of echogenicity and blood flow can easily be made and documented.

Scrotal Imaging Protocol:

1. Image showing both testes (single screen) is the first image obtained. This is important to document the presence of both testes and to compare echogenicity between the testes. If a testis is absent or a prosthetic is in place this should be labeled on the image and documented in the report. Comparative scrotal skin thickness can also be measured on this image (Fig. 16.6).
2. Video clip of survey scan of the left testicle (longitudinal and transverse). The presence of intratesticular and/or extratesticular masses and fluid collections (e.g., hydrocele fluid) are observed for later documentation.
3. Left testicular measurements with the split screen: longitudinal view on left and transverse view on right (Fig. 16.7).

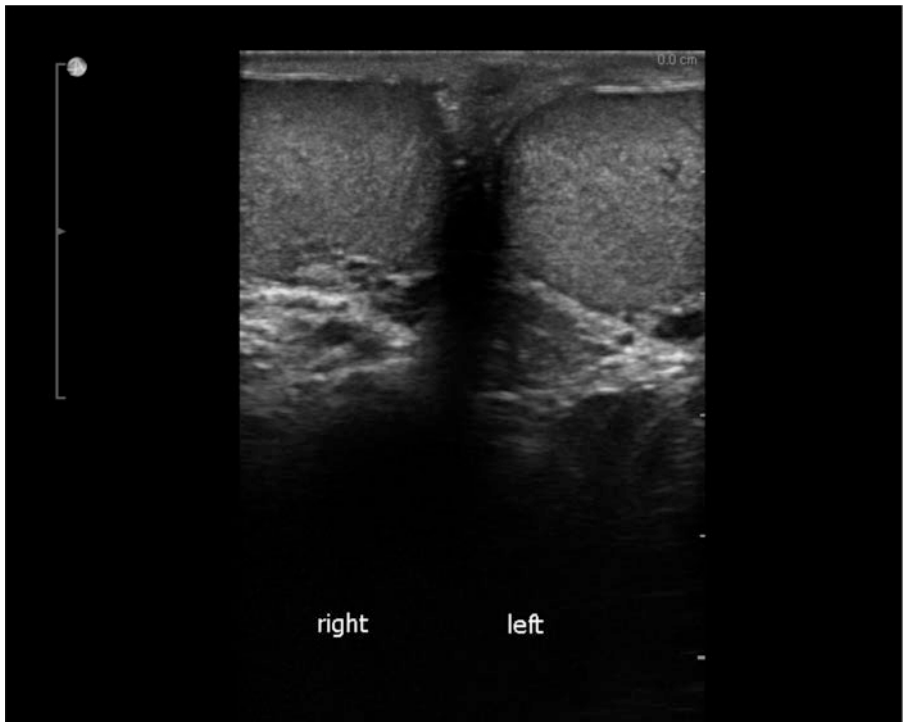

Fig. 16.6 Image showing both testes (single screen image)

4. Video clip of survey scan of the right testicle (longitudinal and transverse).
5. Right testicular measurements with the split screen: longitudinal view on left and transverse view on the right of the screen (Fig. 16.8).
6. Scrotal skin thickness measured (especially important if abnormal).

Split Screen (laterality is when looking at screen)

7. EPIDIDYMIS #1: Epididymal caput (head), right and left side, split screen: right testis on left of screen and left testis on right of screen (Fig. 16.9).
8. EPIDIDYMIS #2: Epididymal corpus (body), right and left side, split screen: right epididymal body on left of screen and left epididymal body on right of screen (Fig. 16.10).
9. EPIDIDYMIS #3: Epididymal cauda (tail), right and left side, split screen: right epididymal body on left of screen and left epididymal body on right of screen (Fig. 16.11).
10. Lateral longitudinal view of the left and right testis: right testis on left of screen and left testis on right of screen (Fig. 16.12).
11. Medial longitudinal view of the left and right testis: right testis on left of screen and left testis on right of screen (Fig. 16.13).
12. Upper (superior pole) transverse view of the left and right testis: right testis on left of screen and left testis on right of screen (Fig. 16.14).
13. Lower (inferior pole) transverse view of the left and right testis: right testis on left of screen and left testis on right of screen (Fig. 16.15).

Color Doppler

14. *Intratesticular blood flow pattern*. Split screen of longitudinal view of both testes with the right testis on left of screen and left testis on right of screen. If a difference in flow pattern is noted this should be documented by obtaining an image and noting in report (Fig. 16.16).

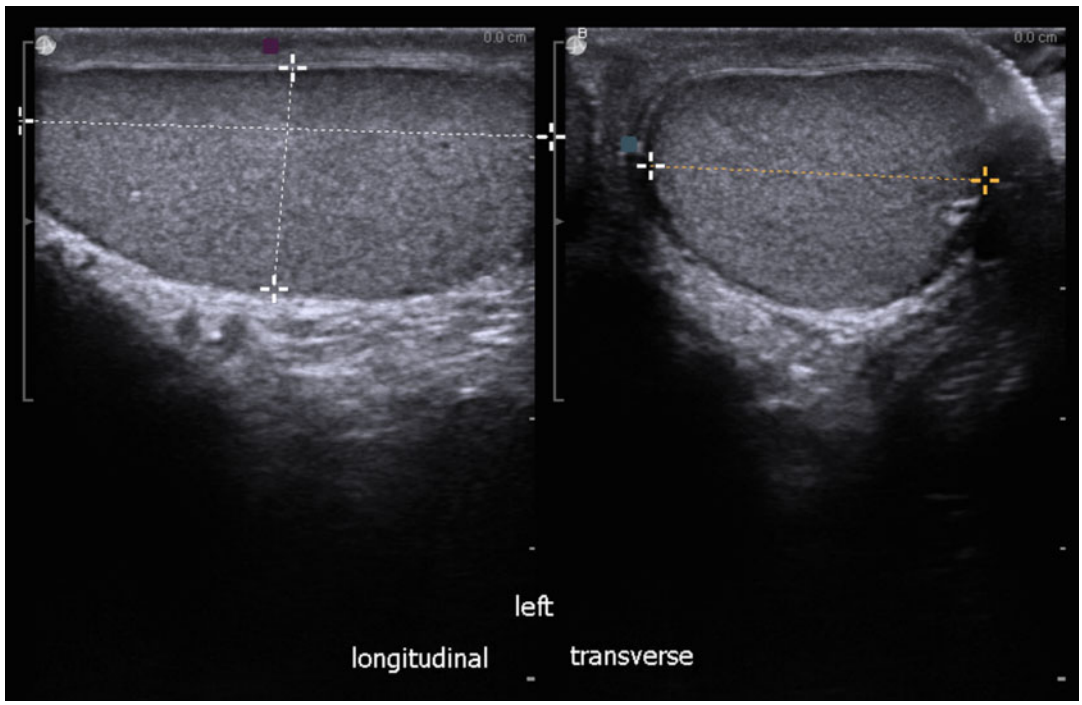

Fig. 16.7 Left testicular measurements (split screen images)

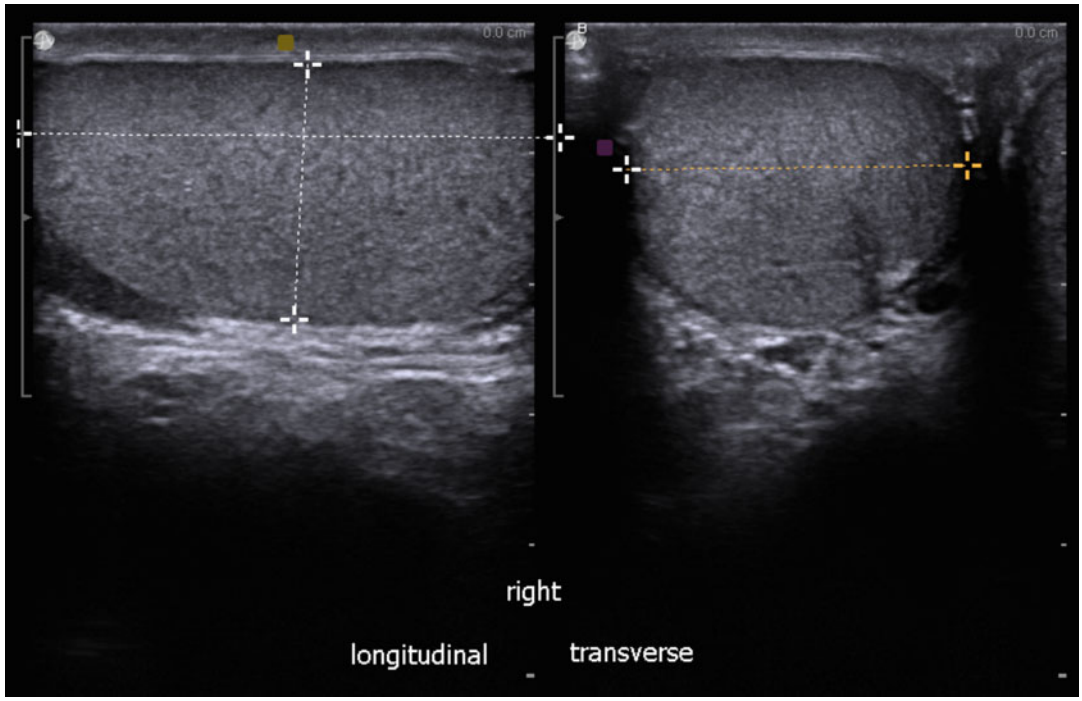

Fig. 16.8 Left testicular measurements (split screen images)

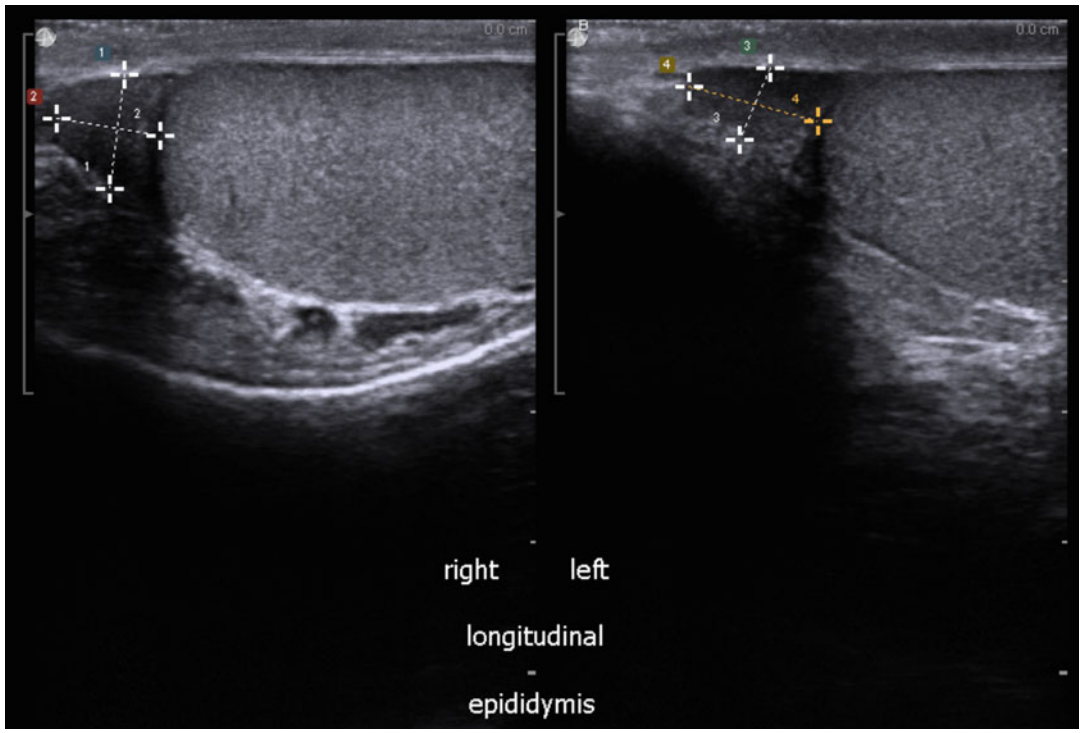

Fig. 16.9 Caput (head) of right and left epididymis (split screen images)

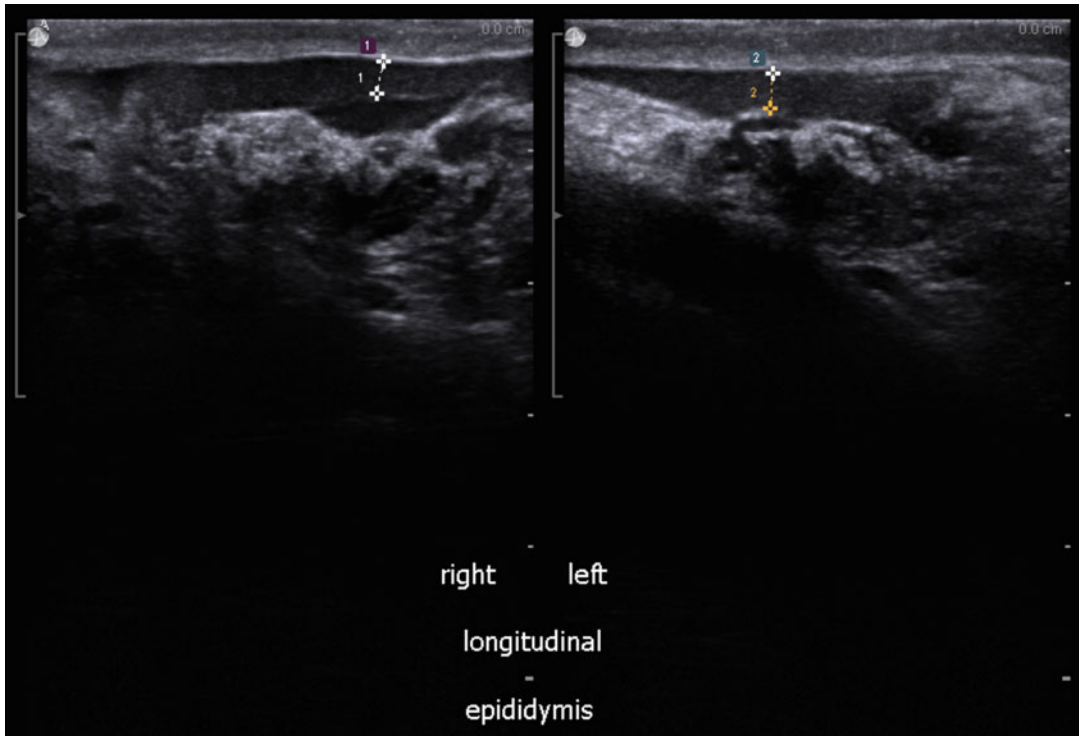

Fig. 16.10 Body of right and left epididymis (split screen images)

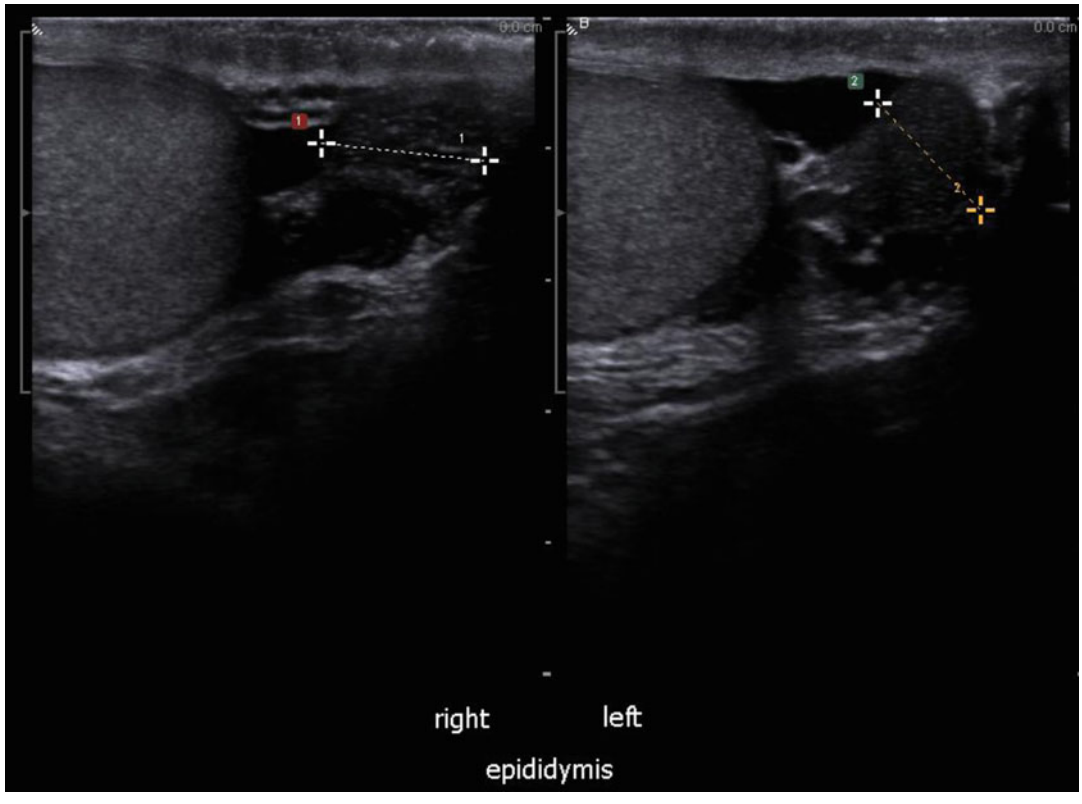

Fig. 16.11 Cauda (Tail) of right and left epididymis (split screen images)

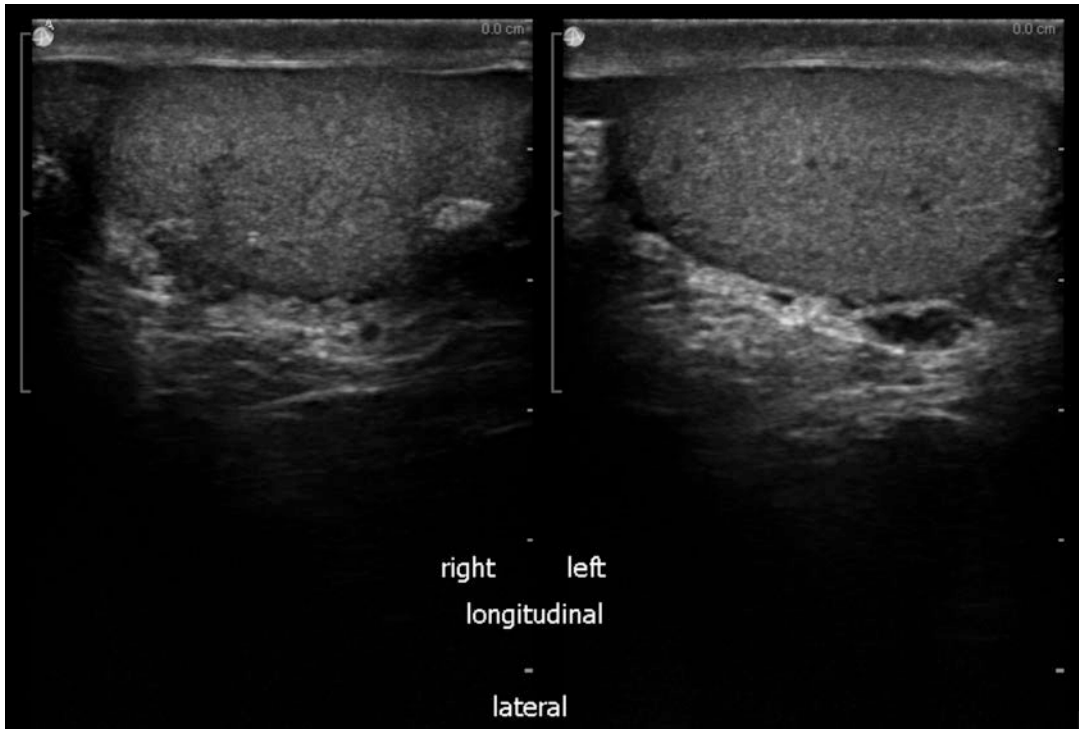

Fig. 16.12 Lateral longitudinal view of the left and right testis (split screen images)

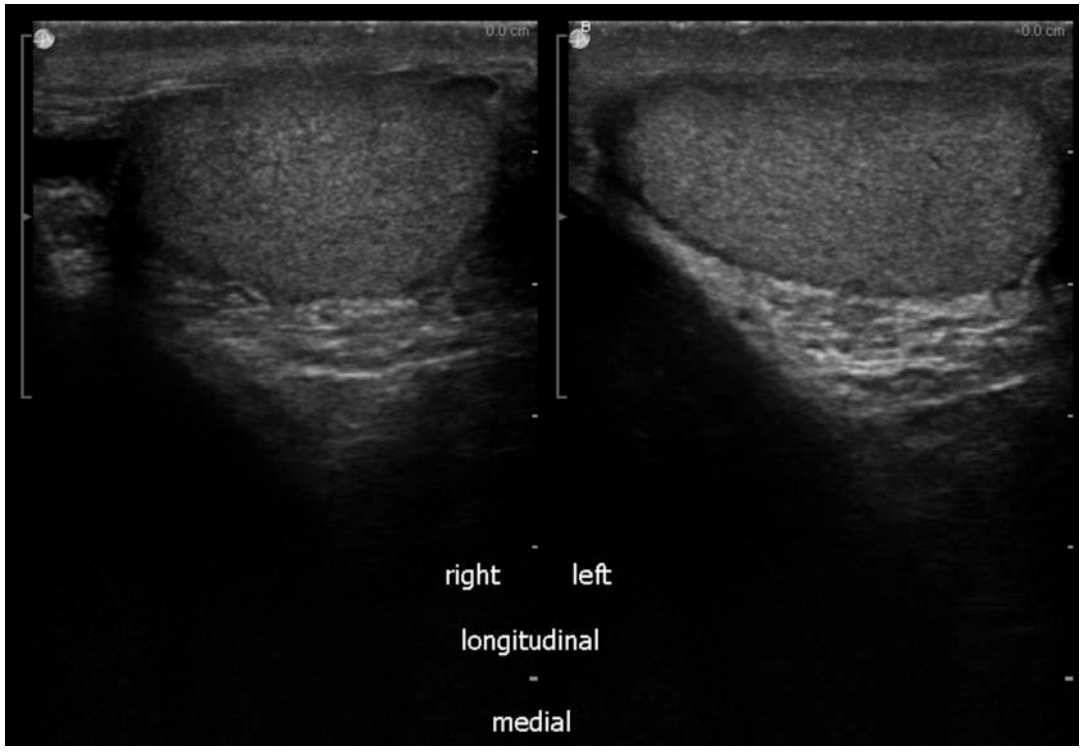

Fig. 16.13 Medial longitudinal view of the left and right testis (split screen images)

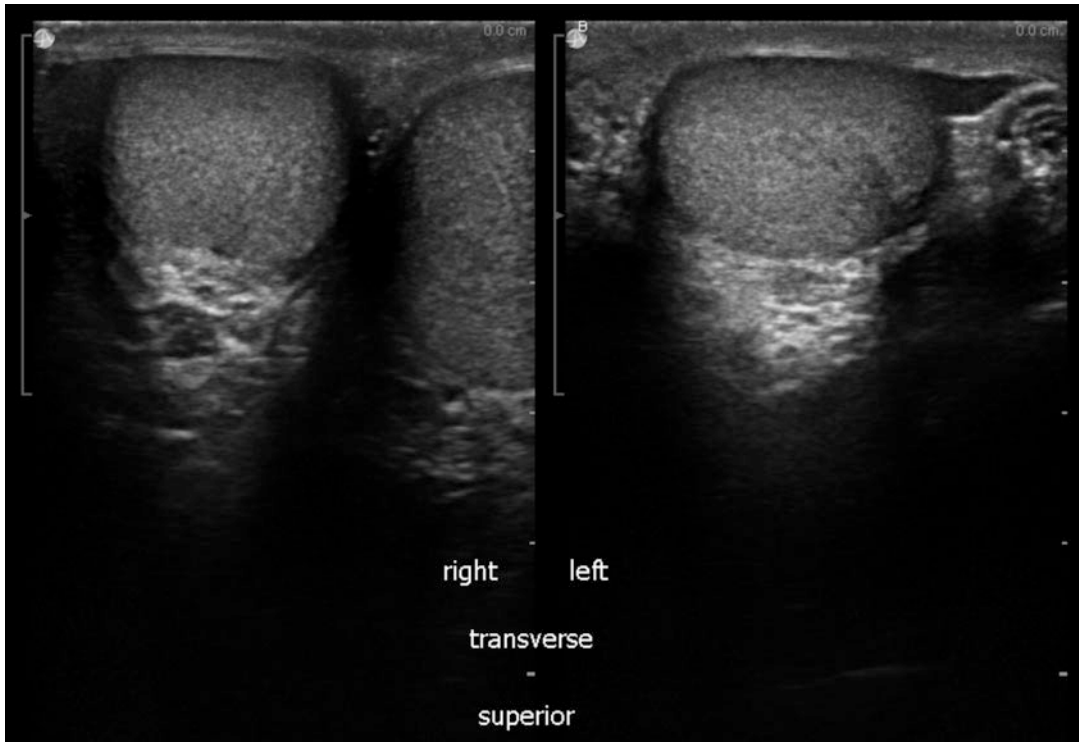

Fig. 16.14 Upper (superior) pole transverse view of the left and right testis (split screen images)

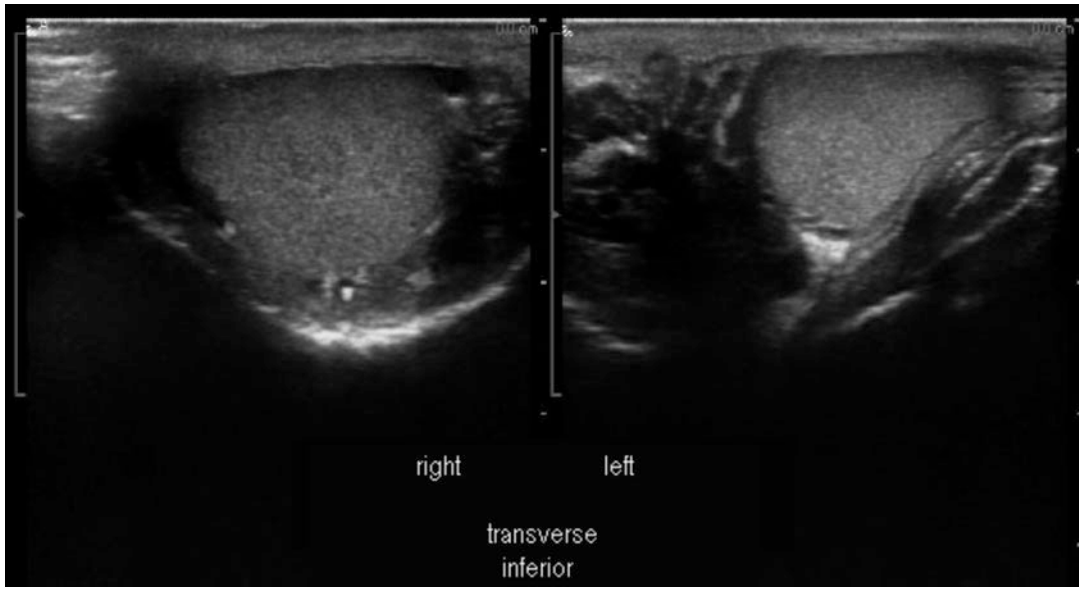

Fig. 16.15 Lower (inferior) pole transverse view of the left and right testis

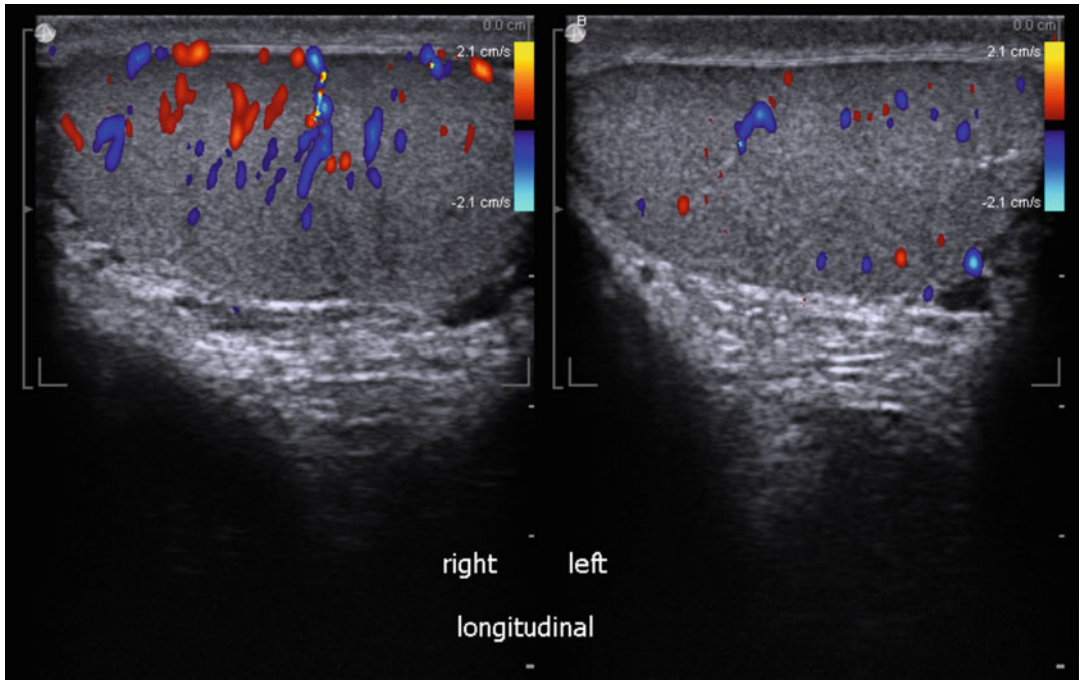

Fig. 16.16 Longitudinal view of Intratesticular blood flow pattern (split screen images)

15. A single screen transverse view of both testes for comparative intratesticular blood flow (Fig. 16.17).
16. *Varicocele evaluation #1*. Longitudinal split screen of spermatochord superior to the testis with the right spermatochord on left of screen and left spermatochord on right of screen. Measurement of inner diameter of largest vein and width of entire complex (Fig. 16.18).
17. *Varicocele evaluation #2*. Longitudinal split screen of spermatochord posterior to the testis with the right spermatochord on left of screen and left spermatochord on right of screen. Measurement of inner diameter of largest vein and width of entire complex (Fig. 16.19).
18. *Optional: Varicocele evaluation #3*. Transverse split screen of spermatochord posterior to the testis with the right spermatochord on left of screen and left spermatochord on right of screen. Measurement of inner diameter of largest vein and width of entire complex (Fig. 16.20).

Spectral Doppler

19. Evaluate a left intratesticular artery with psa, edv, ri and at (acceleration time) at the upper, upper, middle, and lower pole of the testis (Fig. 16.21).
20. Evaluate a right intratesticular artery with psa, edv, ri and at (acceleration time) at the upper, upper, middle, and lower pole of the testis (Fig. 16.22).

Additional Images:

Cine loops (video) of kidneys can be extremely helpful. This is particularly important in the following situations to rule out upper track dilation (hydronephrosis) and/or upper tract masses: (1) varicoceles do not decrease in size in the supine position or no change with valsalva, (2) solitary right varicocele, (3) large varicocele, (4) recurrent varicoceles, and (5) bilateral varicoceles.

Also, if intratesticular or other abnormalities are noted they should be imaged and documented in the report. The image should identify the size, preferably in three dimensions.

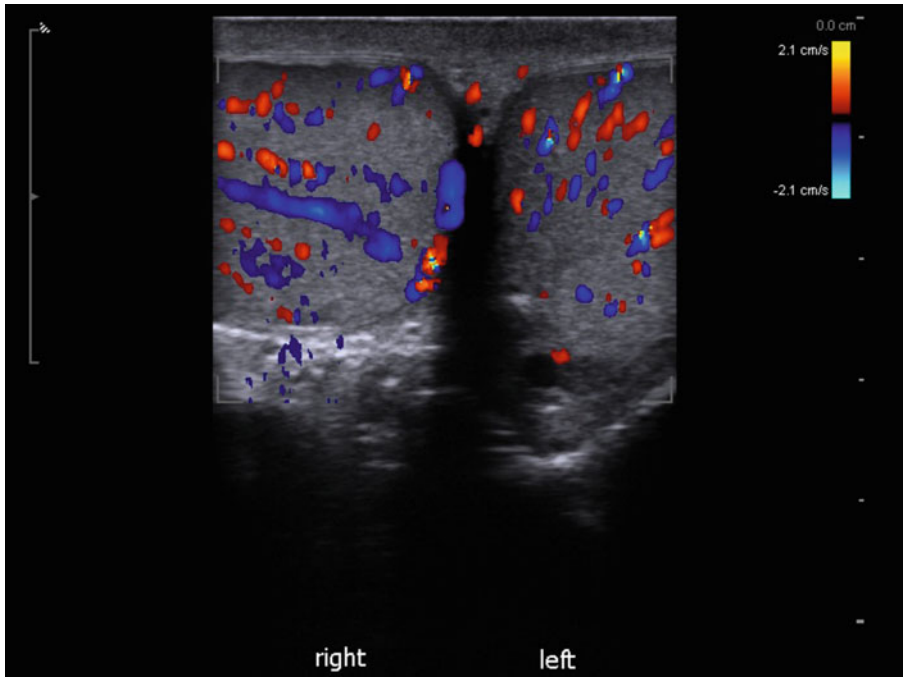

Fig. 16.17 Transverse view of Intratesticular blood flow pattern (split screen images)

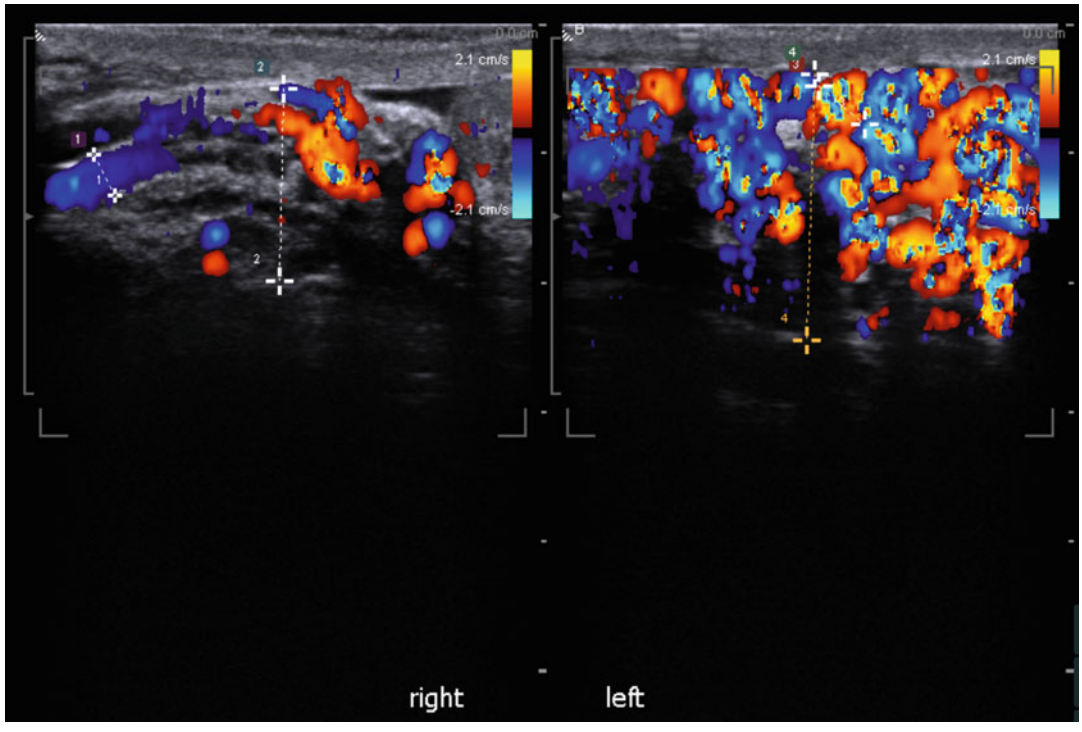

Fig. 16.18 Longitudinal view of spermatic cord for varicocele evaluation (split screen images)

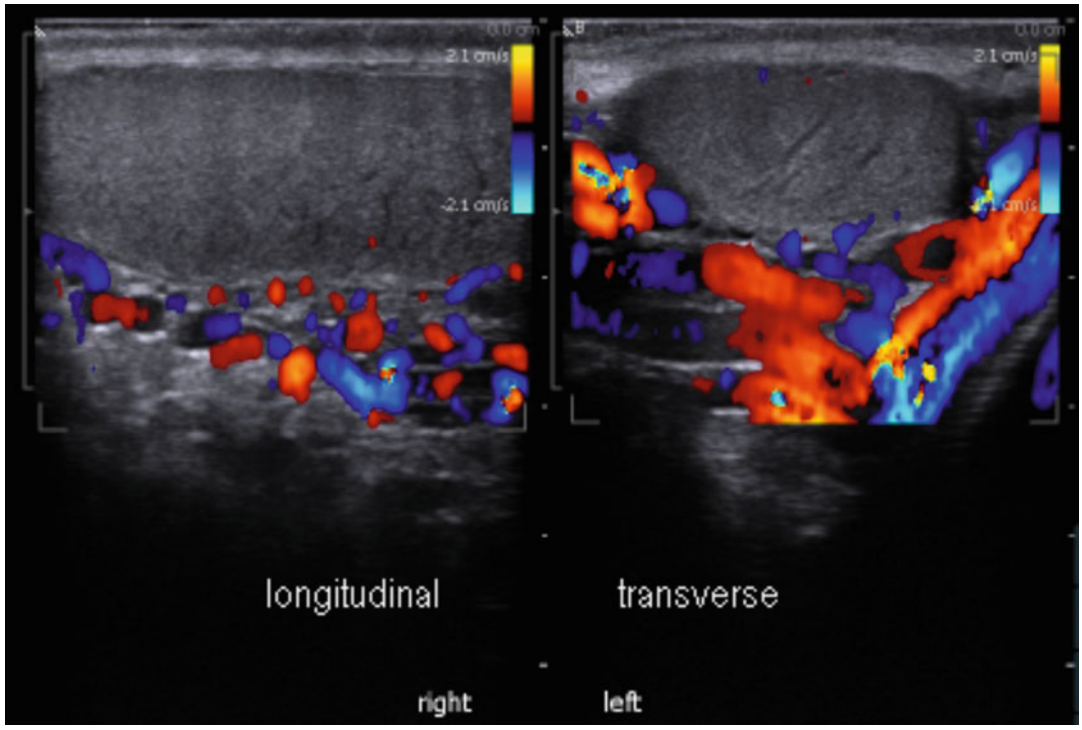

Fig. 16.19 Transverse view of spermatic cord for varicocele evaluation (split screen images)

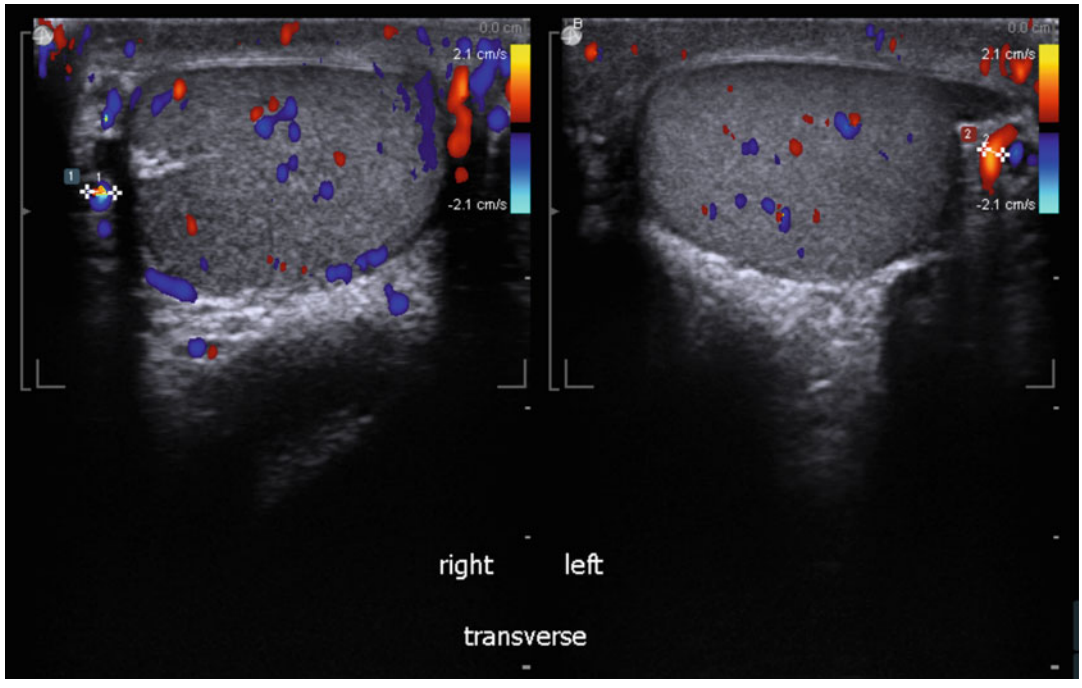

Fig. 16.20 Transverse view of Intratesticular blood flow pattern (split screen images)

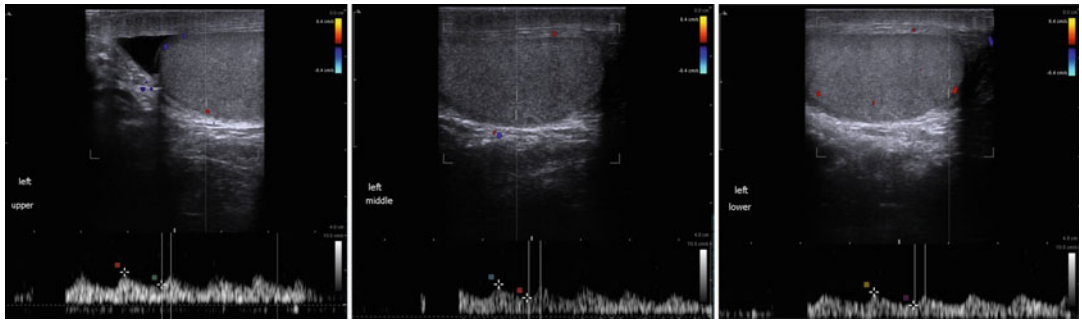

Fig. 16.21 Spectral Doppler of left intratesticular arteries in the upper, upper-middle, and lower pole of the testis (single image view)

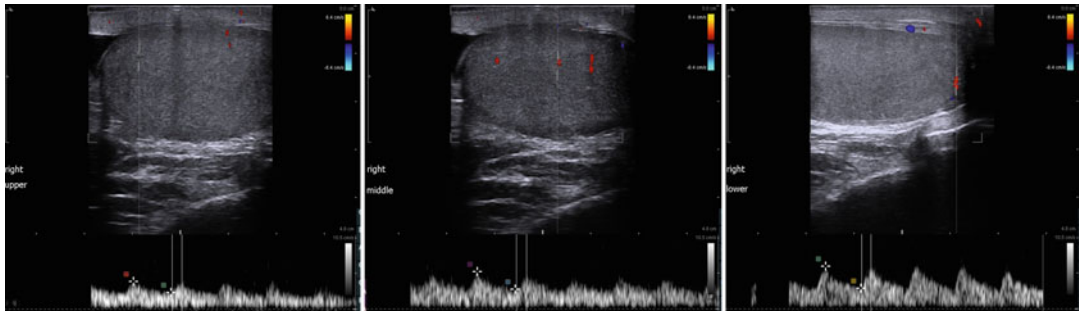

Fig. 16.22 Spectral Doppler of left intratesticular arteries in the upper, upper-middle, and lower pole of the testis (single image view)

If sonoelastography is available it would be useful for intratesticular lesions and potentially for evaluation of spermatogenesis.

Penile Ultrasound

Patient Preparation

The patient should lay comfortably on the examination table in a supine position with legs together providing support for the external genitalia. An alternative position is dorsal lithotomy with the penis lying on the anterior abdominal wall. Regardless of patient position preferred, the area of interest should remain undraped for the duration of the examination, but care should be taken to cover the remainder of the patient as completely as possible including the abdomen, torso, and lower extremities. Ample amounts of ultrasonographic acoustic gel should be used between the transducer probe and the surface of the penis to allow for high-quality images without acoustic interruption.

Routine Survey Scan

As with other ultrasound exams, penile ultrasound uses specific scanning techniques and images targeting the clinical indication prompting the study. Irrespective of the indication for penile ultrasound, routine scanning during penile ultrasound should obtain both transverse and longitudinal views of the penis by placing the transducer probe on the dorsal or ventral aspect of the penis. We will present the technique using a dorsal approach which we find easier for the flaccid phallus. However, the ventral approach is often better with a fully erect phallus. The goal is to

visualize the cross-sectional view of the two corpora cavernosa dorsally and the corpus spongiosum ventrally at different points along the length of the penis from the base of the penile shaft scanning distally toward the glans penis.

The corpora cavernosa appear dorsally, as two homogeneously hypoechoic circular structures, each surrounded by a thin (usually less than 2 mm) hyperechoic layer representing the tunica albuginea that envelops the corpora. The tunica albuginea is a fibroelastic tissue that can become more echogenic and thicker with increased fibrosis. This is often seen in men with Peyronie's disease and erectile dysfunction related to the inability of the emissary veins to be compressed against the inside of the tunica albuginea resulting in a venous leak. The corpus spongiosum is a ventrally located circular structure with homogeneous echotexture, usually more echogenic than the corpora cavernosa. It is well visualized by placing the ultrasound transducer probe on either the dorsal or ventral aspect of the penis; however, it is easily compressible so minimal pressure should be maintained while scanning. For routine anatomic scanning of the penis with ultrasound, all three corpora can be sufficiently viewed from a single dorsal aspect obtained image of the penile shaft. A survey scan is first performed prior to obtaining static images at the proximal (base), mid-portion, and distal (tip) of the corpora cavernosal bodies for documentation. The value of the survey scan cannot be overstated. It often provides the prospective that is necessary to assure absence of coexisting pathology. In addition, a careful survey scan of the phallus will identify abnormalities of the cavernosal vessels, calcified plaques, as well as abnormalities of the spongiosa tissue. All abnormalities should be documented with appropriate measurements if applicable, in static images.

Static images recommended as representative views of this initial surveying scan are as follows: the transverse view at the base of the penile shaft, at the mid-shaft, and at the distal shaft just proximal to the corona of the glans penis. Each image shows transverse sections of all three corporal bodies. Orientation, by convention, is for the right corporal body to be on the left side of the display while the left corporal body is located on the right side of the display. Our preference when viewing a longitudinal projection is to use a split screen view to compare the right and left corporal bodies with measurements of the cavernosal artery diameter taken in this view. We keep the orientation constant, with the projection of the right corporal body on the left side of the display while the left corporal body is located on the right side of the display. Either a dorsal or ventral approach can be used as preferred by the sonographer. A flaccid phallus is often best visualized by the dorsal approach while an erect phallus by the ventral approach.

Penile Ultrasound Protocol

Specifics to be documented on report:

Indication for Procedure: For example, evaluation of penile curvature, evaluation of erectile dysfunction, evaluation of urethral blood supply. Diagnosis code can also be included to document medical necessity.

Transducer: 12–18 MHz linear array transducer with a small footprint.

Please note: if all components of the exam are no seen then the report should document that that component was "Not Seen" and why.

Baseline Study

- Longitudinal and transverse survey scan of the phallus including the corporal bodies and urethra with video clips. This should include views of both corpora cavernosa and corpora spongiosum. Any abnormalities seen should be specifically interrogated and documented. These cine loops will allow for comparative echogenicity of both corpora. If a cine loop is not obtained then a split screen view documenting comparative echogenicity should be obtained.
- Split screen base (proximal), mid and distal view of phallus in transverse plane. This should include views of both corpora cavernosa and corpora spongiosum (Figs. 16.23 and 16.24a, b).

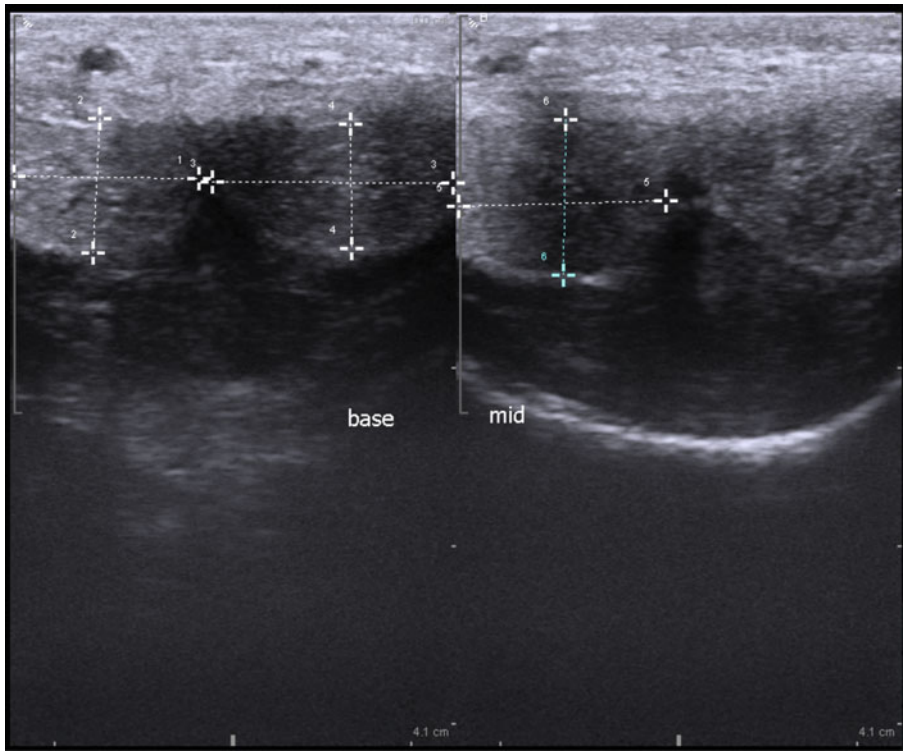

Fig. 16.23 Split screen base (proximal), mid and distal view of phallus in transverse plane with height and width measurements

- Measure height and width of the mid phallus of each corpus cavernosum in transverse projection (Figs. 16.23 and 16.24a, b).
- Split screen longitudinal views of both corpora cavernosa and corpora spongiosum. This should include views of left and right corpora cavernosal artery (Fig. 16.25). Measure height of the proximal, mid and distal phallus of each corpora in the longitudinal projection.
- Baseline Spectral Doppler waveform (with PSV, EDV, RI, and optional measurements Acceleration time and pulsatility index) and inner diameter measurements of longitudinal views of both Left and Right Cavernosal Artery (Fig. 16.26a, b).
- Document abnormalities (e.g., altered echogenicity, plaques, calicifications, corpora tears) in both transverse and longitudinal projections with measurements (Fig. 16.27a–c).
- Baseline spectral Doppler waveform (with PSV, EDV, RI, and optional measurements) including inner diameter measurements of Left and Right Cavernosal Artery.
- Sonoelastography (if available) of phallus in both transverse and longitudinal projections (Fig. 16.27d).
  - Transverse images of Base, Mid phallus, and distal phallus with additional images of areas of interest (e.g., dense tissue, calcifications, etc.).
  - The longitudinal (sagittal) projection should be of the left and right corpora cavernosa centered on the cavernosal artery on the left and right cavernosal artery. The midsagittal projection should also be imaged as should additional images of areas of interest (e.g., dense tissue, calcifications, etc.).

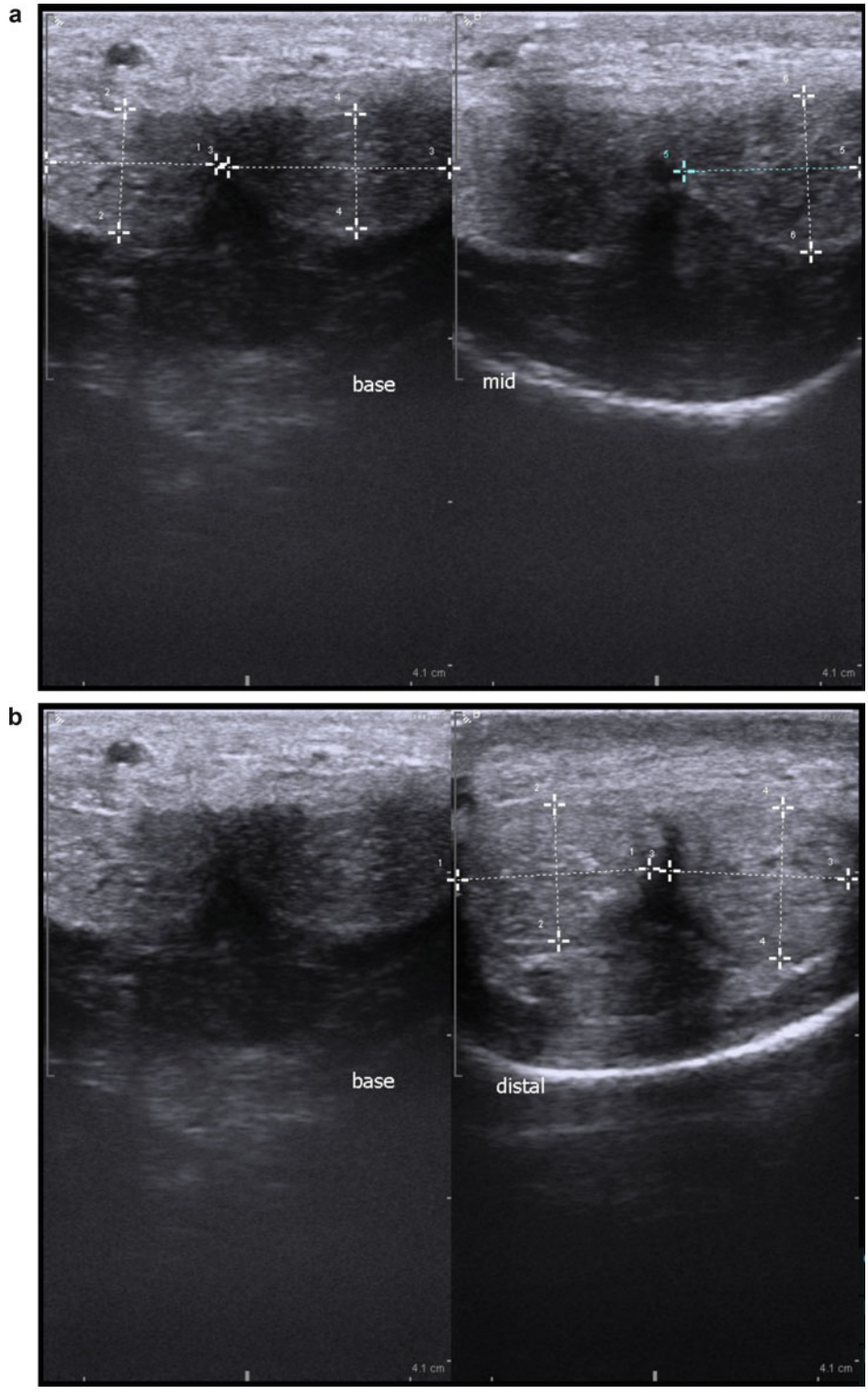

Fig. 16.24 (**a**) Split screen base (proximal), mid and distal view of phallus in transverse plane with height and width measurements. (**b**) Split screen base (proximal), mid and distal view of phallus in transverse plane with height and width measurements

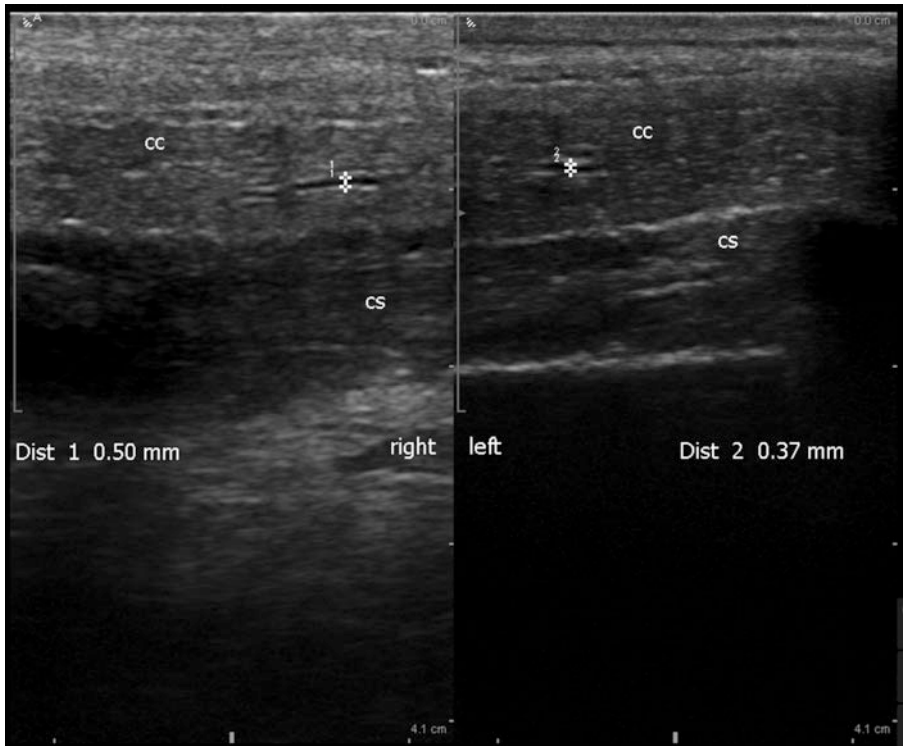

Fig. 16.25 Split screen longitudinal views of both corpora cavernosa (cc) and corpora spongiosum (cs) with measurement of the cavernosal arteries

Penile Study for Vascular Integrity

Technical pointers for Spectra Doppler:

1. Make sure angle of incidence is less than 60°.
2. PSV and EDV measured with at least three waveforms of equal size present.

Postinjection spectral Doppler analysis of the left and right cavernosal artery (performed every 5 min giving an additional medication injection every 10 min, if indicated) (Fig. 16.28a, b).

- Spectral Doppler waveform (with PSV, EDV, RI, and optional measurements)
- Inner diameter measurements of Left and Right Cavernosal Artery
- Subjective assessment of tumescence and rigidity
- Split screen base (proximal), mid and distal view of phallus in transverse plane with height and width measurements at maximal tumescence (Fig. 16.29).

In addition, Sonoelastography (if available) should be performed when maximum corporal dimensions (i.e., maximal tumescence) are achieved and should contain:

- Sonoelastography of phallus in both transverse and longitudinal projections.
  - Transverse images of Base, Mid phallus, and distal phallus with additional images of areas of interest (e.g., dense tissue, calcifications, etc.).
  - The longitudinal (sagittal) projection should be of the left and right corpora cavernosa centered on the cavernosal artery on the left and right cavernosal artery. The mid digital projection should also be imaged as should additional images of areas of interest (e.g., dense tissue, calcifications, etc.).

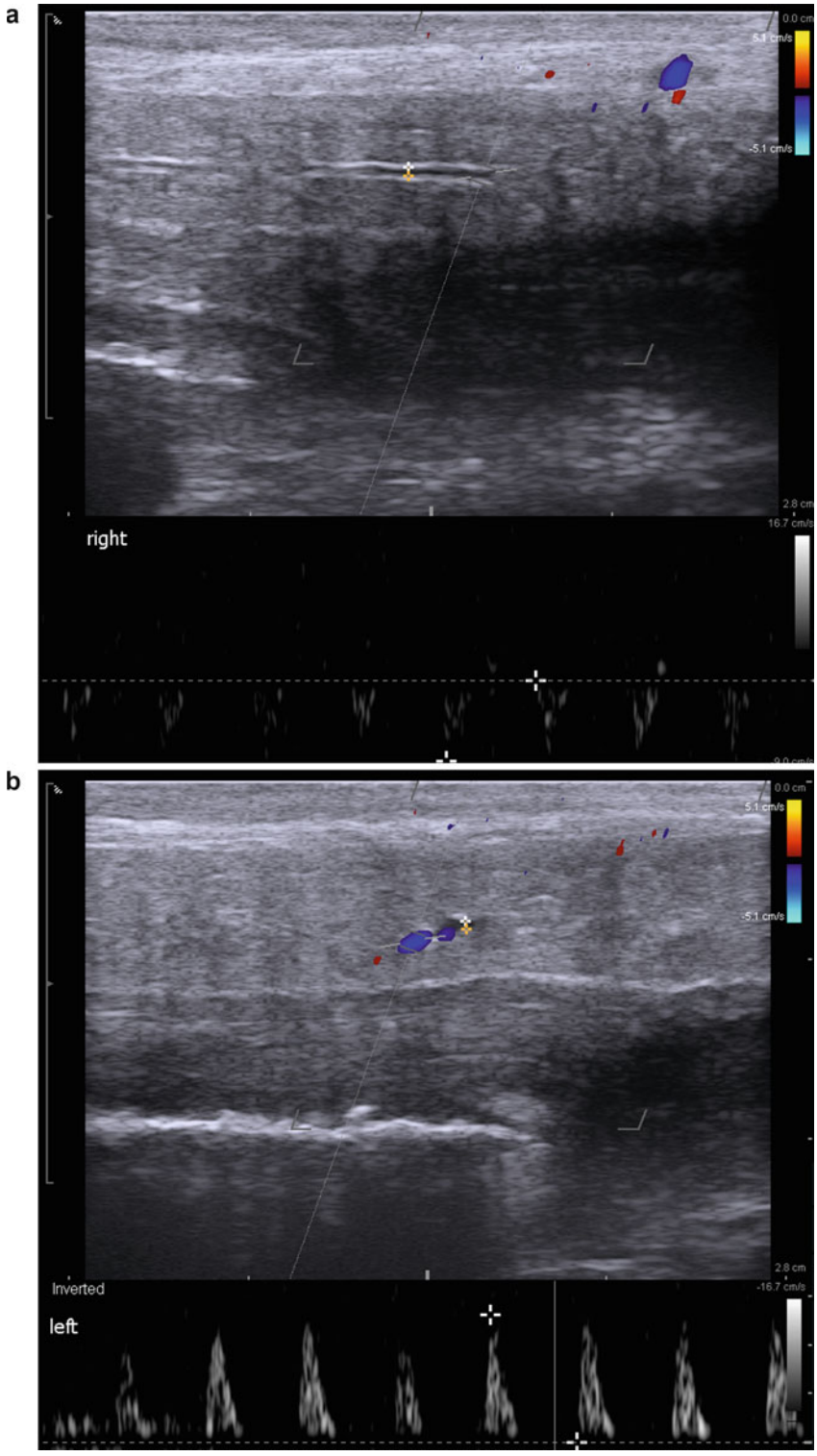

Fig. 16.26 (**a**) Baseline Spectral Doppler waveform of right cavernosal artery. (**b**) Baseline Spectral Doppler waveform of left cavernosal artery

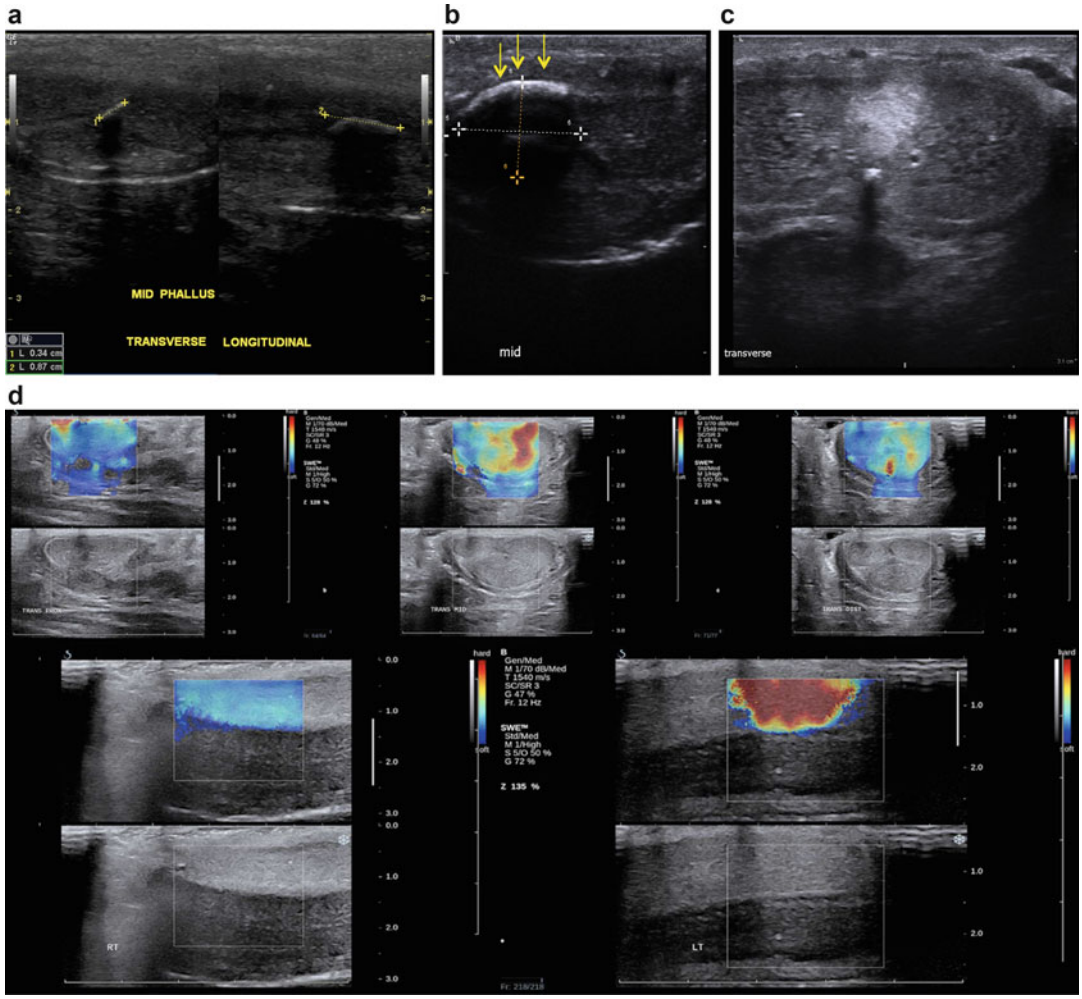

Fig. 16.27 (**a**) Transverse and longitudinal measurements of calcification in penile plaque (split screen images). (**b**) Transverse projection of phallus demonstrating a calcified plaque in the anterior tunica albuginea in the mid phallus on the right (*arrows*). (**c**) Transverse projection of phallus demonstrating a noncalcified dense (echogenic) plaque between the two corpora cavernosa and a small (punctate) calcification inferior to this with posterior shadowing. (**d**) A series of Sonoelastography images of the phallus in both transverse and longitudinal projections demonstrating areas of increased firmness (*red*) in the left corpora as compared to the softer (*blue*) right corpora cavernosa

End of study is achieved when:

- RI equal to or greater than 1.0 or,
- Maximal PSV is reached (i.e., subsequent measurements demonstrate decreasing PSV) or
- Maximal concentration/volume of pharmacologic agent is used.

Perineal (Bulbocavernosal Muscle aka Bulbospongiosus Muscle)

Measurement of the Bulbocavernosal Muscle (BCM) aka Bulbospongiosus Muscle is a novel way of assessing the androgenic effects of testosterone in men. Dabaja et al. [19] (Asian Journal of Andrology 2014, 16, 1–5) have provided

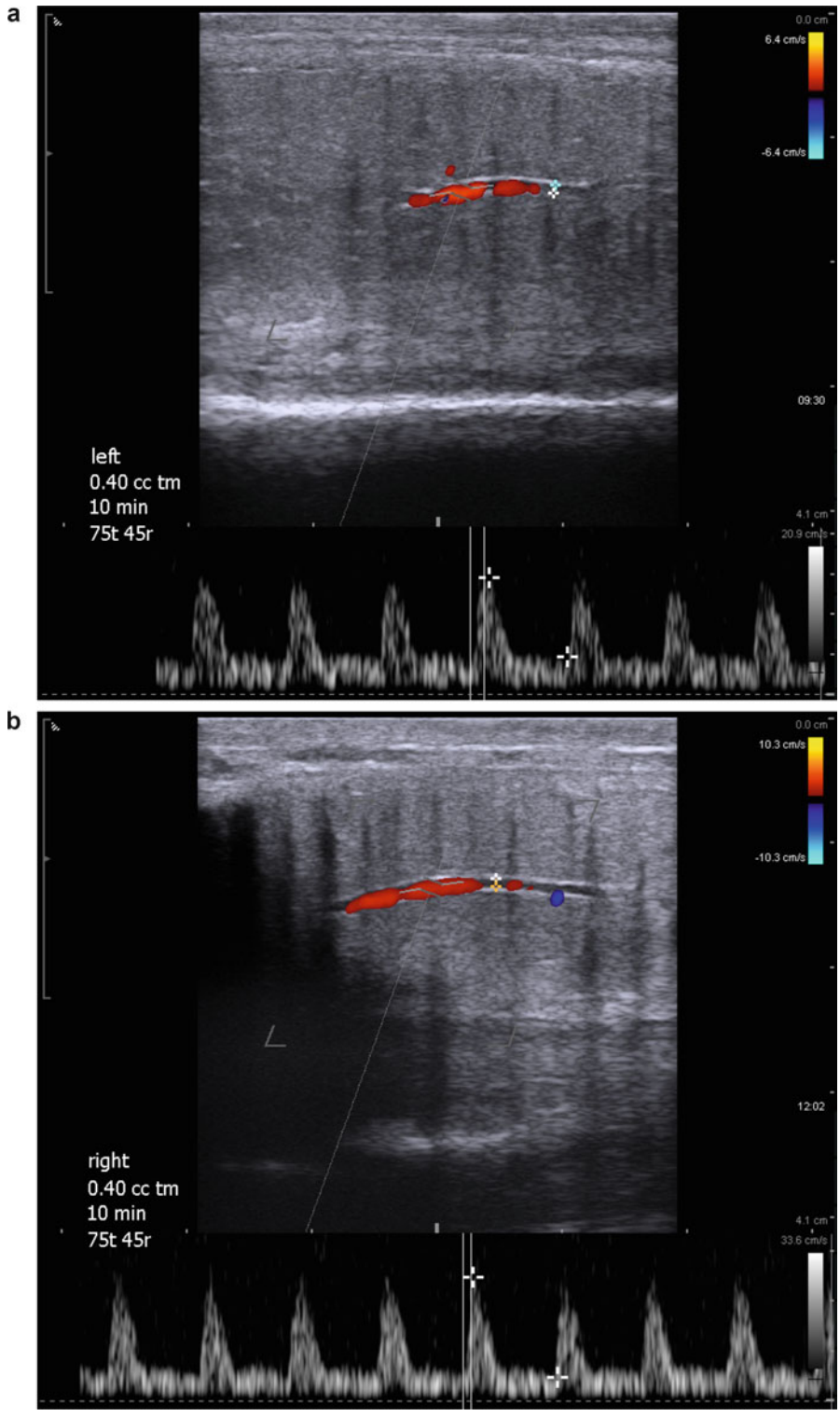

Fig. 16.28 (**a**) 10 min Postinjection spectral Doppler analysis of the left cavernosal artery. (**b**) 10 min Postinjection spectral Doppler analysis of the right cavernosal artery

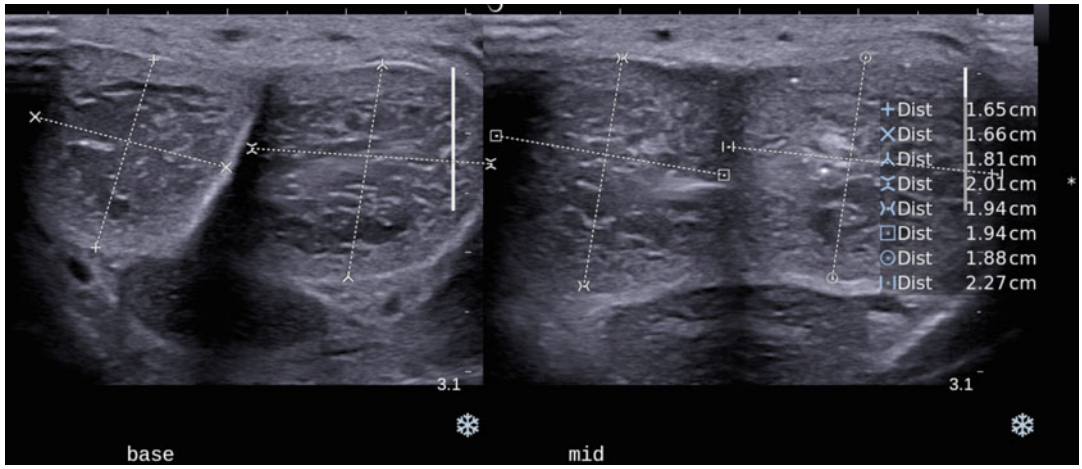

Fig. 16.29 Split screen transverse view of the base (proximal), mid view of the phallus 10 min after injection with measurements

compelling evidence that the BCM area correlates with androgenic activity. They also have compelling data (personal communications) suggesting that BCM area less than 0.75 cm^2 correlates with hypogonadism and that testosterone supplementation results in an increased BCM. This is important since, at present, we have no way, other than assessing serum testosterone and DEXA, to evaluate the efficacy of testosterone replacement therapy. In addition, since the BCM is integral in the ejaculatory process this might provide insight into the etiology of this common malady. We have therefore implemented their protocol in patients presenting with complaints of hypogonadism and/or ejaculatory dysfunction as an additional marker of Low Testosterone prior to institution of therapy. We will also follow this measurement after therapy is initiated. A video can be reviewed at https://www.youtube.com/watch?v=79t3SvINMNE which demonstrates the essential components of this study.

To begin the examination, the patient should be supine with the legs in a 'frog leg' position to enable the sonographer to gain access to the perineum. The area of interest is the anogenital line as indicated in Fig. 16.30.

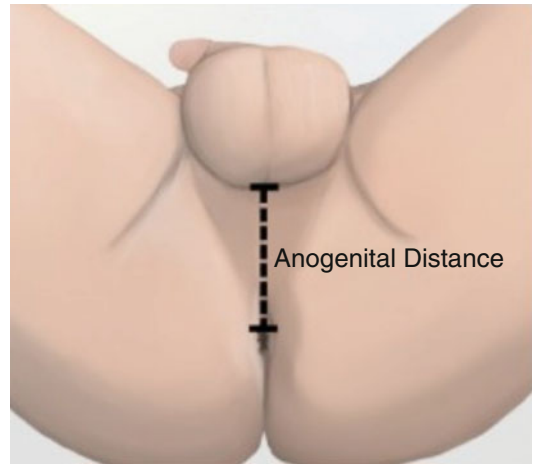

Fig. 16.30 Anogenital line

1. Survey scan of the urethra and cavernosal bodies from distal to proximal in the transverse plane with video clips. The area in red in Fig. 16.31 is the bulbocavernosus muscle draped over the urethra. Imaging of this muscle will use both translational motion and nontranslation techniques termed painting and fanning, respectively.

In the transverse plane, obtain a transverse view in which the urethra cross-section is seen as round (Fig. 16.32). Measure the width of the right (RT BCM) and left (LT BCM) aspects of the bulbocavernosus muscle as well as along the tendinous raphe (AP BCM). Also measure the AP dimension of the urethra (urethra). You should obtain the best transverse image of the bulbocavernosus muscle. This should be where the urethra is seen as round. This orientation will prevent obtaining an oblique view, which might overestimate the

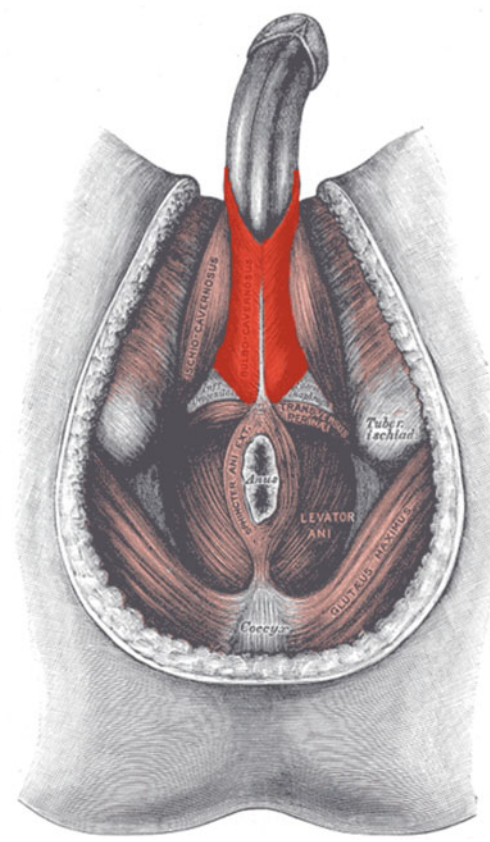

Fig. 16.31 In this schematic the bulbocavernosus muscle also known as the bulbospongiosus muscle is *red* (20th U.S. edition of *Gray's Anatomy of the Human Body*, 1918, open access)

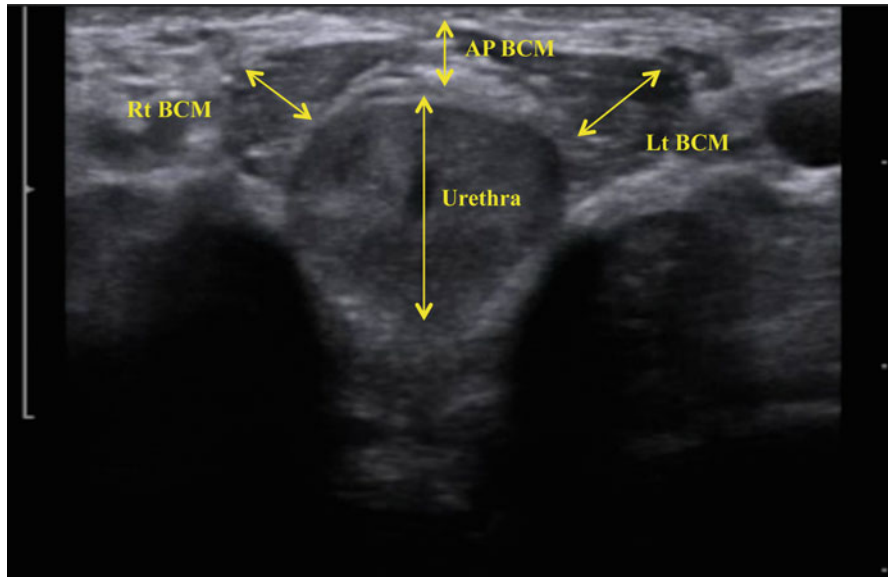

Fig. 16.32 Transverse view in which the urethra cross-section is seen as *round*. Shown are the measurements of the right, mid, and left BCM as well as the urethra

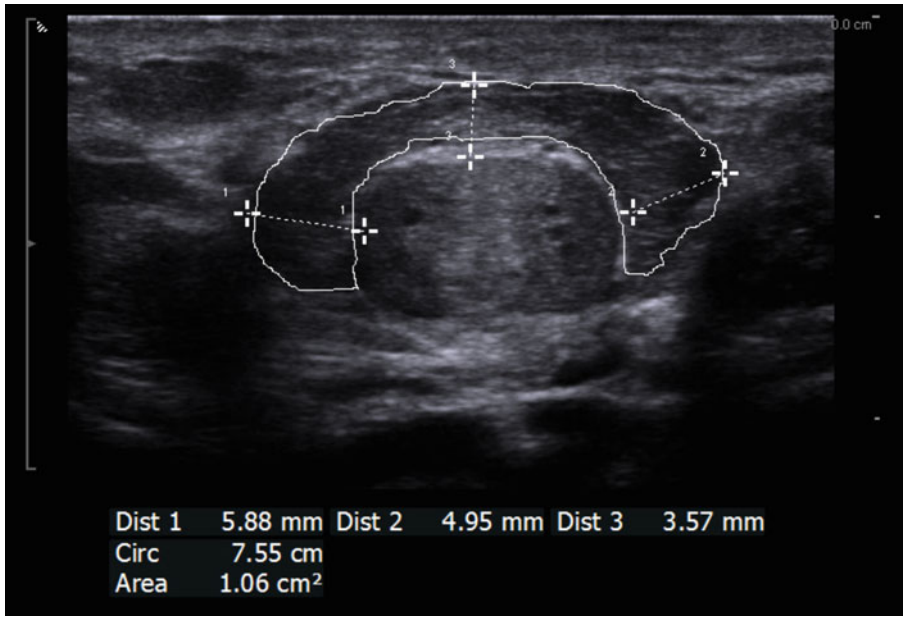

Fig. 16.33 Freehand measurement of the area of the bulbocavernosus muscle

dimensions of the bulbocavernosus muscle. You will then measure the Right and left BCM width as described earlier. In this same projection you should measure the area of the bulbocavernosus muscle (Fig. 16.33). The BCM area is most often obtained by freehand drawing using the trackball on the ultrasound unit. Repeat these measurements on a second image. Report each set of measurements separately as well as reporting the average of the two readings (see BCM template).

2. You will then turn the transducer and perform a survey scan in the longitudinal direction to interrogate the urethra. Perform a longitudinal survey scan of the urethra identifying the area of the bulbar urethra as well as the location of the paired urethral arteries with color Doppler. Try also to follow the cavernosal bodies to their proximal tip and identify the cavernosal artery from its origin and follow it distally. Save a video loop of this survey scan. Also save representative images of the Left Longitudinal BCM (Fig. 16.34), Mid Longitudinal BCM (Fig. 16.35), and Right Longitudinal BCM image (Fig. 16.36). With color Doppler, scan the cavernosal and bulbourethral arteries throughout their course in the perineum (Fig. 16.37) and capture a cine loop of this.

Bladder

Basic Scanning Technique

An even coating of warm conducting gel is placed on the patient's skin prior to beginning the ultrasound examination. Gentle and firm contact is made with the transducer on the lower abdominal wall. Start the examination in the transverse view. Bone inhibits sound waves. Positioning the transducer so that the waves strike the bones of the pubis will produce posterior acoustic shadowing. The image of the bladder may not appear on the screen or only appear in part. Acoustic shadowing from the pubic bone may be avoided by placing the transducer in the transverse view position superior to the pubic bone and then varying the angle of insonation and pressure applied to the transducer as well as fanning inferiorly, to find the echo-free lumen of the bladder.

The machine settings should be adjusted to obtain a good quality image. The image should be of sufficient and uniform brightness, sharp and in focus, of adequate size, with proper image orientation and proper labeling on the image. For this, the Gain-Control setting varies the sensitivity of the transducer to returning sound waves. The Acoustic Output controls the ampli-

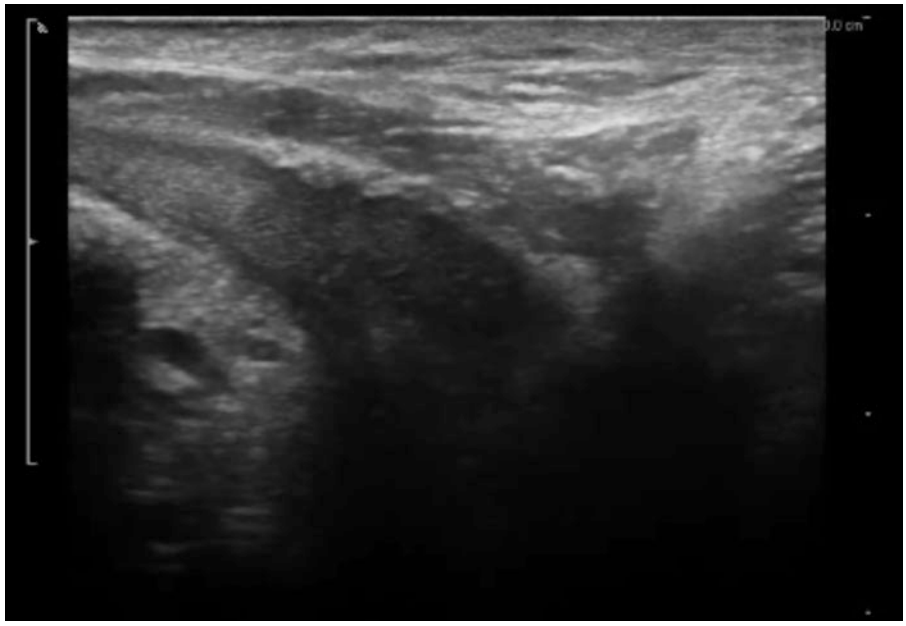

Fig. 16.34 Image of a Longitudinal view of the phallus on the left at the level of where the BCM measurement was taken

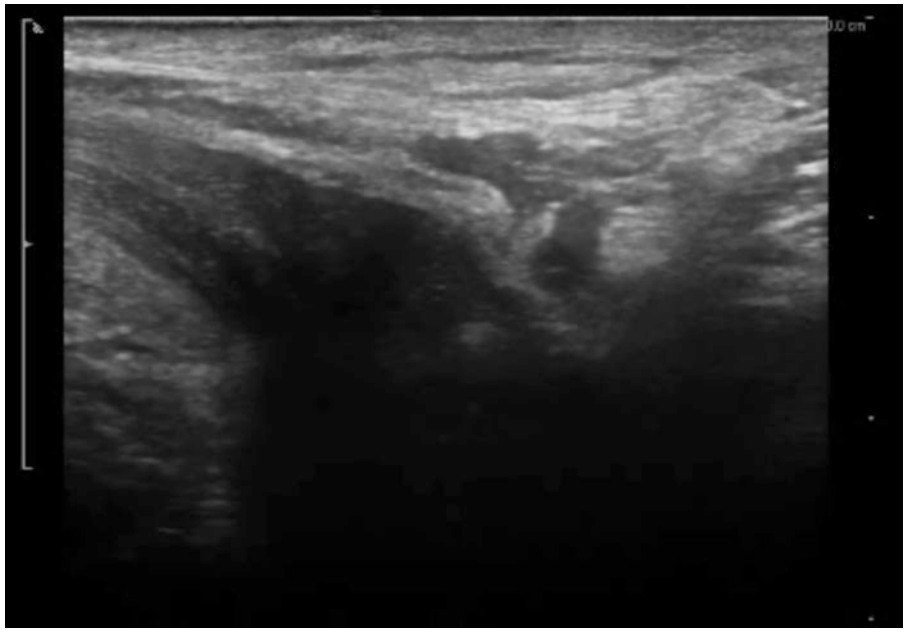

Fig. 16.35 Image of a Longitudinal view of the mid phallus at the level of where the BCM measurement was taken

tude of the generated sound waves; keep the output at a minimal setting. The Time-gain compensation (TCG) is used to obtain uniform tissue echogenicity as one moves away from the transducer. The Focal Zone Setting brackets the structure or organ of primary interest for maximal resolution. Other controls at the examiner's disposal include the depth/size function, the field of view, and cine function for a live recording of the study.

In the transverse view of the bladder, the right side of the bladder should appear on the left side of the screen. In the sagittal view, the superior aspect of the bladder should appear on the left side of the screen. In the transverse bladder view

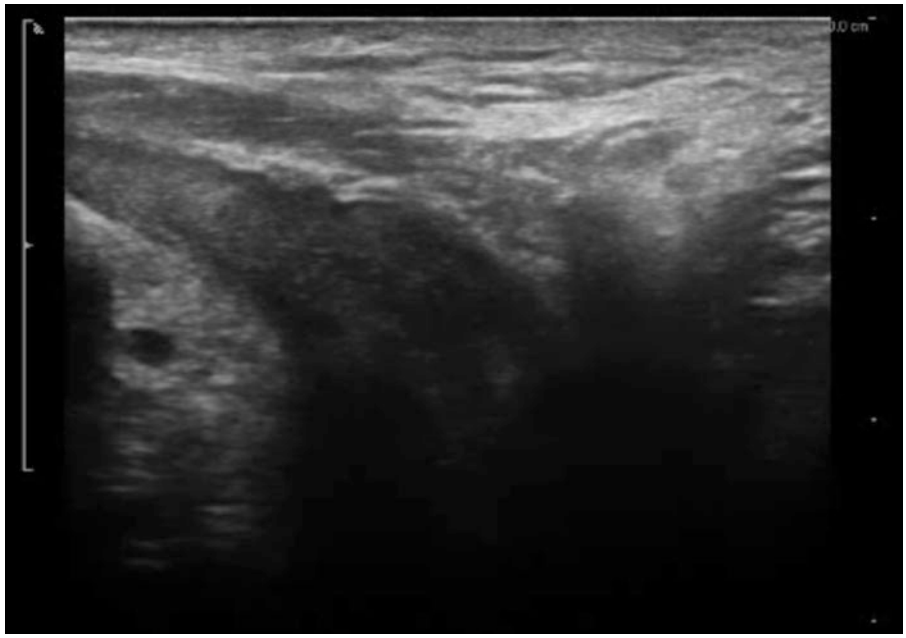

Fig. 16.36 Image of a Longitudinal view of the phallus on the right at the level of where the BCM measurement was taken

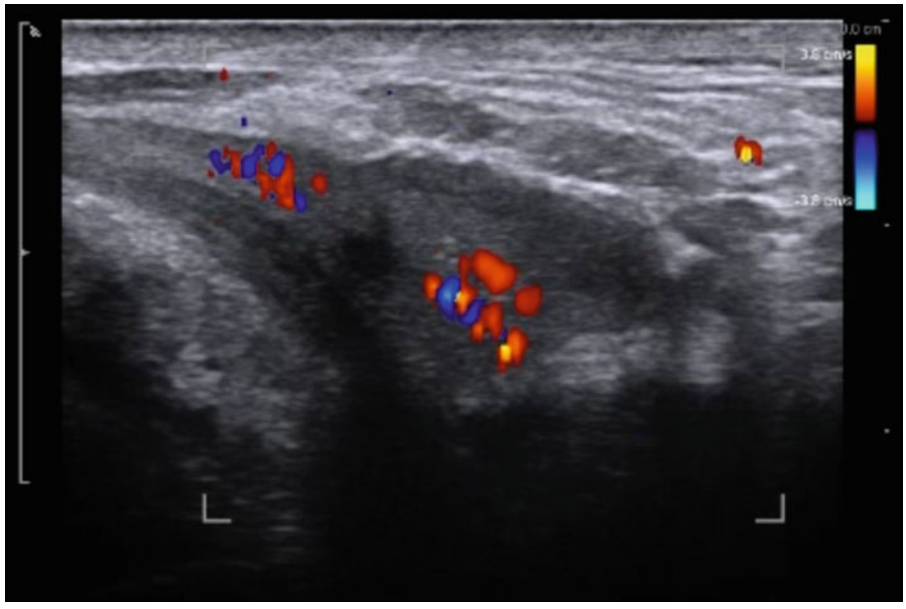

Fig. 16.37 Color Doppler image of a Longitudinal view of the mid phallus at the level of where the BCM measurement was taken

measure the height and width of the bladder. Carefully look at the bladder for anomalies such as trabeculations, best seen on the sagittal view, bladder stones, diverticula, and wall lesions that could represent a transitional cell tumor. Look at the bladder base for the presence of dilated ureters, distal ureteral stones, and ureteroceles. Efflux can be appreciated using power or color Doppler and looking over the site where the orifices would be found.

Measurement of bladder wall thickness is taken, by convention, on a bladder filled with

150 cc. The bladder wall thickness is measured at the posterior wall on the sagital view. If the bladder wall thickness is less than 5 mm, there is a 63 % probability that the bladder is not obstructed. However, if the bladder wall thickness is over 5 mm, there is an 87 % probability that there is bladder obstruction [20].

Further ultrasound study of the bladder can determine the presence of focal lesions, such as bladder tumors. Ultrasound is sensitive for lesions greater than 1 cm in size but has poor specificity. A lesion found on the bladder wall can be further queried by use of color Doppler to confirm the presence of increased blood flow into the lesion.

Power or color Doppler can be utilized, while imaging the bladder base, to show efflux of urine called ureteral jets. The distal ureters can be examined sonographically for the presence of distal ureteral dilation, suggesting obstruction. A hyperechoic lesion might indicate a distal ureteral stone or distal ureteral scar tissue or lesion.

A basic evaluation of the prostate and seminal vesicles is also performed at this time.

Transabdominal Bladder

Specifics to be documented on report:

Indication for Procedure: For example, Lower urinary tract symptoms, total painless gross hematuria. Diagnosis code can also be included to document medical necessity.

Transducer: 3–5 MHz curved array transducer with small footprint.

Please note: if all components of the exam are not seen then the report should document that component was "Not Seen" and why.

Bladder (full bladder >150 cc)

1. Longitudinal and transverse survey scan of bladder with video clips.
2. Bladder (Split screen) midsagittal and midtransverse view with volume, height (AP), width and length measurements (Fig. 16.38).
3. Measurement of bladder wall thickness in at least two locations (posterolateral and dome preferred) (Fig. 16.39).

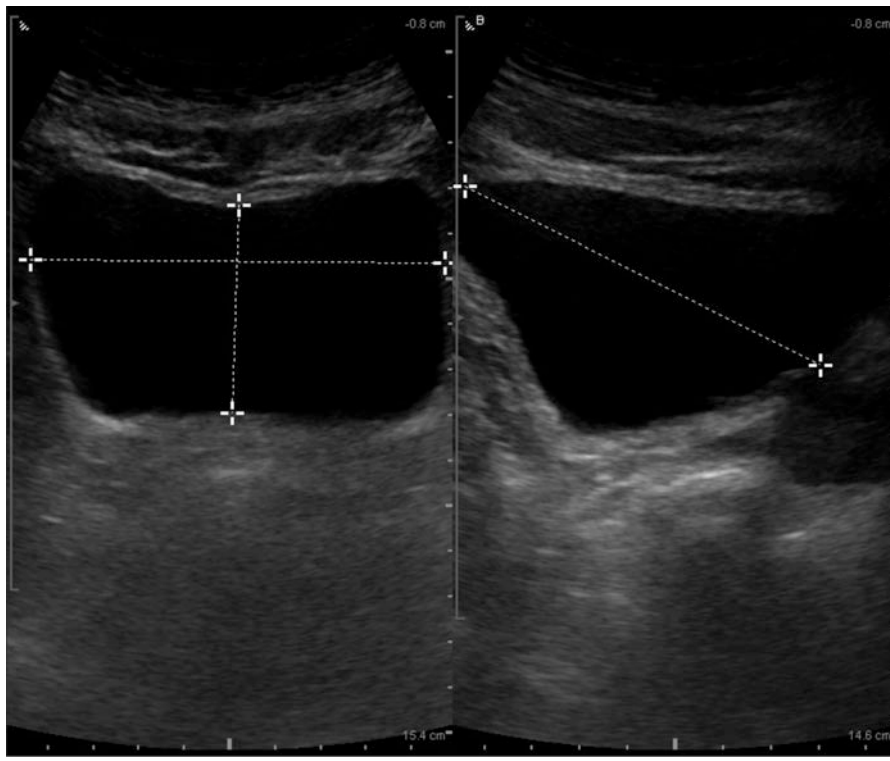

Fig. 16.38 Split screen view of the transverse (*left image*) and midsagittal (*right image*) view of the bladder

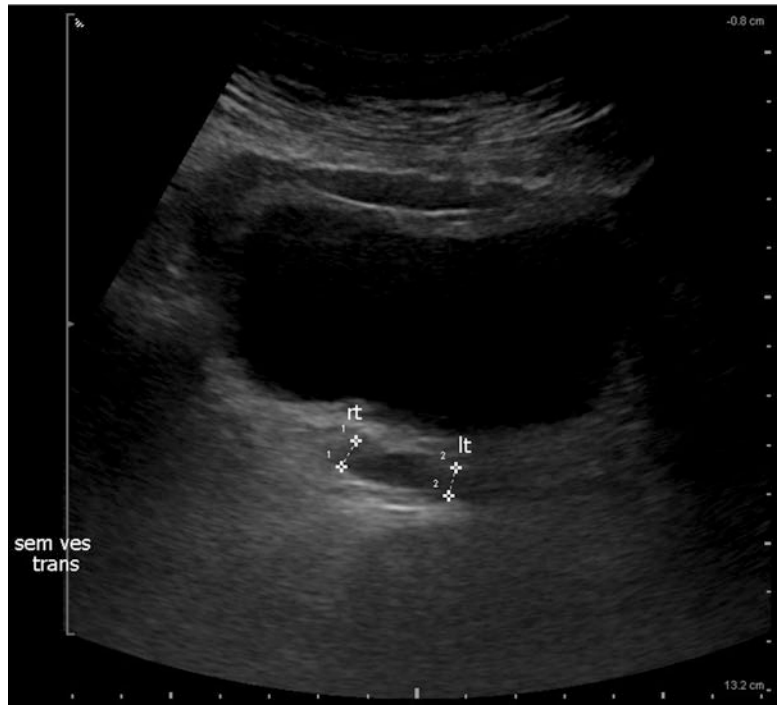

Fig. 16.39 Transverse view of right and left seminal vesicle thickness as seen posterior to the bladder

4. Representative color flow views of left and right ureteral jets with video clip if possible (Fig. 16.40).
5. Document postvoid residual (Fig. 16.41).

Transabdominal Prostate

Once examination of the bladder has been concluded and the images stored, attention is given to the prostate gland in male patients. Both transverse and sagittal views are employed, as in the bladder. To view the prostate, however, the ultrasound probe must be angled to project the ultrasound beam behind the pubic bone. To do this additional pressure is required to be applied against the abdominal wall. Measure the prostate first in the transverse view to obtain the height and width of the prostate. Measure the length of the prostate in the sagittal view. The volume of the prostate is automatically determined by most ultrasound equipment, but may also be calculated using the formula: Length × Width × Height × 0.523. The shape of the middle lobe can be described in the sagittal view. The presence of intravesical prostatic protrusion is present when the middle lobe extends into the bladder lumen. On a line drawn across the bladder neck (BN, TRUS 8), connecting the bladder base on either side, the protrusion of the prostate in centimeters is determined by the length of a vertical line (IPP, TRUS 8) perpendicular to line a. The intraprostatic protrusion (IPP) is Grade I if the line is <0.5 cm; Grade II if >0.7 cm and Grade III if >1 cm. The IPP grade corresponds to the probability of bladder outlet obstruction [21].

In examining the prostate, evaluate for calcification in the parenchyma of the prostate, lucent lesions, cysts, and solid mass effects. Further characterization of prostatic abnormalities can be made with digital rectal examination, transrectal ultrasound, and computerized tomography if necessary.

Abdominal Prostate Imaging

Specifics to be documented on report:

Indication for Procedure: For example, Lower urinary tract symptoms. Diagnosis code can also be included to document medical necessity.

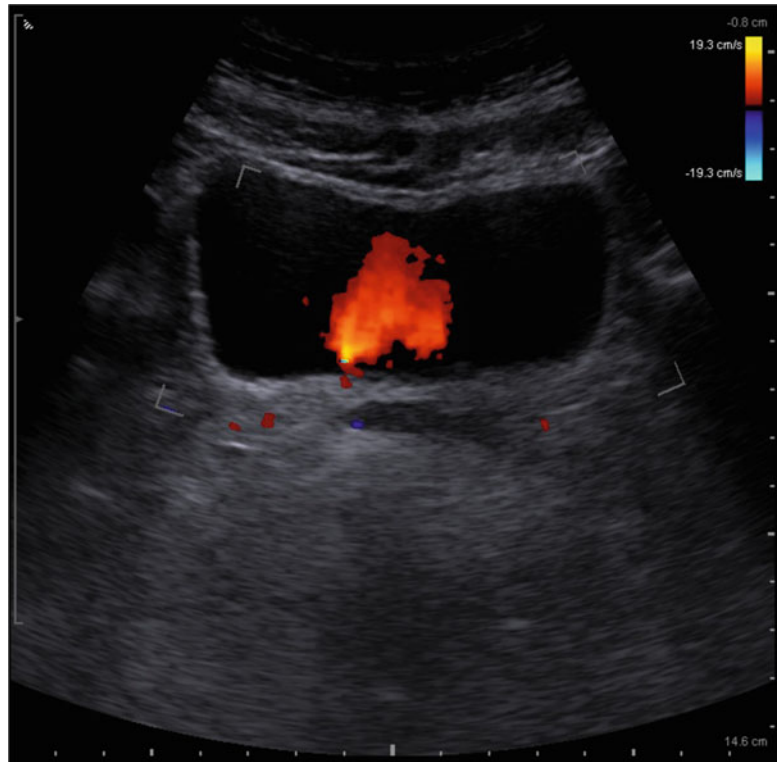

Fig. 16.40 Color Doppler views of left and right ureteral jets

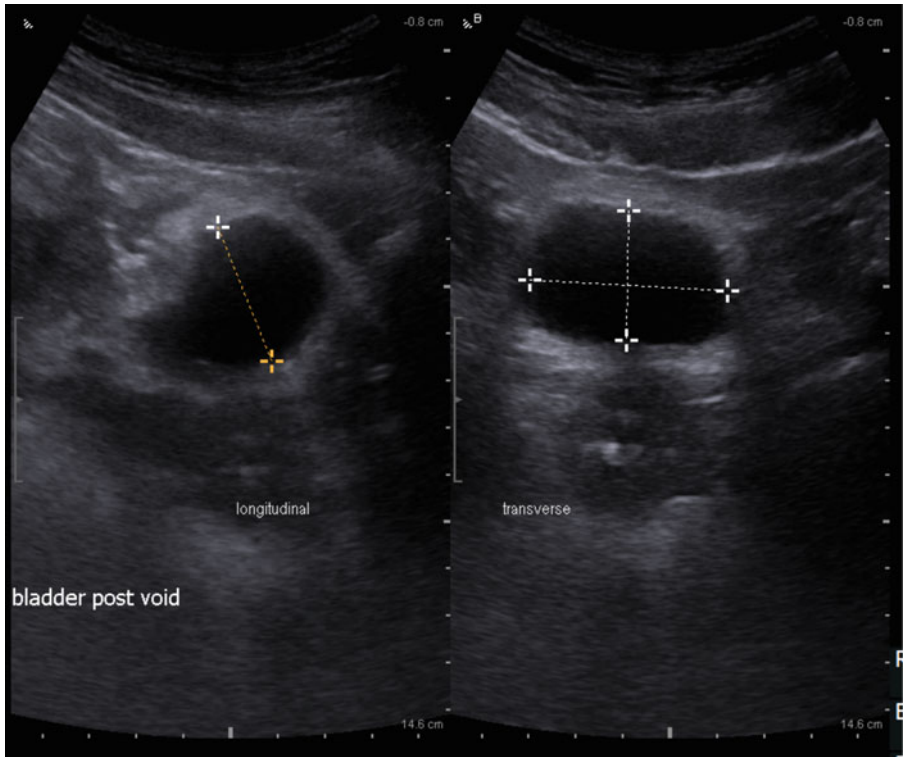

Fig. 16.41 Postvoid residual measurement of the bladder (split screen images)

Transducer: 3–5 MHz curved array transducer with small footprint.

Please note: if all components of the exam are not seen then the report should document that component was "Not Seen" and why.

1. Longitudinal and transverse survey scan of prostate with video clips.
2. Split screen midsagittal and midtransverse view with volume, height (AP), width, and length measurements (Fig. 16.42).
3. Seminal vesicles: transverse views for width measurements (Fig. 16.43).
4. Seminal vesicles: Longitudinal view of left and right seminal vesicle with length and width measurements (Fig. 16.44a, b).

For a complete prostate evaluation, including views of the base and apex as well as evaluation of the seminal vesicles, the transrectal approach is preferred.

Kidneys

A urologic ultrasound examination of the kidneys should include views of the bladder and ureters (if visualized). This is especially important when hydronephrosis is present.

Renal echogenicity should be compared to echogenicity of the adjacent liver or spleen. The kidneys and perirenal regions should be assessed for abnormalities. Dilation of the collecting system or the presence of solid or cystic masses should be noted. Vascular examination of the kidneys by color Doppler is often used:

(a) To assess renal arterial and venous patency.
(b) To evaluate adults suspected of having renal artery stenosis. For this application, angle-adjusted measurements of the peak systolic velocity should be made proximally, centrally, and distally in the extrarenal portion of the main renal arteries when possible.

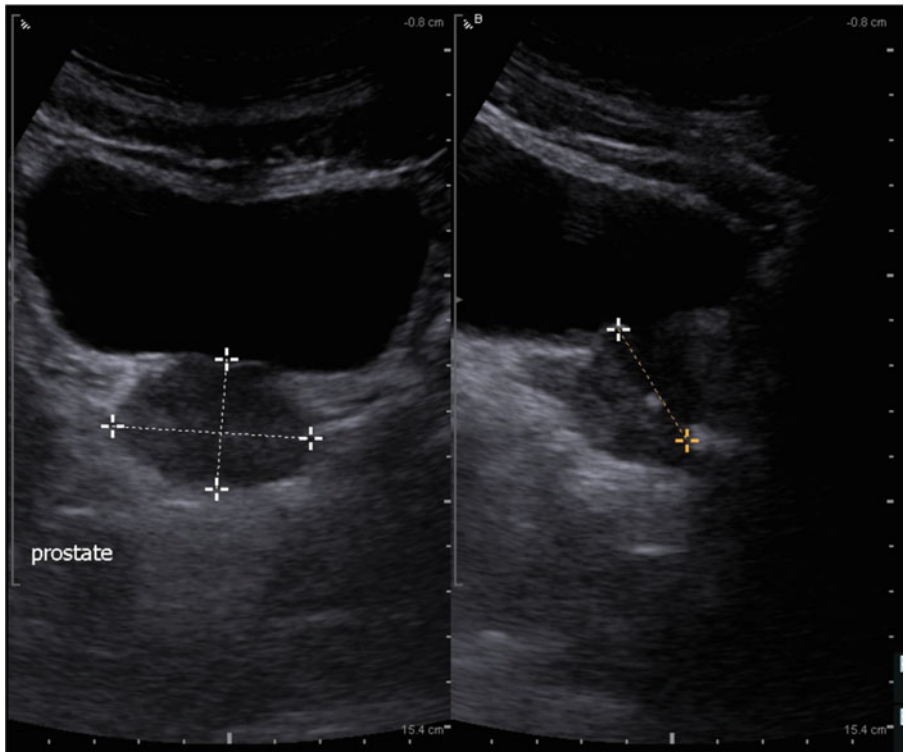

Fig. 16.42 Split screen midtransverse (*left image*) and midsagittal (*right image*) view of the prostate

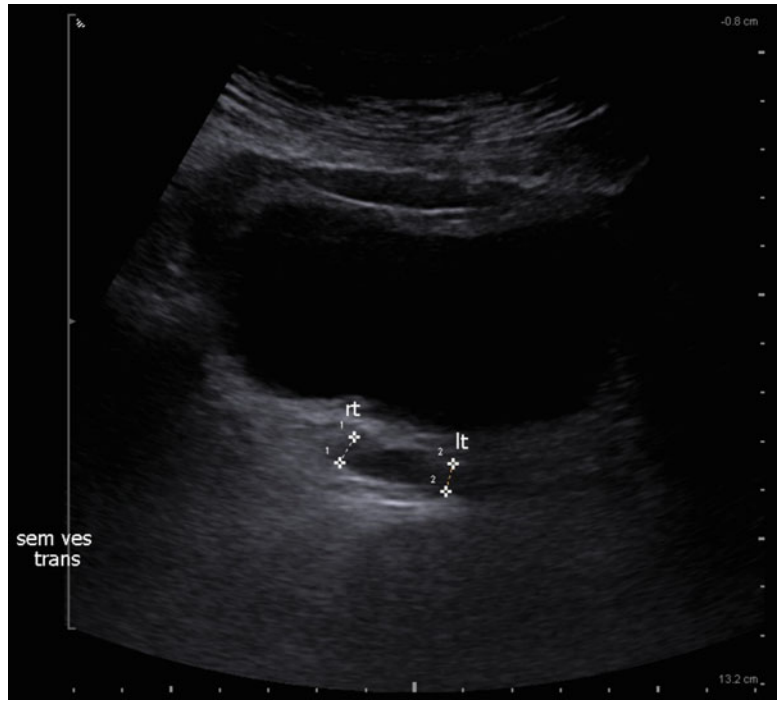

Fig. 16.43 Transverse view of right and left seminal vesicle thickness as seen posterior to the bladder

The peak systolic velocity of the adjacent aorta (or iliac artery in transplanted kidneys) should also be documented for calculating the ratio of renal to aortic peak systolic velocity. Spectral Doppler evaluation of the intrarenal arteries from the upper and lower portions of the kidneys, obtained to evaluate the peak systolic velocity, may be of value as indirect evidence of proximal stenosis in the main renal artery. A ratio of the peak systolic velocity over the peak systolic velocity—end diastolic velocity (resistive index) of an intralobular renal artery can be used to evaluate intrarenal vascular resistance.

Urinary Bladder and Adjacent Structures

When performing a complete ultrasound evaluation of the kidneys, transverse and longitudinal images of the distended urinary bladder and its wall should be included, if possible. Bladder lumen or wall abnormalities should be noted. Dilatation or other distal ureteral abnormalities should be documented. This is especially important when hydronephrosis is present.

Transverse and longitudinal scans may be used to demonstrate any postvoid residual, which may be quantitated and reported. The size and shape of the prostate should be reported when possible.

Renal Ultrasound Protocol

Specifics to be documented on report:

Indication for Procedure: For example, renal calculi, hydronephrosis, hydroureter, collecting system abnormalities, renal tumors. Diagnosis code can also be included to document medical necessity.

Transducer: 3–5 MHz curved array transducer.

Please note: if all components of the exam are not seen then the report should document that component was "Not Seen" and why.

1. Longitudinal and transverse survey scan of both right and left kidney with video clips.
2. Single or Split screen midsagittal and midtransverse view of each kidney with height (AP), width, and length measurements (Fig. 16.45a, b). Also Cortical and parenchymal thickness in at least two areas (Fig. 16.45c). Demonstrate Liver on Right and Spleen on Left (if possible) and comment on comparative echogenicity.

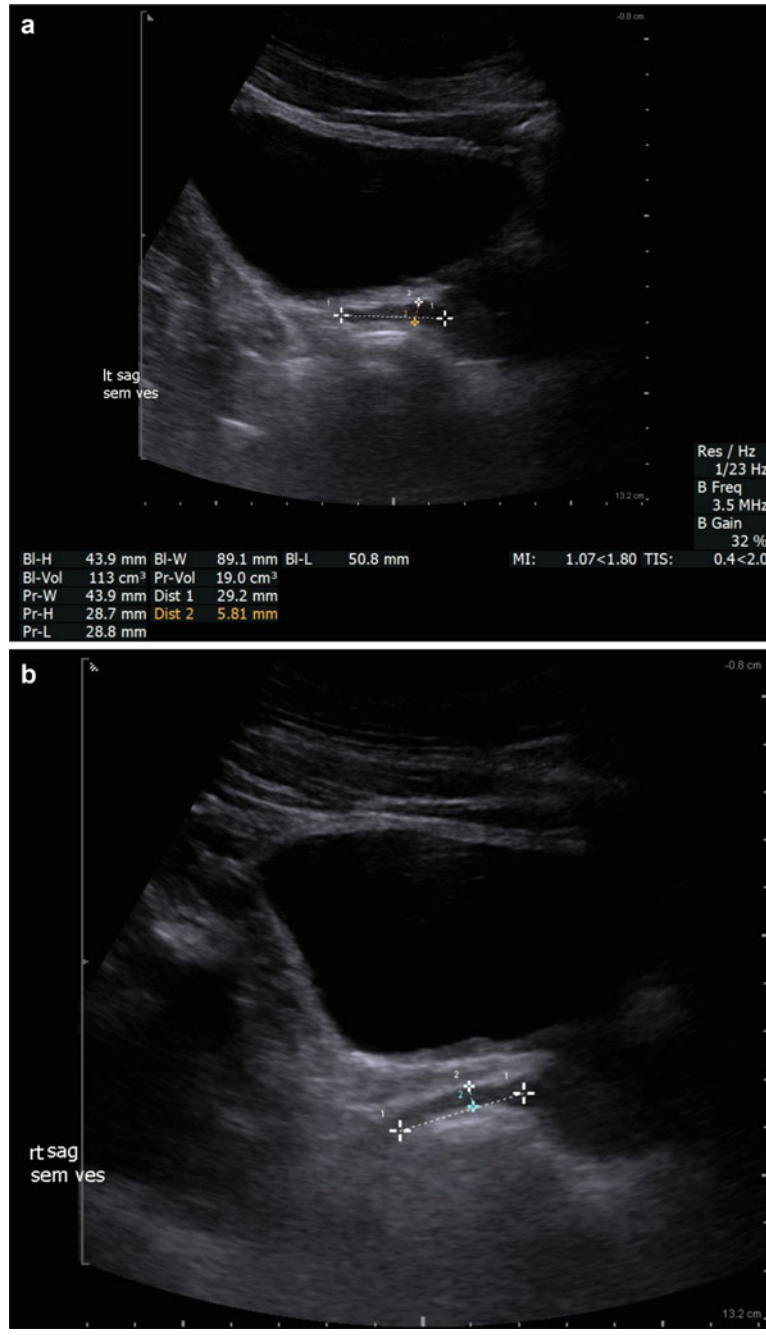

Fig. 16.44 (**a**) Longitudinal view of the left seminal vesicle thickness as seen posterior to the bladder. (**b**) Longitudinal view of the left seminal vesicle thickness as seen posterior to the bladder

3. Medial and Lateral Coronal (longitudinal views) of both kidneys (color Doppler optional) (Fig. 16.46).
4. Upper pole and lower pole transverse views of both kidneys (color Doppler optional) (Fig. 16.47).
5. Consider Spectral Doppler images with RI measurements of interlobar and arcuate vessels in upper, middle, and lower poles if indicated.
6. B-Mode, Color images, spectral Doppler, and/or elastography images of observed abnormalities (Fig. 16.48).

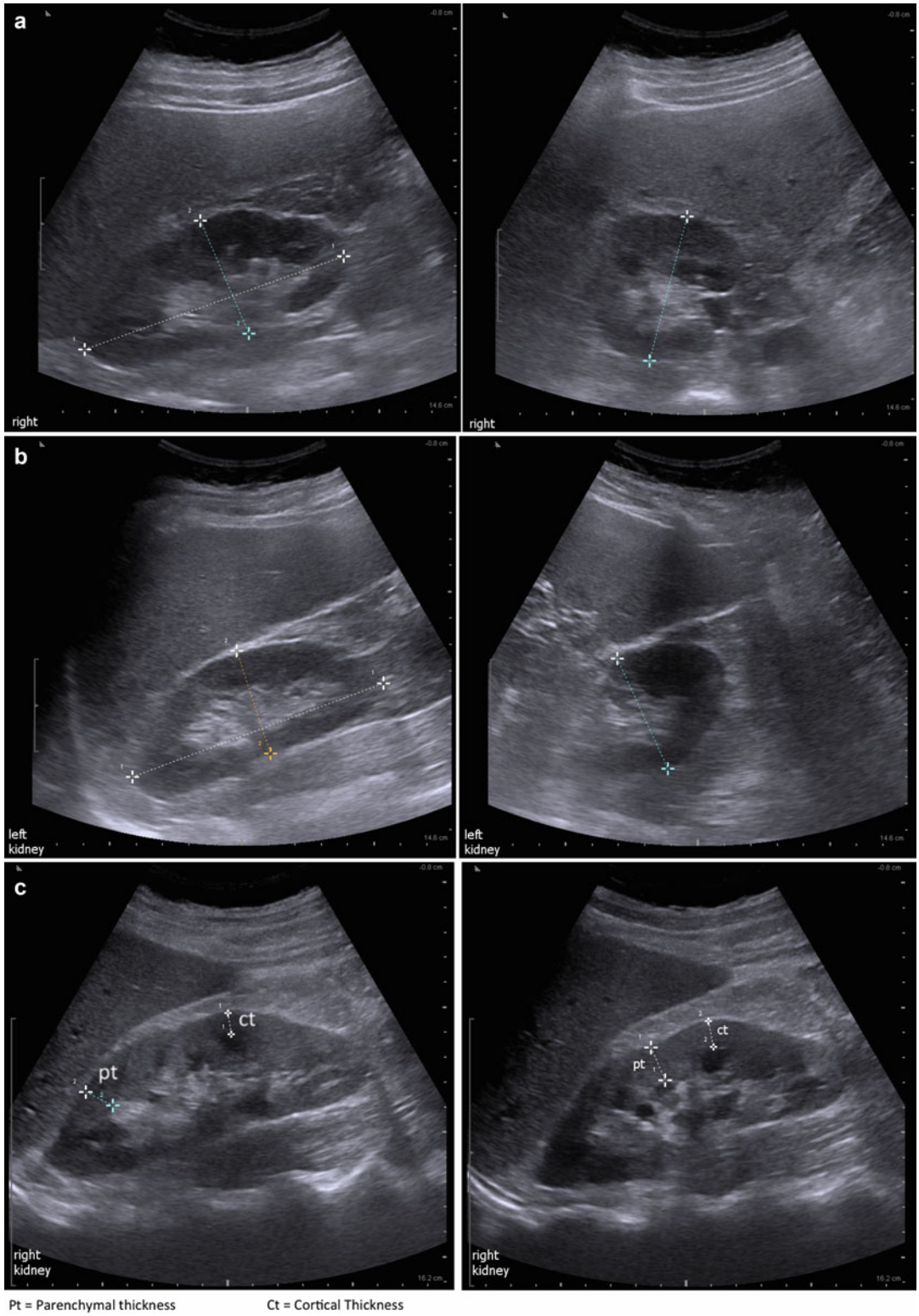

Fig. 16.45 (**a**) Split screen midsagittal (*left image*) and midtransverse (*right image*) view of right kidney. (**b**) Split screen midsagittal (*left image*) and midtransverse (*right image*) view of left kidney. (**c**) Cortical and parenchymal thickness measurements (right kidney)

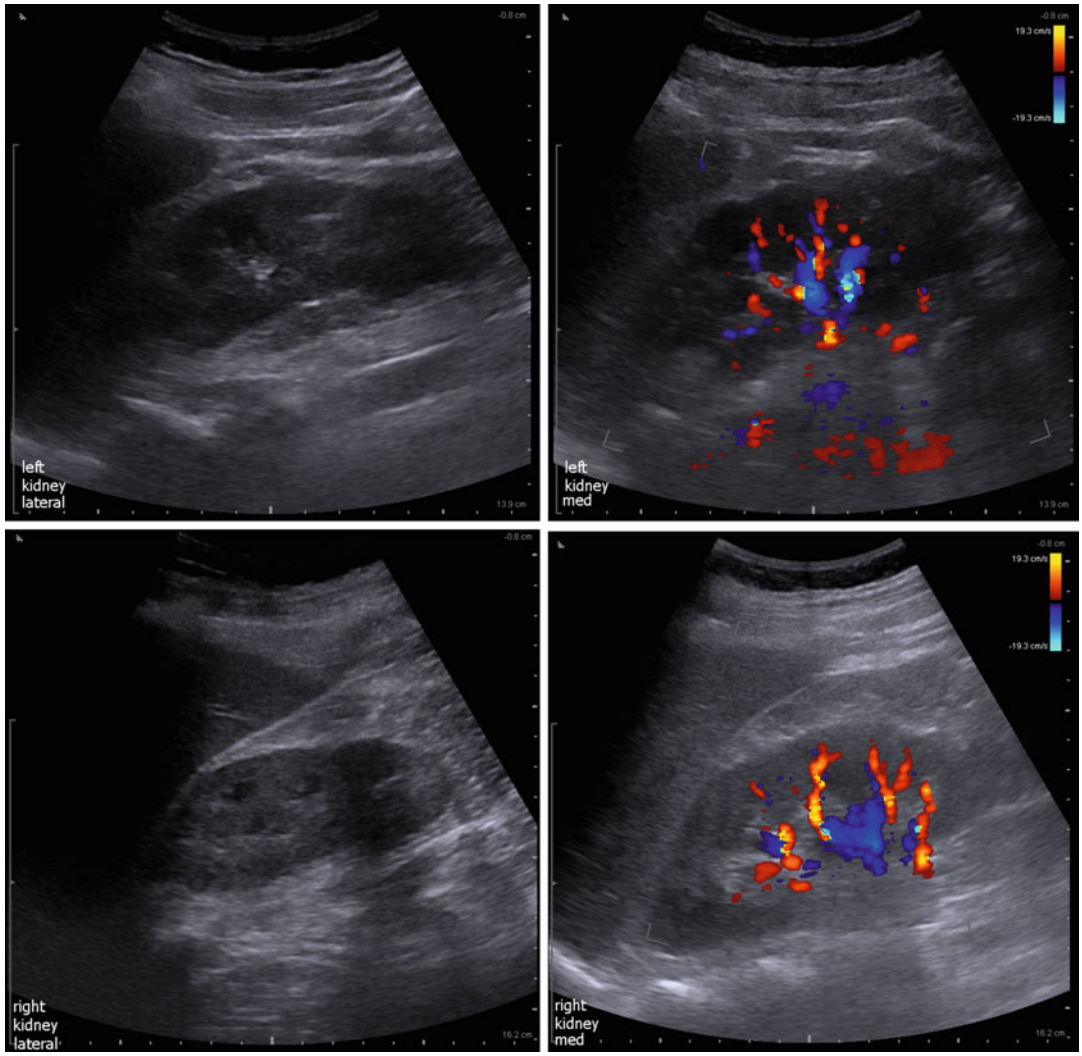

Fig. 16.46 Medial and Lateral Coronal (longitudinal views) of both kidneys

Transabdominal Bladder

Bladder (full bladder >150 cc)

1. Longitudinal and transverse survey scan of bladder with video clips.
2. Bladder (Split screen) midsagittal and midtransverse view with volume, height (AP), width, and length measurements (Fig. 16.38).
3. Measurement of bladder wall thickness in at least two locations (posterolateral and dome preferred) (Fig. 16.39).
4. Representative color flow views of left and right ureteral jets with video clip if possible (Fig. 16.40).
5. Document postvoid residual.

Transabdominal Prostate

1. Longitudinal and transverse survey scan of prostate with video clips.
2. Split screen midsagittal and midtransverse view with volume, height (AP), width, and length measurements (Fig. 16.42).

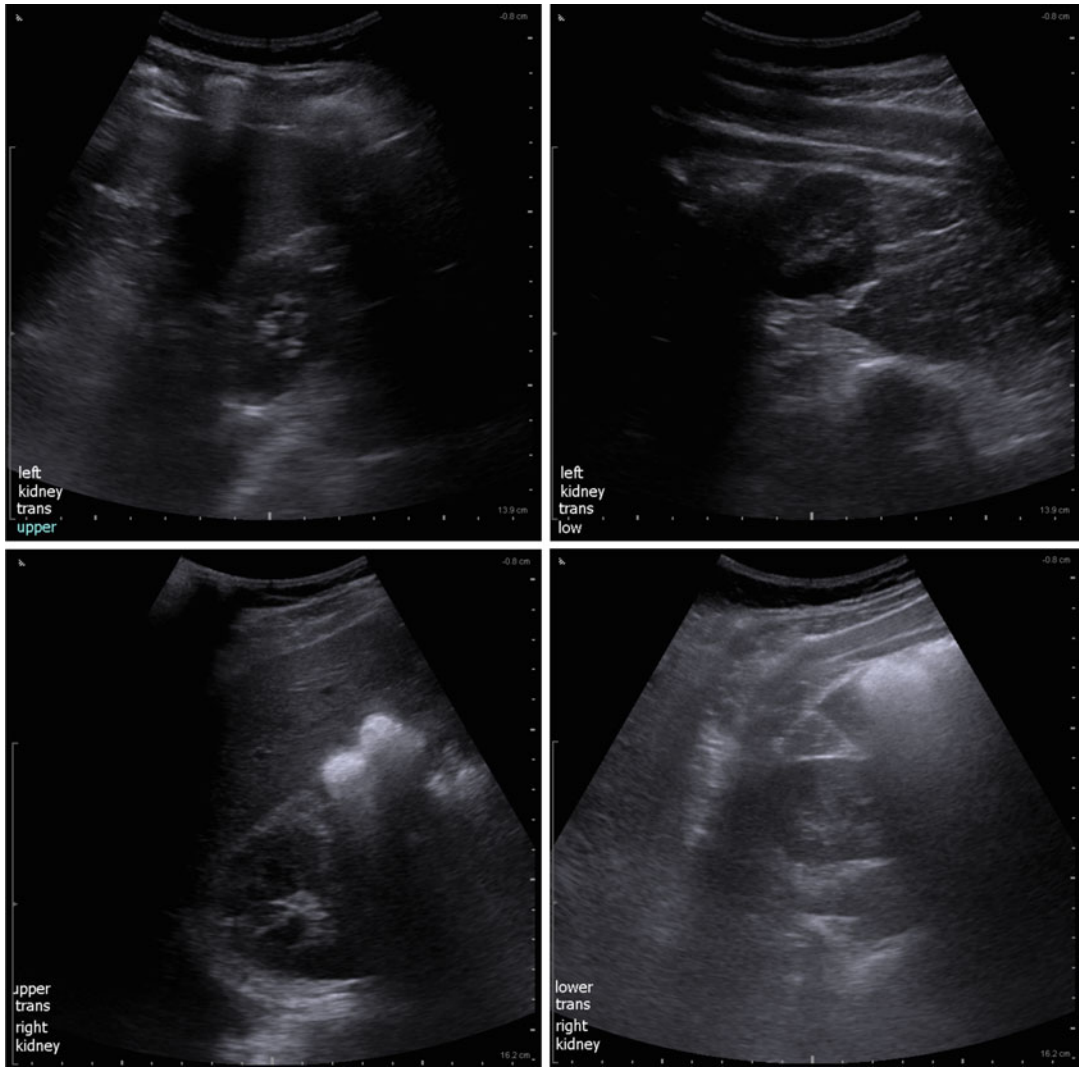

Fig. 16.47 Upper pole and lower pole transverse views of both kidneys

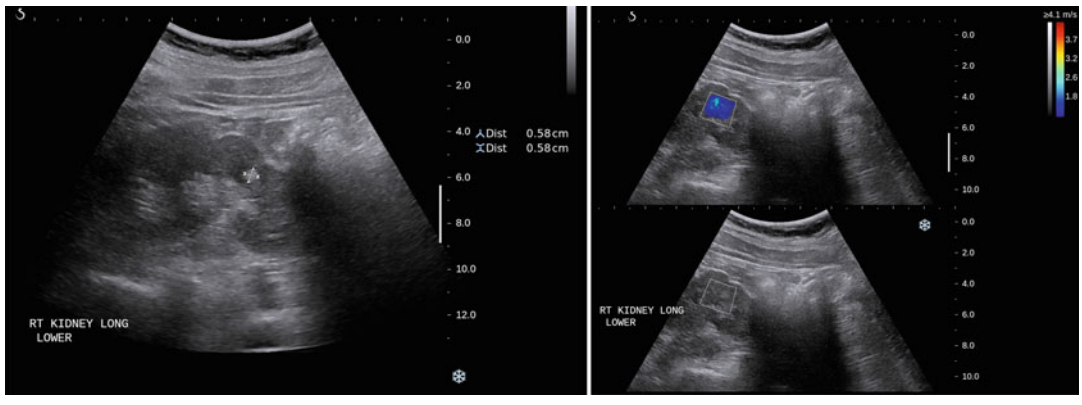

Fig. 16.48 Identification with measurements and color Doppler of observed abnormalities

3. Seminal vesicles: transverse views for width measurements (Fig. 16.43).

Transrectal Prostate Ultrasound (TRUS)

In the young male the prostate is homogenous with zones that are difficult to visualize. A "Sonographic capsule" is seen due to impedance difference between gland and surrounding fat and you can see it well visualized in this image where you have the hypoechoic surrounding fat versus the more isoechoic prostatic tissue. The urethra is seen with surrounding reflectivity of urethral muscles. The normal peripheral zone is often hyperechogenic in comparison to the central and transition zones. The central and transition are often difficult to differentiate. The fibromuscular stroma lies anterior to the urethra. In the older male the glandular and stromal elements enlarge increasing the size of the transition zone and occasionally the peripheral zone. The transition zone is seen independent of other zones. The central zone is usually not visualized or difficult to visualize.

We start the TRUS study, as with all ultrasound studies begins with a survey scan. Orientation is critical. In a transverse view, the abdominal cavity is superior (at the top of the screen) to the prostate while the rectum is inferior (at the lower portion of the screen) to the prostate. In a longitudinal projection the bladder is to the left when looking at the ultrasound screen while the urethra is to the right.

The prostate base is located at the superior aspect of the prostate contiguous with the base of the bladder. The prostate apex is located at the inferior aspect of the prostate continuous with the striated muscles of the urethral sphincter.

We usually utilize a high frequency 5–10 MHz transducer. The transducer can have one, two (bi-planer), or three (Tri-planer) sets of crystals. The patient is usually examined in the left lateral decubitus position with his legs in the knee-to-chest position. Before inserting the probe, a digital rectal exam is performed. Pain or tenderness, rectal stricture, mass, lesion, and/or bleeding that is encountered when performing the rectal exam or when inserting the probe might preclude the transrectal examination being done. After probe insertion, the 'survey' scan of the prostate commences from base to apex including the seminal vesicles and rectal wall. The rest of the examination and documentation follows.

Prostate Ultrasound Protocol (Split Screen Views Preferred When Biplane Transducer Used)

Specifics to be documented on report:

Indication for Procedure: For example, Lower urinary tract symptoms, ejaculatory pain, low volume ejaculate. Diagnosis code can also be included to document medical necessity.

Transducer: 5–10 MHz transducer. This can be end fire, side fire, biplane, or triplaner.

Please note: if all components of the exam are not seen then the report should document that component was "Not Seen" and why.

1. Longitudinal and transverse survey scan of prostate with video clips.
2. Single or Split screen midsagittal and mid-transverse view (transverse view on left and longitudinal view on right and) with volume, height (AP), width, and length measurements. Prostatic urethra demonstrated Fig. 16.49.
3. Seminal vesicles: transverse view for Ampulla diameter and Seminal Vesicle width measurements (Fig. 16.50).
4. Single or Split Screen Base (transverse and longitudinal view) and Rectal Wall thickness measurement (Fig. 16.51).
5. Single or Split Screen Apex (transverse and longitudinal view) and Rectal Wall thickness measurement (Fig. 16.52).
6. Single or Split screen Right lateral longitudinal/sagittal views (split screen transverse and longitudinal projections) with measurements (length and AP) of right seminal vesicle. Periprostatic tissues and vas deferens demonstrated (Fig. 16.53).
7. Single or Split screen Left lateral longitudinal/sagittal views (split screen transverse and longitudinal projections) with measurements (length and AP) of left seminal vesicle. Periprostatic tissues and vas deferens demonstrated (Fig. 16.54).

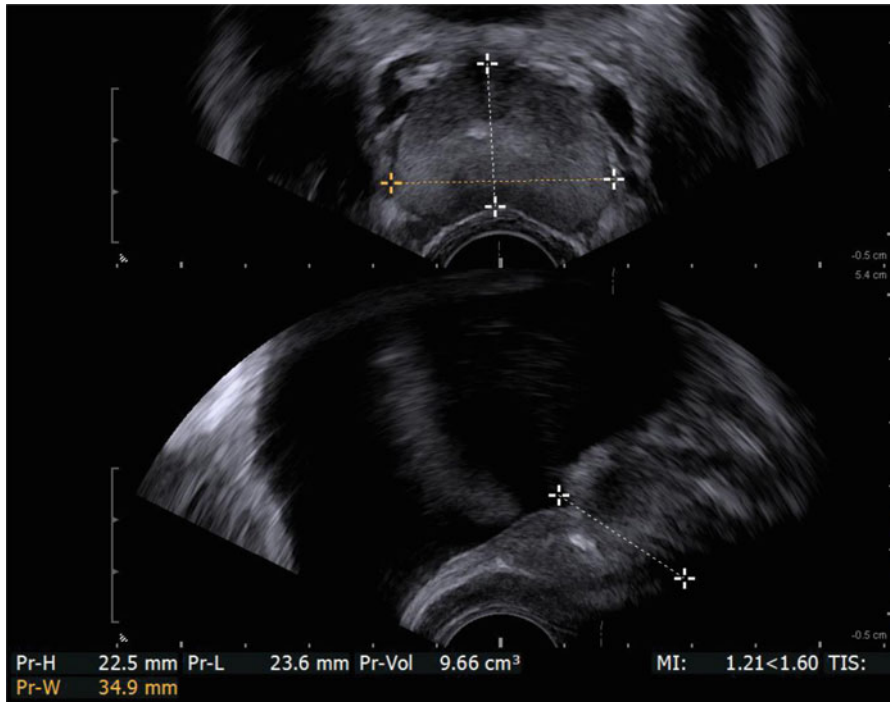

Fig. 16.49 Midtransverse (*top image*) and midsagittal (*lower image*) view of prostate using a biplaner transducer

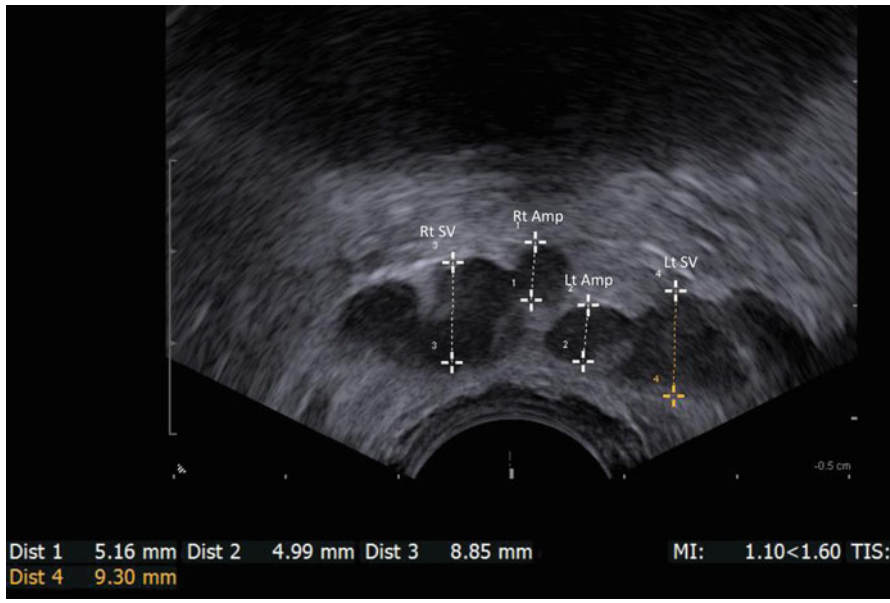

Fig. 16.50 Transverse view of seminal vesicles for Ampulla diameter and Seminal Vesicle width measurements

8. Representative color flow views of prostate (split screen) with both transverse and longitudinal views. Video clips are helpful (Fig. 16.55).
9. If intravesicle lobe: Measure length of intravesicle protrusion in sagittal view beginning at the bladder neck (Fig. 16.56).

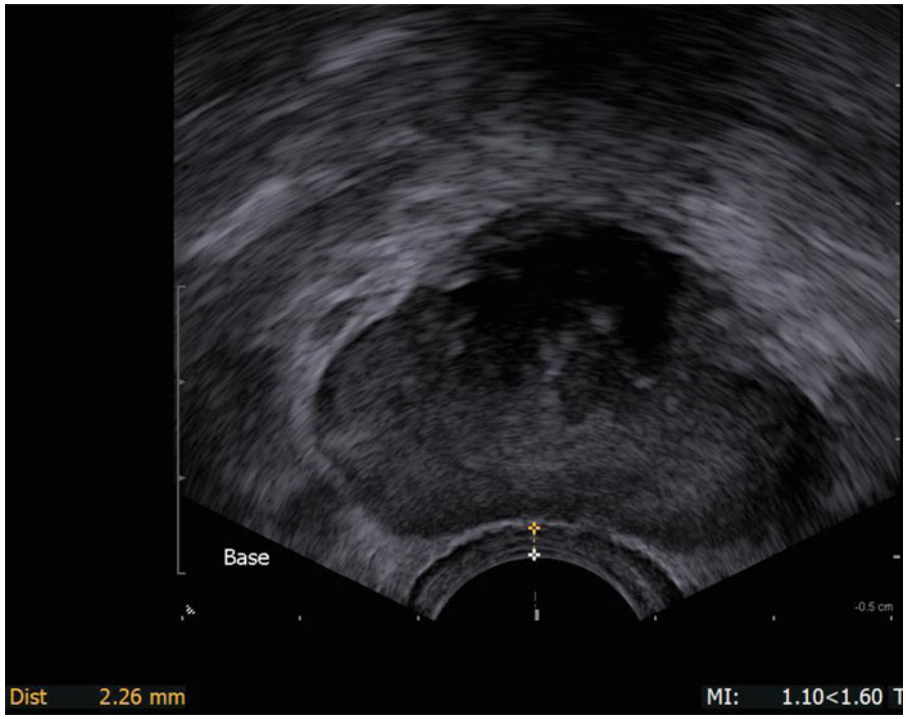

Fig. 16.51 Transverse view at base of prostate for rectal wall thickness measurement

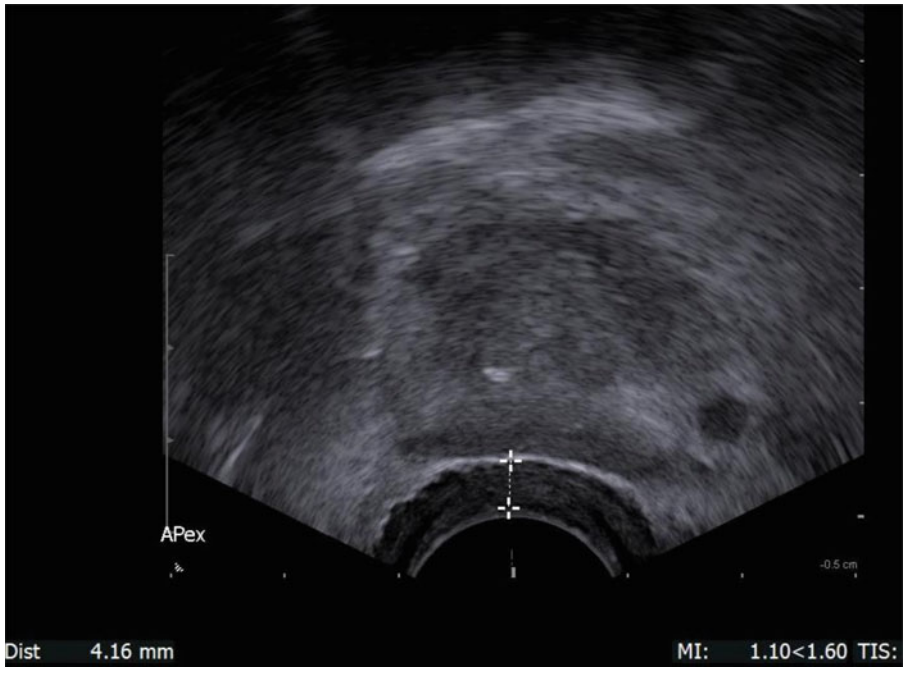

Fig. 16.52 Transverse view at apex of prostate for rectal wall thickness measurement

10. Image documentation of any pathology with appropriate measurements.
11. Bladder:
    - Split screen of the Bladder with measurement of volume, height (AP), width, and length measurements (Fig. 16.57).

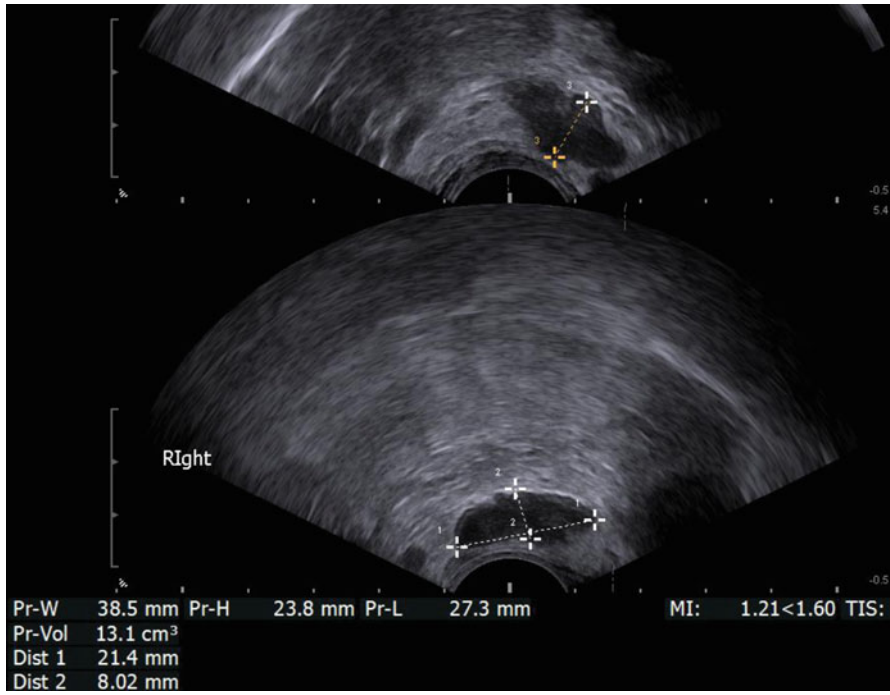

Fig. 16.53 Split screen transverse (*top image*) and longitudinal (*lower image*) view of right seminal vesicle

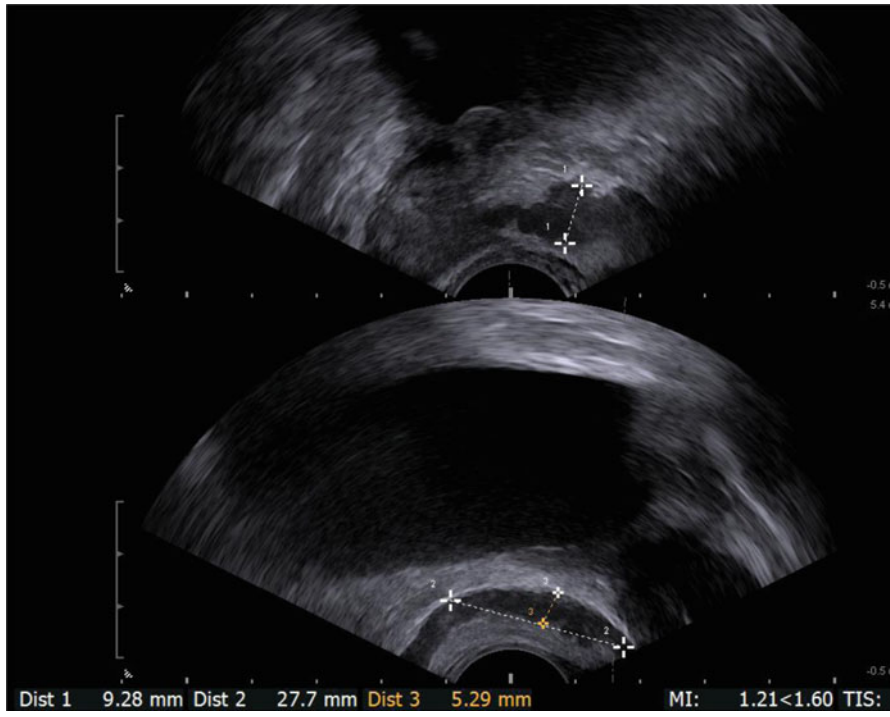

Fig. 16.54 Split screen transverse (*top image*) and longitudinal (*lower image*) view of left seminal vesicle

- Measurement of bladder wall thickness in at least two locations (posterolateral and dome preferred).
- Consider color flow views of left and right ureteral jets with video clip if possible (Fig. 16.58).

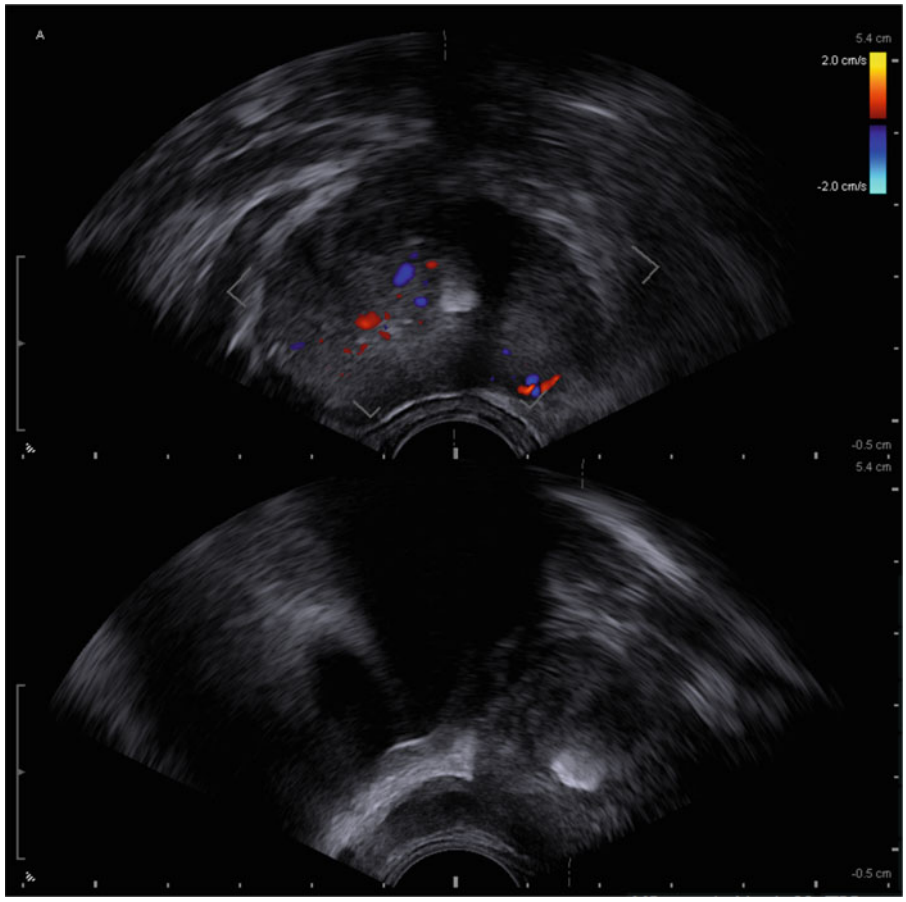

Fig. 16.55 Split screen representative color flow views of prostate with transverse (*top image* with color Doppler) and longitudinal (*lower image*) views

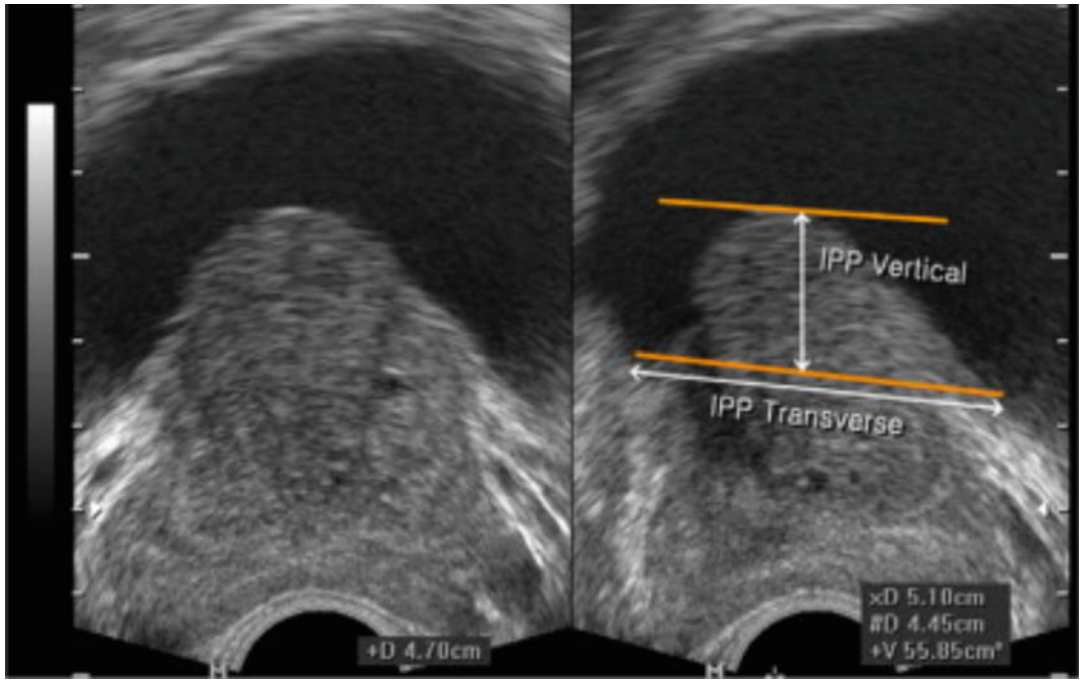

Fig. 16.56 Measure length of intravesicle protrusion in sagittal view beginning at the bladder neck (*transverse image*)

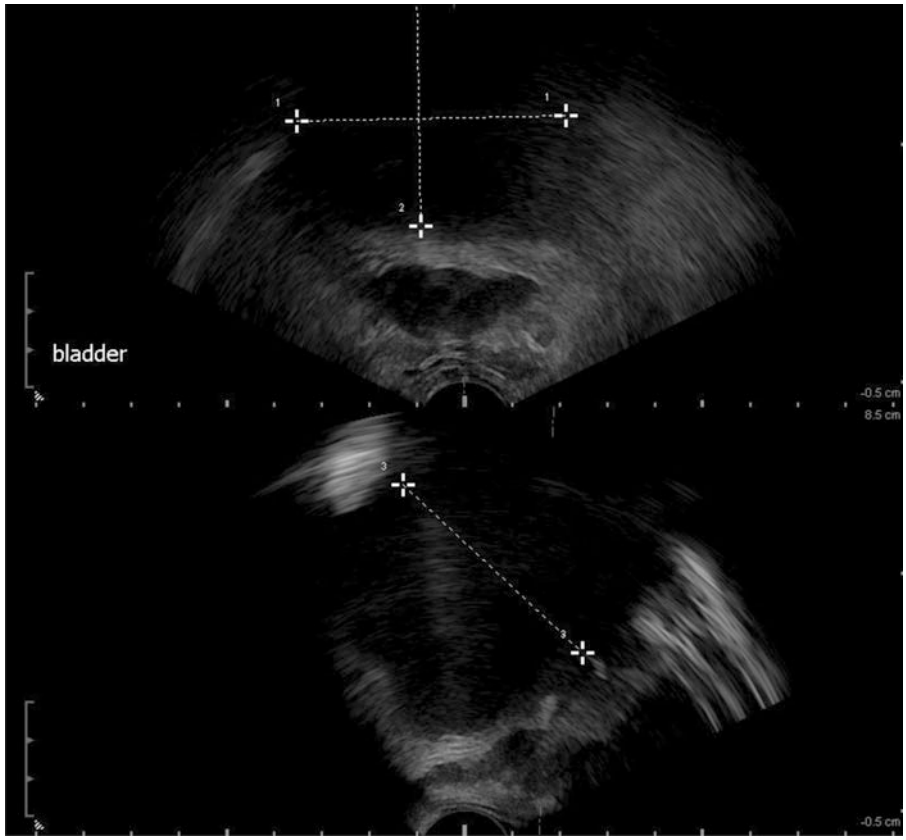

Fig. 16.57 Split screen image of bladder in transverse (*upper image*) and longitudinal (*lower image*)

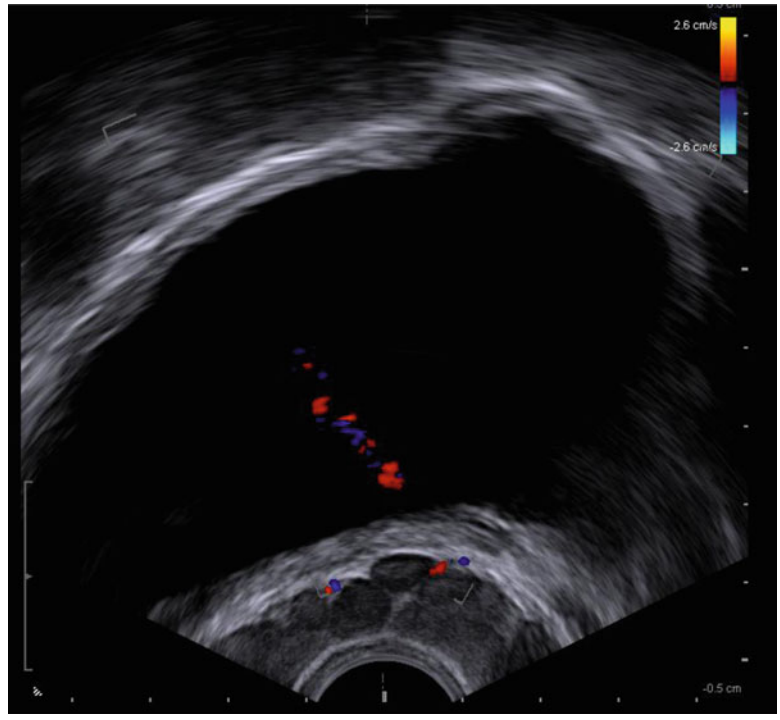

Fig. 16.58 Transverse color Doppler image of left right ureteral jet

Appendix: Legends

See Figs. 16.59, 16.60, 16.61, 16.62, 16.63, and 16.64.

					PATIENT LABEL				
PENILE ULTRASOUND									
DATE OF SERVICE:						BP:			
PROCEDURE:						Pulse:			
	INDICATION:								
	US MACHINE:					TRANSDUCER:			
B-MODE FINDINGS (ATTACH IMAGES)									
RIGHT CORPORA CAVERNOSUM					LEFT CORPORA CAVERNOSUM				
AP LONGITUDINALH (cm)					AP LONGITUDINAL (cm)				
PLAQUE_MASS (size,location):					PLAQUE_MASS (size,location):				
SIZE:		LOCATION:			SIZE:		LOCATION:		
ECHOGENICITY:					ECHOGENICITY:				
CALCIFICATIONS (quantity)					CALCIFICATIONS (quantity)				
INTRACORPORA COMMENTS:									
TRANSVERSE		AP	Width		TRANSVERSE		AP	Width	
PROXIMAL (cm)					PROXIMAL (cm)				
MID (cm)					MID (cm)				
DISTAL (cm)					DISTAL (cm)				
LESION (Y/N):		TYPE:			LESION (Y/N):		TYPE:		
SIZE:		LOCATION:			SIZE:		LOCATION:		
ECHOGENICITY:					ECHOGENICITY:				
COMPARATIVE ECHOGENICITY									
CORPORACAVERNOSUS COMMENTS									
BULBOCAVERNOSUS COMMENTS									
COLOR DOPPLER/DUPLEX FINDINGS (ATTACH IMAGES)									
INDICATION FOR COLOR/DUPLEX STUDY:									
COMMENTS:									
PSV	EDV	RI	Dia (mm)	Time	PSV	EDV	RI	DIA (mm)	Tum/Rig
				Baseline					
				5 MIN					
				10 MIN					
				15 MIN					
				20 MIN					
				30 MIN					
				40 MIN					
PHYSICIAN INTERPRETATION									
DATE/TIME									
			PHYSICIAN SIGNATURE						

Fig. 16.59 Penile ultrasound template

					PATIENT LABEL			
BLADDER ULTRASOUND								
DATE OF SERVICE:								
	INDICATION:							
	US MACHINE:					**TRANSDUCER:**		
B-MODE FINDINGS (ATTACH IMAGES) CPT 76857 (Limited pelvic US)								
BLADDER LENGTH (cm)				**BLADDER URETERAL DILATION (Y/N):**				
BLADDER WIDTH (cm)				**PROSTATE SIZE (cc):**				
BLADDER VOLUME (cc)				**PROSTATE MORPHOLOGY:**				
BLADDER WALL THICKNESS (cm)								
BLADDER DIVERTICULA (Y/N):								
BLADDER TUMOR (Y/N):								
BLADDER PERIVESICAL MASS (Y/N):								
PRE VOID VOLUME (cc)								
POST VOID RESIDUAL (cc)								
BLADDER CALCULUS (Y/N):								
BLADDER FOREIGN BODY (Y/N):								
COMMENTS:								
COLOR DOPPLER/DUPLEX FINDINGS (ATTACH IMAGES) CPT 93975								
INDICATION:	**MASS**	**PELVIC FLOOR**	**URETERAL JETS**					
	LOCATION	**PSV**	**EDV**	**RI**	**AT**			
LEFT								
RIGHT								
COMMENTS:								
PHYSICIAN INTERPRETATION								
DATE/TIME								
			PHYSICIAN SIGNATURE					

Fig. 16.60 Bladder ultrasound template

					PATIENT LABEL			
PERINEAL ULTRASOUND OF BULBOCAVERNOSUS MUSCLE (BCM)								
DATE OF SERVICE:								
	INDICATION:							
	US MACHINE:					TRANSDUCER:		
B-MODE FINDINGS (ATTACH IMAGES) CPT 76857 (Limited pelvic US)								
		#1	#2					
BCM RIGHT (cm)				BCM RIGHT AVG (cm)				
BCM MID (cm)				BCM MID AVG (cm)				
BCM LEFT (cm)				BCM LEFT AVG (cm)				
BCM AREA (cm^2)				BCM AREA AVG (cm^2)				
COLOR DOPPLER/DUPLEX FINDINGS (ATTACH IMAGES) CPT 93975								
	COMMENTS	PSV	EDV	RI	AT			
LEFT								
MID								
RIGHT								
COMMENTS:								
PHYSICIAN INTERPRETATION								
DATE/TIME								
			PHYSICIAN SIGNATURE					

Fig. 16.61 Perineal ultrasound of bulbocavernosus muscle (BCM) template

					PATIENT LABEL				
RENAL ULTRASOUND									
DATE OF SERVICE:									
PROCEDURE:									
	INDICATION:								
	US MACHINE:					TRANSDUCER:			
B-MODE FINDINGS (ATTACH IMAGES)									CPT 76775
RIGHT KIDNEY					LEFT KIDNEY				
LENGTH (cm)					LENGTH (cm)				
WIDTH (cm)					WIDTH (cm)				
HEIGHT (cm)					HEIGHT (cm)				
VOLUME (cm^3)					VOLUME (cm^3)				
SCARRING (Y/N):		LOCATION:			SCARRING (Y/N):		LOCATION:		
STONES (Y/N):					STONES (Y/N):				
SIZE:		LOCATION:			SIZE:		LOCATION:		
COMMENT:					COMMENT:				
MASSES (Y/N):					MASSES (Y/N):				
SIZE:		LOCATION:			SIZE:		LOCATION:		
COMMENT:					COMMENT:				
HYDRONEPHROSIS (Y/N):					HYDRONEPHROSIS (Y/N):				
GRADE:		DESCRIPTION:			GRADE:		DESCRIPTION:		
COMMENT:					COMMENT:				
OBSTRUCTION (Y/N):					OBSTRUCTION (Y/N):				
COMMENT:					COMMENT:				
ECHOGENICITY:					ECHOGENICITY:				
PERINEPHRIC FLUID (Y/N) :					PERINEPHRIC FLUID (Y/N) :				
AMOUNT:		LOCATION:			AMOUNT:		LOCATION:		
RENAL CORTICAL THICKNESS (cm):					RENAL CORTICAL THICKNESS (cm):				
RENAL PARENCHYMAL THICKNESS (cm):					RENAL PARENCHYMAL THICKNESS (cm):				
COMMENTS:									
COLOR DOPPLER/DUPLEX FINDINGS (ATTACH IMAGES)									CPT 93975
INDICATION:	RAS	MASS	Graft						CPT 93976
RIGHT KIDNEY					LEFT KIDNEY				
PSV	EDV	RI	AT	Location	PSV	EDV	RI	AT	Location
PHYSICIAN INTERPRETATION									
DATE/TIME									
					PHYSICIAN SIGNATURE				

Fig. 16.62 Renal ultrasound template

					PATIENT LABEL				
SCROTAL ULTRASOUND									
DATE OF SERVICE:									
	INDICATION:								
	US MACHINE:					TRANSDUCER:			
B-MODE FINDINGS (ATTACH IMAGES)									
RIGHT TESTIS		Mid Sag	Mid Trans		LEFT TESTIS		Mid Sag	Mid Trans	
LENGTH (cm)					LENGTH (cm)				
WIDTH (cm)					WIDTH (cm)				
AP (cm)					AP (cm)				
VOLUME (cm^3)					VOLUME (cm^3)				
☐ MASS (size,location):					☐ MASS (size,location):				
SIZE:		LOCATION:			SIZE:		LOCATION:		
COMPARATIVE ECHOGENICITY									
☐ MICROCALCIFICATIONS (quantity)					☐ MICROCALCIFICATIONS (quantity)				
INTRATESICULAR COMMENTS:					INTRATESICULAR COMMENTS:				
RIGHT EPIDIDYMIS					LEFT EPIDIDYMIS				
CAPUT (cm)					CAPUT (cm)				
CORPUS (cm)					CORPUS (cm)				
CAUDA (cm)					CAUDA (cm)				
LESION (Y/N):		TYPE:			LESION (Y/N):		TYPE:		
SIZE:		LOCATION:			SIZE:		LOCATION:		
COMPARATIVE ECHOGENICITY									
EPIDIDYMAL COMMENTS:					EPIDIDYMAL COMMENTS:				
RIGHT PARATESTICULAR STRUCTURES					LEFT PARATESTICULAR STRUCTURES				
PARATESTICULAR COMMENTS:					PARATESTICULAR COMMENTS:				
RIGHT SCROTAL WALL					LEFT SCROTAL WALL				
COLOR DOPPLER/DUPLEX FINDINGS (ATTACH IMAGES)									
INDICATION FOR COLOR/DUPLEX STUDY:									
RT TESTES					LT TESTES				
☐ VARICOCELE		Dia (mm)	LOCATION		☐ VARICOCELE		Dia (mm)	LOCATION	
PARATESTICULAR STRUCTURES:					PARATESTICULAR STRUCTURES:				
PSV	EDV	RI		LOCATION	PSV	EDV	RI		
				UPPER					
				MIDDLE					
				LOWER					
				AVERAGE					
PHYSICIAN INTERPRETATION									
DATE/TIME									
			PHYSICIAN SIGNATURE						

Fig. 16.63 Scrotal ultrasound template

					PATIENT LABEL			
PROSTATE ULTRASOUND								
DATE OF SERVICE:						PSA:		
	INDICATION:							
	US MACHINE:					TRANSDUCER:		
B-MODE								
DRE					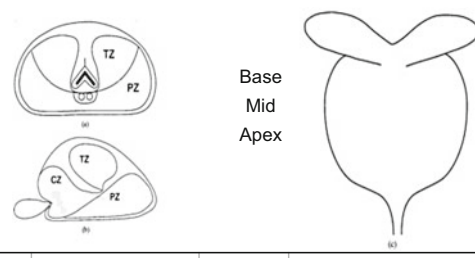			
		LEFT	RIGHT					
SIZE								
LEFT								
RIGHT								
SEMINAL VESICLE								
Length								
Width								
Description								
TRANSVERSE PROSTATE								
BASE:								
MID-GLAND:								
APEX:								
SAGITTAL PROSTATE								
ANTERIOR								
MID-GLAND								
POSTERIOR								
MID-SAGITTAL PROSTATE MEASUREMENTS								
HEIGHT (cm)								
WIDTH (cm)								
LENGTH (cm)								
VOLUME (cm^3)								
COLOR DOPPLER/DUPLEX FINDINGS (ATTACH IMAGES)								
INDICATION FOR COLOR/DUPLEX STUDY:							URETERAL JETS (R/L):	
	LEFT	RIGHT	COMMENTS:					
SV:								
BASE:								
APEX:								
MASS:								
PSV	EDV	RI		LOCATION	PSV	EDV	RI	
				BASE				
				MIDDLE				
				APEX				
				AVERAGE				
PHYSICIAN INTERPRETATION								
DATE/TIME								
			PHYSICIAN SIGNATURE					

Fig. 16.64 Prostate ultrasound template

					PATIENT LABEL

TRUS PROCEDURE RECORD									
DATE OF SERVICE:						RM IN:			
PROCEDURE:	PROSTATE U/S; U/S GUIDANCE/TRUS NEEDLE BX					TIME OUT:			
DIAGNOSIS:	ELEVATED PSA / ABNORMAL DRE / FOLLOW UP					START:			
PHYSICIAN:						FINISHED			
ASSISTANT:						RM OUT:			
LAST ASPIRIN USE						LAST PSA:			
ALLERGIES:						BP:			
VALVES/PROSTHETICS:						PULSE:			
AUA SYMPTOM SCORE:						IIEF:			
TIME OUT:	MD:		NURSE:						
PATEINT TOOK NECESSARY PREPARATIONS AND ANTIBIOTICS FOR PROCEDURE							PATIENT SIGNATURE		
DATE/TIME	Temp	HR	BP	RR	COMMENTS				
POST PROCEDURE INSTRUCTIONS & INFORMATION GIVEN					PATIENT SIGNATURE		WITNESS SIGNATURE		
PATIENT POST PROCEDURE PAIN SCORE:			/ 10						

PHYSICIAN ORDERS			
DATE/TIME	ORDER	SIGNATURE	GIVEN BY

PROCEDURE NOTE									
PSA		DRE			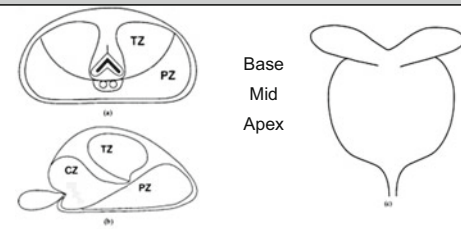				
SEE DICTATED NOTE									
TRANSRECTAL U/S GUIDED NEEDLE BX OF PROSTATE									
1% LIDOCAINE (cc)_____	2% LIDOCAINE(cc)_____								
LEFT (#cores)		RIGHT (#cores)							
_____BASE		_____BASE							
_____MID		_____MID							
_____APEX		_____APEX							
_____TRANSITION ZONE		_____TRANSITION ZONE							
_____TOTAL LEFT		_____TOTAL LEFT							
		_____TOTAL CORES							
PATIENT FOLLOW-UP:									

PHYSICIAN INTERPRETATION									
DATE/TIME									
☐									
			PHYSICIAN SIGNATURE						

Fig. 16.64 (continued)

References

1. AIUM practice guideline for documentation of an ultrasound examination, AIUM practice guidelines.
2. AIUM practice guideline for the performance of an ultrasound examination in the practice of urology. The American Institute for Ultrasound in Medicine, 5 Nov 2011.
3. Health Insurance and Portability Accountability Act of 1996 (HIPAA).
4. HiTech Act of 2009, Health Information Technology for Economic and Clinical Health Act, Federal Register, Vol. 74, No. 79, Monday, 27 Apr 2009.
5. Federal Drug Administration, Code of Federal regulations Title 21 CFR, Part 1270 subpart C, Procedures and Records.
6. Biagiotti G, et al. Spermatogenesis and spectral echocolor Doppler traces from the main testicular artery. BJU Int. 2002;90(9):903–8.
7. Unsal A, et al. Resistance and pulsatility index increase in capsular branches of testicular artery: indicator of impaired testicular microcirculation in varicocele? J Clin Ultrasound. 2007;35(4):191–5.
8. Pinggera GM, et al. Assessment of the intratesticular resistive index by colour Doppler ultrasonography measurements as a predictor of spermatogenesis. BJU Int. 2008;101(6):722–6.
9. Balci A, et al. Long-term effect of varicocele repair on intratesticular arterial resistance index. J Clin Ultrasound. 2008;36(3):148–52.
10. Hillelsohn JH, et al. Spectral Doppler sonography: a non-invasive method for predicting dyspermia. J Ultrasound Med. 2013;32:1427–32.
11. Herati A, et al. Evaluation of impaired spermatogenesis with spectral Doppler ultrasound: correlation with testicular biopsy. MP68-17. J Urol. 2014;191(4):e804–5.
12. Platt JF, Rubin JM, Ellis JH. Acute renal failure: possible role of duplex Doppler US in distinction between acute prerenal failure and acute tubular necrosis. Radiology. 1991;179(2):419–23.
13. Platt JF. Duplex Doppler evaluation of native kidney dysfunction: obstructive and nonobstructive disease. AJR Am J Roentgenol. 1992;158(5):1035–42. http://doi.org/10.2214/ajr.158.5.1566663
14. Onur MR, Poyraz AK, Bozgeyik Z, Onur AR, Orhan I. Utility of semiquantitative strain elastography for differentiation between benign and malignant solid renal masses. J Ultrasound Med. 2015;34(4):639–47. http://doi.org/10.7863/ultra.34.4.639
15. Tan S, et al. Real-time elastography for distinguishing angiomyolipoma from renal cell carcinoma: preliminary observations. AJR Am J Roentgenol. 2013;200(4): W369–75. http://doi.org/10.2214/AJR.12.9139
16. Ozkan F, et al. Interobserver variability of ultrasound elastography in transplant kidneys: correlations with clinical-Doppler parameters. Ultrasound Med Biol. 2013;39(1):4–9. http://doi.org/10.1016/j.ultrasmedbio.2012.09.013
17. Boehm K, Salomon G, Beyer B, Schiffmann J, Simonis K, Graefen M, Budaeus L. Shear wave elastography for localization of prostate cancer lesions and assessment of elasticity thresholds: implications for targeted biopsies and active surveillance protocols. J Urol. 2015;193(3):794–800. http://doi.org/10.1016/j.juro.2014.09.100
18. Postema A, Mischi M, de la Rosette J, Wijkstra H. Multiparametric ultrasound in the detection of prostate cancer: a systematic review. World J Urol. 2015;33(11): 1651–9. http://doi.org/10.1007/s00345-015-1523-6
19. Dabaja AA, Wosnitzer MS, Mielnik A, Bolyakov A, Schlegel PN, Paduch DA. Bulbocavernosus muscle area measurement: a novel method to assess androgenic activity. Asian J Androl. 2014;16:1–5.
20. Manieri C, Carter S, Romano G, Trucchi A, et al. The diagnosis of bladder outlet obstruction in men by ultrasound measurement of bladder wall thickness. J Urol. 1998;159(3):761–5.
21. Chia SJ, Heng CT, Chan SP, Foo KT. Correlation of intravesical prostatic protrusion with bladder outlet obstruction. BJU Int. 2003;91(4):371–4.

Urology Ultrasound Practice Accreditation

17

Nikhil Gupta and Bruce R. Gilbert

Urology Ultrasound Practice Accreditation

As physicians, we strive to provide our patients with the best clinical advice. Therefore, in performing office ultrasound we are committed to assure that our equipment, sonographers, and protocols are the best. Likewise, patients rightfully expect that the ultrasound exam performed uses equipment that is safe and can effectively image the organ of interest. They also trust that their physician can review these images and make appropriate diagnoses and treatment decisions. We constantly endeavor to assure the best care for our patients yet there are few protocols that define what a standard exam consists of. In addition, third-party payers have, for a multitude of reasons, instituted requirements for practices, including urology practices, to follow in order to be compensated for their work in providing ultrasound imaging services. How does the urologist sonographer then assure that their ultrasound exam is compliant with current standards and protocols? One way is through practice accreditation. There are presently two acknowledged accrediting agencies the American College of Radiology (ACR) and the American Institute for Ultrasound in Medicine (AIUM). The AUA and the AIUM have partnered to develop a pathway whereby urology practices can obtain accreditation that is recognized by regulatory authorities and third-party payers. This chapter details the process.

N. Gupta, M.D. (✉)
Smith Institute for Urology, Hofstra University, Northwell Health System, 450 Lakeville Road, Suite M41, Lake Success, NY 11040, USA
e-mail: nkgupta85@gmail.com

B.R. Gilbert, M.D. Ph.D.
The Smith Institute for Urology, Northwell Health System, 450 Lakeville Road, Suite M41, New Hyde Park, NY 11040, USA
e-mail: bgilbert@gmail.com

The Safety of Ultrasound: Primum Non Nocere

Diagnostic ultrasound uses no ionizing radiation, and is therefore generally considered a safe imaging modality. However, sound waves are not entirely benign. The mechanical effects of sound waves may strong enough to break up kidney stones during lithotripsy, or may cause the cavitation of bubbles in tissues containing gas pockets. The friction created as sound waves travel through tissue may result in therapeutic localized heating (desired in physical therapy), or the elevated temperature may have unwanted effects.

In 1985, the US Food and Drug Administration (FDA) developed ultrasound exposure limits for various diagnostic applications: 720 mW/cm^2 spatial peak temporal average (SPTA) for peripheral vascular ultrasound, 430 mW/cm^2 for

P.F. Fulgham, B.R. Gilbert (eds.), *Practical Urological Ultrasound*, Current Clinical Urology,
DOI 10.1007/978-3-319-43868-9_17

cardiac ultrasound, 94 mW/cm^2 for fetal and other ultrasound, and 17 mW/cm^2 for ophthalmic ultrasound. In 1992, the FDA approved the sale of equipment with an SPTA 720 mW/cm^2 for all applications other than ophthalmic as long as the equipment included displayed the newly developed thermal and mechanical indices. With this change, the user, not the manufacturer, has primary responsibility for ensuring the safe use of ultrasound [1, 2].

Much of the research on the safety of diagnostic ultrasound has focused on its use in obstetrics [3]. While attention to ultrasound exposure is critical, the importance of knowledge and experience must not be overlooked [4]. Patients who receive technically inadequate and/or misinterpreted sonograms may not be appropriately managed, require additional studies, or undergo unnecessary procedures. As Merritt wrote in 1989,

> [If] we are really serious in our intention to perform sonographic studies with maximum benefit and minimal risk, the problem of user education, as well as that of bioeffects, must be addressed. In sonography, inadequate user input may be as bad or worse for the patient than excessive acoustic output. The traditional emphasis on the training and practice of the radiologist and the technical and clinical aspects of imaging should encourage our specialty to lead rather than follow our clinical colleagues in the practice and teaching of safe and effective sonography. Only through this approach can we fulfill our fundamental obligation as physicians to protect the patient from unnecessary harm and provide maximum benefit with minimal risk [5].

The History of Ultrasound Practice Accreditation

There are few laws regulating the performance and interpretation of ultrasound examinations. Any licensed physician may purchase an ultrasound machine and begin performing and interpreting sonograms, regardless of whether he or she has received training in the area. Likewise, in most states, any individual can be handed a transducer and told to scan. When an ultrasound exam is indicated, how can patients and their referring physicians know where to go?

In 1995, the American College of Radiology (ACR) and the American Institute of Ultrasound in Medicine (AIUM) began to develop programs to accredit ultrasound practices, and the two organizations accredited their first ultrasound practices in 1996. As of this writing, there are 4401 practices (each site applies as a single practice) with ACR ultrasound accreditation and 1210 (a total of 2039 sites) with AIUM ultrasound accreditation.

The ACR offers ultrasound practice accreditation in breast, general, gynecologic, obstetric, and vascular ultrasound. The AIUM offers an ever expanding list of ultrasound practice accreditation specialties including abdominal/general, breast, diagnostic and interventional musculoskeletal, dedicated thyroid/parathyroid, gynecologic, fetal echocardiography, obstetric, Had and Neck, OB with adjunct detailed fetal anatomic ultrasound, urologic ultrasound, and ultrasound-guided procedures.

Because many leaders of the ultrasound community belong to both organizations, their accreditation programs are similar. Both organizations have developed training guidelines for the interpretation of ultrasound examinations [6–8], and the two organizations have collaborated on the development of guidelines for the performance of a variety of ultrasound exams. Both programs review the qualifications of the physicians and sonographers in the practice, the maintenance and calibration of ultrasound equipment, various policies and procedures, and both programs require the submission of actual case studies. Both programs are accepted by insurers that require ultrasound practice accreditation as a requirement for reimbursement.

The differences between the two organizations can be seen in their mission statements:

> "The ACR serves patients and society by maximizing the value of radiology, radiation oncology, interventional radiology, nuclear medicine and medical physics." [9]

> "The American Institute of Ultrasound in Medicine is a multidisciplinary association dedicated to advancing the safe and effective use of ultrasound in medicine through professional and public education, research, development of guidelines, and accreditation." [10]

AIUM ultrasound physician training guidelines and ultrasound examination guidelines must be relevant to the organizations that are most directly involved with specific ultrasound specialties. For example, AIUM guidelines for the performance of abdominal/retroperitoneal ultrasound examinations were developed in collaboration with ACR, the Society for Pediatric Radiology (SPR), and the Society of Radiologists in Ultrasound (SRU). ACR and the American College of Obstetricians and Gynecologists (ACOG) collaborated on the guidelines for the performance of obstetric ultrasound exams. The participation of the American Urological Association (AUA) was critical in the development of AIUM Training Guidelines for the Performance of Ultrasound in the Practice of Urology [8] and AIUM Practice Guidelines for the Performance of an Ultrasound Examination in the Practice of Urology [9]. This collaboration led to the development of AIUM ultrasound accreditation in the practice of urology.

How does accreditation differ from certification? Certification is granted to an individual who has demonstrated a level of knowledge and who continues to meet the requirements necessary to maintain the certification. The individual remains certified regardless of where he or she practices. Accreditation is granted to a practice (which may be the practice of a solo practitioner) that demonstrates that all of the individuals in the practice, all the relevant policies and procedures, and equipment and maintenance meet certain requirements. Practices must continue to demonstrate compliance at regular intervals, regardless of whether there are changes in personnel, policies, or equipment. An individual who works in an accredited practice cannot go to another practice and claim that the services provided at the second facility are accredited.

Development of Standards in Ultrasound

Standards are essential for the accreditation of practices in ultrasound. Standards provide a universal guideline to compare and assess competency in performing diagnostic examinations. Through the process of accreditation, agencies such as the AIUM are able to vet practices to ensure consistent examination performance across numerous practices and within different fields and specialties. Through reaccreditation, central agencies are able to evaluate practice performance against standard guidelines and track improvement. In a 2004 study, 57 % of studied obstetric practices met minimum AIUM standards and initial accreditation, compared to 86 % of these same practices meeting minimum standards at reaccreditation [11]. Requiring practices to adhere to quality standards improves overall performance and consistency, improving patient outcomes and creating more efficient systems. Thus standards ensure the performance of high quality ultrasound examinations in both academic and community settings.

The primary goal of setting standards is to improve patient care by improving diagnostic accuracy and efficiency. Quality standards also address equipment and patient safety, ensuring a safe environment. Due to lagging and varying equipment and laboratory quality across Europe, the European Association of Cardiovascular Imaging recently set out to standardize these areas by issuing updated standards and processes for accreditation [12]. Practices can also reap benefits by adhering to high quality standards set by well-known agencies. Accreditation by a society known to have high quality standards such as an American College of Radiology can provide a practice prestige and set it apart as compared to other unaccredited practices [13]. Also many state agencies and third-party payers require accreditation with societies such as ACR or AIUM for reimbursement of diagnostic exams.

AIUM Ultrasound Practice Accreditation in Urologic Ultrasound

The AUA has partnered with AIUM to create a path to accreditation for performance of ultrasound in urology practice, utilizing AIUM and an independent third-party reviewer. The application is submitted online at http://aium.org/accreditation/accreditation.aspx, and consists of the following sections.

- Contact information
- Overview of the practice
  - Specialty/specialties in which the practice seeks accreditation
  - The type of practice
  - Ultrasound coverage
  - OSHA compliance

    Practices may consist of one or more fixed sites, may be exclusively mobile (in which case a machine is taken from one location to another), or may be a combination of the two.
- Document Storage and Record-Keeping Policies

  There must be stored images of all relevant normal and abnormal findings. Images and reports must be retained for a period of time that meets or exceeds state or federal requirements [14, 15].
- Patient Safety and Quality Assurance Protocols
  - Steps to ensure that the appropriate study is performed on the correct patient
  - If ultrasound-guided invasive procedures are performed, steps taken to verify patient identification, procedure site, specimen labeling and hand-off
  - Incident reporting
  - Availability of signed final reports
  - Preliminary report policies (if applicable)
  - Universal precautions
  - Disinfection of endocavitary probes
  - Implementation of the ALARA principle
  - Quality assurance

    Final reports must be signed within 24 h of the exam or, for nonemergency cases, by the next business day [14, 15].

    The practice must also meet AIUM transducer cleaning guidelines. Endocavitary probes must undergo high level disinfection after every use, using an FDA-cleared solution [16].

    There must be policies and procedures to protect patients and personnel. The practice must show evidence of practicing the ALARA (As Low As Reasonably Achievable) principle. There must be regular, retrospective efforts to monitor the completeness and technical quality of images and the accuracy and timeliness of reports [14].
- Facility/facilities
  - Address, phone, fax
  - Specialty/specialties performed
  - Annual ultrasound volume
  - Is this site the principal location where each ultrasound specialty is performed?

    A practice may accredit several sites under a single application as long as there is one physician director overseeing the ultrasound operations at all site, the sites follow the same ultrasound examination protocols, reporting policies, etc., and the ultrasound equipment is of comparable quality.
- Ultrasound equipment
  - Location
  - Make, model, serial number, year acquired
  - Frequency of maintenance

    Each ultrasound machine must undergo preventive maintenance and calibration on an annual basis or more frequently [14].
- Interpreting physicians
  - Name
  - Involvement with ultrasound functions
  - Specialty/specialties interpreted, average weekly volume
  - Residency and (if applicable) fellowship
  - Ultrasound training
  - Ultrasound continuing medical education

    Only those physicians in the practice who interpret ultrasound should be listed on the application. All physicians who interpret ultrasound for the practice, even if they only provide occasional coverage, must meet the physician training guidelines (Table 17.1) and be listed on the application. One of the interpreting physicians must be designated as the practice's physician director of ultrasound.

    Each interpreting physician must have participated in at least 100 genitourinary ultrasound examinations prior to submitting the application, and must participate in at least 150 genitourinary ultrasound in the 3 years prior to reaccreditation [14].

    Once the practice is accredited, each interpreting physician must obtain a minimum of ten AMA PRA Category 1 Credits™ in genitourinary ultrasound every 3 years [14].

Table 17.1 Training guidelines for physicians who evaluate and interpret urologic ultrasound examinations

The following is extracted from the AIUM training guidelines approved October 31, 2015. The current training guidelines can be found at http://www.aium.org/officialStatements/53. (Reproduced with permission of the American Institute of Ultrasound in Medicine)
Physicians who perform and/or interpret diagnostic ultrasound examinations in the practice of urology should be licensed medical practitioners who have a thorough understanding of the indications and guidelines for genitourinary ultrasound examinations as well as a familiarity with the basic physical principles and limitations of the technology of ultrasound imaging. They should be familiar with alternative and complementary imaging and diagnostic procedures and should be capable of correlating the results of these other procedures with the ultrasound findings. They should have an understanding of ultrasound technology and instrumentation, ultrasound power output, equipment calibration, and safety. Physicians responsible for diagnostic genitourinary ultrasound examinations should be able to demonstrate familiarity with the anatomic, physiologic, and pathophysiologic characteristics of the anatomic areas that are being examined. These physicians should provide evidence of the training and competence needed to perform and/or interpret diagnostic urologic ultrasound examinations successfully. The training should include methods of documentation and reporting of ultrasound studies
Physicians performing and/or interpreting diagnostic urologic examinations should meet at least one of the following criteria:
1. Completion of an accredited urologic residency that includes training in ultrasound since July 1, 2009 (the year reporting of ultrasound examinations was required by the residency review committee), and is board certified by the American Board of Urology or is board eligible. If completion of certification occurred more than 36 months ago, maintenance of competence must be demonstrated, such as 50 diagnostic urologic ultrasound examinations per year and a total of ten *AMA PRA Category 1 Credits*™ within the previous 36 months[a]
2. Board certification in urology before July 1, 2009, and submission of an attestation of experience including involvement with 100[b] diagnostic urologic ultrasound examinations and training in urologic ultrasound that includes at least a minimum of 12 *AMA PRA Category 1 Credits*™; or level 2 course(s) verifying that the individual has satisfactorily met all specified learning objectives for the level 2 classification course(s) including hands-on demonstration of successfully performing and documenting ultrasound studies. Continuing medical education courses must be approved by the American Urological Association Office of Education or AIUM and include both didactic and hands-on ultrasound. If the level 2 course was completed more than 36 months ago, maintenance of competence must be demonstrated, such as 50 diagnostic urologic ultrasound examinations per year and a total of ten *AMA PRA Category 1 Credits*™ within the previous 36 months[a]
3. Completion of an accredited residency program and/or fellowship or postgraduate training (other than in urology) that includes structured training in diagnostic urologic ultrasound, under the supervision of a qualified physician(s),[c] during which the trainee will have evidence of being involved with the performance, evaluation, interpretation, and reporting of at least 100[b] diagnostic urologic ultrasound examinations
If completion of a residency and/or fellowship program occurred more than 36 months ago:
(a) The supervision and/or performance, interpretation, and reporting of at least 100[b] diagnostic urologic ultrasound examinations in the previous 36 months must be demonstrated; and
(b) Fifteen *AMA PRA Category 1 Credits*™ dedicated to diagnostic urologic ultrasound must be documented within the previous 36 months[a]
4. For completion of an accredited residency program and/or fellowship (other than in urology) in which the physician did not receive the required structured training in diagnostic urologic ultrasound, acceptable clinical experience can be documented by demonstrating:
(a) Evidence of being involved with the performance, evaluation, interpretation, and reporting of at least 100[b] diagnostic urologic ultrasound examinations within the previous 36 months. It is expected that in most circumstances, examinations will be under the supervision of a qualified physician(s);[c] and
(b) Evidence of 30 *AMA PRA Category 1 Credits*™ dedicated to diagnostic urologic ultrasound within the previous 36 months[a]
Maintenance of competence in urologic ultrasound
All physicians performing urologic ultrasound examinations should demonstrate evidence of continuing competence in the interpretation and reporting of those examinations. A minimum of 50 diagnostic genitourinary ultrasound examinations per year is recommended to maintain the physician's skills
Continuing medical education in urologic ultrasound
The physician should complete 10 h of *AMA PRA Category 1 Credits*™ specific to urologic ultrasound every 3 years
Developed in collaboration with the following organization:
American Urological Association

[a]If the physician interprets in multiple specialties, a representative sample of specialties totaling at least 30 *AMA PRA Category 1 Credits*™ dedicated to ultrasound is acceptable

[b]One hundred cases were selected as a minimum number needed to gain experience and proficiency with sonography as a diagnostic modality. This is necessary to develop technical skills, to appreciate the practical applications of basic physics as it affects image quality and artifact formation, and to acquire an experience base for understanding the range of normal and recognizing deviations from normal

[c]A qualified physician is one who, at minimum, meets the criteria defined above in this document

Cases presented as preselected, limited-image sets, such as in lectures, case conferences, and teaching files, are excluded. The ability to analyze a full image set, determining its completeness and the adequacy of image quality, and performing the diagnostic process, distinguishing normal from abnormal, is considered a primary goal of the training experience

- Sonographers (if applicable)
  - Name
  - Involvement with ultrasound functions
  - Certification
  - Training
  - Specialty/specialties performed
  - Length of time with practice

    Each sonographer or other nonphysician who performs ultrasound examinations for the practice must be or become appropriately certified prior to reaccreditation (in 3 years). The AIUM currently recognizes certification in abdominal ultrasound by the American Registry of Diagnostic Medical Sonography (ARDMS) and general sonography certification granted by the American Registry of Radiologic Technologists (ARRT) obtained after January 1, 2013 [14].
- Additional personnel (if applicable)
  - Name
  - Involvement with ultrasound functions

Within 1 week of submitting the online application, the practice must submit the following to the AIUM:

1. Payment (if not already paid online).

   The nonrefundable accreditation fee is automatically calculated based on the number of specialties in which the practice seeks accreditation, the number of sites the practice would like to have accredited, and the number of machines the practice has [17].
2. The Accreditation Agreement.

   The Accreditation Agreement defines the relationship between the AIUM and the practice seeking accreditation. It includes a HIPAA addendum by which the practice names the AIUM as its Business Associate. Review of the application cannot begin without this agreement. The AIUM will also sign the agreement and forward you a copy for your HIPAA records [18].
3. Supporting documents, including medical licenses and residency and/or fellowship certificates for each interpreting physician, current registry cards for all sonographers (if applicable), and preventive maintenance records for each of your ultrasound machines [19].
4. Case studies. The case studies are the most important component of the accreditation application.

   The practice must upload digital images and reports from four cases in the area or areas most commonly performed by the practice at its principal site. For example, a practice that mostly sees males with a history of infertility, most or all of the cases submitted are likely to be scrotal sonograms. Another practice may choose to submit (in triplicate) the images and reports from one renal study, two prostate studies, and one penile study.

   If the practice has more than one site or mobile unit, it must submit one additional case study and report (in triplicate) from each additional site or mobile unit [20].

   Important points:

(a) The practice must retain all original studies.
(b) The copies must be identical in content and quality.
(c) Cases performed using automated bladder scanners are not acceptable.
(d) Only diagnostic studies performed within the last 12 months are acceptable.
(e) If there are multiple interpreting physicians and/or sonographers, the cases must reflect as many of the physicians and/or sonographers as possible. Studies performed or interpreted by someone who is not listed on the application will not be accepted.

The AIUM Accreditation Review Process

Once the online application, signed accreditation agreements, payment, supporting documents, and case studies have been received, one copy of the agreement, now also signed by the AIUM, is returned to the practice with a note that the application is complete and is being sent out for review.

The online portion of the application and the supporting documents are reviewed internally.

The case studies are sent out to two independent reviewers, and, if their scores are discrepant, may be sent to a third reviewer as well. All studies are scored based on their compliance or noncompliance with the relevant ultrasound examination guidelines.

Once all of the scores have been reconciled and review of the online application is complete, the practice will be sent a findings letter that summarizes any areas that need clarification or revision, as well as reports of any deficient areas noted in the case studies. The practice will be given 30 days to respond to the letter and, if one or more case studies receive failing scores, submit a new case or cases showing that the practice has implemented changes to correct any deficiencies.

Once the response has been received, the application will be presented to the AIUM Ultrasound Practice Accreditation Council, which will decide whether to grant accreditation.

The Effect of Ultrasound Practice Accreditation

To date, there have been few studies on the impact of ultrasound practice accreditation.

In 2004, Brown et al. published a retrospective review of asymptomatic patients who were referred for surgical evaluation for carotid endarterectomy on the basis of carotid arteries studies performed at nonaccredited facilities [21]. All patients underwent additional scans at an accredited facility. The authors found that technical errors by the unaccredited facilities led to overestimation of disease in 18 % of the cases, and underestimation of disease in 26 % of cases. Patient management was significantly altered on the basis of the repeat studies performed at the accredited facility in 61 % of patients.

There were significant limitations to this study, which based its conclusions on findings from "several" nonaccredited facility and one accredited practice. All analysis was based on the reports from the nonaccredited practices; no images from these practices were reviewed, and the findings from the accredited practice were used as the standard; no angiograms were obtained.

Another study by Abuhamad et al. was also published in 2004 [11]. In this study, the scores of practices applying for AIUM reaccreditation were compared to the scores the same practices had received on their initial applications 3 years earlier. The scores of the practices applying for reaccreditation were also compared to the scores of practices submitting initial applications at the same time (and in the same specialties) as the reaccreditation applications. Because most of the applications received at that time were in obstetric and/or gynecologic ultrasound, only those specialties were reviewed.

The scores of practices applying for reaccreditation were significantly higher than their initial scores ($p<0.001$ for all). The scores of the practices applying for reaccreditation were also significantly higher than those of practices applying for initial accreditation at the same time although it was noted that the scores of practices applying for initial accreditation at that time were higher than the initial scores of the practices now applying for reaccreditation. The findings confirmed that the process of accreditation played a significant role in the improvement of scores at reaccreditation, and the authors suggested that growing familiarity with AIUM standards and guidelines may have contributed to the higher scores earned by initial applicants applying for accreditation when compared to the scores earned by practices that initially applied for accreditation 3 years earlier.

"In conclusion," the authors wrote, "our study shows that ultrasound accreditation adds value to the practice by improving compliance with AIUM minimum standards and guidelines for the performance of ultrasound examinations, which should translate into enhancement of the quality of the ultrasound practice."

Popowski et al. [22] compared performance of ultrasound by GYN residents before and after a short training session and before and after an accreditation training process. The short training session consisted of a 1-h class taught by a board-certified Ob-Gyn expert in ultrasound and received a written standardized imaging protocol. The residents who underwent the full accreditation training process had higher quality scores fon ultrasound examinations as compared to

residents who only underwent the short training session [22]. Thus the accreditation process raises the quality of ultrasound performance and allows for quality control of examinations.

A Urology Practice Perspective

The process of practice accreditation is not without challenges to both the urologists and the urology practice. Urologists have traditionally viewed imaging as a tool, very much like a stethoscope, that assists them in providing care for their patients. The process of accreditation changes this by requiring both the urologist and the urology practice to expend resources to meet the requirements of accreditation. As the Physician Director of an AIUM accredited urology practice (BRG) I first needed make sure that all members of our group understood the benefits of practice accreditation and were supportive of the endeavor. A concern of my colleagues was that if any did not meet the physician requirements for credentialing by the date of accreditation that physician could no longer order, review, or bill for these studies until that individual satisfied the requirements. To maximize the number of credentialed physicians we arranged with the AUA to have a Hands-On ultrasound course that would satisfy the training requirements as specified above.

A second challenge, which actually turned out to be a tremendous benefit of going through the accreditation process, was the organization of our ultrasound program. A Policy and Procedure (P&P) manual was developed that organized our quality assurance program. Preventative maintenance logs were updated and placed on recurring cycles with our vendors. Protocols were developed with the sonographers to assure quality and consistency in all ultrasound exams. An image archival system (PACS) was purchased and integrated with our electronic medical records for image and report archiving. Twenty-four hours physician review and sign-off was therefore easily attained. We have also instituted monthly meetings with the physician director of ultrasound and sonographers at which time we review random studies and reports and adjust our protocols as needed.

ARDMS, the American Registry for Diagnostic Medical Sonography, certifies ultrasound technicians in performing specific sonographic examinations. The ARDMS also runs programs for physician certification in certain areas of performing ultrasound such as in echocardiography and vascular ultrasound. At this point ARDMS does not have any physician-oriented certification for urology-associated ultrasound imaging so the urologist does not yet need to consider ARDMS certification.

Overall the accreditation process has greatly helped organize our approach and markedly improved the quality of our process. This has translated into improved diagnostic examinations and, in turn, patient care. In addition, it has allowed us to obtain reimbursement from third-party payers that have been denying claims based on our prior lack of accreditation.

References

1. Miller DL. Safety assurance in obstetrical ultrasound. Semin Ultrasound CT MR. 2008;29(2):156–64.
2. Nelson TR, Fowlkes JB, Abramowicz JS, Church CC. Ultrasound biosafety considerations for the practicing sonographer and sonologist. J Ultrasound Med. 2009;28:139–50.
3. Houston LE, Odibo AO, Macones GA. The safety of obstetrical ultrasound: a review. Prenat Diagn. 2009; 29:1204–12.
4. Filly RA, Crane JP. Routine obstetric sonography. J Ultrasound Med. 2002;21:713–8.
5. Merritt CRB. Ultrasound safety: what are the issues? Radiology. 1989;173:304–6.
6. ACR-SPR-SRU practice guideline for performing and interpreting diagnostic ultrasound examinations. http://www.acr.org/~/media/ACR/Documents/PGTS/guidelines/US_Performing_Interpreting.pdf
7. AIUM training guidelines for physicians who evaluate and interpret ultrasound examinations. http://aium.org/resources/viewStatement.aspx?id=14
8. AIUM training guidelines for the performance of ultrasound in the practice of urology. http://aium.org/resources/viewStatement.aspx?id=44
9. ACR history and mission. http://www.acr.org/About-Us
10. AIUM mission statement. http://aium.org/aboutUs/constitution.aspx
11. Abuhamad AZ, Benacerraf BR, Woletz P, et al. The accreditation of ultrasound practices: impact on compliance with minimum performance guidelines. J Ultrasound Med. 2004;23:1023–9.

12. Popescu BA, Stefanidis A, Nihoyannopoulos P, et al. Updated standards and processes for accreditation of echocardiographic laboratories from The European Association of Cardiovascular Imaging. Eur Heart J Cardiovasc Imaging. 2014;15(7):717–27.
13. Tomory M. ACR ultrasound accreditation: how does that impact equipment maintenance? Biomed Instrum Technol. 2010;44(5):402–3.
14. AIUM standards and guidelines for the accreditation of ultrasound practices. http://aium.org/resources/viewStatement.aspx?id=26
15. AIUM practice guideline for documentation of an ultrasound examination. http://aium.org/resources/guidelines/documentation.pdf
16. AIUM guidelines for cleaning and preparing endocavitary ultrasound transducers between patients. http://aium.org/resources/viewStatement.aspx?id=27
17. Accreditation fee calculator. http://aium.org/accreditation/fees.pdf
18. Accreditation agreement. http://aium.org/accreditation/agreement.pdf
19. Accreditation application checklist. http://aium.org/accreditation/checklist.pdf
20. Case study submission requirements. http://aium.org/accreditation/caseStudyRequirements/urologic.pdf
21. Brown OW, Bendick PJ, Bove PG, et al. Reliability of extracranial carotid artery duplex ultrasound scanning: value of vascular laboratory accreditation. J Vasc Surg. 2004;39:366–71.
22. Popowski T, Huchon C, Fathallah K, et al. Impact of accreditation training for residents on sonographic quality in gynecologic emergencies. J Ultrasound Med. 2015;34(5):829–35.

ERRATUM TO

Physical Principles of Ultrasound

Pat F. Fulgham

P.F. Fulgham, B.R. Gilbert (eds.), *Practical Urological Ultrasound*, Current Clinical Urology,
DOI 10.1007/978-3-319-43868-9_2

DOI 10.1007/978-3-319-43868-9_18

The published version of this book included error in the image Fig 2.20. This image has been updated.

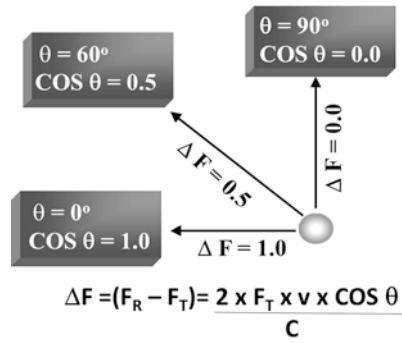

The updated online version of the original chapter can be found under
http://dx.doi.org/10.1007/978-3-319-43868-9_2

P.F. Fulgham, B.R. Gilbert (eds.), *Practical Urological Ultrasound*, Current Clinical Urology,
DOI 10.1007/978-3-319-43868-9_18

Index

P.F. Fulgham, B.R. Gilbert (eds.), *Practical Urological Ultrasound*, Current Clinical Urology,
DOI 10.1007/978-3-319-43868-9